

RAS 12277

DOCKETED
USNRC

NEDO-24154-A
78NED290R1
CLASS I
AUGUST 1986

2006 SEP 19 PM 3:37

OFFICE OF THE SECRETARY
NUCLEAR REGULATORY COMMISSION
ADJUDICATIONS STAFF

DOCKET NUMBER
PROD. & UTIL. FAC. 50-271-01A

LICENSING TOPICAL REPORT

QUALIFICATION OF THE ONE-DIMENSIONAL CORE TRANSIENT MODEL FOR BOILING WATER REACTORS VOLUME 1

U.S. NUCLEAR REGULATORY COMMISSION

In the Matter of Entergy Nuclear Vermont Yankee LLC

Docket No. 50-271 Official Exhibit No. Entergy 26

OFFERED by Applicant/Licensee Intervenor (Incl. Staff 15, 16)

NRC Staff _____ Other _____

IDENTIFIED on 9/13/06 Witness/Panel Nichols/Casillas

Action Taken: ADMITTED REJECTED WITHDRAWN

Reported/Clerk MAC

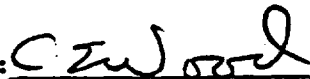
GENERAL  ELECTRIC

NEDO-24154-A
78NED290R1
Class I
August 1986

LICENSING TOPICAL REPORT

QUALIFICATION OF THE ONE-DIMENSIONAL
CORE TRANSIENT MODEL FOR BOILING WATER REACTORS
VOLUME 1

Approved:



J. E. Wood, Manager
Core & Fuel Technology

Approved:



D. L. Fischer, Manager
Core Nuclear Design

NUCLEAR ENERGY BUSINESS OPERATIONS • GENERAL ELECTRIC COMPANY
SAN JOSE, CALIFORNIA 95125

GENERAL  ELECTRIC

NEDO-24154-A

DISCLAIMER OF RESPONSIBILITY

Neither the General Electric Company nor any of the contributors to this document makes any warranty or representation (express or implied) with respect to the accuracy, completeness, or usefulness of the information contained in this document or that the use of such information may not infringe on privately owned rights; nor do they assume any responsibility for liability or damage of any kind which may result from the use of any of the information contained in this document.



UNITED STATES
NUCLEAR REGULATORY COMMISSION
WASHINGTON, D. C. 20555

FEB 4 1981

Dr. G. G. Sherwood, Manager
Safety and Licensing
General Electric Company
175 Curtner Avenue
San Jose, California 95114

Dear Dr. Sherwood:

SUBJECT: ACCEPTANCE FOR REFERENCING GENERAL ELECTRIC LICENSING TOPICAL
REPORT NEDO-24154/NEDE-24154P

The Nuclear Regulatory Commission has completed its review of the General Electric Company Licensing Topical Report NEDO-24154 Volumes I and II and NEDE-24154 Volume III entitled "Qualification of the One-Dimensional Core Transient Model for Boiling Water Reactors" and the supplemental information submitted by R. H. Buchholz, letter (MFN 155-80) dated September 5, 1980. This report describes the General Electric transient analysis code, ODYN. This code is to be used for transient analyses of the following eight transients:

A. For Thermal Limit Evaluation

<u>Event</u>	<u>Thermally Limiting or Near Limiting (Typically)</u>
1. Feedwater Controller Failure - Maximum Demand	X
2. Pressure Regulator Failure - Closed	
3. Generator Load Rejection	X
4. Turbine Trip	X
5. Main Steamline Isolation Valve Closures	
6. Loss of Condenser Vacuum	
7. Loss of Auxiliary Power - All Grid Connections	X

FEB 4 1981

Dr. G. G. Sherwood

-2-

B. For ASME Vessel Overpressure Protection Pressure Limiting

1. MSIV Closure with Position Switch
Scram Failure (i.e., MSIV Flux Scram) X

Other transients and anticipated operational occurrences may be analyzed with the REDY Code described in NEDO-10802.

For all operating BWRs and those currently under operating license review, we propose that the following pressurization events be reanalyzed using ODYN: generator load rejection/turbine trip without bypass (whichever is limiting), feedwater controller failure-maximum demand and main steam isolation valve closure-flux scram (to satisfy ASME code pressure requirements). These are the same pressurization events presently included in reload submittals. As discussed in the September 5, 1980 letter from R. H. Buchholz (GE) to USNRC subject: "Response to NRC Request for Information on ODYN Computer Model," the events not included are considered to be bounded by these three.

This letter also provides the information required for application of ODYN and justification for continued plant operation during transition from transient analyses based on ODYN. The safety evaluation and a supplementary safety evaluation are enclosed.

As a result of our review, we find the Licensing Topical Report NEDO-24154 Volumes I and II/NEDE-24154P Volume III as augmented by GE/Buchholz letter No. MFN 155-80 dated September 5, 1980 acceptable for referencing in applications for operating license within the conditions specified in the topical report, the supplemental letter and the attached safety evaluation and supplement.

We do not intend to repeat the review of the safety features described in the topical report and found acceptable in the attachment. Our acceptance applies only to the features described in the topical report and under the conditions discussed in the attachment.

In accordance with established procedure, it is requested that General Electric Company publish an approved version of these reports, proprietary and non-proprietary, within three months of receipt of this letter. The revisions are to appropriately incorporate the supplementary information into the body of the report and incorporate this letter and the attached safety evaluation and supplement following the title page and thus just in front of the abstract. The report identifications of the approved reports are to have a -A suffix.

Dr. G. G. Sherwood

-3-

FEB 4 1961

Should Nuclear Regulatory Commission criteria or regulations change such that our conclusions as to the acceptability of the report are invalidated, General Electric and/or the applicants referencing the topical report will be expected to revise and resubmit their respective documentation or submit justification for the continued effective applicability of the topical report without revision of their respective documentation.

Sincerely,



Robert L. Tedesco, Assistant Director
for Licensing
Division of Licensing

Enclosure:
As Stated

SAFETY EVALUATION
FOR THE
GENERAL ELECTRIC TOPICAL REPORT
QUALIFICATION OF THE ONE-DIMENSIONAL
CORE TRANSIENT MODEL FOR
BOILING WATER REACTORS
NEDE-24154 and NEDE-24154-P
Volumes I, II and III

Prepared By
Reactor Systems Branch, OSI

Reviewers
F. Odar, Lead (RES)
L. Baltracchi
D. B. Fieno
G. M. Holahan
M. M. Mendonca
J. Voglewede

June 1980

TABLE OF CONTENTS

	<u>Page</u>
I. SUMMARY OF THE TOPICAL REPORT.....	I-1
A. INTRODUCTION.....	I-1
B. SCOPE.....	I-2
C. SUMMARY OF ANALYTICAL MODELS.....	I-2
II. STAFF EVALUATION.....	II-1
A. REVIEW OF ANALYTICAL MODELS.....	II-2
1. Recirculation and Control System.....	II-2
a. Recirculation Loop Model.....	II-2
b. Control System Model.....	II-6
c. Steam Separator Model.....	II-9
d. Upper Plenum, Vessel Dome and Bulkwater Model.....	II-11
2. Steam Line Model.....	II-12
3. Core Thermal Hydraulics Model.....	II-14
a. Drift Flux Model.....	II-15
b. Mechanistic Boiling Model.....	II-19
4. Core Physics Model.....	II-20
a. Assumptions in the Neutronics Model.....	II-20
b. Derivation of Equations for the One-Group, One-Dimensional, Time-Dependent Neutronic Model.....	II-21
c. Calculation of Input Parameters.....	II-23
5. Fuel Heat Transfer Model.....	II-25
6. Summary of Code Uncertainties.....	II-31
a. Margin in ACPR Calculations.....	II-31
b. Margin in Pressure Calculation.....	II-33
B. QUALIFICATION OF THE ODYN CODE.....	II-35
1. Qualification of Neutronics Model - Comparison of ODYN with BWR Core Simulator.....	II-35
2. Qualification of Thermal Hydraulic Model.....	II-38

TABLE OF CONTENTS (Continued)

	<u>Page</u>
3. Qualification Using Integral Tests.....	II-40
a. Peach Bottom Tests.....	II-40
b. KKM Test.....	II-54
4. Qualification Using Another Computer Code - Audit Calculations.....	II-59
a. Development of Computational Method.....	II-59
b. Peach Bottom Tests and Audit Calculations.....	II-61
5. Summary of Code Qualification.....	II-75
C. EVALUATION OF THE MARGIN.....	II-76
III. STAFF POSITION.....	III-1
IV. REFERENCES.....	IV-1

I. SUMMARY OF TOPICAL REPORT

A. INTRODUCTION

Between April 9, 1977 and April 27, 1977, three turbine trip tests were performed at the Peach Bottom, Unit 2, to examine the validity of the General Electric transient analysis methods and verify the computer codes. The first scram signal which normally would have been initiated on the position of the turbine stop valve, was bypassed in order to provide a transient comparable in severity to the worst transients analyzed in FSARs. Using the transient analysis method and the REDY computer code used in the licensing applications at that time, General Electric made pre-test predictions of pressure, neutron flux and Δ CPR on a best estimate basis. The neutron flux and Δ CPR predictions were significantly nonconservative and the pressure predictions were somewhat nonconservative.

After the tests General Electric performed post-test predictions of pressure, neutron flux and Δ CPR using the actual or measured plant parameters with best estimate modeling assumptions as well as the licensing model assumptions. The Δ CPR and the neutron flux predictions were again nonconservative for both sets of calculations. The pressure peaks were predicted conservatively. It should be noted that General Electric showed that the predictions of pressure and Δ CPR were conservative with licensing basis inputs when the first scram signal initiated on turbine stop valve position was not bypassed, i.e., under normal conditions.

The comparisons of the test results and the REDY code, the licensing basis model, confirmed the existence of a steam line pressure wave propagation phenomenon in a turbine trip transient and time varying nature of the axial core

power distribution. General Electric accelerated its model development program to include steam line dynamics and representation of the core physics and thermal hydraulics in space-time domain and produced the ODYN computer code which is the subject of this review.

B. SCOPE

The scope of this review is the evaluation of the ODYN code for use in the analysis of certain transients in Chapter 15 of the FSARs.

C. SUMMARY OF ANALYTICAL MODELS

The overall system model in the ODYN code consists of a one-dimensional representation of the reactor core, and the recirculation and control system model. These two models are coupled to each other. A steady state initialization is made initially, and then the parameters for the transient are calculated.

First, the recirculation and control systems are solved for the steady state conditions. Some of the initial conditions are input and they may be plant unique. Other initial hydraulic values such as core pressure drop and bypass flow fraction, which are also input to the steady state recirculation and control model, are calculated elsewhere. These parameters are calculated in the steady state multi-channel core code (Reference 1). Using all these input values, the steady state recirculation and control model calculates the remaining hydraulic parameters in the plant. The steady state initialization in the recirculation and control model provides the loop pressure drop, core exit pressure, core inlet flow and enthalpy to the one-dimensional reactor core model. These values are used in the reactor core model to calculate the neutron kinetics, thermal hydraulics and fuel parameters for the steady state conditions.

The steady state axial power distribution is calculated by the neutronics model. The model uses cross section fits obtained from an analysis about cross sections for different relative coolant densities and control states and that are radially averaged for each axial plane. The fits are such that the axial power in the one dimensional model is required to yield the same axial behavior as in the three-dimensional BWR Core Simulator solution. The steady state thermal hydraulic solution permits the calculation of the steady state fuel temperature distribution.

During the transient, the recirculation and control system model calculates the time derivatives. At the end of the time step, the recirculation and control system model supplies the new external boundary conditions to the reactor core model. The reactor core model calculates the new neutron flux, thermal hydraulic parameters and fuel temperatures. It also provides reactor core exit quality, flow and pressure as input to the recirculation and control system model. The recirculation and control system model calculates the loop pressure drop and the reactor core model calculates the core pressure drop. These pressure drops are compared. If they are not equal within a certain limit, the recirculation and control system model derivatives are modified and the time step calculations are repeated.

The recirculation system is modeled by solving the mass, energy and momentum conservation equations for the steam line, reactor vessel and recirculation loop components which included jet pumps, recirculation pumps and associated piping. The control system is modeled as a series of connected gains, filters,

integrators, and nonlinearities (limiters and function generators). The control system output is valve position and thus flow control. The one-dimensional core model comprises equations describing the neutron kinetics, thermal-hydraulics and heat transfer behavior of the core.

Major assumptions used in the modeling of the recirculation system are as follows:

1. Pressure variations in the system are described with ten nodes. One node is used for the reactor inlet; another node is used for the reactor vessel dome, and the remaining eight nodes are used to describe the behavior of the steam line.
2. Liquid and vapor mass volume balances are used to predict the reactor vessel water level changes.
3. The recirculation loop model can simulate any combination of multi-loop systems. The entire recirculation loop is assumed to be subcooled and incompressible.
4. Steam in the steam line is treated as single phase flow. Condensation of steam in the steam line is precluded during the transient.

Major assumptions used in the reactor core model are as follows:

1. A one-dimensional neutron kinetics model is assumed. The neutron flux varies axially with time. One energy group diffusion theory and six delayed

neutron groups are used. Decay heat is modeled using a simple exponential decay heat model. The one dimensional neutron diffusion parameters are obtained by collapsing the parameters obtained from the GE three-dimensional BWR Core Simulator (Reference 2).

2. A single active heated channel represents the core average conditions and another single channel represents the core bypass. A five equation model representing mass and energy conservation for the liquid and vapor, and the mixture momentum conservation are used to calculate core thermal-hydraulic behavior.

3. Heat transfer to the moderator and fuel temperatures are calculated using an average fuel and cladding model at each axial location of the core. The gap conductance is an input parameter which may vary axially in time. The conduction parameters are temperature dependent. A radially uniform (flat) power distribution is assumed in the fuel rods.

II. STAFF EVALUATION

The staff evaluation was performed in three parts:

- A. Review of the analytical models in the ODYN code and determination of uncertainties in the code modeling.
- B. Review of the qualification of the code. This part of the review is accomplished in three areas:
 1. Comparison of specific models in the code with separate effects test data.
 2. Comparison of integral response of the code with the integral test data.
 3. Comparison of the code predictions with the predictions of an independent code; i.e., audit calculations.
- C. Review of the safety margin; i.e., evaluation of the margin when the code is used with the uncertainties assigned in the licensing basis transient. The uncertainties of the calculations were evaluated as part of the calculational model review.

The measure of all code uncertainties is made in terms of $\Delta\text{CPR}/\text{ICPR}$ ratio. The "CPR" is an acronym for critical power ratio. It is the ratio of the critical power of the limiting bundle in the core to the power of the same bundle at the operating power of interest. The critical power is an artificial bundle power obtained by increasing the power analytically until the critical quality is reached. The analysis is performed using the GEXL correlation. Since the hydraulic and neutronic parameters change during the transient, CPR also changes during the transient. The minimum value of the CPR is called MCPR and

the difference between the initial critical power ratio, ICPR, and MCPR is the Δ CPR. Hence, the ratio of Δ CPR/ICPR is a measure of the relative severity of the transient.

The uncertainties in the code are determined by making sensitivity studies. An independent parameter in the code is perturbed and the resulting change in Δ CPR/ICPR is calculated for a turbine trip without bypass transient, which is generally limiting. These independent parameters pertain to the various models such as the parameter of C_0 in the Zuber drift flux model or frictional loss coefficients in the steamline. They do not pertain to system parameters which determine the actuation of the valves since licensing basis analysis require limiting settings for these systems parameters.

A. REVIEW OF ANALYTICAL MODELS

1. Recirculation and Control System

a. Recirculation Loop Model

The recirculation loop system consists of the upper plenum, steam separators, vessel dome, jet pump and recirculation loop. Mass, energy and momentum conservation equations are used to describe thermal and hydraulic behavior of the components. These equations are solved using an explicit finite differencing method which is presented in Reference 3.

During the steady-state initialization, the time derivatives are set equal to zero. A multi-channel steady state hydraulics code provides the steady state core pressure drop and the bypass flow fraction to the recirculation system model. This code is presented in

Reference 1 and has been reviewed and approved by NRC (Reference 4). The other inputs used by the recirculation system model are plant specific such as dimensions related to plant geometry, pressure loss coefficients, separator carryunder fraction and jet pump and recirculation pump characteristics.

In the initial steady state conditions the jet pump drive and suction flows can be determined from the equation of continuity and the jet pump "m" ratio. This ratio is defined as the ratio of the suction to the drive flow. It is valid for the rated conditions which are selected to correspond to steady state initial operating conditions. Using the momentum equation and the "m" ratio, the suction flow and the suction flow loss coefficient are determined. During the transient the ratio changes. The jet pump suction and drive flows (consequently recirculation loop and core inlet flows) are calculated using the momentum equations keeping the suction flow loss coefficient constant. The sum of the suction and drive flows provide the recirculation loop flow and the sum of all recirculation loop flows provide the core inlet flow.

The recirculation system models used in the ODYN and REDY codes are the same. The REDY code (Reference 5) has been reviewed for ATWS analyses and the recirculation system model has been found acceptable with some limitations (Reference 6). The following discusses and evaluates the recirculation system model. This evaluation, except for the uncertainties, is the same both for ODYN and REDY codes. The

limitations found in the REDY code are equally applicable in the QOYN code.

During the transient, momentum equations are used to calculate the jet pump suction and drive flows. Hence, the form loss coefficients in the recirculation system affect the core flow and consequently the calculated ΔCPR . A sensitivity study performed by General Electric using the QOYN code by decreasing the diffuser form loss coefficient by 10% showed an increase of 0.001 in $\Delta\text{CPR}/\text{ICPR}$. General Electric estimated uncertainties in the jet pump loss coefficients about 20%. These uncertainties are inferred from the uncertainty in the jet pump "m" ratio. General Electric noted that the decrease in the jet pump pressure drop loss on the order of 20% changed $\Delta\text{CPR}/\text{ICPR}$ by 0.01. This is the biggest uncertainty estimated by General Electric in the recirculation system. According to General Electric reasonable variations in other parameters such as drive flow L/A, jet pump areas or lengths (which are manufactured to close engineering tolerances) and loss coefficients at the nozzle, plenum and bulkwater did not change $\Delta\text{CPR}/\text{ICPR}$ ratios significantly. Based on these sensitivity studies, the impact of these uncertainties on the values of $\Delta\text{CPR}/\text{ICPR}$ in the generally limiting transient is small.

During the transient, the transient terms of the momentum equation representing inertia may become important in determining the core flow. Recirculation pump trip tests were performed at 50%, 75%, and 100% power levels in the Oyster Creek plant and reported in Reference 5. Good agreement exists between the measured and REDY calculated

core flows for the transient. This shows that the momentum equations were solved correctly to predict flow transients. Recirculation pump trip tests were also performed in Dresden-2 and they were reported in Reference 5. However, in these tests measured core flows were higher than those calculated because the actual pump inertia was higher than the value used in the analysis.

One of the jet pump modeling assumptions is that the region from the nozzle to the throat is considered to have no inertia. In order to validate the transient modeling of the jet pump, transient jet pump tests were conducted at the Moss Landing Generating facility, Reference 5. In these tests the jet pump drive flows were oscillated at several frequencies and measurements were made of the gain and phase relationship of the drive flow. Comparison of the measurements and model predictions showed good agreement up to 5 Hz. The model did not predict a resonance condition in the cold test data at 6.5 Hz; consequently, the use of the model is limited to 5 Hz. This limitation means that the code will have errors if recirculation loop flow variations are sudden. The harmonic components of the flow variation should be less than 5 Hz.

Another assumption which has been validated by tests is the assumption of complete mixing at the core inlet. Tests were performed in Monticello to verify this assumption. Core flow distributions for three core flow rates, at 25%, 50% and 85% of rated flow rates, were measured for symmetric operation of the recirculation pumps, Reference 7. Tests results indicate that the bundle flow rate does not vary more than 2.8% from that in the average

bundle with 95% confidence level. This indicates that the assumption of uniform pressure distribution at the inlet of the core and complete mixing is a valid assumption for the recirculation system modeling.

The review of the analytical models and the comparison of the predictions with the tests above indicate that the recirculation loop model and the impact of associated uncertainties on ACPR/ICPR as presented by General Electric are acceptable. The harmonic components of the flow variation should be less than 5 Hz and the model should be valid for the analysis of transients where the fluid in the recirculation loop, downcomer and core inlet remains subcooled (incompressible). In the transients to be analyzed by the DDYN code, it is expected that these limits will not be exceeded.

b. Control System Model

The control system models were evaluated for structure as well as the methodology for evaluating plant specific properties. Plant specific properties consist of response functions, gains, and time constants for the control system.

The system models are composed of transfer functions, limiters and function generators. The transfer functions are based on typical filters and proportional, integral, derivative control laws. Limiters and function generators are used in the modeling of flow valves as a means of linearizing the gain within control loops. We have reviewed the model structure for the motor generator flow control

model, the feedwater control model and the pressure regulation with the Mechanical Hydraulic Control. We find the structure of these models acceptable and typical of the type of modeling conducted with classical control system theory.

With respect to the description of the control models, the following models were evaluated:

- (a) Valve Flow Control System
- (b) Motor-Generator Flow Control
- (c) Feedwater Flow
- (d) Pressure Regulator and Turbine Controls
- (e) Reactor Safety Systems

For input signals, the Valve Flow Control model receives a turbine governor signal, a sensed steamflow signal, a filtered neutron flux signal, a recirculation drive flow signal and a manual setpoint signal. The control system is modeled as a series of connected gains, filters, integrators, and nonlinearities (limiters and function generators). The control system output is valve position and thus flow control.

For input signals, the Motor-Generator Flow Control model receives a load demand error, a master manual or automatic signal as well as a loop manual or automatic signal. The control system is modeled as a series of gains, integrators, function generators, and with actuators of a drive motor, variable speed coupler, generator, and motor pump. The controlled variable is recirculation drive flow.

For input signals, the Feedwater Control System receives feedwater flow disturbances, vessel pressure corrections, a level setpoint signal, a mixture level signal, and a steam flow signal. These signals are operated on by a control modeled as a series of connected gains, integrators, filters, and non-linearities (limiters and function generators). The controlled variable is feedwater flow.

For input signals, the Pressure Regulator receives a turbine inlet pressure signal, a pressure setpoint, a turbine speed setpoint and a turbine load setpoint. These signals are operated on by a control modeled as a series of gains, filters, control laws, control valve servos and non-linearities. The controlled variable is turbine inlet pressure.

The staff review finds that these models are conditionally acceptable. Technically, the models are composed of transfer function, gains, filters, and synthesized nonlinearities such as deadbands and saturation limits. The technical form of the control system models is acceptable to the staff.

However, the model is used to establish initial control system settings such as gains, time constants, and control functions. Since the selection of these settings is made on a plant specific basis, the staff requires that each applicant's Safety Analysis Report reference a clearly defined basis for making these selections. The design criteria must be provided for each control system of the plant. The initial control system characteristics shall be verified as conforming to the design criteria for each control system of the plant.

c. Steam Separator Model

The separator is modeled using a one dimensional momentum conservation equation whereas the flow in a separator is rotational and clearly multi-dimensional. However, using separator test results (Reference 8), it was possible for General Electric to develop an empirical one dimensional momentum equation describing the flow behavior. Tests indicated that the thickness and configuration of the layer of swirling water along separator walls is independent of the inlet flow (for 200,000 lb/hr < Flow < 800,000 lb/hr) but dependent on the inlet quality. The water layer primarily affects the effective L/A in the momentum equation of the separator. Due to differences between the densities of steam and water, the primary inertial effects are due to the liquid. The tests of Reference 8 provided a relationship between the effective L/A and the inlet quality, and an empirical separator pressure drop coefficient.

General Electric states that the value of pressure drop coefficient has a conservative bias in it. The higher the pressure drop or the pressure drop coefficient, the higher is the value of $\Delta\text{CPR}/\text{ICPR}$. However, General Electric did not quantify the conservatism in this model in terms of $\Delta\text{CPR}/\text{ICPR}$ relative to actual plant conditions. Therefore, no credit is given to this conservatism.

General Electric performed sensitivity studies decreasing the value of L/A by 30%. This resulted in an increase of 0.002 in $\Delta\text{CPR}/\text{ICPR}$. In order to assess if the scatter of 30% in the separator L/A is sufficient, the staff reviewed the separator data in Reference 8.

The data indicates that the scatter in the separator L/A values can be high. The thickness of water layer can be used to make a fairly good estimate for L/A. Tests indicate that the thicknesses of water layer for the same conditions can vary from each other by a factor of four. Reference 8 describes the reason for these variations as an instability.

Discussions with General Electric indicate that the value of L/A used in the ODYN code included the value of L/A for the standpipe and therefore, the scatter was not a factor of 4 but it was judged to be 30%. The staff has no information how these separate L/A effects (one due to the separator and the other due to the standpipe) can be assessed.

Reviewing the analytical model we find that the separator model is acceptable; however, based on available information we judge that a factor of 2 in separator L/A variation (rather than 30%) would be more appropriate in assessing the uncertainty. Hence, we estimate the component of that Δ CPR/ICPR uncertainty for L/A will increase from ± 0.002 to ± 0.015 .

d. Upper Plenum, Vessel Dome and Bulkwater Model

These components are modeled using mass, energy and momentum conservation equations. Peach Bottom tests indicate that dome pressures calculated to predict the data are higher than the experimental values. In the opinion of General Electric, the reason for the overprediction is that the energy equation for the dome

region predicts that the bulk water mass very quickly becomes subcooled, the system becomes stiff, and therefore, the pressure rises very quickly. Since the rapid pressure rise leads to a rapid void collapse the staff concludes that the model is conservative. However, the Peach Bottom tests also indicate that Δ CPR predictions are not conservative. This implies that the conservatism of the bulk water model is offset by the nonconservatism somewhere else. General Electric did not quantify the conservatism in this particular model. In view of Peach Bottom tests where a trade off has occurred, no credit for conservatism can be given.

We find that the analytical methods used in these models are acceptable; however, as stated, no credit for conservatism will be given.

2. Steam Line Model

The steam line is modeled assuming single phase mass and energy conservation equations which are solved using an explicit finite differencing method. The steam is assumed to behave isentropically. The steam line is nodalized into six segments while the bypass line is modeled using two nodes. Safety and relief valve flow rates are treated as separate flow branches.

Sensitivity studies were performed by General Electric for various numbers of nodes for a sample test problem wherein the inlet pressure is kept constant and at the outlet turbine stop valve closure is simulated. These sensitivity studies were performed using nodal arrangements of 3,4,5,6,7,

8, 20, and 40 nodes and compared with the analytical model predictions using the method of characteristics. The analyses indicate that a minimum of 7 nodes is required to predict frequencies to a reasonable degree. The comparison of amplitudes of pressure oscillations between the 8 node model and the analytical model is also reasonable. The conservatism of a model is dependent upon the integral of the pressure oscillations over a relatively short period of time since it is the integral of the pressure that is imposed on the core. The void collapse and the subsequent power increase is dependent upon the rate of change of this integral pressure. Judging from the pressure oscillations calculated from the 8 node model and the analytical model based on the method of characteristics the staff concludes that the integrated pressures are approximately the same for both models and perhaps there is a very slight conservatism in the 8 node model. Consequently, we find that the finite differencing scheme and the solution method employed in the streamline model are acceptable.

Other uncertainties in the model are in the form of friction loss coefficients and in the value of the average specific heat ratio. General Electric conducted sensitivity studies by varying the specific heat ratio and form loss coefficients. The Peach Bottom tests indicated an average specific heat ratio of 1.15. The change of this ratio to 1.25 caused an increase of 0.01 in the $\Delta CPR/ICPR$ ratio.

We reviewed the values of the average specific heat ratios for steam at 1000 psia. The value of 1.15 is valid for saturated steam with very little amount of droplets in it. The value of 1.25 is valid for a slightly superheated steam. Since there is a pressure drop along the

steam line, we do not expect steam to be superheated. Hence, the value of 1.15 is acceptable. We also find the calculation of uncertainty of 0.01 in $\Delta\text{CPR}/\text{ICPR}$ ratio acceptable.

General Electric also performed a sensitivity study by decreasing the loss coefficient by 20%. This was based on the upper limit of steamline loss coefficient uncertainty. Decreasing the loss coefficient by 20% increases the ratio of $\Delta\text{CPR}/\text{ICPR}$ by 0.01. Decreasing the loss coefficient by 20% is a reasonable assumption and we find the calculation of uncertainty of 0.01 in $\Delta\text{CPR}/\text{ICPR}$ due to pressure loss coefficients acceptable.

In conclusion, our review indicates that the analytical methods used in steam line modeling and associated uncertainties are acceptable.

3. Core Thermal-Hydraulics Model

Two-phase mass, energy and momentum conservation equations were used to predict the behavior of the thermal-hydraulics of the core. Two mass and two energy conservation equations representing each phase separately and one momentum equation representing the mixture comprised the five equation model. In addition to these equations, correlations for 1) interfacial heat flux, 2) Zuber drift flux model (Reference 9), 3) two-phase pressure drop, and 4) heat transfer, are used.

The interfacial heat transfer correlation is based on the "mechanistic model" presented in Reference 9. The selection of the heat transfer correlations is based on the flow regimes. In the single-phase liquid region, the Dittus-Boelter correlation is used. In the subcooled and bulk

boiling regions, the Jens-Lottes and Chen correlations are used, respectively. Two-phase pressure drop correlations are based on the Martinelli-Nelson correlation. The five equation model together with the correlations are solved using a fully implicit finite differencing method in the space-time domain. The space domain is one dimensional in the axial direction and the core is represented using 24 axial nodes.

To improve the accuracy of predictions within a node, a boiling boundary concept is defined. This concept defines a location in the axial direction for which the mixture enthalpy is equal to the enthalpy at which point subcooled boiling begins. This location establishes the boundary between the liquid and two-phase regions within an axial node at each time step and the program selects the appropriate correlation for the appropriate region. The variables solved for each node are volumetric flux, vapor fraction, pressure, vapor enthalpy and liquid enthalpy.

Two models are particularly significant in the assessment of uncertainties in the five equation model; they are Zuber drift flux and the subcooled boiling models. These are discussed in the following sections.

a. Drift Flux Model

The choice of two parameters, C_0 and V_{gj} is important in this model. The first coefficient (C_0) is the concentration parameter which describes the slip due to cross sectional averaging of a nonuniform void fraction profile. The second term (V_{gj}) is the drift velocity which describes the local slip between the phases. The value of C_0 is strongly dependent on the flow regimes and geometry. This

dependence has been shown in many tests (Reference 9). The drift velocity is dependent on the density differences between the phases as well as on the flow regimes.

In the model used by General Electric, these parameters are empirically determined in the form of correlations based on the test data. The data were obtained both from tubes and channels, and are reported in References 10 through 14. When the vapor fractions obtained from these parameters were used to calculate power shapes observed in BWRs, some discrepancies were observed. Consequently, General Electric introduced another correlation for C_0 , and a concept of neutron effective void fraction, to provide a better fit with measured power shapes. Based on physical considerations it is conceivable why C_0 used in thermal hydraulic calculations is different from C_0 for neutron power calculations. The thermal hydraulic C_0 is based on tube geometry while neutron effective C_0 is obtained from actual core geometry. The value of C_0 should be different for tubes and rod bundles because of different vapor fraction profiles and flow regimes. However, in a telecon General Electric stated that C_0 valid for thermal hydraulics gave good agreement with Atlas data and C_0 valid for neutron effective void fraction gave good agreement with the core data. Hence, the differences cannot be explained based on geometrical considerations alone and there is an artificial fix in the model. According to Reference 34, this fix is necessary to compensate for deficiencies in lattice physics methods.

General Electric estimates that the uncertainty in the concentration parameter, C_0 , is about $\pm 3\%$ at a void fraction of .70 for neutron effective vapor fraction calculations. This corresponds to a $\pm 5\%$ uncertainty in void reactivity coefficient which leads to an uncertainty of ± 0.008 in the value of $\Delta\text{CPR}/\text{ICPR}$. However, General Electric uses $\pm 10\%$ uncertainty in the value of C_0 for thermal hydraulic calculations. We find no reason that the uncertainty in C_0 for neutron power calculations should be different because the correlation is used to calculate voids the same way as in the thermal hydraulics. General Electric does not state any uncertainty in V_{gj} for neutron power calculations but states an uncertainty of $\pm 20\%$ for thermal hydraulic calculations.

Based on Reference 15, we assessed the uncertainties for thermal hydraulic $C_0 \pm 20\%$ and $V_{gj} \pm 30\%$ respectively. Reference 15 has a different data base from the references that the General Electric used. Extrapolating the General Electric results, we estimate that $\pm 20\%$ uncertainty in C_0 would result in $\pm 33\%$ uncertainty in the void fraction or void reactivity coefficient.

We also reviewed the void fraction data taken in the FRIGG loop, Reference 16. The FRIGG tests were performed using rod bundles. The review of the data indicated that the scatter of $\pm 30\%$ in void fraction was reasonable in the low quality region. This finding also substantiated the estimate of $\pm 20\%$ uncertainty in the value of C_0 .

Assuming the same uncertainty for the neutron effective C_0 and extrapolating the General Electric results, we have estimated that the uncertainty of $\pm 20\%$ in C_0 resulting in $\pm 33\%$ uncertainty in the void fraction or in the void reactivity coefficient would produce an uncertainty of ± 0.053 in $\Delta\text{CPR}/\text{ICPR}$. We presented these findings in the ACRS hearing, Reference 30.

In response to the above staff assessment, General Electric submitted additional information, Reference 31, requesting the reduction of the uncertainty in $\Delta\text{CPR}/\text{ICPR}$. The primary argument was that the uncertainty of $\pm 20\%$ in the value of C_0 (seven times the uncertainty of $\pm 3\%$ which had been proposed by General Electric) leading to an uncertainty of approximately $\pm 30\%$ in void fraction was applicable for a low quality and a low vapor fraction region. The uncertainty becomes smaller at higher qualities. In addition, General Electric submitted another sensitivity study using neutron effective $C_0 = 1.0$ and noted that this would be the bounding value for ΔCPR calculations. General Electric also noted that the transient results were weakly dependent on void fractions at low qualities in the subcooled region, Reference 32.

We reviewed the new information submitted in Reference 31, and agree with General Electric that uncertainties in vapor fraction can be reduced at higher qualities and that $C_0 = 1.0$ is a bounding value for bulk boiling. General Electric stated an uncertainty of $\pm 5\%$ in void reactivity coefficient at a void fraction of 70%. This corresponds approximately to an uncertainty of $\pm 5\%$ in void fraction. Further

review of the void fraction data in the FRIGG loop shows a scatter of $\pm 10\%$ in void fraction at qualities of 5% and 10%. These qualities are considered relatively high and they correspond to vapor fractions of 40% and 60% respectively. It appears that the FRIGG loop data show a larger scatter of void fraction than that assumed by General Electric. At high qualities, the uncertainty of $\pm 10\%$ in void fraction corresponds to approximately $\pm 10\%$ uncertainty in C_0 . However, the theoretical limit for C_0 in the bulk loading region is 1.00. It can be higher but not lower in this region. The scatter of 10% on neutron effective C_0 would bring the value of C_0 below 1.00. Some of the scatter in the FRIGG data was due to measurement errors which could be as high as $\pm 10\%$. Hence, we accept the limit of $C_0 = 1.00$ as bounding for the uncertainty studies. Further, sensitivity studies performed in Reference 32 indicate that the transient is weakly dependent on changes of neutron effective C_0 in low quality region. Hence, we accept the calculation of uncertainty of ± 0.011 in $\Delta CPR/ICPR$ as suggested in Reference 31. This is approximately 30% larger than that originally proposed by General Electric.

b. Subcooled Boiling Model

The phenomenon of subcooled boiling is modeled by the "Mechanistic" subcooled boiling model developed by R. T. Lahey in Reference 9. The model provides a relationship for interfacial heat flux between the bubbles and surrounding liquid. It consists of two terms: one term shows the effect of the temperature difference between the phases and the other shows the effect of the wall heat flux.

The model has been verified using the data obtained by S. Z. Rouhani (References 17 and 18). These data were obtained from a vertical annular channel. In determining the uncertainty of the correlation, General Electric provided a sensitivity study using a coefficient "n" in the correlation. The nominal value of "n" is 1.0. For n = 1.25, a change of 0.009 in $\Delta\text{CPR}/\text{ICPR}$ is obtained. If 1.50 is assumed, the change in $\Delta\text{CPR}/\text{ICPR}$ is 0.014. GE states that the value of 1.25 provides a reasonable uncertainty for the model but does not provide any supporting evidence or data.

We reviewed the void fraction vs. axial height curves drawn for various "n" values and find that the void fraction difference between the two curves drawn for n = 1.0 and n = 1.5 is about 3.5% in absolute or 18% relative to the average measured value of the void fraction in the subcooled region. Some of the rod bundle experiments performed in the Frigg loop (Reference 15) show 100% (relative) scatter of the data. In general, the scatter is 15 - 30% relative to the average void fraction. We believe $\pm 30\%$ scatter is a reasonable estimate of uncertainty. Therefore, we increased the uncertainty in ΔCPR by a factor of 1.67 (30/18) which results in ± 0.023 in the uncertainty value of $\Delta\text{CPR}/\text{ICPR}$ for the subcooled boiling model. We estimate the corresponding minimum and maximum values of "n" to be 0.5 and 2.0 respectively. General Electric is required to make sensitivity studies to verify that these values correspond to ± 0.023 uncertainty in $\Delta\text{CPR}/\text{ICPR}$.

The review of the analytical models describing the thermal-hydraulic behavior of the core indicates that these models are acceptable provided the uncertainties of various components are increased to the values recommended by the staff.

4. Core Physics Model

a. Assumptions in the Neutronics Model

The neutronics model of ODYN is based on time-dependent, one-dimensional, one-group, diffusion theory. The model includes the effect of delayed neutrons and the calculation is performed in the axial dimension of a BWR. Radial effects due primarily to Doppler, moderator, and control state are taken into account in collapsing a three-dimensional model to the one-dimensional axial model. Of the three effects, the control state variation due to scram during a transient is the most important. Some care must, therefore, be taken in choosing the initial weighting functions to account for these effects.

We have reviewed the assumptions in this neutronic model with the current state-of-the-art for performing space-time coupled neutronic and thermal-hydraulic calculations. We conclude, based on our review, that the assumptions on which the neutronic model of ODYN are based are acceptable.

b. Derivation of Equations for the One-Group, One-Dimensional, Time-Dependent Neutronic Model

We have followed in a step-by-step manner the derivation of the one-group, space-time neutronics model presented primarily in

Appendix A of Volume I of the report. This derivation proceeds from the time-dependent form of the three-dimensional neutron diffusion equation for the fast flux as used by the General Electric three-dimensional reactor simulator (Reference 2) along with appropriate equations for delayed neutrons. The three-dimensional time-dependent neutron flux is represented as a product of radial and axial time-dependent components. Weighting functions are next introduced to make this factorization unique and to minimize errors in the procedure in some sense. The weighting functions are taken, according to the adiabatic approximation, as the solution to a steady-state eigenvalue problem to be solved at various points in time. In practice, the weighting functions are calculated only at time zero for as many BWR operating states as is necessary. This procedure results in the final form used for the one-group, one-dimensional, time-dependent equations along with defining equations for the nuclear parameters that are used. The derivation also includes discussion of the average axial power distributions, initial normalization procedures, and boundary conditions.

Section 5 of Volume I of the report discusses the integration of the spatial and time variables to obtain the discrete form of the one-group, one-dimensional, time-dependent equations. The procedures used for this are straight forward. This section also discusses the radial weighting function and the treatment of the control state. Cross section related parameters are functions of axial core height, control state, and relative water density. These parameters are fit to quadratics in the relative water density.

Our review of the derivation of the equations for the one-group, one-dimensional, time-dependent neutronics model has been performed by deriving and verifying each of the equations presented in Volume I of the report. We conclude, based on our step-by-step review of all the neutronic equations, that the derivation of nuclear parameters and equations for the one-group, one-dimensional, time-dependent model is acceptable.

c. Calculation of Neutronic Input Parameters

General Electric uses its Lattice Physics Model and its Three-Dimensional BWR Core Simulator to process nuclear data for the ODYN code. The Lattice Physics Model is described in Reference 19. The Three-Dimensional BWR Core Simulator is described in Reference 2. Both of these codes have been reviewed and approved by the NRC for use in BWR applications.

The Lattice Physics Model, as its name implies, is used to generate nuclear parameters for use as input to the BWR Core Simulator. This data is generated as a function of fuel type, control, temperature, void fraction, void history, and exposure. Before being used by the BWR Core Simulator, the data is transformed from the Lattice Physics Model void fraction to the Neutron Effective Void (NEV) model void fraction. This empirical procedure was developed by GE to remove a discrepancy between BWR Core Simulator results and operating reactor data. The BWR Core Simulator is used to perform the three-dimensional analyses that are required for obtaining the data for processing into parameters and cross sections for the ODYN code.

Our review of the calculation of neutronic input parameters is based on the use of NRC reviewed and approved codes and on comparisons of three-dimensional and ODYN steady-state neutronic analyses. The approved codes are (1) the Lattice Physics Model (NEDE-20913-P, "Lattice Physics Methods," C. L. Martin, June 1976 and NEDO-20939, "Lattice Physics Methods Verification," C. L. Martin, June 1976) and (2) the BWR Core Simulator (NEDO-20953, "Three-Dimensional BWR Core Simulator," J. A. Woolley, May 1976 and NEDO-20946, "BWR Simulator Methods Verification," G. R. Parkos, May 1976). The steady-state calculations compared the BWR Core Simulator and ODYN results for scram reactivity and core averaged axial power distributions, among other things, for a number of different reactors and operating states.

Some of the uncertainty values used by General Electric in response to our Question 12 need to be revised in our judgement. We believe that the Doppler reactivity coefficient uncertainty should be increased from ± 6 percent to about ± 10 percent. This increase is based on the uncertainties inherent in the calculation of Uranium-238 resonance absorption, the calculation of the Dancoff factor in the complex BWR lattice, the calculation of spatial weighting factors, and the computation of effective fuel temperatures. This change in the Doppler uncertainty will have very little effect on the calculated $\Delta\text{CPR}/\text{ICPR}$ ratio. We estimate that this will increase the uncertainty in $\Delta\text{CPR}/\text{ICPR}$ from ± 0.0015 to ± 0.002 . We believe that the scram reactivity uncertainty should be increased from ± 4 percent to about ± 10 percent. This increase is based on the uncertainties

inherent in calculating the initial scram reactivity rate and total control rod worths. We estimate that this will increase the uncertainty in $\Delta\text{CPR}/\text{ICPR}$ from ± 0.01 to ± 0.02 . The General Electric values for the Lattice Physics Model and BWR Core Simulator uncertainties in the void reactivity coefficient calculation are acceptable as given in response to our Question 12.

Since the uncertainties in the neutron effective void fraction are assessed in the thermal hydraulic section, we did not consider it as part of void reactivity uncertainty. Hence, the uncertainty in $\Delta\text{CPR}/\text{ICPR}$ value is reduced from ± 0.020 to ± 0.018 .

We conclude, based on our review, that the procedures and calculations performed to provide the neutronic parameters for input to the ODYN code are acceptable.

5. Fuel Heat Transfer Model

Heat transfer to the coolant and temperatures within the fuel are calculated assuming a single cylindrical fuel element for each axial location. The fuel heat transfer model used in the ODYN code calculates fuel temperatures as a function of time in the transient as input to the Doppler reactivity calculation. The cladding wall temperatures are also calculated as input to the transient cladding-to-coolant heat transfer model. The ODYN code allows for axial variation of the neutron flux, as well as of coolant flow, density, and pressure. This results in an axially varying set of input conditions for the fuel heat transfer model. The resulting temperature calculations are then solved for a series of discrete axial elevations in the core.

The fuel and cladding conductivity and heat capacity are assumed to be temperature dependent. A gap thickness is specified between the fuel and the cladding and an input gap conductance is used. Axial and time variations in the gap conductance may be given, but a constant value is used for safety analyses. The external heat transfer coefficient and coolant temperature are obtained from the thermal-hydraulic portion of the code. The heat generation rate in the fuel pellet is obtained from the axial power distribution which is determined by the neutronics segment of ODYN. The radial heat distribution in the fuel rod is assumed to be independent of axial position and independent of time.

General Electric derived the fuel heat transfer model from the general heat flow equation. The equation is expressed with axisymmetry and zero axial conduction assumed. The resulting, one-dimensional, transient heat conduction equation is solved by the Crank-Nicholson finite-difference technique. The solution is approximate, but the procedure is widely practiced and is well documented in the open literature. General Electric has limited its description of the fuel heat transfer model to the formulation of this final equation.

The resulting heat conduction equation is applied to a single rod with a radially averaged heat generation rate. This rod is used to represent all of the fuel rods in the reactor core. Because axial conduction is assumed to be negligible, the equation can be solved independently for each discrete axial position in the core. The finite-difference technique also requires a radial nodalization of the fuel rod. The nodes may be of arbitrary size. General Electric has assumed that the fuel pellet is

divided into seven radial nodes and the cladding into two nodes. The coefficients for both the steady-state and transient forms of the resulting finite-difference equations are given in Tables 7-1 and 7-2 of the model description.

A number of limiting assumptions have been considered in our review of the fuel heat transfer model.

1. The ODYN core transient model is designed to handle short-term events which occur on a time scale of seconds. This makes it possible to ignore the effects of long-term fuel behavior phenomena, such as creep and swelling. Pre-transient conditions, such as the average fuel-to-cladding gap size, are calculated with more detailed fuel performance codes, such as GEGAP-III (Reference 20) and subsequently used as input to ODYN.
2. The ODYN core transient model is designed to handle average, rather than extreme, fuel conditions. The fuel rod input parameters represent an average of all fuel rods at a given axial location. Bounding input parameters are, in general, more difficult to establish and thus are more critical in the overall analysis. However, the ODYN code, as a whole-core analysis, requires only the average conditions. In this respect, we note that the ODYN transient model does not have a hot channel capability, where extreme fuel conditions would be required as input.

Both of these limiting assumptions were considered in our review of the gap conductance values used by the ODYN code. We have reviewed (Reference 21) the selection of the axial and time variation of gap conductance to determine whether the selected values are appropriate for different transients. General Electric stated that the core average gap conductance values are calculated by GEGAP-III (Reference 20) which is approved by NRC. The calculated conductance is input for all axial nodes and is kept constant during the transient.

A sensitivity study was also performed for the most limiting pressurization event in which the Δ CPR decreases when axial varying gap conductance is used. It was shown that most of the high power axial nodes have higher than core average gap conductance. During the transient, higher gap conductance will lead to faster heat transfer from the fuel to the moderator/coolant which generates more steam voids. This results in lower stored heat in the higher power nodes. In addition, the faster conversion of fuel stored energy to steam voids in the core helps to mitigate the transient due to negative void reactivity feedback. Therefore, the transient with axial varying gap conductance is less severe than that with constant gap conductance.

During limiting pressurization transients, it is expected that the fuel gap conductance will be higher than its initial steady-state value due to the increase in the thermal expansion of the fuel pellet. As discussed above, higher gap conductance leads to a less severe transient. General Electric has not taken credit for this fact, but has stated that the use of constant conductance throughout the transient compensates for uncer-

tainties in thermal conductivity and specific heat of the fuel and cladding. We have examined these properties and find that they are appropriate over the temperature range specified by GE (300-1500 °K for fuel thermal conductivity). Therefore, it is concluded that the use of a constant, core average gap conductance in the proposed OQYN licensing calculations is appropriate.

We have also questioned the use of a specific core average gap conductance value of 1000 Btu/hr-ft²-°F for the analysis of the Peach Bottom Unit-2 turbine trip event. General Electric has shown (Q-11, Volume II) the calculated peak neutron flux as a function of time for gap conductance values of 500, 1000, and 1500 Btu/hr-ft²-°F. Small differences in neutron flux are observed for the 500 and 1000 Btu/hr-ft²-°F values. This is because the entire flux pulse is only a few tenths of a second wide and a fast fuel time constant is needed to produce a moderate density feedback through the rod heat flux. The peak neutron flux is minimum for the 1500 Btu/hr-ft²-°F value, showing that large values of gap conductance will mitigate the calculated flux response. This conclusion is in agreement with that found for axial and time varying conductance values. It also shows that a core average gap conductance value of 1000 Btu/hr-ft²-°F is not, in itself, an adequately qualified conductance value for core transient analyses. We conclude that conductance values should be based on an approved fuel performance code.

We have also reviewed the use of a radially averaged heat generation rate rather than a radially-dependent heat generation rate. We questioned the conservatism of this assumption because flux depressions, and therefore a

radially-dependent heat generation rate is expected in BWR fuels. General Electric has acknowledged that the radial power distribution within the fuel rod is not uniform. This is because the plutonium build-up and self-shielding of the fuel results in a radial power shape peaked sharply at the outside of the fuel pellet. Heat transfer from the inside of the pellet to the cladding occurs by diffusion through the fuel material. When the power is peaked at the outside of the pellet, the average distance from the area of maximum heat generation to the edge of the pellet is less. This results in a shorter time constant than in the uniform power production case. A reduction in the thermal time constant results in faster feedback of heat flux to the moderator/coolant and reduces the consequences of the pressurization transient in the same manner that higher gap conductance does. Hence, a uniform power distribution assumption inside the fuel pellet is conservative from the moderator/coolant standpoint.

Although the use of a uniform radial pin power distribution and small gap conductance values lead to conservative moderator/coolant conditions, these assumptions also lead to higher fuel temperatures. The higher fuel temperatures, in turn, lead to increased Doppler broadening in the fuel pin which is non-conservative for transient analysis. The ODYN code assumes that all fuel at the same axial location in the core has the same temperature profile. Analyses have shown that this approach may tend to underestimate the Doppler reactivity effects because the fuel pins which have the greatest resonance capture rates are near the bundle periphery and operate at higher average temperature than that calculated by the code. This assumption is valid only for fuel assemblies with uniform

enrichment. However, the Doppler reactivity contribution to BWR transient analysis appears to be of lesser importance than the scram and moderator void reactivity contributions. The use of a uniform radial pin power distribution is therefore appropriate in the analysis of events where Doppler reactivity effects are small.

We have also questioned the application of the Crank-Nicholson method to the fuel heat transfer equation. This method suffers complications when heat generation varies with position and time, when thermal properties vary and when non-linear boundary conditions are used. General Electric has stated that the method of solution suffers complications only when the time steps are too large relative to the fuel thermal time constant or when the fuel properties change more rapidly than the time step of the solution. It was further stated that the BWR fuel thermal time constant is in the range of 5-8 seconds compared to 0.01 second time steps taken by the ODYN code. Such extensive time stepping is required for the hydraulic analysis and will accommodate all non-linearity problems of the fuel behavior. It was also noted that the gap conductance is conservatively held constant in the transient calculation. We therefore conclude that the method of solution is appropriate for safety analyses.

In summary, we find that the ODYN fuel heat transfer model is appropriate for whole-core analysis of short-term events. We note that the code is used for whole-core analysis and is not proposed for hot channel calculations. We have also examined the list of events selected (Volume III, table 2-1) for analysis with ODYN and find that these events are of short duration or are limited in expected fuel temperature increase. We

conclude, therefore, that the ODYN fuel heat transfer model is appropriate for the safety analysis of these events.

6. Summary of Code Uncertainties

a. Margin in Δ CPR Calculations

In summary, the staff agrees with some of the code uncertainties calculated by General Electric. However, some of the code uncertainties are low and the staff recommends higher values. A comparison of the code uncertainties and the corresponding bounding values as recommended by General Electric and the staff is presented in Table I.

General Electric claims an expected conservative bias of 0.02 (Table 3-3, Volume III) in the calculation of the value of Δ CPR/ICPR due to the modeling of the gap conductance. However, the sensitivity studies performed using different values of gap conductance (Q-11, Volume II) as well as the comparison of the Peach Bottom test data with the ODYN predictions do not indicate that such a conservatism in Δ CPR calculations exists. Consequently, we do not believe that the predictions have a conservative bias.

Our review shows that the ODYN code is a best estimate code and there is no inherent conservatism in predictions of Δ CPR/ICPR when best estimate input values are used. Consequently, we do not give credit for this claimed conservatism of 0.02.

General Electric estimated the total code uncertainty (Table 3-3, Volume III) using the method of linearization. This method can

TABLE-I

COMPARISON OF CODE UNCERTAINTIES AND CORRESPONDING
BOUNDING VALUES AS ESTIMATED BY
GENERAL ELECTRIC AND THE STAFF

	GE		STAFF	
	Bounding Values of Parameters	\pm ACPR ICPR	Bounding Values of Parameters	\pm ACPR ICPR
I. Reactor Core Model				
(1) Nuclear Model				
(a) Void Coefficient	$\alpha_v \pm 13\%$	0.020	$\alpha_v \pm 11\%$	0.018
(b) Doppler Coefficient	$\alpha_d \pm 6\%$	0.002	$\alpha_d \pm 10\%$	0.002
(c) Scram Reactivity	$\alpha_s \pm 4\%$	0.010	$\alpha_s \pm 10\%$	0.020
(d) Prompt Neutron Heating		0.006		0.006
(2) Thermal Hydraulic Model				
(a) Drift Flux Parameters	$C_o \pm 3\%$ $V_{gj} \pm 20\%$	0.008	$C_o = 1.00$ $V_{gj} \pm 30\%$	0.011
(b) Subcooled Void Model	$n = 1.25$	0.009	$n = 0.5$ 2.0	0.023
(3) Fuel Heat Transfer Model				
(a) Pellet Heat Distribution	(Conservative)		-	-
(b) Pellet Heat Transfer Parameters	(Conservative)		-	-
II. Recirculation System Model				
(1) System Inertia	(L/A) \pm 200%	0.002	L/A \pm 200%	0.002
(2) Jet Pump losses	K = 20%	0.010	K = 20%	0.010
(3) Core Pressure Drop	$\Delta + 1.5$ psf	0.005	$\Delta + 1.5$ psf	0.005
(4) Separator (L/A)	-30%	0.002	-200%	0.015
(5) Separator ΔP	(Conservative)		-	-
III. Steam Line Model				
(1) Pressure Loss Coefficients	K = 20%	0.010	K = 20%	0.010
(2) Specific Heat Ratio	$\gamma + .10$	0.010	$\gamma + .10$	0.010
Total:		0.031		0.044

estimate the output distribution only approximately. The method also assumes the independence of the parameters. The appropriateness of the linear method should be verified by response surface and Monte Carlo analyses. However, as will be shown subsequently, the results of the statistical analyses performed in Volume III are not acceptable. New statistical analyses, if performed by General Electric, should be based on code uncertainties based on comparison of code predictions with the test data. Consequently, we use the value of total code uncertainty calculated from model sensitivity studies and method of linearization in determining the margin of $\Delta\text{CPR}/\text{ICPR}$ in Option A (to be presented in Staff Position) where statistical analysis is not required. The total code uncertainty in Table 3-3 of Volume III as per General Electric is ± 0.031 . Based on our review we increase this value to ± 0.044 .

b. Margin in Pressure Calculations

General Electric has not performed analyses to determine the uncertainties in the calculation of pressure. Hence, it will be necessary for General Electric to perform these calculations using staff recommended values of the parameters listed in Table I for the Main Steam Isolation Valve closure event. We believe that there is sufficient conservatism in the ASME vessel overpressure limit to permit General Electric to use approximate linear methods to determine the uncertainty in the output. This uncertainty (2σ) should be added to the QDYK calculated pressure. If General Electric demonstrates that this uncertainty is very small (e.g., by a factor of 10 or more) relative to the uncertainty in determining ASME vessel overpressure limit, no addition of uncertainty to the calculations of pressure is needed.

B. QUALIFICATION OF THE ODYN CODE

1. Qualification of Neutronics Model - Comparison of ODYN with BWR Core Simulator

One of the ways in which the ODYN code may be qualified is by comparison of ODYN results with those obtained by using other codes and analytical methods. These comparisons should include both steady-state and dynamic calculations. A calculation of a BWR turbine trip without bypass licensing basis transient is compared in a later section to a calculation performed by our consultants at Brookhaven National Laboratory (BNL). This section will discuss some steady-state comparisons made by General Electric of ODYN and the BWR Core Simulator.

The BWR Core Simulator Code (NEDO-20953, "Three-Dimensional BWR Core Simulator," J. A. Woolley, May 1976 and NEDO-20946, "BWR Simulator Methods Verification," G. R. Parkos, May 1976) has been reviewed and approved by the NRC. This code, as used by General Electric, predicts measured power distribution peak to average ratios as follows:

- (a) Axial power distribution
 - 5% for uncontrolled assemblies
 - 10% for controlled assemblies

- (b) Radial power distribution
 - 5% underestimate relative to the process computer

- (c) Nodal power distribution
 - 4% for gamma scan data
 - 7 to 8% for process computer data

The BWR Core Simulator calculation of the criticality of first cycle and reload BWRs results in a small bias which is taken into account for reactivity determinations of cold, xenon-free and hot operating conditions. The standard deviation of these criticality calculations is about 0.002 in units of reactivity.

The quantities to be compared are the core averaged axial power shape, the scram reactivity, and the void reactivity coefficient. These neutronic parameters were selected for comparison because of their importance in the turbine trip without bypass licensing basis transient. In addition, it is the space time evaluation of these quantities that distinguishes the ODYN calculation from a point kinetics evaluation of pressurization type transients.

The comparison of the core averaged axial power distribution, as computed by the BWR Core Simulator and ODYN, is given by the response by GE to our Question 36. This response states that the collapsing scheme employed in the generation of nuclear parameters ensures that the steady-state core averaged axial power distribution and criticality computed by ODYN are identical to the BWR Core Simulator results. The response also indicates that, for a number of plants and operating states, The ODYN core averaged axial power distribution agreed to within 0.5 percent of the results obtained with the three-dimensional BWR Core Simulator.

The scram reactivity was compared for three BWR-4 reactor operating states. The initial scram rate (ISR), defined as the scram reactivity insertion rate during the first second from the time scram is initiated,

is the quantity chosen for comparison rather than the total scram worth. The ISR has been shown to be a critical quantity for short duration power burst transients of the load rejection type.

One operating state was for the beginning of cycle 2 but with all control rods out. ODYN results for the neutron flux and scram reactivity as a function of control rod insertion (or time) compared well with results obtained with the BWR Core Simulator. The ISR for ODYN was about 0.93 of the value obtained with the BWR Core Simulator. The second comparison was for the same BWR-4 but with some control rods inserted to achieve a critical condition. The ISR for ODYN was about 0.86 of the value obtained with the BWR Core Simulator. The third comparison was for another BWR-4 at 50 percent of full rated power and 100 percent of full rated core flow. This reactor had a considerable control rod inventory and, therefore, provides a severe test for the ODYN code. The ISR for ODYN was about 0.94 of the value obtained with the BWR Core Simulator. For all three comparisons the ODYN result for ISR was smaller than that obtained with the BWR Core Simulator and was therefore conservative.

The void reactivity coefficient derived from ODYN calculations was compared to the void reactivity coefficient derived from the BWR Core Simulator. This coefficient is obtained by knowing the core averaged void fraction and reactivity at two different reactor operating states. The different reactor operating states were obtained by changing either the reactor pressure or flow. For the variety of cases examined, GE states that the ODYN and BWR Core Simulator void reactivity coefficients agree to within 5%.

Our review of the comparison of steady-state BWRs calculated using the one-dimensional ODYN code with comparable calculations using the three-dimensional BWR Core Simulator code has been performed (1) by reviewing GE results for the scram reactivity and void reactivity coefficients and (2) by reviewing the GE response to our request for additional information on steady-state comparisons between the two codes.

We conclude, based on our review, that steady-state ODYN code calculation of core averaged axial power distributions, scram reactivity, and void reactivity coefficients are either in good agreement with or conservatively calculated with respect to comparable steady-state results obtained with the BWR Core Simulator code.

2. Qualification of the Thermal Hydraulic Model

Several comparisons of the ODYN thermal hydraulic model to standard GE design models were performed. The standard GE design model was submitted in Reference 1 and was approved by NRC in Reference 4. Both steady state and transient conditions were analyzed.

The steady state analysis first compared the thermal hydraulic characteristics (void fraction vs. axial location) of two typical BWR fuel channels (high and low power channel). The results of this comparison show good agreement between the models. This was expected since both models are very similar. The maximum void fraction variation between these models was approximately 5% for the high power channel and about 17% for the low power channel. These variations are for the axial locations where the void reactivity change is expected to be most significant for

the transient calculations, i.e., >4 ft. axial height. The steady state analysis also compared the change in void fraction vs. axial location for a 10 psi pressure change. The maximum void fraction variation between the models for this comparison was approximately 0.5% for the high power channel and about 5% for the low power channel. These variations are within the range of uncertainty for these type of thermal hydraulic calculations. See also discussions in Section II.A.3.a and b.

For the transient analysis comparison, the ODYN channel thermal hydraulic model result was compared to an analytical solution for exponential flow decay. The comparison required that ODYN be modified to include a constant axial heat flux distribution, and steam and drift flux properties. This was done because the tests were run with a uniform axial heat flux and calculational convenience required the choice of constant steam and drift flux properties. The tests were performed using a single heated tube containing Freon-114 at relatively low pressures and temperatures; about 125 psia and 160°F respectively. There is $\pm 10\%$ uncertainty in the measurements of the void fraction. The calculational uncertainty seems to be on the order of $\pm 5\%$. These tests verified that the analytical modeling technique including the drift flux model is acceptable and can be used to predict the vapor fraction. Judging the comparisons between the predictions and the test data and the special nature of these tests, the staff estimates that an uncertainty of $\pm 30\%$ in transient void fraction in low qualities and $\pm 5\%$ in high qualities for a rod bundle geometry during reactor transients is reasonable and consistent with the findings in the analytical model review in the previous section.

3. Qualification Using Integral Tests

In the past several years General Electric has undertaken a test program to verify the analytical methods for reactor pressurization transients. The tests of major interest for the current discussion consist of four turbine trip experiments. Three of these tests were performed at Peach Bottom Unit 2 (PB-2) in April 1977 and the remaining test was performed at a foreign reactor (KKM) in June 1977. These tests provide the experimental data base for verification of the ODYN code. The test results will be summarized in this section. A detailed description of the PB-2 test is presented in Reference 22.

General Electric stated that ODYN has been developed from first principles and independent of these results. The staff notes that in the ODYN code the only artificial fix is the neutron effective void correlation. The comparisons with integral plant tests provide an independent check of the ODYN code. The evaluation concentrates on the differences between test results and corresponding ODYN predictions. The parameters which are considered in these comparisons are steamline pressure, reactor vessel dome pressure, core exit pressure, and transient neutron flux distribution. These parameters are of primary importance in simulation of the pressurization transient. An accurate, ODYN simulation of these parameters would provide some verification of the assumptions for the transient models.

a. Peach Bottom Tests

The inputs used for this comparison were best estimate or measured values for the current (April 1977) Peach Bottom Unit 2 EDC2 conditions. The three Peach Bottom Unit 2 (PB-2) tests were conducted at

power levels of 47.4, 61.6, and 69.1 percent of full rated power. The tests were intended to be conducted at 100 percent of the rated flow. However, the second test was conducted at 82.1 percent of rated flow due to xenon. These three tests had different control rod distributions and fractions. For these three tests the first scram signal on the position of the turbine stop valve was disabled so that the scram would occur on high neutron flux. Disabling of the primary scram signal was necessary to obtain a significant power increase as a function of time for tests. Control rod insertion was assumed to vary linearly with time and was based on measured data. A constant value of 1000 BTU/hr-ft²-°F was used for the fuel rod gap conductance. Sensitivity studies performed by General Electric showed that the neutron flux as a function of time was insensitive to large changes in the gap conductance for these tests (See Q-II, Volume II).

The GE BWR Core Simulator was used to generate three-dimensional power distributions and to collapse the nuclear parameters according to the ODYN procedures. The initial core averaged axial power distribution calculated with ODYN can then be compared with power distributions obtained with the PB-2 process computer. Comparison shows that ODYN agrees quite well with the process computer core average axial power distributions for all three tests. This means that the GE neutronic procedures for generating nuclear parameters are internally consistent and provides the proper initial conditions for the start of the transient calculations.

A comparison of the total core power as a function of time provides an integral test of the important reactivity feedback due to scram and moderator density changes. This comparison would also be indicative of the adequacy of the core pressure and inlet flow calculations. The comparison shows that ODYN predicts the initial and fall-off part of the turbine trip transients correctly but overpredicts the peak total core power response for all three tests. It should be noted that the calculated consequences of the turbine trip tests are sensitive to scram delay time and the power fraction for prompt moderator heating. It should also be noted that small changes in reactor operating state conditions such as, for example, core pressure, cause relatively large changes in the flux transient because of the large net reactivity of the transients.

The reactivity components displayed for these ODYN calculations show that when scram occurs the power burst is quickly quenched. This is due to the control rod distribution and fraction for each test. The Doppler reactivity component plays only a secondary role. The reactivity components again demonstrate the necessity for their accurate assessment in any calculations of these type of transients.

A further indication of the adequacy of the ODYN calculation can be ascertained by comparing the core power as a function of time at the Local Power Range Monitor (LPRM) detector positions. The miniature fission detectors that comprise this LPRM system are distributed both radially and axially within the reactor core. Analysis of the PB-2 data shows that the radial variation of the neutron power with

time is similar for each detector on an axial level. This means that a one-dimensional axial calculation such as ODYN should be an adequate representation for these tests. The neutron power as a function of time does vary, however, with axial position as shown by the experimental data for the A, B, C, and D level LPRMs which are located at 1-1/2, 4-1/2, 7-1/2, and 10-1/2 feet from the bottom of the core. Comparison of the ODYN results for the neutron power as a function of time for these four detector levels with test data shows similar trends as observed for the total core power. The ODYN results and test data agreement for each LPRM level is similar to that for the total core power for each of the tests. This indicates that the ODYN calculation correctly models the axial neutron flux variations as a function of time for these PB-2 turbine trip tests.

Figures 1 through 3 (reproduced from NEDO-24154) present comparisons of axial neutron flux variations as measured (calculated by the process computer) and calculated by the ODYN code before the initiation of the tests. Figures 4 through 6 present comparisons of prompt neutron power as measured and calculated by the ODYN code during the tests.

The ODYN calculated steamline pressure compares well with the PB-2 data for predicted wave travel time and frequency of pressure oscillations. However, the calculated pressure curves are more spread out and the amplitudes are smaller than the measured steamline pressure. General Electric has attributed this difference to the coarseness of the spatial mesh in the steamline modeling. As

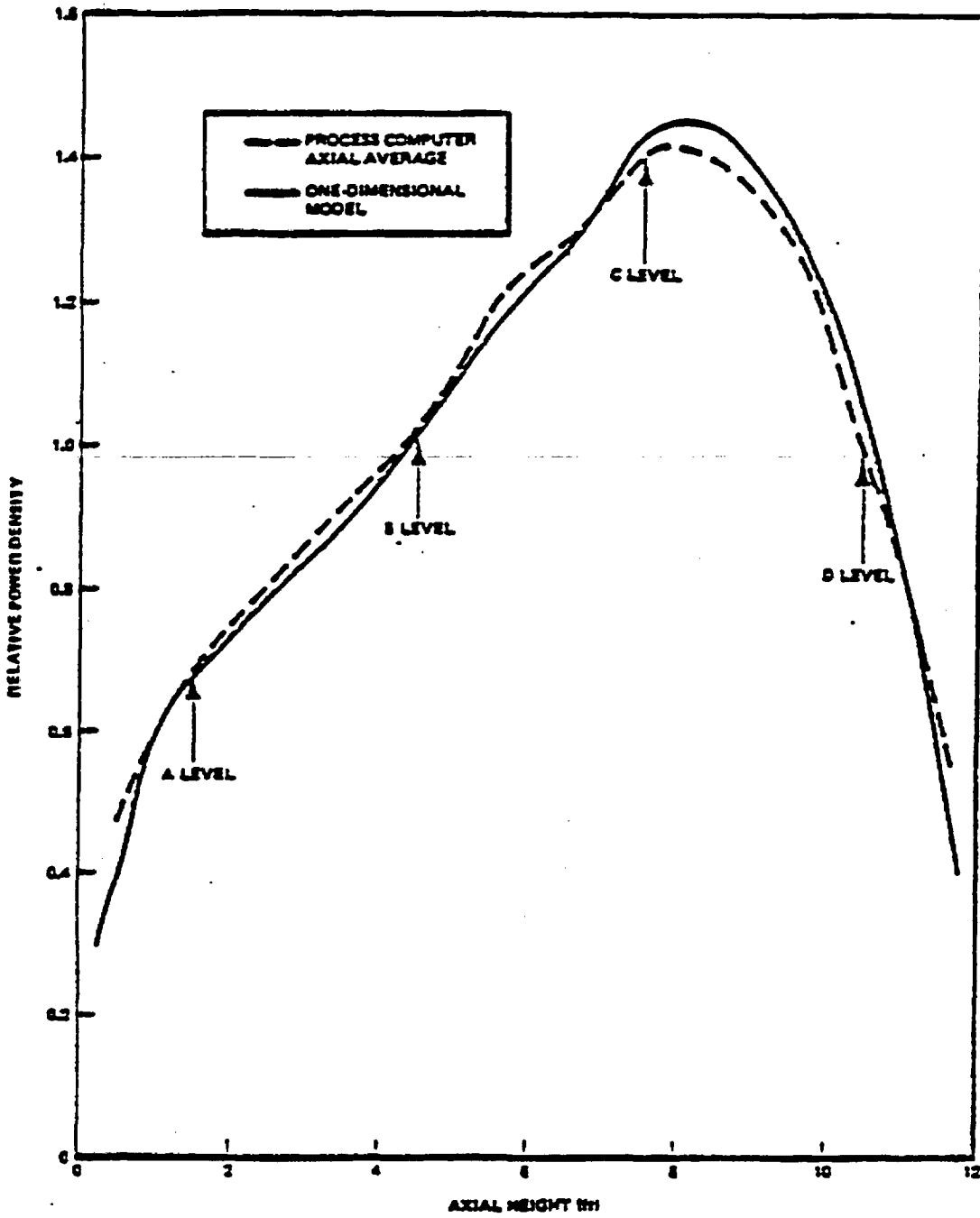


Figure 1 Axial Power Profile Turbine Trip 1

II-43

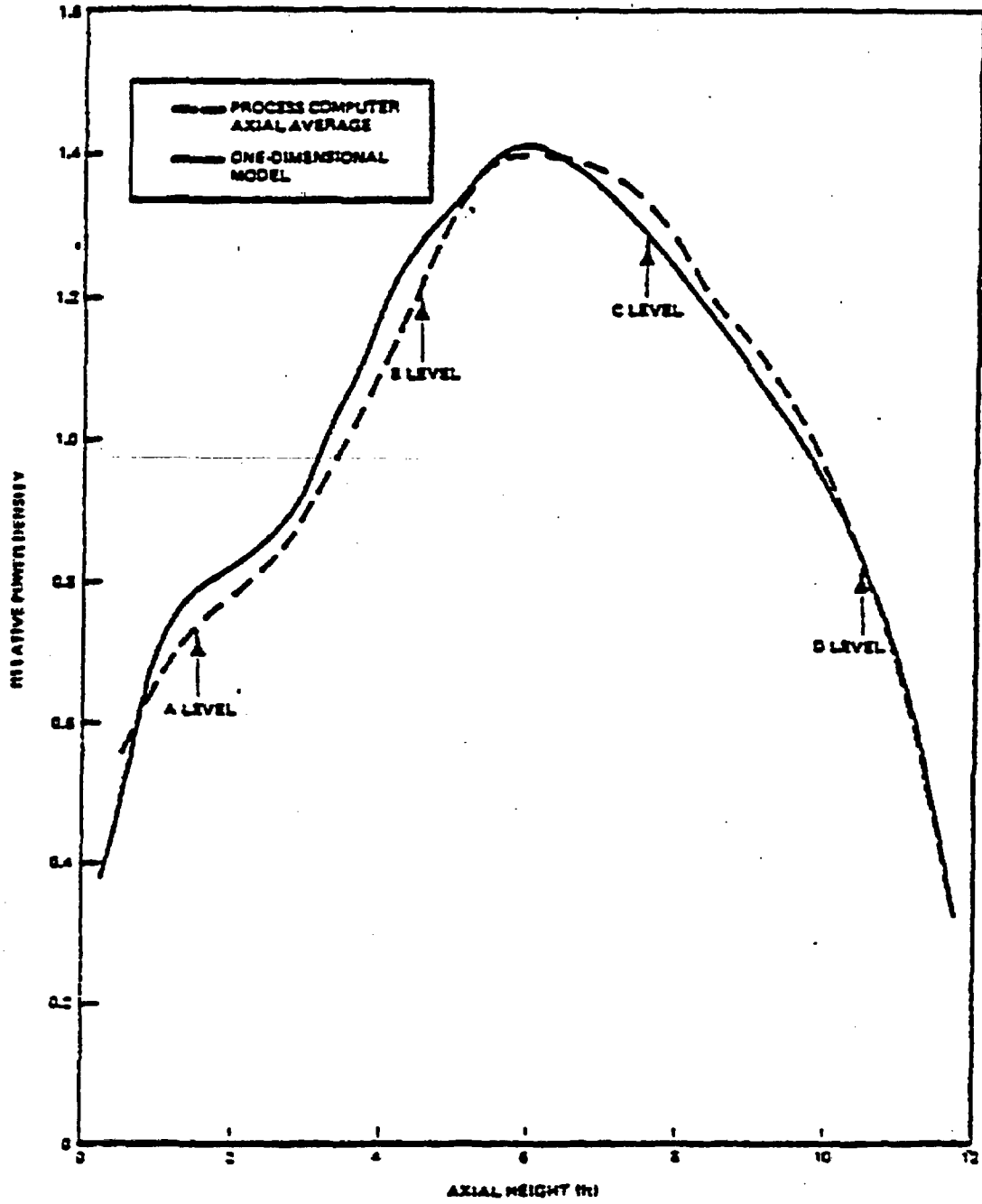


Figure 2 Axial Power Profile Turbine Trip 2

II-44

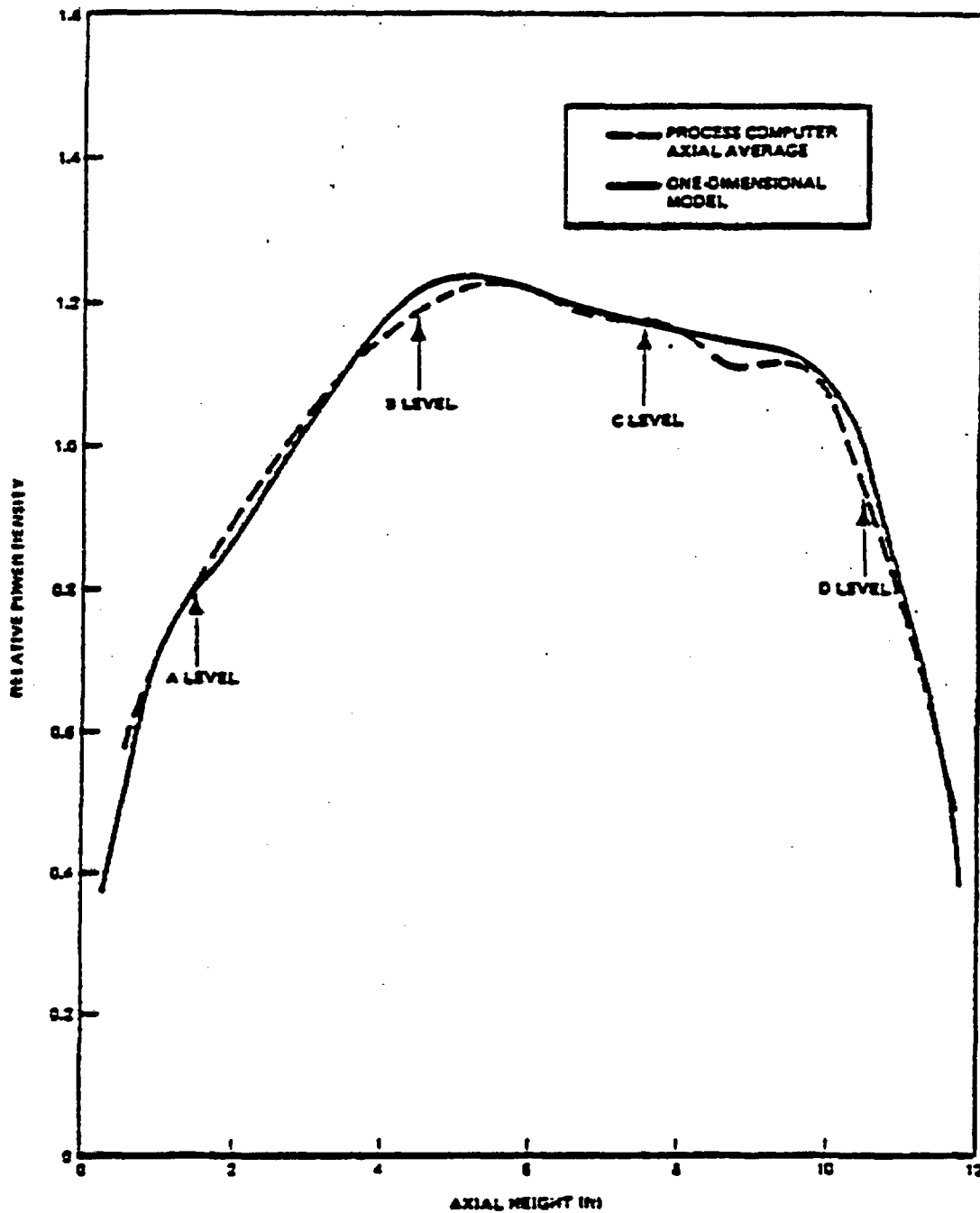
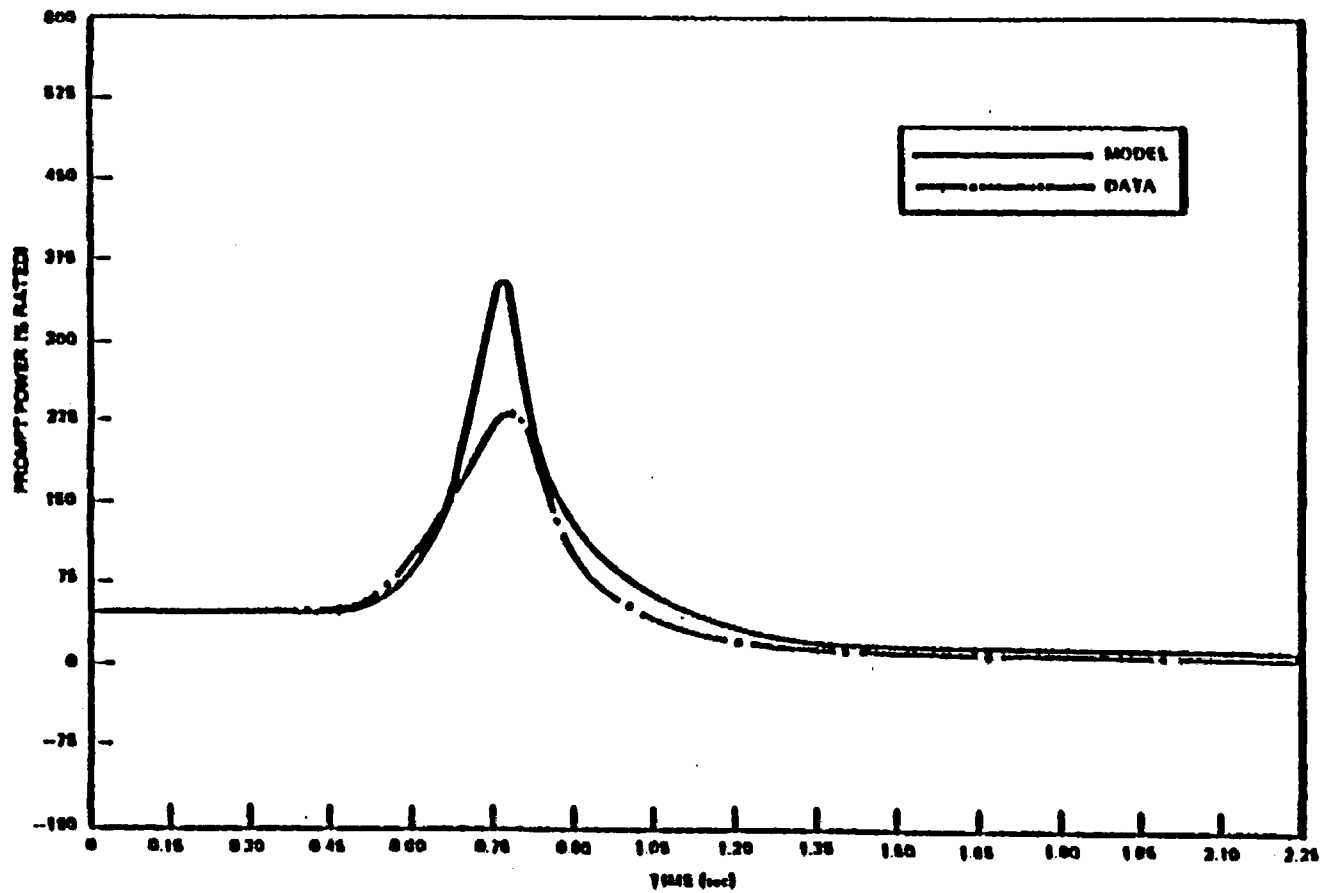


Figure 3 Axial Power Profile Turbine Trip 3

II-45

11-11

98-11

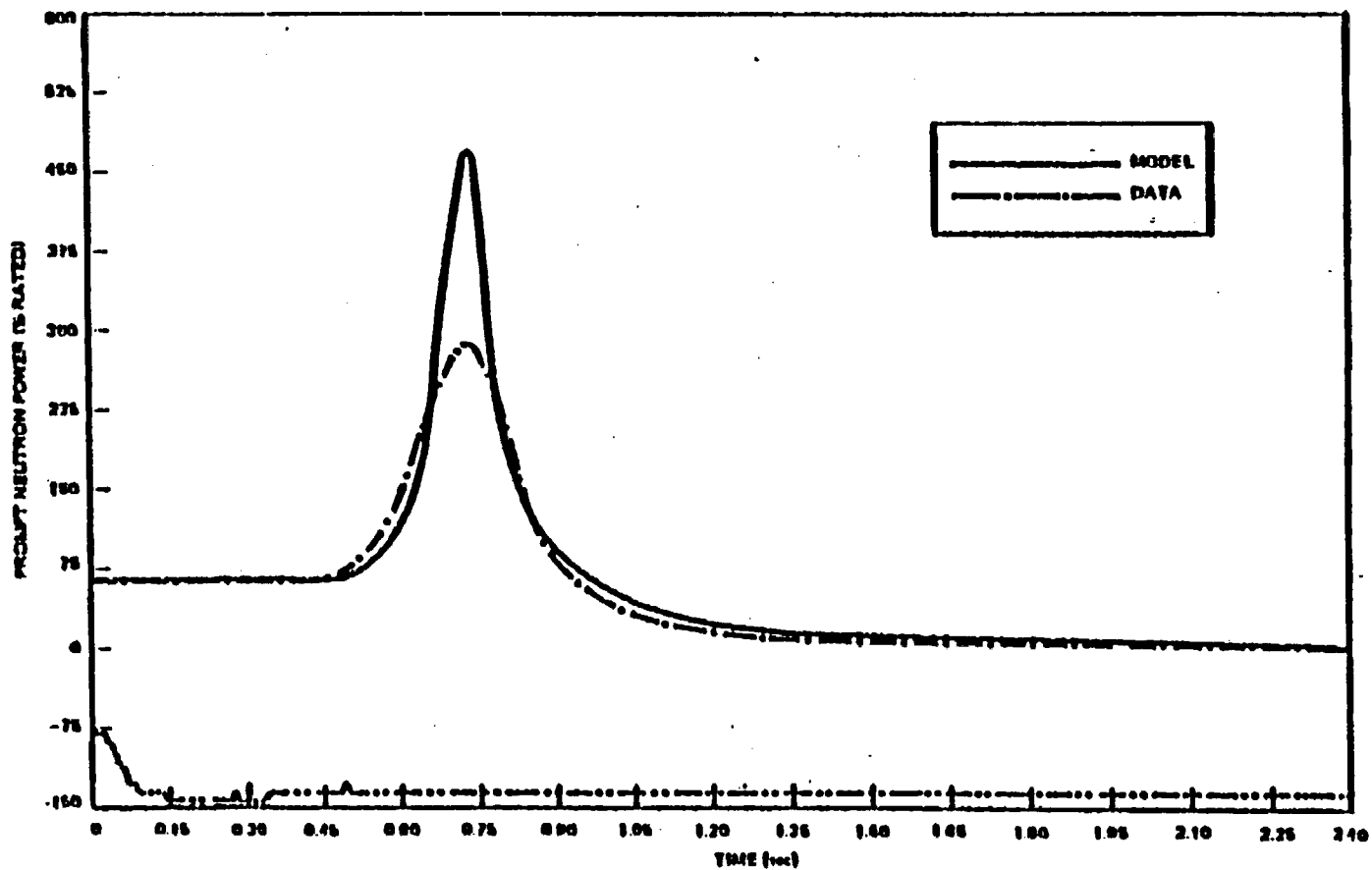


EPDO-24154

Figure 4 Peach Bottom-2 Turbine Trip 1 Prompt Neutron Power

IX113

II-47

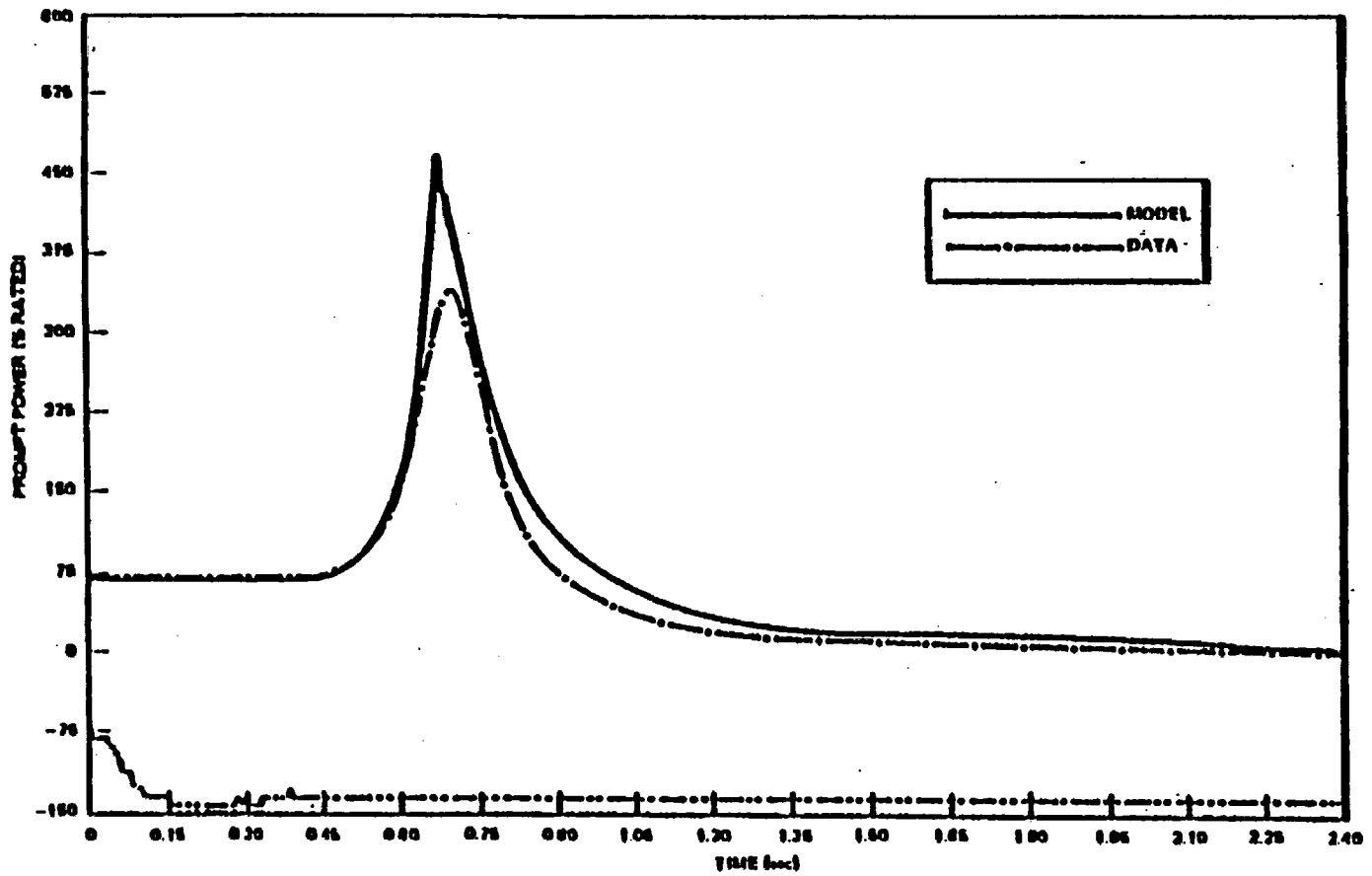


NEED-26154

Figure 5 Peach Bottom-2 Turbine Trip 2 Prompt Neutron Power

TEXT

II-48



NEO-24154

Figure 6 Peach Bottom-2 Turbine Trip 3 Prompt Neutron Power

evidence of this hypothesis, General Electric showed that the steamline pressure calculation for the KKM test, which had a finer spatial mesh, was quite accurate. General Electric has also pointed out that the steamline pressure response shape is not as important to the transient behavior as is the integrated value of the steamline pressure response.

We do not agree entirely with General Electric. In answer to Q-19 in Volume I, General Electric performed a sensitivity study showing the effect of nodalization (different mesh sizes) and comparing the results with the analytical model which uses method of characteristics. The difference in amplitudes in this comparison is on the order of 10% while the difference in amplitudes in Peach Bottom tests and ODYN predictions is 50%. In addition, expected differences have opposite trends. The accuracy claimed by General Electric in the KKM test can be due to the adjustment of the valve opening time. This adjustment was made by General Electric to obtain a better agreement with the measured pressure data. It appears that the steamline model does not predict the amplitudes of oscillations accurately. This is also substantiated by the staff audit calculations. However, we agree with General Electric that the integrated steamline pressure response is more important in determining the transient behavior than the amplitude of individual oscillations occurring at these frequencies. The Peach Bottom tests indicate that the dome pressures do not oscillate and this is the pressure to which the reactor is subjected. Comparison of the dome pressures indicate that the dome pressure calculations performed by the ODYN code are conservative

relative to data; i.e., the overall rate of pressure rise as well as the magnitude of the calculated pressure were higher than the data indicate.

The initial dome pressure rise for the PB-2 tests was predicted accurately by ODYN. The calculation overpredicts the pressure rise near the peak of the first pressure oscillation, thus conservatively modeling void collapse for reactivity feedback. ODYN appears to overpredict the peak vessel pressure rise which demonstrates a conservative basis for overpressure protection analyses. General Electric states (Reference 23) that the overprediction is due to the assumption made in the energy equation for the dome region. The overprediction of dome pressure is considered a desirable conservatism. Within the period of time that the neutron flux pulse occurs, the dome pressure overprediction is approximately 15 to 28% higher than the data.

Reviewing the steamline and dome pressure transients and based on the sensitivity studies performed by General Electric, we require that the steamline be modeled by at least 8 nodes with maximum size of 100 ft for a node.

The core exit pressure is one of the most important parameters for the prediction of the pressurization transient neutron flux response. As was the case in dome pressure comparisons, the initial rise in core exit pressure was followed well by the model for all three tests. From the comparisons of ODYN to the PB-2 test results,

General Electric has concluded that the steamline dome and vessel thermal hydraulic models simulate the overall core pressure rise rather well in all three experiments. This lends confidence to the code predictions through the full range of power levels. Measurements indicate some oscillations in core exit pressure. These oscillations have been attributed to instrument line effects by General Electric. This is corroborated by the lack of associated oscillations in neutron flux measurements.

The neutron flux predictions by the ODYN code were conservative relative to data. We estimate that the peak neutron flux is higher by 54 to 86% than the data and the integral of the nuclear power (which is a measure of the amount of energy generated) is also higher by approximately 16 to 42% than the data. Hence, the neutron fluxes were predicted conservatively in all three tests.

As a final step, General Electric has presented a calculation of $\Delta CPR/ICPR$ for test and model. We reviewed the calculational procedure and consider it appropriate. The results show that the $\Delta CPR/ICPR$ for ODYN predicted transient conditions is within 0.01 of the values which would be predicted from test conditions; i.e., the $\Delta CPR/ICPR$ values calculated using the measured flow from jet pump ΔP measurements, the measured pressure and the measured power during the tests. The ODYN transient conditions predicted two out of three $\Delta CPR/ICPR$ values conservatively. The differences are between -5.1% and 6.8% relative to values calculated using the data (minus means nonconservative). The differences in these three test results in

terms of $\Delta\text{CPR}/\text{ICPR}$ give $\mu = 1.14\%$ which represents a very slight conservatism for the mean and $\sigma = \pm 6.39\%$ for the standard deviation. Since the data (three points) are very limited, the results do not have a high degree of confidence. Table II presents these values of $\Delta\text{CPR}/\text{ICPR}$.

TABLE II
COMPARISON OF MAXIMUM $\Delta\text{CPR}/\text{ICPR}$ VALUES FOR
PEACH BOTTOM AND KKM TESTS

<u>Test</u>	<u>Initial CPR</u>	<u>$\Delta\text{CPR}/\text{ICPR}$ (Data)</u>	<u>$\Delta\text{CPR}/\text{ICPR}$ (ODYN)</u>
<u>Peach Bottom</u>			
Turbine trip 1	2.536	0.170	0.173
Turbine trip 2	2.115	0.136	0.129
Turbine trip 3	2.048	0.132	0.141
<u>KKM</u>			
Turbine trip	1.279	0.077	0.084

Review of the test results indicate that all model conservatisms claimed by General Electric such as conservatism in calculation of the steam dome pressures and neutron flux, conservatism in collapsing of 3-D core neutronics and thermal hydraulics, conservatism in the gap conductance input parameters and any other conservatism claimed in the computer model are either so small that it did not make any difference in calculating ΔCPR for these three tests or all of these claimed conservatisms are offset by an unidentified nonconservatism somewhere else, perhaps in calculation of flow. It is evident that the calculations of ΔCPR are not conservative for all of the tests.

They can only be regarded as best estimate or accurate predictions. Hence, based on the Peach Bottom tests we do not give any credit for the conservatism in the models used in the ODYN code. The code will be regarded as best estimate for Δ CPR calculations and any discrepancy between the test results and the code will be treated as an uncertainty or an error. Further tests would be needed to reduce these uncertainties.

b. KKM Test Comparison

A brief summary of the test conditions is contained in Volume II. KKM plant has an unusual configuration, in that, it has two turbines and two sets of steamlines with a reheater line in each steamline. It presents some special model considerations for ODYN simulation. A special version of ODYN was developed to simulate this configuration.

Also unique to this test comparison as opposed to the PB-2 comparison is the modeling of turbine stop valve and bypass valve actuations. Measured turbine stop valve and bypass valve positions between initial and end of actuation were not available for this transient. The stop valve behavior can be reasonably estimated from the opening to closing time. However, the transient response is quite sensitive to the bypass valve behavior. The bypass valve opening speed of the ODYN model was adjusted until the calculated transient turbine inlet pressure agreed with measurement. This adjustment was made for only the initial bypass valve opening speed and, thereafter bypass valve position was controlled based on the plant control parameters. The remainder of the test modeling is similar to that of the PB-2 test

comparison. The fuel rod gap heat transfer coefficient was selected to be 600 Btu/hr-ft²-°F.

The turbine trip test conducted at KKM provided a reactor and operating state that was quite different from PB-2. The test at KKM corresponded to an end-of-cycle condition with all control rods fully withdrawn and with the reactor at 77 percent of full rated power and 85.5 percent of full rated core flow. The reactor itself is considerably smaller in size than PB-2 and has a somewhat different system including two turbo-generating units. The turbine trip test at KKM resulted in a milder transient than the tests at PB-2. The ODYN results compared to the test data showed the same general agreement as was observed for PB-2 for the response of the core power as a function of time. The calculated steamline pressure response for the KKM turbine trip appears to be in good agreement with measurement. The KKM comparisons appear to be in slightly better agreement with measurement than do the PB-2 comparisons. As previously discussed, the characteristics of the bypass valve were adjusted to give a good agreement with the measured steamline pressure.

The measurements of dome pressure showed some oscillations. Since these oscillations did not manifest themselves in the neutron flux measurements, they were attributed to instrument line disturbances and were not considered to be actual pressure oscillations. There were also oscillations in core exit pressure measurements. Similar oscillations were not observed in the PB-2 tests. These oscillations

were also attributed to the instrument line disturbances since no oscillations were observed in neutron flux.

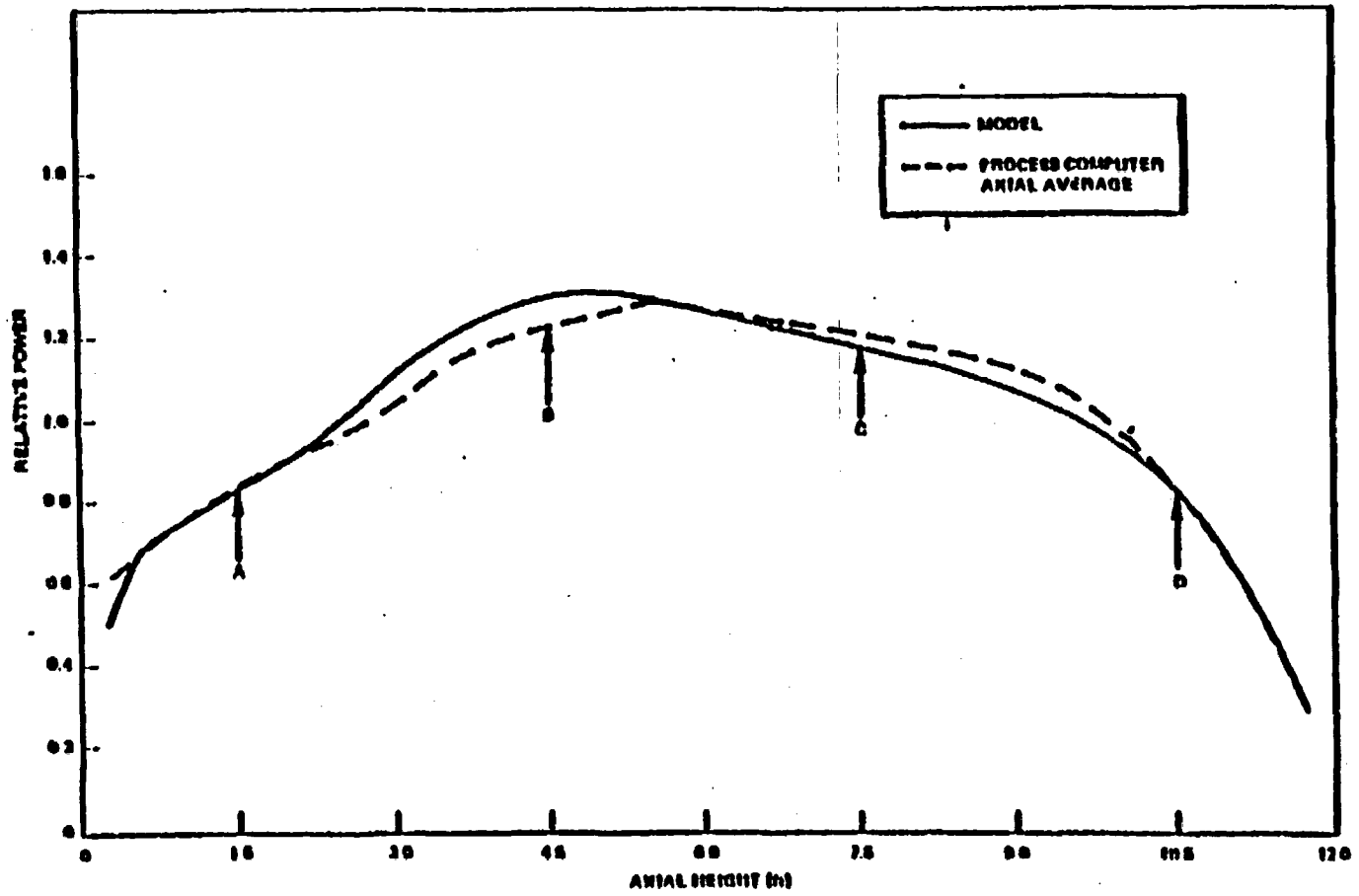
The calculated pressure responses pass through the data up to 1.8 seconds of the transient time. After 1.8 seconds the calculated pressure are higher than those measured. The calculated core exit pressure had a 40 millisecond delay behind the data. This was attributed to the modeling of steam separator inertia. We agree with General Electric that the overall shape of the core exit pressure response is duplicated well by the ODYN code. The agreement between the calculated and measured pressures in the dome and the steamline is also reasonably good. There is no conservatism in calculation of pressures up to 1.8 second of transient time.

The measurement of neutron flux indicates a double peak behavior. This double peak was attributed to an oscillation in core pressure which was thought to be enhanced by KKM bypass characteristics. The ODYN code overpredicted the initial neutron flux peak by approximately 53% and underpredicted the second peak. We estimated that the integral of the calculated nuclear power was higher by approximately 20% than the data. Figures 7 and 8 present the comparisons of measured and calculated axial neutron and prompt neutron fluxes respectively.

The calculated value of $\Delta\text{CPR}/\text{ICPR}$ was about 9.1% conservative relative to the value calculated using measured quantities (see Table II).

11-56

11-56

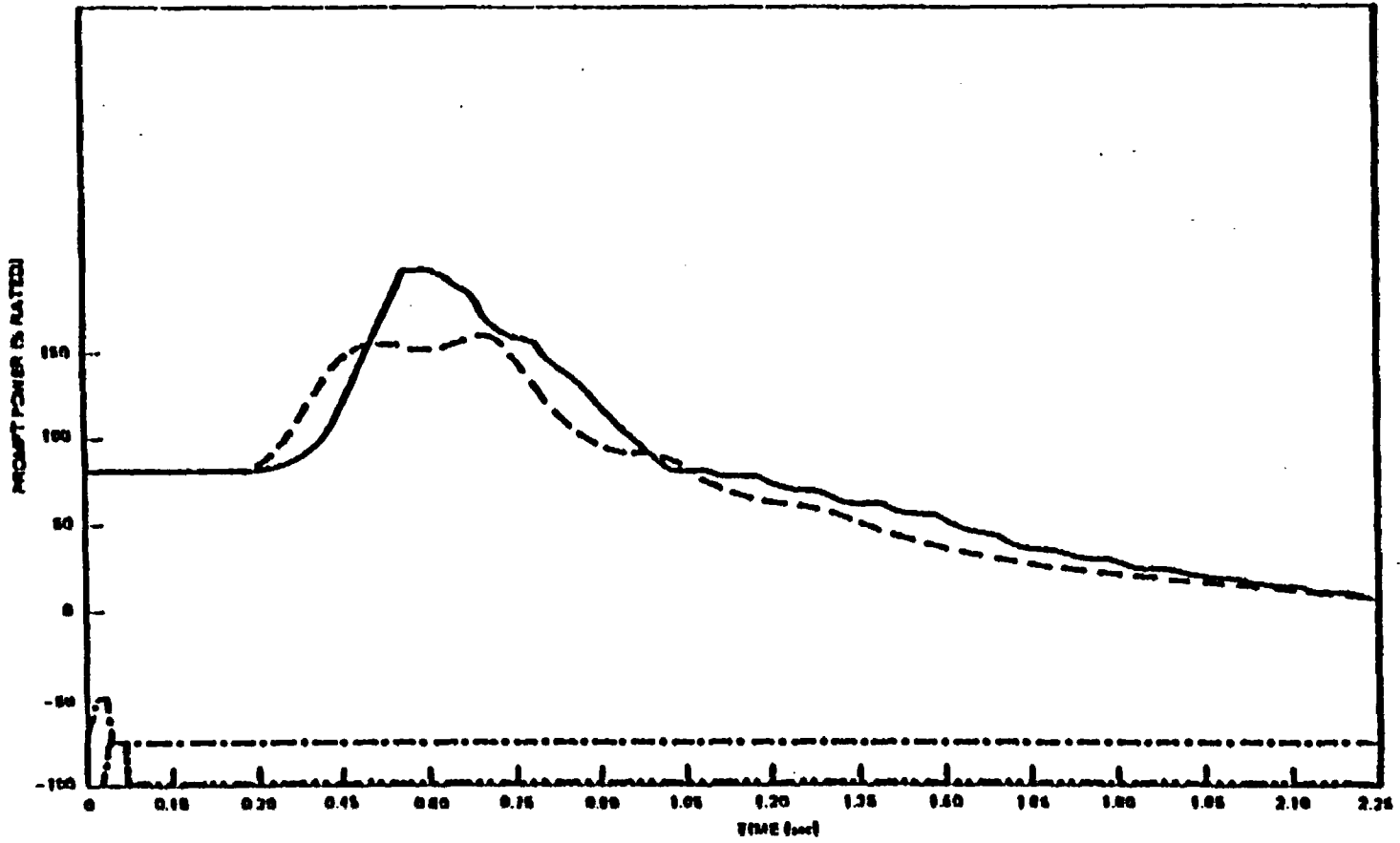


11-56

Figure 7 Average Axial Power KKH Test Conditions

111111

11-57



NEED-24154

Figure 8 KKH Turbine Trip Prompt Neutron Power

Although there is conservatism of 9.1% in $\Delta\text{CPR}/\text{ICPR}$, the difference in absolute values is small; i.e., 0.007 in terms of $\Delta\text{CPR}/\text{ICPR}$. Since the value of ICPR was 1.279, the value of ΔCPR is approximately 0.01. According to General Electric the maximum practical accuracy in ΔCPR is 0.01 (Volume III). In addition, KKM transient is a relatively mild transient. Hence, we do not give any credit for conservatism in $\Delta\text{CPR}/\text{ICPR}$ prediction.

4. Qualification Using Another Computer Code - Audit Calculations

Another important means of qualifying a code is to compare the results of calculations with the results obtained from another code. The two codes should be as independent as possible including the neutronic input parameters. The BNL-TWIGL (Reference 24) and RELAP-3B (Reference 25) codes are fully capable of analyzing these BWR turbine trip tests and satisfy the requirement of independence. The nuclear data base for deriving the input for the BNL-TWIGL/RELAP-3B codes also satisfies the requirement of independence.

a. Development of Computational Method

A calculational method for the analysis of the turbine trip transients was developed at BNL using the RELAP3B and BNL-TWIGL computer codes. This method was developed under two NRC Technical Assistance Programs supplementing each other, and uses the codes in an iterative manner. The details of the method are presented in Reference 26. The RELAP3B code is used to perform the system transient analysis for the audit calculations. The BNL-TWIGL code is used to calculate the reactivity feedbacks and core power transient. The BNL-TWIGL code performs a

space-time analysis of core neutronics and thermal hydraulics with feedback in two dimensions (reference 21).

The BNL-TWIGL code has a number of advantages over the ODYN code. The calculation can be performed with two neutron energy groups in two-dimensional (r,z) cylindrical geometry. It has the capability of allowing for five radial scram zones. Any important radial effects will, therefore, be calculated by BNL-TWIGL. The BNL-TWIGL code also has two disadvantages relative to the ODYN code. These disadvantages are: (1) the lack of a bypass flow channel, and (2) the independence of the Doppler reactivity with void fraction. Weighing these advantages and disadvantages of BNL-TWIGL relative to the ODYN code, it is our judgment that they will not adversely affect the comparison of the two codes for the turbine trip transient discussed herein.

The calculational method was developed using the Peach Bottom tests as a bench mark. Assuming the measured power history (power vs. time) in the core as input, RELAP3B calculates the system thermal-hydraulic parameters and provides the BNL-TWIGL code with the time dependent core inlet boundary conditions, i.e., pressure, flow and temperature variations with time. Then, the BNL-TWIGL code performs the space-time analysis of the core neutronics and thermal-hydraulics. The calculated power history is then compared with the measured power which was input to the RELAP3B code. If the differences are large the calculated power history is used in the RELAP3B code and the calculations are repeated until the power history calculated by the BNL-TWIGL code is in good agreement with the power history input to

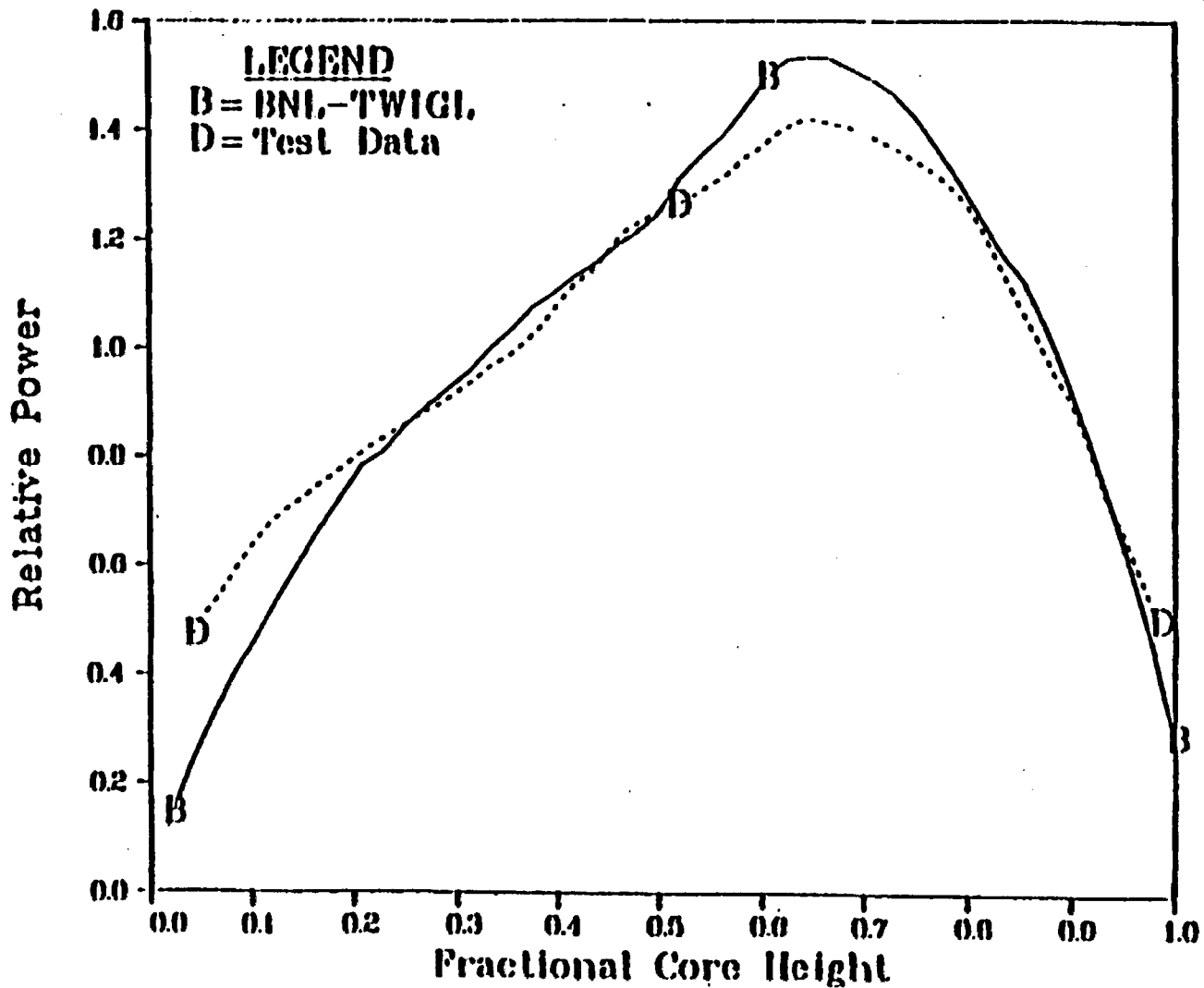
the RELAP3B code. This method was used for both the Peach Bottom tests and the licensing audit calculations (turbine trip without bypass transient).

b. Peach Bottom Tests and Audit Calculations

The RELAP3B/BNL-TWIGL calculational method described above was employed by BNL to analyze the Peach Bottom transient tests. The calculated power history agreed well with the measured power history. There is also good agreement between the other calculated and measured parameters. The core physics results that were obtained by BNL are presented in Reference 25. Reference 25, also discusses the geometric modeling, the neutron cross sections, and the initialization of the transients. These calculations confirmed the adequacy of the BNL-TWIGL/RELAP-3B modeling for computing BWR turbine trip transients. Figures 9 through 14 show samples of these agreements. "Revised BNL" curves in Figures 12 through 14 refer to a more detailed BNL model which will be explained subsequently.

Calculations performed with the ODYN code also agreed very well with the experimental results although the neutron flux predictions were slightly conservative. We believe that this can be attributed to the slightly higher ODYN pressure predictions during the transient. The power history calculated by BNL provides better agreement with the experimental data on a best estimate basis than the ODYN code predictions.

Peach Bottom 2 Turbine Trip Test 1, Initial Power



11-61

Figure 9
11-61

Peach Bottom 2 Turbine Trip Test 2, Initial Power

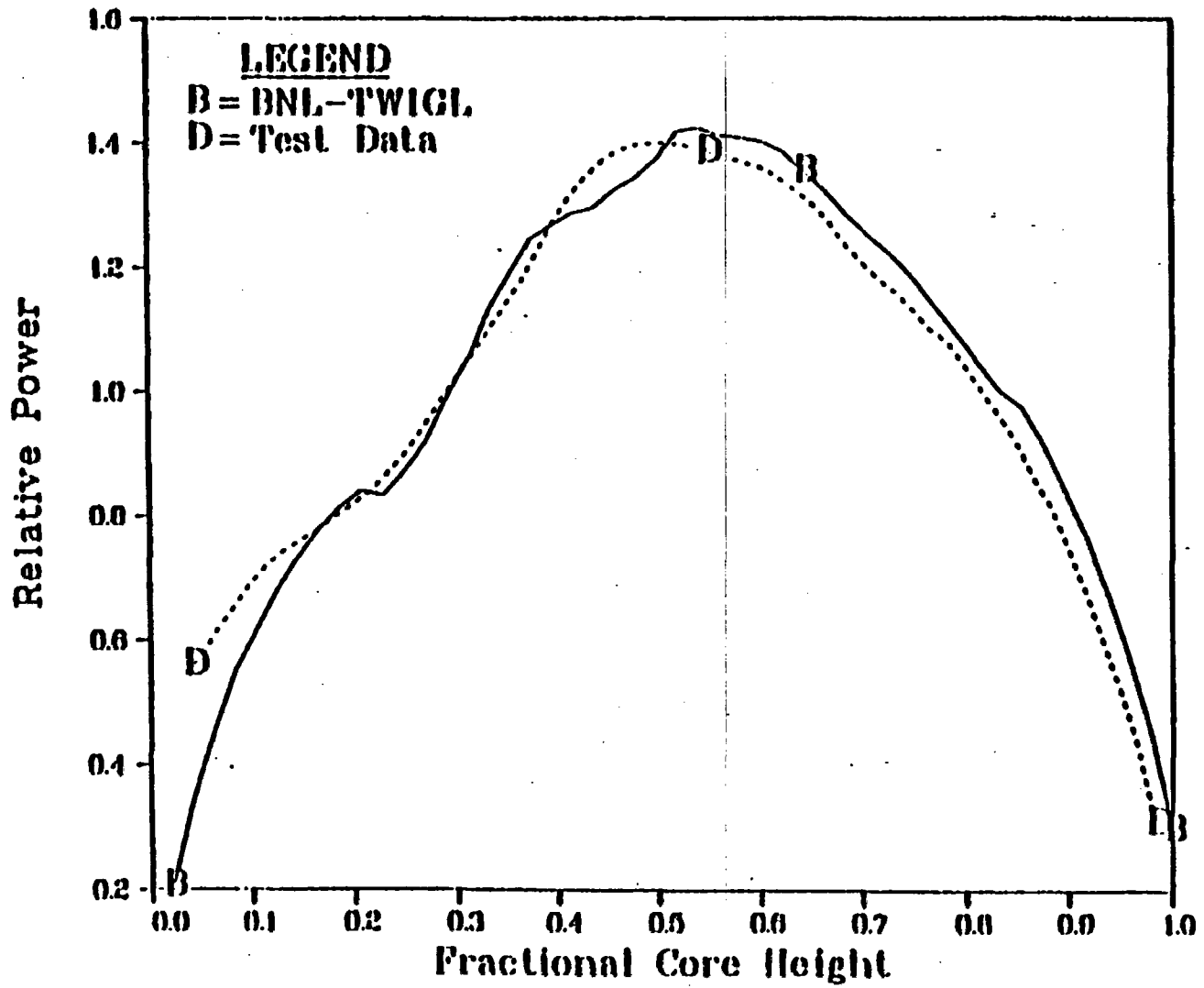


Figure 10
11-62

11-62

Peach Bottom 2 Turbine Trip Test 3, Initial Power

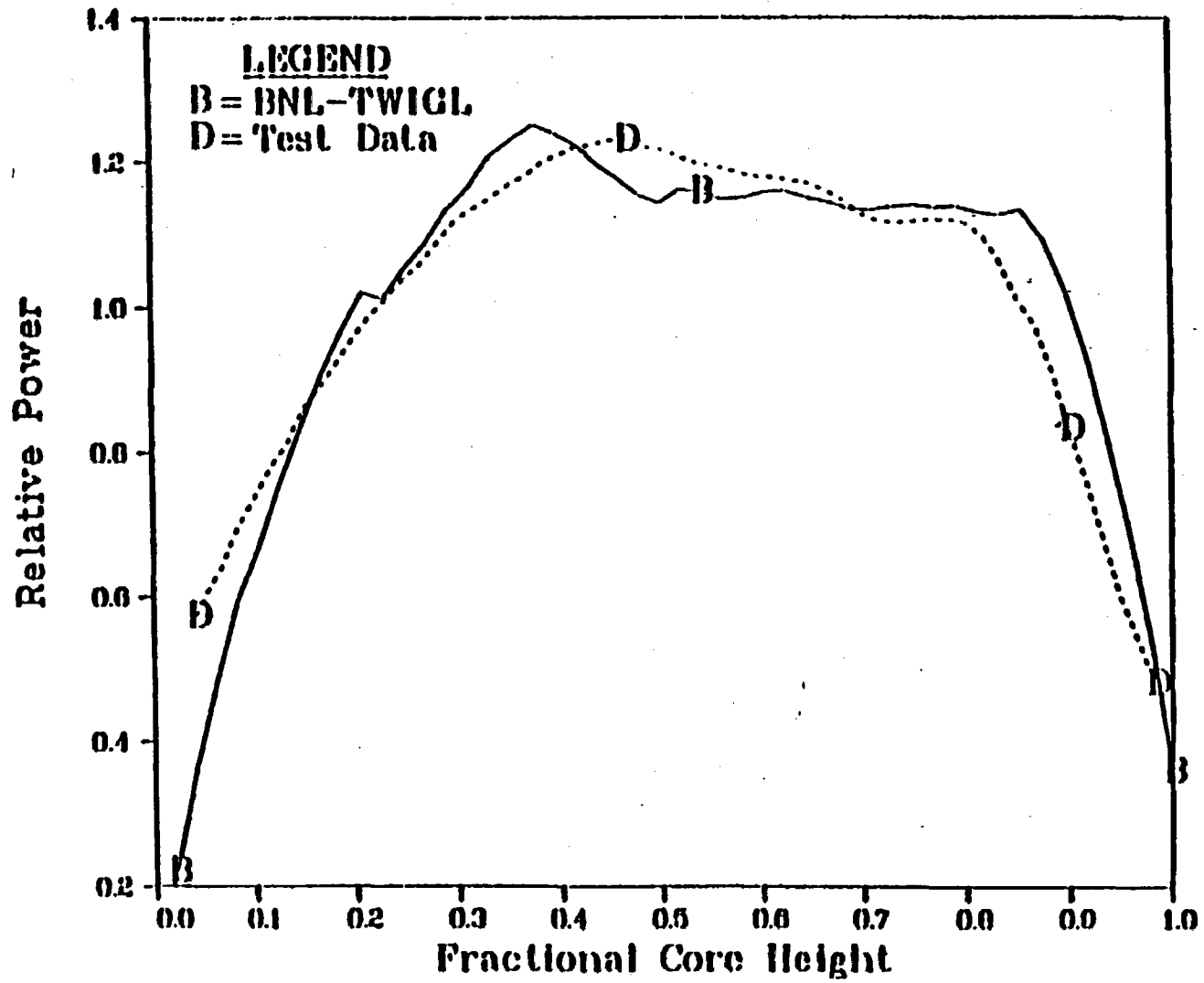


Figure 11
11-63

11-63

Peach Bottom 2, Turbine Trip, Test 1

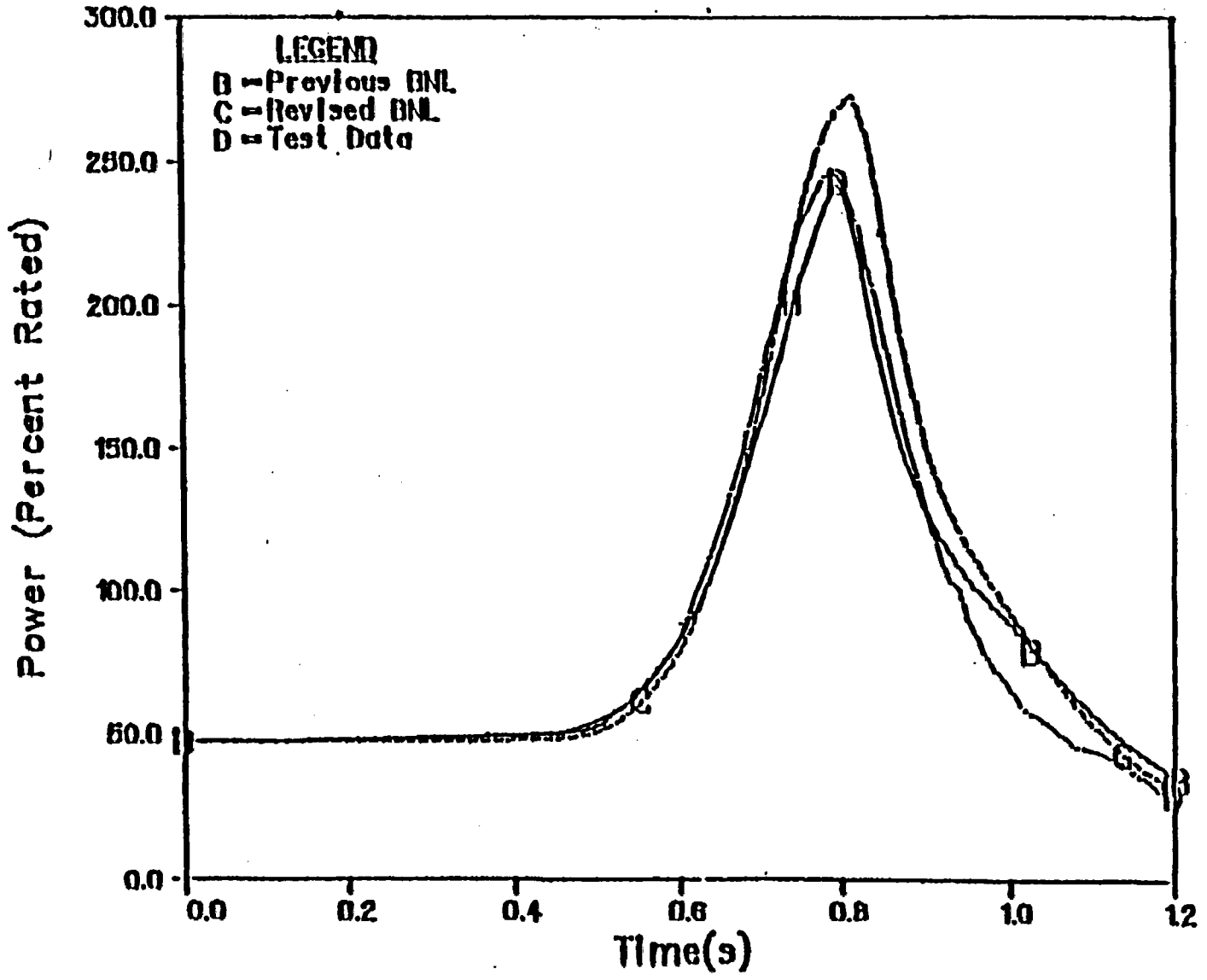
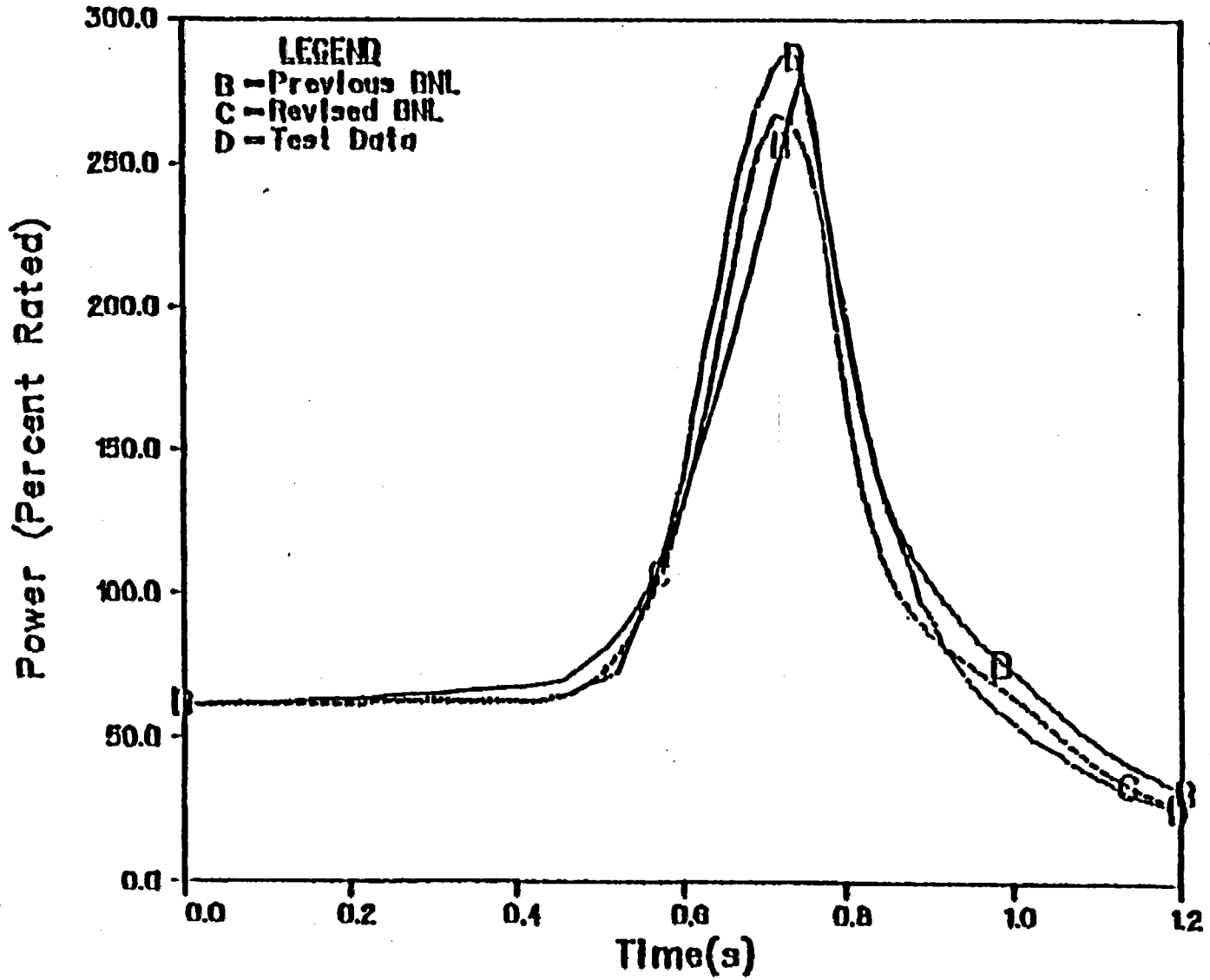


Figure 12
11-64

1000

Peach Bottom 2, Turbine Trip, Test 2



1000

Figure 13
11-65

Peach Bottom 2, Turbine Trip, Test 3

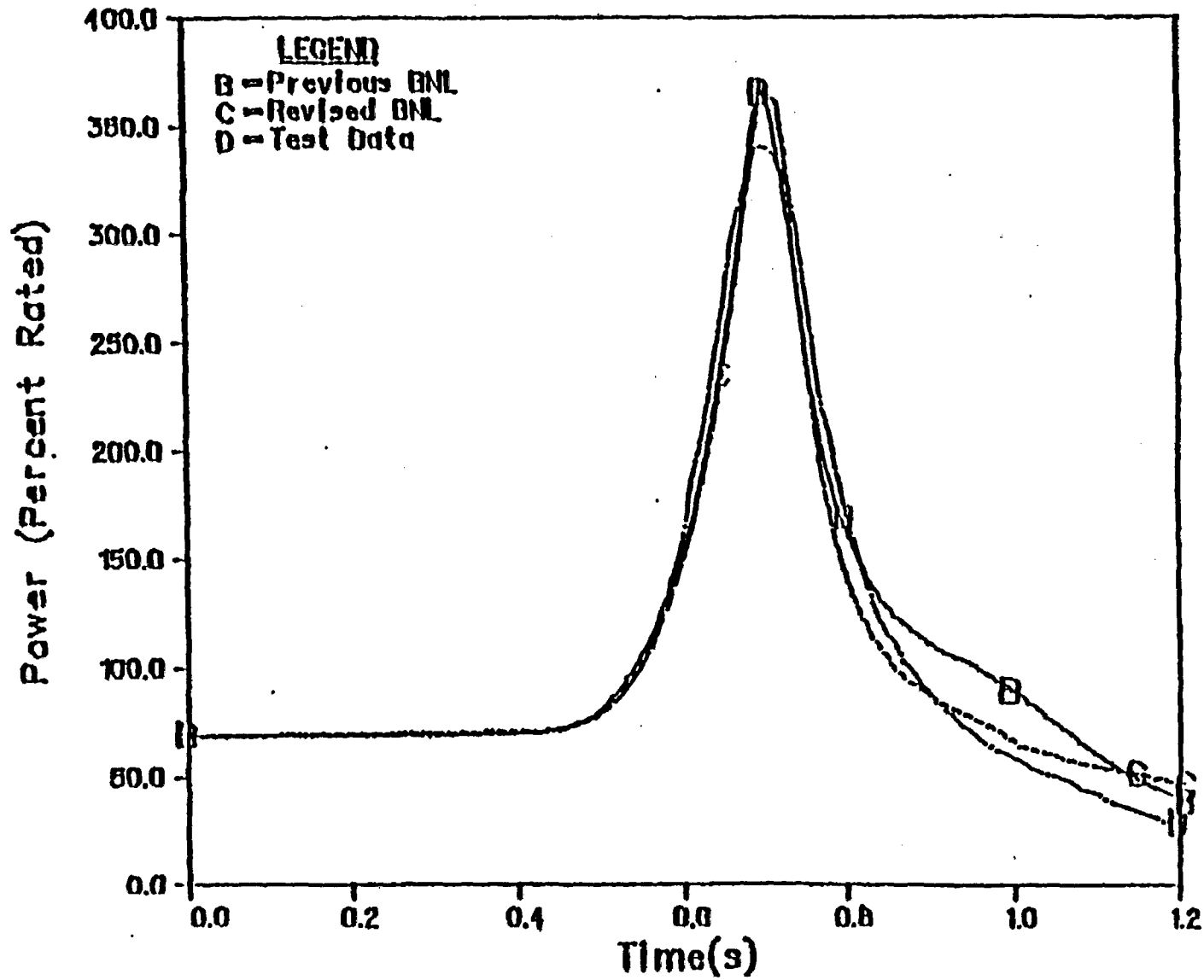


Figure 14
11-65

150001

At a meeting on July 14, 1978 attended by GE and our consultants from BNL, a turbine trip without bypass transient (TTWOB) was defined for calculation by GE with the ODYN code and by BNL with the BNL-TWIGL/RELAP-3B codes. This TTWOB transient was for PB-2 at end-of-cycle 2 with the reactor at an all rods out condition and with a Haling core power distribution. The reactor trip was assumed to occur from the primary trip signal for this transient, i.e., the position of the turbine stop or control valve. All of the system input parameters were discussed and values were assigned. The reactor was assumed to be operating at a 104.5 percent of full rated power and at 100 percent of rated core flow.

The initial calculations by GE and BNL differed considerably. The total core power as a function of time calculated by BNL was about 60 percent greater in energy output although the initial rise and falloff of the power was about the same. The BNL calculation predicted a peak power of over 7 times the initial core power at about 0.9 seconds. The GE calculation resulted in a peak power of about 4 times the initial core power at about 1.0 second.

A GE evaluation of its calculation resulted in finding two significant errors that led to a new GE calculation. One of the errors was the steamline length. It had originally been input as 460 feet whereas the value should have been 400 feet. GE also found that one of its processing codes had improperly accounted for the Doppler reactivity feedback variation with void fraction. This new GE calculation resulted in a more severe transient than the earlier

calculation. The new GE prediction of peak power was about 5.3 times the initial core power at about 0.9 seconds. This GE calculation had an earlier rise and an earlier fall-off of the total core power than the BNL calculation. The BNL calculation still predicted a greater energy output for the transient by about 20-25 percent. A comparison of the reactivity components showed that the void, scram, Doppler, and net reactivities as a function of time differed significantly between the BNL and new GE calculation. As an example, the BNL calculation resulted in a prompt critical calculation with a maximum net reactivity of over one dollar. The GE calculation resulted in a maximum net reactivity somewhat less than 0.8 dollars.

Since it was our expectation that the BNL and GE calculations would be in better agreement, a meeting with General Electric at BNL was held to resolve differences between the calculations. This meeting was held from September 27 through September 29, 1978 with GE, BNL, and NRC in attendance, Reference 27. The main differences noted between the two calculations are listed below.

<u>ITEM</u>	<u>REMARK</u>
1. Relief valves	
(a) Set Points	GE values too large
(b) Delay time	BNL did not include
(c) Bank capacities	BNL did not use GE values
(d) Time constant for full flow	BNL did not include
2. Turbine inlet pressure	GE value too large
3. Steam separator modeling	
(a) Separator L/A	BNL value low
(b) Separator mass	BNL water inventory too low

<u>ITEM</u> (Cont.)	<u>REMARK</u> (Cont.)
4. Doppler reactivity feedback	BNL does not include variation with void fraction
5. Bypass heating effects	BNL does not include
6. Fuel gap conductance	BNL used variable value (400-500) whereas GE used a constant value of 1000

In addition, some of the BNL neutronic data were also compared to corresponding GE data. The beginning-of-cycle infinite multiplication factor (K_{∞}) was compared for a number of fuel types both with and without a control blade and as a function of void fraction. Only small differences were noted between the various sets of data. The initial axial K_{∞} distribution was also compared and again only small differences were noted. It was also noted that the BNL control worth was about 15 percent larger than that of GE. These neutron cross section and K_{∞} data as a function of fuel exposure and void fraction were later provided to the staff by GE for the two dominant fuel types in the PB-2 core (References 28 and 29).

Void reactivity coefficients extracted from the BNL and GE TTWO8 calculations indicate that the BNL value at the start of the transient is larger in magnitude by about 14 percent than the GE value. This larger BNL void coefficient is consistent with the lattice physics data that is used. However, the neutron effective void correlation used by General Electric compensates for a large part of this difference (Reference 34).

A reanalysis of the turbine trip without bypass transient was performed by BNL. Both analyses were presented in Reference 33.

Some sensitivity studies were also performed. Some of the differences noted in the meeting did not change the BNL results substantially. However the difference in the separator inventories and the required renodalization around the separators to accommodate proper inventories inside and outside of the separators and inclusion of a separate flow path between the steam dome and outside of the separators (bulkwater), reduced the neutron power and the total energy output in the licensing basis transient (TTWOB). The total energy output, the integral of the neutron power, predicted by BNL during the transient was less than that in the second calculation performed by General Electric. However, the General Electric calculation still indicated an earlier rise and an earlier fall-off of the total core power than the BNL calculation. Figure 15 presents these two BNL calculations as well as the General Electric calculation.

The primary reason for the change in the energy outputs as well as disagreement in the shape of the neutron power transient was the new inlet core flow calculation by the BNL. The core inlet flow in the second BNL calculation was in closer agreement with the second GE calculation in that it exhibited similar oscillatory behavior. However, there were still some differences in amplitudes. It should be noted that the differences in flow variation during the transient between the two BNL calculations were within 15% of each other. Judging from the BNL studies, Reference 33, we conclude that the modeling of separators is significant in predicting the core inlet flow. We also note that the BNL modeling of the separators is still deficient in that the inertia term, L/A , does not depend on the

BWR Licensing-basis Transient

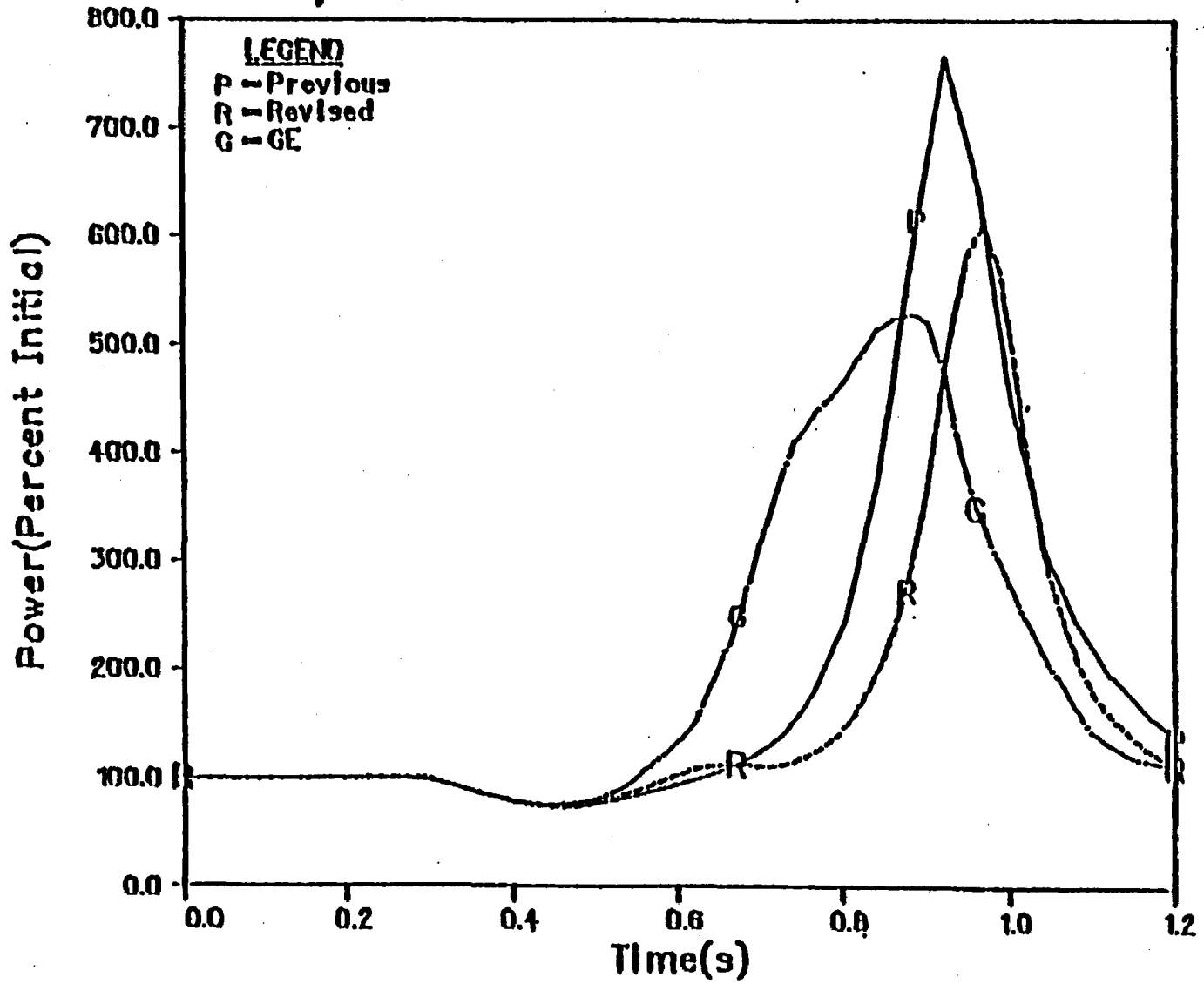


Figure 15
11-71

11-71

quality at the entrance of the separators. The ODYN code contains the modeling of the L/A term which derived its basis from experimental data obtained from separators. Hence, we judge that the ODYN model should predict the core inlet flow more accurately than does the BNL model, and that the neutron power transient should also be more accurately predicted by the ODYN code.

Reference 33 indicates that previous and revised BNL models predict almost similar core inlet flow variations at the beginning of the Peach Bottom turbine trip tests. However, there are large differences between predictions after 0.8 sec. Since the power peaks occur before 0.8 sec in the Peach Bottom tests, these large differences in inlet flow predictions do not alter the predictions of neutron powers as illustrated in Figures 12 through 14. However, as shown in the analysis of licensing basis transient, the separator inertia term and its modeling is important in predicting the transient behavior (or amplitude of oscillations) of the core inlet flow.

Reference 33 also indicated that the heat flux predictions in the second BNL calculation were lower for the portion of the transient where highest Δ CPRs were expected to occur than those calculated by General Electric. This was expected since the integral of neutron flux in the second BNL calculation was smaller than that calculated by General Electric. BNL did not perform Δ CPR calculations. However, the predictions of heat flux would suggest, and we would expect that the second BNL calculations would produce less Δ CPR than that calculated by General Electric.

BNL did not report heat fluxes in their first calculations. However, the integral of the neutron flux was almost the same as that calculated by General Electric. Hence, we expect similar severity for Δ CPR values if Δ CPR calculations were made using the first calculations performed by BNL.

A third analysis of the TTWOB transient was performed by BNL using GE calculated values of the core exit pressure and core inlet flow. The BNL-TWIGL calculation now predicted a transient with similar initial power rise and fall-off characteristics as the GE ODYN calculation although the peak power was higher in the BNL calculation. A sensitivity calculation with a 5 percent change in the void reactivity feedback resulted in a BNL-TWIGL power transient that compared very well with the corresponding GE results. The change of 5% in void reactivity or the coefficient is well within the calculated uncertainty of 11% as presented in Section II.A.6.

These audit calculations established the fact that core inlet flow is a very sensitive parameter. The core inlet flow measurements (i.e., the jet pump Δ p measurements) in the Peach Bottom tests contained some errors. In Section II.B.3.a, where qualification of the ODYN code using Peach Bottom tests was evaluated, many comparisons between various parameters (such as pressure and neutron flux) were made and these parameters were always found to be conservative relative to data. However, despite these conservative features, the calculated values of Δ CPR cannot be considered as conservative. This was also pointed out in Section II.B.3.a. Based on the information submitted,

it is our judgment that there is some nonconservatism in core inlet flow calculation in the ODYN code overcoming all other conservatisms.

We conclude that, although a precise audit of the GE ODYN code was not obtained by the BNL-TWIGL/RELAP-3B codes for this licensing basis TTWOB transient, the analyses performed by BNL provided us with valuable insights concerning this transient. We conclude that the primary reason for the disagreement of the BNL-TWIGL/RELAP-3B TTWOB results with the GE results is due to core inlet flow differences. Judging from the audit calculations as well as Peach Bottom test results, we also conclude that differences in predictions on the order of 20% in prediction of peak neutron flux can be expected using different computer codes which represent the state of the art.

5. Summary of Code Qualification

In summary, we find that the ODYN is a best estimate code containing models developed from first principles and provides good predictions of existing experimental data. The experimental data were obtained from separate effects and integral plant tests. The separate effects tests include core power measurements from various plants and heated tube tests to verify the void fraction model. Integral plant tests were performed at Peach Bottom Unit 2 and KKM. Comparison of the test data and calculations indicates that the agreement is within the uncertainties calculated in Section A. We find that the Δ CPR predictions from the ODYN and SCAT codes are neither conservative nor nonconservative. They predict the available data well.

The ODYN-SCAT prediction of the three Peach Bottom transient tests and one KKM transient test demonstrated a 2σ uncertainty of approximately 37% of $\Delta\text{CPR}/\text{ICPR}$ at a 95% confidence level. We have determined this using χ^2 distribution. No credit was given for measurement errors. This results in a $2\sigma \Delta\text{CPR}/\text{ICPR}$ uncertainty of 0.068 for a transient which degrades the CPR from an initial value of 1.30 to the limit of 1.06. Since these tests represent a very limited data base, it is likely that the 2σ uncertainty can be reduced significantly by the acquisition of additional test data for comparison to code predictions. Hence, we recommend that additional integral plant tests be performed to qualify the code with a higher confidence.

C. EVALUATION OF THE MARGIN

The ODYN statistical analysis was performed by General Electric at our request in order to provide a quantitative basis for determining if the ODYN licensing basis contains an acceptable level of conservatism. Two quantities were calculated in this analysis: the probability of the expected ΔCPR exceeding the licensing basis ΔCPR ; and the probability of exceeding the thermal-hydraulic design basis (i.e., probability of exceeding 0.1% of fuel in Boiling Transition).

The ODYN Code is intended to be used to calculate the change in Critical Power Ratio (CPR) during rapid pressurization transients such as the loss of load and feedwater controller failure transients. This information is used in combination with the General Electric Thermal Analysis Basis (GETAB) CPR safety limit to establish the operating limit CPR. GETAB is a statistical analysis

which determines the value of CPR which corresponds to 0.1% of the fuel rods in Boiling Transition. The GETAB analysis considers the effects of uncertainties on input parameters such as power, coolant temperature and flow as well as uncertainties in the GEXL correlation.

Uncertainties in the ODYN Code need to be considered since these will affect the probability of exceeding the thermal-hydraulic design basis. One method of accounting for the effects of ODYN code uncertainties is to include uncertainties directly into the GETAB statistical analysis. A second method is to assure that the ODYN licensing calculation gives a sufficiently conservative value of Δ CPR to assure that the thermal-hydraulic design basis is not exceeded. GE has chosen to use the second method in demonstrating the acceptability of the ODYN licensing basis.

We have determined that this approach is acceptable in principle. In addition, we have determined that an acceptable level of conservatism for the ODYN licensing basis corresponds to a 5% probability of exceeding the thermal-hydraulic design basis.

General Electric has provided statistical analyses of the loss of load (Turbine Trip) and feedwater controller failure transients. These analyses use Monte Carlo calculations to predict Δ CPR with a second order response surface which simulates ODYN calculations. The input parameters in the response surface are: initial power; control rod drive (CRD) speed; exposure index (a measure of axial power shape effects); ODYN code uncertainty; and response surface fitting uncertainties.

The response surface was generated through a regression analysis of Δ CPR calculations performed using input from the ODYN Code. The accuracy of the response surface was tested by General Electric by comparing the results of ODYN calculations to the results of response surface calculations. The accuracy checks were done for 15 load rejection transients for a BWR/3 EOC-6 and for 15 load rejection transients for a BWR/4 EOC-4. These comparisons showed good agreement between the two methods. In addition, a regression fitting error was developed from these comparisons and this fitting error was added to the response surface. This error was found to have a range of one standard deviation values of 0.0076 Δ CPR/ICPR to 0.0126 Δ CPR/ICPR depending on the plant type, the time in cycle, and the transient of interest. This range of errors is three to four times smaller than General Electric's estimate of the ODYN code uncertainty (0.031 Δ CPR/ICPR) or our estimate of (0.044 Δ CPR/ICPR) - see Table I. This indicates that the response surface is a faithful reproduction of the ODYN calculational results and that the response surface can be used to establish the effect of ODYN code uncertainties on the probability of exceeding the thermal-hydraulic design basis.

The distribution functions of each of the input variables (initial power, CRD speed, exposure index, and code uncertainty) were reviewed. The uncertainties of the ODYN code are discussed extensively in the code review section of this report and will not be repeated here. The uncertainty on initial power level used by GE was + 2%. We requested additional information to substantiate this value and were given extensive information on the various elements in the plant energy balance and the uncertainties associated with each of these elements. The elements of the energy balance were checked against the ASME standard for determining energy output from a nuclear plant, "ASME Performance Test Codes,

Test Code for Nuclear Steam Supply Systems (PTC 32.1-1969)." In addition, the uncertainty values for each element were reviewed and found to be reasonable. We have concluded that the 2% uncertainty (at one standard deviation) is an acceptable value for power measurement uncertainty.

In support of the assumed distribution of CRD speeds, General Electric has provided the results of tests from 13 operating BWRs. The total data base includes 3,985 individual CRD scrams. The information was presented in considerable detail, including the mean values and standard deviations of the times to 5%, 20%, 50% and 90% insertion for various plant types and for full core and partial core scram tests. An extensive and convincing statistical analysis of the data was also presented. Each data set was tested to determine if it could be tested as part of a larger data set; and only those data set which were found to be statistically alike, at a high confidence level, were treated together. Statistical tests were performed by General Electric to determine the significance of: variations among BWR designs; variations between full core tests and partial core tests; variations among operating plants; variations among scram tests; and variations among individual drives within scram tests. We conclude that these CRD scram tests are indicative of past operating experience and that the mean values and standard deviations of CRD speed can be chosen for the statistical analysis of the OQYN code. However, we cannot conclude that these CRD scram tests will be indicative of future reactor scram speed performance. In addition, it is also necessary to demonstrate that the scram characteristics of an individual reactor to be licensed can be represented by the distribution used in the analysis. The scram characteristics of an individual reactor should belong to the same population. General Electric should provide an assurance or appropriate

modifications to Technical Specifications to demonstrate that the scram characteristics indeed belong to the same population or can be represented by the same distribution. General Electric should also assess the impact of the use of best estimate distributions on providing this assurance.

The transient response to rapid overpressure events is dependent on the core average axial power distribution and axial exposure distribution since these strongly influence both the void and control rod reactivity feedback. General Electric has defined Exposure Index as a measure of the axial exposure distribution. Exposure Index indicates the extent to which an actual axial exposure distribution differs from the ideal, design axial exposure distribution (Haling distribution). ODYN licensing calculations use the Haling distribution as input. General Electric proposed to show the conservatism associated with this assumption by establishing that the axial exposure distributions actually encountered during operation are more favorable than the Haling distribution. This conservatism was quantified as part of the overall ODYN statistical analysis by including Exposure Index as one of the input variables in the response surface.

To establish a basis for the expected distribution of Exposure Indices, General Electric presented data from 11 operating reactors at end of cycle conditions and 15 data points for 5 operating reactors at mid-cycle conditions. In response to a request for additional data on observed Exposure Index, General Electric provided 8 additional data points. Because of the limited number of data points and the large scatter in the data we were led to question the assumption that the data was normally distributed. The individual data points obtained from General Electric were subjected to the W-test for normality by

the NRC, Applied Statistics Branch. This test indicated that there was not a sufficient reason to reject the assumption that the data were normally distributed. Based on this information, the inclusion of Exposure Index in the statistical analysis as a normally distributed variable is acceptable. As in the case with the use of measured CRD speeds, the implications of using best estimate values of Exposure Index based on past operating experience and the associated need for assurance and modifications to Technical Specifications to demonstrate continued acceptable performance were not addressed. Since we cannot determine appropriate modifications necessary for demonstration of the conservatism due to inability to operate at Haling power shape for each reactor to be licensed, we find that the use of the variation of power shape from that of a Haling shape in the statistical analysis is not appropriate.

General Electric has performed the statistical analysis using several different sets of assumptions relative to the response surface input parameters. The probability of exceeding the ODYN licensing basis Δ CPR was calculated for each case. This corresponds to the probability of exceeding the GETAB CPR safety limit. The probability of exceeding the criteria of 0.1% of fuel rods in Boiling Transition was also calculated for some of these cases. Since General Electric has proposed that the safety limit for BWRs be based on the GETAB CPR safety limit, it is appropriate to use the probability of exceeding this value as the basis for accepting the proposed licensing method. As stated previously, we have determined that a 5% probability of exceeding the GETAB CPR limit is acceptable. Unless the safety limit for BWRs is redefined by General Electric and reevaluated by the staff, the use of the probability of exceeding 0.1% of fuel in boiling transition is not an appropriate basis for judging the acceptability of the ODYN licensing basis.

In conclusion, we recommend that General Electric reperform the statistical analysis to demonstrate the appropriateness of the margin to the GETAB limit. This statistical analysis should not take credit for conservatism in the Haling power distribution. It may take credit for distribution in scram speeds if General Electric demonstrates that the distribution used in the analysis is applicable to the plant specific case. The analysis should also be performed using the code uncertainties as revised by the staff ($\pm 0.068 \Delta\text{CPR}/\text{ICPR}$) which was based on the plant test data. General Electric may wish to convolute additional variables in the statistical analysis if assurance for conservatism for each specific application is provided.

III. STAFF POSITION

We stated our position on the ODYN code and its application in Reference 35. The following is a statement of that position.

I. ΔCPR Calculations

The analysis for ΔCPR must be performed in accordance with either approach A or approach B.

A. ΔCPR Calculations with Margin Penalty

This approach is comprised of the three step calculation which follows:

1. Perform ΔCPR calculations using the ODYN and the improved SCAT (Reference 36) codes for the transients in Table III and using the input parameters in the manner proposed in pages 3-1 through 3-4 of NEDE-24154-P. The sensitive input parameters are listed in Table IV.
2. Determine ICPR (operating initial critical power ratio) by adding ΔCPR calculated in step 1 above to the GETAB safety limit. Calculate ΔCPR/ICPR.
3. Determine the new value of ICPR by adding 0.044 to the value of ΔCPR/ICPR calculated in step 2 above. Apply this margin to Chapter 15 analysis of the FSARs submitted for OLS, and CPs and to reloads.

The margin of 0.044 is obtained from consideration of uncertainties in components listed in Table I.

A sample calculation is presented below:

Step 1

Assume that ΔCPR calculations using the ODYN licensing basis have been performed and the result is

$$\Delta\text{CPR}_c = .14$$

where the subscript c refers to calculations.

Step 2

Calculate ICPR based on the calculations.

$$\text{ICPR}_c = 1.06 + .14 = 1.20$$

where the GETAB limit is 1.06.

$$\frac{\Delta\text{CPR}_c}{\text{ICPR}_c} = \frac{.14}{1.20} = .117$$

Step 3

$$\frac{\Delta\text{CPR}_{\text{new}}}{\text{ICPR}_{\text{new}}} = .117 + 0.044 = .161$$

$$\Delta\text{CPR}_{\text{new}} = \frac{\frac{\Delta\text{CPR}_{\text{new}}}{\text{ICPR}_{\text{new}}}}{\frac{\Delta\text{CPR}_c}{\text{ICPR}_c}} \Delta\text{CPR}_c = \frac{.161}{.117} .14 = .192$$

$$\text{ICPR}_{\text{new}} = 1.06 + .19 = 1.25$$

B. Statistical Approach for Reduction of Margin Penalty

General Electric assessed the probability of the Δ CPR during a limiting transient exceeding the Δ CPR calculated for the proposed licensing basis transient (NEDE-25154-P response to question 4). The General Electric study demonstrated that this probability, based on operating data over several fuel cycles from a group of plants, is very low. The key parameters in the study are scram speed, power level, power distribution, and an estimate of ODYN uncertainties. The proposed approach utilizes the conservatism inherent in the statistical deviation of the actual operating conditions from the limiting conditions assumed for the first three parameters in licensing basis calculations to compensate for potential non-conservatism from the ODYN uncertainties.

The staff has concluded that the use of end-of-cycle power distributions from multi-cycles for several reactors to obtain credit for margin conservatism relative to Haling power distribution is not appropriate. There is no assurance that the end-of-cycle power distribution conservatism obtained from operating reactor history are representative of the end-of-cycle conditions which will exist for the specific core. We have also concluded that scram speed data used in the GE statistical assessment must be proved applicable to specific license and reload applications. In order to take credit for conservatism in the scram speed performance for reloads, it must be demonstrated that there is insufficient reason to reject the plant-specific scram speed as being within the distribution assumed in the statistical analysis. For CP and OL, the scram speed

distribution for the specific plant must be demonstrated consistent with those used in the statistical approach. Similar design and prototypic performance characteristics coupled with appropriate technical specifications on scram speed performance could provide acceptable evidence of the applicability of the data base.

Statistical convolution of the power measurement uncertainties to take credit for full power operation at a power level value below that used in licensing calculations is acceptable to the staff. However, plant specific procedures to operate within the licensing limit must be taken into account in these calculations.

The code uncertainty penalty (0.044 in $\Delta\text{CPR}/\text{ICPR}$) applied to the licensing calculations described in (A) does not account for unknown contributors. Past experience has shown that additional margin in safety calculations is often needed to compensate for unknown non-conservatism in licensing calculations due to code errors or other factors. The ODYN prediction of three Peach Bottom transient tests and one KKM transient test demonstrated a 2σ uncertainty of approximately 37% of $\Delta\text{CPR}/\text{ICPR}$ at a 95% confidence level. This was determined using χ^2 distribution. No credit was given for measurement errors. This results in a 2σ $\Delta\text{CPR}/\text{ICPR}$ uncertainty of 0.068 for a transient which degrades the CPR from an initial value of 1.30 to the limit of 1.05. Since these tests represent a very limited data base, it is likely that the 2σ uncertainty can be reduced significantly by the acquisition of additional test data for comparison to code predictions. Therefore, the magnitude of the code uncertainty used in the statistical convolution may be reduced to a value consistent with the 2σ

value of $\Delta\text{CPR}/\text{ICPR}$ uncertainty at a 95% confidence level when such a reduction can be justified by additional transient test data.

In summary, the staff has concluded that the statistical approach to compensate for potential non-conservatism from the ODYN uncertainties is acceptable with the following limitations.

1. Power distribution conservatisms should be excluded.
2. Scram speed conservatisms must be demonstrated to be applicable to plant specific cases.
3. Calculations should be performed using a code uncertainty value which is 37% of the $\Delta\text{CPR}/\text{ICPR}$ for a limiting transient to account for code uncertainties, including unknown contributors (e.g., code errors), based on the approved transient test data base. This results in a value of ± 0.068 in $\Delta\text{CPR}/\text{ICPR}$ uncertainty for a transient extending over a CPR range of 1.30 to 1.06.
4. The transient test data base must be expanded and submitted for staff review to justify any reduction in the value of ODYN Code uncertainty (2 σ value of $\Delta\text{CPR}/\text{ICPR}$ at a 95% confidence level).
5. A new statistical analysis conforming with these limitations must be provided.

An acceptable licensing basis using the Option B statistical approach is a 95/95 Δ CPR/ICPR for the limiting event. This can be established in one of two ways:

- a. Option B can be applied on a plant-specific basis - i.e., statistical analyses performed on a particular plant to determine its 95/95 Δ CRR/ICPR. The statistical analysis procedures to be used are those defined in the ODYN Licensing Topical Report (LTR), Volume 3, except for the modifications required by the NRC in Reference 35.

- b. Option B can be applied on a generic basis. This involves the establishment of generic Δ CPR/ICPR adjustment factors for groupings of similar-type plants (the groupings used in the ODYN LTR are considered to be an acceptable matrix) which can then be applied to the plant-specific Δ CPR/ICPR calculations from the ODYN LTR deterministic approach to derive the estimated 95/95 values. Each plant group and transient type correction factor is based on an analysis of a typical plant in that group (e.g., BWR 2/3, 4/5, and 6), in which the differences between the 95/95 Δ CPR/ICPR calculated per the ODYN LTR deterministic approach is determined for a specific transient (e.g., load rejection without bypass). The difference, which may be positive or negative, is designated the plant group adjustment factor for that transient. The generic Δ CPR/ICPR adjustment factors established for the various plant groupings must be submitted to the NRC for review.

II. PRESSURE CALCULATIONS

Calculations should be performed for the Main Steam Isolation Valve closure event with position switch scram failure using the values listed in Table I^x as per staff evaluation to arrive at the overall code uncertainty in pressure calculation. Add this uncertainty to the ODYN calculated pressure for this event in OL, CP and reload applications. If General Electric can demonstrate that this uncertainty is very small (e.g., by a factor of 10 or more) relative to the bias in determining ASME Vessel Overpressure limit, no addition of uncertainty to the calculations of pressure is needed.

^xWe note that there is an error in Enclosure 2 of Reference 35. The bounding values of the drift flux parameters should have been in conformance with Table I as per staff evaluation.

TABLE III
TRANSIENTS TO BE ANALYZED USING THE ODYN CODE

A. For Thermal Limit Evaluation

<u>Event</u>	<u>Thermally Limiting or Near Limiting (Typically)</u>
1. Feedwater Controller Failure - Maximum Demand	X
2. Pressure Regulator Failure - Closed	
3. Generator Load Rejection	X
4. Turbine Trip	X
5. Main Steamline Isolation Valve Closures	
6. Loss of Condenser Vacuum	
7. Loss of Auxiliary Power - All Grid Connections	X

B. For ASME Vessel Overpressure Protection

Pressure Limiting

1. MSIV Closure with Position Switch Scram Failure (i.e., MSIV Flux Scram)	X
---	---

TABLE IV
INPUT PARAMETERS SENSITIVE FOR THE ANALYSES

1. CRD scram speed - at technical specification limit.
2. Scram setpoints - at technical specification limits.
3. Protection-system logic delays - at equipment specification limits.
4. Relief valve capacities - minimum specified.
5. Relief valve setpoints and response - all valves at specified upper limits of setpoints and slowest specified response.
6. Pressure drop from vessel to relief valves - maximum value.
7. Steamline and vessel geometry - plant-unique values.
8. Initial power and steam flow - maximum plant capability.
9. Initial pressure and core flow - design values at maximum plant capability.
10. Core exposure/power distribution - consistent with Haling mode of operation.
11. Feedwater conditions - maximum temperature (maximum core average void content).

III. Other Limitations

1. Listing of important input variables such as listed in Table IV and initial plant parameters including but not limited to control system characteristics as depicted in Figures 4-13 through 4-16 of NEDO-24154, Vol. 1, but with numerical values provided should be provided with each submittal. The initial control system characteristics, including the model used in the selection of initial settings, shall be defined and substantiated in terms of the design basis for each control system of the plant. We understand that neutronic parameters which were originally obtained from the GE 3-D Core Simulator and collapsed to provide input to the ODYN code, are best estimate. If there is a significant change in this calculational method altering the input parameters, General Electric should submit the new procedure to NRC for its evaluation. The code uncertainty value of $\pm 0.068 \Delta\text{CPR}/\text{ICPR}$ based on the Peach Bottom and KKM test data includes uncertainties in this calculational method since this method was used in comparison of test data with code predictions. Hence, any significant change in this procedure will change the code uncertainty.
2. A minimum of eight nodes should be used to represent the steam line. However, the maximum length of any node should not be more than 100 ft.
3. The code cannot predict accurately core inlet flow oscillations with frequencies above 5 Hz. Although we do not expect any inlet flow oscillation above frequency of 5 Hz for the transients listed in Table III, General Electric should verify that the harmonic components above 5 Hz are indeed very small if very rapid variations of flow in these transients are predicted.

-
4. The transients listed in Table III are short term licensing transients. If the code is intended to be used for long term transients or different types of overpressurization transients such as ATWS, appropriate modifications should be made.

References

1. NEDE-24011-P, "Generic Reload Fuel Application," Chapter 4, Hydraulic Model Description, May 1977.
2. NEDO-20953, "Three-Dimensional BWR Core Simulator," J. A. Wooley, May 1976.
3. NEDO-20566, "General Electric Company Analytical Model for Loss-of-Coolant Analysis in Accordance with 10 CFR 50, Appendix K, Volume 2," January 1976.
4. NRC letter from D. G. Eisenhut to R. Gridley, dated May 12, 1978.
5. NEDO-10802, Amendments 10802-01 and 02, "Analytical Methods of Plant Transient Evaluations of the General Electric Boiling Water Reactor," R. B. Linford, February 1973.
6. NUREG-0460, V. II, Anticipated Transients Without Scram for Light Water Reactors, April 1978.
7. NEDO-10299, "Core Flow Distribution in Modern Boiling Water Reactor as Measured in Monticello," January 1971.
8. APED-4762, "Performance Tests of Axial Flow Primary Steam Separators," C. H. Robbins, January 1965.
9. NEDO-13388, "2-Phase Flow in Boiling Water Nuclear Reactors," R. T. Lahey, July 1974.
10. Isbin, H. S., Sher, H. C., Eddy, K. C., "Void Fractions in Two-Phase Steam-Water Flow," AIChE Journal, Vol. 3, No. 1, 136-142, March, 1957.
11. Isbin, H. S., Rodriguez, H. A., Larson, H. C., and Pattie, B. D., "Void Fractions in Two-Phase Flow," AIChE Journal, Vol. 5, No. 4, 427-432, Dec. 1959.
12. Marchaterre, J. F., "The Effect of Pressure on Boiling Density in Multiple Rectangular Channels," ANL-522, Feb., 1956.
13. Janssen, E., Kesvinen, J. A., "Two-Phase Pressure Drop in Straight Pipes and Channels; Water-Steam Mixtures at 600 to 1400 psia," GEAP-4616, May 1964.
14. Cook, W. H., "Boiling Density in Vertical Rectangular Multichannel Sections with Natural Circulation," ANL-5621, Nov. 1956.
15. Ishii, M., "One-Dimensional Drift-Flux Model and Constitutive Equations for Relative Motion Between Phases in Various Two-Phase Flow Regimes," ANL-77-47, October 1977.

16. Frigg Loop Project, Frigg-2, AB Atomenergi, Stockholm, Sweden, 1968.
17. Rouhani, S. Z., "Void Measurements in the Region of Subcooled and Low Quality Boiling," Symposium on Two-Phase Flow, University of Exeter, Devon, England, June 1965.
18. Rouhani, S. Z., "Void Measurements in the Region of Subcooled and Low-Quality Boiling," Park II, AE-RTL-788, Aktiebolaget Atomenergi, Studsvik, Sweden, April, 1966.
19. NEDO-20913-P, "Lattice Physics Methods," C. L. Martin, June 1976.
20. "GEGAP-III: A Model for the Prediction of Pellet-Cladding Thermal Conductance in BWR Fuel Rods," General Electric Report NEDC-20181, November, 1973.
21. D. F. Ross (NRC) letter to E. D. Fuller (GE) dated June 2, 1978.
22. EPRI NP-564, "Transient and Stability Tests at Peach Bottom Atomic Power Station Unit 2 at End of Cycle 2," L. A. Carmichael and R. G. Niemi, June 1978.
23. Letter from K. W. Cook to R. L. Tedesco, MFN 3137-78, "Transmittal of Responses to Round 2 Questions on the ODYN Transient Model," dated Dec. 13, 1978.
24. BNL-NUREG-21925, "BNL-TWIGL, A Program for Calculating Rapid LWR Core Transients," D. J. Diamond, Ed., October 1976.
25. BNL-NUREG-22011, "User's Manual for RELAP-3B-MOD 110: A Reactor System Transient Code," 1977.
26. BNL-NUREG-24903, "Core Analysis of Peach Bottom-2 Turbine Trip Tests," H. S. Chang, D. J. Diamond, September 1978.
27. Memo from F. Odar to Z. R. Rosztoczy, "Meeting with General Electric at Brookhaven National Laboratory," October 17, 1978.
28. Letter from K. W. Cook of GE to Frank Schroeder of NRC, October 10, 1978 on Potential Differences between GE and BNL Models.
29. Letter from K. W. Cook of GE to Frank Schroeder of NRC, October 26, 1978, on Transmittal of Exposure Dependent Data.
30. Transcript of ACRS hearings held on March 19-20, 1979, Los Angeles, California.
31. Letter from K. W. Cook of GE to R. L. Tedesco, Clarification of ODYN Model Uncertainties, MFN 123-79, dated April 30, 1979.
32. Letter from K. W. Cook of GE to R. P. Denise, Additional Void Fraction Information Requested for ODYN Review, MFN-219-79, August 27, 1979.

33. BNL-NUREG-26684, "Analysis of Licensing Basis Transients for a BWR/4," M. S. Lu, H. S. Cheng, W. G. Shier, D. J. Diamond, M. M. Levine, September 1979.
34. BNL-NUREG-23501, "A Space-Time Analysis of Void Reactivity Feedback in Boiling Water Reactors," H. S. Cheng, M. S. Lu, D. J. Diamond, October 1977.
35. Letter from R. P. Denise (NRC) to G. G. Sherwood (General Electric), dated January 23, 1980.
36. Letter from K. W. Cook (General Electric) to F. Schroeder and D. G. Eisenhut (NRC), MFN 171-79, "Implementation of a Revised Procedure for Calculating Hot Channel Transient Δ CPR," July 20, 1979.

Supplemental Safety Evaluation
For The
General Electric Topical Report
Qualification Of The One-Dimensional
Core Transient Model For
Boiling Water Reactors
NEDO-24154 and NEDE-24154P
Volumes I, II and III

Prepared By

Reactor Systems Branch, DSI

The Safety Evaluation Report on the ODYN code (Reference 2) is primarily an evaluation of the calculational model with little discussion of implementation requirements. Reference 3 provides the information required to bridge the gap between evaluation and implementation. Specifically, there are eight items covered in Reference 3; these are:

1. ODYN Option B statistical adjustment factors,
2. Control rod drive scram insertion time conformance procedure for plants licensed under ODYN Option B,
3. Uncertainty in ODYN pressure calculations,
4. ODYN model temperature limits,
5. Uncertainty in subcooled boiling model,
6. Description of electronic hydraulic control model,
7. Listing of ODYN input variables,
8. Comparison of minimum critical power ratio operating limits established by REDY and ODYN.

Each of these items is discussed below.

Item 1. Statistical Adjustment Factors

Page III-6 of Reference 2 allows two statistical approaches; one is a plant-specific statistical analysis and the other is a generic analysis for plant groups (e.g. BWR/2, 3, 4, 5, 6) and transients. The second approach involves the establishment of generic $\Delta\text{CPR}/\text{ICPR}$ adjustment factors for groupings of similar-type plants which can be applied to plant-specific $\Delta\text{CPR}/\text{ICPR}$ calculation from the ODYN licensing topical report (LTR) deterministic approach. Reference 3 provides the statistical adjustment factors for the three transients which are normally limiting transients (load rejection or turbine trip without

bypass, feedwater controller failure to maximum demand and pressure regulator downscale failure). These generic statistical adjustment factors are shown in Table 1; we find them to be acceptable.

Item 2. CRD Scram Insertion Time Conformance Procedure

Page III-3 of Reference 2 states "In order to take credit for conservatism in the scram speed performance for reloads, it must be demonstrated that there is insufficient reason to reject the plant-specific scram speed as being within the distribution assumed in the statistical analysis. For CP and OL, the scram speed distribution for the specific plant must be demonstrated consistent with those used in the statistical approach."

General Electric presents the following procedure as one which satisfies the Staff's objectives for scram conformance. It should be noted that some utilities using ODTK Option 3 may desire to establish their own conformance procedures.

The procedure consists of testing, at the 5% significance level, the scram surveillance data at the 20% insertion position which is generated several times each cycle as required in the Reactivity Control System Technical Specification (20% insertion is representative of that portion of the scram most affecting the pressurization transient). The unique rod notch position closest to 20% (and the appropriately adjusted time of insertion) is expected to be utilized in actual plant application of this generic concept. For most plants, the surveillance requirements are as follows:

- (1) all control rods are measured at beginning of cycle (BOC), and
- (2) X of control rods are measured every 120 days during cycle (X is plant-dependant and ranges from 10 to 50).

At the completion of each surveillance test performed in compliance with the technical specification surveillance requirements, the average value of all surveillance data at the 20% insertion position generated in the cycle to date is to be tested at the 5% significance level against the distribution assumed in the ODTK analyses. The surveillance information which each plant using this procedure will have to retain throughout the fuel cycle is the number of active control rods measured for each surveillance test (the first test is at the BOC and is denoted N_1 ; the i th test is denoted N_i) and the average scram time to the 20% insertion position for the active rods measured in test i (τ_i). The equation used to calculate the overall average of all the scram data generated to date in the cycle is:

$$\tau_{ave} = \frac{\sum_{i=1}^n N_i \tau_i}{\sum_{i=1}^n N_i} \quad (2-1)$$

where

n = number of surveillance tests performed to date in the cycle;

$\sum_{i=1}^n N_i$ = total number of active rods measured to date in the cycle; and

$\sum_{i=1}^n N_i \tau_i$ = sum of the scram times to the 20% insertion position of all active rods measured to date in the cycle to comply with the Technical Specification surveillance requirements.

The average scram time, τ_{ave} , is tested against the analysis mean using the following equation:

$$\tau_{ave} \leq \tau_B \quad (2-2)$$

where

$$\tau_B = \mu + 1.65 \left(\frac{\sum_{i=1}^n N_i}{n} \right)^{1/2} \sigma \quad (2-3)$$

The parameters μ and σ are the mean and standard deviation of the distribution for average scram insertion time to the 20% position used in the ODYN Option B analysis.

If the cycle average scram time satisfies the Equation 2-2 criterion, continued plant operation under the ODYN Option B operating limit minimum critical power ratio (OLMCFR) for pressurization events is permitted. If not, the OLMCFR for pressurization events must be re-established, based on a linear interpolation between the Option B and Option A OLMCFRs. The equation to establish the new operating limit for pressurization events is given below:

$$OLMCFR_{New} = OLMCFR_{Option\ B} + \frac{\tau_{ave} - \tau_B}{\tau_A - \tau_B} \Delta OLMCFR \quad (2-4)$$

where

- τ_{ave} and τ_B are defined in Equations 2-1 and 2-3, respectively;
- τ_A = the present technical specification limit on core average scram time to the 20% insertion position; and
- $\Delta OLMCFR$ = the difference between the OLMCFR calculated using Option A and that using Option B for pressurization events.

Note that Equation 2-3, which establishes the maximum allowable scram insertion time for operation under Option B, may also be expressed in the following manner:

$$\tau_3 = v + A\sigma \quad (2-5)$$

where

$$A = 1.65 \left(\frac{\bar{x}_1}{\sum_{i=1}^n x_i} \right)^{1/2} \quad (2-6)$$

The relationship between the coefficient, A, and the amount of surveillance data generated during the cycle is illustrated in Figure 2-1. As more data become available through the performance of in-cycle surveillance-tests, the coefficient decreases, as does the acceptance criterion, τ_3 . Thus, the scram speed criterion is being tightened as the cycle progresses, based on the assumption that, as more scram data become available during the cycle, the uncertainty in the mean value calculation should decrease.

We find the scram insertion time conformance procedure to be acceptable.

Item 3. Uncertainty in ODDN Pressure Calculations

Page III-7 of Reference 2 states that if GE can demonstrate that the uncertainty in calculated pressure is small (e.g. by a factor of 10 or more) relative to the bias in determining ASME vessel overpressure limit, no addition of uncertainty to the calculation's of pressure is needed. A sensitivity study varying ODDN input parameters over the range of Table 1 of Reference 2 shows the RMS uncertainty in the peak vessel pressure to be 11 psi. GE estimates the bias in the ASME code to account for the material uncertainty to be approximately 310 psi. Therefore, there is no need to account for pressure uncertainty in

the ODYN calculations.

Item 4. ODYN Model Temperature Limit

An early draft of the ODYN SER limited the code calculation to fuel temperatures less than 1500°K (approximately 2240°F). This was because Figure 8-2 of Reference 1 limited the thermal conductivity of UO₂ to 1500°K. The actual equation used in ODYN,

$$K = \frac{38.24}{402.4+T} + 6.07123 \times 10^{-13} (T+273)^3$$

where T = fuel temperature (°C) and

K = thermal conductivity (watts/Cm°C)

is based on data which extended to the UO₂ melting temperature (3080°K).

Therefore, the fuel temperature limit for ODYN analyses is the UO₂ melting temperature (3080°K or 5100°F).

Item 5. Uncertainty in Subcooled Boiling Model

Page II-19 of Reference 2 states "We estimate the corresponding minimum and maximum values of 'n' to be 0.5 and 2.0 respectively. General Electric is required to make sensitivity studies to verify that these values correspond to ± 0.023 uncertainty in $\Delta\text{CPR}/\text{ICPR}$." GE analyzed the turbine trip without bypass transient for n = 2.0, as requested for a 251 BWR/4. The peak core average heat flux (% rated) increased from 121.6% (for n = 1.0) to 124.0 (for n = 2.0). This leads to a $\Delta\text{CPR}/\text{ICPR}$ sensitivity of about 0.024. It is concluded that the Staff's estimate of ± 0.023 for n values between 0.5 and 2.0 is valid.

Item 6. Description of Electronic Hydraulic Control Model

An early draft of Reference 2 stated "Wherein electronic hydraulic controls are used in the design, the model used in selection of initial control setting shall be submitted for staff review." This statement was made because Reference 1 provided information only for the mechanical hydraulic control. GE claims that there is no functional difference between the two types of control. However, they provided a description of the model in Reference 3. We agree with the GE claim that there is no functional difference between the two types of control.

Item 7. Listing of ODYN Input Variables

Page III-10 of Reference 2 states "Listing of important input variables such as listed in Table IV and initial plant parameters including but not limited to control system characteristics as depicted in Figures 4-13 through 4-16 of NEDO-24154, vol. 1, but with numerical values provided should be provided with each submittal. The initial control system characteristics, including the model used in the selection of initial settings, shall be defined and substantiated in terms of the design basis for each control system of the plant." Item 7 of Reference 3 lists typical values of these initial parameters which may be included by reference into individual plant submittals provided the values are appropriate to the individual submittals.

Item 8. Comparison of MCPR Operating Limits Established by REDY and ODYN

The Staff requested GE to provide a comparison of CPR operating limits based on REDY and ODYN prediction. The purpose of such a comparison was to

evaluate the appropriateness of continued plant operation under the current REDY-based operating limits during the transition period in which ODYN is implemented for rapid pressurization events.

In addition, the Staff indicated that the initial ODYN analysis for each BWR operating plant must include all the pressurization events identified in Table 2-1, Volume 3 of Reference 1, unless justification could be provided that fewer events (such as the limiting events presently analyzed for reload submittals) would be sufficient.

Table 2 shows ODYN and REDY-based CPR operating limits for the limiting pressurization events (load rejection without bypass and feedwater controller failure-maximum demand) for plants in which both ODYN and REDY calculations are available. Two sets of ODYN numbers are provided: ODYN deterministic calculations per the GE letter (Reference 1), labelled "ODYN-GE LTR" in Table 2; and ODYN Option B statistical calculations, labelled "ODYN Option B" in Table 2. Also included in the table are the plant minimum operating limits, based on all the abnormal events, when using REDY, ODYN GE LTR, and ODYN Option B to calculate the rapid pressurization events.

Because the overall plant operating limits are, in all cases, either unaffected or improved, GE concludes that implementation of ODYN will not represent a significant change to the operating limits for BWR plants. For those plants which use ODYN Option B, it is generally expected to either produce no change to the limit or else to improve it slightly. We agree with this conclusion.

The events for which ODTK has been qualified and approved are listed in Reference 1, Volume 3, and include the following: (1) feedwater controller failure-maximum demand; (2) pressure regulator failure-closed direction; (3) generator load rejection with and without bypass operation; (4) main steamline isolation valve closure (trip scram and flux scram); (5) loss of condenser vacuum; (6) turbine trip with and without bypass; and (7) loss of auxiliary power - all grid connections. GE proposes that only the following three events be reported for reload submittals or safety analysis report revisions: generator load rejection/turbine trip without bypass (whichever is limiting), feedwater controller failure-maximum demand, and main steamline isolation valve closure-flux scram (to satisfy ASME code pressure requirements). These are the same pressurization events presently included in reload submittals, and reflect the consistency in the ODTK and RDT results. The events not included in the submittal are much less severe, for the reasons discussed below.

1) Turbine/Generator Trips With Bypass

These events are considerably less severe than the transients in which the bypass system is assumed to fail. Typical turbine bypass capacities range from 25-40% of rated steamflow. This bypass capacity results in a considerably milder thermal and overpressurization event.

2) Pressure Regulator Failure - Closed Direction

The standard event evaluated in SAR analysis is one in which the controlling pressure regulator is assumed to fail in the closed direction. Under these failure conditions, the backup regulator takes over control of the turbine admission valves, preventing any serious transient. The disturbance is mild and similar to a pressure set point change with no significant reductions of fuel thermal margins occurring. As shown in the SARs, this event is considerably less severe than the generator and turbine trips without bypass.

3) Loss of Condenser Vacuum

Various system malfunctions can cause a loss of condenser vacuum due to some single equipment failure. The reduction or loss of vacuum in the main turbine condenser will sequentially trip the main and feedwater turbines and bypass system and, for some plants, close the main steamline isolation valves. While these are the major events occurring, other resultant actions will include scram (from stop valve closure) and bypass opening with the main turbine trip. Because the protective actions are actuated at various levels of condenser vacuum, the severity of the resulting transient is directly dependent upon the rate at which the vacuum pressure is lost. Normal loss of vacuum due to loss of cooling water pumps or steam jet air ejector problem produces a very slow rate of loss of vacuum (minutes, not seconds). If corrective actions by the reactor operators are not successful, then simultaneous trips of the main and feedwater turbines, and ultimately complete isolation by closing the bypass valves (opened with the main turbine trip) and the MSIVs, will occur. This event is bounded by the turbine trip without bypass event.

4) Loss of Auxiliary Power - All Grid Connections

This event is initiated by a generator load rejection. Since the turbine bypass system is assumed to operate during the initial portion of this event, it is comparable to the load rejection with bypass and is considerably less severe than the without bypass events.

5) MSIV Closure - Trip Scram

This event has a slower shutoff of steam flow than the turbine trip without bypass event. Therefore, the transient is not as severe. This has been confirmed by OGTN calculations.

The staff agrees with the GE assessment of the relative severity of the transients listed. Therefore, the following events should be reanalyzed with ODYN for plants which have analyses of record using REDY:

- 1) generator load rejection/turbine trip without bypass
- 2) feedwater controller failure maximum demand
- 3) main steam line isolation valve closure-flux scram.

If for a particular plant another event should be more limiting than those just listed, then the other event should also be reanalyzed with ODYN. For the new plants with transient analyses supplied by GE, all of the events listed in Table 3 of Reference 1 should be analyzed with ODYN.

References

1. NEDO-24154 and NEDE-24154P, Volumes I, II and III, "Qualification of the One-Dimensional Core Transient Model for Boiling Water Reactors," October, 1978.
2. Memorandum for T. Novak and R. Tedesco from P. S. Check, "Safety Evaluation for Qualification of the One-Dimensional Core Transient Model for Boiling Water Reactors," NEDO-24154 and NEDE-24154P, Volumes I,II and III," October 22, 1980.
3. Letter to P. S. Check (NRC) from R. H. Buchholz (GE), MFN-155-80, "Response to NRC Request for Information on ODYN Computer Model," September 5, 1980.

Table 1
SUMMARY OF GENERIC STATISTICAL ADJUSTMENT FACTORS (Δ CPR/ICPR)

<u>Plant Groupings</u>	<u>LR/TIWOEP*</u>	<u>FNCF</u>	<u>PRDF</u>
BWR 2/3 - EOC	+0.006	-0.016	—
BWR 4/5 w/o RPT - EOC	-0.039	-0.009	—
BWR 4/5 w/o RPT - MOC	-0.111	-0.009	—
BWR 4/5 w/RPT - EOC	-0.024	+0.016	—
BWR 4/5 w/RPT - MOC	-0.001	+0.026	—
BWR 6 - EOC	-0.021	+0.003	+0.017

*With the exception of FNCF or PRDF events, this set of adjustment factors will be applied to all pressurization events analyzed with the ODYN code to establish the CPR operating limit, since they typically involve generator or turbine trips.

Table 2
COMPARISON OF REND/ODYN RESULTS

Operating CPR Limits

<u>Plant</u>	<u>IA w/o BP</u>			<u>FWCF</u>			<u>Plant Minimum</u>		
	<u>RENY</u>	<u>ODYN (GE Ltr)</u>	<u>ODYN (Option B)</u>	<u>RENY</u>	<u>ODYN (GE Ltr)</u>	<u>ODYN (Option B)</u>	<u>RENY</u>	<u>ODYN (GE Ltr)</u>	<u>ODYN (Option B)</u>
BWR/3-209 EDC6	1.46	1.36	1.37	1.41	1.36	1.39	1.46	1.36	1.38
BWR/4-189 EDC5	1.42	1.33	1.27	1.31	1.25	1.23	1.42	1.33	1.27
BWR/4-210 ⁽³⁾ EDC4	1.18	1.20	1.17	1.13	1.12	1.14	1.21 ⁽²⁾	1.21	1.21 ⁽²⁾
BWR/6-238 EDC3	1.16	1.10	1.08	1.14	1.11	1.12	1.20 ⁽¹⁾	1.20 ⁽¹⁾	1.20 ⁽¹⁾

Notes: (1) Limited by Rod Withdrawal Error
 (2) Limited by Loss of 100°F Feedwater Heating
 (3) Plant with RPT

ERT/111

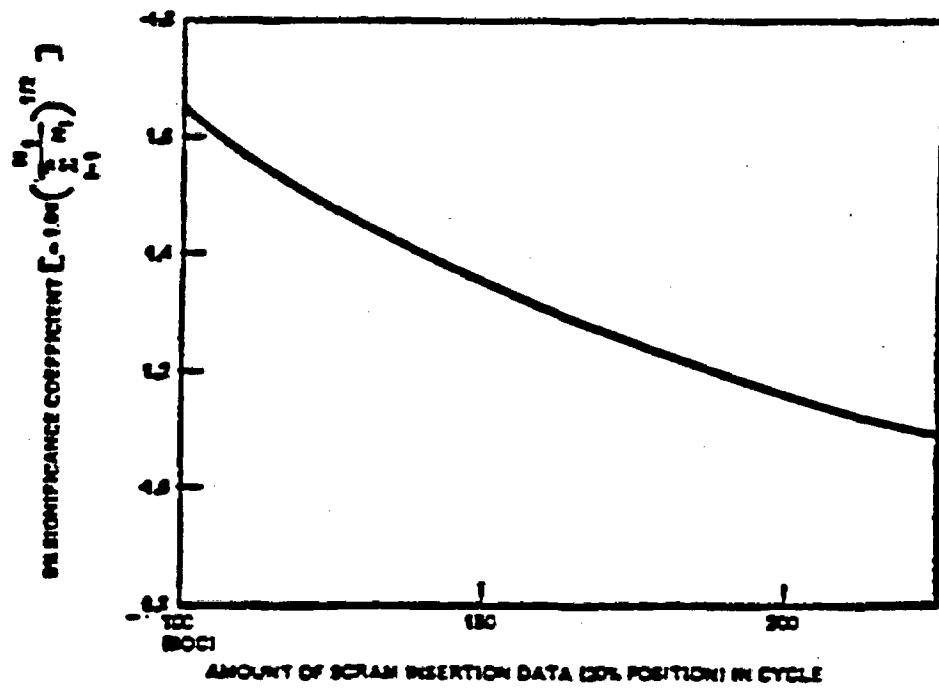


Figure 2-1. 5% Significance Coefficient (A) vs. Surveillance Data in Cycle

GENERAL ELECTRIC

NUCLEAR POWER
SYSTEMS DIVISION

GENERAL ELECTRIC COMPANY, 175 CURTNER AVE., SAN JOSE, CALIFORNIA 95125
MC 682, (408) 925-5722

MFN-013-81

January 19, 1981

U.S. Nuclear Regulatory Commission
Division of Systems Integration
Office of Nuclear Reactor Regulation
Washington, DC 20555

Attention: Paul S. Check, Assistant Director of Plant Systems

Gentlemen:

SUBJECT: ODDYN ADJUSTMENT METHODS FOR DETERMINATION OF OPERATING LIMITS

References: 1) Telecon, H. C. Pfefferlen, R. E. Engel and R. T. Hill (GE) with M. W. Hodges (NRC), January 5, 1981
2) R. P. Denise to G. G. Sherwood, January 23, 1980

The purpose of this letter is to document the agreement reached in the Reference 1 telecon concerning the application of the Initial Critical Power Ratio (ICPR) adjustment factors in conjunction with ODDYN analysis results.

Option A

The ICPR adjustment method to be used with the non-statistical approach (Option A) for rapid pressurization events is that given in Step 3 of Reference 2. This method is to be considered a definition for use specifically with the NRC derived adjustment factor of 0.044.

The application of the adjustment factor in this case can be defined as:

$$\text{ICPR}_{\text{new}} = 1.044 (\text{ICPR})_c$$

where $(\text{ICPR})_c$ = calculated value of ICPR

Option B

The method to be used with the statistical approach (Option B) has been defined to be consistent with the adjustment factors derived by General Electric. This method requires the addition of the

adjustment factor (AF) to the ratio of the calculated values of ΔCPR and ICPR ($\Delta\text{CPR}/\text{ICPR}$)_c:

$$\left(\frac{\Delta\text{CPR}}{\text{ICPR}}\right)_{\text{new}} = \left(\frac{\Delta\text{CPR}}{\text{ICPR}}\right)_{\text{c}} + \text{AF}$$

This equation can be simplified to:

$$\text{ICPR}_{\text{new}} = \frac{\text{SL}}{1 - \left[\left(\frac{\Delta\text{CPR}}{\text{ICPR}}\right)_{\text{c}} + \text{AF}\right]}$$

Where SL = Safety Limit MCPR

It should be noted that in both the Option A and Option B cases, the ICPR is defined as Safety Limit plus ΔCPR for the event being analyzed.

If you have any additional questions or comments, please contact me or H. C. Pfefferlen on (408) 925-3392 of my staff.

Very truly yours,

RHBuchholz

R. H. Buchholz, Manager
BWR Systems Licensing
Safety and Licensing Operation

RHB:sem/1158-59 1F

cc: L. S. Gifford
M. W. Hodges

PREFACE

This document represents a compilation of the information provided to the Nuclear Regulatory Commission by the General Electric Company for the staff's review of GE's One-Dimensional Core Transient Model. Volume I of this report contains the One-Dimensional Core Transient Model description, as well as the questions/responses associated with the staff review of this description document.

Volume II of this report contains the document for Qualification of the One-Dimensional Core Transient Model for Boiling Water Reactors, as well as the associated staff questions/responses.

Volume III of this report contains two parts: Part I provides the General Electric proposal for application of the One-Dimensional Core Transient Model, as well as the staff questions/responses related to the proposal; Part II provides two questions/responses related to the model description which involve information proprietary to the General Electric Company.

The questions referenced within this report were transmitted to General Electric by letter from the NRC staff: untitled letter, D. F. Ross to E. D. Fuller, dated June 2, 1978.

TABLE OF CONTENTS

	<u>Page</u>
ABSTRACT	cx1-i
1. INTRODUCTION AND SUMMARY	1-1
2. MODEL-MODEL COMPARISONS	2-1
2.1 Nuclear Model Comparisons	2-1
2.1.1 Scram Reactivity	2-1
2.1.2 Void Coefficient	2-2
2.2 Thermal-Hydraulic Model Comparisons	2-3
3. ANALYSIS OF TURBINE TRIP EXPERIMENTS	3-1
3.1 Peach Bottom Turbine Trips	3-1
3.1.1 Test Summary	3-1
3.1.2 Model Inputs	3-2
3.1.3 Data Comparisons	3-3
3.1.3.1 Transient Pressure	3-3
3.1.3.2 Neutron Flux	3-4
3.1.3.3 Critical Power Ratio	3-7
3.1.4 Conclusions	3-8
3.2 KKM Turbine Trip	3-8
3.2.1 Test Summary	3-9
3.2.2 Special Model Considerations	3-10
3.2.3 Model Inputs	3-10
3.2.4 Data Comparisons	3-11
3.2.4.1 Transient Pressure	3-11
3.2.4.2 Neutron Flux	3-13
3.2.4.3 Critical Power Ratio	3-15
3.2.5 Conclusions	3-15
REFERENCES	3-74

APPENDICES

A	RESPONSE TO NUCLEAR REGULATORY COMMISSION QUESTIONS ON SECTIONS 1 THROUGH 3 OF VOLUME II	A-1
---	--	-----

LIST OF ILLUSTRATIONS

<u>Figure</u>	<u>Title</u>	<u>Page</u>
2-1	Plant A (BWR/4) All-Rods-Out Scram	2-6
2-2	Plant A All-Rods-Out Scram Reactivity	2-7
2-3	Plant A Initial Control Rod Pattern in Nodes Withdrawn (24 is Completely Out)	2-8
2-4	Plant A Critical Rod Pattern Scram Reactivity	2-9
2-5	Plant B Rod Pattern in Number of Nodes Withdrawn (24 is Completely Out)	2-10
2-6	Plant B (BWR/4) Scram Reactivity	2-11
2-7	Plant B Transient Axial Power	2-12
2-8	Steady-State Void Fraction Profile High Power Channel	2-13
2-9	Steady-State Void Fraction Profile Low Power Channel	2-14
2-10	Change in Void Fraction from 10 Psi Pressure Change High Power Channel	2-15
2-11	Change in Void Fraction from 10 Psi Pressure Change Low Power Channel	2-16
2-12	Void Fraction Versus Time Exponential Flow Decay Problem	2-17
3-1	Axial Power Profile Turbine Trip 1	3-19
3-2	Axial Power Profile Turbine Trip 2	3-20
3-3	Axial Power Profile Turbine Trip 3	3-21
3-4	Peach Bottom-2 Rod Insertion Fraction Versus Time	3-22
3-5	Peach Bottom Eight-Node Steamline Schematic	3-23
3-6	Peach Bottom-2 Turbine Trip 1 Steamline Pressure	3-24
3-7	Peach Bottom-2 Turbine Trip 2 Steamline Pressure	3-25
3-8	Peach Bottom-2 Turbine Trip 3 Steamline Pressure	3-26
3-9	Peach Bottom-2 Turbine Trip 1 Dome Pressure	3-27
3-10	Peach Bottom-2 Turbine Trip 2 Dome Pressure	3-28
3-11	Peach Bottom-2 Turbine Trip 3 Dome Pressure	3-29
3-12	Peach Bottom-2 Turbine Trip 1 Core Exit Pressure	3-30
3-13	Peach Bottom-2 Turbine Trip 2 Core Exit Pressure	3-31
3-14	Peach Bottom-2 Turbine Trip 3 Core Exit Pressure	3-32
3-15	Peach Bottom-2 Turbine Trip 1 Prompt Neutron Power	3-33
3-16	Peach Bottom-2 Turbine Trip 2 Prompt Neutron Power	3-34
3-17	Peach Bottom-2 Turbine Trip 3 Prompt Neutron Power	3-35
3-18	Peach Bottom-2 Reactivity Turbine Trip 1	3-36

LIST OF ILLUSTRATIONS (Continued)

<u>Figure</u>	<u>Title</u>	<u>Page</u>
3-19	Peach Bottom-2 Reactivity Turbine Trip 2	3-37
3-20	Peach Bottom-2 Reactivity Turbine Trip 3	3-38
3-21	Peach Bottom-2 A Level LPRM's Turbine Trip 1	3-39
3-22	Peach Bottom-2 B Level LPRM's Turbine Trip 1	3-40
3-23	Peach Bottom-2 C Level LPRM's Turbine Trip 1	3-41
3-24	Peach Bottom-2 D Level LPRM's Turbine Trip 1	3-42
3-25	Peach Bottom-2 A Level Flux Turbine Trip 1	3-43
3-26	Peach Bottom-2 B Level Flux Turbine Trip 1	3-44
3-27	Peach Bottom-2 C Level Flux Turbine Trip 1	3-45
3-28	Peach Bottom-2 D Level Flux Turbine Trip 1	3-46
3-29	Peach Bottom-2 A Level Flux Turbine Trip 2	3-47
3-30	Peach Bottom-2 B Level Flux Turbine Trip 2	3-48
3-31	Peach Bottom-2 C Level Flux Turbine Trip 2	3-49
3-32	Peach Bottom-2 D Level Flux Turbine Trip 2	3-50
3-33	Peach Bottom-2 A Level Flux Turbine Trip 3	3-51
3-34	Peach Bottom-2 B Level Flux Turbine Trip 3	3-52
3-35	Peach Bottom-2 C Level Flux Turbine Trip 3	3-53
3-36	Peach Bottom-2 D Level Flux Turbine Trip 3	3-54
3-37	Schematic of KKM Steamline Model	3-55
3-38	Average Axial Power KKM Test Conditions	3-56
3-39	Control Rod Motion Pattern KKM Turbine Trip Test	3-57
3-40	Turbine Pressure Turbine A KKM Turbine Trip	3-58
3-41	Turbine Pressure Turbine B KKM Turbine Trip	3-59
3-42	KKM Turbine Trip Steamline Pressure, Turbine A	3-60
3-43	KKM Turbine Trip Steamline Pressure, Turbine B	3-61
3-44	KKM Turbine Trip Dome Pressure	3-62
3-45	KKM Turbine Trip Core Exit Pressure	3-63
3-46	KKM Turbine Trip Prompt Neutron Power	3-64
3-47	Reactivity Components KKM Turbine Trip	3-65
3-48	A Level LPRM Flux KKM Turbine Trip	3-66
3-49	B Level LPRM Flux KKM Turbine Trip	3-67
3-50	C Level LPRM Flux KKM Turbine Trip	3-68

NEDO-24154-A

LIST OF ILLUSTRATIONS (Continued)

<u>Figure</u>	<u>Title</u>	<u>Page</u>
3-51	D Level LPRM Flux KKM Turbine Trip	3-69
3-52	A Level Flux KKM Turbine Trip	3-70
3-53	B Level Flux KKM Turbine Trip	3-71
3-54	C Level Flux KKM Turbine Trip	3-72
3-55	D Level Flux KKM Turbine Trip	3-73
11-1	Peach Bottom-2 Turbine Trip 3 (69% Power) Neutron Flux	A11-2
15-1	Peach Bottom-2 Turbine Trip 1 Core Exit Pressure (35% Bypass)	A15-3
15-2	Peach Bottom-2 Turbine Trip 2 Core Exit Pressure (35% Bypass)	A15-4
15-3	Peach Bottom-2 Turbine Trip 3 Core Exit Pressure (35% Bypass)	A15-5

NEDO-24154-A

LIST OF TABLES

<u>Table</u>	<u>Title</u>	<u>Page</u>
2-1	Comparison of Void Coefficients Obtained with Three-Dimensional and One-Dimensional Core Models	2-5
2-2	Summary of Hydraulic Channel Conditions	2-5
3-1	Peach Bottom-2 Turbine Trip Test Conditions	3-16
3-2	Peach Bottom-2 Dynamic Test Signals	3-16
3-3	Peak Vessel Pressure	3-17
3-4	Maximum Δ CPR Values for Peach Bottom Turbine Trip Tests	3-17
3-5	KKM Turbine Trip Test Conditions	3-17
3-6	KKM Dynamic Test Signals	3-18
3-7	Maximum Δ CPR Values for the KKM Turbine Trip Test	3-18
5-1	Peak Flux Values as a Function of Scram Delay Time	A5-2
6-1	Summary of One Dimensional Model Sensitivity Studies	A6-2
15-1	Summary of ACPR/ICPR Results for Peach Bottom Turbine Trips	A15-2

NEDO-24154-A

ABSTRACT

A transient model for the boiling water reactor (BWR) has been developed which contains a one-dimensional neutronic and thermal-hydraulic simulation of the reactor core, as well as a nodal representation of the pressure variations in the main steamline. Comparisons are made between various parts of the core model and other nuclear and thermal hydraulic models. Model results are also compared to data acquired from turbine trip experiments carried out at the Peach Bottom and KKM Atomic Power Stations.

1. INTRODUCTION AND SUMMARY

The transient behavior of a boiling water reactor (BWR) power plant depends not only on the mechanical response of the recirculation and control systems but also on the power behavior of the reactor core. Previous computer models¹ for the BWR system have used a point model to describe the thermal-hydraulic and neutronic response of the reactor core. The dynamic steamline response has been described by a lumped compressible steamline node. An improved BWR transient model, which includes a more detailed description of the reactor core and steamline, has been constructed and is described in detail in Reference 2. This report describes qualification studies supporting the one-dimensional core transient model. These studies include comparisons with other computer models, as well as comparison with data from actual BWR pressurization transients.

The improved transient model consists of an integrated one-dimensional reactor core model which is coupled to recirculation and major system control models. The recirculation and control system models are, for the most part, identical to the point reactor model described in Reference 1. The reactor core is hydraulically coupled to the recirculation loop through the core exit pressure and core inlet flow. The core exit quality and pressure drop are computed by the core model, which, in turn, interacts with the loop parameters.

The improved model also contains a more detailed description of the pressure variations in the main steamline. The model includes a nodalized description of the mass and momentum balances in the steamline and is capable of predicting the wave phenomenon present in the steamline during transients such as turbine trips.

The reactor core model allows for spacial variation of the neutron flux, fuel temperature, coolant flow, coolant density and pressure in the axial direction. The neutron kinetics behavior is described by one energy group diffusion theory with six delayed neutron groups. The thermal-hydraulic model contains separate conservation and energy equations for the vapor and liquid phases as well as a mixture momentum equation. Fuel rod heat conduction equations are solved for each axial elevation in the core.

NEDO-24154-A

Two types of studies will be presented in this report; model-model comparisons and model comparisons with experimental data. The model-model comparisons are designed to show that the one-dimensional nuclear and thermal-hydraulic models of the reactor core are consistent with core models currently used in BWR design. Also, the collapsed one-dimensional nuclear model is compared with transient results obtained from more detailed three-dimensional simulations. The model comparisons with experimental data consist of calculations of four instrumented turbine trips conducted with a delayed direct scram by bypassing of the direct trip scram, such that the scram occurred following a high flux trip. The experiments were performed at the Peach Bottom-2 and KKM BWR power plants. The model data comparisons are given for a large number of transient variables, including system pressure, reactor flow, and neutron flux. The model-data comparisons form the basis for the qualification of the one-dimensional transient model.

The nuclear model-model comparisons show that the one-dimensional model agrees well with three-dimensional results for scram calculations with no thermal feedback. Also, good agreement with three-dimensional simulator results are obtained for static void reactivity coefficients. The thermal-hydraulic model steady-state results agree well with results obtained with the standard BWR design models. The comparison of transient thermal-hydraulic results is carried out on a simplified flow decay problem for which an analytic solution exists.

Turbine trip data were acquired at the Peach Bottom Atomic Power Station Unit 2 (Peach Bottom-2) for three power levels: 48%, 62% and 69% of rated power. The comparisons show good agreement between data and calculation for all three turbine trips. The experimental data show a steamline wave phenomenon which is duplicated by the model calculation. The model also shows good agreement in total neutron flux. The axial shift of the flux during the transient is apparent in the data and is duplicated by the calculation. Thermal margin calculations carried out using both the experimental and calculated transient heat generation rates showed that the calculated transient change in critical power ratio (ΔCPR) divided by the initial CPR (ICPR) is within 0.01 of the change inferred from the experimental data for all three experiments.

NEDO-24154-A

An additional turbine trip experiment was carried out at the KKM plant in Muehleburg, Switzerland. This turbine trip was initiated from 77% of rated power and approximated end-of-cycle conditions. The KKM reactor is a two-turbine plant and contains a more complicated steamline configuration. Therefore, modifications were made to the model described in Reference 2 to adequately describe this complexity. The results of this comparison again show good agreement between data and calculation. The calculated change in critical power ratio agrees with the change inferred from the data to within 0.01 Δ CPR/ICPR.

The four turbine trip experiments represent the most significant part of the one-dimensional transient model qualification data base. The comparisons shown in this document show that the one-dimensional model is successful in calculating all four turbine trips, which were initiated from different power levels and core conditions.

2. MODEL-MODEL COMPARISONS

The comparison of computer model results to experimental data obtained from actual reactor plant transients is the most desirable qualification basis. However, comparisons with other models are also useful in showing that a specific assumption yields accurate results or is consistent with other approved design methods.

2.1 NUCLEAR MODEL COMPARISONS

The solution techniques employed in the one-dimensional nuclear model are described in Section 5 of Reference 2. The one-dimensional diffusion parameters are derived by collapsing three-dimensional steady-state solutions obtained from the General Electric three-dimensional BWR simulator³. This collapsing process is described in detail in Appendix A of Reference 2. The ability of the one-dimensional core model to calculate scram reactivity and void coefficients will be examined in this section.

2.1.1 Scram Reactivity

In order to test the validity of the one-dimensional collapsing procedures described in Section 5 of Reference 2, a series of scram calculations has been compared with the one-dimensional solutions with three-dimensional solutions obtained with the three-dimensional BWR simulator. These scram calculations have no void feedback and represent a test of the collapsed one-dimensional model in properly estimating scram reactivity worth. The basic nuclear data used in the two calculations are identical and the one-dimensional parameters have been obtained from the steady-state three-dimensional solution. Three cases are considered here. The first case examined is a BWR/4 core at the beginning of Cycle 2 (Plant A). To simulate an end-of-cycle scram situation, all of the control rods were assumed to be withdrawn. Figures 2-1 and 2-2 show a three-dimensional, one-dimensional comparison of total neutron flux and scram reactivity versus time. The agreement is quite good over the entire scram range. The second example, shown in Figure 2-4, shows the same core in a critical rod pattern shown in Figure 2-3. In this case, the flux and scram reactivity agreement is still good, although not quite as good as the all-rods-out case. This second case is more difficult to calculate because of the rapid

radial flux changes caused by the motion of the inserted rods. The third example shows a BWR/4 reactor at 50% power, 100% flow (Plant B). In this case, there is a considerable number of control rods in the core, as shown in Figure 2-5. Also, the radial power distribution is complicated because of the lower power level and the complicated rod pattern. Here the agreement is still good, especially in the early part of the scram, which is the important region in the analysis of turbine trip accidents. Finally, a comparison of axial power shapes for the third example is shown in Figure 2-7 for a number of times during the scram.^{Q7*} The change in average axial shape is followed quite well by the one-dimensional model. In summary, the collapsing procedures used in generating the one-dimensional neutron kinetics model yield results which compare well with three-dimensional scram calculations.

2.1.2 Void Coefficient

The one-dimensional nuclear model must accurately predict the void reactivity response of the core in order to follow the neutron flux response during BWR transients such as turbine trips. Table 2-1 contains a comparison of void coefficient values obtained with the one-dimensional nuclear model and the three-dimensional BWR Simulator. In each case, the void coefficient is calculated as the following eigenvalue difference:

$$\text{Void Coefficient} = \frac{1}{\beta} \frac{\kappa(\alpha_1) - \kappa(\alpha_2)}{\alpha_1 - \alpha_2}$$

where α_1 and α_2 are core averaged void fractions at two different reactor states.^{Q8} The two reactor states were generated by varying the reactor pressure and flow, which undergo the greatest change during a turbine trip transient. In all cases, the one-dimensional and three-dimensional coefficients agree to within 5%. A wide variety of power levels and control rod configurations has been covered in the cores analyzed. Thus, the one-dimensional model is expected to favorably reproduce the three-dimensional transient void reactivity response.

*Q7 - Replies to NRC questions on the text are documented in Appendix A. The symbol Q7 denotes that this topic is discussed further in the reply to NRC Question 7.

2.2 THERMAL-HYDRAULIC MODEL COMPARISONS

Steady-state comparisons between the thermal-hydraulic model described in Section 6 of Reference 2 and the standard GE BWR channel hydraulic model have been carried out. Figures 2-8 and 2-9 show axial void fraction profiles for a high power and low power channel. Some differences exist in the subcooled void region because of different numerical treatments of the subcooled boiling process. Also, small differences exist at the top of the channel because the current model allows pressure and saturation enthalpy to vary along the channel, while the standard GE model assumes constant pressure and saturation enthalpy. Considering the above model differences, the overall agreement is good, to within 0.003 in void fraction. These same two channels were also run at 10 psi higher pressure and the change in void fraction calculated as a function of axial height. The results obtained by the two models are compared in Figures 2-10 and 2-11 for the low and high power channels, respectively. Note that excellent agreement is obtained for the change in void profile generated by a pressure change.^{Q9}

These calculations show that the channel hydraulic model gives steady-state results consistent with standard GE design tools, which have been verified against void fraction measurements in test assemblies.

In the transient mode, model-model comparisons are more difficult because the five-equation model is more detailed than currently employed design models. However, a closed form solution exists for the one-dimensional vapor continuity equation with constant steam and drift flux properties.⁵ The initial conditions for the transient considered are listed in Table 2-2. During the transient, the axial heat flux distribution is constant and uniform. The time-dependent boundary condition is:

$$\text{Inlet volumetric flux} = 0.0002 (1 + 29986.495e^{-5t}), \text{ ft/sec}$$

The one-dimensional hydraulic model was modified to include constant steam properties and drift flux correlations and then used to obtain a solution to the above problem. Spacial nodes were placed every 0.5 ft up the channel.

NEDO-24154-A

This solution is compared with the closed form solution in Figure 2-12. The transient void fraction at 0.5 and 12 ft from the channel entrance is plotted. The maximum deviation at 0.5 ft is 0.006 in void fraction. The maximum deviation at 12 ft is 0.0003. This numerical test shows that the overall numerical procedures employed in the thermal-hydraulic model are adequate.

NEDO-24154-A

Table 2-1

COMPARISON OF VOID COEFFICIENTS OBTAINED WITH
THREE-DIMENSIONAL AND ONE-DIMENSIONAL CORE MODELS

<u>Plant</u>	<u>Percent of Rated Power (%)</u>	<u>Percent of Rated Flow (%)</u>	<u>Average Void Fraction</u>	<u>Perturbation Mechanism</u>	<u>3-D Void Coefficient (c/ΔV)</u>	<u>1-D Void Coefficient (c/ΔV)</u>
Plant B (BWR/4)	48	100	0.232	Pressure change	-33.9	-33.2
Plant B (BWR/4)	62	80	0.289	Pressure change	-29.9	-31.5
Plant B (BWR/4)	69	100	0.301	Pressure change	-28.5	-29.2
Plant C (BWR/5)	104	100	0.413	Pressure change	-21.3	-22.0
Plant C (BWR/5)	104	100	0.413	Flow change	-24.2	-24.0
Plant D	77	93	0.321	Pressure change	-26.3	-27.6

Table 2-2

SUMMARY OF HYDRAULIC CHANNEL CONDITIONS

<u>Label</u>	<u>Inlet Volumetric Flux (ft/sec)</u>	<u>Bundle Power (MW)</u>	<u>Sub- cooling (Btu/lb)</u>	<u>Flow Area (ft²)</u>	<u>Hydraulic Diameter (ft)</u>	<u>Channel Length (ft)</u>	<u>Pressure (psi)</u>
High Power Channel	6.45	6.55	23.4	0.1065	0.0433	12.5	1055
Low Power Channel	4.305	1.64	23.4	0.1065	0.0433	12.5	1055
Transient Calcula- tion	5.997	1.00	0	0.1115	0.0484	12	1000

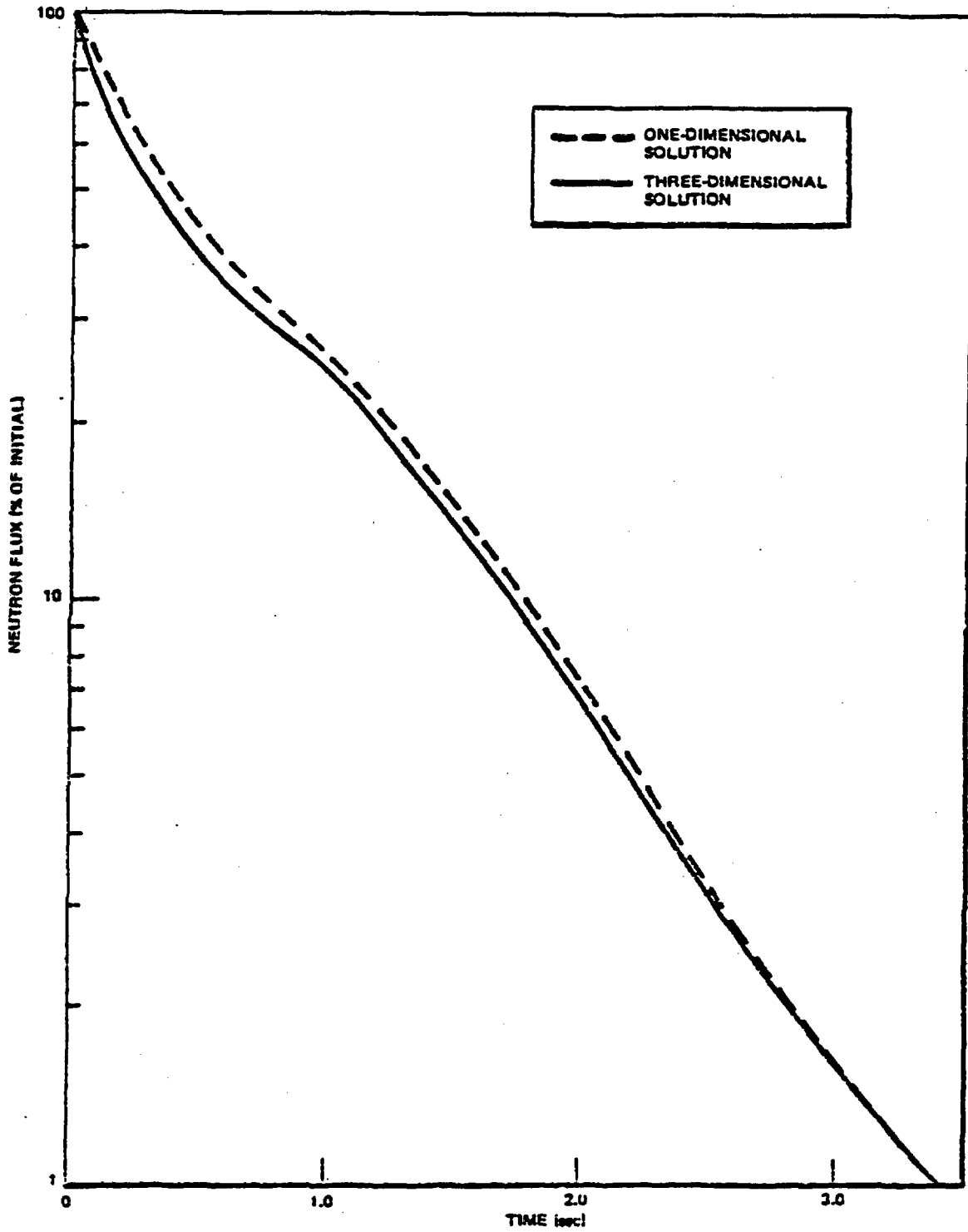


Figure 2-1. Plant A (3WR/4) All-Rods-Out Scram

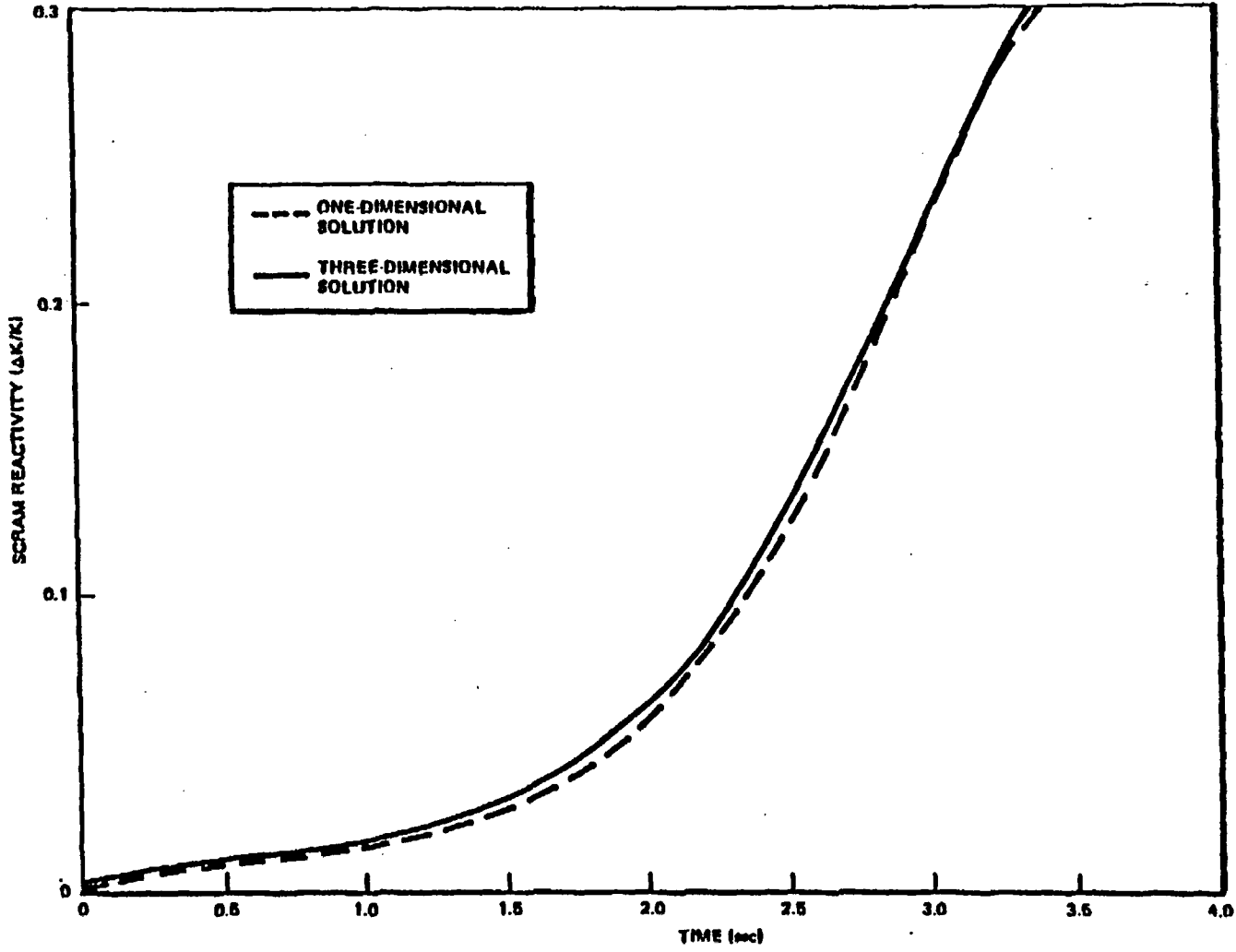


Figure 2-2. Plant A All-Rods-Out Scram Reactivity

NEDO-24154-A

INITIAL CONTROL ROD ARRAY

J/I	1	3	5	7	9	11	13
1							
3						20.42	
5			12.43				0.45
7				14.43		18.42	
9					0.45		0.45
11		20.42		18.42			
13			0.45		0.45		0.45

Figure 2-3. Plant A Initial Control Rod Pattern in Nodes Withdrawn (24 is Completely Out)

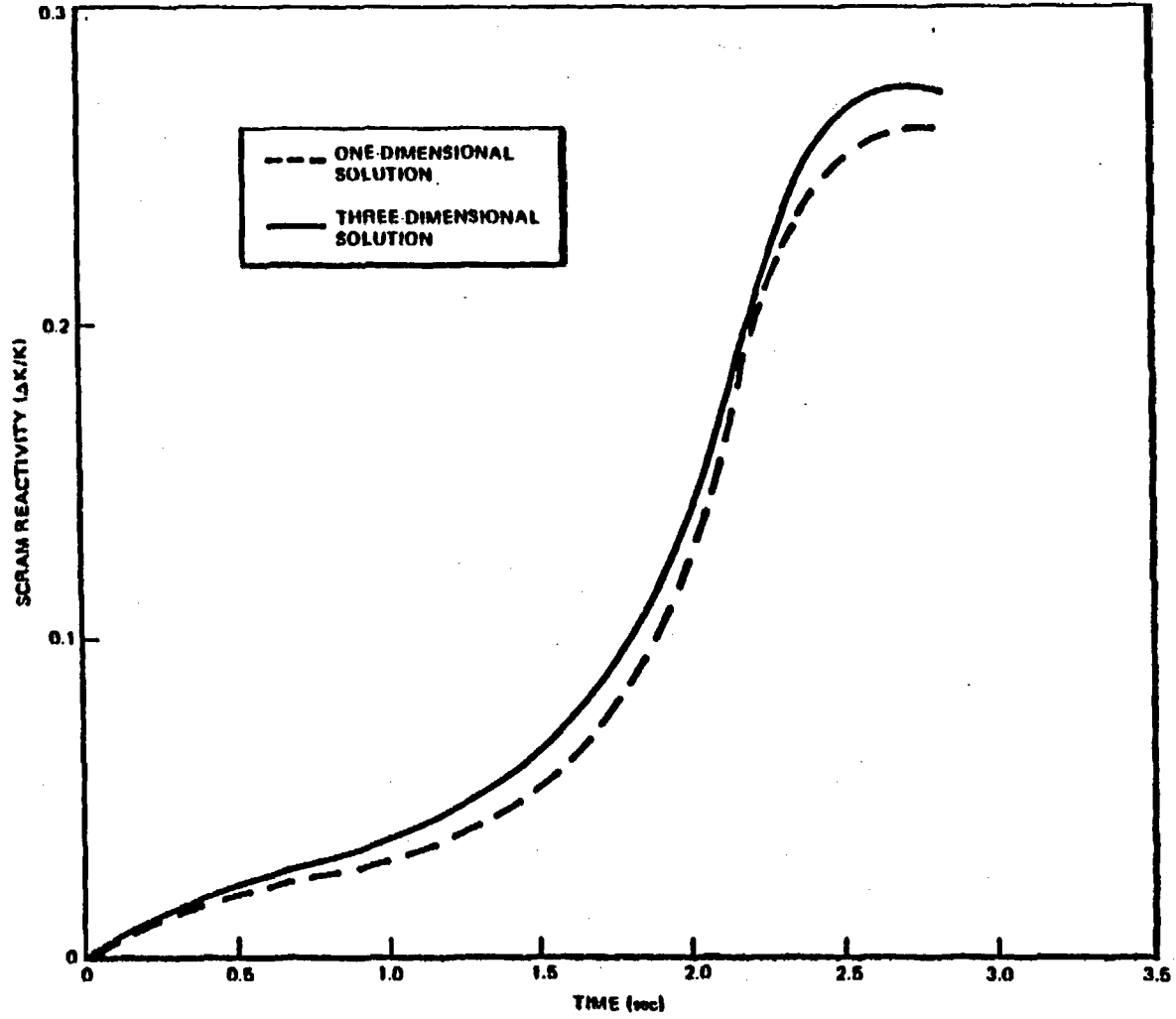


Figure 2-4. Plant A Critical Rod Pattern Scram Reactivity

INITIAL CONTROL ROD ARRAY

J/I	1	3	5	7	9	11	13	15	17	19	21	23	25	27	29
1															
3						10.17		14.17		19.17					
6					0.17		0.17		0.17		0.17				
7				20.17		10.17		8.17		10.17		20.17			
8			0.17		0.17		0.17		0.17		0.17		0.17		
11		10.17		10.17		20.17				20.17		10.17		19.17	
13			0.17		0.17		0.17		0.17		0.17		0.17		
15		14.17		8.17				20.17				8.17		14.17	
17			0.17		0.17		0.17		0.17		0.17		0.17		
19		19.17		10.17		20.17				20.17		10.17		19.17	
21			0.17		0.17		0.17		0.17		0.17				
23				20.17		10.17		8.17		10.17		20.17			
25					0.17		0.17		0.17		0.17				
27						19.17		14.17		19.17					
28															

2-10

NEEO-24154-A

Figure 2-5. Plant B Rod Pattern in Number of Nodes Withdrawn (24 is Completely Out)

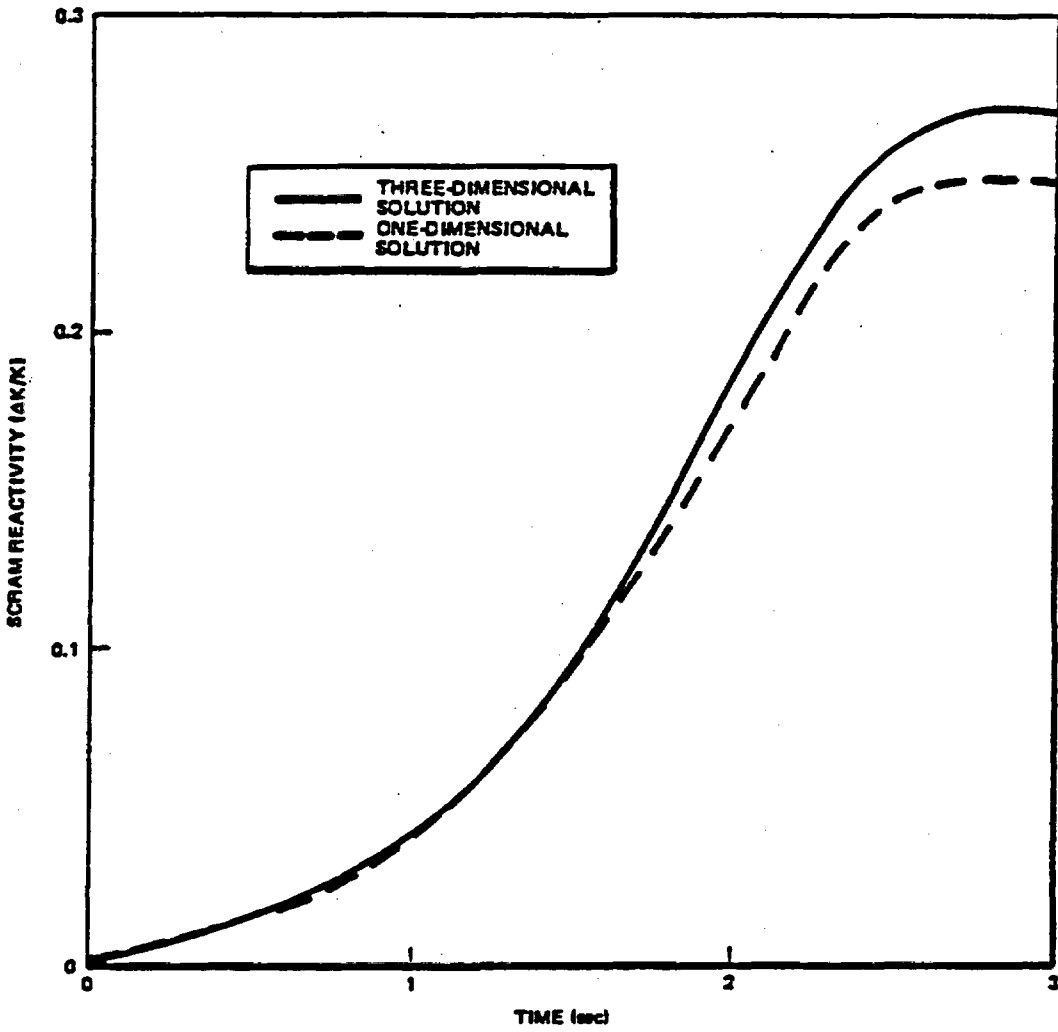


Figure 2-6. Plant B (BWR/4) Scram Reactivity

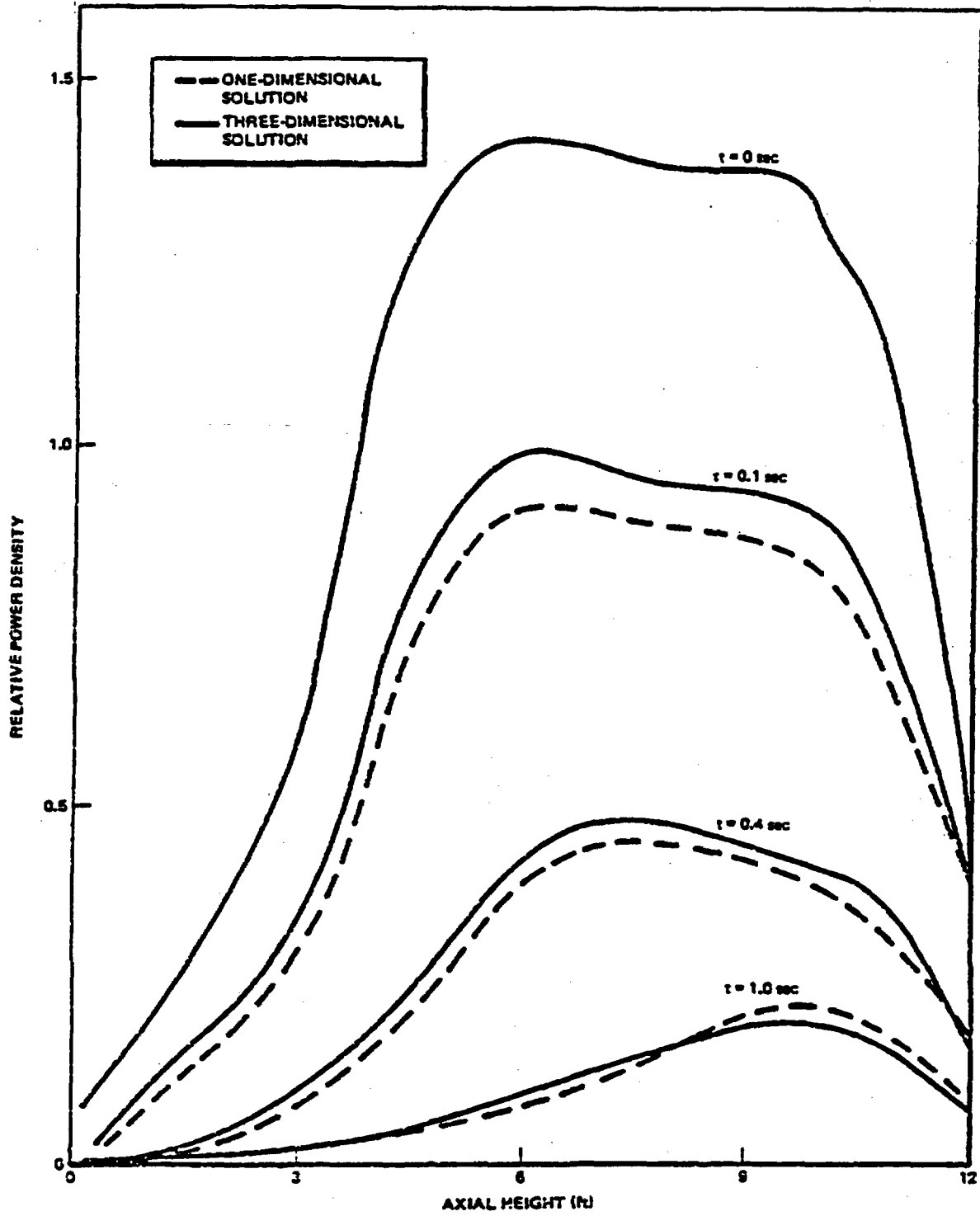


Figure 2-7. Plant B Transient Axial Power

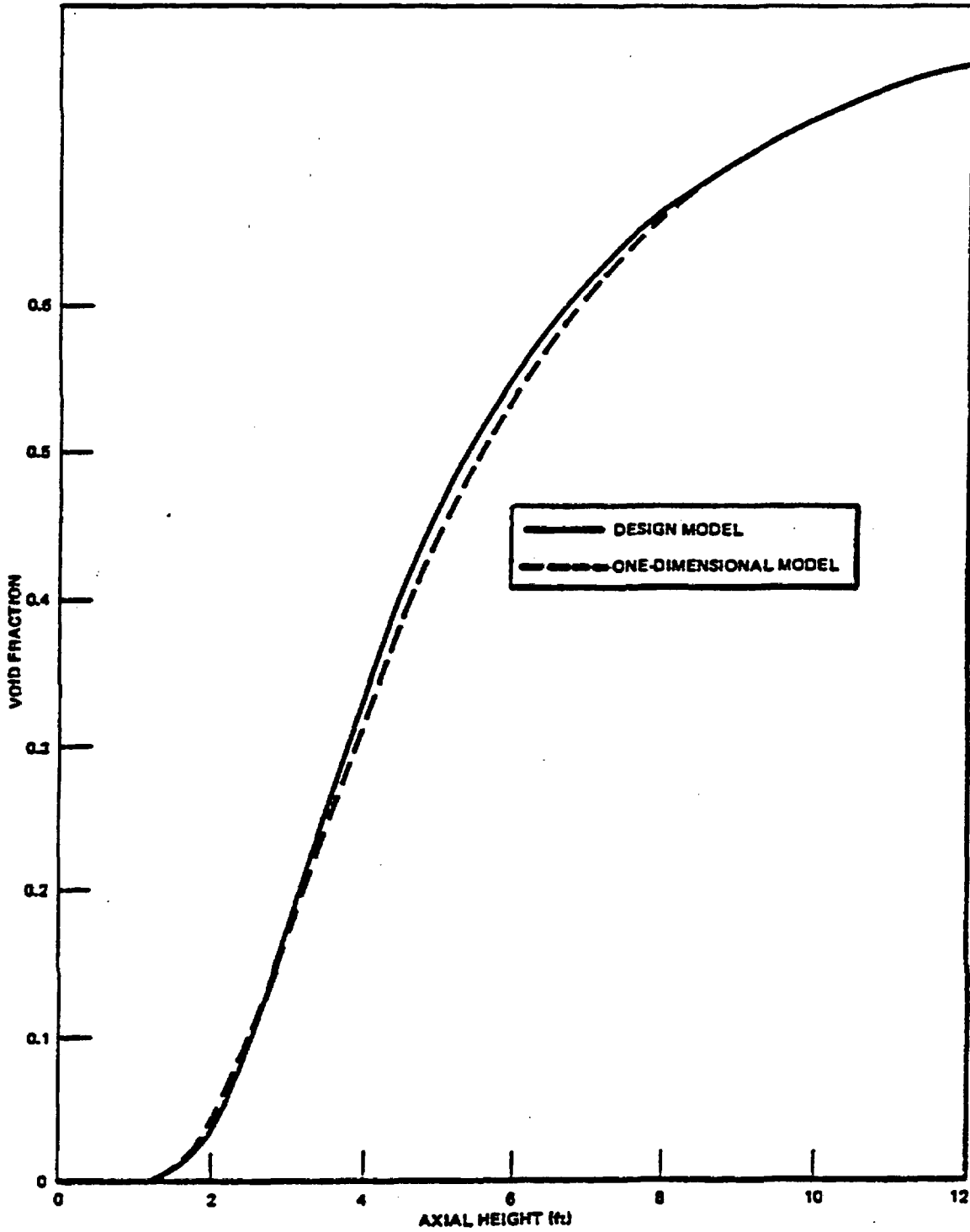


Figure 2-8. Steady-State Void Fraction Profile High Power Channel

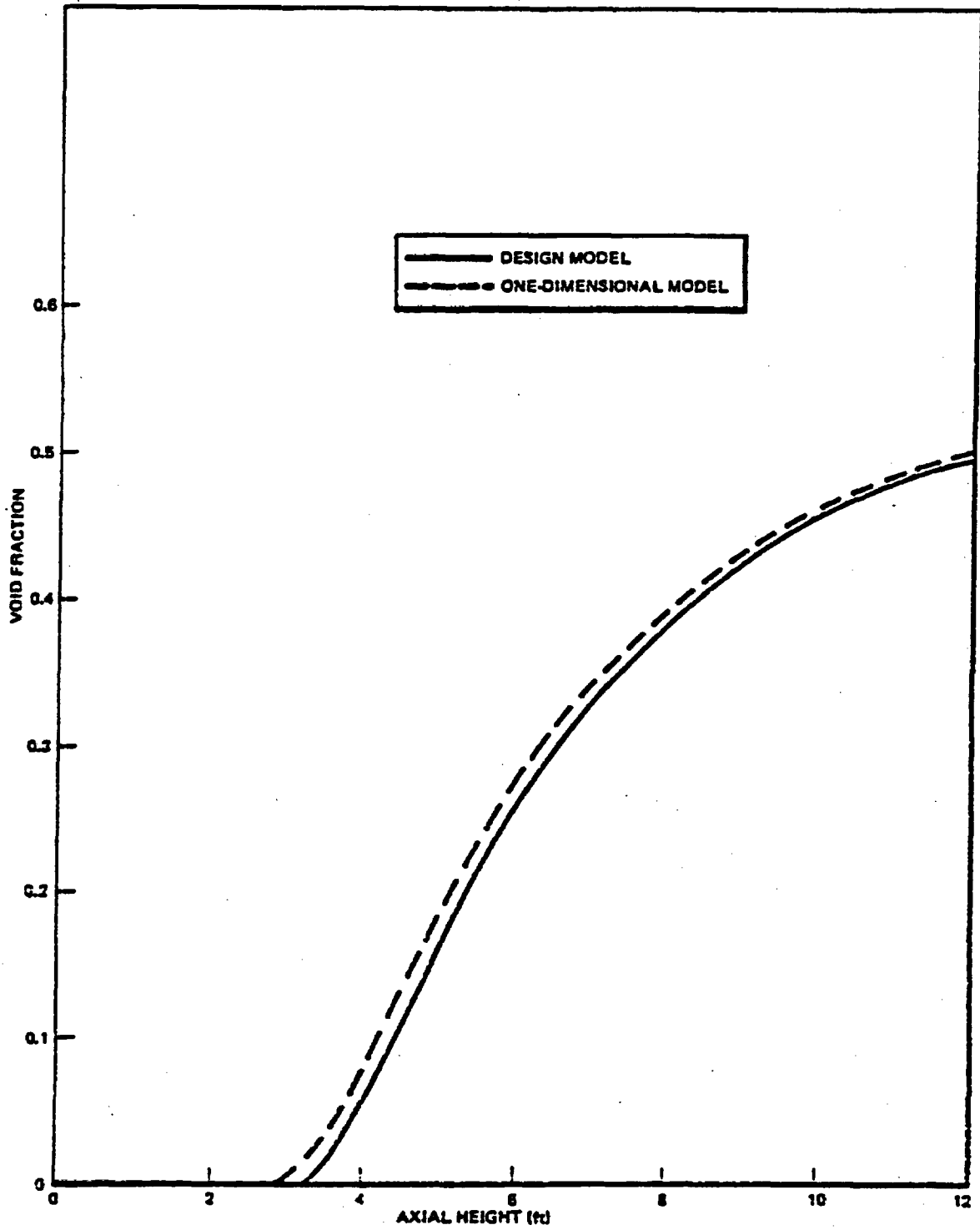


Figure 2-9. Steady-State Void Fraction Profile Low Power Channel

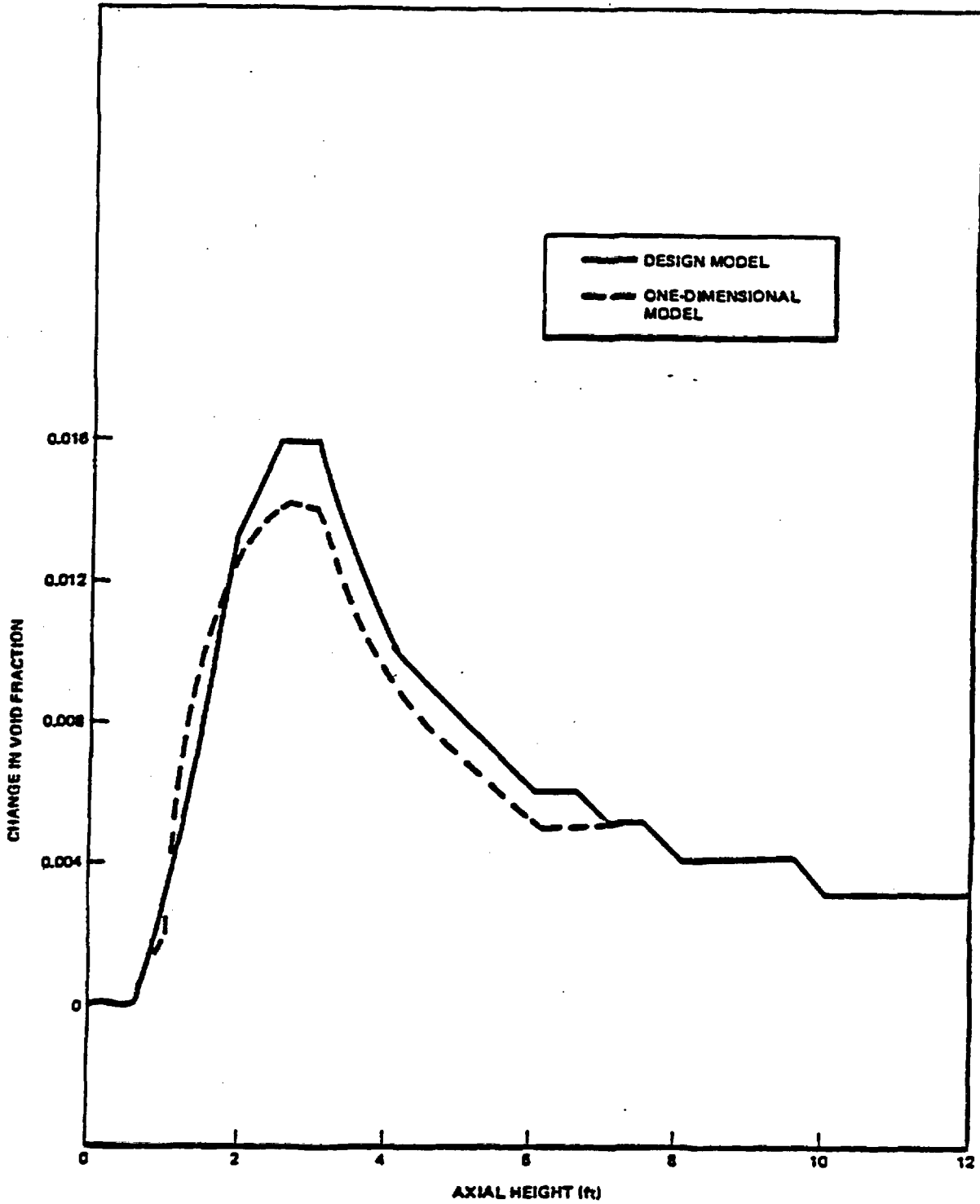


Figure 2-10. Change in Void Fraction from 10 Psi Pressure Change High Power Channel

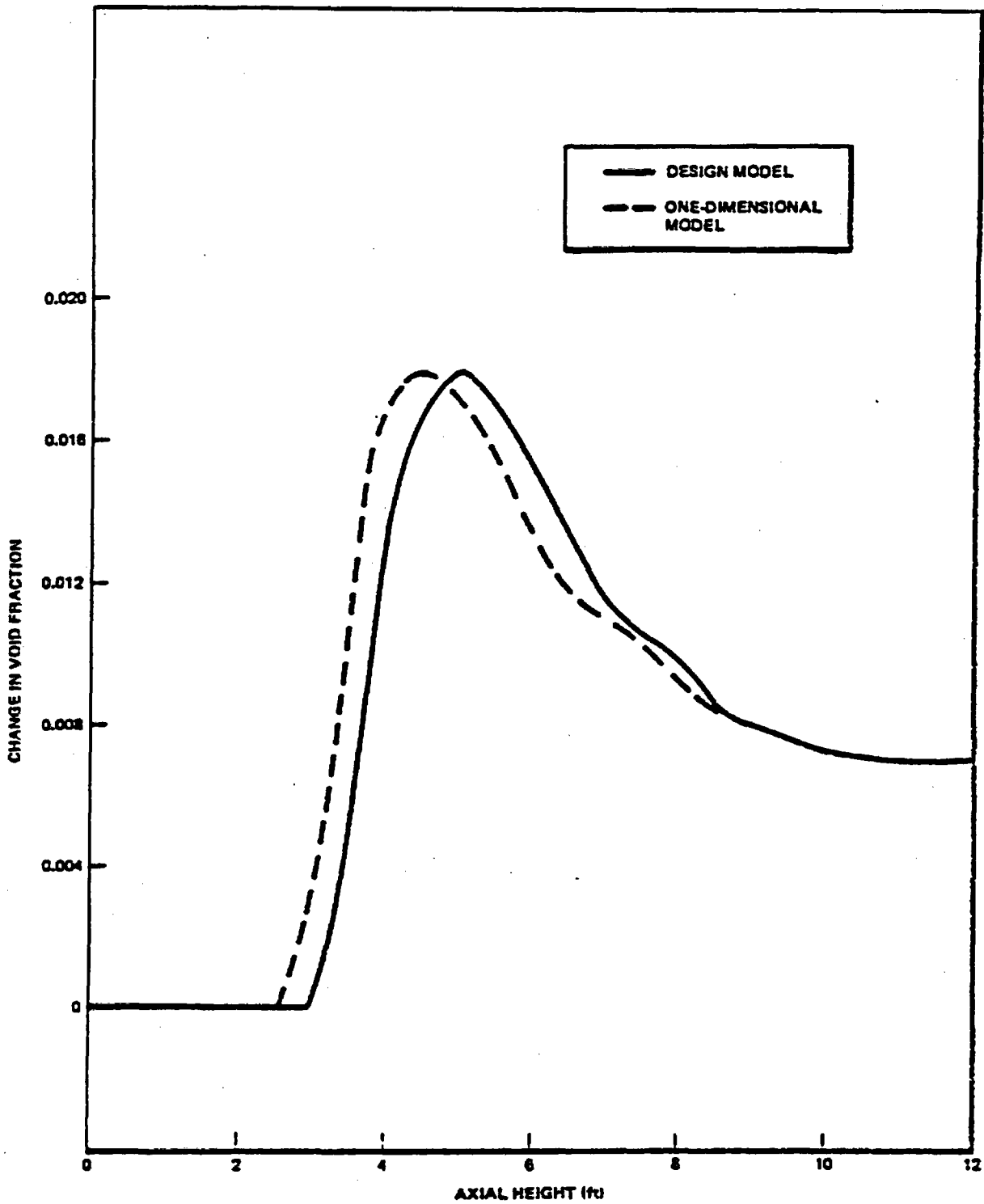


Figure 2-11. Change in Void Fraction from 10 Psi Pressure Change Low Power Channel

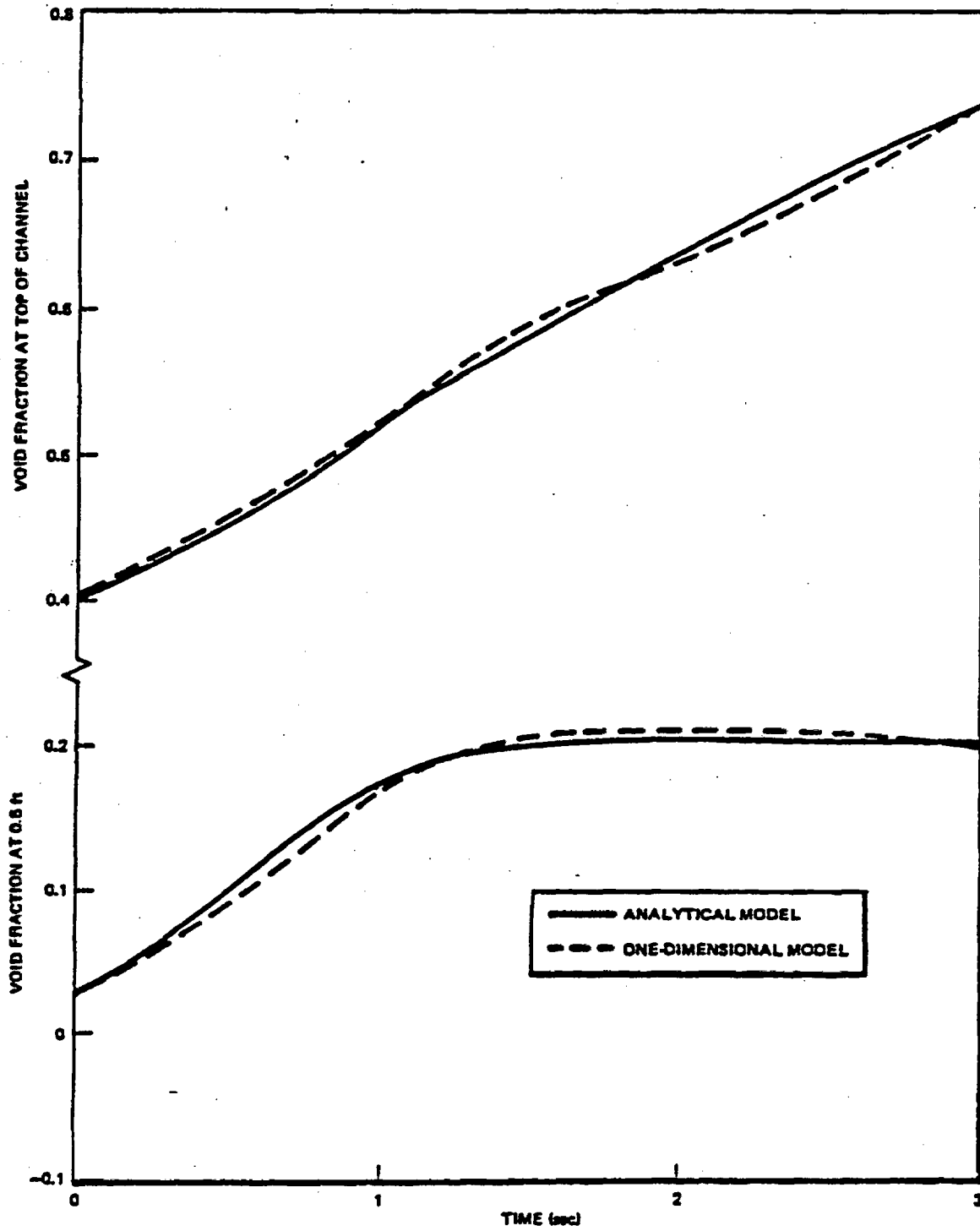


Figure 2-12. Void Fraction Versus Time Exponential Flow Decay Problem

3. ANALYSIS OF TURBINE TRIP EXPERIMENTS

Four special turbine trip experiments were carried out on BWR reactors during 1977. An extensive amount of data was taken at each event, providing an outstanding set of benchmarks for transient model qualification. These tests were specifically designed to obtain data which would be useful in verifying assumptions for transient models. The first three turbine trips were carried out on the Peach Bottom-2 reactor and the fourth on the KKM reactor in Switzerland.

3.1 PEACH BOTTOM TURBINE TRIPS

Three instrumented turbine trips were carried out at the Peach Bottom-2 reactor during April 1977. These tests were conducted with the direct scram on stopvalve position bypassed such that a trip on high flux was obtained. This departure from the normal reactor condition was required to obtain a sufficiently large flux response to allow a model-test comparison. A detailed description of the test conditions and measurement process can be found in Reference 4.

3.1.1 Test Summary

The initial power and flow conditions for each test are shown in Table 3-1. These test conditions were selected in order of increasing power along a line of constant reactor flow. Prior to the second turbine trip test, it was necessary to reduce core flow to hold the power to within 1% of planned test power level due to the xenon level in the core at the time of the test. In each of the three tests, the trip scram was disabled and the flux scram setpoint adjusted. The scram setpoints are also listed in Table 3-1.

A total of 153 signals were recorded by a digital data acquisition system. A summary of the measured quantities appears in Table 3-2. The comparisons presented here will concentrate on important aspects of both the one-dimensional reactor core model and distributed steamline model.

3.1.2 Model Inputs

As pointed out in Reference 2, most of the mathematical modeling for the recirculation and control system part of the BWR is identical to the model currently used for transient design analysis.¹ The vast majority of the external loop description for the Peach Bottom plant is identical to that used in design and licensing analysis, and is taken from a description of the plant conditions found in Reference 7. A few quantities have been changed to be compatible with the one-dimensional core and eight-node steamline models. These changes are all discussed in this section.

The initial conditions for all three tests were used by the GE BWR Simulator to generate three-dimensional power distributions. These nuclear data were then collapsed into one-dimensional parameters according to the procedures outlined in Reference 2. A comparison of process computer output and the resulting one-dimensional axial power profiles appears in Figures 3-1, 3-2, and 3-3.

The control rod motion pattern was taken from measured data. A linear rod motion pattern as shown in Figure 3-4 was assumed. Figure 3-4 also shows the measured rod positions as a function of time after the trip signal. The same motion pattern was assumed for all three turbine trips.

The steamline representation is shown in Figure 3-5. The lengths and areas associated with each node are also shown. The coefficients for pressure losses were calculated by considering the geometry of the steamline and using pressure drop correlations⁶ to compute the appropriate losses over each section of pipe. These coefficients are also shown in Figure 3-5. The resistance quantity K_1 is defined in Reference 2. The core thermal-hydraulic geometry used a weighted average of the dimensions from the 576 7x7 bundles and the 188 8x8 bundles.^{Q10} Temperature-dependent conduction parameters were used for the fuel pellet and cladding. A value of 1000 Btu/hr-ft²-°F was used for gap conductance.

For the three turbine trip test conditions, the transient flux response was found to be a very weak function of gap conductance. That is, variations of 100% in gap conductance produced only 5% changes in peak neutron flux.^{Q11}

NEDO-24154-A

This low sensitivity results from the fast nature of the Peach Bottom flux transients, where thermal feedback contributes only a small part to the reactivity shutdown.

Turbine stopvalve and bypass valve positions were also recorded during each transient⁴ and were then used to describe valve motion in the calculation.

3.1.3 Data Comparisons

3.1.3.1 Transient Pressure Comparisons

Dynamic pressure measurements were recorded at the turbine inlet, in the steamline 90 ft downstream from the vessel, the vessel dome, and near the core exit plenum. In all of the pressure comparisons listed in this section, the data shown are the unfiltered data as recorded by the pressure sensors. The sensors are connected to the appropriate measurement locations by water-filled sensor lines. These sensor lines have their own second-order response which can often give rise to oscillations in the recorded data. Further discussion of the sensor line effects is contained in Reference 4.

Figures 3-6 through 3-8 show comparisons of calculation and data for the pressure measured in the steamline near the safety/relief valves. Note that the model accurately predicts the wave travel time down the steamline and the frequency of pressure oscillations. However, the calculated waves are more spread out and the amplitudes are smaller than the measured waves. The spreading out of the calculated wave is due to the coarseness of the spatial mesh.^{Q1} However, this change in shape does not appreciably affect the dome pressure profile because the vessel dome pressure is influenced in large part by the total steamline flow, which is proportional to the integral of the steamline pressure. Hence, the area under each oscillation is of more interest than the detailed shape.

Plots of dome pressure over the first 1.2 sec of the transient are shown in Figures 3-9 through 3-11. Note that the calculation simulates the initial pressure rise rate quite well in all three tests. Note also that the calculation overpredicts the pressure rise near the peak of the first pressure oscillation. The peak dome pressure occurs about 2.5 sec into the transient. Values for the peak dome pressure are listed in Table 3-3. The transient model

overpredicts the peak pressure by approximately 30 psi in all three cases.^{Q2,Q4} The overprediction of peak pressure is thought to be due to the bypass flow model used in the transient model. The rated bypass capacity of 26% of total steam flow was assumed. It is felt that the real bypass capacity is somewhat larger than 26%. Also, the model calculations assume choked flow through the bypass valve for all valve positions. It is possible that, immediately after the valve opening, the bypass flow will overshoot the steady-state value. If this is true, the peak pressure could be overcalculated by the model.

The core exit pressure is compared in Figures 3-12 through 3-14. Accurate prediction of the core exit pressure is most important in determining the core neutron flux response. Note that, again, the initial rise in pressure is followed well by the model for all three test conditions. The oscillations in the data between 0.4 and 0.7 sec are thought to be caused by the second-order behavior of the instrument line. Note that after 0.7 sec, large oscillations occur.^{Q4} These oscillations begin just about the time that control rod motion starts and could be connected with a disturbance caused by the initial motion of the control rods. No oscillations in neutron flux are observed during this period, so that it is most likely that these oscillations are connected with an instrument line disturbance.

In evaluating the model against the measured data, the steamline and dome model simulate the overall core pressure rise rather well in all three experiments. As the power level is changed, the model tracks the experimental behavior and that about the same differences are observed in all three experiments. There are, however, localized portions of the transient where the model overpredicts the pressure rise. In some cases, these differences can be important, such as the portion of each curve between 0.7 and 0.8 sec where the peak neutron flux is observed. In this region, small changes in pressure can have noticeable effects on neutron flux. This behavior will be discussed further in Section 3.1.3.2.

3.1.3.2 Neutron Flux Comparisons

The most important and demanding test of this transient model is the neutron flux response. The severity of the flux transient determines the transient critical power ratio and its prediction requires not only good core pressure

calculations, but an accurate scram and void reactivity feedback model. The total flux results are shown in Figures 3-15 through 3-17 for the three turbine trips. Note that in all three cases excellent agreement is obtained over the initial rise and falloff portions of the flux spike. The calculation always tends to overpredict the peak flux value.

This overprediction near the peak flux value is primarily due to the fact that the core exit pressure rise is overcalculated during this time period.

Figures 3-18 through 3-20 show the reactivity components as a function of time during the transient as calculated by the one-dimensional model. The definitions of the reactivity components are given in Appendix A of this report. Note that near the peak of the total reactivity curve, the net reactivity is about $\rho = 0.80$. When the overall reactivity level is this large, small changes in reactivity can cause large changes in peak flux levels because the prompt change in flux is proportional to $1/(1-\rho/\beta)$: where ρ is the net reactivity and β is the delayed neutron fraction. For the Peach Bottom transients a 1 psi change in core pressure will generate a change of about 0.02 in the ratio ρ/β , which, in turn, will cause about a 10% change in peak neutron flux. Note also that this sensitivity exists over a short time span and that 0.04 sec after the scram motion begins, the calculated flux agrees again with the data.

A second contributor to the peak flux differences is the assumed scram motion model. The model assumes that all control rods start at the same time and move with the same speed, whereas there is actually a spread of starting times and speeds. This model approximation tends to overestimate the peak flux but also will overestimate the initial fall off rate in the neutron flux. A change in scram initiation time of 0.02 sec results in a 5% change in peak neutron flux, so that this effect is not as large as the pressure effect noted above.^{Q5}

The reactivity curves also show that for the Peach Bottom test conditions, the scram reactivity is very strong and almost immediately turns the flux transient around. This is due to the fact that many control rods are inserted in the core, giving rise to a strong scram reactivity.

The Doppler feedback is small for the Peach Bottom Transients and the final answer is not sensitive to the Doppler coefficient. Turbine trips initiated from higher power will have larger Doppler sensitivities, but even in those cases, changes in Doppler coefficients of 30 to 40% are required to materially influence peak heat flux results.

In addition to the total APERM response, LPRM signals were recorded at 80 locations in the core. The LPRMs are located at four axial levels, which are 1.5, 4.5, 7.5 and 10.5 ft above the bottom of the fuel. These locations will be referred to as the A, B, C and D levels, respectively. Figures 3-21 through 3-24 show plots of all the Turbine Trip No. 1 LPRM signals for each level plotted as a percent of initial signal. All the LPRM signals for a given level have the same time behavior, which indicates that there is very little radial flux change during the transient. The transient behavior is not the same between the four levels, indicating that there are axial flux shifts during the transient. The magnitude of the flux shift is considerable. The A level fluxes increase to 350%, whereas the D level increases to 550%. These trends are observed in all three turbine trip experiments (Reference 4). Based on this information, a one-dimensional model appears to be appropriate to describe the transient nuclear behavior of the core. Figures 3-25 through 3-36 show comparisons between calculation and data for the A, B, C and D level flux response for the three turbine trips.

The largest flux rise occurs near the top of the reactor core, which has the largest void fraction and the largest void coefficient. Detector A is below the boiling boundary for these experiments and experiences the smallest flux rise. Figure 2-10 shows that the largest void changes occur near the boiling boundary in the low quality regions. In the reactor, the boiling boundary is different in each channel and the variation in void fraction with axial position is smaller than the one-dimensional estimate, which contains a single thermal-hydraulic channel. For this reason, the one-dimensional model will overestimate flux changes near the boiling boundary. This trend can be noticed in the Peach Bottom results in comparing the B level flux response with the other levels.^{Q17} However, the magnitude of this overestimate near the boiling boundary is relatively small, and the A, B, C and D level comparisons are almost identical to those observed for the total flux for all three transients.

This indicates that the one-dimensional model is accurately predicting the axial flux shifts which take place during the transient.

3.1.3.3 Critical Power Ratio

The critical power ratio (CPR) is a calculated quantity which is a measure of how close conditions in a particular channel are to transition boiling. A good measure of the relative severity of a particular reactor transient is the maximum change in CPR, divided by the initial or steady-state CPR (ICPR).

For the Peach Bottom turbine trips, the CPR comparisons have been made by driving a hot channel transient thermal-hydraulic calculation with both experimentally determined and calculated inlet flow, pressure, and fuel heat generation rate. The pressure input was taken from the core pressure signal, which was filtered with a 5Hz low pass filter. The transient fuel heat generation rate was taken to be proportional to the total APERM response. Core flow was obtained from pressure drop measurements taken across four of the jet pumps throughout the three turbine trips. Changes in core flow can be detected by assuming the jet pump pressure drop to be proportional to the square of the flow. In practice, however, this is not an accurate measure of core flow because of the large amount of noise in the jet pump pressure drop signal. In this case, a 5 Hz filter was applied to the four jet pump signals to reduce the noise component and then averaged to obtain a pressure drop. The steady-state flow was normalized to the recorded flow at the beginning of each transient.

In both cases, the initial conditions and channel properties are identical. Only the transient pressure, flow and flux responses are different so that a good measure of bias in CPR is obtained.

For the transient CPR calculations driven by the experimental data, uncertainties in the input quantities will contribute to an uncertainty in the ratio CPR/ICPR. Reference 4 quotes a ± 2 psi uncertainty in core pressure. This pressure uncertainty, coupled with a $\pm 3\%$ uncertainty in flow, results in a ± 0.01 uncertainty in the ratio CPR/ICPR.^{Q15, Q18} This CPR uncertainty is obtained from sensitivity calculations carried out on pressurization type transients.

The results of the transient CPR calculations are summarized in Table 3-4. In each case, the model driven CPR/ICPR is within 0.01 of the data driven value. This excellent agreement is an indication of the overall quality of the calculated results and shows that, while differences exist in detail between model calculation and experiment, their overall impact on CPR is small.

3.1.4 Conclusions

A great deal of information has been assembled for the three turbine trips carried out at Peach Bottom. The one-dimensional BWR transient model compares well with the measured pressure responses in the vessel dome and core exit. The steamline pressure comparisons show the model underpredicting the magnitude of the pressure oscillations but this does not affect the dome pressure response. The peak steamline and dome pressures are overcalculated by the model, indicating the possibility of larger bypass flow than assumed by the model.

The flux response agreement is good for all three experiments. The model overpredicts the peak neutron flux due to a slight overcalculation of pressure near the time of maximum neutron flux. The initial and final portions of the flux show excellent agreement. The axial response is also followed well, as evidenced by comparisons with A, B, C, and D level LPRM signals.

Finally, the good qualitative agreement obtained in the pressure, flow and flux responses results in excellent transient CPR comparisons. Overall confidence in the model is strengthened by the fact that about the same degree of agreement was obtained for all three turbine trip tests. Model input assumptions were identical for all three tests except for the core power level, core flow and known changes in valve actions and scram setpoints. This agreement indicates that the model can also follow changes in transient behavior due to changes in power level and flow and can be used to predict full power turbine trip transients.

3.2 KKM TURBINE TRIP

An instrumented turbine trip was carried out at the KKM power plant in Muehleburg, Switzerland on June 30, 1977. The KKM Plant is unique for BWR's, having two turbines and a bypass capacity of 110% of full rated steam flow. At the time of the

test, the reactor core was near the end of a fuel cycle and all the control rods were out of the core at rated conditions. These test conditions provide an additional, valuable transient benchmark because they realistically simulate end-of-cycle conditions. However, the two-turbine configuration and large bypass capacity provided additional challenges for the steamline and valve flow portions of the one-dimensional transeint model. As in the case of the tests conducted at the Peach Bottom-2 plant, the direct trip scram on stopvalve position was bypassed to obtain a significant flux response during the test.

3.2.1 Test Summary

The initial conditions for the KKM turbine trip test are summarized in Table 3-5. The KKM plant was designed with a large bypass capacity in order to avoid a full reactor scram following a turbine trip. Therefore, only selected rods are inserted following the turbine trip signal. For this test, the select rod insertion was disabled. The flux scram setpoint was not changed and remained at 120% of rated for the test. The normal bypass capacity at KKM is 110% of rated steam flow. Each turbine has two bypass valves which are located in the same valve chest with the turbine stopvalves. One of these bypass valves was disabled on each turbine, thereby reducing the total bypass capacity to 55% of rated steam flow for this test.

As in Peach Bottom, a digital data acquisition system was used to record a total of 118 signals. The signals (summarized in Table 3-6) are essentially the same as those recorded at Peach Bottom. Unlike Peach Bottom, however, the signals recording the turbine stopvalve and bypass valve positions were not available. The KKM plant has a mechanical control system to regulate bypass flow and a continuous signal recording valve position was not available. Therefore, additional position switches were installed on these valves, but their signals were lost due to equipment problems. The only signals available are the valve initial opening time and the time at which the valve is in the full open position. The comparisons presented here will concentrate on the pressure and flux measurements which form the qualification base for the distributed steamline and reactor core models.

3.2.2 Special Model Considerations

The one-dimensional transient model used for the description of the Peach Bottom turbine trips is described in Reference 2. Separate models exist for valve flow control and motor generator plants, so that with one exception all BWR/3 through 6 plants can be described. This exception is KKM, which has two turbines and two sets of steamlines. Also, each steamline has a reheater line, a feature which is not present on any domestic BWR's. Therefore, a special version of the one-dimensional transient model has been constructed which contains two steamlines and also correctly simulates the reheater line. The physical dimensions of both steamlines are identical, so the same constants are used for both lines. A schematic of the steamline model appears in Figure 3-37, along with the dimensions and pressure drop constants.

The pressure control system in use at KKM was also simulated, along with a description of the other unique control features of the KKM plant. These other KKM unique model approximations had little effect on the calculated turbine trip transient response.

3.2.3 Model Inputs

With the exception of those items mentioned in Section 3.2.2, the mathematical modeling for the KKM transient model is identical to that described in Reference 2. The recirculation system parameters are based on the input procedures used for other GE transient analyses.

As in the Peach Bottom tests, the GE BWR Simulator was used to generate a steady-state three-dimensional power distribution for the test configuration. These nuclear data were then collapsed into one-dimensional parameters according to the procedures outlined in Reference 2. A comparison of the resultant one-dimensional power profile and the process computer output is shown in Figure 3-38. A total of 32 control rod drift relay signals were recorded, which were then used to determine the control rod bank position with time. From these data, a linear rod motion pattern was established. This pattern is shown in Figure 3-39 along with the measured position of a few control rods. The time zero is established as that point when the flux reaches the trip setting, which in this case is 120% of full rated power.

A special steamline model was constructed for this analysis and is discussed in Section 3.2.2. The model dimensions and loss coefficients are listed in Figure 3-37.

The gap conductance used in the KKM analysis is $600 \text{ Btu/hr-ft}^2\text{-}^\circ\text{F}$. As in the Peach Bottom analysis, the severity of the test transient is not very large, and the calculated flux response is not sensitive to gap conductance. The core thermal-hydraulic geometry was determined from a weighted average of the dimensions from the 12 7x7 bundles and the 228 8x8 bundles in the core at the time of the experiment.

As pointed out before, measured turbine stopvalve and bypass valve positions were not available for this transient. Because of the large bypass capacity, the calculated dome pressure and core flux response is sensitive to the bypass valve opening characteristics. In order to arrive at a realistic transient value response, the bypass valve opening time was set at 0.1 sec, which was the observed time, and the bypass valve opening speed was adjusted until the calculated transient turbine inlet pressure response agreed with the measured data. This adjustment affected only the initial valve opening speed. After the initial bypass valve opening, the KKM pressure controller system was allowed to change the valve position based on the plant control parameters and the calculated pressure controller inputs. It should be pointed out that the adjusted bypass valve opening speed was more rapid than the value currently used in the KKM design calculations.

3.2.4 Data Comparisons

3.2.4.1 Pressure Calculations

Figures 3-40 and 3-41 show the transient pressure comparisons at the two turbine inlets. Upon the manual trip signal, the B turbine stopvalve motion was initiated first, followed by the A turbine stopvalve motion 0.024 sec later. The stopvalve motion closing time was 0.042 sec for both turbines. All of the plots in this section place time equal to zero at the beginning of turbine B stopvalve motion. Initially, the pressure rises and then begins to decrease about 0.2 sec after the start of stopvalve motion. This decrease is due to the opening of the bypass valve, which begins its motion at 0.1 sec.

Other oscillations are due to the wave nature of the steamline transient pressure response. The turbine pressure response from 0.2 to 0.6 sec is sensitive to the bypass valve motion. The best calculated response was obtained with a very rapid valve opening time (≈ 0.08 sec), which is more rapid than that used in normal design calculations. The opening time of 0.08 sec agrees quite well with opening times of 0.07 to 0.09 sec observed in the KKM startup test results obtained from the turbine vendor. The overall agreement is about the same in the A and B steamlines, the only difference being that the A results are displaced about 0.024 sec in time and the initial pressure rise is somewhat slower in the B turbine.

Figures 3-42 and 3-43 show a comparison of transient steamline pressure for steamlines A and B, respectively. The first pressure peak is narrower than those observed in Peach Bottom; the magnitude of the peak is reduced by the opening of the bypass valve. The model predicts a slightly slower wave travel time. The 20 to 30 msec delay in the first calculated pressure peak relative to the data still represents good agreement between experiment and model but will contribute to a slight delay in the initial core pressure rise. After the first pressure peak, the calculations show a 3 Hz oscillation in the steamline pressure. This same frequency is also present in the data. Note that the detailed wave shape is somewhat different in the data and calculation. The KKM model does not undercalculate the magnitude of the initial steamline pressure peak, as observed in the Peach Bottom results. This is due to the finer node structure in the KKM steamline simulation. The KKM used 7 nodes to simulate a 330 ft steamline, whereas the Peach Bottom model used 6 nodes to simulate a 400 ft steamline. The impact of the steamline pressure differences is reduced because the reactor vessel pressure will depend in large part on the change in total steamline flow, which is proportional to the integral of the transient steamline pressure.

The dome pressure comparison is shown in Figure 3-44. The data show a large number of oscillations. These oscillations are due to a disturbance in the instrument line. This can be verified in the test data because similar oscillations are not detected in the core pressure or neutron flux response. Because of this behavior, detailed comparison between data and calculations is difficult. The calculated response does pass through the data, but it is difficult to determine if the timing of the pressure wave is being calculated

accurately. The dome pressure compares quite well out to 1.8 seconds, when the data starts to decrease and the calculated pressure continues to increase. No relief valve opening was observed during the test and the cause of the decrease in the observed pressure is not known nor important in the determination of the core flux response.

Figure 3-45 shows a comparison of the measured and calculated core exit pressure. Although there is some oscillation in the data after 0.42 sec, an overall pattern can be determined. Again, it is felt that these oscillations are due to instrument line response because no oscillations are observed in the neutron flux. The calculated pressure response lags about 40 msec behind the data, reaching an initial peak at about 0.5 sec. Better agreement between calculation and experiment could be obtained with an improved inertia model for the steam separators. The current model assumes the steam to be mixed with the water in the separators, which tends to overestimate its inertia. The model used here still yields reasonable agreement and also provides a conservative estimate of the neutron flux.

In evaluating the total steamline and vessel model, it is important to note that all of the significant aspects of the transient pressure behavior have been duplicated. The plotted data are the raw instrument data, and the instrument line effects are still present so that precise comparisons cannot be made at this time. However, it is apparent that the overall shape of the core exit pressure response is duplicated quite well by the model.

3.2.4.2 Neutron Flux Comparisons

The neutron flux response from the KKM Turbine Trip is compared in Figure 3-46. The KKM transient flux response is interesting because of its double peak behavior. This double peak behavior is caused by an oscillation in the core exit pressure. The pressure rises initially to a peak around 0.4 sec, falls off slightly, then reaches a second peak at 0.72 sec. The control rod scram motion starts at 0.6 sec and reduces the magnitude of the second flux peak. Careful examination of the calculated core exit pressure shows that the model delays the initial pressure rise somewhat, then overestimates the first pressure rise and underestimates the second pressure peak. This results in a calculated flux which does not have the double peak behavior, but which

overestimates the initial flux peak and underestimates the second flux peak. Note, however, that these are shape differences and that the overall magnitude of the transient is slightly overpredicted by the model. Also note that differences between calculated and observed flux response correlate quite well with differences between calculated and observed core pressure. This indicates that the one-dimensional reactor core model responds quite accurately to pressure and scram changes.

The calculated reactivity components are plotted in Figure 3-47. The initial reactivity rise is due to void collapse. However, the scram does not begin until the transient has turned around. Note that the scram reactivity curve has a smaller slope than observed in Peach Bottom. This is due to the all-rods-out configuration.

As a further test of the reactor core model, the A, B, C and D level LPRM signals were also compared. Figures 3-48 through 3-51 show the A, B, C, and D level LPRMs all plotted as a percent of initial power. Note that the overall behavior is one-dimensional, similar to the observed behavior at Peach Bottom. A comparison between calculated A, B, C and D level response and the average observed response at each level is shown in Figures 3-52 through 3-55. In each case, the calculated curve differs from the measured response. However, the deviation in each case is about the same as observed in the total flux. Note that the A level flux decreases much more rapidly after the scram begins because of its close proximity to the control rods, whereas the D level flux has only decreased to 120% of initial after 1.2 sec. This same pattern is also evident in the calculated values.

In attempting to evaluate the one-dimensional model's ability to calculate neutron flux response, it should be pointed out that the KKM transient is a mild one compared to the Peach Bottom transients. In Peach Bottom the neutron flux peak value was as high as 550% of initial, whereas the maximum KKM increase was 220%. Because of its larger bypass capacity and subsequent reduced pressure rise, the detailed flux response was more sensitive to small oscillations in the pressure, which, in turn, was influenced by the turbine and bypass valve behavior. Even with the differences in flux shape, the total energy release is approximated quite well by the one-dimensional model. The impact on the transient critical power ratio is discussed in Subsection 3.2.4.4.

3.2.4.3 Critical Power Ratio

Critical power ratio calculations were also carried out for the KKM transient using both the model transient and the data transient as inputs to the hot channel calculation. The CPR results are summarized in Table 3-7. Note that good agreement is achieved between the data driven and model driven maximum Δ CPR values. The uncertainty on the data driven Δ CPR/ICPR values is ± 0.01 .

3.2.5 Conclusions

Analysis of the KKM turbine trip presented a few unique challenges for the one-dimensional transient model. The two-turbine configuration and the large bypass capacity required careful consideration of the steamline model and the turbine stopvalve and bypass valve characteristics. The final dome pressure and core pressure response was followed quite well by the model, although the exact shape of the transient pressure response was not duplicated. The overall magnitude of the flux response was duplicated quite well, even though the double peak shape was not duplicated by the model. However, the success of the model in duplicating the transient is demonstrated by the excellent agreement obtained in the transient CPR values.

The KKM transient was in many ways quite different from those at Peach Bottom, yet the transient model was successful in duplicating its behavior as well, lending additional confidence to its ability to calculate pressurization transients.

NEDO-24154-A

Table 3-1

PEACH BOTTOM-2 TURBINE TRIP TEST CONDITIONS

	<u>Core Power</u>		<u>Core Flow</u>		<u>Flux Scram</u>
	<u>(MWT)</u>	<u>(% Rated)</u>	<u>(10⁶ lb/hr)</u>	<u>(% Rated)</u>	<u>Setting</u>
					<u>(% Rated)</u>
Turbine Trip 1	1562	47.4	101.3	100.3	85
Turbine Trip 2	2030	61.6	82.9	82.1	95
Turbine Trip 3	2275	69.1	101.9	100.9	77

Table 3-2

PEACH BOTTOM-2 DYNAMIC TEST SIGNALS

<u>No. of Signals</u>	<u>Test Signal Description</u>
<u>Recorded</u>	
80	LPRM Signals
4	APRM Signals
2	TIP Signals
4	Jet Pump (Calib) dPs
1	CORE dP
2	Steamflow Nozzle dPs
2	Steamflow Nozzle Upstream Pressures
2	Turbine Inlet Pressures
1	Reactor Vessel Pressure
1	Core Exit Pressure
2	Reactor Feedpump Flows
1	Reactor Feedwater Temperature
2	Recirculation Loop Flows
2	Recirculation Pump Inlet Temperatures
2	Reactor Water Level
31	Control Rod Drift Relays
1	Scram Solenoid Relay
4	Turbine Stop Valve Position Switches (2 at 10% and 2 at 90%)
4	Turbine Bypass Valve Position Switches (2 at 10% and 2 at 90%)
1	Turbine Bypass Position
4	Turbine Stop Valve Position

NEDO-24154-A

Table 3-3
PEAK VESSEL PRESSURE

	<u>Data*</u>	<u>Model Calculation</u>
Turbine Trip 1	1042	1070
Turbine Trip 2	1052	1072
Turbine Trip 3	1069	1100

*Data value is biased to the same initial value as calculation.

Table 3-4
MAXIMUM ΔCPR VALUES FOR PEACH BOTTOM TURBINE TRIP TESTS

	<u>Initial CPR</u>	<u>ΔCPR/ICPR (Data)</u>	<u>ΔCPR/ICPR (Model)</u>
Turbine Trip 1	2.536	0.170	0.173
Turbine Trip 2	2.115	0.136	0.129
Turbine Trip 3	2.048	0.132	0.141

Table 3-5
KKM TURBINE TRIP TEST CONDITIONS

Core Power	769 MWt 77% Rated
Core Flow	25.69 x 10 ⁶ lb/hr 86.5% Rated
Flux Scram Setting	120% Rated
Vessel Pressure	1023 psi

NEDO-24154-A

Table 3-6
KKM DYNAMIC TEST SIGNALS

No. of Signals Recorded	Test Signal Description
52	LPRM Signals
4	APRM Signals
2	TIP Signals
4	Jet Pump (Calib) dPs
1	Core dP
2	Steamflow Nozzle dPs
2	Steamflow Nozzle Upstream Pressures
2	Steamline Header Pressures
2	Turbine Inlet Pressures
1	Reactor Vessel Pressure
1	Core Exit Pressure
32	Control Rod Drift Relays
1	Scram Solenoid Relay
2	Relief Valve Positions
2	Relief Valve Downstream Pressures
4	Turbine Stop Valve Position Switches (2 at 10% and 2 at 90%)
4	Turbine Bypass Valve Position Switches (2 at 10% and 2 at 90%)

Table 3-7
MAXIMUM ΔCPR VALUES FOR THE
KKM TURBINE TRIP TEST

Initial CPR	1.279
ΔCPR/ICPR (Data)	0.077
ΔCPR/ICPR (Model)	0.084

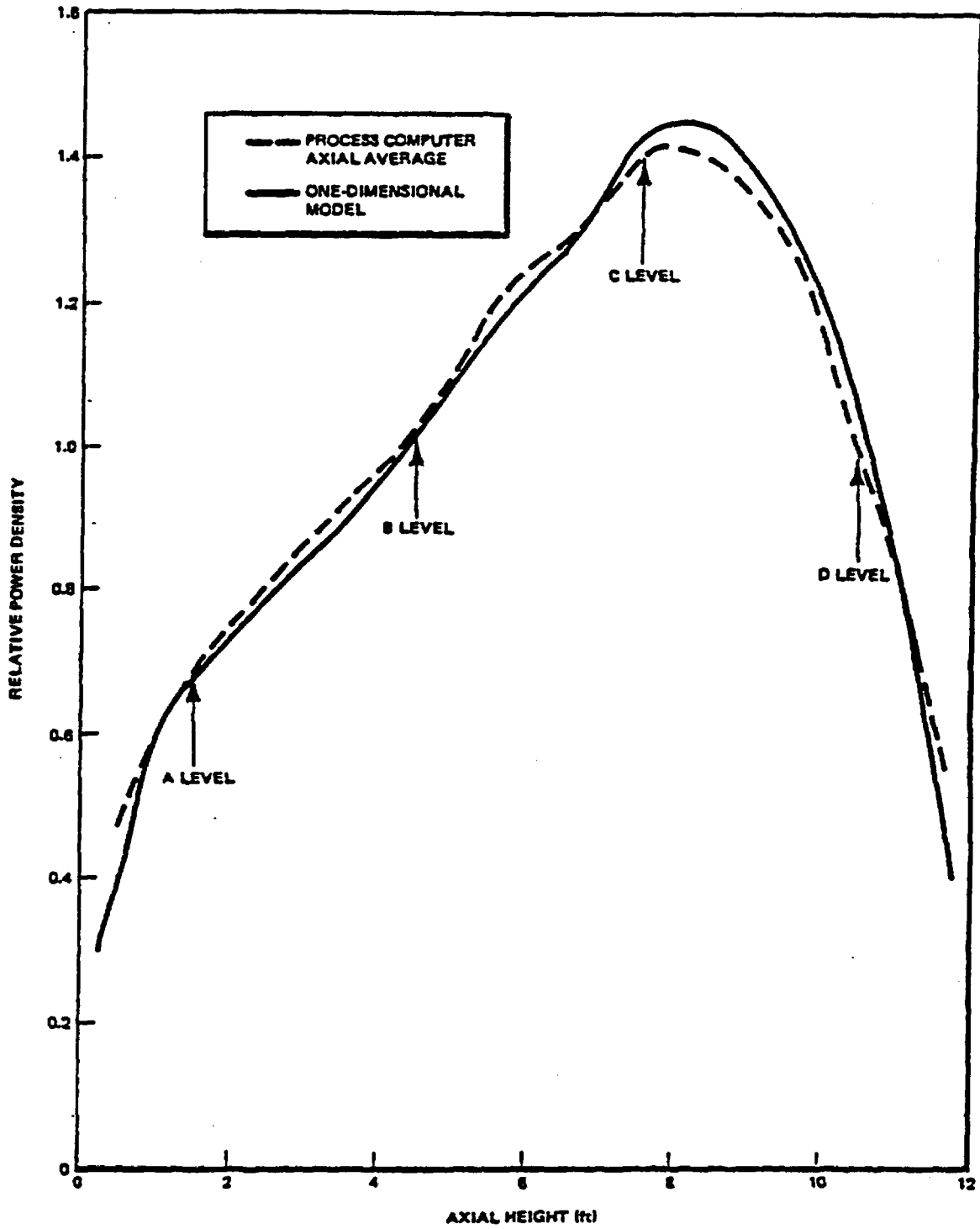


Figure 3-1. Axial Power Profile Turbine Trip 1

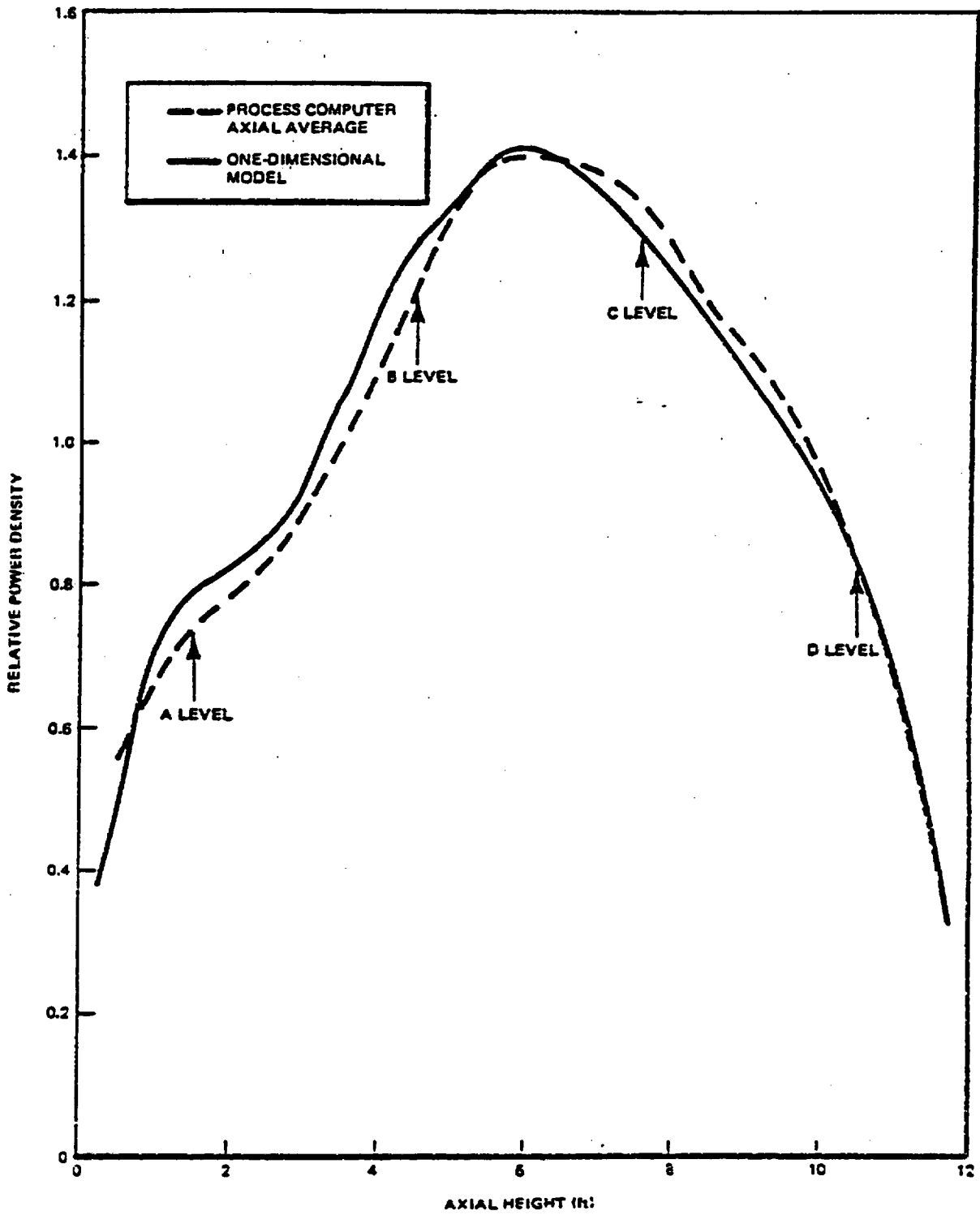


Figure 3-2. Axial Power Profile Turbine Trip 2

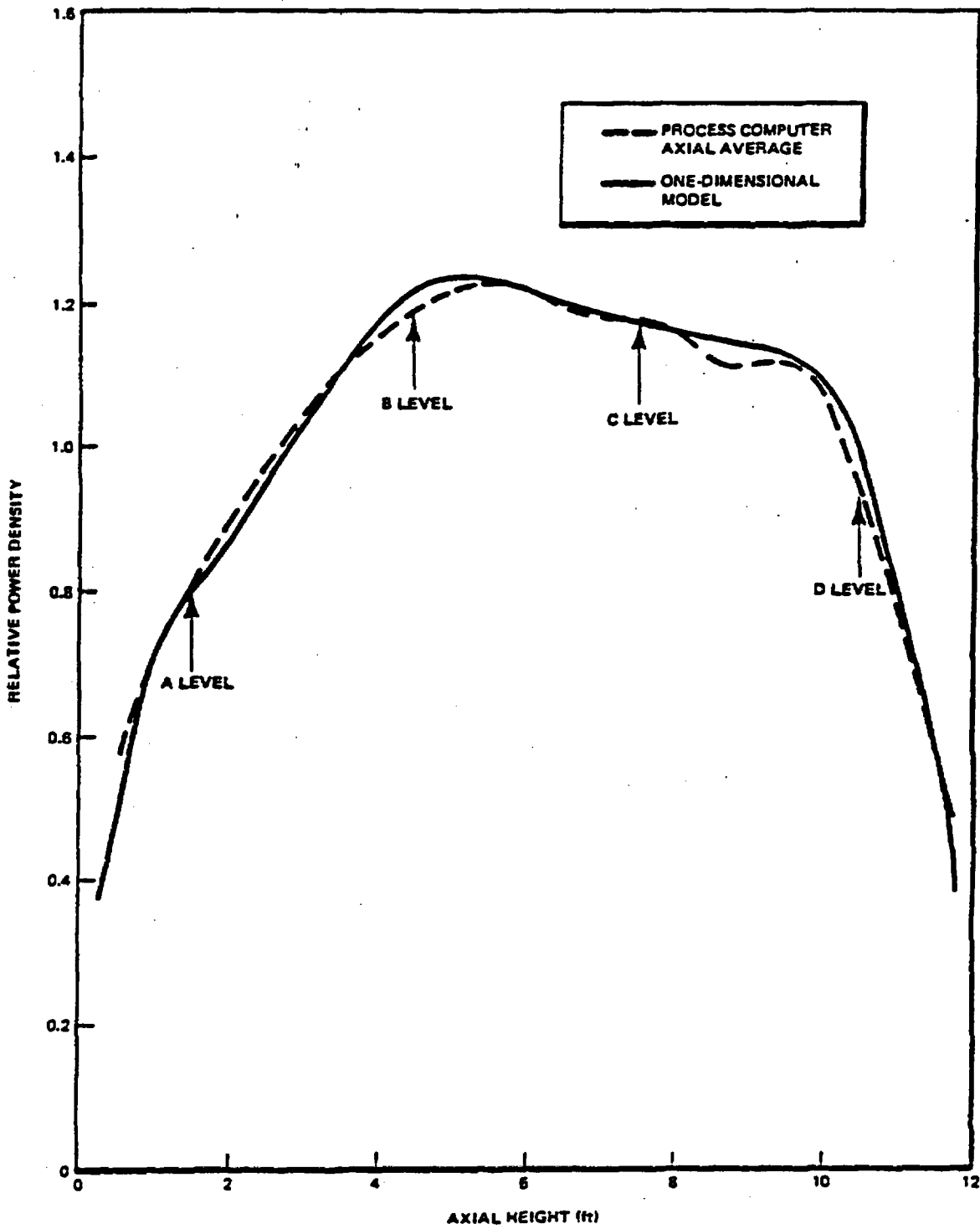


Figure 3-3. Axial Power Profile Turbine Trip 3

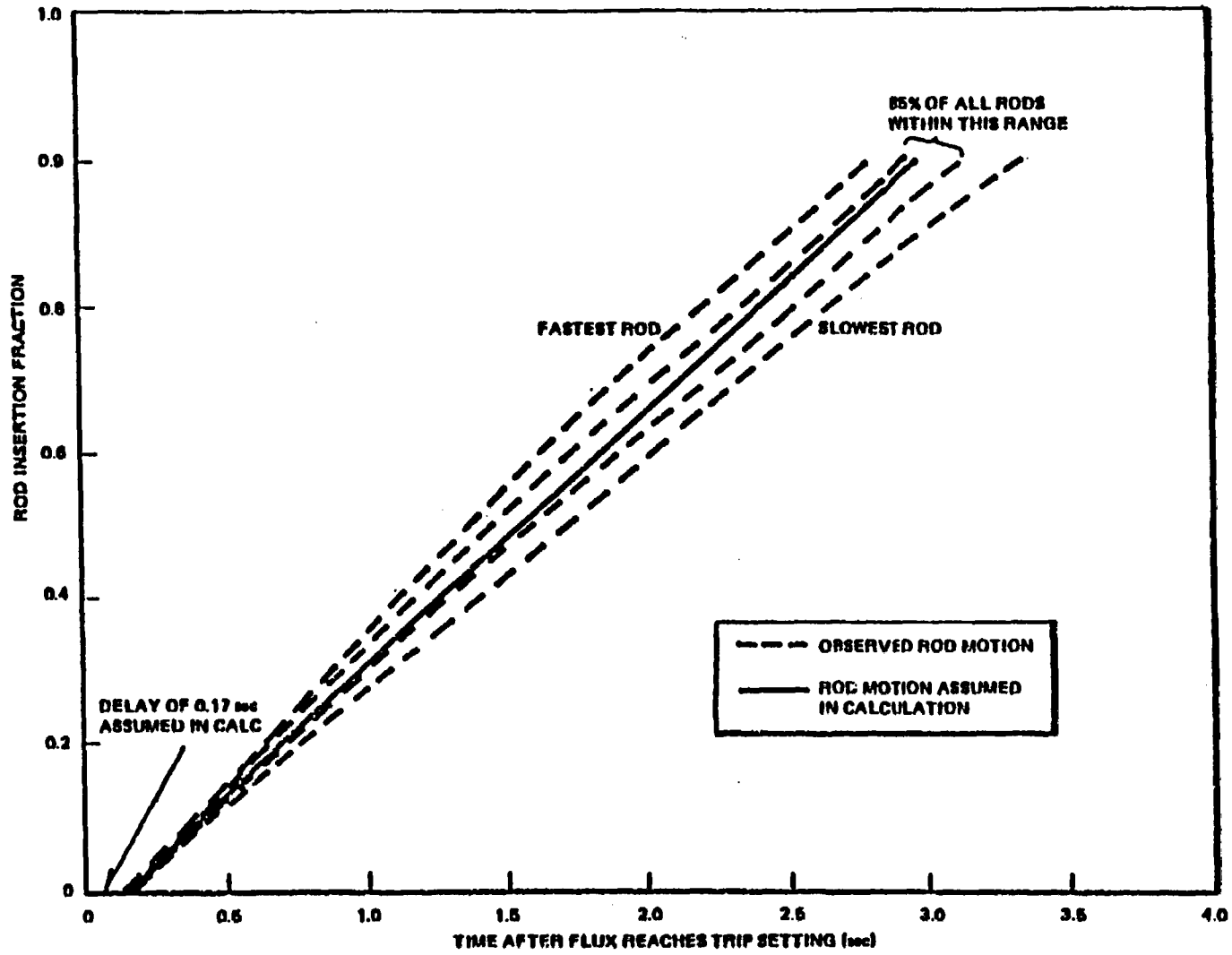
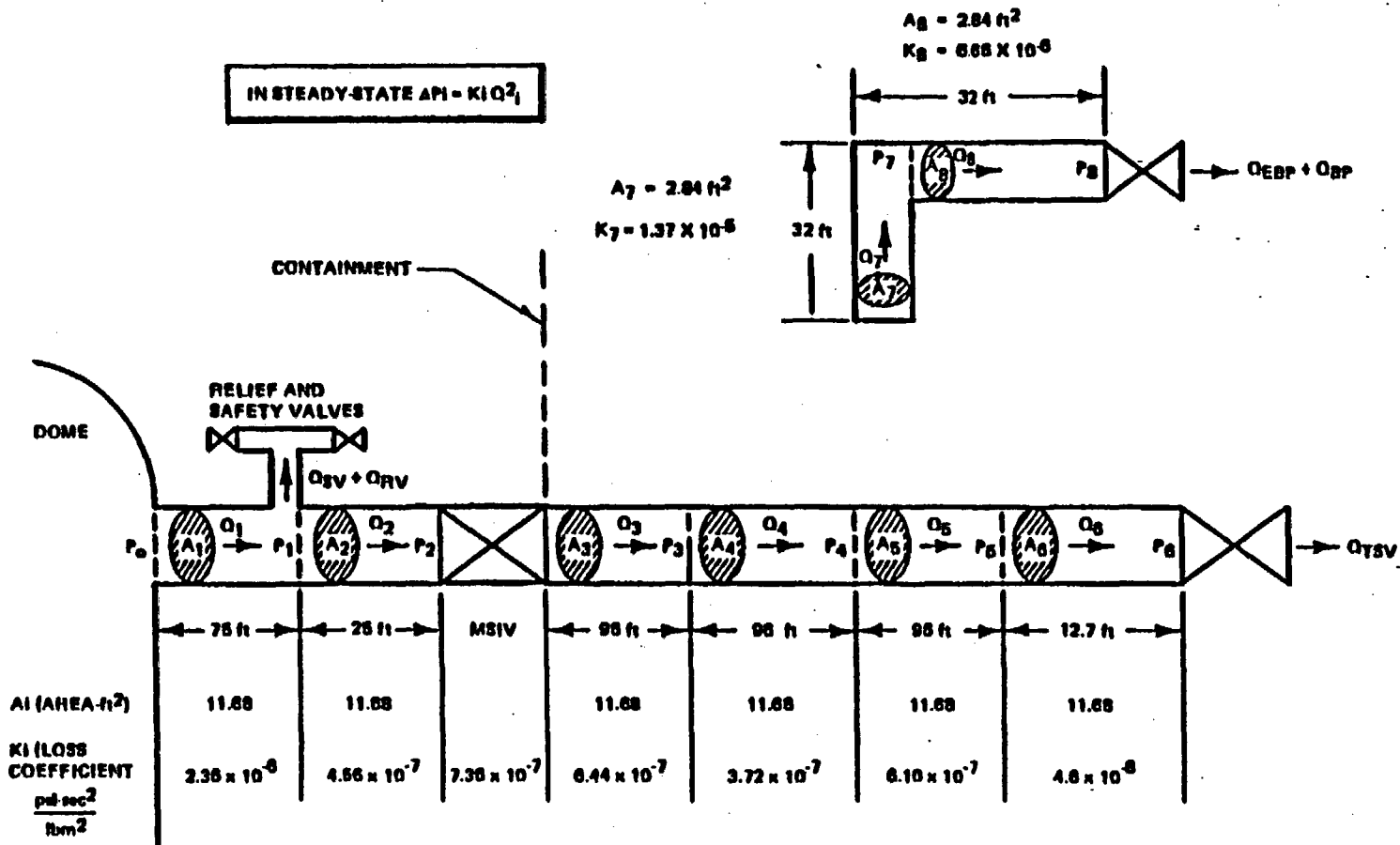


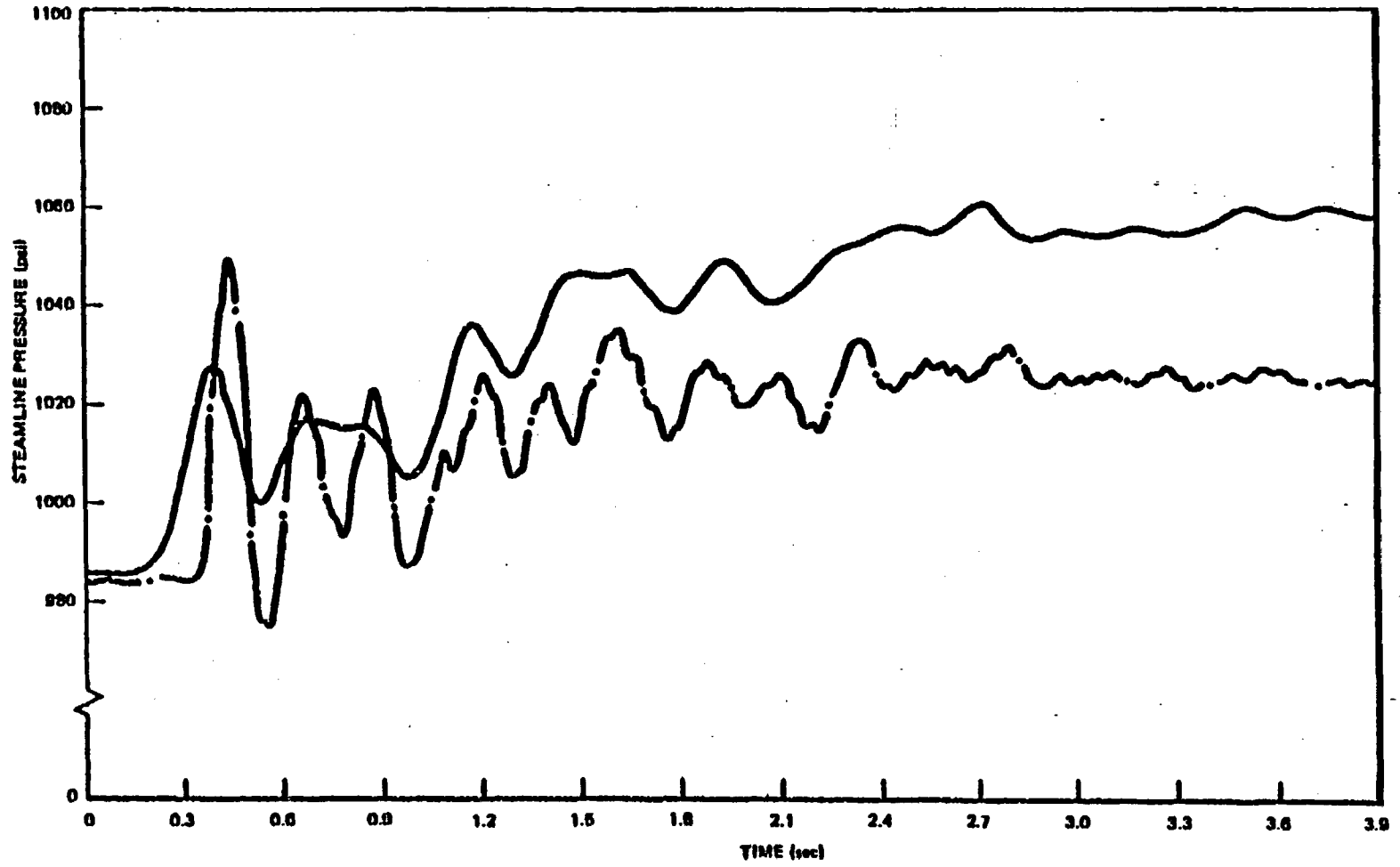
Figure 3-4. Peach Bottom-2 Rod Insertion Fraction Versus Time



NEED-24154-A

Figure 3-5. Peach Bottom Eight-Node Steamline Schematic

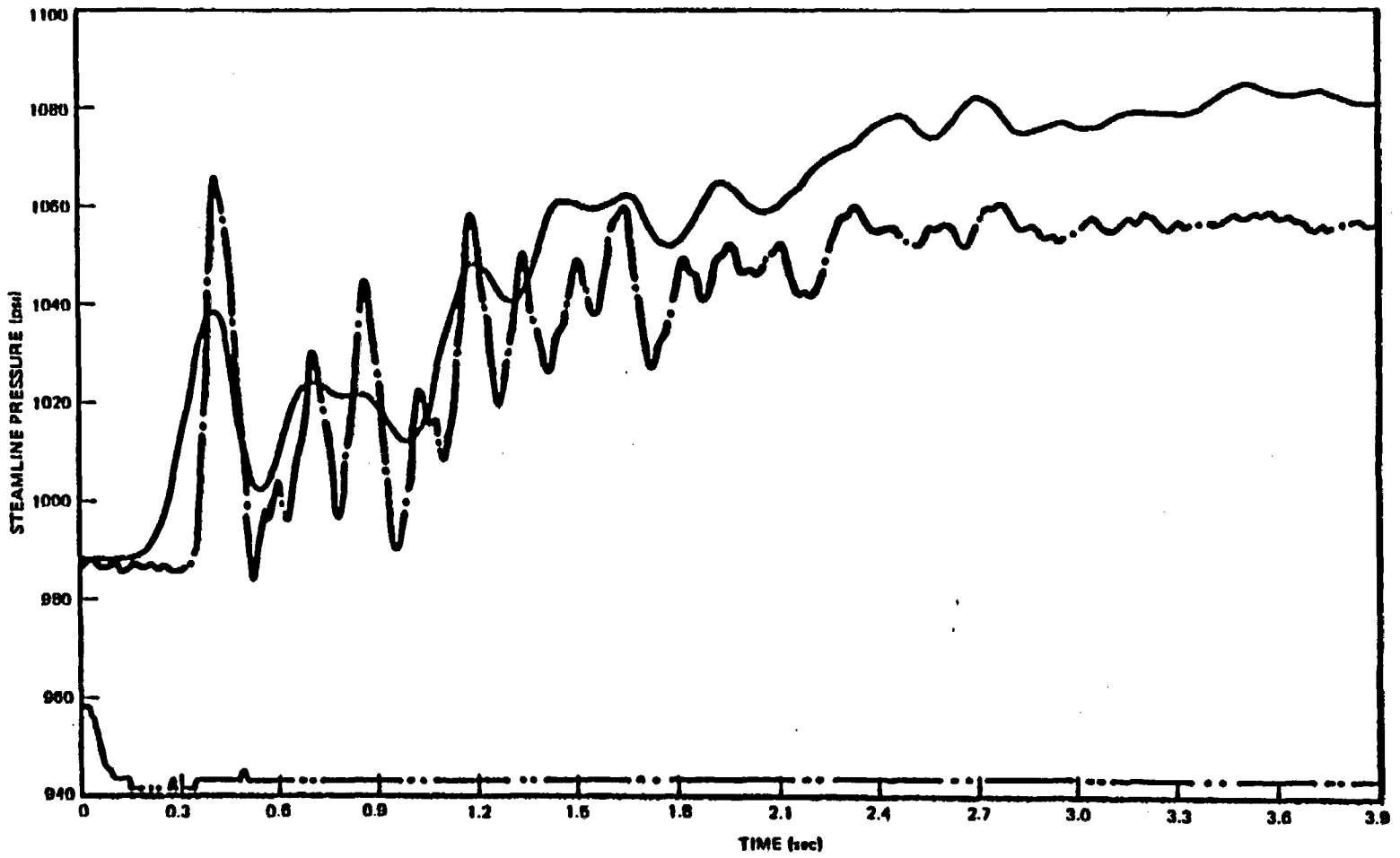
3-24



NEDO-24154-A

Figure 3-6. Peach Bottom-2 Turbine Trip 1 Steamline Pressure

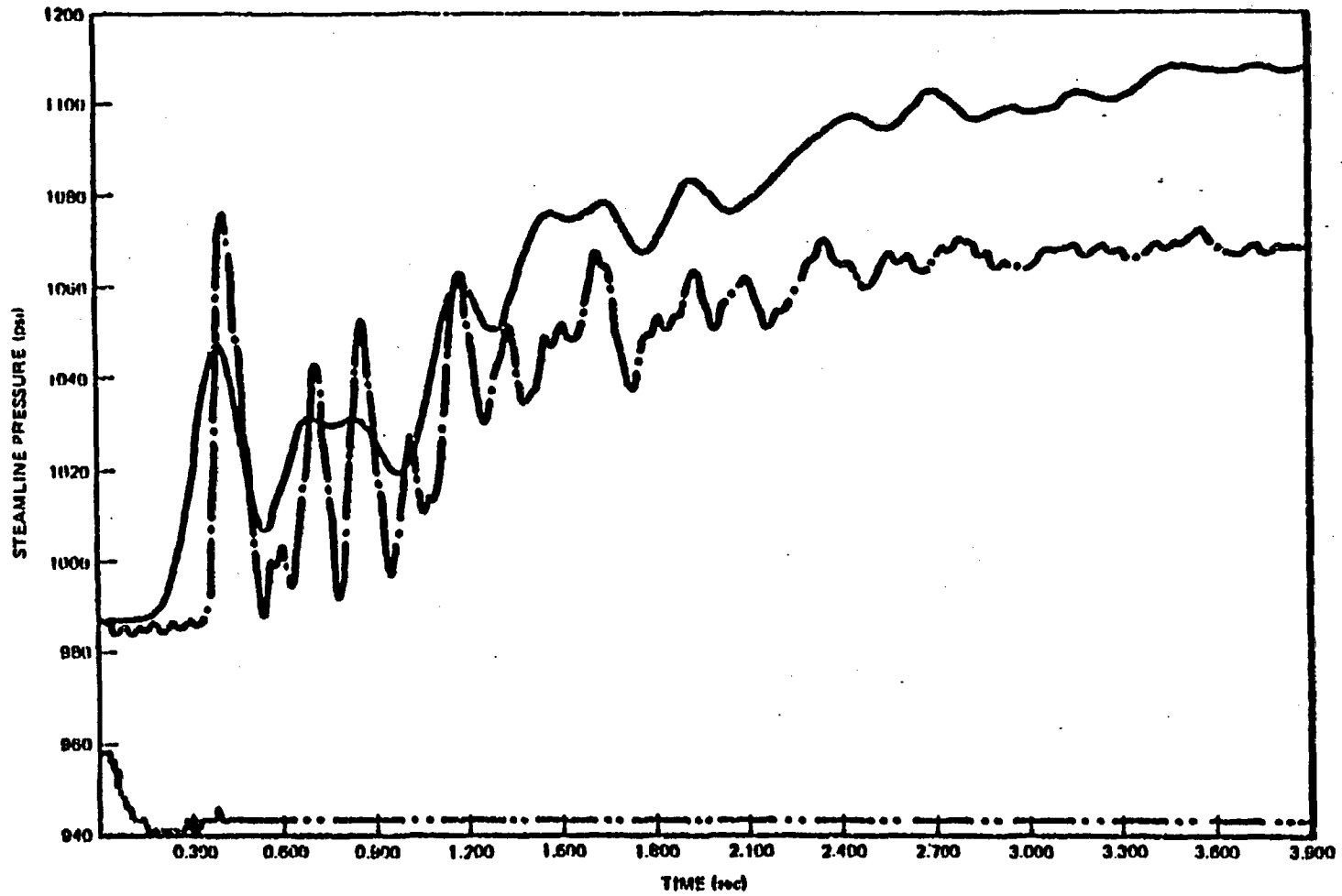
3-25



NEDO-24154-A

Figure 3-7. Peach Bottom-2 Turbine Trip 2 Steamline Pressure

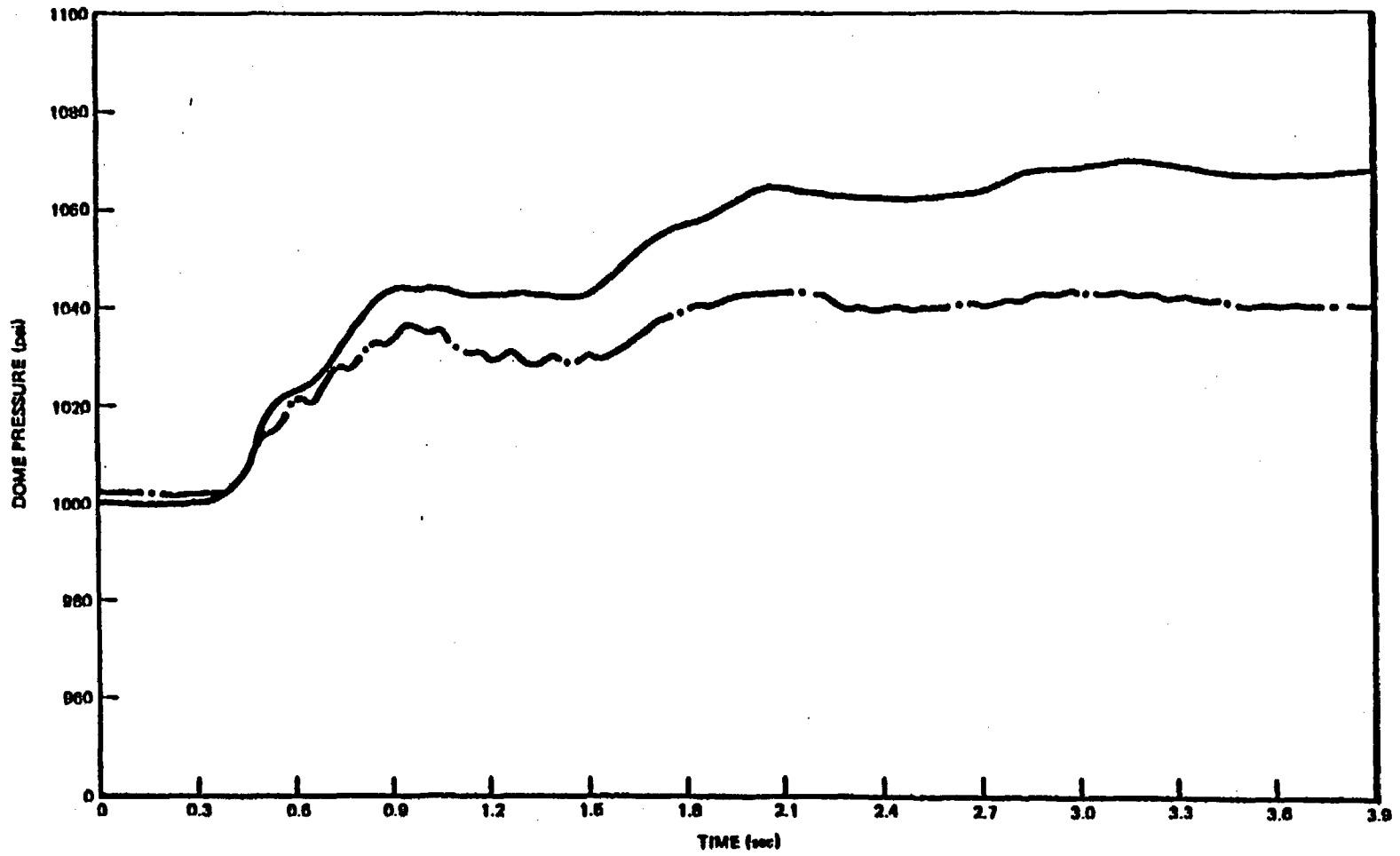
3-26



NEED-24154-A

Figure 3-8. Peach Bottom-2 Turbine Trip 3 Steamline Pressure

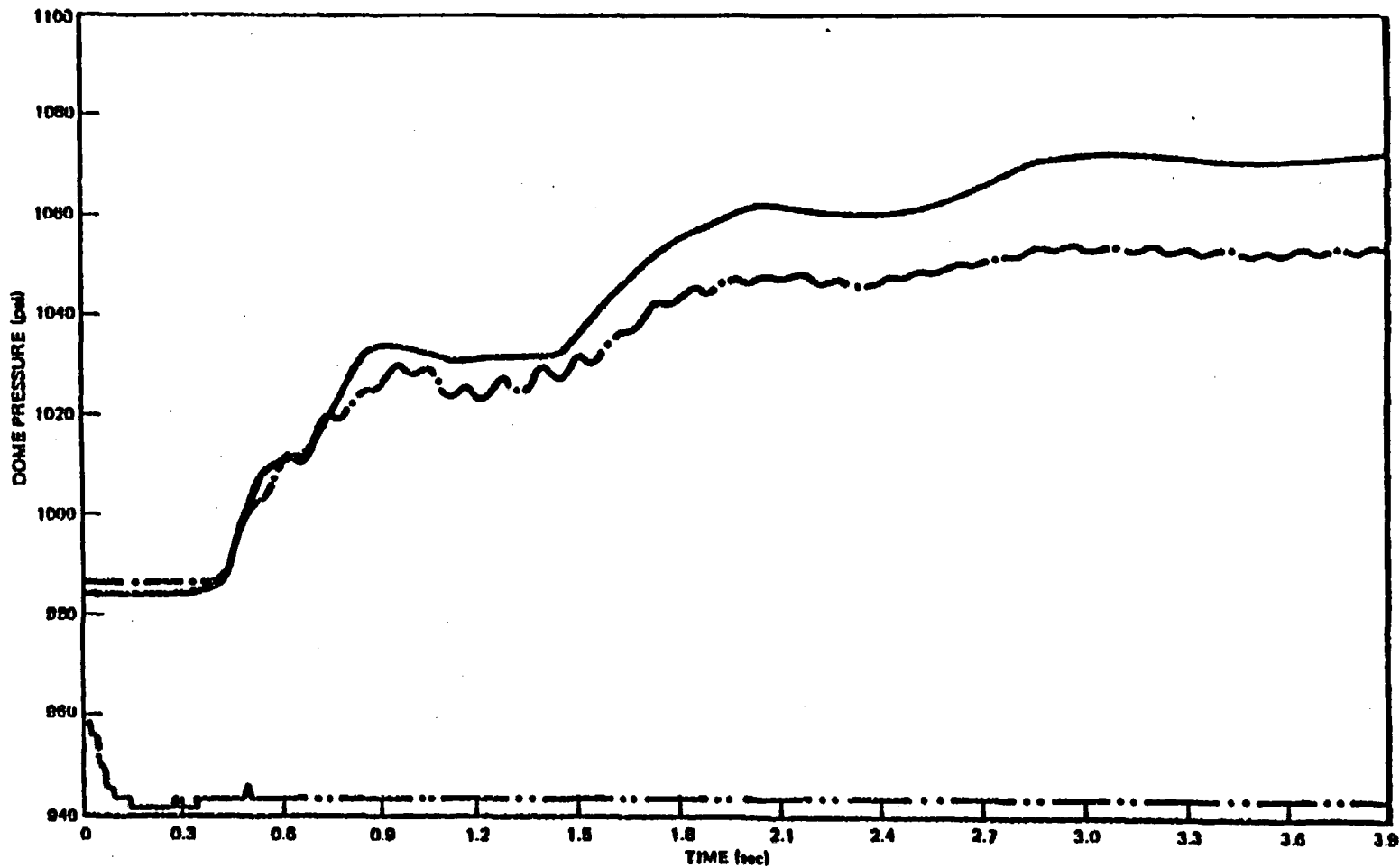
3-27



NEDO-24154-A

Figure 3-9. Peash Bottom-2 Turbine Trip 1 Dome Pressure

3-28



NEDO-24154-A

Figure 3-10. Peach Bottom-2 Turbine Trip 2 Dome Pressure

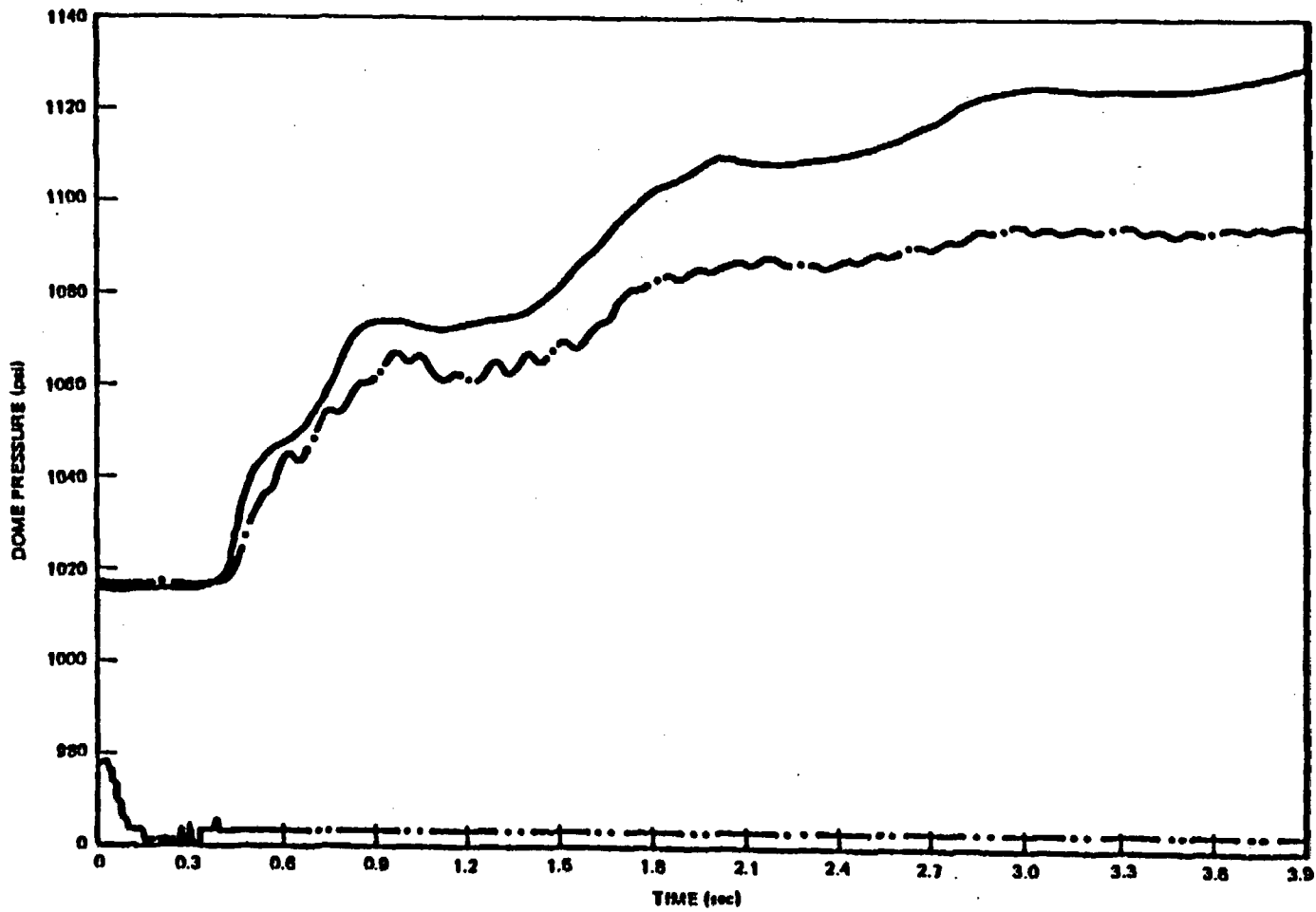
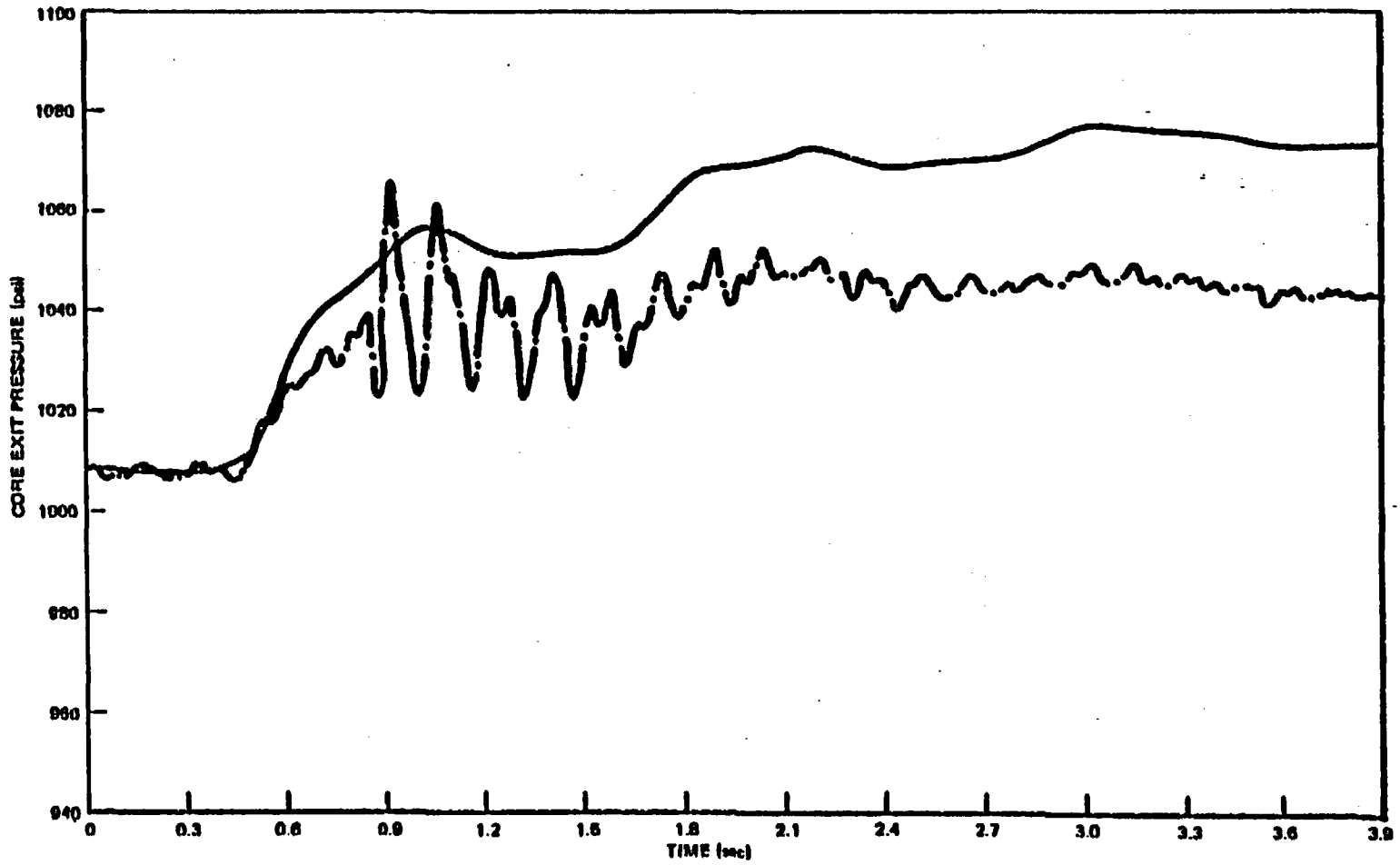


Figure 3-11. Peach Bottom-2 Turbine Trip 3 Dome Pressure

3-30



NEEO-24154-A

Figure 3-12. Peach Bottom-2 Turbine Trip 1 Core Exit Pressure

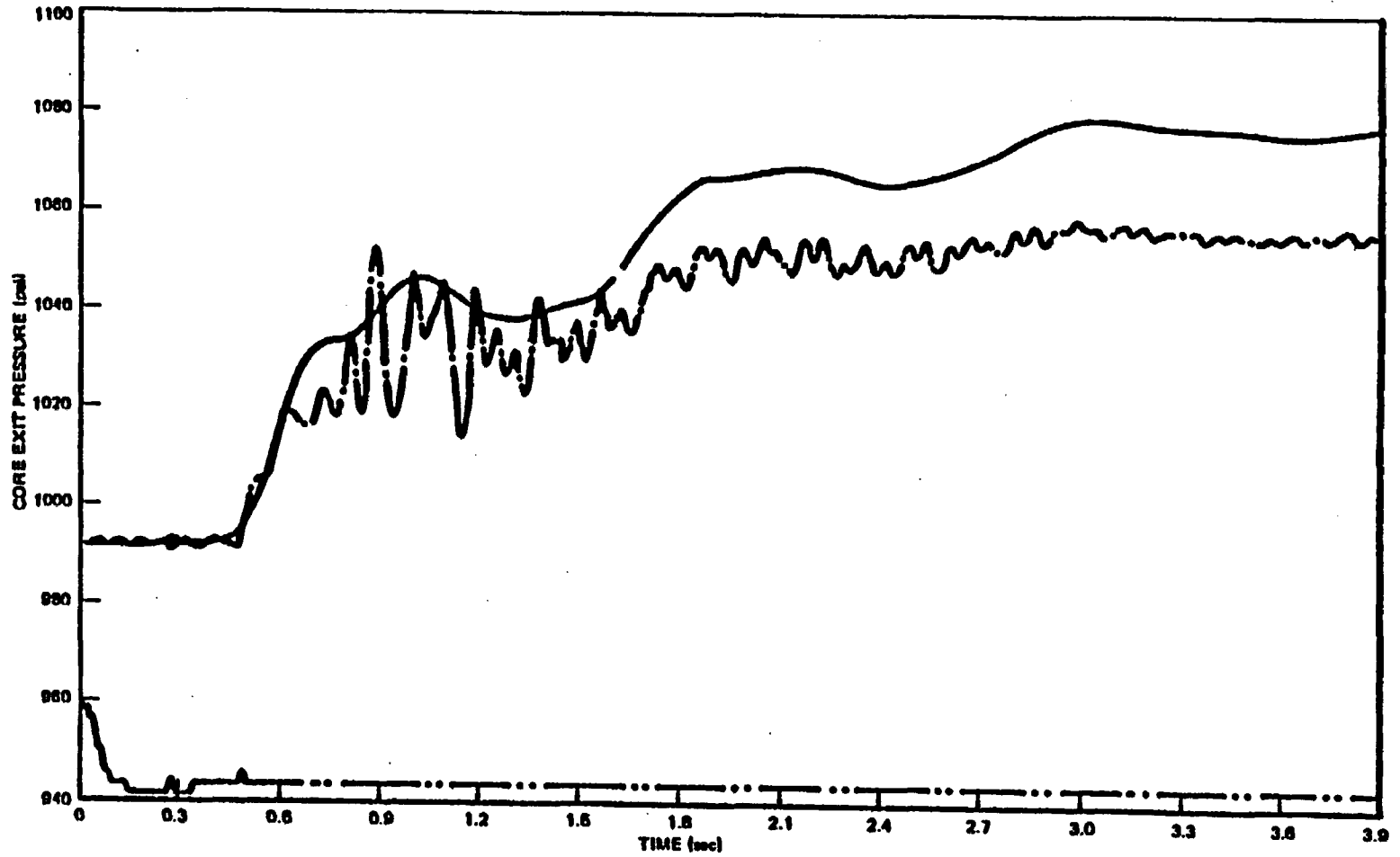
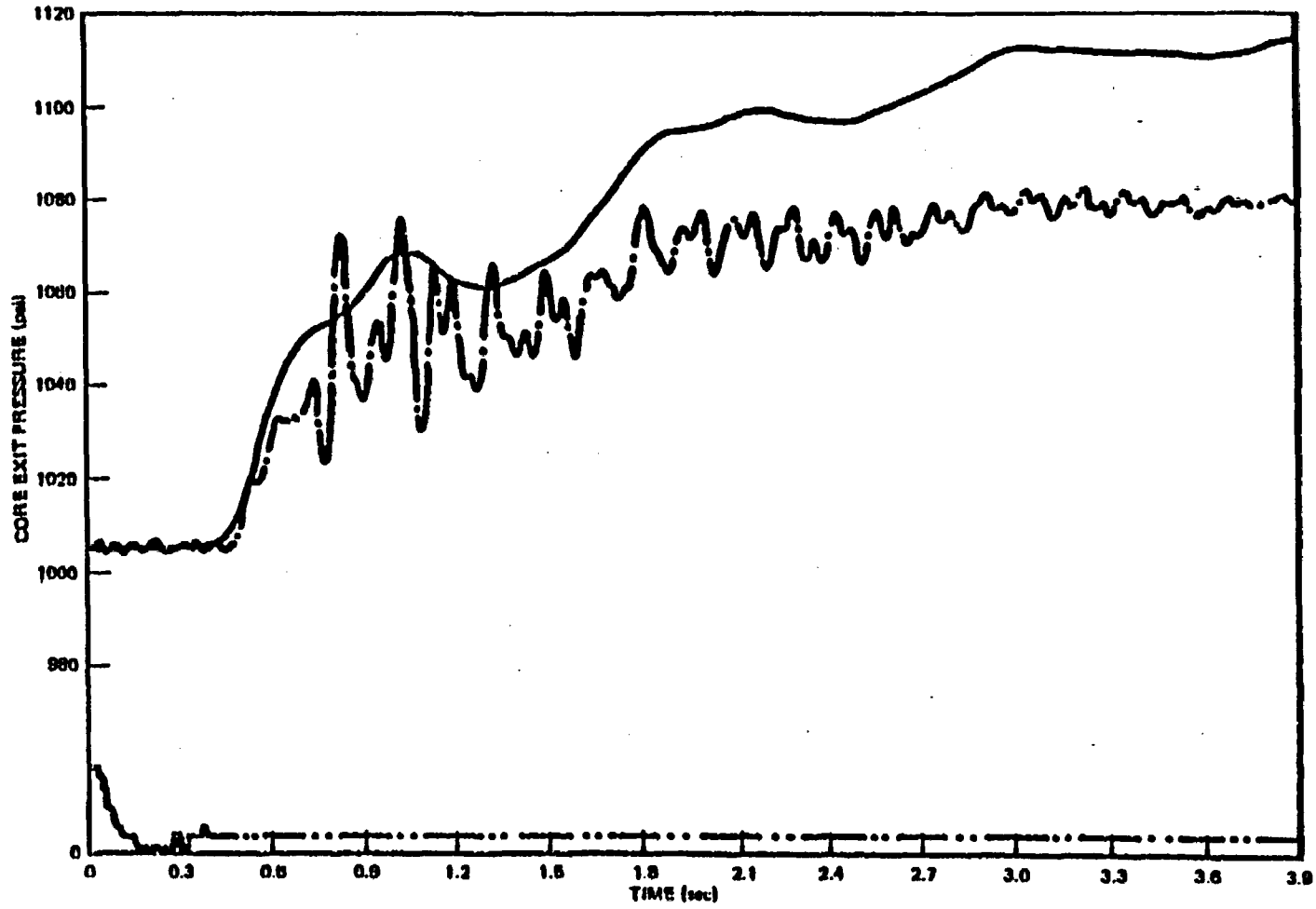


Figure 3-13. Peach Bottom-2 Turbine Trip 2 Core Exit Pressure

3-22



NEED-24154-A

Figure 3-14. Peach Bottom-2 Turbine Trip 3 Core Exit Pressure

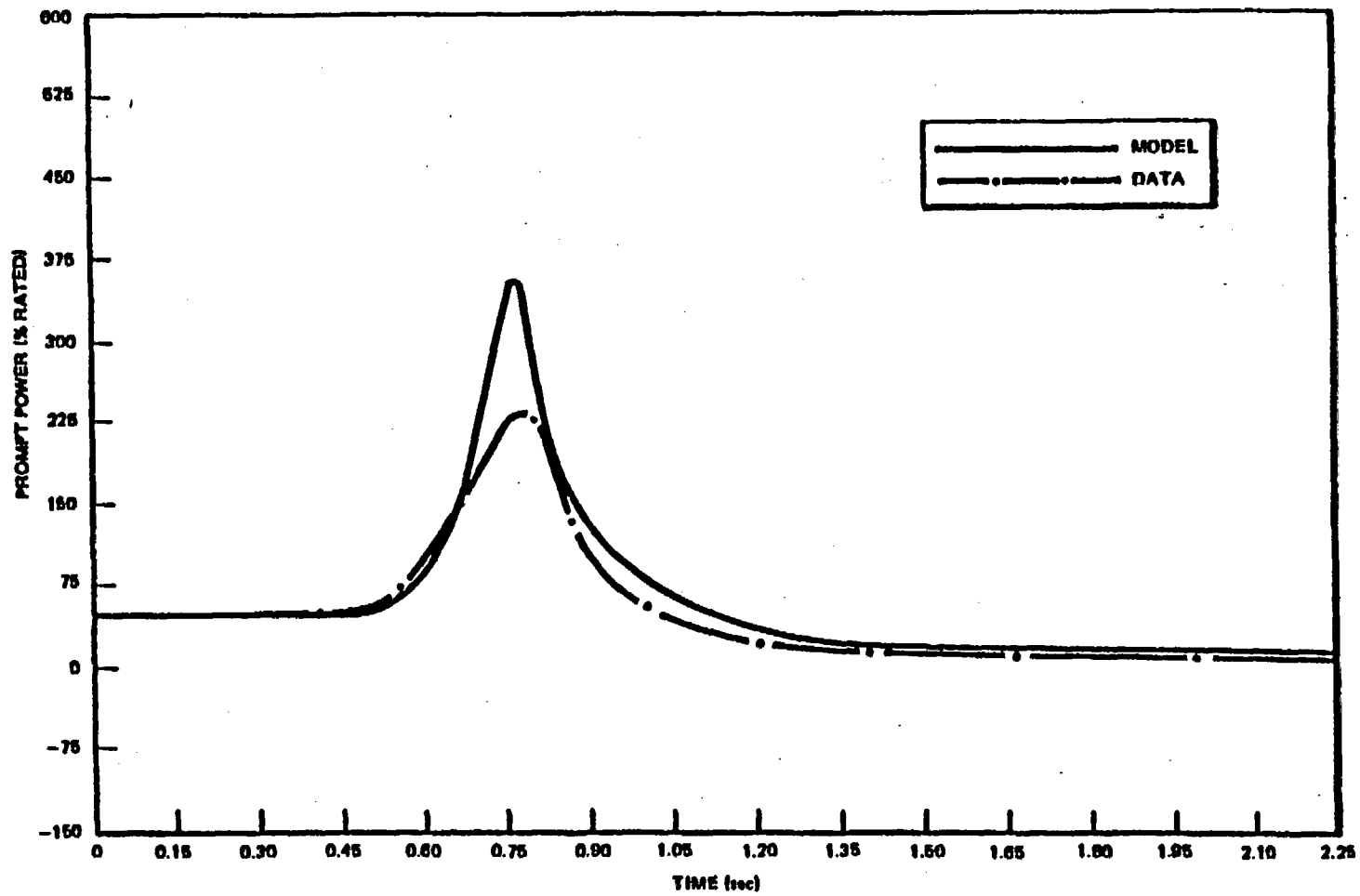
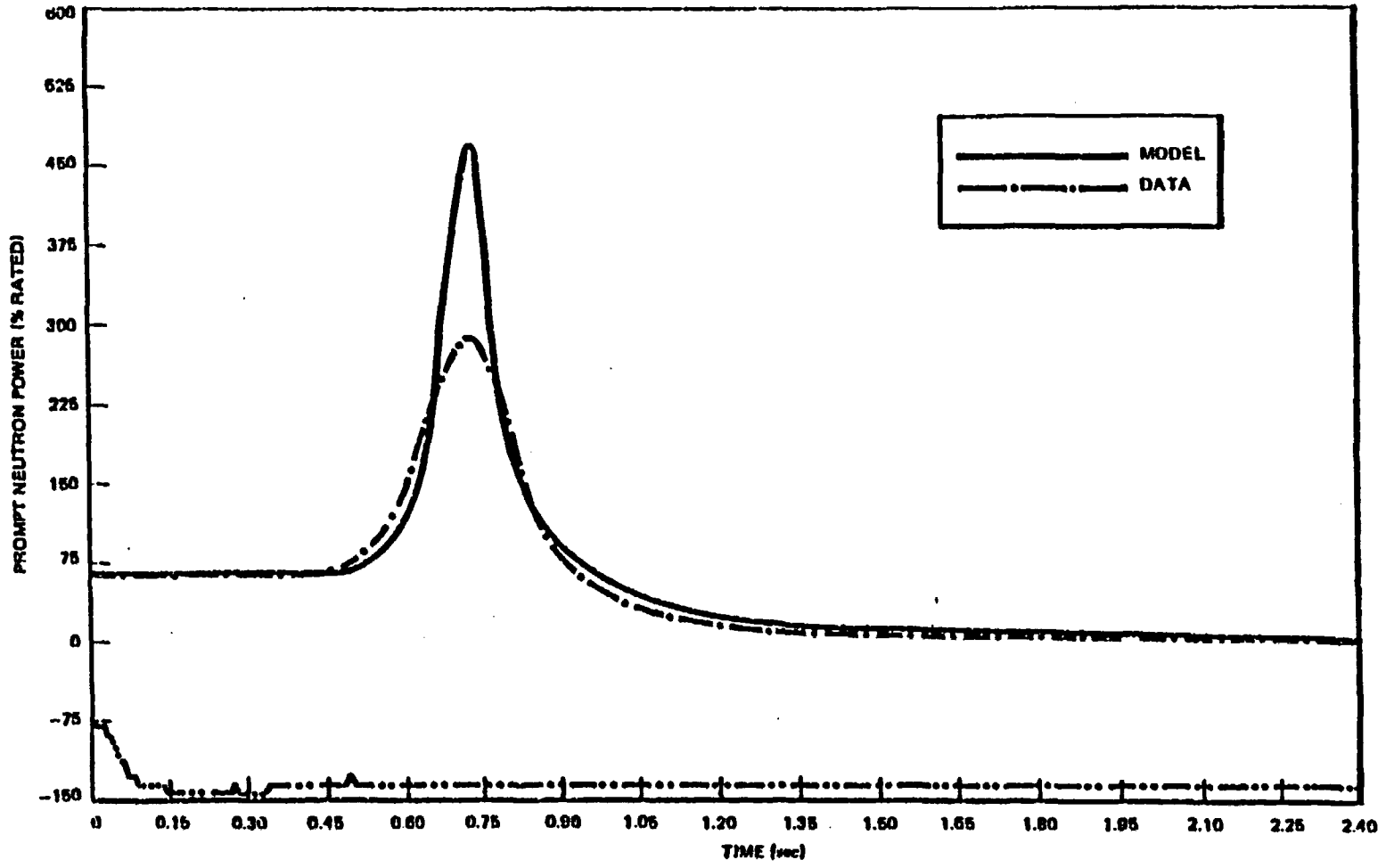


Figure 3-15. Peach Bottom-2 Turbine Trip 1 Prompt Neutron Power

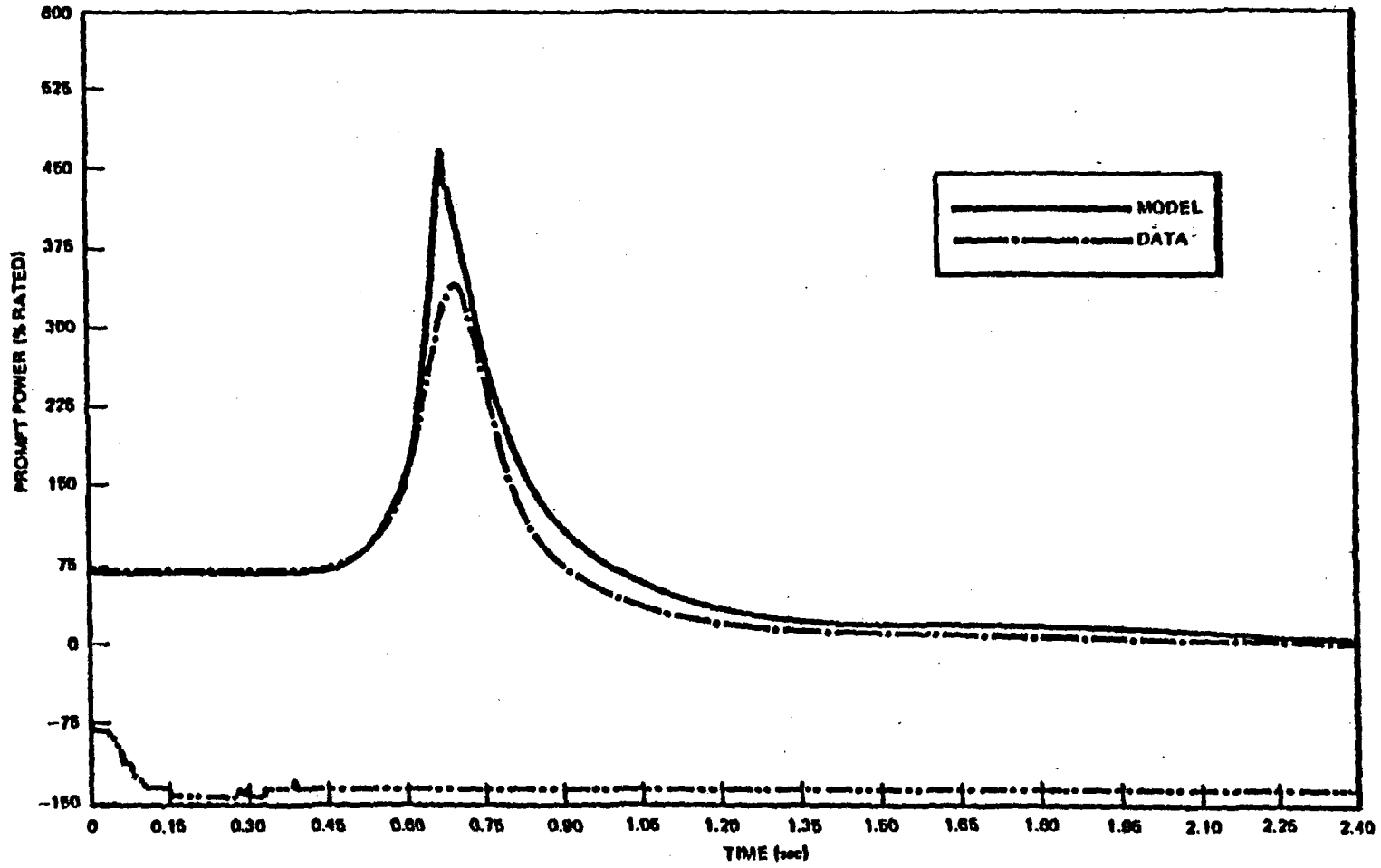
3-34



NEEDO-24154-A

Figure 3-16. Peach Bottom-2 Turbine Trip 2 Prompt Neutron Power

3-35



NEDO-24154-A

Figure 3-17. Peach Bottom-2 Turbine Trip 3 Prompt Neutron Power.

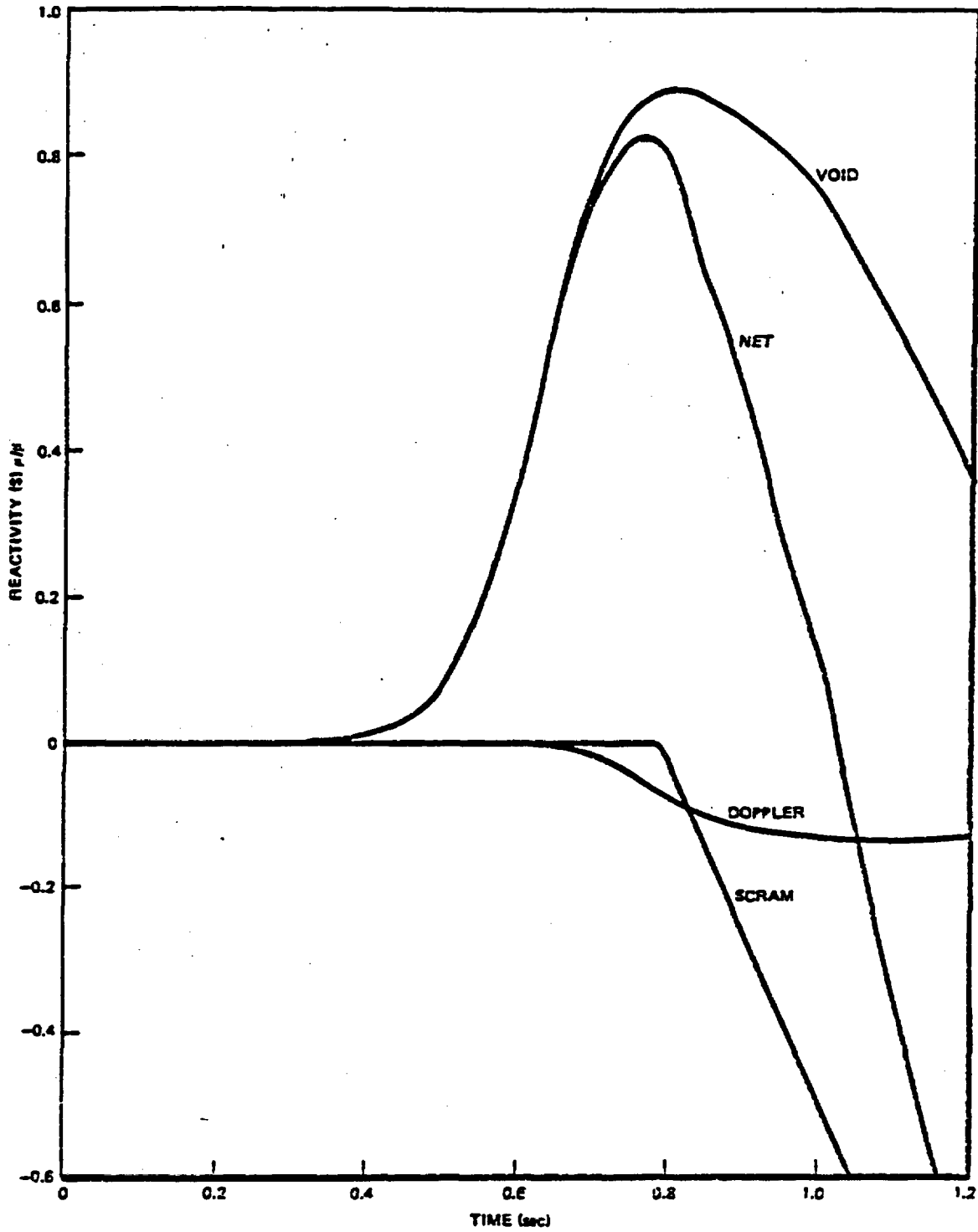


Figure 3-18. Peach Bottom-2 Reactivity Turbine Trip 1

NEDO-24154-A

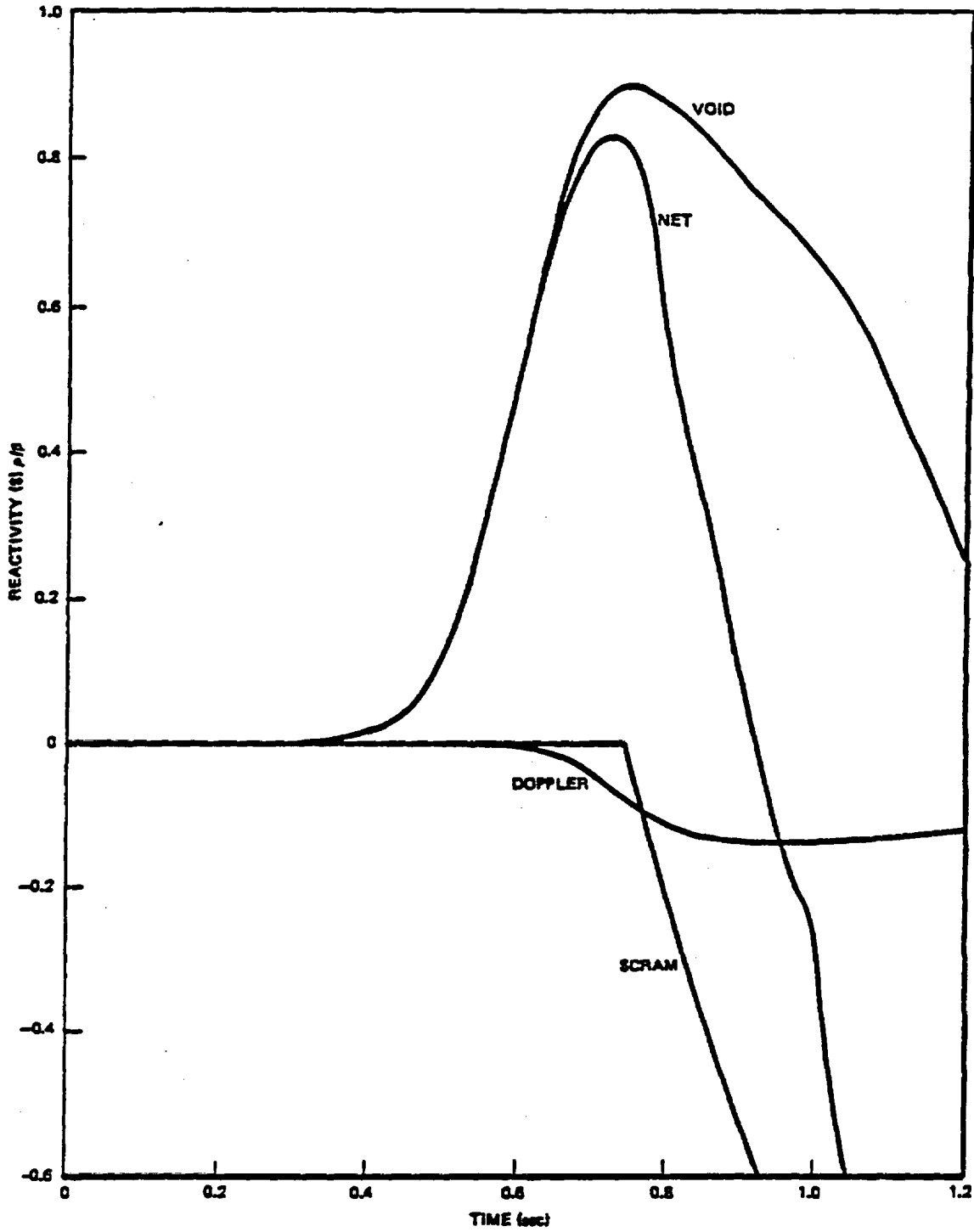


Figure 3-19. Peach Bottom-2 Reactivity Turbine Trip 2

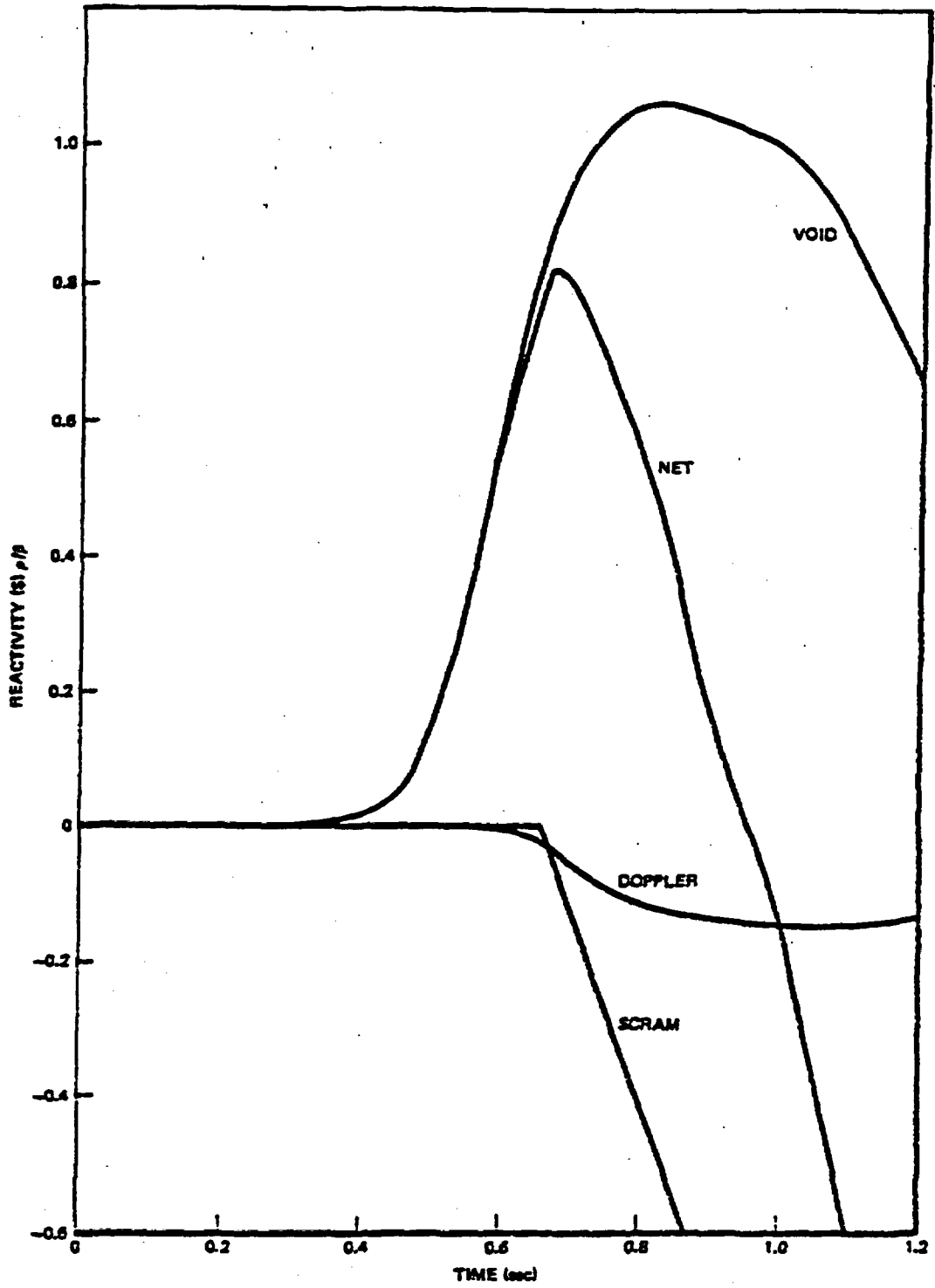


Figure 3-20. Peach Bottom-2 Reactivity Turbine Trip 3

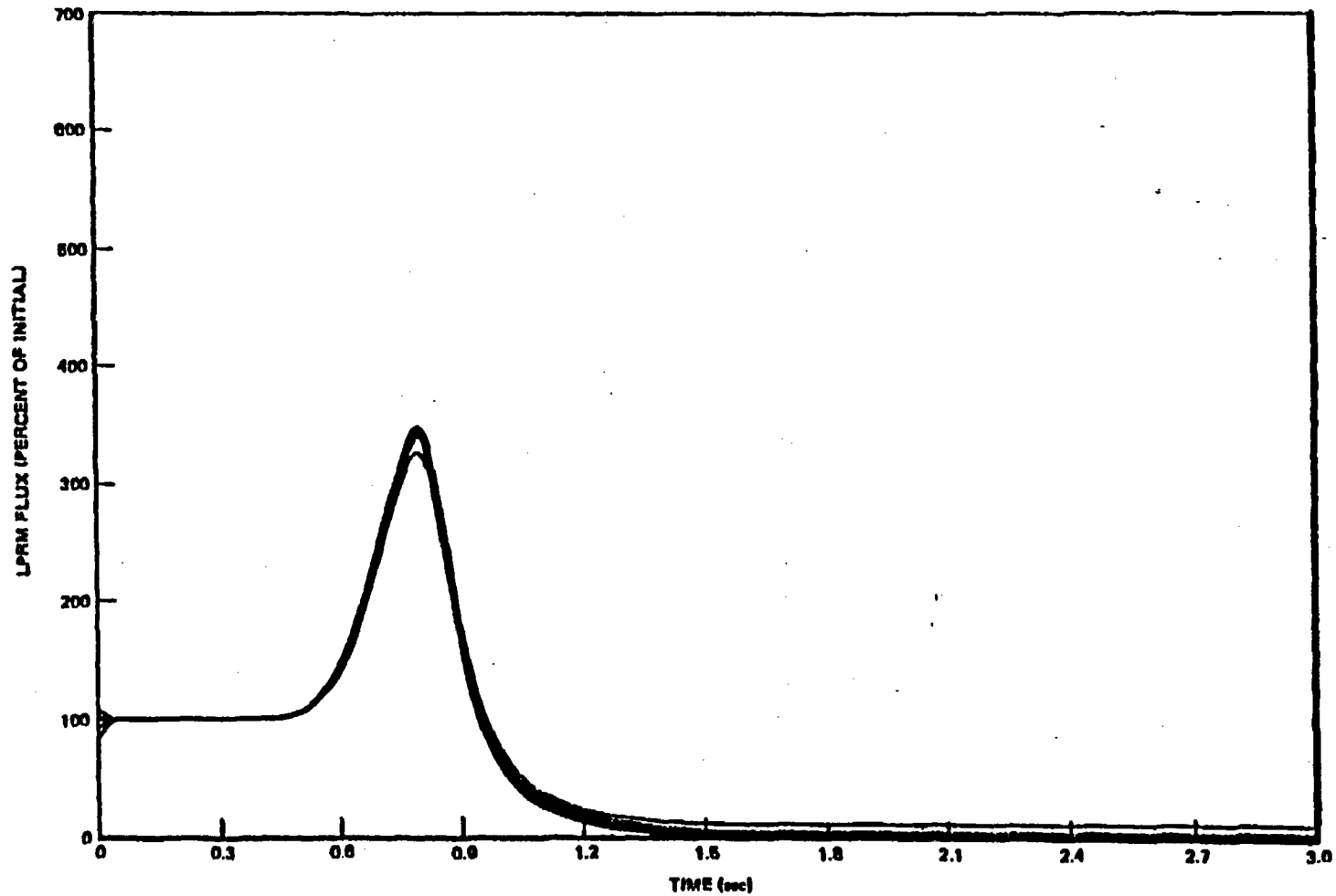
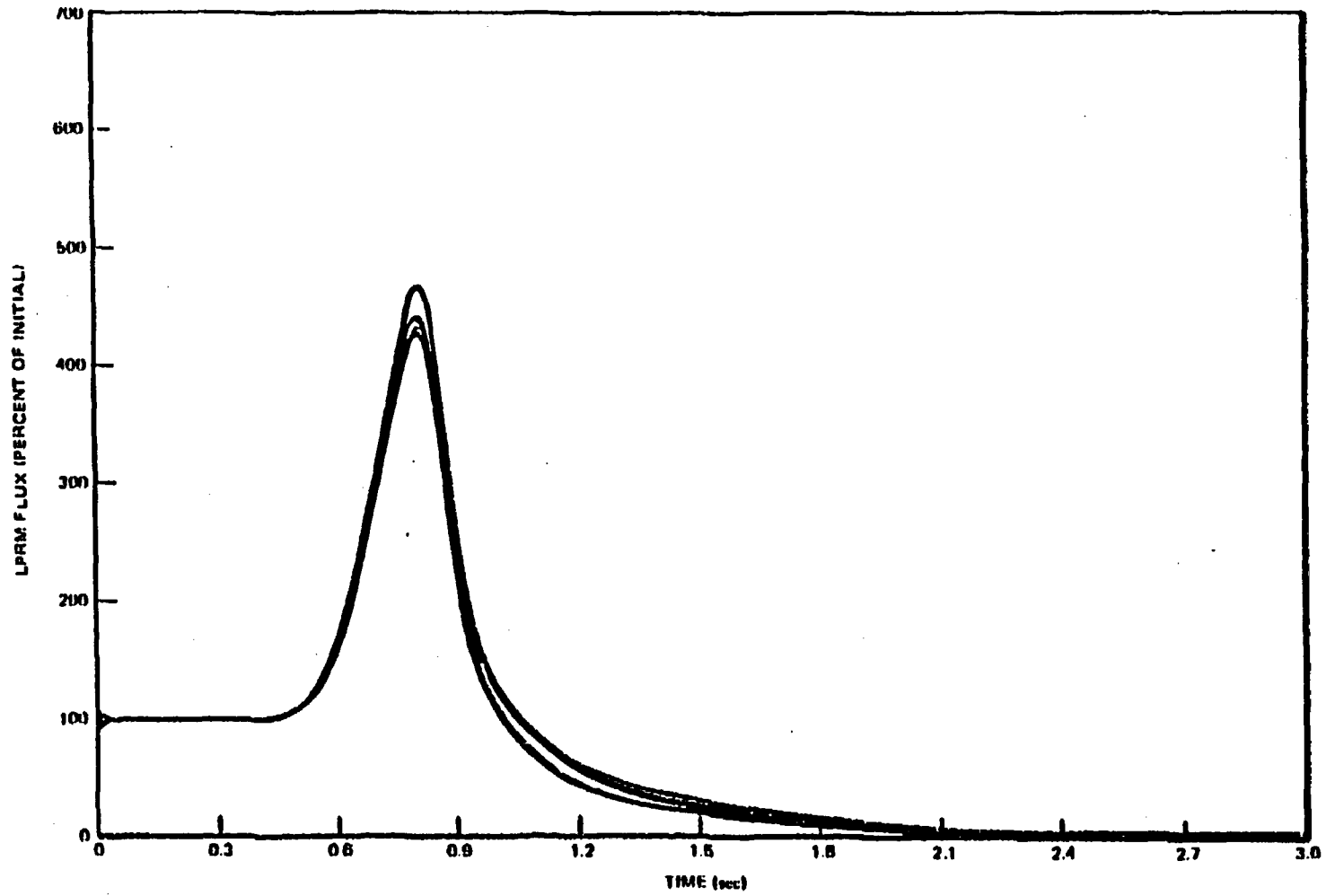


Figure 3-21. Peach Bottom-2 A Level LPRM's Turbine Trip 1

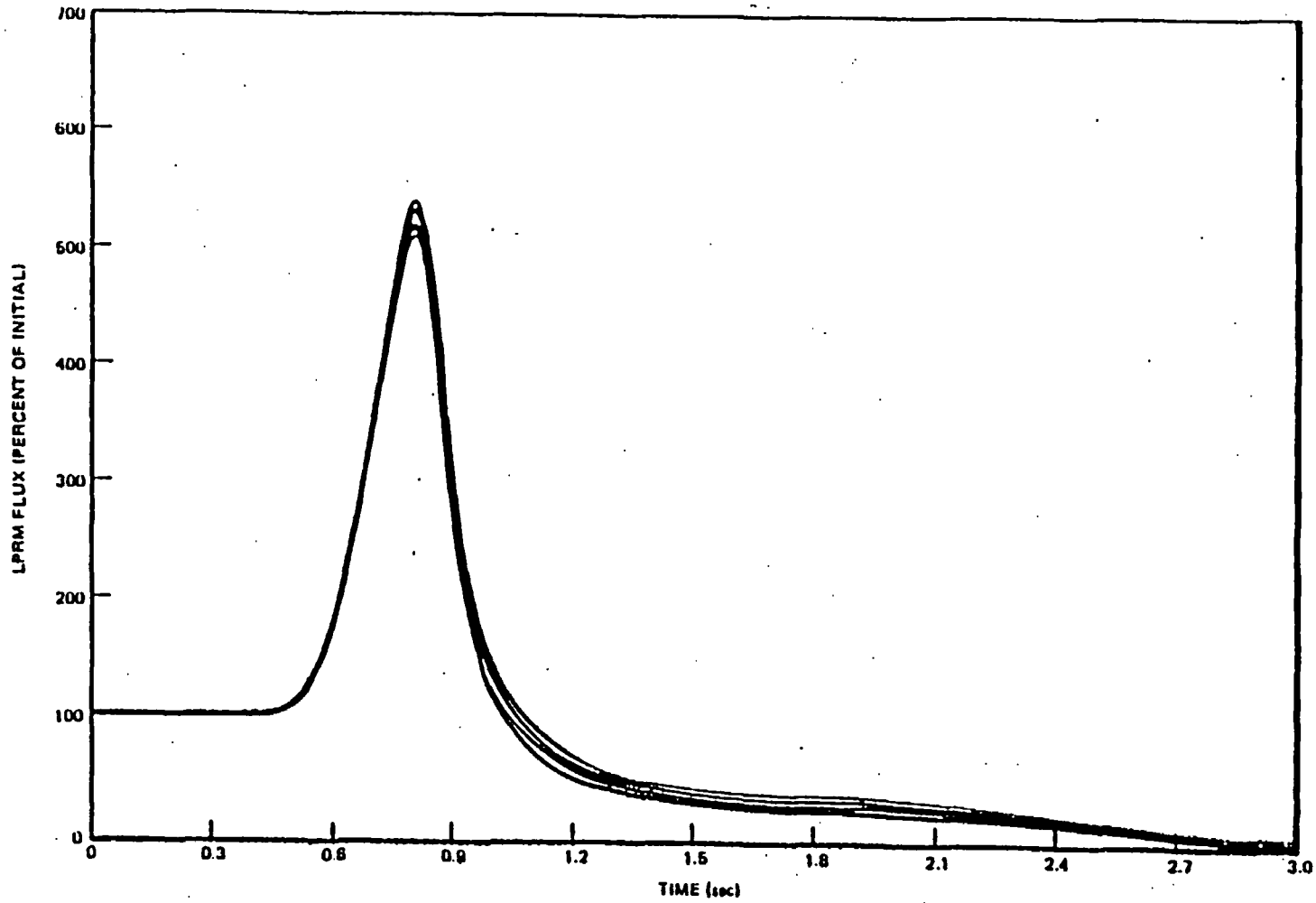
3-40



NEEDO-24154-A

Figure 3-22. Peach Bottom-2 B Level LPRM's Turbine Trip 1

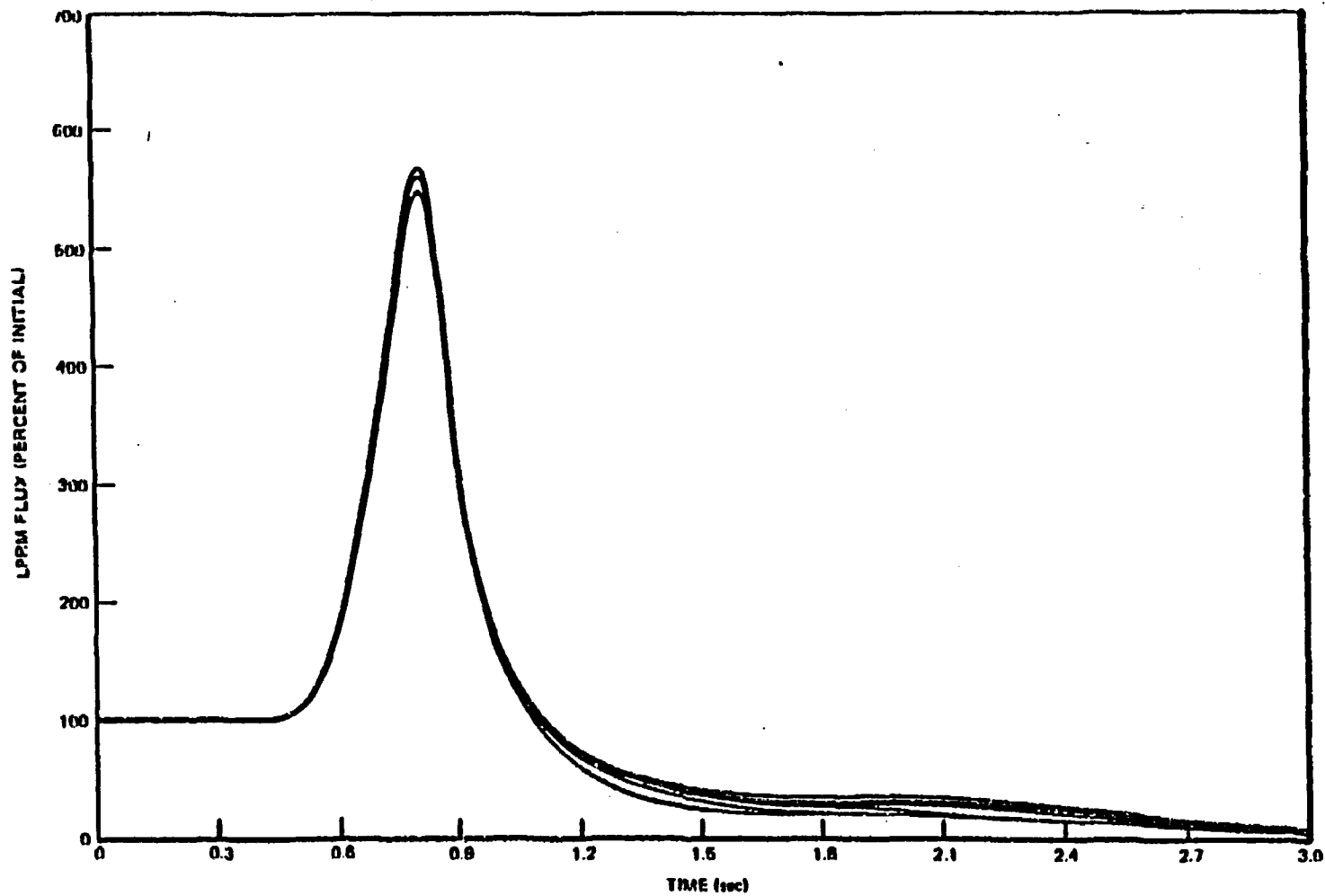
3-41



NEDO-24154-A

Figure 3-23. Peach Bottom-2 G Level LPRM's Turbine Trip 1

3-42



NEED-24154-A

Figure 3-24. Peach Bottom-2 D Level LPRM's Turbine Trip 1

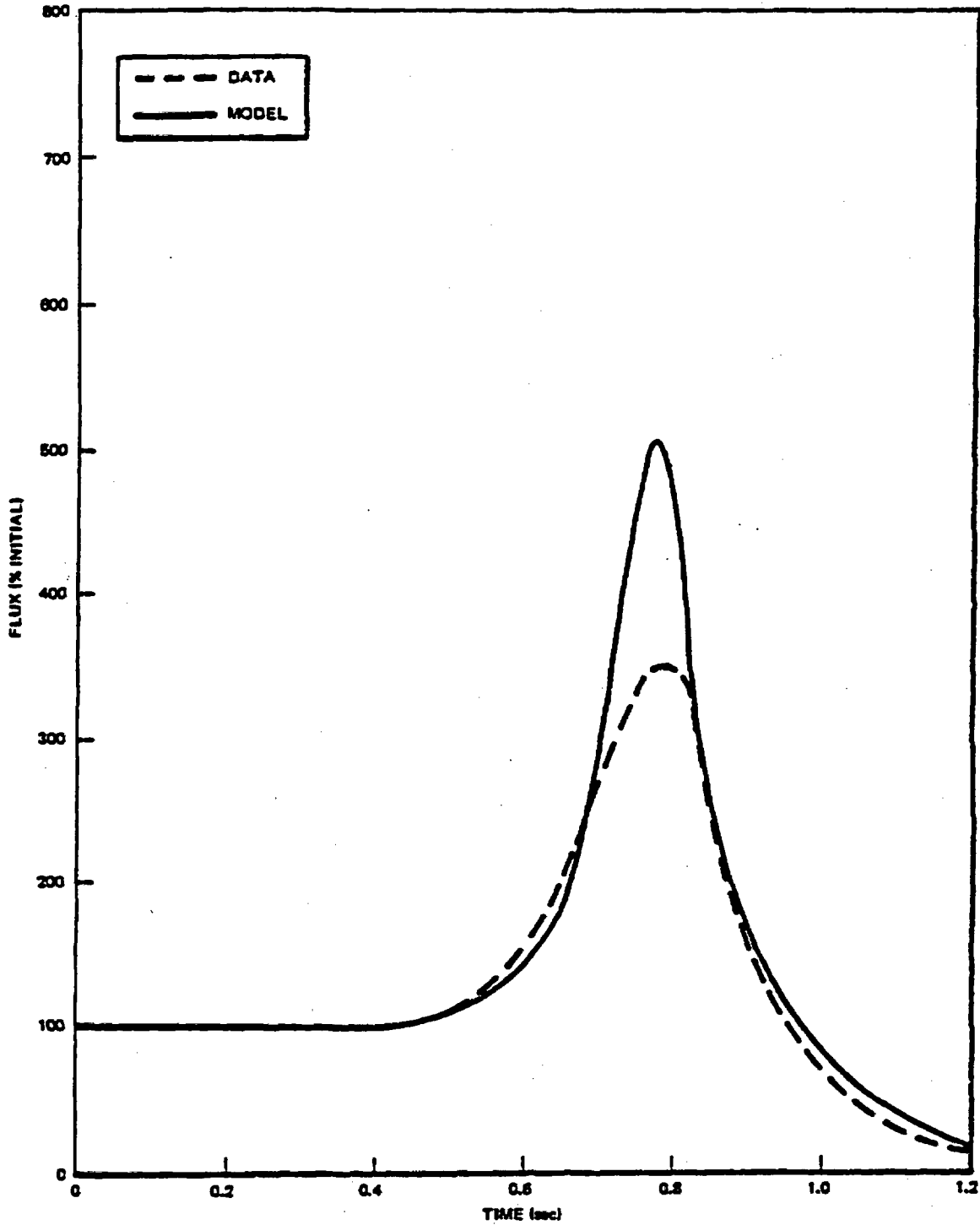


Figure 3-25. Peach Bottom-2 A Level Flux Turbine Trip 1

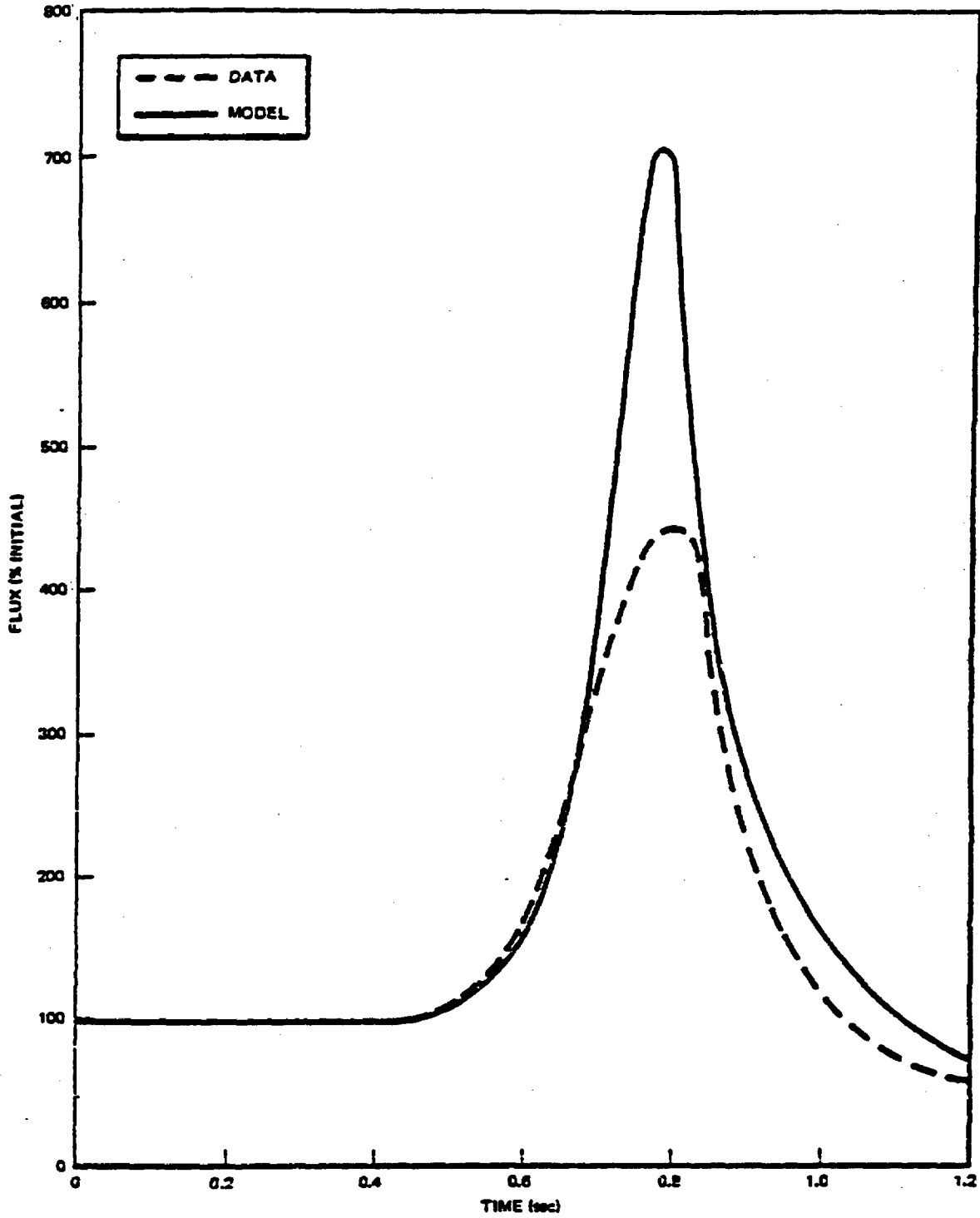


Figure 3-25. Peach Bottom-2 E Level Flux Turbine Trip 1

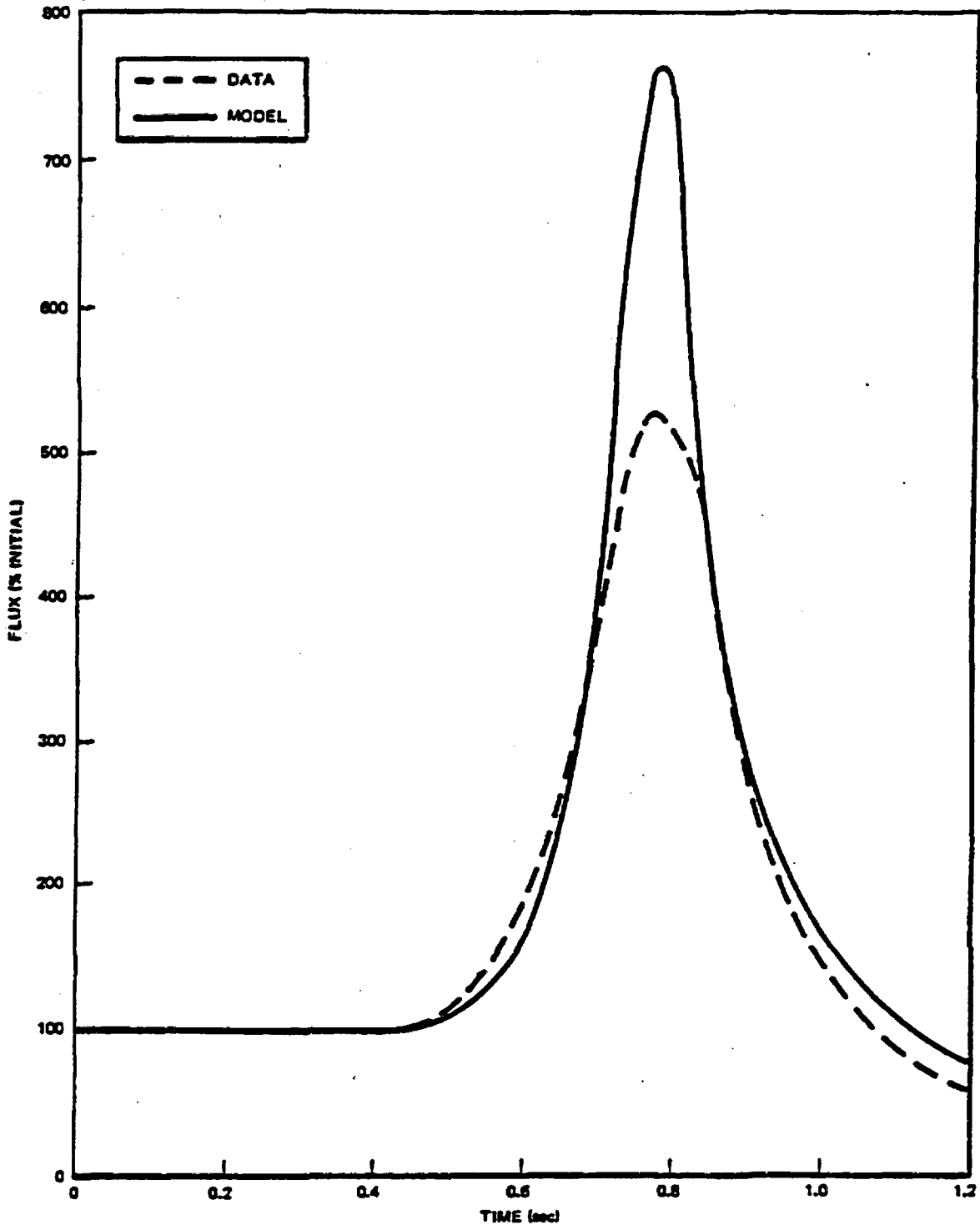


Figure 3-27. Peach Bottom-2 C Level Flux Turbine Trip 1

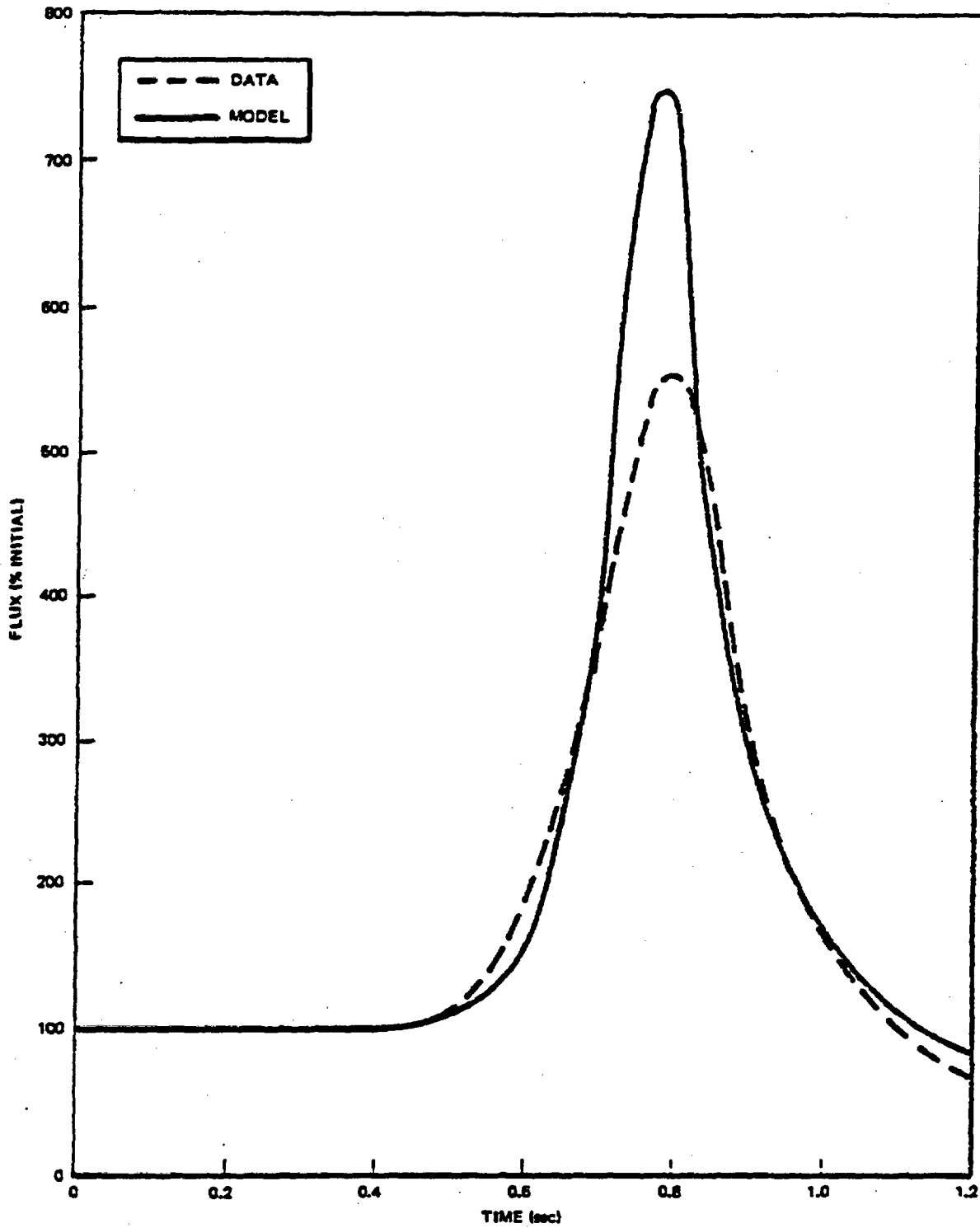


Figure 3-28. Peach Bottom-2 D Level Flux Turbine Trip 1

NEDO-24154-A

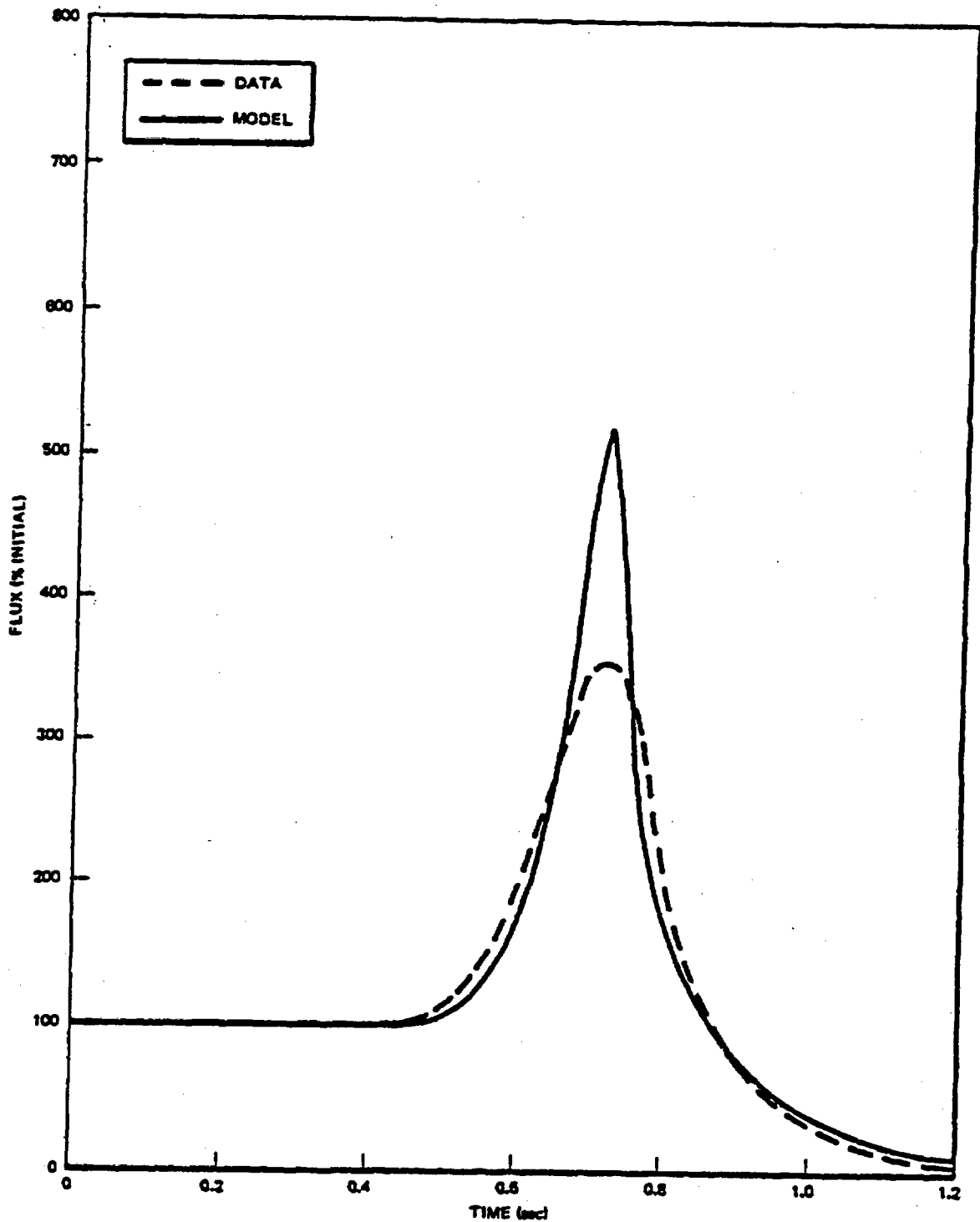


Figure 3-29. Peach Bottom-2 A Level Flux Turbine Trip 2

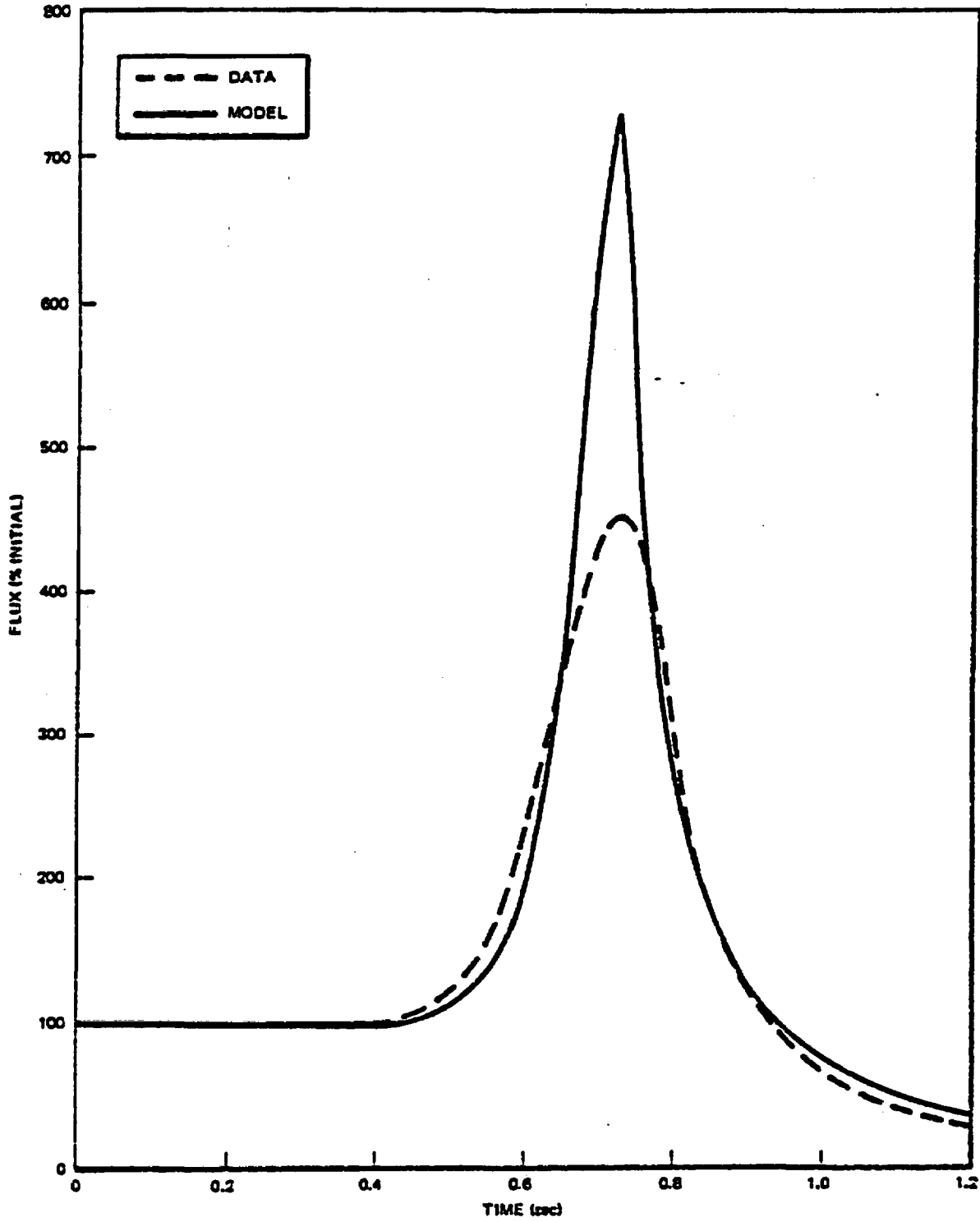


Figure 3-30. Peach Bottom-2 B Level Flux Turbine Trip 2

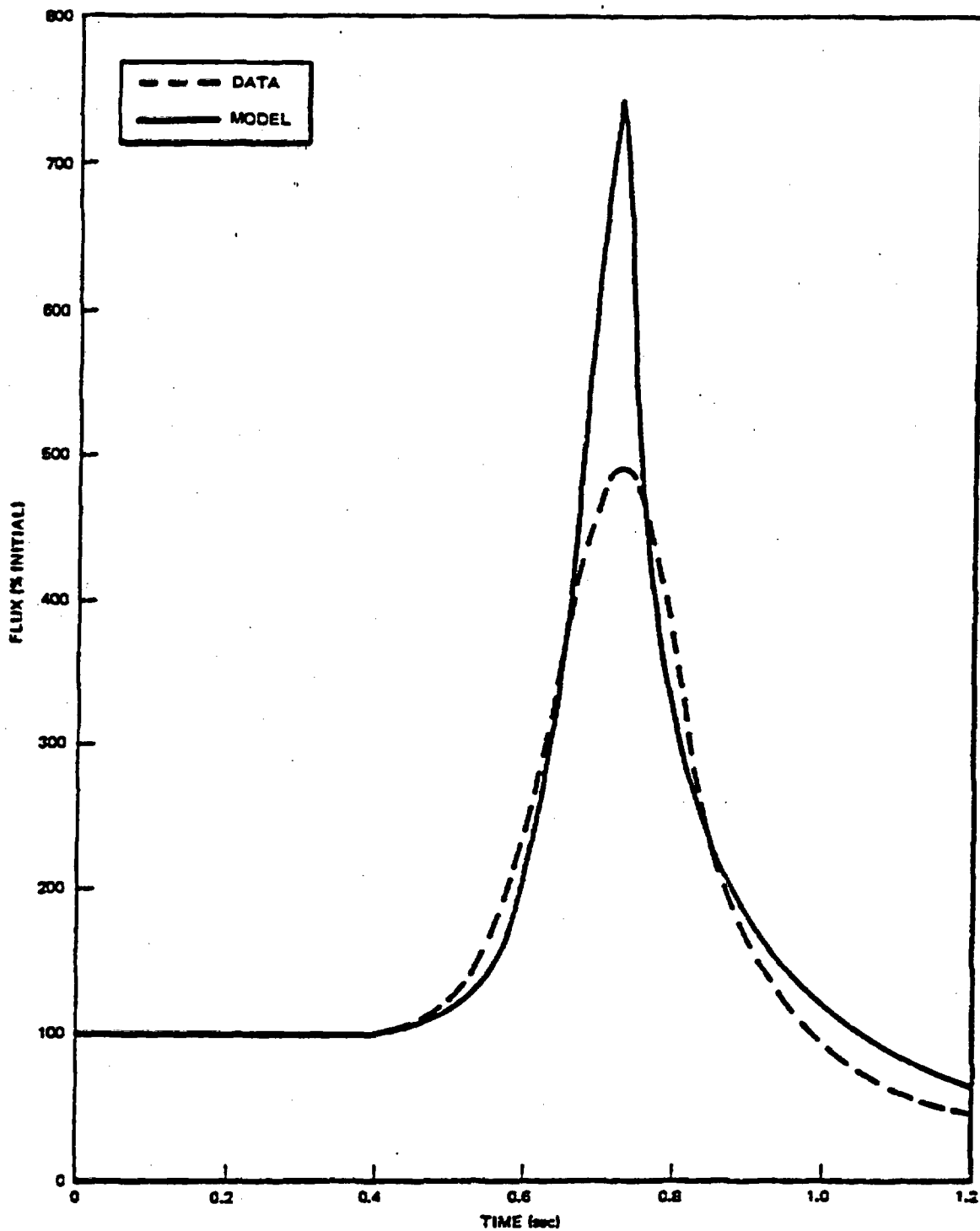


Figure 3-31. Peach Bottom-2 C Level Flux Turbine Trip 2

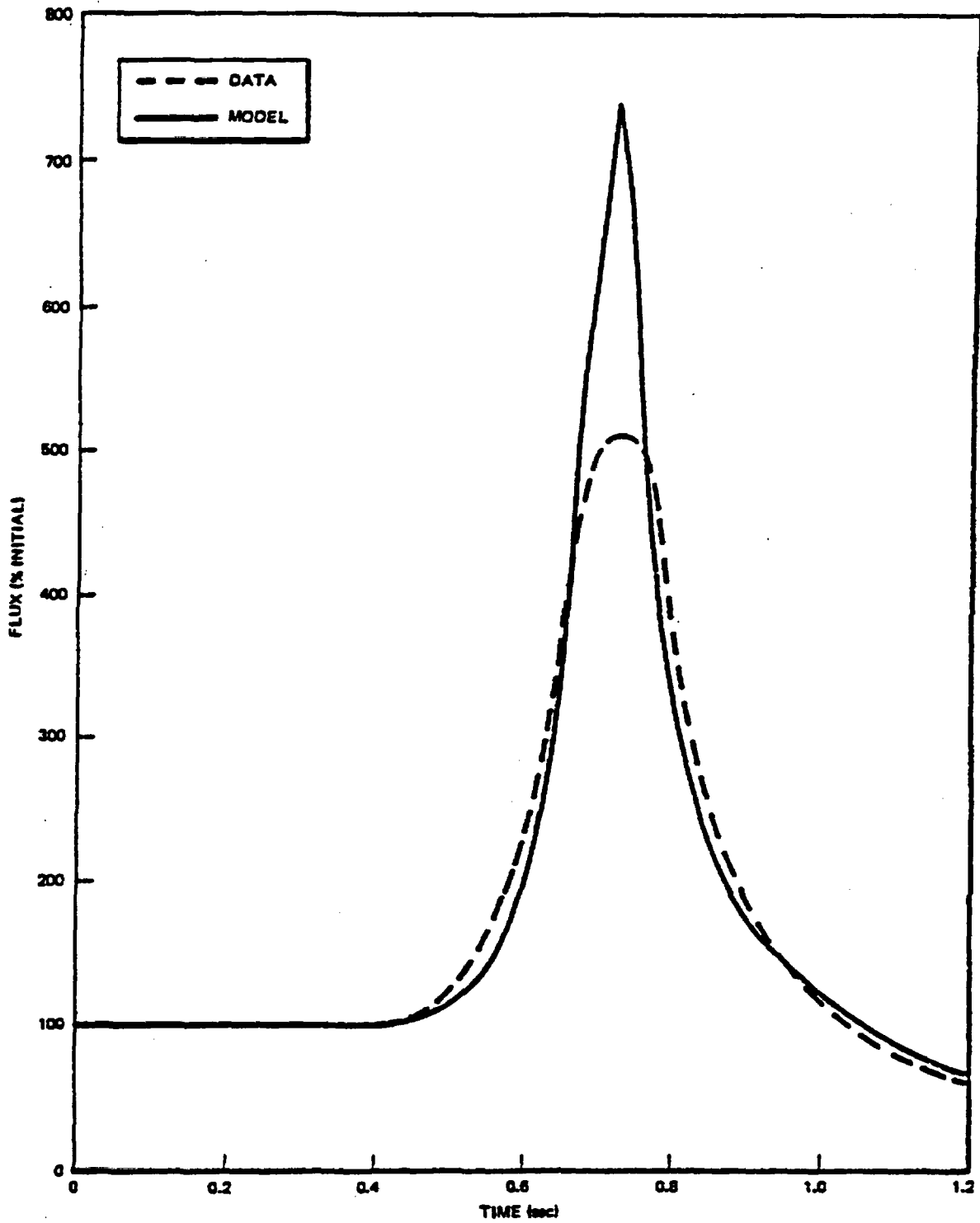


Figure 3-32. Peach Bottom-2 D Level Flux Turbine Trip 2

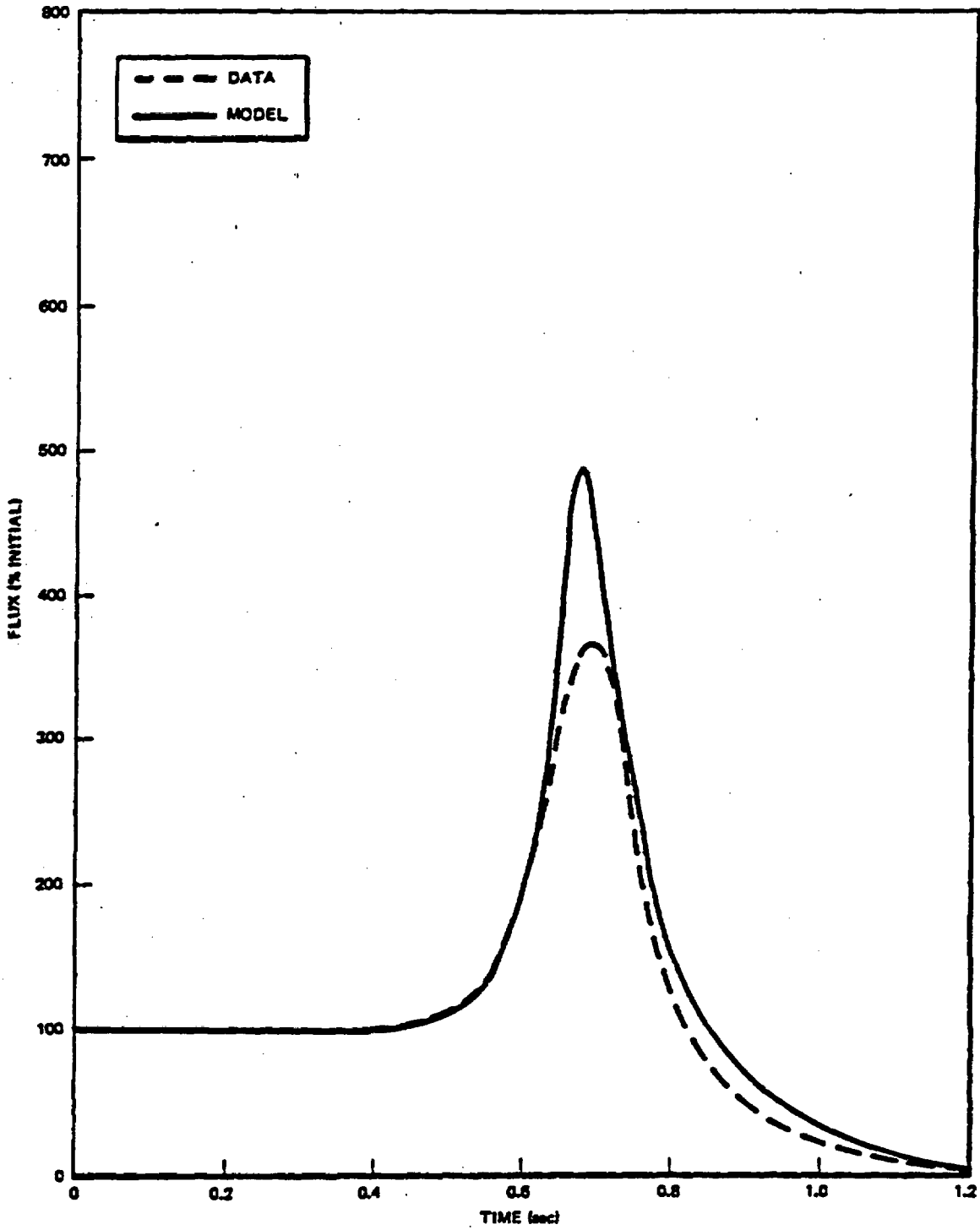


Figure 3-33. Peach Bottom-2 A Level Flux Turbine Trip 3

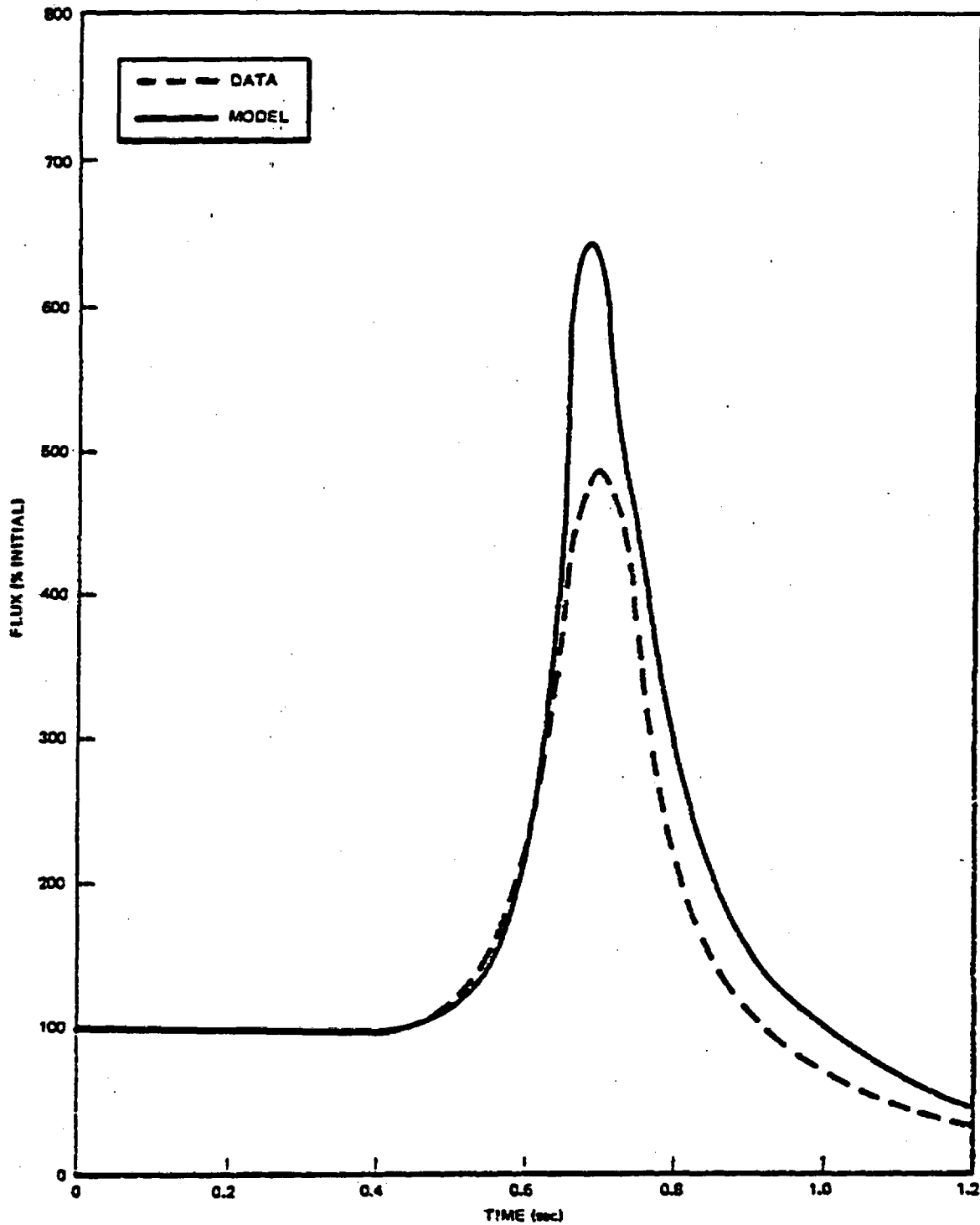


Figure 3-34. Peach Bottom-2 B Level Flux Turbine Trip 3

NEDO-24154-A

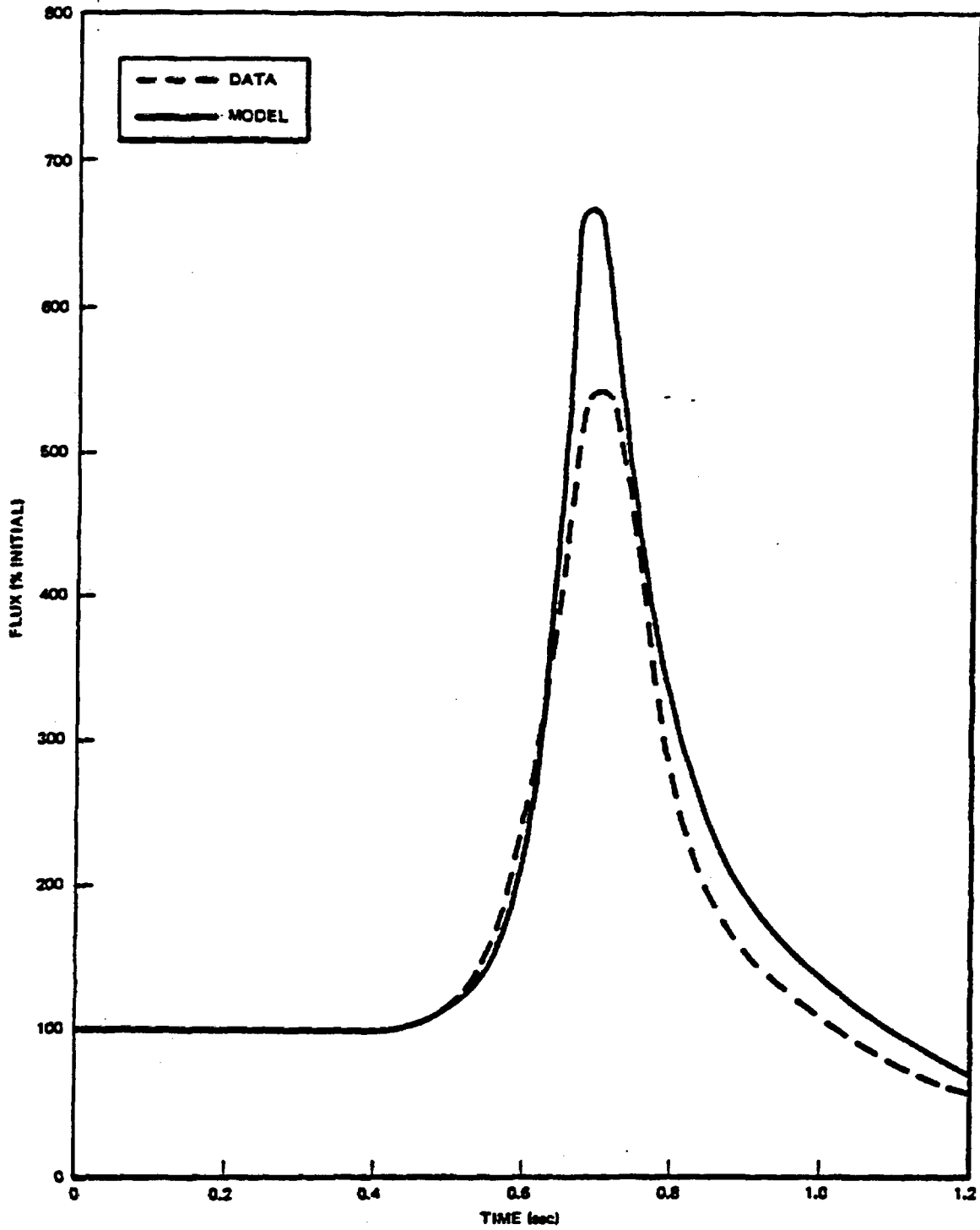


Figure 3-35. Peach Bottom-2 C Level Flux Turbine Trip 3

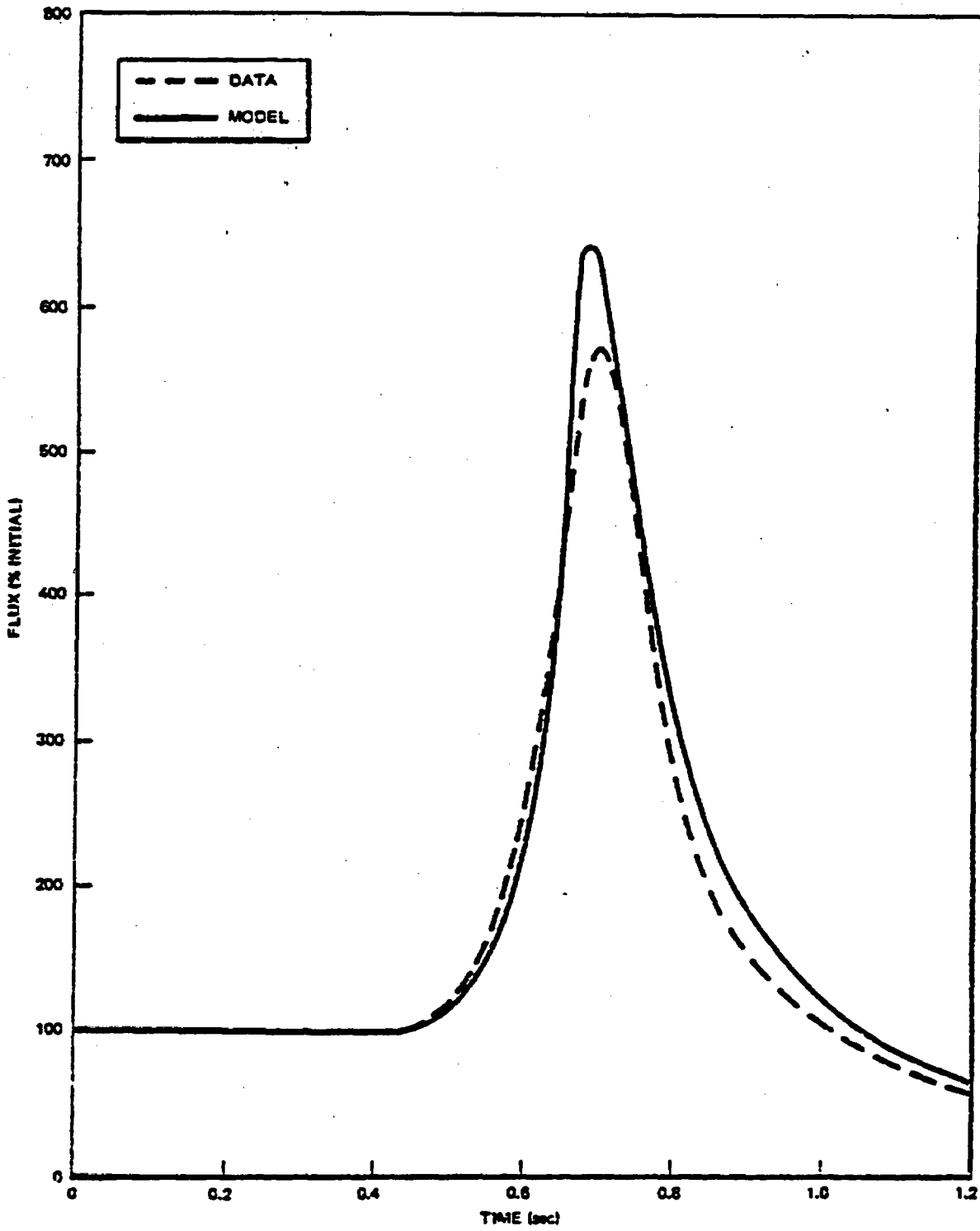
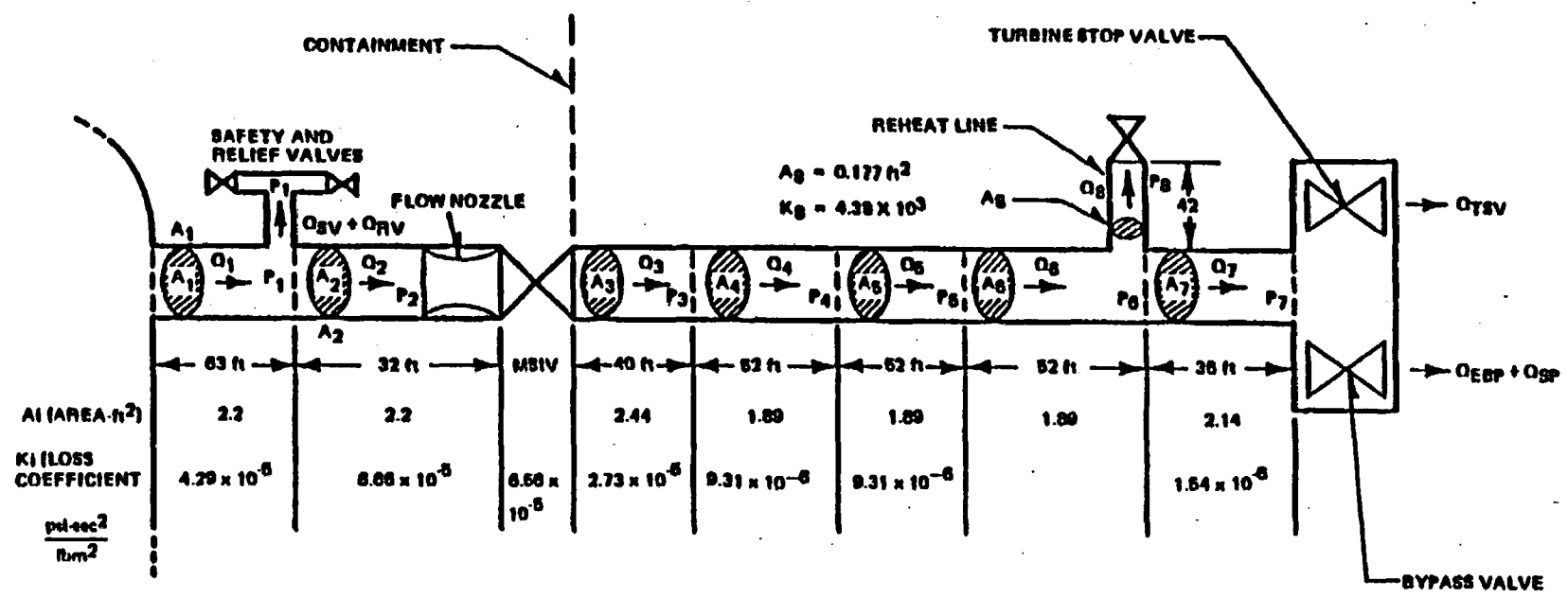


Figure 3-36. Peach Bottom-2 D Level Flux Turbine Trip 3

IN STEADY STATE, $\Delta P_i = K_i Q_i^2$

3-55



NEDO-24154-A

Figure 3-37. Schematic of KKM Steamline Model

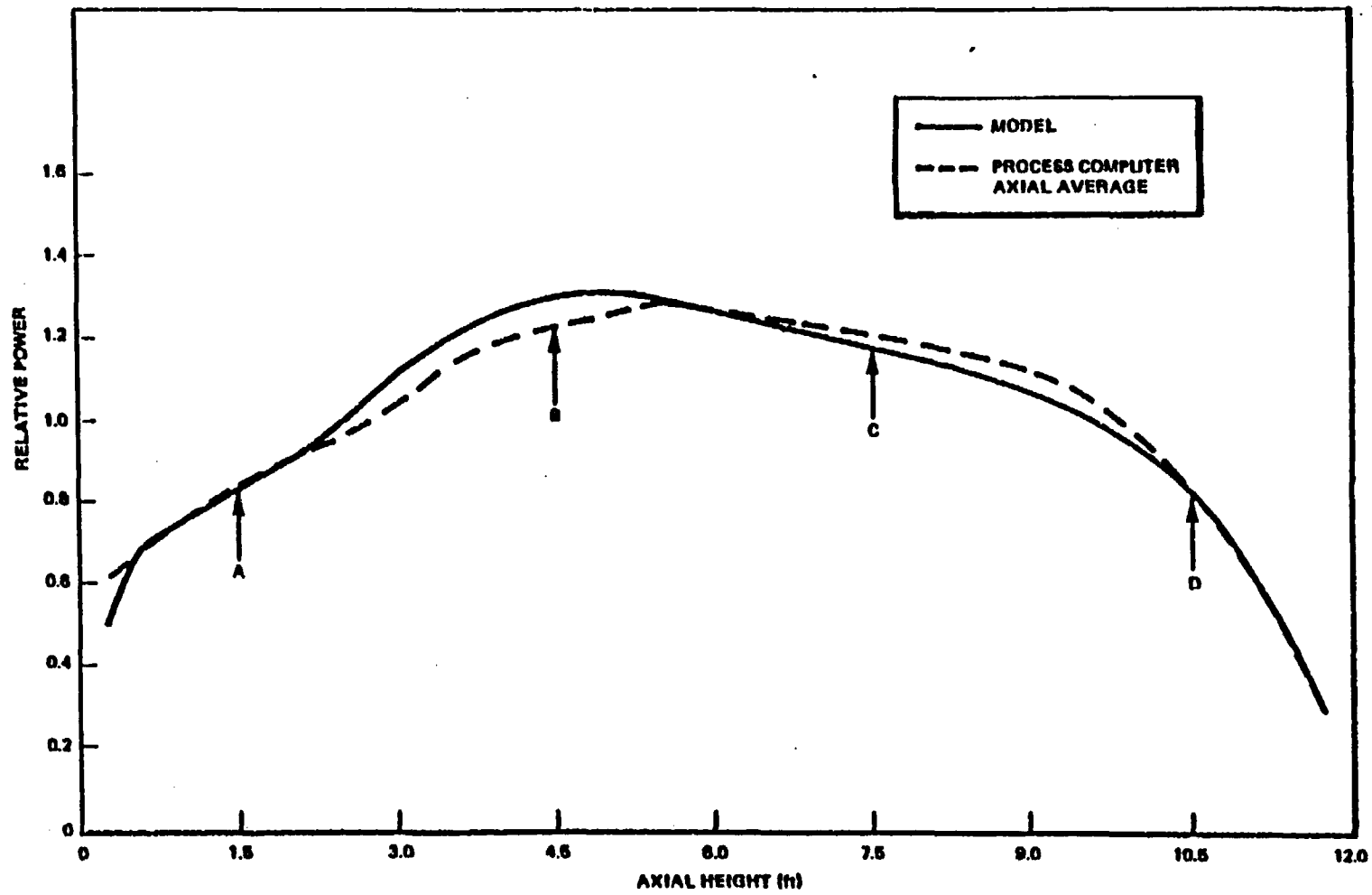


Figure 3-38. Average Axial Power KKM Test Conditions

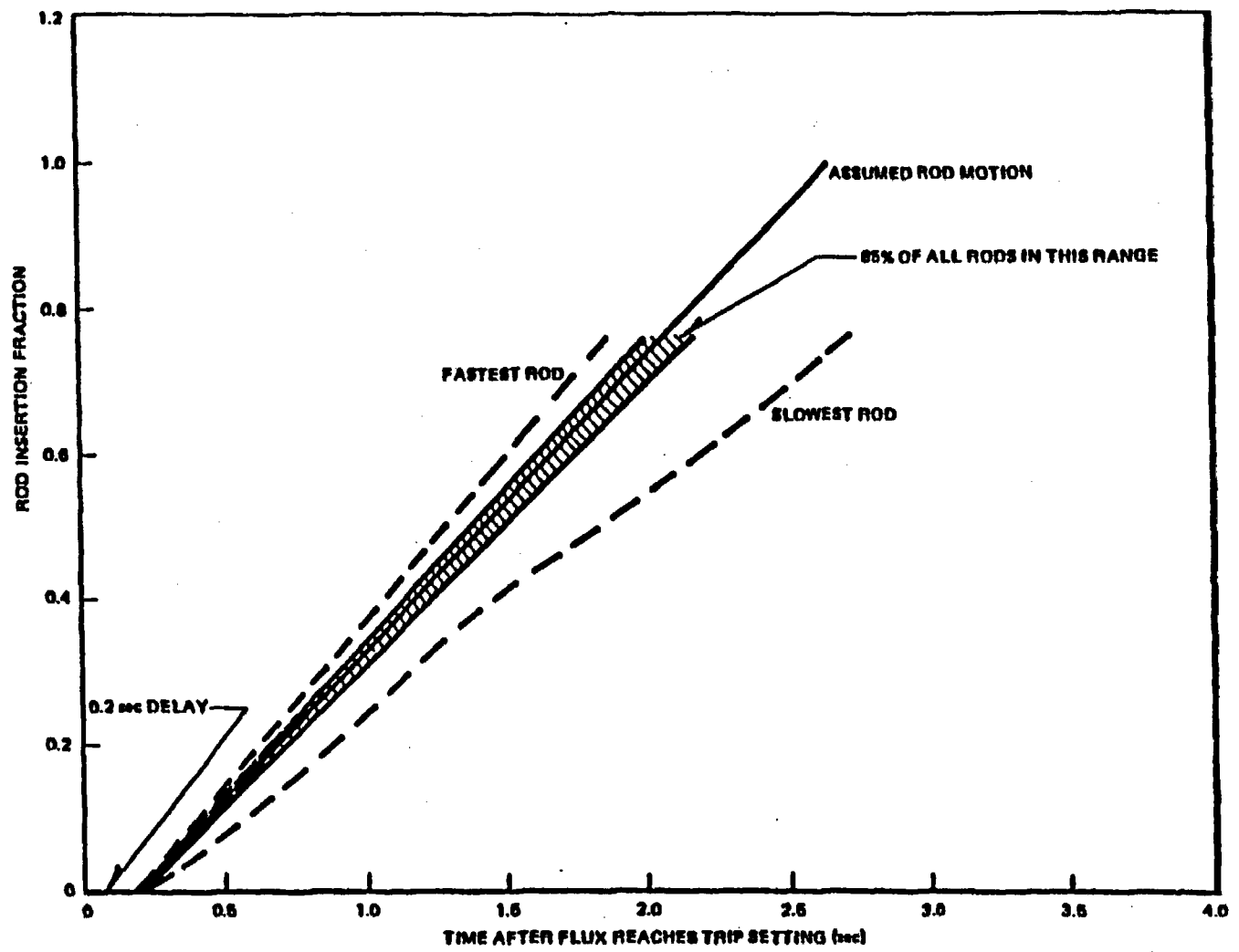


Figure 3-39. Control Rod Motion Pattern KKM Turbine Trip Test

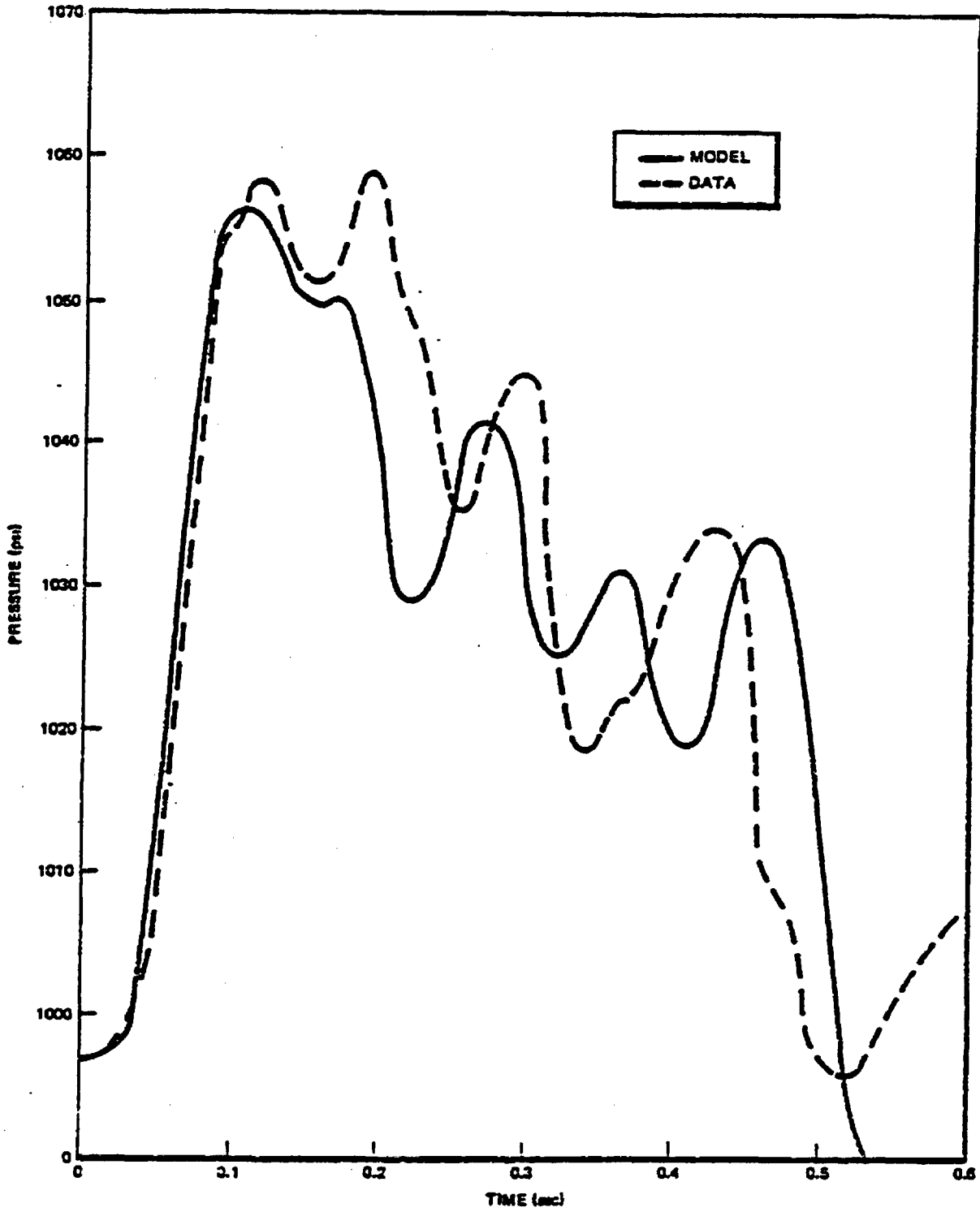


Figure 3-40. Turbine Pressure Turbine A KKM Turbine Trip

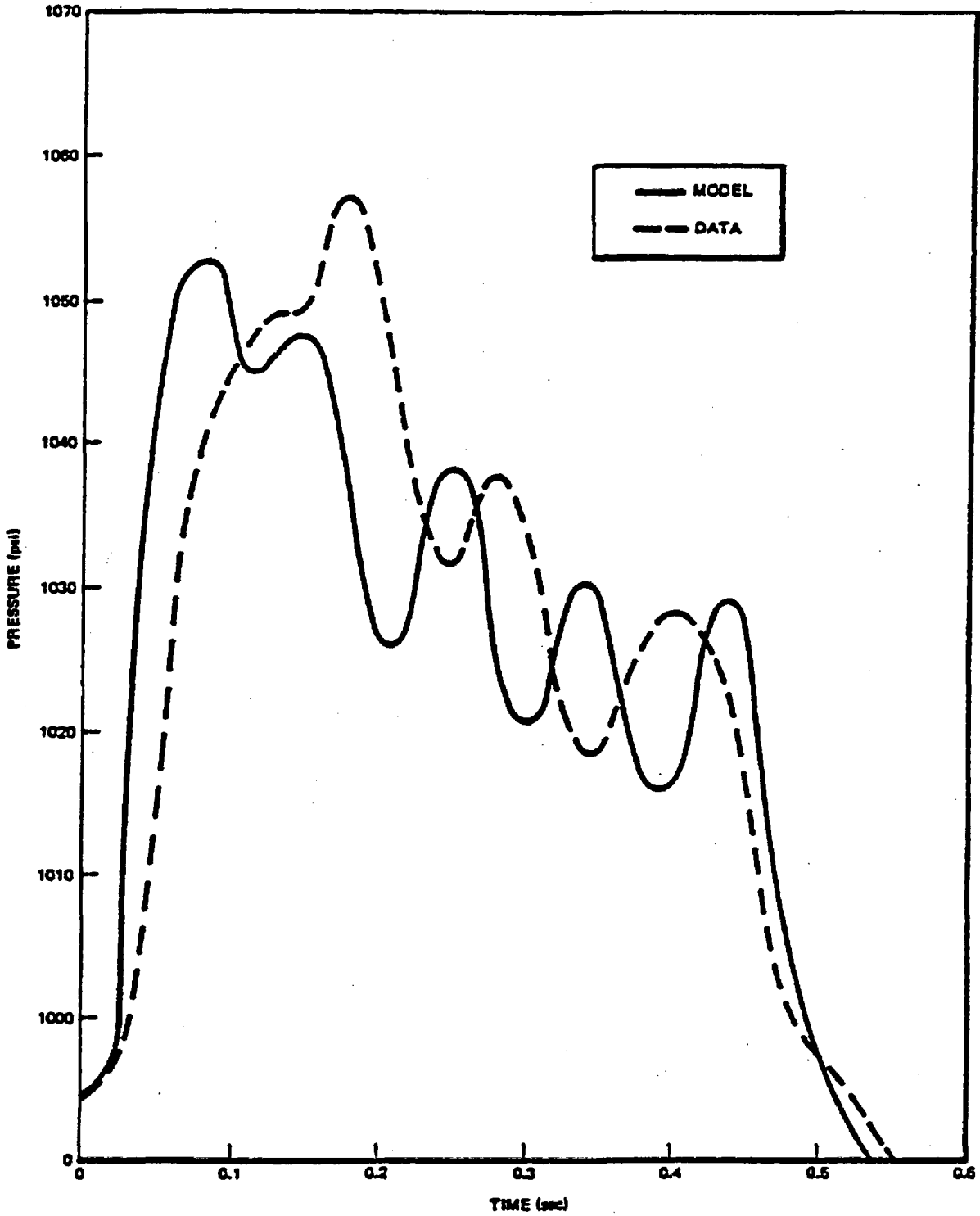


Figure 3-41. Turbine Pressure Turbine B KKM Turbine Trip

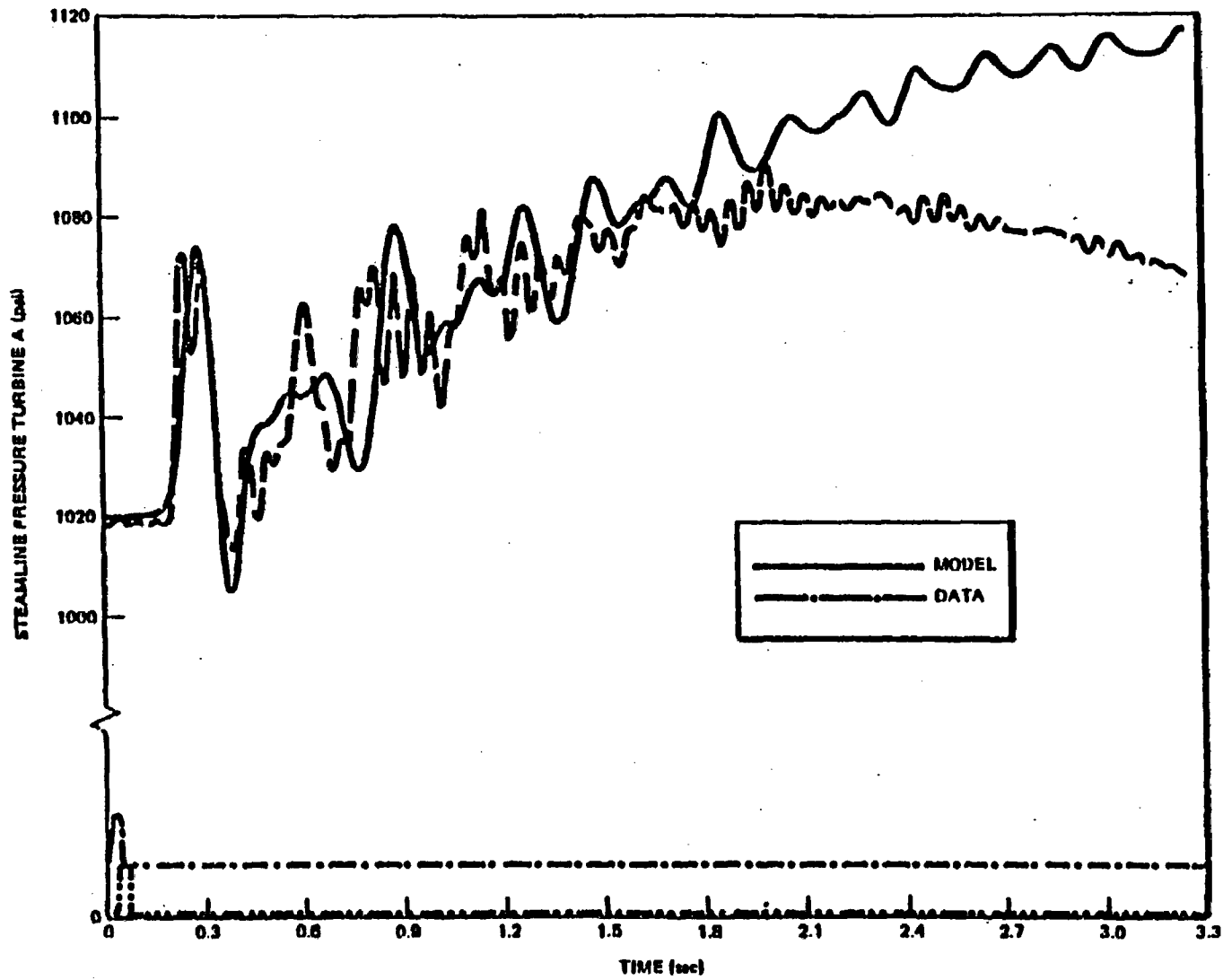


Figure 3-42. KKM Turbine Trip Steamline Pressure, Turbine A

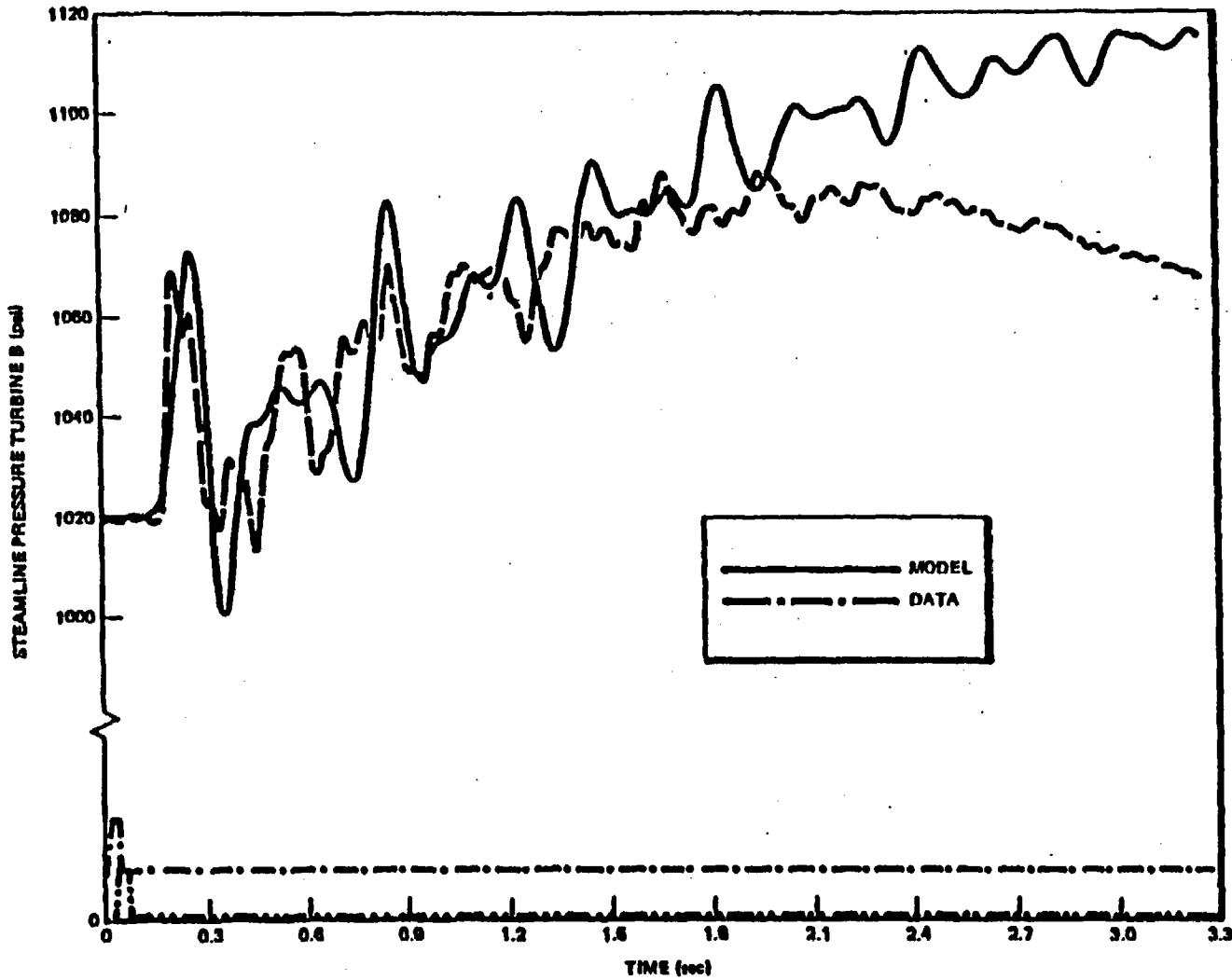
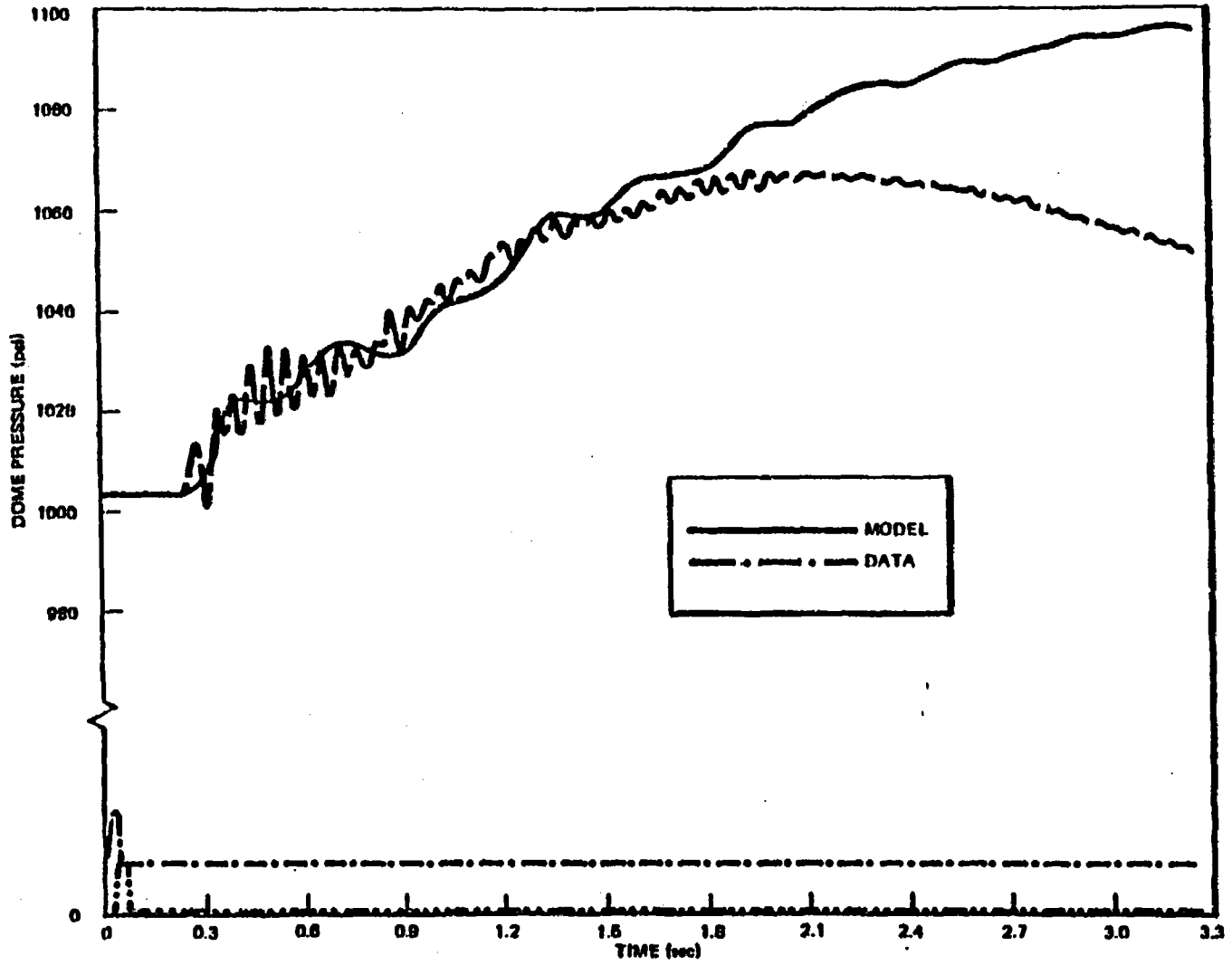


Figure 3-43. KKM Turbine Trip Steamline Pressure, Turbine B

3-52



NEDO-24154-A

Figure 3-44. KKM Turbine Trip Dome Pressure

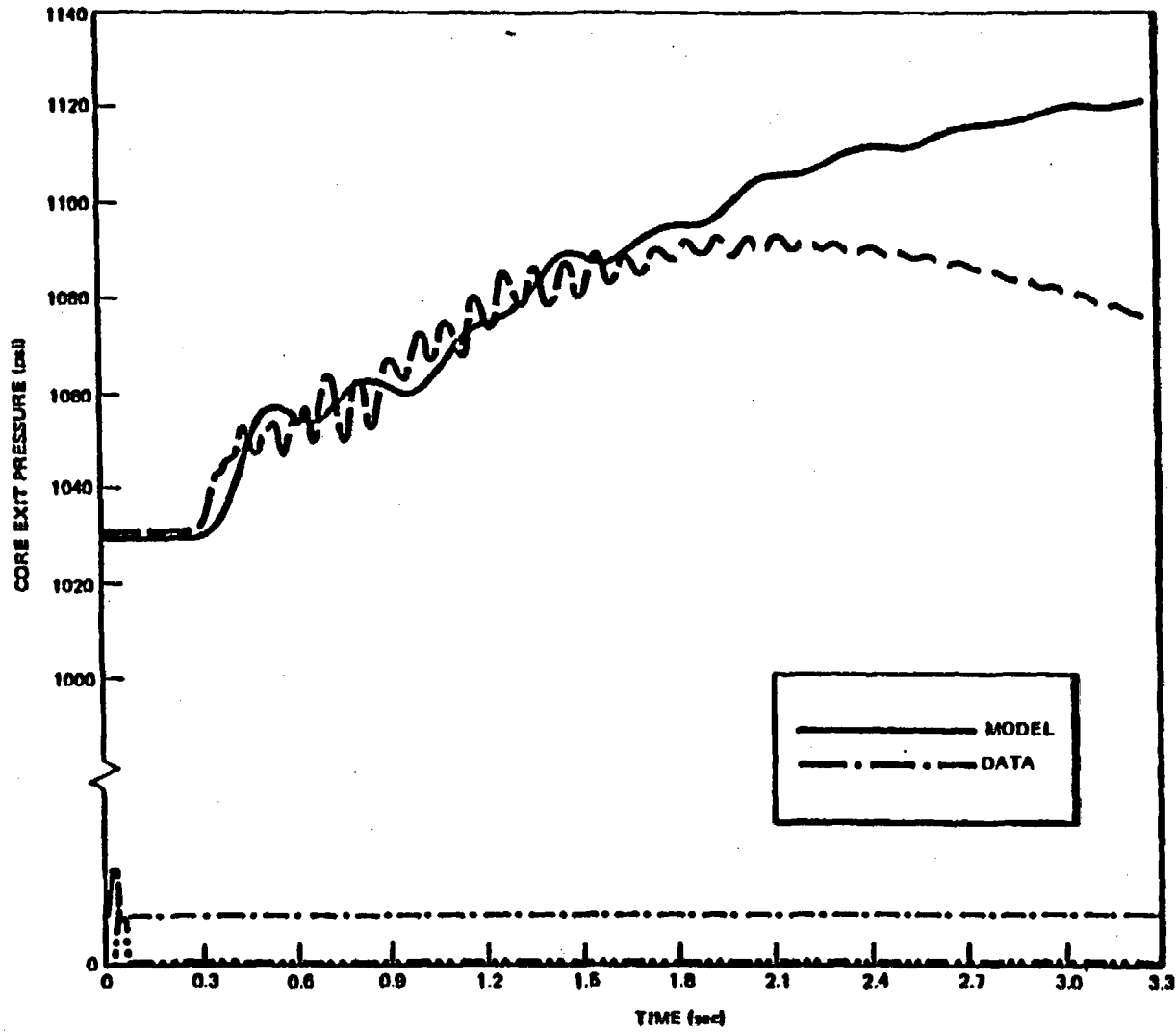
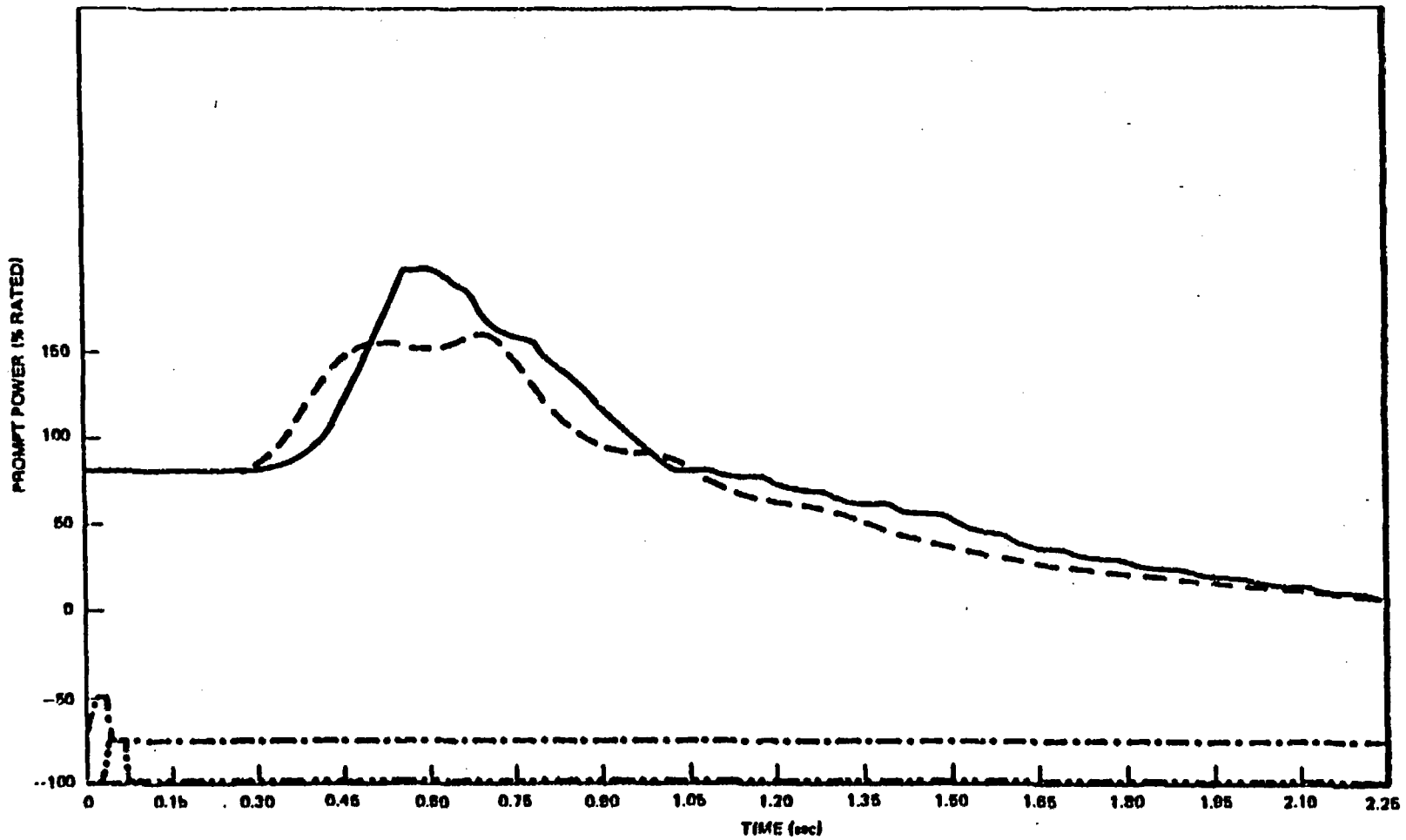


Figure 3-45. KKH Turbine Trip Core Exit Pressure

3-54



NEEO-24154-A

Figure 3-46. KKM Turbine Trip Prompt Neutron Power

NEDO-24154-A

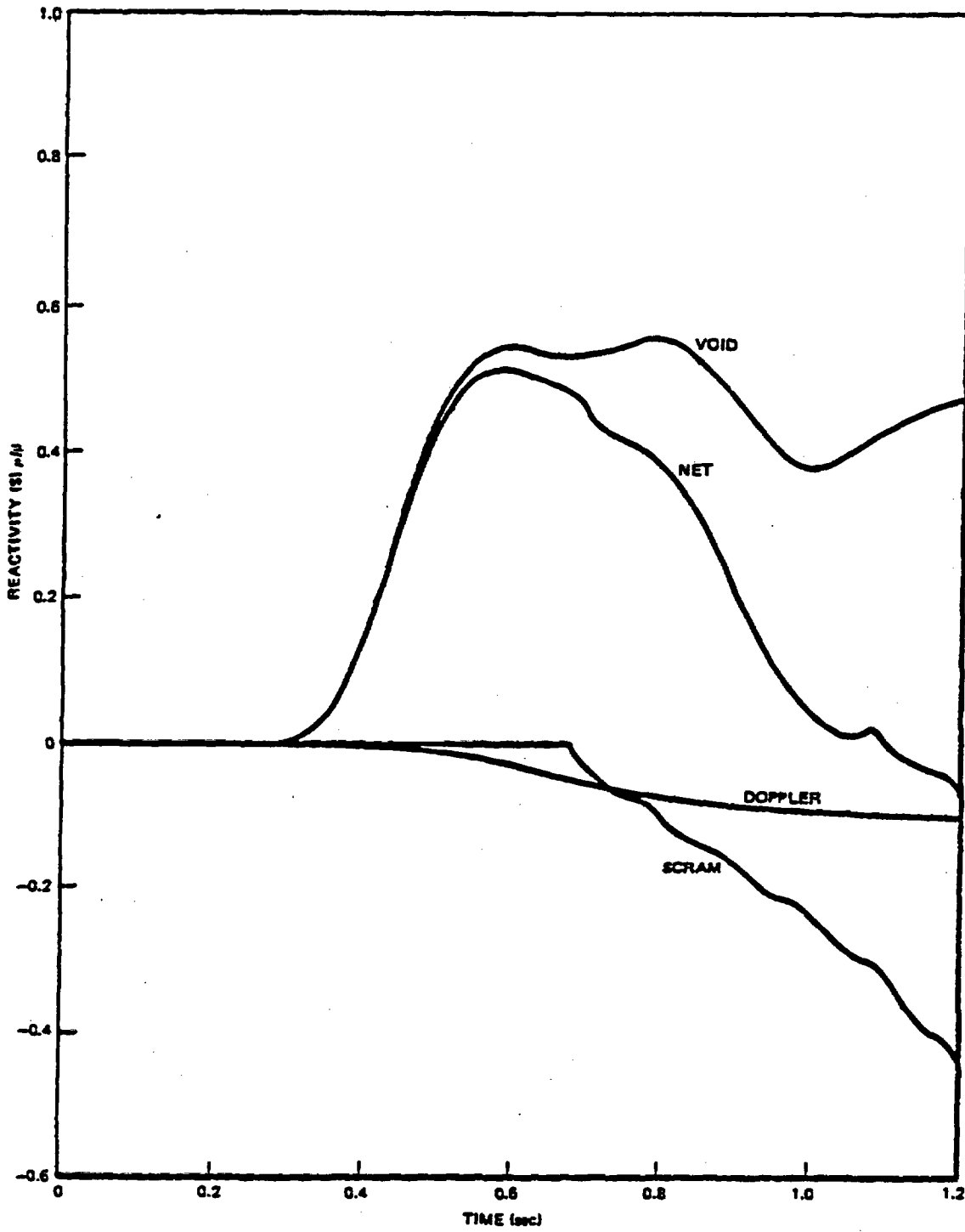


Figure 3-47. Reactivity Components KKM Turbine Trip

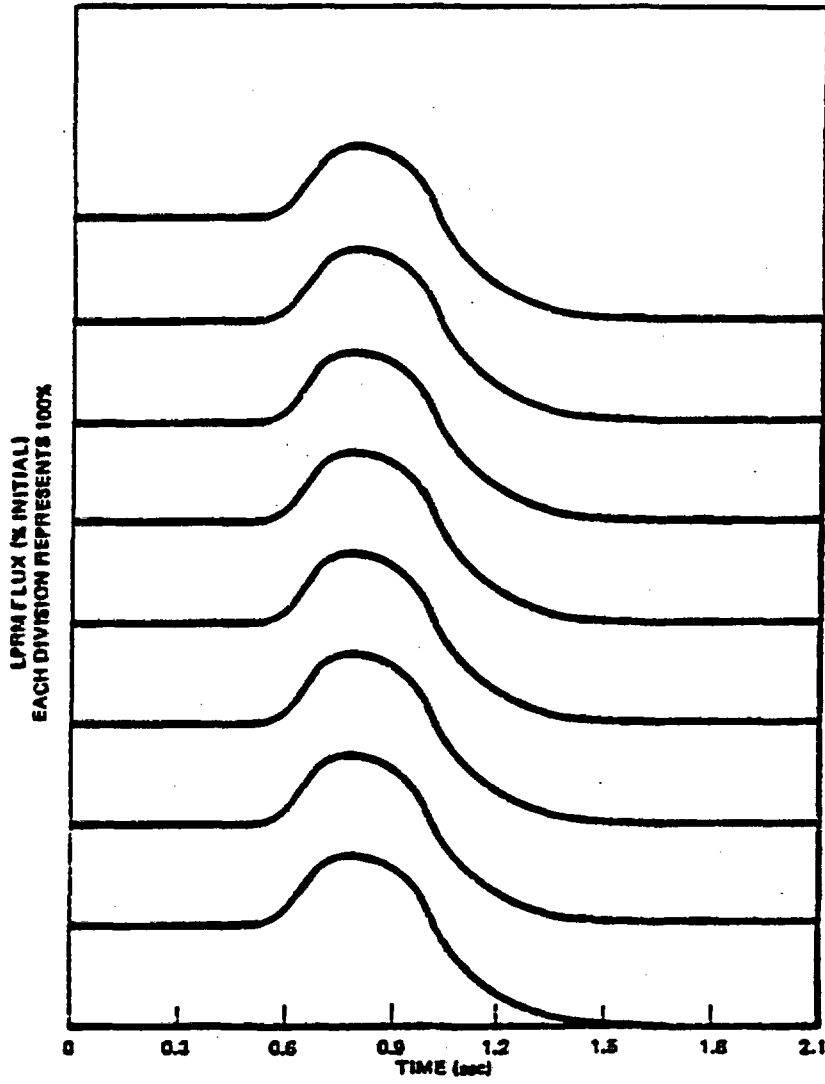


Figure 3-48. A Level LPRM Flux KRM Turbine Trip

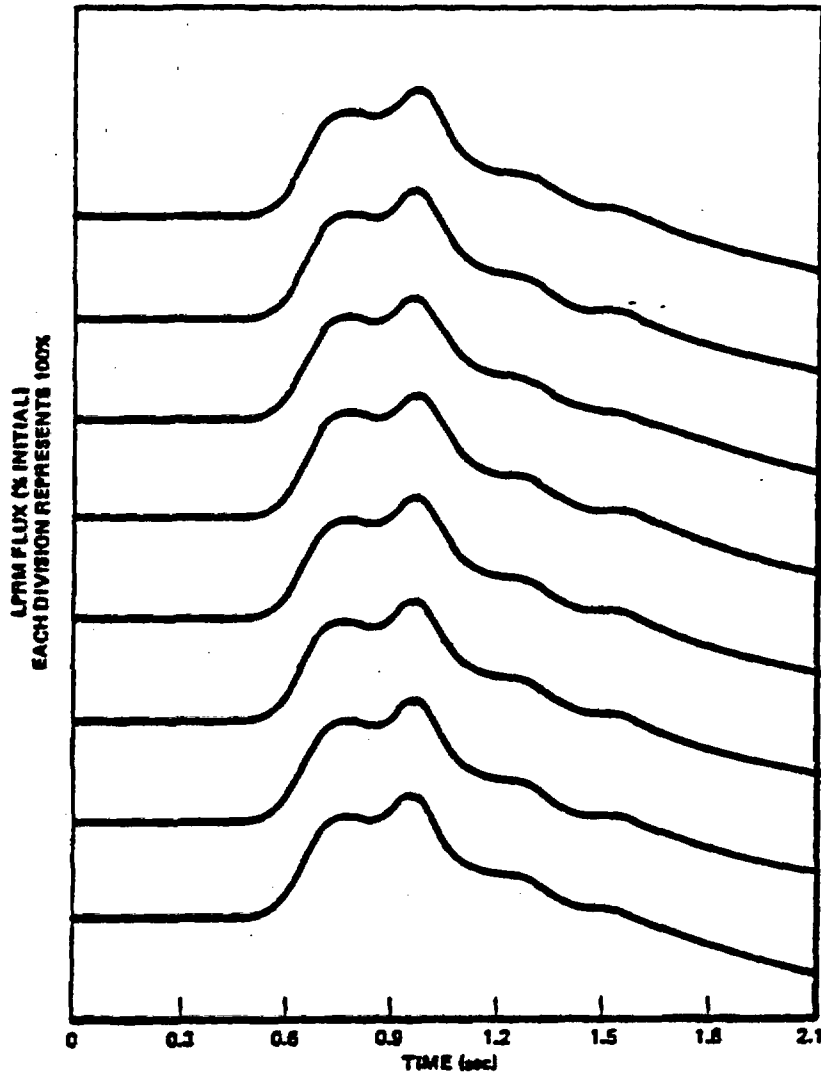


Figure 3-49. B Level LPRM Flux KKM Turbine Trip

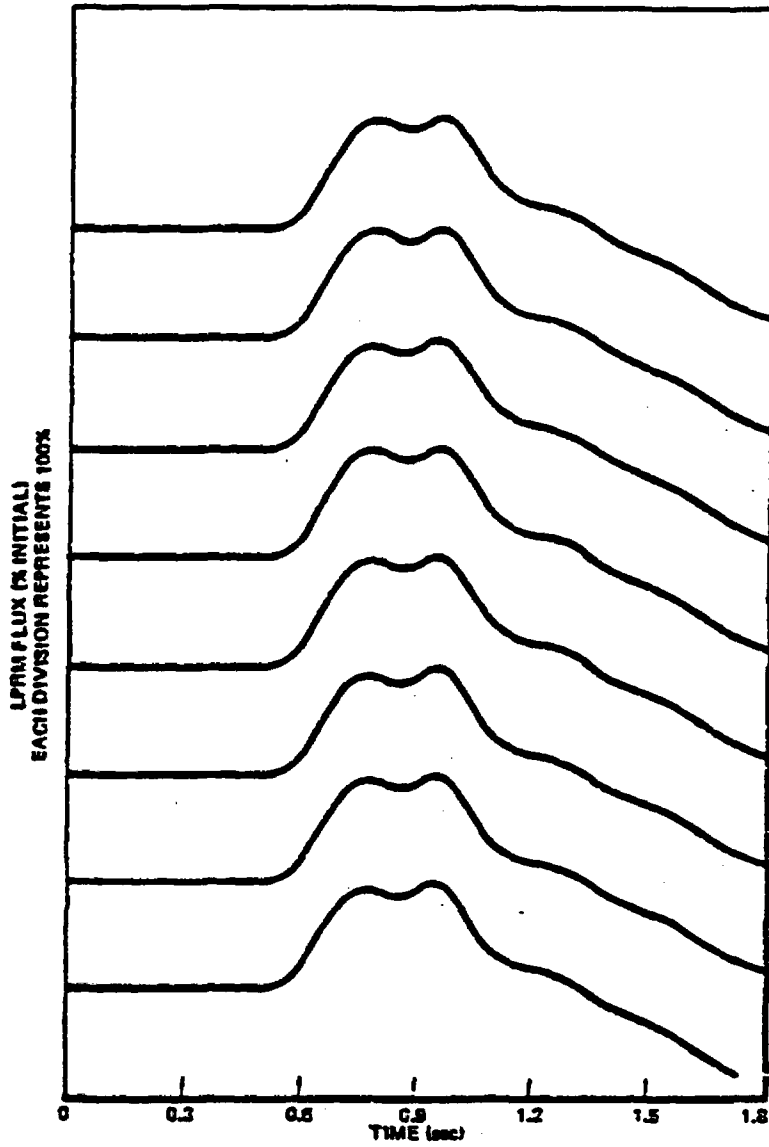


Figure 3-50. C Level LPRM Flux KKM Turbine Trip

NEDO-24154-A

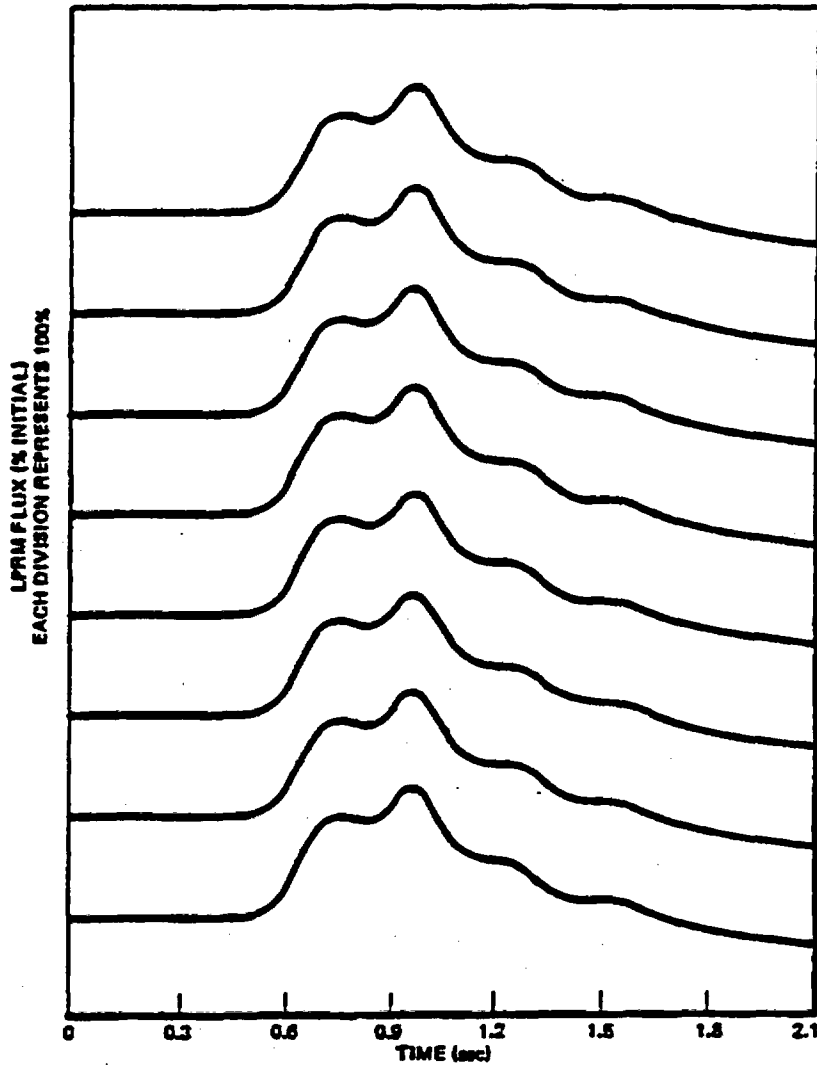


Figure 3-51. D Level LPRM Flux KKM Turbine Trip

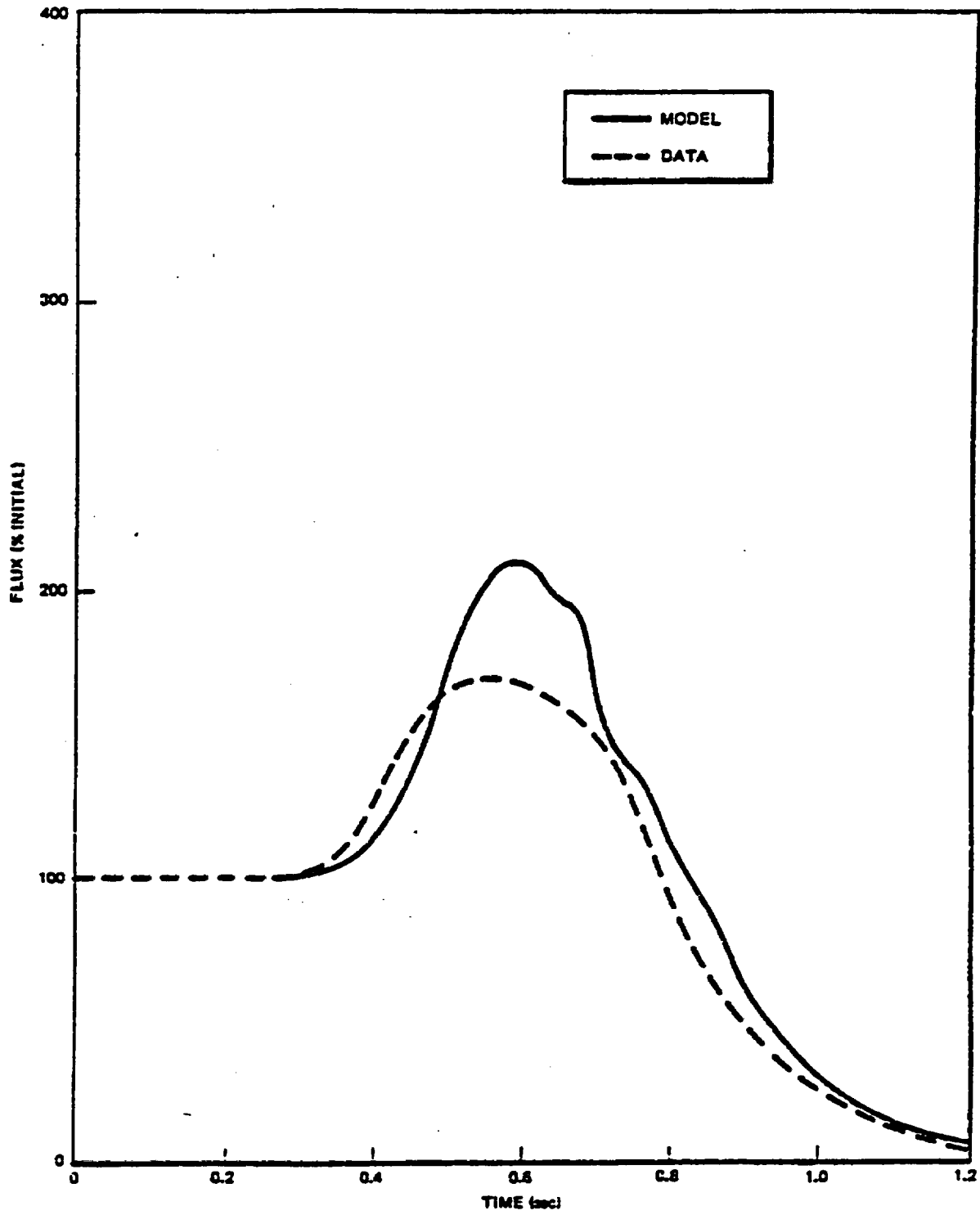


Figure 3-52. A Level Flux KKM Turbine Trip

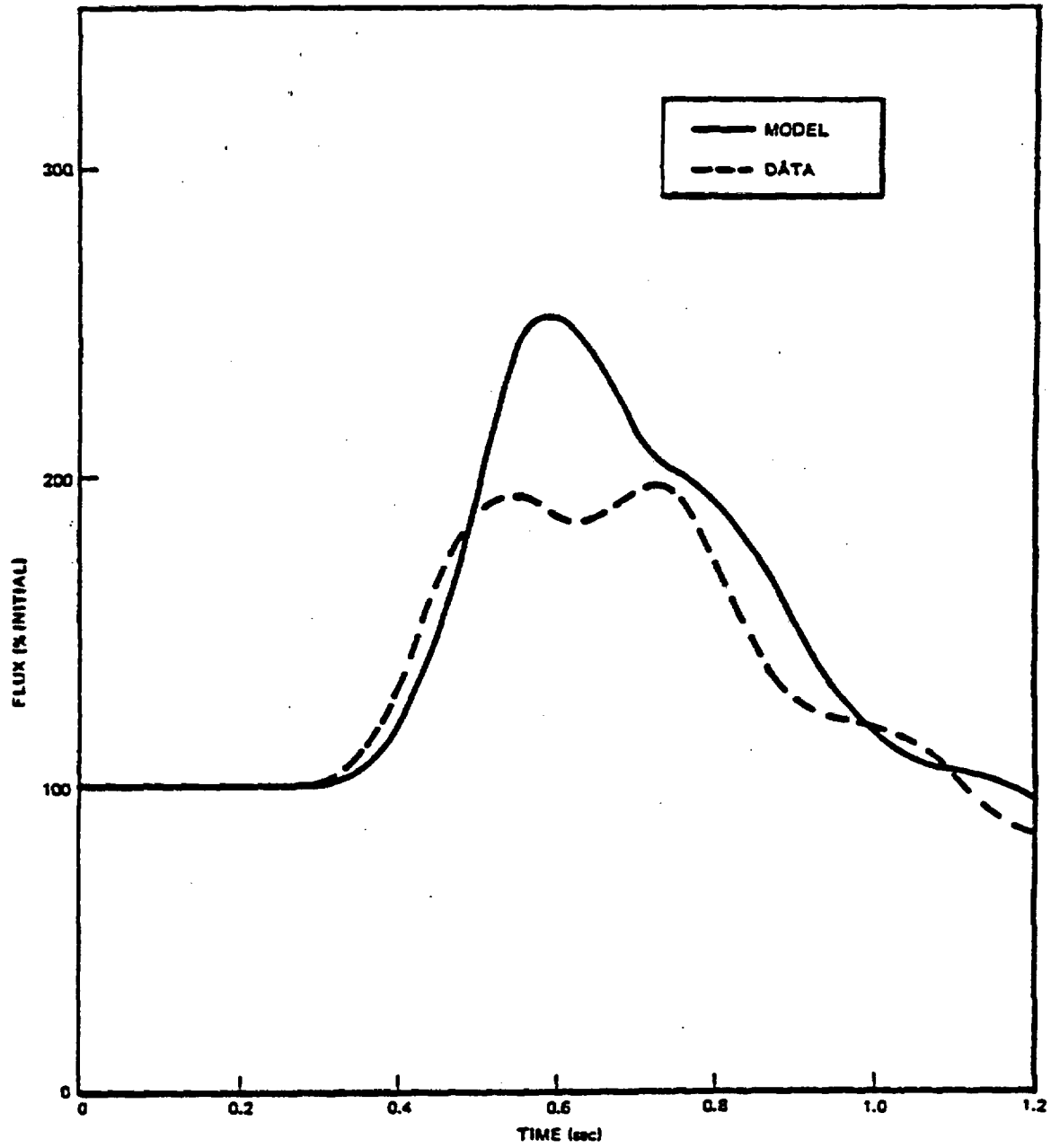


Figure 3-53. B Level Flux KKM Turbine Trip

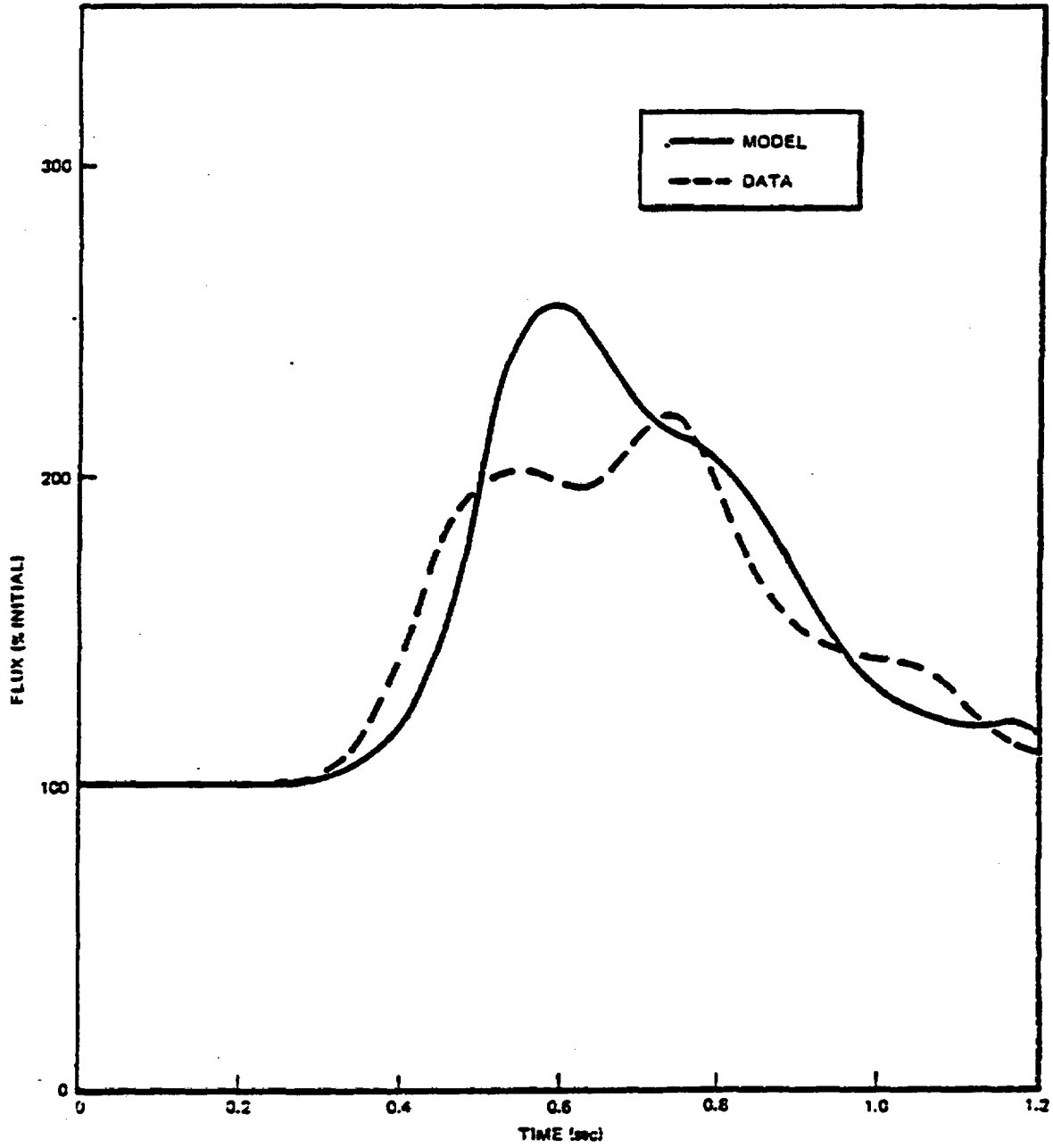


Figure 3-54. C Level Flux KCM Turbine Trip

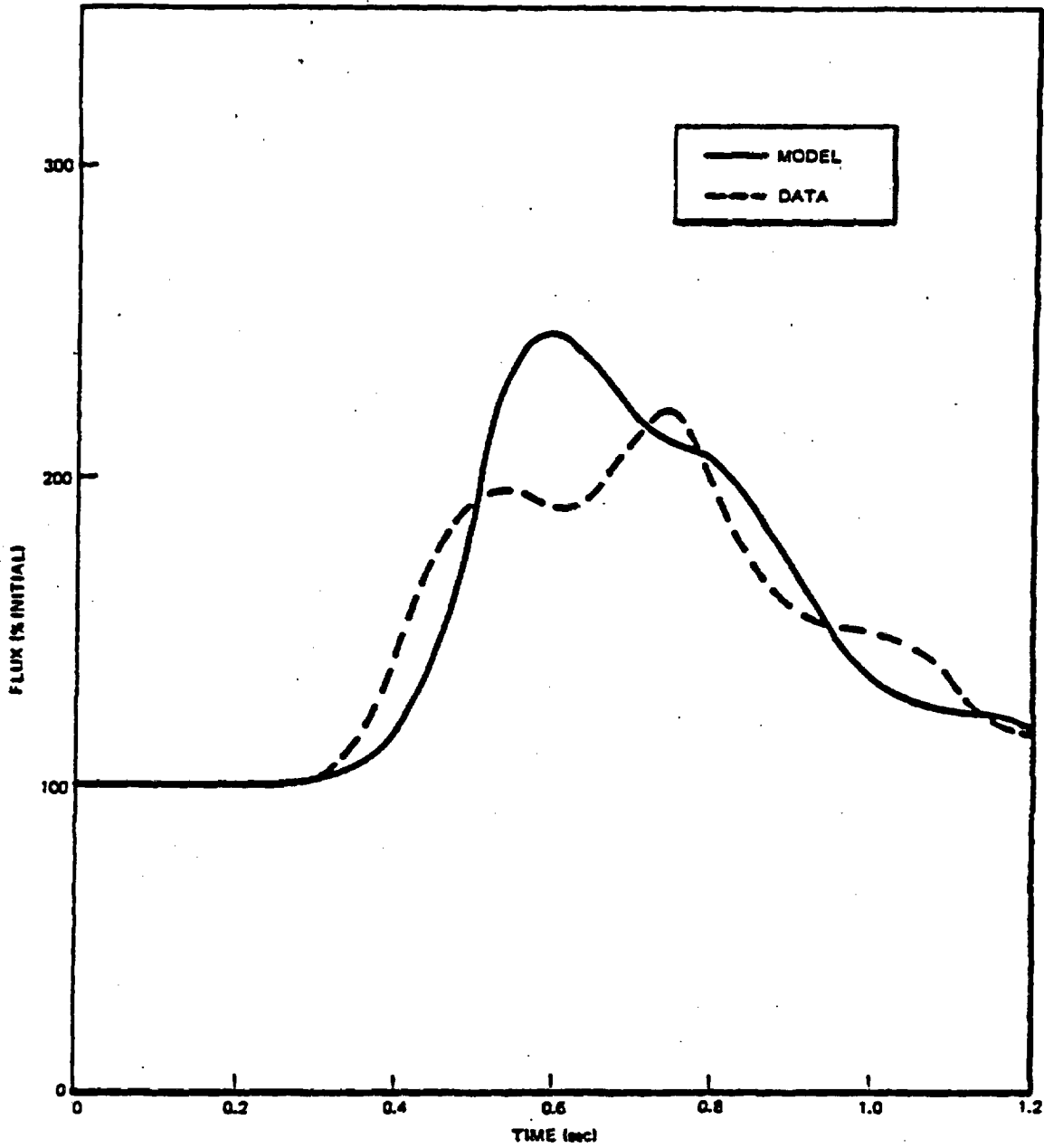


Figure 3-55. D Level Flux KKM Turbine Trip

REFERENCES

1. R. B. Linford, *Analytical Methods of Plant Transient Evaluations of the General Electric Boiling Water Reactor*, NEDO-10802, February 1973.
2. *One-Dimensional Core Transient Model*, NEDO-24154, Vol. 1, October 1978.
3. J. A. Woolley, *Three-Dimensional BWR Core Simulator*, NEDO-20953-A.
4. L. A. Carmichael and R. O. Niemi, *Transient and Stability Tests at Peach Bottom Atomic Power Station Unit 2 at End of Cycle 2*, EPRI NP-564, June, 1978.
5. R. T. Lahey, B. S. Shiralkar, J. M. Gonzalez, L. E. Schnebly, *The Analysis of Transient Critical Heat Flux*, GEAP-13249, April 1972.
6. *Flow of Fluids Through Valves, Fittings and Pipe*, The Crane Co. Technical Paper No. 410, 1969.
7. N. E. Larsen, *Core Design and Operating Data for Cycles One and Two of Peach Bottom-2*, EPRI-NP563, June 1978.
8. *Generic Reload Fuel Application*, NEDE 24011-P-3, May 1977.

4. RECIRCULATION AND CONTROL SYSTEM MODEL

The recirculation and control system is simulated by solving the mass, energy, and momentum balances over all of the appropriate steam line, vessel, and recirculation loop components. The control and safety system functions are simulated through digital logic in the transient model. The model Block diagram is shown in Figures 4-1a and 4-1b. These figures can be used to reference the equations in this section.

4.1 VESSEL AND STEAM LINE HYDRAULIC MODEL

The saturated regions of the reactor vessel and steam lines are simulated by lumped transient mass, energy, and volume balances. This division is represented schematically in Figure 4-1c.^{Q18}

4.1.1 Upper Plenum Model

In formulating the mass, energy, and momentum balances, the following assumptions are employed:

1. A homogeneous mixture of steam and liquid phases exists in all regions.
2. Thermodynamic equilibrium exists.
3. Inertial and friction momentum losses can be ignored in the core exit plenum.
4. Mass and energy storage variations in the separators are negligible.
5. Friction dissipation of energy is negligible in exit plenum regions.

The mass balance is written,

$$\dot{M}_1 = \dot{m}_{fC} + \dot{m}_{fB} + \dot{m}_{gC} + \dot{m}_{gB} + \dot{m}_{cs} - \dot{m}_{21} - \dot{m}_{11} \quad (4-1)$$

^{Q18} - Responses to NRC questions on the text are documented in Appendix B. The symbol ^{Q18} denotes that this topic is discussed further in the response to NRC Question 18.

where m_{fC} , m_{fB} , m_{gC} and m_{gB} are obtained from the core hydraulics model (see Section 3.2) and m_{21} and m_{11} are the vapor and liquid flow leaving the upper plenum. The plenum density is given by

$$\bar{\rho}_1 = M_1/V_1 \quad (4-2)$$

The liquid and vapor masses and plenum quality are given as

$$M_{gl} = V_1/v_{fgl} - (v_{fl}/v_{fgl}) M_1, \quad (4-3)$$

$$M_{fl} = M_1 - M_{gl}, \quad (4-4)$$

$$X_1 = M_{gl}/M_1. \quad (4-5)$$

The momentum balance is given by

$$0 = 144 (P_e - P_{le}) - \frac{g \bar{\rho}_1 l_1}{g_c}. \quad (4-6)$$

The energy and volume balances can be used to obtain the following energy equation:

$$\begin{aligned} & \frac{h_{fgl}}{v_{fgl}} (m_{gC} + m_{gB} - m_{11}) v_{gl} + (m_{fC} + m_{fB} - m_{21} + m_{cs}) v_{fl} \\ & + m_{cs} (h_{cs} - h_{fl}) = \left[\left(M_{gl} \frac{dh_g}{dP} + M_{fl} \frac{dh_f}{dP} - \frac{144V_1}{J} \right) \right. \\ & \left. - \frac{h_{fgl}}{v_{fgl}} \left(M_{gl} \frac{dv_g}{dP} + M_{fl} \frac{dv_f}{dP} \right) \right] \frac{dP_1}{dt} \end{aligned} \quad (4-7)$$

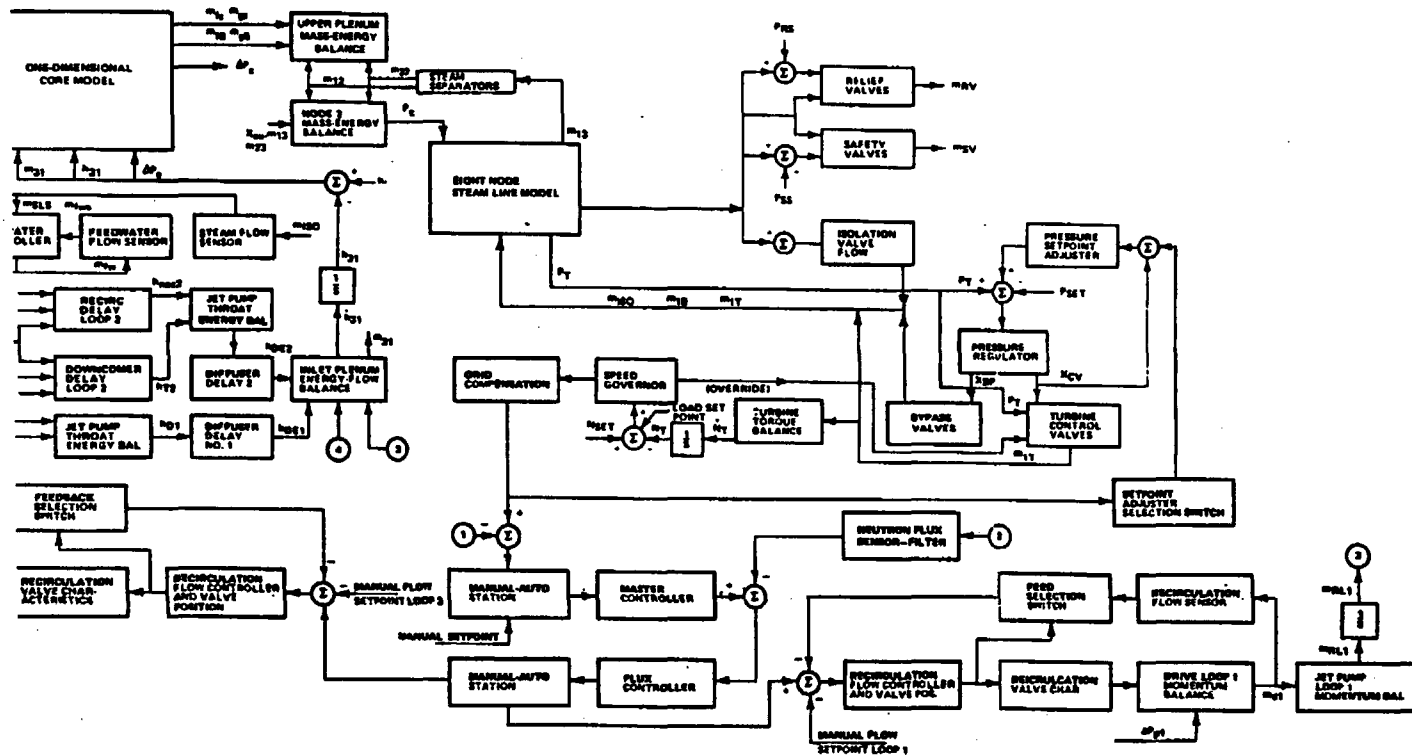
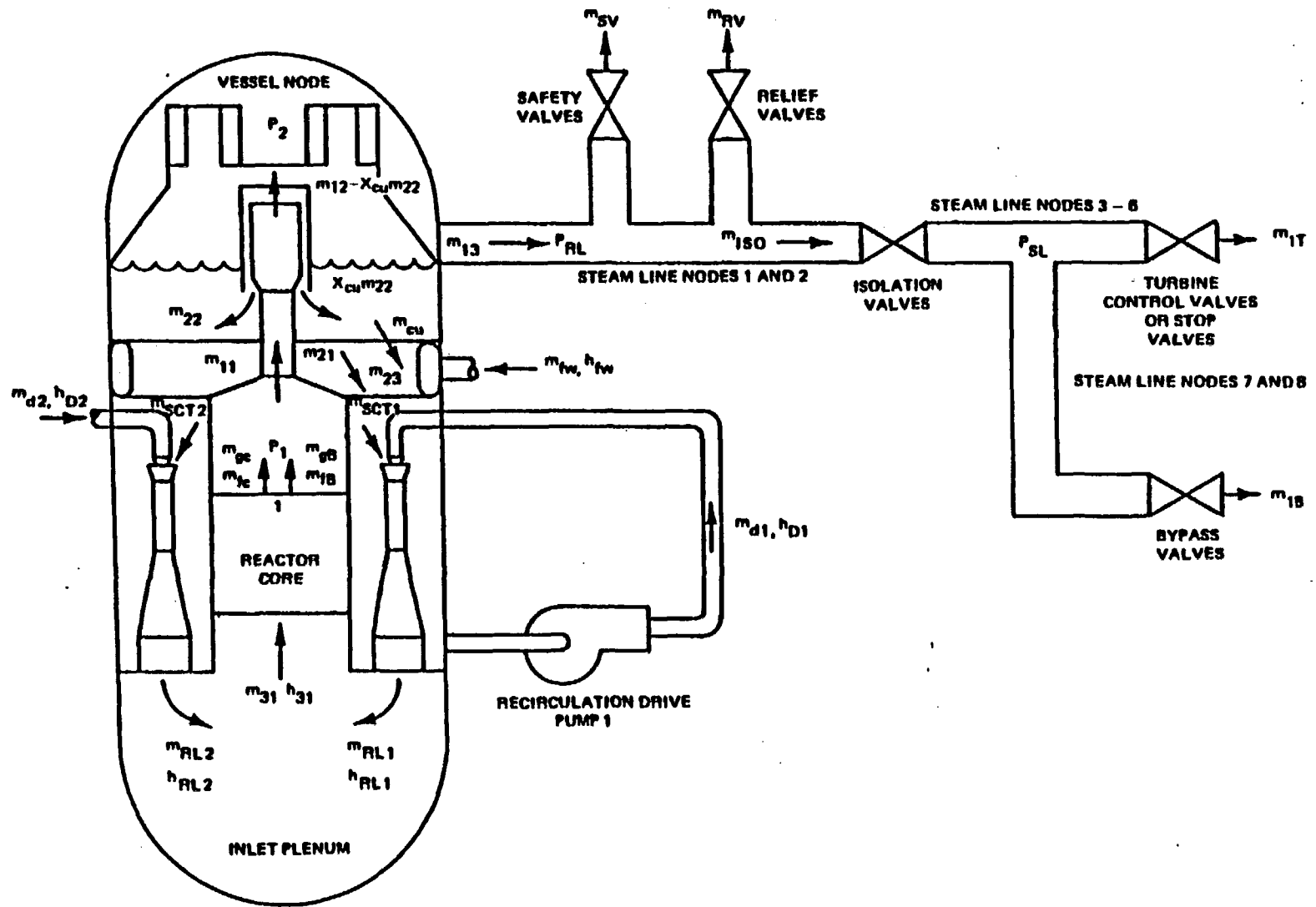


Figure 4-1b. Model Block Diagram with Valve Flow Control

4-7



NEDO-24154-A

Figure 4-1c. Thermodynamic Model Schematic

4.1.2 Separator Model

As the separator mixture leaves the core plenum pressure node, it must undergo a slight adjustment in quality because of the change in saturated properties from the core plenum to the vessel pressure node. The quality in the vessel pressure node can be determined from the following assumptions:

1. The quality of the saturated mixture entering the separators is the average plenum quality.
2. The saturated mixture entering the vessel node undergoes a free expansion in a massless region at the separator inlet.

From an energy balance, the quality of the mixture entering the vessel node is given by

$$X_2 = \frac{X_1 h_{f1} + h_{f1} - h_{f2}}{h_{fg2}} \quad (4-8)$$

Assuming the average density of the fluid in the separator barrel to be approximately the same as that in the plenum and standpipes, the mass of steam in the separators is given approximately by

$$M_{gs} = \bar{\rho}_1 X_1 V_s \quad (4-9)$$

The saturated liquid mass is then

$$M_{fs} = \bar{\rho}_1 V_s - M_{gs} \quad (4-10)$$

The transient steam separator flow equation can be derived based on the following assumptions:

1. The transient behavior of the steam separators is adequately described by the dynamic response of one average separator.

2. The compressible flow effects in the separators can be neglected.
3. The steam separates near the inlet of the separator, giving a central core of vapor and a layer of liquid spiraling up the separator wall.
4. The principal inertial effects are due to the layer of liquid. (All other l/A terms are small compared to this value.)

A force balance on the liquid flow spiraling along the wall gives

$$\left(\frac{1}{g_c} \frac{\hat{l}}{A}\right) \frac{m_{21}}{N_{sep}} = 144(P_{1e} - P_2) - \frac{g \bar{\rho}_1 (l_{sep1} + l_{sp})}{g_c} - \Delta P_{sep} \quad (4-11)$$

where separator geometry is given in Figure 4-2.

Experimental steady-state measurements of the pressure drop across the separator⁽⁵⁾ are correlated by

$$\Delta P_{sep} = C_{sep} m_{3s}^2 / \bar{\rho}_1 N_{sep}^2 \quad (4-12)$$

An estimate of the effective length-to-area ratio in the separator barrel, and hence its calculated inertia, may vary considerably from the physical dimensions if it is assumed that an average particle of fluid must travel a spiral path from the inlet to the outlet.^{Q15}

Studies concerning design, analysis, and testing of the separators have led to further understanding of the liquid layer thickness, velocities, and effective \hat{l}/\hat{A} (flow length/area) relationships. These studies showed several important relationships which led to the model simulated here.

1. The water layer along the separator was virtually independent of the total flow (200,000 < Flow < 800,000 lb/h).
2. This water layer thickness (and thereby the effective \hat{l}/\hat{A}) was dependent upon the quality at the separator inlet.

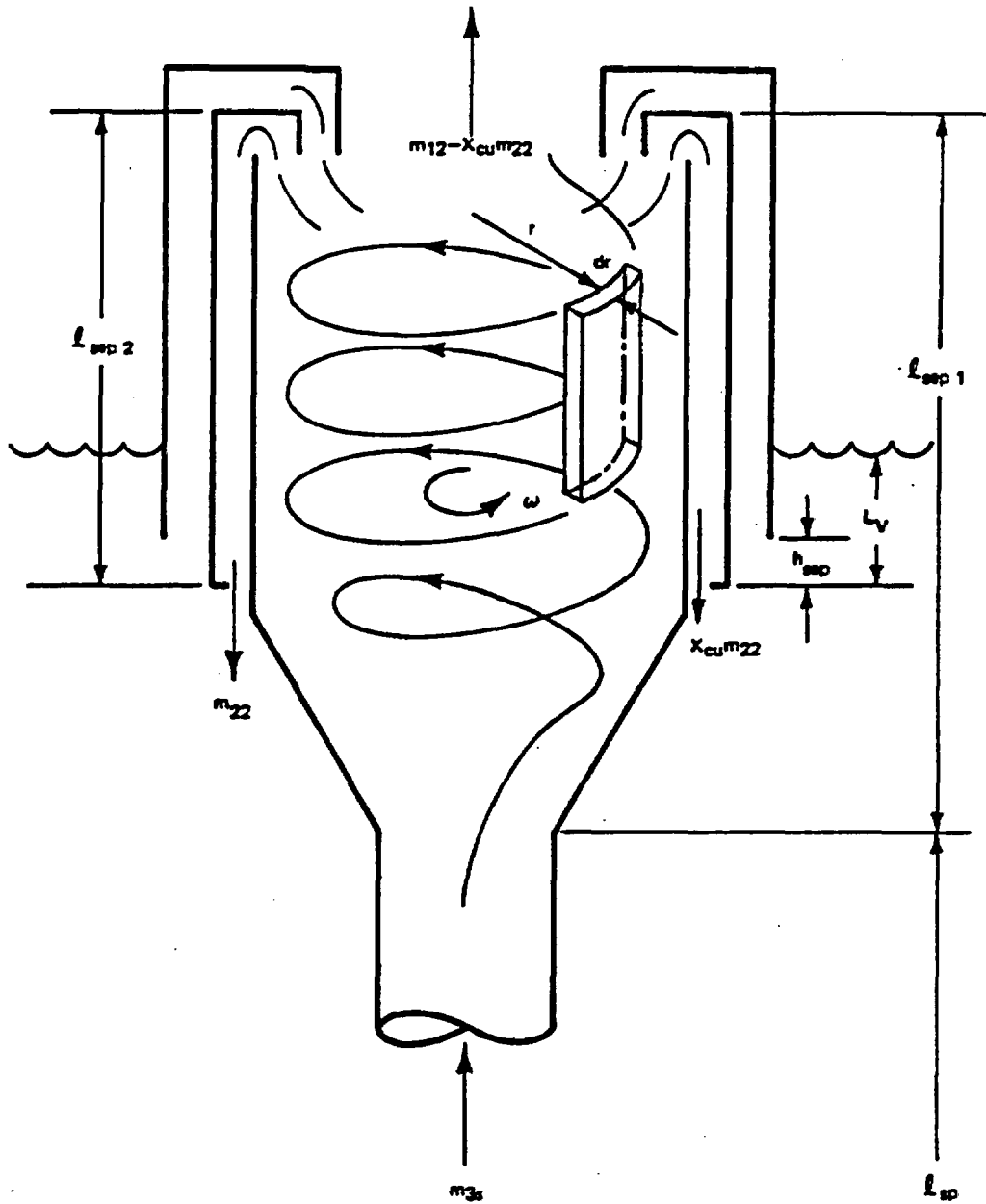


Figure 4-2. Steam Separator Schematic

Typical variation of \hat{l}/\hat{A} with quality is shown in Figure 4-3. The other length-to-area ratio in equation may be evaluated directly from physical dimensions.

The steamflow entering the vessel is then obtained from:

$$\dot{m}_{12} = X_2 \dot{m}_{3s} \quad (4-13)$$

and liquid flow from

$$\dot{m}_{22} = \dot{m}_{3s} - \dot{m}_{12} \quad (4-14)$$

4.1.3 Vessel Dome and Bulkwater Model

4.1.3.1 Vessel Pressure Rate

The analysis of the transient thermodynamic conditions in the vessel pressure node is derived on the basis of the following assumptions:

1. The rates of mass transfer at the steam/water interfaces, other than carryunder in the bulkwater, are negligible.
2. When the vessel pressure rate is positive and the carryunder mass in the bulk water is zero, the bulk water is subcooled.
3. Enthalpy changes in the bulk water due to pressure changes are negligible when the bulk water is subcooled.
4. The mixing of feedwater, bulk water, and carryunder occurs in a massless region whose position is independent of time.
5. The mass of liquid in the separators always remains saturated.
6. Heat loss from the vessel and intervals is neglected. ^{Q48}

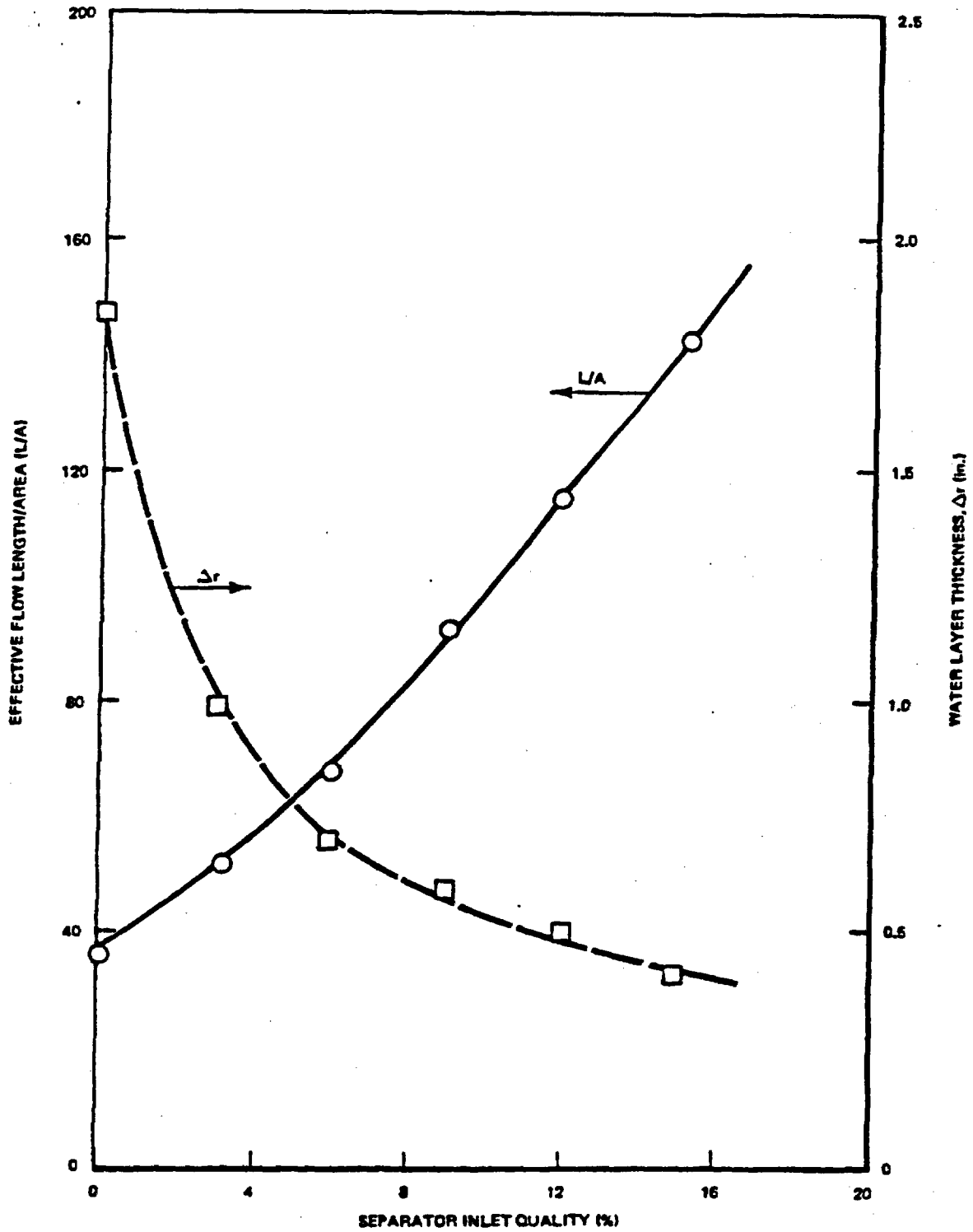


Figure 4-3. Centrifugal Steam Separator Characteristics versus Inlet Quality - 200,000 < total flow < 800,000 lb/hr

The mass, volume, and energy balances for the vessel pressure node are:

Mass Balances

$$\dot{M}_{g2} = \dot{m}_{12} - \dot{m}_{gfb} - \dot{m}_{cu} - \dot{m}_{13} \quad (4-15)$$

$$\dot{M}_{f2} = \dot{m}_{22} + \dot{m}_{gfb} - \dot{m}_{23} \quad (4-16)$$

Volume Balance

$$\dot{V}_2 = \frac{\dot{M}_{g2}}{\rho_{g2}} + \frac{\dot{M}_{f2}}{\rho_{f2}} \quad (4-17)$$

Energy Balance

$$\begin{aligned} (\dot{m}_{12} - \dot{m}_{cu} - \dot{m}_{13}) h_{g2} + (\dot{m}_{22} - \dot{m}_{23}) h_{f2} &= \dot{M}_{g2} u_{g2} \\ &+ \frac{\dot{M}_{f2}}{\rho_{f2}} u_{f2} + \frac{144 P_2 \dot{V}_2}{J} \end{aligned} \quad (4-18)$$

Noting that $\dot{V}_2 = 0$, the combination of Equations 4-15, 4-16, and 4-17 gives the expression for the vessel pressure rate,

$$\frac{h_{fg2}}{v_{fg2}} \left[v_{f2} (\dot{m}_{22} - \dot{m}_{23}) + v_{g2} (\dot{m}_{12} - \dot{m}_{13} - \dot{m}_{cu}) \right] = D_2 \dot{P}_2 \quad (4-19)$$

where for $M_{gb} > 0$,

$$\begin{aligned} D_2 &= \left[(M_{fb} + M_{fs}) \frac{dh_{f2}}{dP} + (M_{gd} + M_{gb}) \frac{dh_{g2}}{dP} - \frac{144V_2}{J} \right] \\ &- \frac{h_{fg2}}{v_{fg2}} \left[(M_{fb} + M_{fs}) \frac{dv_{f2}}{dP} + (M_{gd} + M_{gb}) \frac{dv_{g2}}{dP} \right] \end{aligned} \quad (4-20)$$

and for $M_{gb} = 0$, and $\dot{P}_2 > 0$; $m_{cu} = 0$ and

$$D_2 = \left[M_{fs} \frac{dh_{f2}}{dP} + M_{gd} \frac{dh_{g2}}{dP} - \frac{144V_2}{J} \right] - \frac{h_{fg2}}{v_{fg2}} \left[M_{fs} \frac{dv_{f2}}{dP} + M_{gd} \frac{dv_{g2}}{dP} + M_{fb} \frac{dv_s}{dP} \right] \quad (4-21)$$

4.1.3.2 Mass Balance

The total mass of the vessel bulk water can be obtained from the mass balance,

$$\dot{M}_{fb} = m_{22} + m_{gfb} - m_{23} \quad (4-22)$$

and the carryunder entrained in the bulkwater is obtained from

$$\dot{M}_{gb} = X_{cu} m_{22} - m_{cu} - m_{gfb} \quad (4-23)$$

The mass of steam in the vessel dome is obtained from the mass balance in the dome

$$\dot{M}_{gd} = m_{12} - X_{cu} m_{22} - m_{13} \quad (4-24)$$

The volume of bulk water and entrained carryunder above the feedwater sparger is given by

$$V_{b+cu} = \frac{M_{fb}}{v_{f2}} + \frac{M_{gb}}{v_{g2}} - V_s \quad (4-25)$$

4.1.3.3 Downcomer Flow

The carryunder flow entering the downcomers is proportional to the product of the mass ratio of entrained steam to bulk water and the liquid flow from the vessel,

$$m_{cu} = \frac{M_{gb}}{M_{fb}} m_{23} \quad (4-26)$$

At the feedwater sparger, the application of flow continuity yields:

$$m_{31} = m_{23} + m_{fw} + m_{cu} + m_{ci} \quad (4-27)$$

Using (4-26) for m_{cu} , it is possible to solve (4-27) for m_{23}

$$m_{23} = (m_{31} - m_{fw} - m_{ci}) / \left(1 + \frac{M_{gb}}{M_{fb}}\right) \quad (4-28)$$

4.1.3.4 Carryunder Condensation Rate

Because of the carryunder from the steam separators, an entrained mass of steam bubbles will be present in the bulk water of the vessel. This mass of steam has an influence on the pressure rate in the vessel, and consideration of its dynamics is included for that reason. Mass and energy balances can be written for vessel bulk water and carryunder as follows:

Mass Balances

$$\dot{M}_{gb} = X_{cu} m_{22} - m_{cu} - m_{gfb} \quad (4-29)$$

$$\dot{M}_{fb} = m_{22} + m_{gfb} - m_{23} \quad (4-30)$$

Energy Balance

$$m_{22} h_{f2} + X_{cu} m_{22} h_{g2} - m_{23} h_{f2} - m_{cu} h_{g2} = \frac{\dot{M}_{gb} u_{g2}}{J} + \frac{\dot{M}_{fb} u_{f2}}{J} + \frac{144V_B P_2}{J} \quad (4-31)$$

Combining the above two equations leads to an expression for carryunder condensation rate

$$m_{gfb} = \frac{1}{h_{fg2}} \left[M_{gb} \frac{dh_{g2}}{dP} + M_{fb} \frac{dh_{f2}}{dP} - \frac{144(V_{gb} + V_{fb})}{J} \right] \frac{dP_2}{dt} \quad (4-32)$$

If carryunder completely condenses,

$$m_{gfb} = X_{cu} m_{22} \quad (4-33)$$

At the feedwater sparger, the saturated liquid, carryunder, and any high pressure core injection flow is assumed to mix perfectly with the subcooled feedwater.

The enthalpy of the fluid entering the downcomer is given by:

$$h_{33} = (h_{fw} m_{fw} + h_{f2} m_{23} + h_{g2} m_{cu} + m_{ci} h_{ci}) / m_{31} \quad (4-34)$$

4.1.3.5 Vessel Level

Referring to Figure 4-4, it is apparent that the vessel level change per unit volume, bulk water, and carryunder will vary with vessel level. Defining level in the model to be the height of carryunder and bulk water above the bottom of the separator, the vessel level may be expressed as follows:

$$L_v = \frac{V_{b+cu} - V_{b+cu,0}}{A_{L1}}, \quad L_v < 0 \quad (4-35)$$

$$L_v = \frac{V_{b+cu} - V_{b+cu,0}}{A_{L2}}, \quad h_{sep} > L_v \geq 0 \quad (4-36)$$

$$L_v = \frac{V_{b+cu} - V_{b+cu,0} - A_{L2} h_{sep}}{A_{L3}} + h_{sep}, \quad (l_{sepl} > L_v \geq h_{sep}) \quad (4-37)$$

$$L_v = \frac{V_{b+cu} - V_{b+cu,0} - A_{L2} h_{sep} - A_{L3}(l_{sepl} - h_{sep})}{A_v} + l_{sepl}$$

$$L_v > l_{sepl} \quad (4-38)$$

where $V_{b+cu,0}$ is the bulkwater volume when $L_v = 0$ (volume of the bulkwater region below the separator discharge skirt)

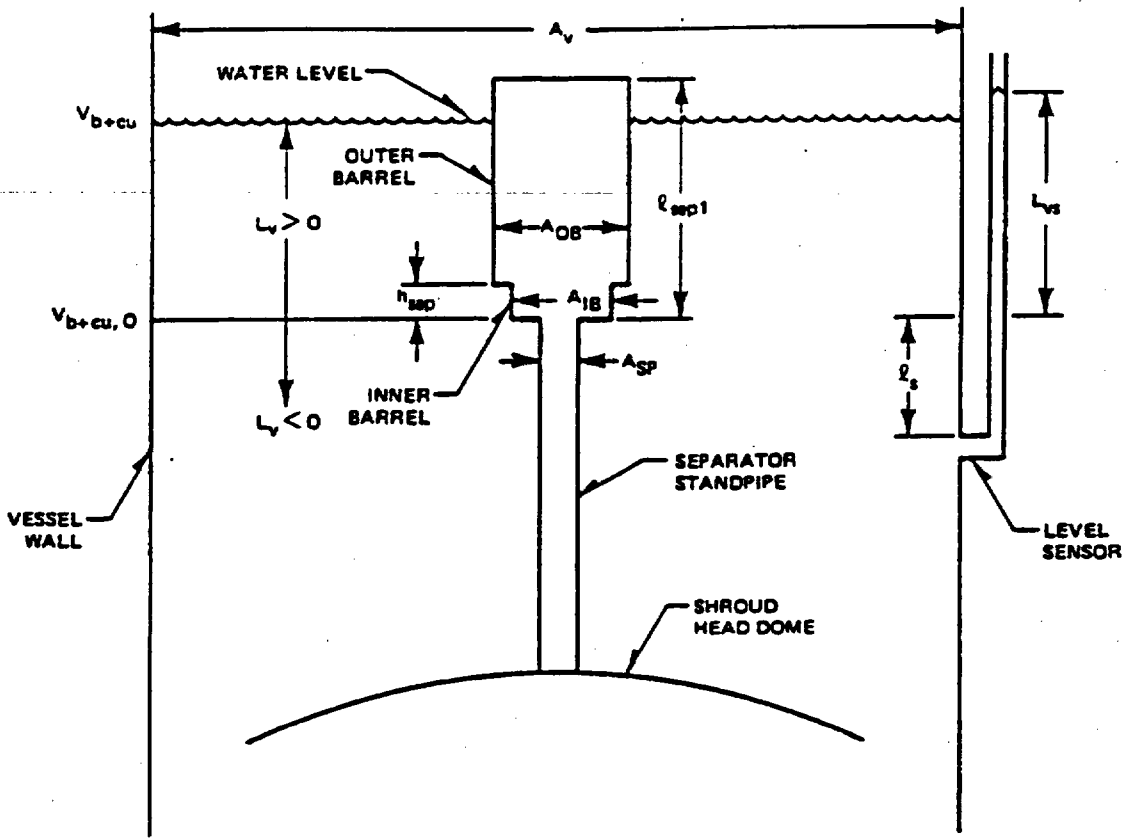


Figure 4-4. Vessel Level Schematic

and

$$A_{L1} = A_v - N_{sep} A_{SP} \quad (4-38a)$$

$$A_{L2} = A_v - N_{sep} A_{IB} \quad (4-38b)$$

$$A_{L3} = A_v - N_{sep} A_{OB} \quad (4-38c)$$

The level sensor measures the differential static pressure between a tap on the side of the vessel and the bottom of a reference leg of water, maintained at constant temperature. The level signal appearing at the input to the feedwater control system, in terms of height of saturated water, is given by

$$L_{vs} = \frac{(l_s + L_v) \rho_{b+cu}}{\rho_{f2}} - l_s \quad (4-39)$$

where

$$\rho_{b+cu} = \frac{1}{V_{b+cu}} (M_{fb} + M_{gb}) \quad (4-40)$$

4.1.4 Steam Line Model Description

The pressure and flow behavior in the steam line is described by the conservation of mass and momentum equations:

$$\frac{\partial c}{\partial t} = - \frac{\partial Q}{\partial x} \quad (4-41)$$

$$\frac{\partial Q}{\partial t} = - \frac{\partial P}{\partial x} - \frac{KQ|Q|}{\rho} \quad (4-42)$$

where ρ is the density of the steam, P is the pressure, Q is the mass flow per units area, and x is the distance along the steamline. The flow-squared term in Equation 4-42 represents losses due to friction. The steam is assumed to behave isentropically, so that the energy balance is described as,

$$\frac{P}{\rho^\gamma} = \text{constant} \quad (4-43)$$

where γ is the ratio of specific heats for steam.

Differentiating Equation 4-43 with respect to time yields

$$\frac{\partial \rho}{\partial t} = \frac{\rho}{\gamma P} \frac{dP}{dt} \quad (4-44)$$

permitting Equation 4-41 to be expressed as,

$$\frac{\partial P}{\partial t} = - \frac{\gamma P}{\rho} \frac{\partial \rho}{\partial x} \quad (4-45)$$

Equations 4-42 and 4-45 are solved by nodalizing the steam and bypass lines. An eight node steam line is shown schematically in Figure 4-5. Note that the main steam line is divided into six segments, or nodes, and the bypass steam line is described by two nodes.^{Q19} The first node incorporates the steam line volume between the vessel and the safety and relief valves, while the second node includes the remaining volume up to the MSIV's. The four nodes downstream of the MSIV's describe the remainder of the main steam line and their dimensions can be adjusted to provide for varying cross-sectional pipe areas and to allow correct placement of the bypass line which can be attached at nodes 3, 4, 5, or 6. Associated with each node are six physical quantities. These quantities are: A_1 , node cross-sectional area; l_1 , node length; Q_1 , flow through node; P_1 , pressure at end of node; ρ_1 , density of steam within node; and K_1 , a frictional loss coefficient. In addition, in this model the dome is treated as a pure source of pressure, P_0 , which varies according to the thermodynamic response of the vessel dome during system transients. Equations 4-42 and 4-45 are integrated over each node segment to obtain

$$\dot{Q}_1 = \frac{P_{i-1} - P_i - R_i Q_i |Q_i|}{L_1} \quad (4-46)$$

and

$$\dot{P}_1 = \frac{Q_1 - Q_{1+1} - Q_B}{C_1} \quad (4-47)$$

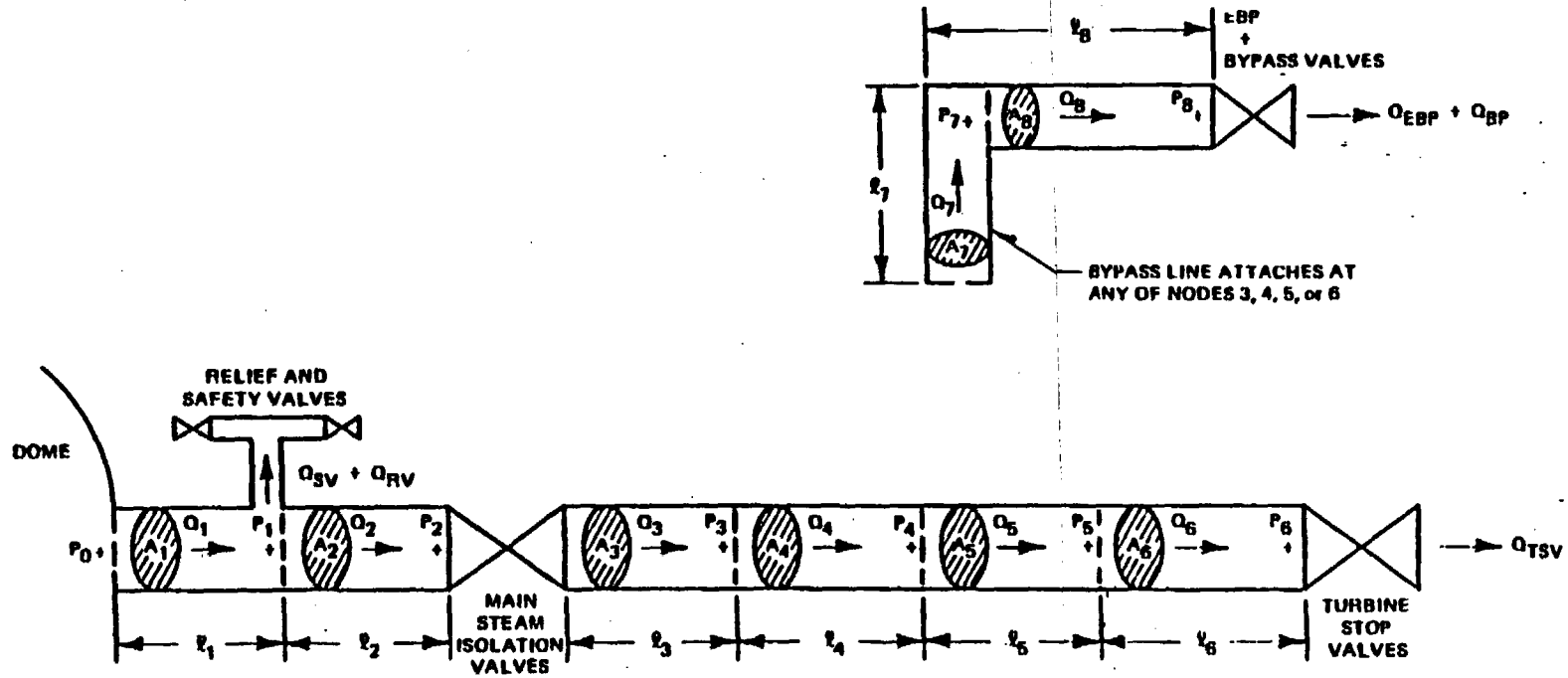


Figure 4-5. Eight Node Steam Line Schematic

where

$$R_i = \frac{(K_i + K_{MSIV})}{\rho_i} \quad (4-48)$$

$$L_i = \frac{l_i}{(144)(32.2) A_i} \quad (4-49)$$

$$C_i = \frac{l_i A_i \rho_i}{\gamma P_i} \quad (4-50)$$

The quantity Q_B represents the flow through a branch contained in node i . This branch may be the bypass line, in which case it is Q_7 , the flow through the first bypass node. It also may represent the safety and relief valve flow. At the end of the steam line, Q_{i+1} is replaced by the turbine or bypass valve flows. These flows are based on total steam flow and valve position.

It is seen that each of the R , L , and C elements are dependent on readily available parameters. The lengths and areas of each node vary with the plant being simulated, values of K are obtained from initial pressure drop data, and the density, ρ_i , is calculated at any time using Equation 4-64. Near 1000 psia (typical operating pressure), γ varies from 1.26 to 1.05 based on quality and steam temperature and is obtained from steam tables.

4.1.4.1 Safety and Relief Valve Model

The relief and safety valves provide high-pressure relief for the vessel if their setpoints are exceeded. The location of the relief and safety valves is along the steam line prior to the isolation valves. Generally, the relief and safety valves do not reseal at the setpoint pressure where they open. The typical valve lift characteristics for pop-action relief and spring-action

safety valve operation are shown in Figure 4-6. The flow through the relief valves is governed by

$$\dot{m}_{RU} = (m_{RC} - m_{RU})/\tau_{RV} \quad (4-51)$$

$$m_{RV} = \begin{cases} m_{RU} \left(\frac{P_{RL}}{P_{RL,0}} \right), & \text{if } P_{RL} > P_{RS,0} \text{ or } P_{RL} > P_{RR,i} \text{ after } P_{RL} > P_{RS,i} \\ 0 & \text{otherwise} \end{cases} \quad (4-52)$$

where $P_{RL,0}$ is the initial line pressure.

The total relief valve rated capacity, m_{RC} , is obtained from the individual relief capacity at initial line pressure

$$m_{RC} = N_{RV} C_{RV} (P_{RL,0}) \quad (4-53)$$

The safety valve flow is determined similar to the relief valve flow

$$\dot{m}_{SU} = (m_{SC} - m_{SU})/\tau_{SV} \quad (4-54)$$

$$m_{SV} = \begin{cases} m_{SU} \left(\frac{P_{RL}}{P_{RL,0}} \right), & \text{if } P_{RL} > P_{ss,i} \text{ or } P_{RL} > P_{SR,i} \text{ after } P_{RL} > P_{ss,i} \\ 0 & \text{otherwise.} \end{cases} \quad (4-55)$$

Because of the characteristics of the relief and safety valves can be different, the rated capacity of the safety valves is

$$m_{SU} = \sum_{\substack{\text{all open} \\ \text{groups, } i}} N_{SVi} C_{SV} (P_{RL,0}) f_{SV} (P_{RL}, P_{ss,i}) \quad 4-56$$

where $f_{SV} (P_{RL}, P_{ss,i})$ is the lift characteristic of the individual safety valve set to open at $P_{ss,i}$. The function f_{SV} can, of course, be used to simulate a wide variety of characteristics, including those of the relief valves if the characteristics are the same. Q20

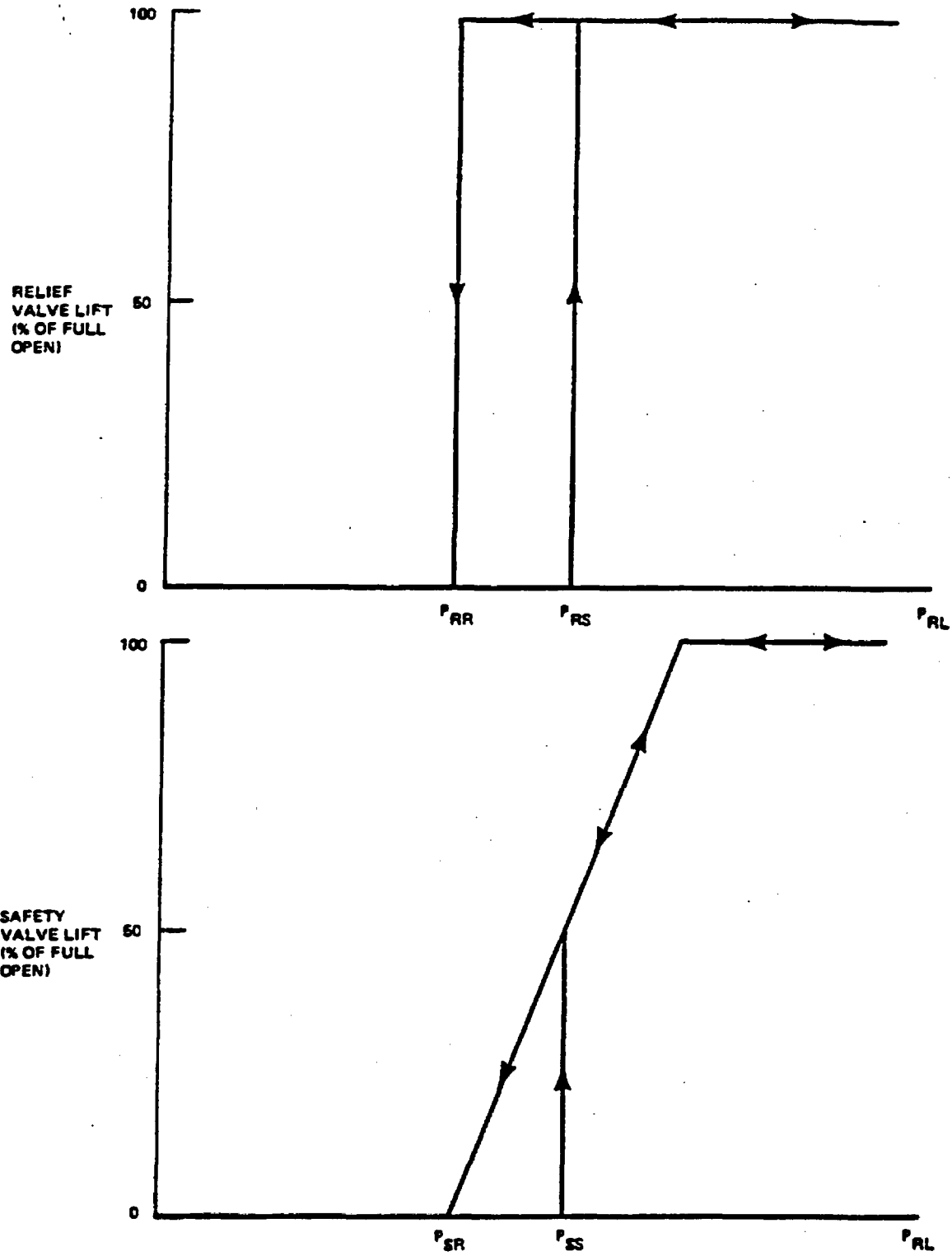


Figure 4-6. Typical Safety and Relief Valve Characteristics

4.1.5 Core Inlet Plenum Enthalpy Balance

There is a time delay before a perturbation in feedwater enthalpy affects the drive and driven flows in jet pump plants. In non-jet pump plants, the delay also exists through the recirculation loops, but due to the separation of downcomer flow into a drive and driven flow in jet pump recirculation systems the jet pump plant time delays affect the recirculation flow in a more complicated fashion. All model flow time delays are obtained in the same manner. They begin by considering an enthalpy balance on a length of line in which no back mixing occurs with negligible heat loss, i.e.,

$$-\frac{\partial h}{\partial x} m_{31} = A_D \rho_l \frac{\partial h}{\partial t} \quad (4-57)$$

with the boundary condition that

$$h = h_{33}(t) \text{ at } x = 0 \text{ (feedwater sparger)}$$

where h is the enthalpy and ρ is the density of the fluid.

4.1.5.1 Jet Pump Recirculation Systems

The enthalpy balances of the core inlet plenum and jet pump regions depend on the following assumptions:

1. Perfect mixing of suction and drive flow occurs in the jet pump throat.
2. Perfect mixing occurs in the vessel inlet plenum.
3. The liquid entering the core is at the average enthalpy of the plenum.
4. The inlet plenum is incompressible so that pressure rate effects on properties and enthalpy can be neglected.

The solution to Equation 4-57 at the jet pump throat entrance is the familiar delay solution

$$h_{ti} = h_{33}(t - \tau_{DC}), \quad t > \tau_{DC} \quad (4-58)$$

$$h_{ti} = h_{33}(0) \quad t \leq \tau_{DC} \quad (4-59)$$

where

$$\int_{t-\tau_{DC}}^t m_{RL} \bar{c}_r dt' = V_D / N_L \quad (4-60)$$

There is an additional delay through the recirculation loop so that drive flow enthalpy at the nozzle exit becomes

$$h_{nozi} = h_{33}(t - \tau_{DC} - \tau_{Ri}) - H_{los}/m_{31}, \quad t > \tau_{DC} + \tau_{Ri} \quad (4-61)$$

$$h_{nozi} = h_{33}(0) - H_{los}/m_{31}, \quad t \leq \tau_{DC} + \tau_{Ri} \quad (4-62)$$

Again the time delay, τ_{Ri} , can be obtained from a volume balance similar to τ_{DC}

$$\int_{t-\tau_{Ri}}^t m_{d1} \bar{c}_r dt' = \frac{V_{NE}}{N_L} + V_R \quad (4-63)$$

Finally, the diffuser exit enthalpy is the mixing throat enthalpy delayed by flow transport similar to the enthalpy delay through the other parts of the recirculation system

$$h_{DE1}(t) = h_{D1}(t - \tau_{DE1}) \quad t > \tau_{DE1} \quad (4-64)$$

$$\int_{t-DE}^t \frac{m_{RL1}}{\rho_r} dt' = V_{Diff} \quad (4-65)$$

$$h_{DE1}(t) = h_{D1} \quad t < \tau_{DE1} \quad (4-66)$$

The quantities h_{D1} and m_{d1} are obtained from the following mass and energy balances:

Jet pump mass balance (loop 1)

$$m_{RL1} = m_{SCT1} + m_{d1} \quad (4-67)$$

Energy balance inside jet pump

$$m_{RL1} h_{D1} = m_{SCT1} h_{t1} + m_{d1} h_{nozi} \quad (4-68)$$

Energy balance of driven flow entering inlet plenum

$$m_{31} h_{3v} = h_{DE1} N_1 m_{RL1} + h_{DE2} N_2 m_{RL2} \quad (4-69)$$

4.1.5.2 Non-Jet Pump Recirculation Systems

Assumptions 2 through 4 of Subsection 4.1.5.1 also apply to non-jet pump recirculation systems.

The non-jet pump plant recirculation flow enthalpy at the lower plenum is due to a single delay through the entire downcomer-recirculation loop:

$$h_{LP1} = h_{33}(t - \tau_{NJ1}) - H_{1os}/m_{31}, \quad t > \tau_{NJ1} \quad (4-70)$$

$$h_{LP1} = h_{33}(0) - H_{1os}/m_{31}, \quad t \leq \tau_{NJ1} \quad (4-71)$$

where τ_{NJ1} is obtained by solving

$$\int_{t-\tau_{NJ1}}^t \frac{m_{RL1}}{\rho_r} dt' = \frac{V_D}{N_L} + V_R \quad (4-72)$$

The energy balance of inlet flow is expressed as

$$m_{31} h_{3v} = \frac{N_1}{I} m_{RL1} h_{LP1} \quad (4-73)$$

4.1.5.3 Lower Plenum Enthalpy Balance (Applied to Jet Pump and Non-Jet Pump Plants)

$$\dot{h}_{31} = \frac{m_{31}}{V_{LP} \rho_r} (h_{3v} - h_{31}) \quad (4-74)$$

The core inlet subcooling is given by

$$\Delta h = h_f - h_{31} \quad (4-75)$$

4.2 RECIRCULATION FLOW MODEL

4.2.1 Vessel Inlet Flow

4.2.1.1 Jet Pump Recirculation Systems

Refer to Figure 4-7 for a diagram of a jet pump and terminology used in this part of the analysis. While the model shown includes only a single-nozzle jet pump, it is possible to simulate multi-nozzle jet pumps by varying the area of throat and nozzle and adjusting the friction coefficients for flow through the recirculation loops to correspond to the multi-nozzle loop. The momentum balance equations are based on the following assumptions:

1. All recirculation flow liquid is subcooled, incompressible, and one dimensional.

2. Velocity heads in the bulk water, downcomer, and lower plenum are negligible.
3. Flow mixing in the jet pump throat occurs in an inertia and loss-free region which extends from the nozzle downstream to complete momentum exchange.
4. Static pressure is uniform across the suction and drive flow area at the nozzle exit.
5. Inertia in the suction flow jet pump entrant region is negligible.
6. Mixing of suction and drive flow is not appreciable until the jet pump throat entrance is reached by both flows.

The drive flow loop momentum balances are,

1. P_{dwn} to vessel outlet

$$\left(\frac{l_D}{A_D}\right) \frac{\dot{m}_{di}}{g_c} = 144 (P_{\text{dwni}} - P_{\text{voi}}) + \frac{g}{g_c} \bar{\rho}_r \Delta Z_D - K_{\text{dwn}} m_{di}^2 \quad (4-76)$$

2. Vessel outlet to nozzle exit

$$\begin{aligned} \left(\frac{l_{RL}}{A_{RL}}\right) \frac{\dot{m}_{di}}{g_c} &= 144 (P_{\text{voi}} + \Delta P_{pi} - P_{\text{jeti}}) - (K_d + K_{\text{noz}}) m_{di}^2 \\ &- \frac{m_{di}^2}{\left(2\bar{c}_r g_c A_{\text{noz}}^2\right)} - \frac{g}{g_c} \bar{\rho}_r \Delta Z_{RL} \end{aligned} \quad (4-77)$$

3. Summing 1 and 2 above

$$\begin{aligned} \frac{1}{g_c} \left(\frac{l_D}{A_D} + \frac{l_{RL}}{A_{RL}}\right) \dot{m}_{di} &= 144 (P_{\text{dwni}} + \Delta P_{pi} - P_{\text{jeti}}) \\ &- (K_{\text{dwn}} + K_d + K_{\text{noz}}) m_{di}^2 - \frac{m_{di}^2}{2\bar{c}_r g_c A_{\text{noz}}^2} \end{aligned} \quad (4-78)$$

The downcomer pressure is calculated from,

$$P_{\text{dwni}} = P_2 + \left[\frac{g}{g_c} \bar{\rho}_b (\Delta Z_b + L_v) - \frac{\lambda_b}{A_b} \frac{\dot{m}_{RL1}}{g_c} - K_b \dot{m}_{RL1}^2 \right] / 144 \quad (4-79)$$

The total driven flow is given by

1. P_{dwni} to P_{jeti}

$$P_{\text{jeti}} = P_{\text{dwni}} - \frac{1}{144} \left(K_{\text{SCT}} - \frac{1}{2g_c \bar{\rho}_b A_{\text{sct}}^2} \right) \dot{m}_{\text{SCT1}}^2 \quad (4-80)$$

2. P_{thi} to core inlet

$$\left(\frac{l_{\text{LP}}}{A_{\text{LP}}} + \frac{l_{\text{dif}}}{A_{\text{dif}}} \right) \frac{\dot{m}_{RL1}}{g_c} = 144(P_{\text{thi}} - P_I) + \frac{g}{g_c} \Delta Z_{\text{dif}} \bar{\rho}_r - \left(K_{\text{dif}} - \frac{1}{2g_c \bar{\rho}_r A_{\text{th}}^2} \right) \dot{m}_{RL1}^2 \quad (4-81)$$

$$\dot{m}_{31} = N_1 \dot{m}_{RL1} + N_2 \dot{m}_{RL2} \quad (4-82)$$

Summing Equations 4-79, 4-80, and 4-81 with the additional substitution for \dot{m}_{31} from differentiation of Equation 4-82 gives the overall momentum equation for each loop: Q24

$$\frac{1}{g_c} \left[\frac{l_{\text{dif}}}{A_{\text{dif}}} + \frac{l_{\text{LP}}}{A_{\text{LP}}} + \frac{l_b}{A_b} \right] \dot{m}_{RL1} = 144(P_{\text{thi}} - P_{\text{jeti}}) + 144(P_2 - P_e) + \frac{g}{g_c} \left[\bar{\rho}_r \Delta Z_{\text{dif}} + \bar{\rho}_b (\Delta Z_b + L_v) \right] - \left[K_b + K_{\text{dif}} - \frac{1}{2g_c A_{\text{th}}^2 \bar{\rho}_r} \right] \dot{m}_{RL1}^2 - \left[K_{\text{SCT}} + \frac{1}{2g_c A_{\text{sct}}^2 \bar{\rho}_b} \right] \dot{m}_{\text{SCT1}}^2 - 144\Delta P_C \quad (4-83)$$

The jet pump mixing region pressure difference, ΔP_{jet} , is calculated by performing a momentum balance in the momentum exchange of the jet pump. Since this region is small, it can be considered inertia free. The inertia-free momentum balance for the momentum exchange region can be written generally for one-dimensional flow in the following form:

$$\Sigma F = (\dot{m}_{out} V_{out} - \dot{m}_{in} V_{in}) / g_c \quad (4-84)$$

The V_{in} and V_{out} are the velocities in and out of the region, respectively, and are assumed to indicate flow direction at this point. The idealized geometry of the nozzle, suction channel and throat regions is shown in Figure 4-8. ^{Q21}
For forward flow in both loops, it is possible to write the following mass and momentum balance equations:

$$\dot{m}_{RL1} = \dot{m}_{di} + \dot{m}_{SCT1} \quad (4-85)$$

$$\dot{m}_{out} V_{out} = \dot{m}_{RL1} V_{RL1} = \frac{\dot{m}_{RL1}^2}{\rho_r A_{th}} \quad (4-86)$$

$$\dot{m}_{in} V_{in} = \dot{m}_{SCT1} V_{SCT1} + \dot{m}_{di} V_{di} \quad (4-87)$$

$$\dot{m}_{in} V_{in} = \frac{\dot{m}_{SCT1}^2}{\rho_r A_{sct}} + \frac{\dot{m}_{di}^2}{\rho_r A_{noz}} \quad (4-88)$$

The force balance on the momentum exchange region is:

$$\Sigma F = (P_{jet} (A_{noz} + A_{SCT}) - P_{thi} A_{thi}) 144 \quad (4-89)$$

$$\Sigma F = 144 (P_{thi} - P_{jet}) A_{th} = 144 (-\Delta P_{jet} A_{th}), \quad (4-90)$$

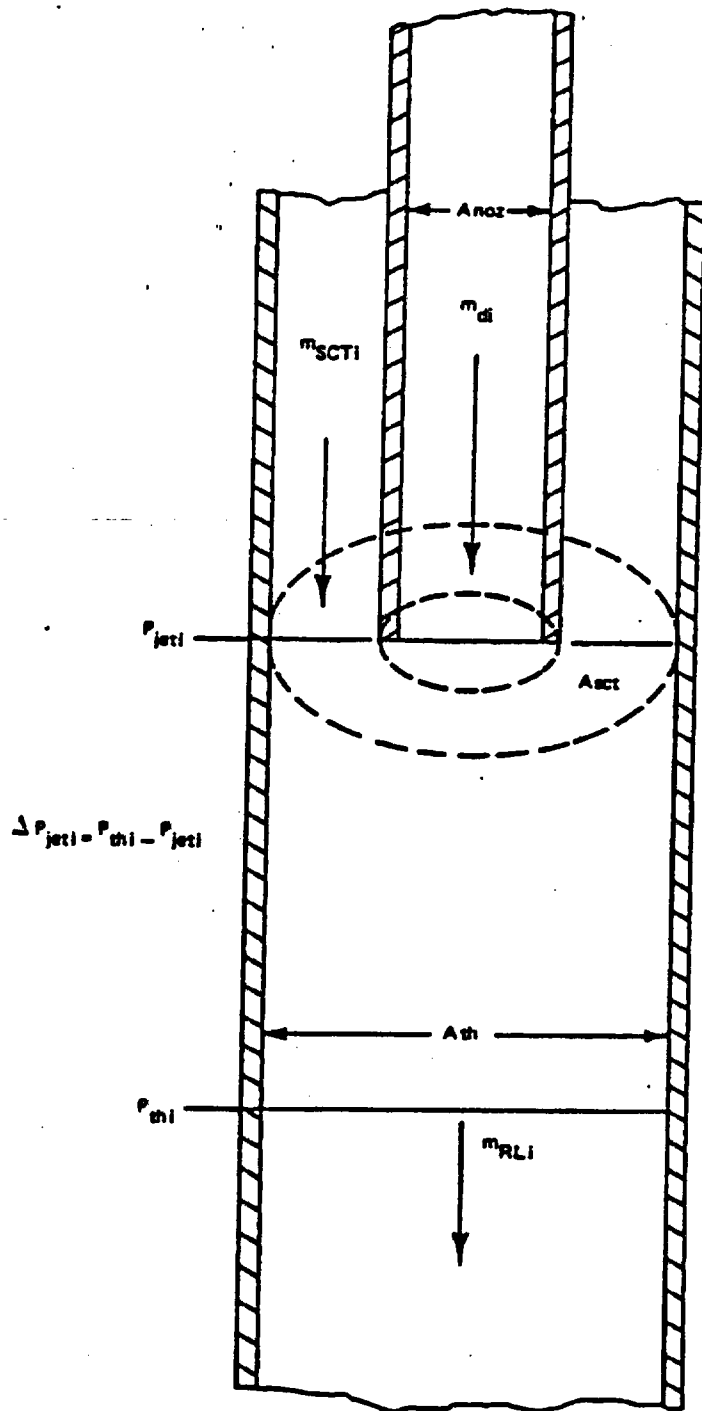


Figure 4-8. Jet Pump Throat Diagram

hence

$$\Delta P_{jet} = \left(\frac{m_{di}^2}{A_{noz}} + \frac{m_{SCT}^2}{A_{sct}} - \frac{m_{RLi}^2}{A_{th}} \right) / 144 \bar{\rho}_T g_c A_{th} \quad (4-91)$$

The result of Equation 4-91 holds in all flow cases for the geometry of Figure 4-8. The specific cases are: (1) all flows forward, (2) suction flow reversed ($m_d = m_{SCT} + m_{RL}$), (3) suction and diffuser flow reversed with forward drive flow ($m_{SCT} = m_d + m_{RL}$), and (4) all flows reversed ($m_{RL} = m_d + m_{SCT}$).^{Q22}

4.2.1.2 Non-Jet Pump Recirculation Systems

Refer to Figure 4.7a for a diagram illustrating the non-jet pump terminology. Summing the momentum balance equations from the vessel outlet through the recirculation system and back into the vessel inlet plenum, gives

$$\begin{aligned} \frac{1}{g_c} \left(\frac{l_{RL}}{A_{RL}} \right) \dot{m}_{RLi} &= 144(\Delta P_{pi} - P_I + P_{voi}) + \frac{g}{g_c} \Delta Z_{RL} \bar{c}_r \\ &- K_{RL} m_{RLi}^2 - K_{LP} m_{RLi}^2 \end{aligned} \quad (4-92)$$

This equation describes the transient loop flow through either recirculation loop of the system.

The equation for the flow in the downcomer is

$$\begin{aligned} \frac{l_D}{g_c A_D} \dot{m}_{RLi} &= 144(P_2 - P_{voi}) + \frac{g}{g_c} (\bar{\rho}_r \Delta Z_D + \bar{\rho}_b L_v + \bar{\rho}_b \Delta Z_b) \\ &- K_D m_{RLi}^2 \end{aligned} \quad (4-93)$$

Differentiating the mass balance in the lower plenum yields

$$\frac{dm_{3l}}{dt} = \sum_i N_i \frac{dm_{RLi}}{dt} \quad (4-94)$$

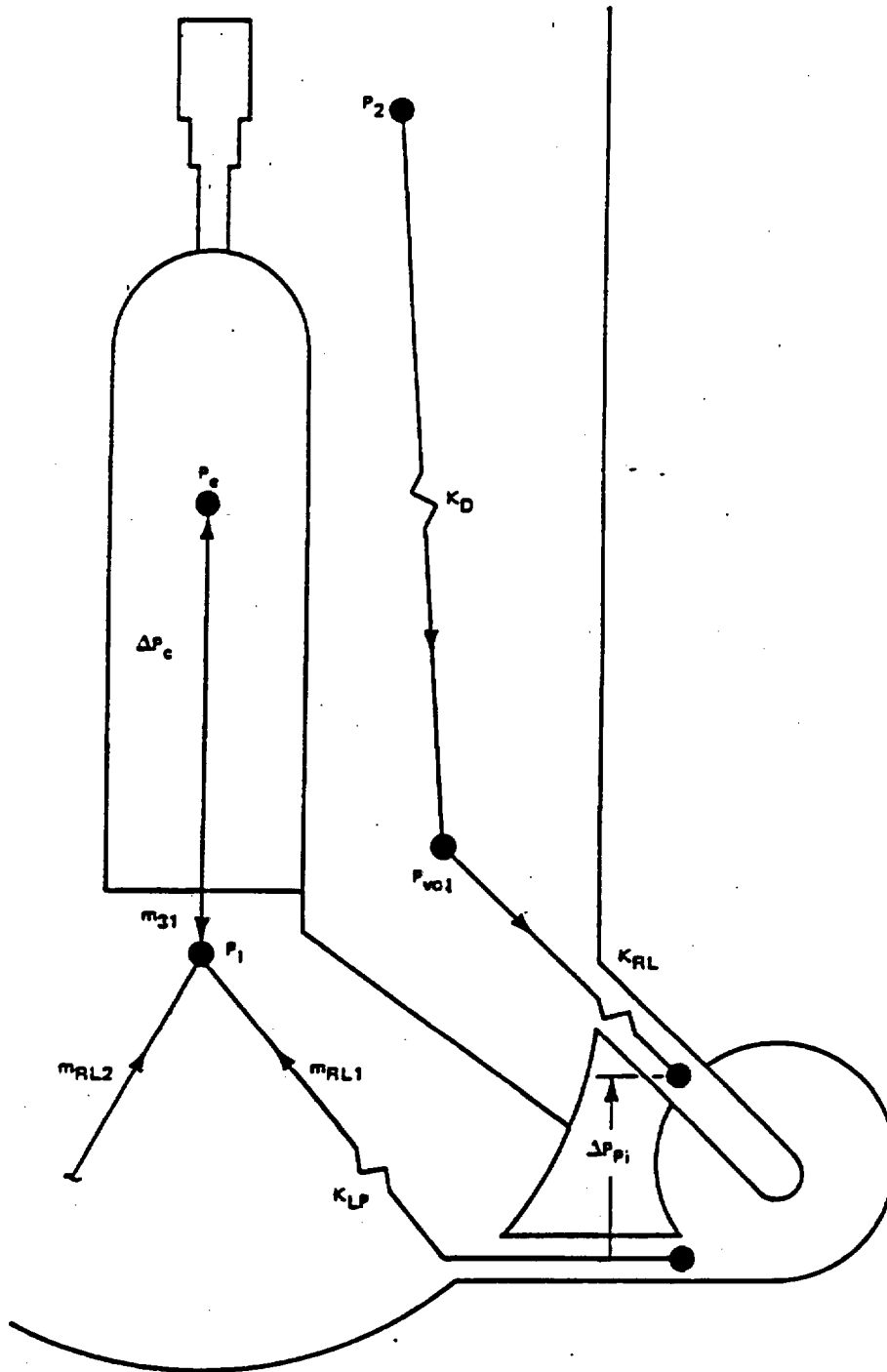


Figure 4-7a. Non-Jet Pump Schematic

Substituting Equation 4-94 into Equation 4-92 and adding Equations 4-92 and 4-93 yields the following equation describing the transient flow in loop 1

$$\frac{1}{g_c} \left[\frac{l_{RL}}{A_{RL}} + \frac{l_D}{A_D} \right] \dot{m}_{RL1} = 144(P_2 - P_e + \Delta P_{pi}) + \bar{\rho}_b (L_v + \Delta Z_b) \frac{g}{g_c} + \frac{g}{g_c} \bar{\rho}_r (\Delta Z_D + \Delta Z_{RL}) - K_{RL} m_{RL1}^2 - (K_D + K_{LP}) m_{RL1}^2 \quad 144 \Delta P_C \quad (4-95)$$

where ΔP_C is obtained from the core model. Q23

4.2.2 Recirculation Pump Drive Systems

4.2.2.1 Pump and Pump Drive Motor

The recirculation pump drive motor power comes from either a drive motor connected to a generator unit through a fluid coupler or the power plant output directly. In either case, the pump torque requirements and pressure head produced can be approximated by the following equation "fits" to the manufacturer's curves as a function of pump flow and shaft speed,

$$T_{mi} = K_{PT1} n_{pi}^2 + K_{PT2} m_{pi} n_{pi} + K_{PT3} (m_{pi} + K_{PT4} n_{pi}) |m_{pi} + K_{PT4} n_{pi}| \quad (4-96)$$

and

$$\Delta P_{pi} = K_{PH1} n_{pi}^2 + K_{PH2} m_{pi} + K_{PH3} (m_{pi} + K_{PH4}) |m_{pi} + K_{PH4}| \quad (4-97)$$

for forward and reversed flow operation. Typical curves are shown in Figures 4-9 and 4-10. The equation describing pump-motor shaft speed is

$$\frac{\pi J_p}{30g_c} \frac{dn_{pi}}{dt} = (T_{eli} - T_{mi}) \quad (4-98)$$

Disregarding small motor time constants, the electrical drive-motor torque is found from its torque-speed characteristic. Typical curves are shown in Figure 4-11.

$$T_{eli} = T_{eli}(n_{pi}) \quad (4-99)$$

In analyses of a specific plant, it is, of course, necessary to use the pump curves appropriate for the equipment installed in the plant.

4.2.2.2 Motor-Generator Units

If pump motor power comes from an M/G set, the response of the fluid coupler must be included in the transient model of the plant. Torque transmitted by the coupler is related to slip between the drive motor and generator and the coupling position of the scoop tube by fitting the following formula to the manufacturer's curves

$$T_{ci} = T_{C,rated} X_{ci}^3 \left\{ K_{CT1} \left| \frac{n_{di} - n_{gi}}{n_{d,rated}} \right|^3 + K_{CT2} \right\} \left(\frac{n_{di} - n_{gi}}{n_{d,rated}} \right) \quad (4-100)$$

Typical curves of T_{ci} are indicated in Figure 4-12 neglecting small time constants.

The drive motor shaft speed is obtained from the torque balance between electrical and coupler drive torques,

$$\frac{\pi J_{di}}{30g_c} \frac{dn_{di}}{dt} = T_{edi} - T_{ci} \quad (4-101)$$

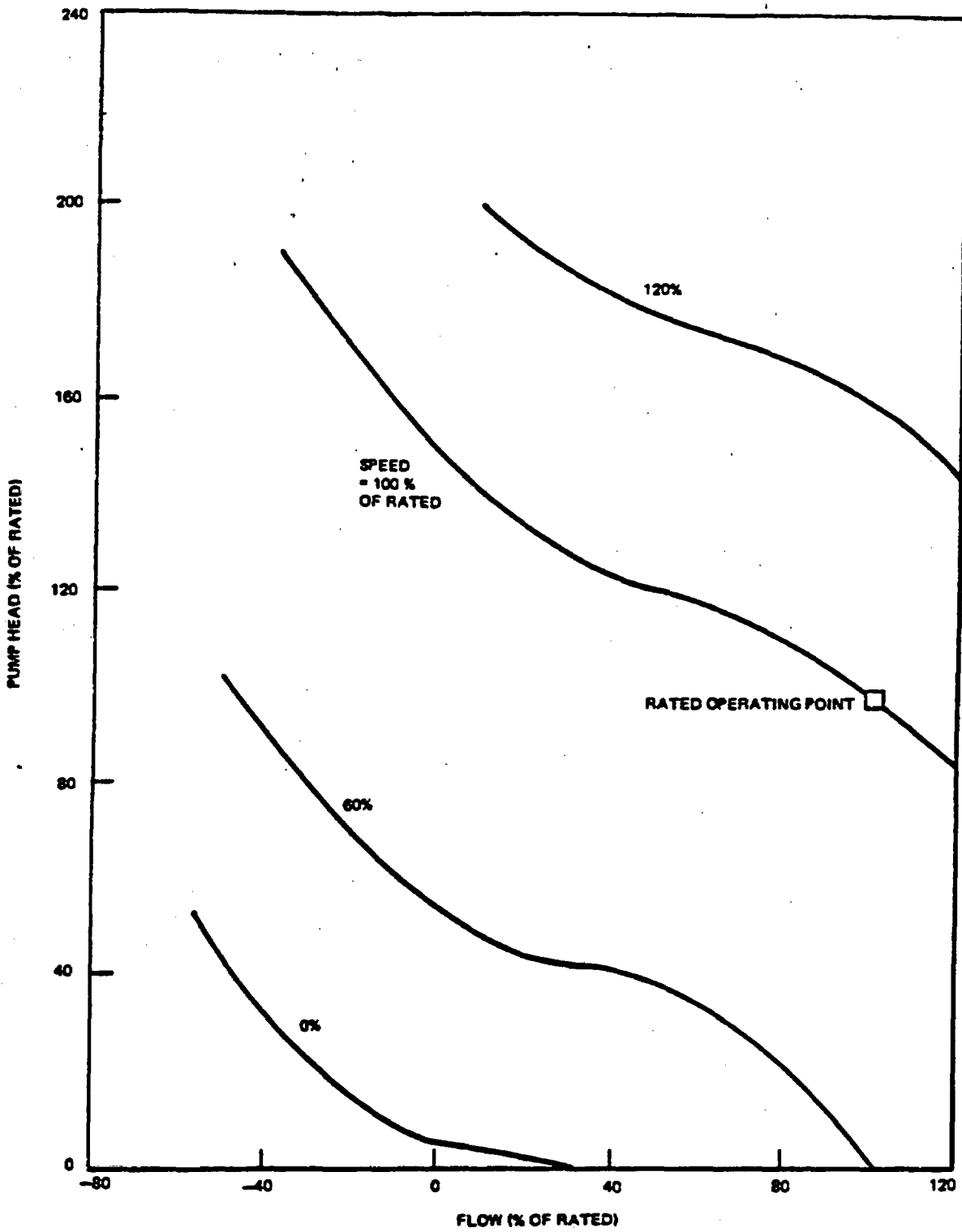


Figure 4-9. Typical Recirculation Pump versus Flow and Speed

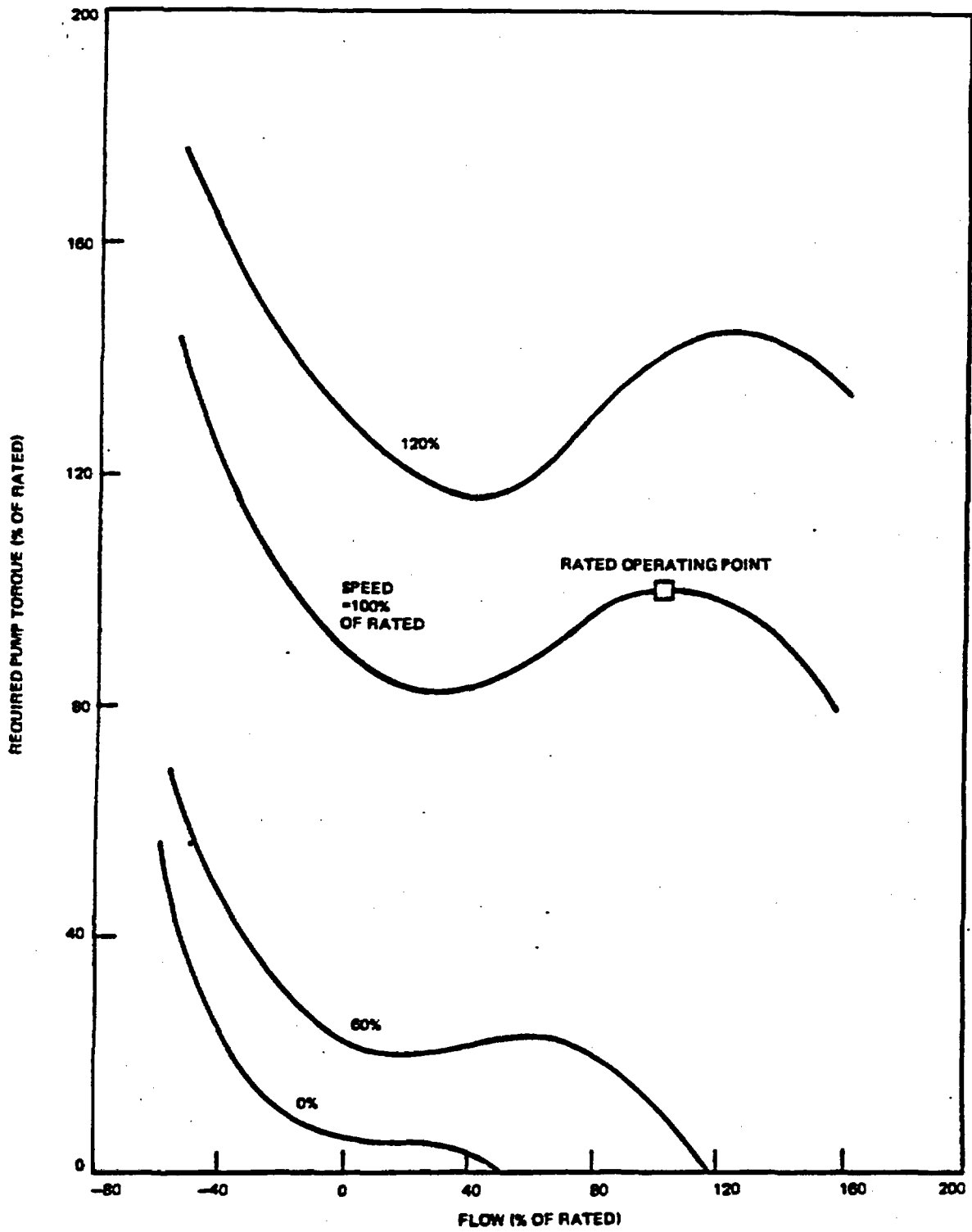


Figure 4-10. Typical Pump Torque Characteristic versus Flow and Speed

NEDO-24154-A

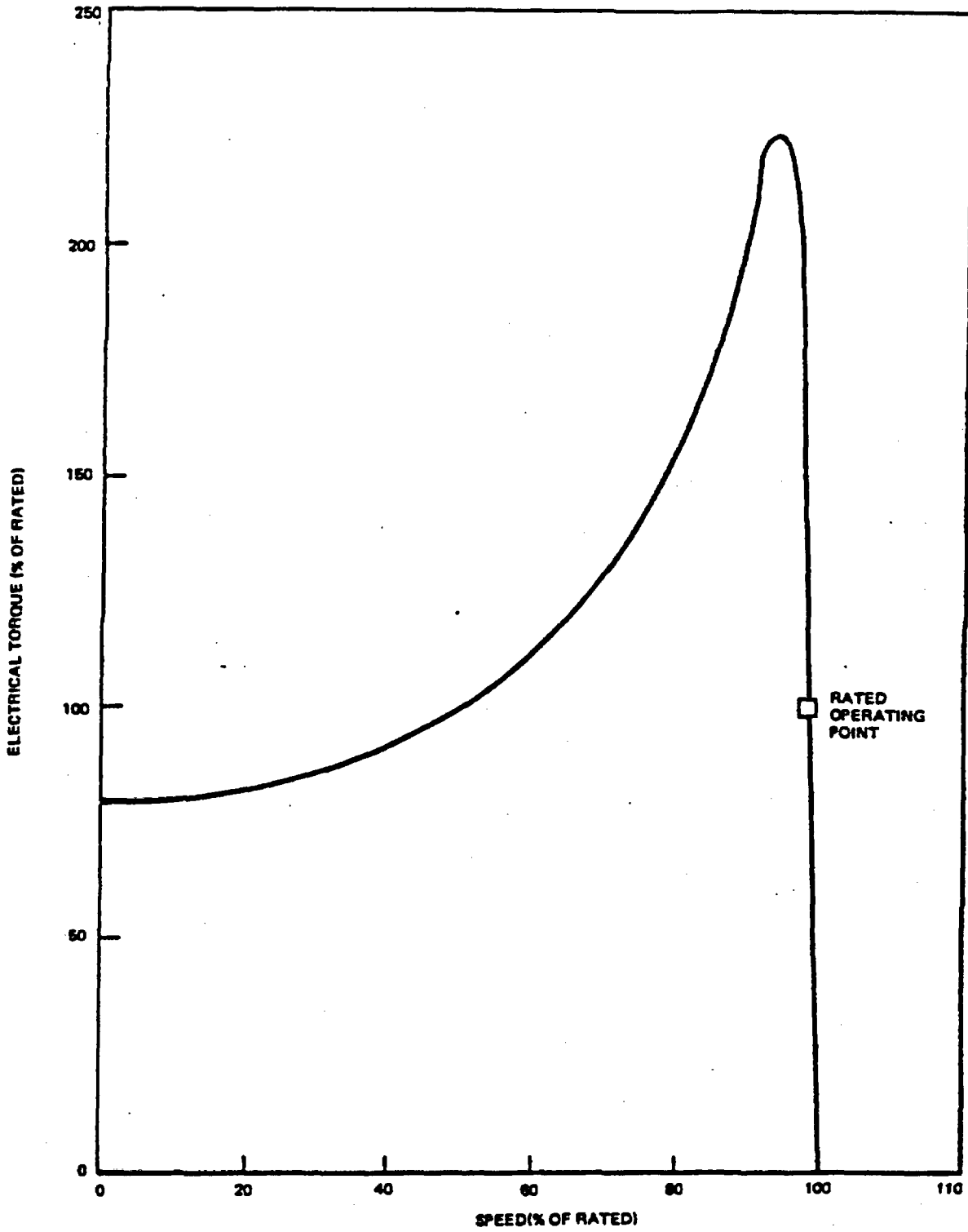


Figure 4-11. Typical Recirculation Pump Motor Electrical Torque versus Speed (Constant Excitation Voltage)

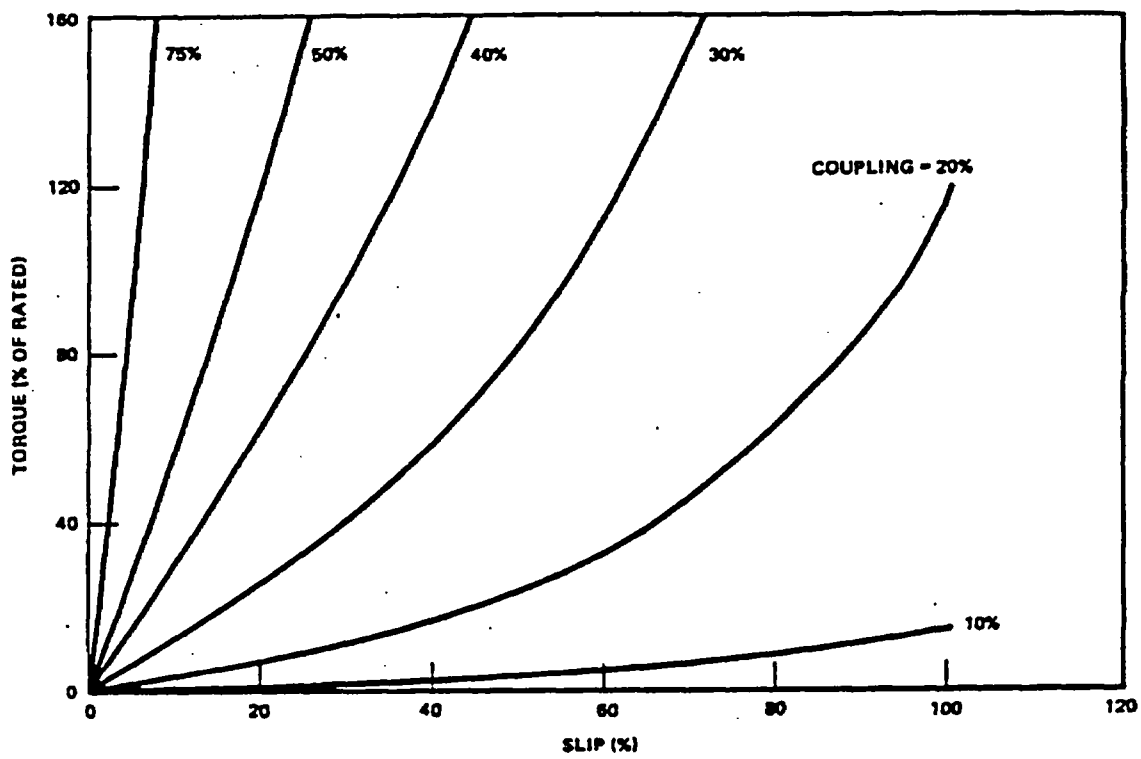


Figure 4-12. Typical Transmitted Coupler Torque versus Slip and Coupling

The electrical torque to the drive motor, T_{edi} , is obtained from the manufacturer's torque speed characteristics which will be similar to Figure 4-11.

The generator shaft speed follows from the torque balance between the coupler output and pump motor power requirements

$$\frac{\pi J_{gi}}{30g_c} \frac{dn_i}{dt} = T_{ci} - T_{gi} \quad (4-102)$$

The recirc pump electrical torque, T_{e2i} is coupled to the generator torque through the pumping power and the efficiency of the generator and pump units

$$T_{gi} = \frac{\eta_{pi} T_{e2i}}{\eta_{gi} \eta_{gen} \eta_{pump}} \quad (4-103)$$

4.3 CONTROL SYSTEMS

4.3.1 Valve Flow Control

The valve flow control block diagrams are shown in Figures 4-1b and 4-13. Gains, time constants, and limiters must be input for the specific plant design. ^{Q42}

4.3.2 Motor-Generator Flow Control

The motor-generator flow control block diagrams are shown in Figures 4-1a and 4-14. Gains, time constants, and limiters must be input for the specific plant design. ^{Q43}

4.3.3 Feedwater Flow

The three-element feedwater control system used in the transient model is presented in Figure 4-15. By proper choice of the steam flow gain, K_{LS} , the steady-state level may be programmed with power, depending on the requirements of steam separator performance. The transient response of steam-driven

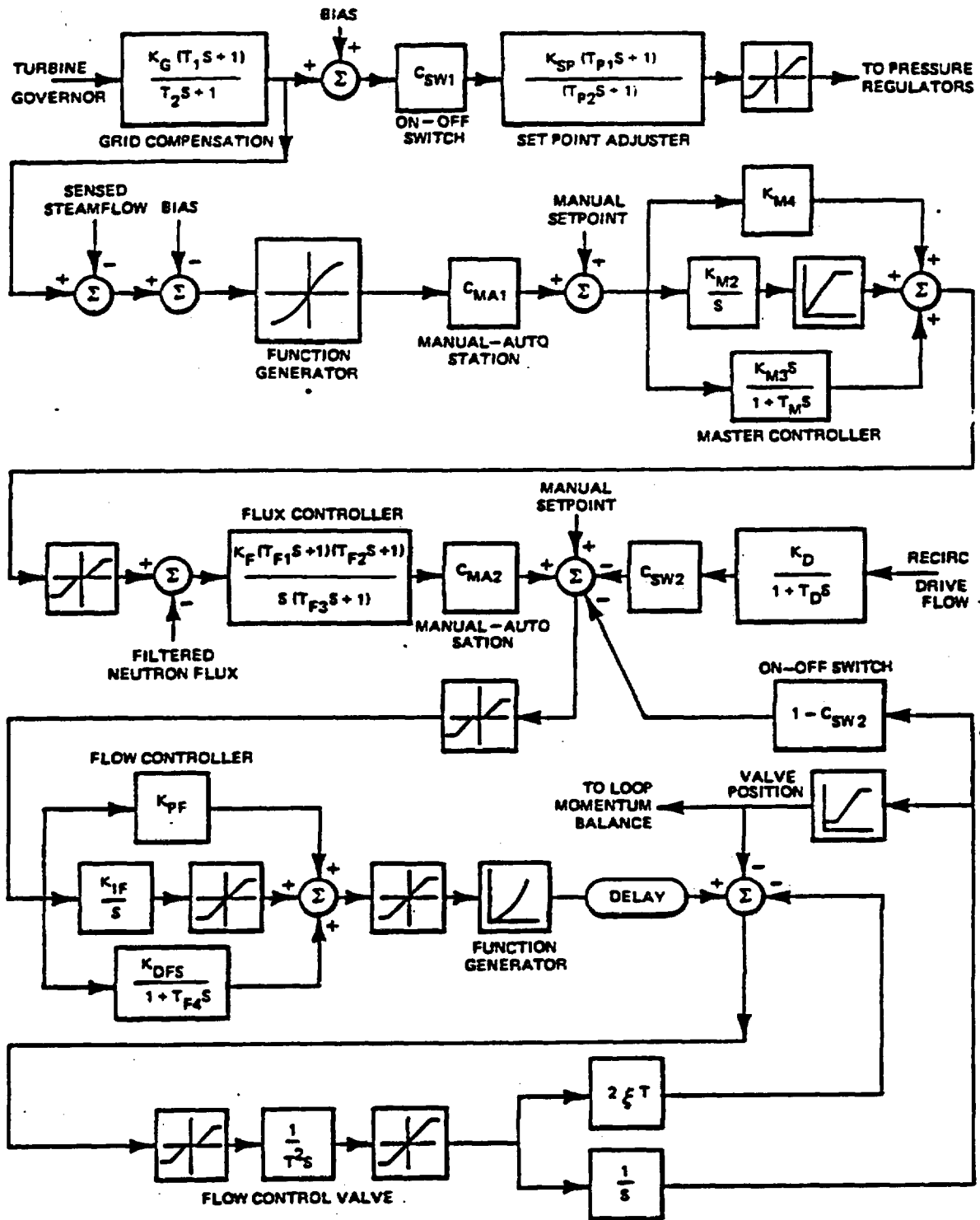


Figure 4-13. Valve Flow Control Block Diagram

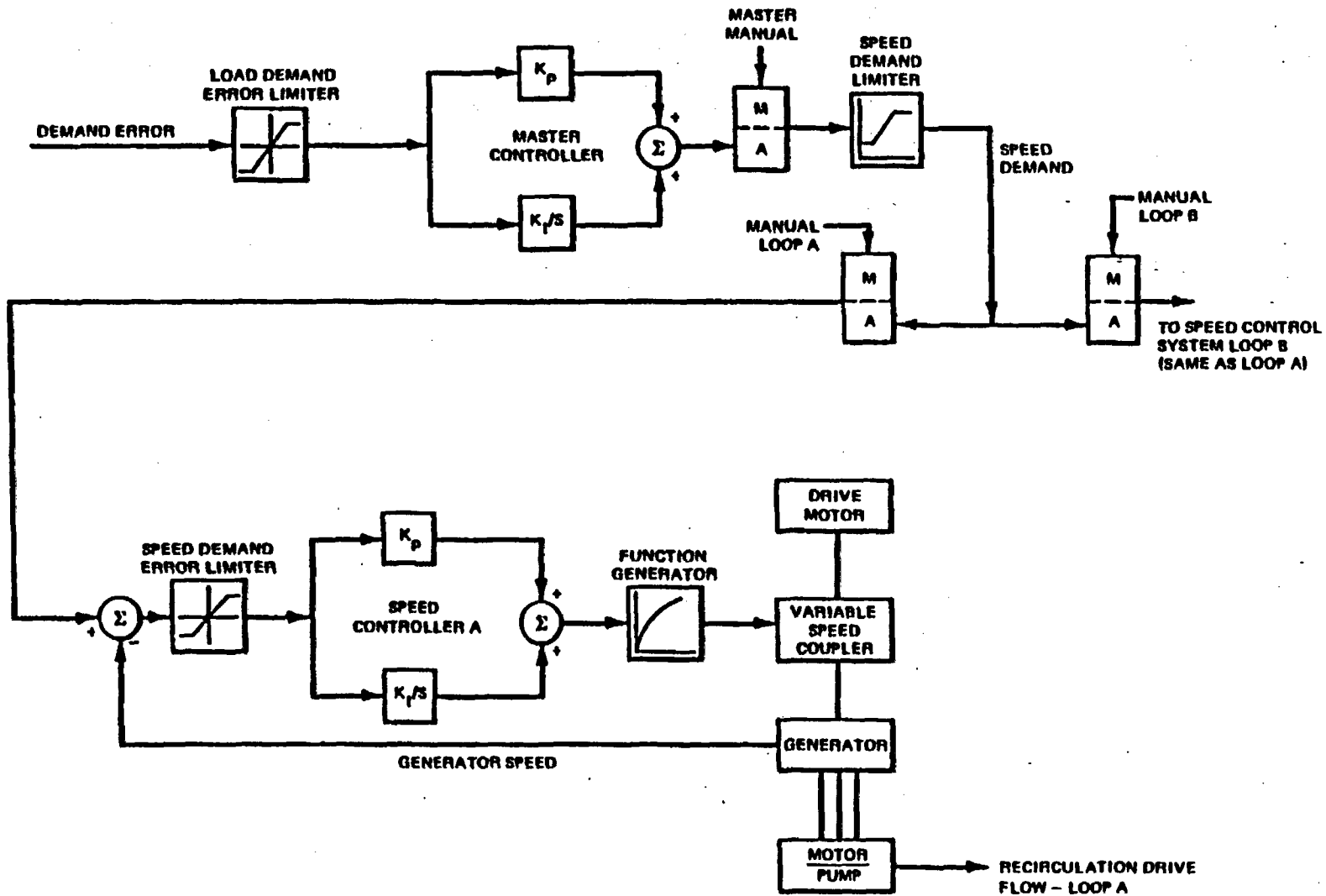


Figure 4-14. Motor-Generator Flow Control Block Diagram

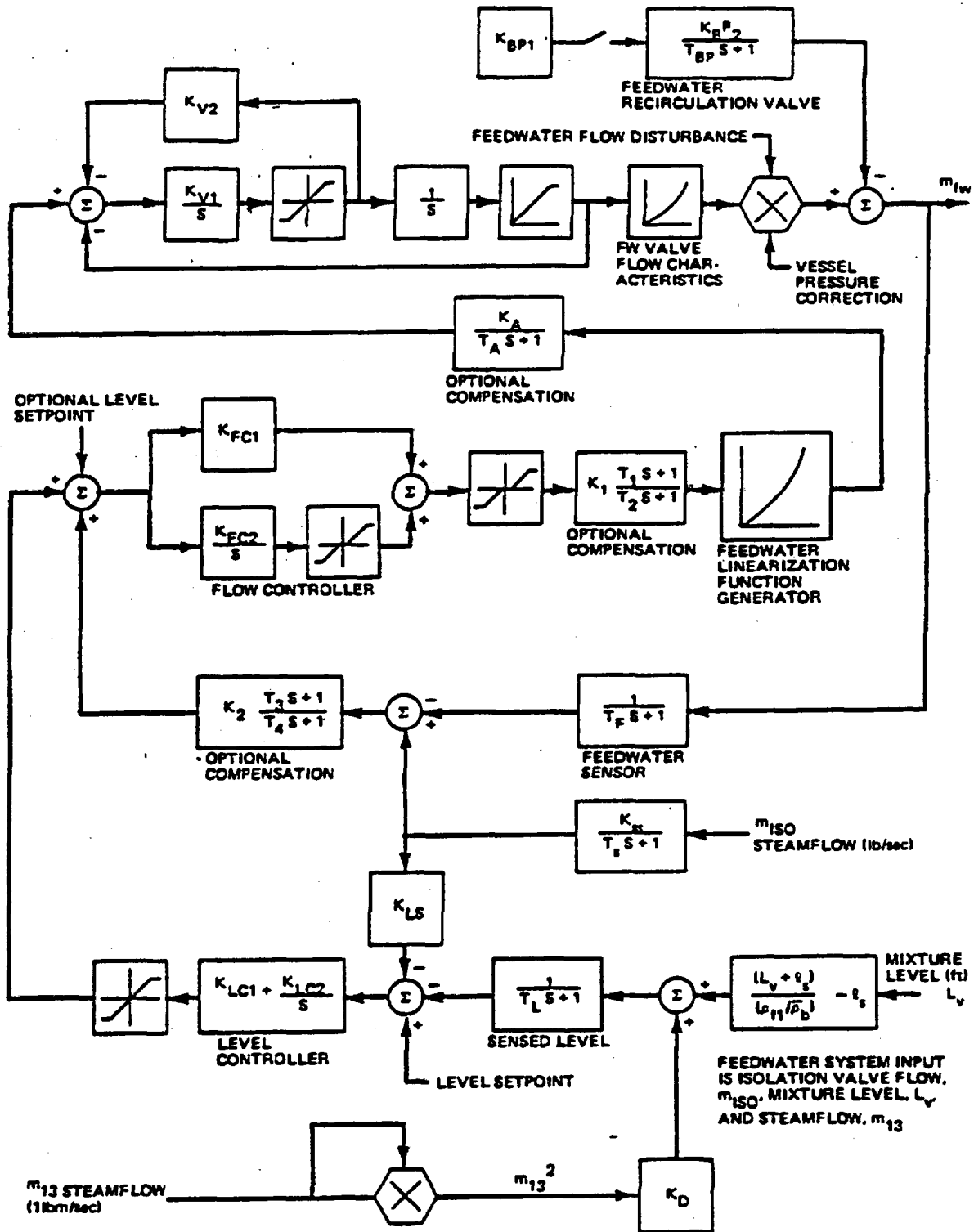


Figure 4-15. Feedwater Control

feedwater pumps is simulated through the use of the optional compensator and constants K_A and T_A .^{Q44}

4.3.4 Pressure Regulator and Turbine Controls

A typical pressure regulator and turbine control system simulation used in the transient model is presented in block diagram form in Figure 4-16. Numerical values for gains and time constants must be input for each plant design.^{Q45, Q47}

4.4 REACTOR SAFETY SYSTEMS

That part of the reactor safety system concerned with the high flux scram, the high vessel pressure scram, and the manual scram, is simulated through digital logic in the transient model. The safety system model includes the differential equations describing a flux filter which may be switched in or out of the high flux scram circuit. With this circuit active, true neutron flux is related to the circuit output by

$$n_s = \frac{K_s (1 + T_2 s)(1 + T_3 s)}{(1 + T_1 s)(1 + T_4 s)} n \quad (4-104)$$

where

$$T_1 < T_2 < T_3 < T_4$$

Automatic scram of the reactor occurs when neutron flux or pressure exceed the scram setpoint. In the case of neutron flux, the setpoint can be adjusted with the sensed recirculation loop flow. The sensed flow is related to the actual flow through a sensor time constant. In Laplace transform variables, this relationship is:^{Q46, Q47}

$$m_s = \frac{m_{31}}{1 + T_{Cs} s} \quad (4-105)$$

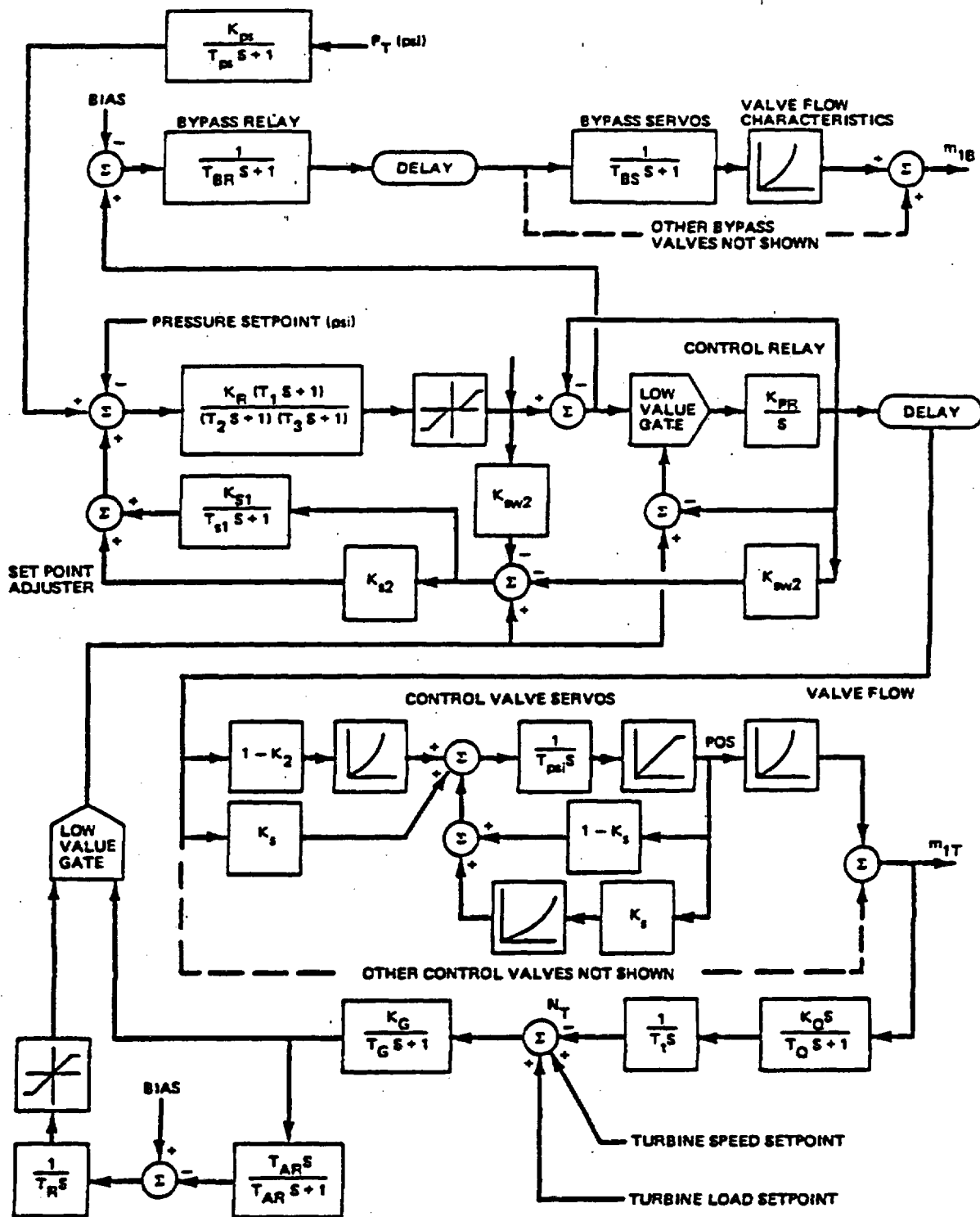


Figure 4-16. Pressure Regulator Block Diagram

The flux scram set point then becomes

$$n_{set} = n_{set0} + \frac{\partial n_{set}}{\partial m_{31}} \left(\frac{m_s}{m_{31, rated}} - 1 \right), \quad m_s < m_{31}, \quad (4-106)$$

If the sensed flow, m_s , exceeds the rated flow, the setpoint of the flux scram is the full-power flux scram setpoint, n_{set0} . Thus,

$$n_{set} = n_{set0}, \quad m_s \geq m_{31, rated} \quad (4-107)$$

4.5 NOMENCLATURE

A_D	Bulkwater and downcomer flow area, ft^2
A_D	Downcomer flow cross section, ft^2
A_{LP}	Inlet plenum flow cross section, ft^2
A_P	Vessel plenum flow cross section, ft^2
A_{RL}	Recirculation line cross section, ft^2
A_{sp}	Separator standpipe cross section, ft^2
A_{IB}	Separator inner downcomer cross section, ft^2
A_{OB}	Separator outer downcomer cross section, ft^2
\hat{A}	Effective separator rotational flow cross section, ft^2
A_v	Pressure vessel cross section, ft^2
A_{th}	Jet pump throat area, ft^2
A_{open}	Full open area of isolation valves, ft^2
$A(t)$	Isolation valve area at time t , ft^2
A_{noz}	Jet pump nozzle area, ft^2
A_{sct}	Jet pump suction area, ft^2
A_{L1}	Vessel area at standpipes, ft^2
A_{L2}	Vessel area at inner separator downcomer barrel, ft^2
A_{L3}	Vessel area at outer separator downcomer barrel, ft^2

NEDO-24154-A

C_{sep}	Separator friction coefficient
$C_{RV}(P_{RL,0})$	Capacity of individual relief valve open at $P_{RL,0}$, lb/sec
$C_{SV}(P_{RL,0})$	Capacity of individual safety valve open at $P_{RL,0}$, lb/sec
D_2	Denominator of vessel pressure rate equation, Btu/psi
$f_B(X_{Bj})$	Characteristic of bypass valve, per unit
$f_{SV}(P_{RL}, P_{ss,i})$	Safety valve capacity characteristic, per unit
$f_T(X_{Tj})$	Characteristic of j^{th} turbine control valve, per unit
g	Acceleration of gravity, ft/sec ²
g_c	Newton's law, conversion factor lb-ft/sec ² -lb _c
h_{3v}	Mixed enthalpy at lower plenum inlet, Btu/lb
h_{31}	Mixed enthalpy at core inlet, Btu/lb
h_{33}	Enthalpy in vessel downcomer, Btu/lb
h_{cs}	High pressure core spray enthalpy, Btu/lb
h_{fi}	Liquid saturation enthalpy in i^{th} pressure node, Btu/lb
h_{gi}	Steam saturation enthalpy in i^{th} pressure node, Btu/lb
h_{fgi}	Heat of vaporization, Btu/lb
h_{ci}	Enthalpy of high pressure coolant injection flow, Btu/lb
\bar{h}_{sci}	Average enthalpy of subcooled liquid in core, Btu/lb
h_{fw}	Feedwater enthalpy entering vessel, Btu/b
h_{sep}	Vertical height above skirt where steam separator diameter changes, ft
h_{LP}	Enthalpy of recirculation flow entering inlet plenum for non-jet pump plants, Btu/lb
h_{Di}	Recirculation enthalpy at jet pump throat - i^{th} loop, Btu/lb
h_{DEi}	Diffuser exit enthalpy - i^{th} loop, Btu/lb
h_{ti}	Suction flow enthalpy - i^{th} loop, Btu/lb
h_{nozi}	Drive flow enthalpy at i^{th} jet pump nozzle, Btu/lb

NEDO-24154-A

Δh	Core inlet subcooling, Btu/lb
H_{los}	Energy lost in Recirculation system, BTI/sec
J_{di}	Drive motor inertia, lb_m-ft^2
J_{gi}	Generator inertia, lb_m-ft^2
J	Mechanical equivalent of heat, lb/Btu
J_p	Pump-motor inertia, lb_m-ft^2
K_i	Flow squared loss coefficient for steamline node; $Psi-sec^2/lb_m$
K_{MSIV}	Flow squared loss coefficient for MSIV valves, $Psi sec^2/lb_m$
K_b	Bulkwater friction coefficient, $psi/(lb/sec)^2$
K_{CTI}	Constants in coupler torque numerical fit
K_{dif}	Jet pump diffuser friction coefficient, $psi/(lb/sec)^2$
K_{Pl}	Exit plenum friction coefficient, $psi/(lb/sec)^2$
K_{dwn}	Downcomer friction coefficient - jet pump throat to vessel outlet, $psi/(lb/sec)^2$
K_d	Drive loop friction coefficient, $psi/(lb/sec)^2$
K_{noz}	Jet pump nozzle exit coefficient, $psi/(lb/sec)^2$
K_s	Gain in flux suppression filter
K_{SL1}	Flow coefficient for steam line to pressure relief valves, $in-ft^{3/2}/sec$
K_{SL2}	Steam line flow coefficient for flow from relief valves to isolation valves to turbine, $in-ft^{3/2}/sec$
$K_{ISO}(t)$	Steam flow coefficient for flow through isolation valves, $in-ft^{3/2}/sec$
K_{RL}	Recirculation line friction coefficient, $psi/(lb/sec)^2$
K_{LP}	Vessel lower plenum friction coefficient, $psi/(lb/sec)^2$
K_D	Downcomer friction coefficient, $psi/(lb/sec)^2$ (non jet pump plant)
K_{PTI}	Constant in numerical fit of pump torque curve
K_{PHI}	Constant in numerical fit of pump head curve

NEDO-24154-A

K_{SCT}	Jet pump suction coefficient, $\text{psi}/(\text{lb}/\text{sec})^2$
L_V	True vessel mixture level relative to separator skirt, ft
L_{VS}	Sensed vessel level relative to separator skirt, ft
L_f	Length of active fuel, ft
L_c	Length of total core, ft
l	effective separator length, ft
l_D	Length of flow path in downcomer, below jet pump throat, ft
l_b	Length of bulkwater and downcomer flow path to jet pump throat, ft
l_{LP}	Length of flow path in inlet plenum, ft
l_i	Length of streamline node 1
l_1	Length of flow path in upper plenum, ft
l_s	Elevation difference between level sensor tap and separator discharge skirt (ft)
l_{RL}	Length of recirculation line, ft
l_{sep1}	Length of separator barrel, ft
l_{sep2}	Length of separator downcomer, ft
l	Effective length of flow path in separator, ft
l_{sp}	Length of separator standpipe, ft
\bar{l}_{dif}/A_{dif}	Effective jet pump diffuser length to area ratio, ft^{-1}
m_{31}	Core inlet flow, lb/sec
m_{3s}	Total separator flow, lb/sec
m_{11}	Steam flow leaving plenum, lb/sec
m_{21}	Liquid flow leaving plenum, lb/sec
m_{12}	Steam flow leaving separators, lb/sec
m_{ISO}	Steam flow through isolation valves, lb/sec
m_{22}	Liquid flow leaving separators, lb/sec
m_{13}	Steam flow leaving vessel, lb/sec
m_{23}	Liquid flow leaving vessel, lb/sec

NEDO-24154-A

\dot{m}_{IT}	Steam flow entering turbine admission valves, lb/sec
\dot{m}_{LB}	Steam flow entering bypass valves, lb/sec
\dot{m}_{SV}	Steam flow entering safety valves, lb/sec
\dot{m}_{RV}	Steam flow entering relief valves, lb/sec
\dot{m}_{CS}	High pressure core spray flow, lb/sec
\dot{m}_{CU}	Carryunder steam flow entering downcomer, lb/sec
\dot{m}_{gfb}	Carryunder condensation rate in vessel bulk water, lb/sec
\dot{m}_{fw}	Feedwater flow, lb/sec
\dot{m}_{RLi}	Recirculation flow in i^{th} loop, lb/sec
\dot{m}_{SCTi}	Recirculation suction flow in i^{th} loop, lb/sec
\dot{m}_{di}	Recirculation drive flow in i^{th} loop, lb/sec
\dot{m}_{BV}	Bypass valve capacity, lb/sec
\dot{m}_{TVj}	Capacity of j^{th} turbine control valve, lb/sec
\dot{m}_{pi}	Recirculation pump flow = \dot{m}_{di} for jet pumps, = \dot{m}_{RLi} for full flow recirculation (lb/sec)
\dot{m}_s	Sensed recirculation loop flow, lb/sec
\dot{m}_{ci}	High pressure coolant injection flow, lb/sec
\dot{m}_{SV}	Uncompensated safety valve flow rate, lb/sec
\dot{m}_{RC}	Relief capacity at setpoint of valves, lb/sec
\dot{m}_{RU}	Uncompensated relief valve flow rate, lb/sec
\dot{m}_{SC}	Safety capacity at steam line pressure P_{RL} , lb/sec
M_{fs}	Mass of saturated liquid in separators, lb
M_{gs}	Mass of saturated steam in separators, lb
M_{g1}	Mass of steam in vessel plenum, lb
M_{f1}	Mass of saturated liquid in vessel plenum, lb
M_{g2}	Mass of steam in vessel, lb
M_{f2}	Mass of saturated liquid in vessel, lb

NEDO-24154-A

M_{gd}	Mass of steam in vessel dome, lb
M_{fb}	Mass of saturated liquid in bulk water, lb
M_{gb}	Mass of steam entrained in vessel bulk water, lb
M_{c+p}	Total mass of fluid in plenum and core, lb
M_1	Total mass of fluid in vessel plenum, lb
n_{gi}	Generator speed in i^{th} loop, rpm
n_{di}	Drive motor speed in i^{th} loop, rpm
$n_{d, \text{rated}}$	Rated drive motor speed, rpm
n_{ps}	Pump drive synchronous speed, rpm
n_s	Output of flux suppression network, per unit
n_{set}	flux scram setpoint, per unit
n_{set0}	Full power flux scram setpoint, per unit
n_{pi}	Pump speed in i^{th} recirculation loop, rpm
N_1	Number of recirculation loops represented by model loop 1
N_2	Number of recirculation loops represented by model loop 2
N_i	Number of loops of a given flow, m_{RLi}
N_f	Number of fuel rods in core, dimensionless
N_{sep}	Number of separators, dimensionless
N_{BV}	Number of open bypass valves, dimensionless
N_{RV}	Number of open relief valves, dimensionless
N_{set}	Flow adjustable flux scram set point, %
$N_{\text{SV}i}$	Number of safety valves in group i , dimensionless
N_{TV}	Number of open turbine control valves, dimensionless
$P_{\text{dwn}i}$	Pressure in downcomer of i^{th} loop, psi
P_i	Pressure in i^{th} node, psi
P_1	Upper Plenum Pressure, psi
P_I	Core inlet pressure, psi
P_{jet}	Jet pump nozzle exit pressure in i^{th} loop, psi

NEDO-24154-A

P_{1e}	Plenum exit pressure, psi
P_{RL}	Steam line pressure at pressure relief valves, psi
$P_{RR,i}$	Reset pressure of i^{th} relief valve, psi
$P_{SR,i}$	Reset pressure of i^{th} safety valve, psi
P_{SL}	Steam line pressure at turbine stop valve, psi
$P_{ss,i}$	Setting of i^{th} relief valve, psi
P_{voi}	Pressure at vessel outlet, for loop, psi
$P_{RS,i}$	Setting of i^{th} safety valve, psi
P_T	Turbine inlet pressure, psi
P_{thi}	Jet pump throat pressure in i^{th} loop, psi
$\Delta P_{jet i}$	Pressure drop across jet pump mixing region in i^{th} loop, psi
ΔP_{pi}	Pump head in i^{th} recirculation line, psi
ΔP_C	Core pressure drop, psi
s	Laplace transform variable, sec^{-1}
t	Time, sec
T_i	Flux filter constants
T_{mi}	Mechanical shaft torque of i^{th} recirculation pump drive, ft-lb
T_{eli}	Electrical torque of i^{th} recirculation pump drive, ft-lb
$T_{C, \text{rated}}$	Coupler rated torque, ft-lb
T_{ci}	Torque transmitted from drive motor to generator by fluid coupler in i^{th} loop, ft-lb
T_{cs}	Recirculation flow time constant, sec
T_{edi}	Drive motor electrical torque in i^{th} loop, ft-lb
u_{fi}	Internal energy of saturated liquid in i^{th} pressure node, Btu/lb
u_{gi}	Internal energy of saturated steam in i^{th} pressure node, Btu/lb
v_{fi}	Specific volume of liquid in i^{th} pressure node, ft^3/lb
v_{gi}	Specific volume of steam in i^{th} pressure node, ft^3/lb

NEDO-24154-A

v_{fgi}	$v_{gi} - v_{fi}$
v_s	Specific volume of subcooled bulk water, ft^3/lb
V_{gb}	Volume of steam entrained in vessel bulk water, ft^3
$V_{b+cu,0}$	Volume of bulk water region below separator discharge skirt, ft^3
V_{b+cu}	Volume of steam and liquid above feedwater sparger, ft^3
V_{fb}	Volume of bulk water liquid, ft^3
V_D	Volume of vessel downcomer, ft^3
V_{LP}	Volume of vessel inlet plenum, ft^3
V_1	Volume of core exit plenum, ft^3
V_s	Volume of steam separators, ft^3
V_B	Volume of bulk water and separators, ft^3
V_R	Volume of recirculation line, ft^3
V_{Diff}	Volume of jet pump - throat to diffuser exit, ft^3
V_{NE}	Volume of downcomer from jet pump throat to vessel outlet, ft^3
X_{ci}	Coupler position, %
X_{ec}	Core exit quality, dimensionless
X_1	Plenum exit quality at separator inlet, dimensionless
X_2	Quality at separator outlet, dimensionless
X_{cu}	Carryunder fraction, dimensionless
X_{Bj}	Bypass valve (j^{th}) opening, per unit
X_r	Control rod insertion location, dimensionless
X_{Tj}	Position of j^{th} turbine control valve, per unit
ΔZ_b	Flow elevation change, bottom of separators to downcomer, ft
ΔZ_D	Flow elevation change, downcomer to vessel exit, ft
ΔZ_{dif}	Flow elevation change, diffuser of jet pump to core inlet, ft
ΔZ_{PL}	Flow elevation change, exit plenum, ft
ΔZ_{RL}	Flow elevation change, recirculation system, ft

NEDO-24154-A

η_{gen}	Recirculation drive generator efficiency, dimensionless
η_{pump}	Recirculation pump efficiency, dimensionless
ρ_{fi}	Density of saturated liquid in node i, lb/ft ³
ρ_{gi}	Density of saturated vapor in node i, lb/ft ³
$\bar{\rho}_r$	Recirculation loop average density, lb/ft ³
ρ_b	Bulk water density, lb/ft ³
τ_{DC}	Downcomer transport delay, sec
τ_{Ri}	Recirculation transport delay from i th loop downcomer at jet pump suction, sec
τ_{Nji}	Recirculation loop delay, non jet pump plant, sec
τ_{DEi}	Transport delay through i th loop diffuser, sec
τ_{RV}	Relief valve time constant, sec
τ_{SV}	Safety valve time constant, sec

5. NEUTRON KINETICS MODEL

The time-dependent neutron flux distribution is calculated assuming a single energy group, six delayed neutron groups, and time-dependent diffusion only in the axial direction. The three-dimensional neutron diffusion parameters used in the GE BWR Simulator are collapsed into equivalent one-dimensional parameters by procedures which are described in Appendix A of this report. This section describes the solution of the one-dimensional kinetics equations and the techniques used to obtain diffusion parameters for use in transient calculations.

5.1 THE ONE-DIMENSIONAL KINETICS EQUATION

The one-dimensional equation derived in Appendix A is written,

$$\frac{\bar{I}}{v} \frac{\partial \phi'}{\partial t} = \frac{\partial}{\partial z} \bar{D} \frac{\partial \phi'}{\partial z} - \overline{DB}^2 \phi' + (1 - \bar{\beta}) \bar{F} \phi' - \bar{\Sigma}_r \phi' + \sum_1 \lambda_1 C_1 \quad (5-1)$$

$$\frac{\partial C_1}{\partial t} = \beta_1 \bar{F} \phi' - \lambda_1 C_1 \quad i = 1 - 6 \quad (5-2)$$

where the diffusion parameters are derived and defined in Appendix A.

At time t , the boundary conditions are

$$-\frac{\bar{D}(t)}{\phi'} \frac{\partial \phi'}{\partial z} \Big|_{z=b} = \Gamma_b \left(1 - \frac{\bar{D}(t)}{\bar{D}(t=0)} \right) \quad (5-3)$$

where Γ_b is the steady-state neutron current to flux ratio at boundary b . Q31

Once the quantity $\phi'(z,t)$ is obtained, the axial power distribution is given by

$$P(z,t) = f(z,t) \phi'(z,t) \quad (5-4)$$

The definition of $f(z,t)$ can be found in Appendix A.

Q31 - Responses to NRC questions on the text are documented in Appendix B. The symbol Q31 denotes that this topic is discussed further in the response to NRC Question 31.

During a specific transient, the diffusion parameters will change due to changes in water density, fuel temperature, and control rod motion. The resultant changes in ϕ' and hence, $\Psi(z,t)$ are determined by solving Equations 5-1 and 5-2 numerically. This process is described in Section 5.2.

5.2 NEUTRON KINETICS EQUATION SOLUTION

This section discusses the numerical solution of Equations 5-1 and 5-2. The numerical techniques are quite straightforward and have been used in other GE neutron kinetics models.⁶ The model is outlined here for completeness. The time difference equations are found by integrating Equations 5-1 and 5-2 from t_k to t_{k+1}

$$\begin{aligned} \frac{1}{v}(\phi^{k+1}(z) - \phi^k(z)) &= \int_{t_k}^{t_{k+1}} \left\{ \frac{\partial}{\partial z} \bar{D} \frac{\partial \phi'}{\partial z} - \overline{DB}_r^2 \phi' + (1 - \beta) \bar{F}\phi' - \bar{\Sigma}_r \phi' \right\} dt \\ &+ \sum_i \bar{\lambda}_i \int_{t_k}^{t_{k+1}} c_i dt \end{aligned} \quad (5-5)$$

$$c_i^{k+1}(z) - c_i^k(z) = -\bar{\lambda}_i \int_{t_k}^{t_{k+1}} c_i dt + \bar{\beta}_i \int_{t_k}^{t_{k+1}} \bar{F}\phi' dt \quad (5-6)$$

where

$$c_i^k(z) = c_i(z, t_k) \quad (5-7)$$

$$\phi^k(z) = \phi'(z, t_k) \quad (5-8)$$

Note that Equation 5-5 contains an integral of $C_1(z,t)$ over time. The first step in eliminating this integral is to assume that $C_1(z,t)e^{-\lambda_1 t}$ varies linearly from t_k to t_{k+1} . Then using Equation 5-6, we find

$$\sum_1 \lambda_1 \int_{t_k}^{t_{k+1}} c_1(z,t) dt = \sum_1 \left[\lambda_1 \gamma_1^k c_1^k \Delta t_k + \beta_1 (1 - \gamma_1^k) \int_{t_k}^{t_{k+1}} F\phi' dt \right] \quad (5-9)$$

where

$$\Delta t_k = t_{k+1} - t_k \quad (5-10)$$

$$\gamma_1^k = \frac{1}{1 + \alpha_1^k \lambda_1 \Delta t_k} \quad (5-11)$$

$$\alpha_1^k = \left(\frac{1}{1 - e^{-\lambda_1 \Delta t_k}} - \frac{1}{\lambda_1 \Delta t_k} \right) \quad (5-12)$$

Substituting Equation 5-9 into Equation 5-5 yields Equation 5-13, which now only involves time integrals of the flux ϕ' ; i.e.,

$$\begin{aligned} \frac{\bar{1}}{v} (\phi^{k+1}(z) - \phi^k(z)) &= \int_{t_k}^{t_{k+1}} \left\{ \frac{\partial}{\partial z} \bar{D} \frac{\partial \phi'}{\partial z} - \frac{D \bar{B}}{r} \phi' \right. \\ &\quad \left. + (1 - \hat{\beta}) k \bar{F} \phi' - \bar{I} \phi' \right\} dt \\ &\quad + \sum_1 \lambda_1 \gamma_1^k c_1^k(z) \Delta t_k \end{aligned} \quad (5-13)$$

where

$$\hat{B}_k = \sum_1 \gamma_1^k \bar{B}_1 \quad (5-13a)$$

Equation 5-13 involves integrals of the form

$$\int_{t_k}^{t_{k+1}} A(t) \phi' dt$$

which are approximated as

$$\int_{t_k}^{t_{k+1}} A(t) \phi' dt = \Delta t_k \left(\alpha_\phi A^{k+1} \phi^{k+1} + (1 - \alpha_\phi) A^k \phi^k \right) \quad (5-14)$$

where α_ϕ is an interpolation parameter.^{Q33} Following a change in cross section, the flux behaves as $e^{+\Sigma v t}$. Hence,

$$\alpha_\phi = \left(\frac{1}{1 - e^{-\Sigma v \Delta t_k}} - \frac{1}{\Sigma v \Delta t_k} \right) \quad (5-15)$$

For most time step sizes of practical interest, the parameter α_ϕ is essentially 1.0 and, hence, the flux integration is purely implicit. The resultant spatial equations are (including α_ϕ for generality):

$$\begin{aligned} & \alpha_\phi \left[\frac{\partial}{\partial z} \bar{D}^{k+1} \frac{\partial}{\partial z} \phi^{k+1} - \overline{DB}_r^{2k+1} \phi^{k+1} + (1 - \hat{\beta}) \bar{F}^{k+1} \phi^{k+1} \right. \\ & \left. - \left(\frac{\Sigma_r^{k+1}}{\Sigma_r} + \frac{1}{\bar{v} \Delta t_k \alpha_\phi} \right) \phi^{k+1} \right] + (1 - \alpha_\phi) \left[\frac{\partial}{\partial z} \bar{D}^k \frac{\partial}{\partial z} \phi^k - \overline{DB}_r^{2k} \phi^k + (1 - \hat{\beta}) \bar{F}^k \phi^k \right. \\ & \left. - \left(\frac{\Sigma_r^k}{\Sigma_r} - \frac{1}{\bar{v} \Delta t_k (1 - \alpha_\phi)} \right) \phi^k \right] + \sum_1 \lambda_1 \gamma_1^k c_1^k = 0 \quad (5-16) \end{aligned}$$

In order to obtain the spatial solution, the core axis is divided into a number of equally spaced nodes, as shown in Figure 5-1. Integrating Equation 5-16 from z_{j-} to z_{j+} yields the following equation:

$$\begin{aligned} & \alpha_{\phi} \left[\frac{D_j^{k+1}}{h} \frac{d\phi^{k+1}}{dz} \Big|_{z_{j-}}^{z_{j+}} + hG_j^{k+1} \phi^{k+1} - \frac{h}{\bar{v}\Delta t_k \alpha_{\phi}} \phi_j^{k+1} \right] \\ & + (1 - \alpha_{\phi}) \left[\frac{D_j^k}{h} \frac{d\phi^k}{dz} \Big|_{z_{j-}}^{z_{j+}} + hG_j^k \phi_j^k + \frac{h}{\bar{v}\Delta t_k (1 - \alpha_{\phi})} \phi_j^k \right] \\ & + \sum_i \lambda_i \gamma_i^k c_{i,j}^k h = 0 \end{aligned} \quad (5-17)$$

where

$$\phi_j^k = \frac{1}{h} \int_{z_{j-}}^{z_{j+}} \phi_i^k(z) dz \quad (5-18)$$

$$c_{i,j}^k = \frac{1}{h} \int_{z_{j-}}^{z_{j+}} c_i^k(z) dz \quad (5-19)$$

$$h = z_{j+} - z_{j-} \quad (5-20)$$

and Q34

$$G_j^k = (1 - \beta^k) F_j^k - \frac{D_j^k}{h} B^{2k} - \frac{\bar{\Sigma}_j^k}{h} \quad (5-21)$$

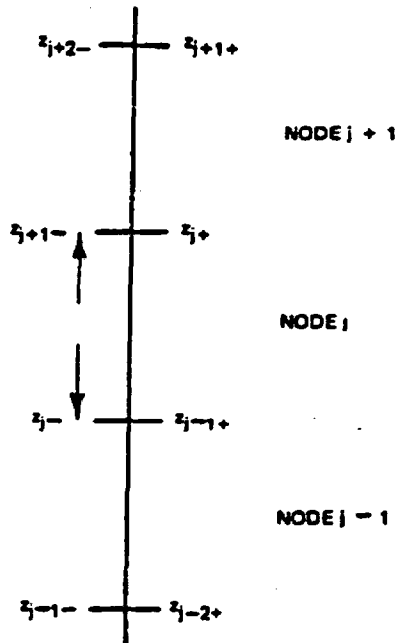


Figure 5-1. Neutron Kinetics Spatial Mesh

All of the nuclear parameters are assumed to be constant over node j. The derivative term $D \frac{d\phi}{dz} \Big|_{z_{j-}}^{z_{j+}}$ is evaluated using a difference expression for $\frac{d\phi}{dz}$ at the node boundary and applying the current continuity condition at the node boundaries. The result is

$$D_j^k \frac{d\phi^k}{dz} \Big|_{z_{j-}}^{z_{j+}} = \frac{1}{h} \sum_{l=j-1}^{j+1} D_{lj}^k (\phi_l^k - \phi_j^k) \quad (5-22)$$

where

$$\overline{D}_{lj}^k = \frac{2D_l^k D_j^k}{D_l^k + D_j^k} \quad (5-23)$$

Defining a matrix A^k with elements

$$A_{j-1,j}^k = \frac{1}{h^2} D_{j-1,j}^k \quad (5-24)$$

$$A_{j+1,j}^k = \frac{1}{h^2} D_{j+1,j}^k$$

$$A_{j,j}^k = A_{j-1,j}^k - A_{j+1,j}^k + G_j^k \quad (5-25)$$

$$A_{1j}^k = 0, \quad 1-j \geq 2_1$$

the discretized form of the neutron kinetics equations can be written,

$$\left[\alpha_\phi A^{k+1} - \frac{1}{v\Delta t_k} I \right] \phi^{k+1} = - \left[(1 - \alpha_\phi) A^k + \frac{1}{v\Delta t_k} I \right] \phi^k - \sum_i \lambda_i \gamma_i^k c_i^k \quad (5-26)$$

where ϕ^k and c_i^k are vectors with elements ϕ_j^k and $c_{i,j}^k$. The vector ϕ^{k+1} can be obtained from equation 5-26 and c_i^{k+1} is given by,

$$c_i^{k+1} = c_i^k \left[1 - \gamma_i^k \lambda_i \Delta t_k \right] + \bar{\beta}_i \gamma_i^k \left[\alpha_\phi F^{k+1} \phi^{k+1} + (1 - \alpha_\phi) F^k \phi^k \right] \quad (5-27)$$

Thus, the flux and precursor solution (ϕ^{k+1} and c_i^{k+1}) can be determined once A^{k+1} and ϕ^k are known. The steady-state solution is normalized such that ϕ^k is constant (See Appendix A).

5.3 RADIAL FLUX APPROXIMATIONS

The choice of the three-dimensional radial weighting function $\psi(r,t)$ is an important factor in the success of the one-dimensional neutron model in accurately predicting the transient neutronic behavior. In the steady-state condition, an "exact" solution is available from the 3-D reactor simulator.² However, during a specified transient the application of the adiabatic approximation requires a large number of additional three-dimensional flux calculations which would make its strict application impractical. Therefore, the approach taken in the current one-dimensional model is to make use of the initial 3-D steady-state solution to estimate $\psi(r,t)$ throughout the entire transient. In choosing approximate forms for $\psi(r,t)$ and the weighting function $\phi(\bar{r},t)$, it is important to know how $\psi(\bar{r},t)$ varies in the radial (x,y) direction, because

$$\psi(\bar{r},t) = \phi(\bar{r},t)/\phi(z,t) \quad (5-28)$$

where $\phi(\bar{r},t)$ is the three-dimensional flux distribution and $\phi(z,t)$ is the average axial distribution. Therefore, attention should be directed to the possible radial flux changes in a transient when choosing $\psi(\bar{r},t)$.

There are three main mechanisms which cause flux changes in a transient. These are fuel temperature (Doppler) changes, moderator density changes, and control rod motion. In this model, it is assumed that radial flux shape changes due to Doppler and void effects are small, and that the steady-state ($t=0$) radial distribution holds if only moderator density and Doppler change. Control rod motion, however, can have a significant impact on radial flux shape. When a group of control rods enters a given axial region, the radial shape may change drastically because the flux will drop in those regions near the control rods and will change by a smaller amount in regions away from control rods.

For transient analysis, the most common control rod motion pattern is the control rod scram. Therefore, the procedures developed here for approximating $\psi(r,t)$ are designed to predict flux changes during a reactor scram. Figure 5-2 is a schematic diagram showing a typical steady-state control rod pattern in a BWR. Note the divisions defining radial "control states."

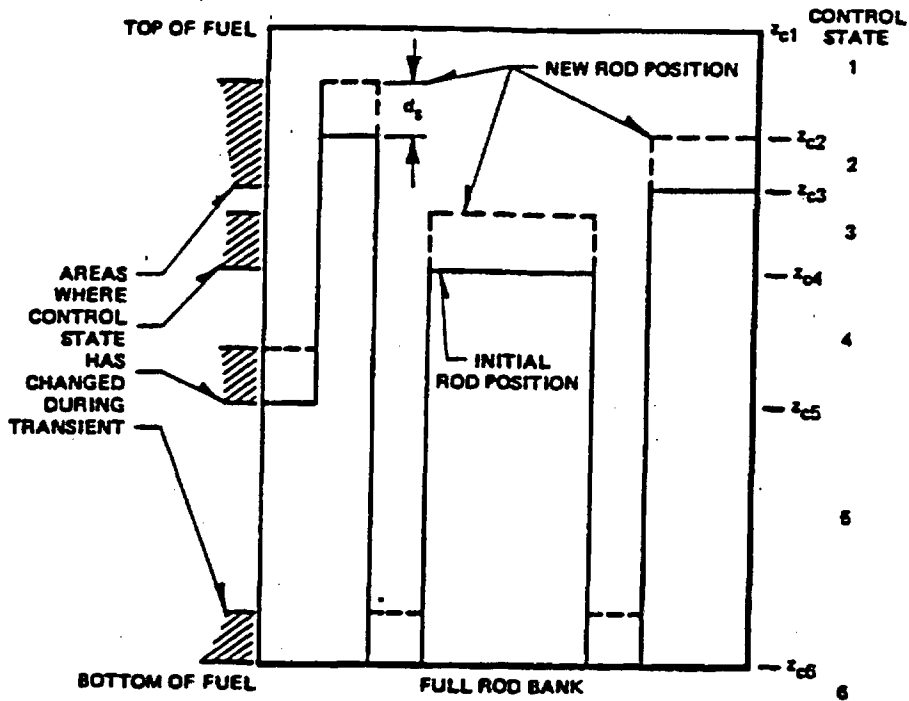


Figure 5-2. Control State Schematic

A control state is defined as a unique radial rod pattern. In this example there are six unique control states, including the full rod bank which in this case is fully withdrawn. Also shown is the height of each control state z_{c_i} . At some time t_g in the transient, let us assume that the control rods have moved some distance d_g . Note that for certain regions of the core (denoted by the shaded area), the control state has changed. For these regions, therefore, the radial flux is also changed and approximated as

$$\psi(x,y,z,t_g) = \psi(x,y,z_{c_i},0) \quad (5-29)$$

where c_i is the new control state at z at time t_g . This procedure amounts to assuming that the radial flux in the vicinity of the control rod tip remains constant as the control rod moves up the core during a scram. It is important to ensure that the flux near the control state interfaces are calculated accurately because in most transients involving scram, the first several inches

of control rod motion is most important, and the greatest reactivity change occurs near the control rod tips. The weighting function is

$$\phi(x,y,z,t) = \phi(z,0) \psi(x,y,z_{c1},0) \quad (5-30)$$

The radial flux approximations employed in this section permit the generation of one-dimensional parameters, using only the steady-state 3-D distribution obtained from the BWR Simulator, while still accounting for radial flux changes during a reactor scram.^{Q2}

5.4 NEUTRON PARAMETER FITS

All of the parameters in Equation 5-1 can be calculated from the list of quantities listed in Table 5-1. Their definition can be found in Appendix A. The quantity \bar{F} in Equation 5-1 is evaluated from^{Q35}

$$\bar{F} = \frac{1}{k_0} \left[\overline{K\bar{\Sigma}} (1 + \overline{CDOP} (\sqrt{T} - \sqrt{T_0})) \right] - \bar{\Sigma} + \bar{\Sigma}_1 \quad (5-31)$$

The flux-to-power conversion factor is given by

$$\bar{F} = k_0 \bar{\Sigma} \left[\frac{\overline{K\bar{\Sigma}}}{\bar{\Sigma}} (1 + \overline{CDOP} (\sqrt{T} - \sqrt{T_0})) - 1 \right] + k_0 \bar{\Sigma}_1 \quad (5-32)$$

where we have assumed that

$$\overline{CDOP} = \overline{CDOP} \quad (5-33)$$

and

$$\overline{K\bar{\Sigma}} = \frac{\overline{K\bar{\Sigma}}}{\bar{\Sigma}} \bar{\Sigma} \quad (5-34)$$

Table 5-1
NEUTRON PARAMETERS

	Symbol	Definition	Defining Equation
1	$\bar{1}/v$	Inverse neutron speed	(A-64)
2	\bar{D}	Diffusion coefficient	(A-65)
3	\overline{DB}_r^2	Radial leakage	(A-66)
4	\overline{KE}	v-fission cross section	(A-68)
5	\overline{CDOP}	Doppler correction coefficient	(A-69)
6	$\bar{\Sigma}$	Absorption cross section	(A-72)
7	$\bar{\Sigma}_1$	Removal cross section	(A-73)
8	$\bar{\Sigma}$	Flux weighted absorption	(A-88)
9	$\bar{\Sigma}_1$	Flux weighted removal	(A-91)
10	$\bar{\beta}$	Delayed neutron fraction	(A-67)
11	$\bar{\lambda}_i$	Decay constant for precursor i	(A-74)
12	ϕ'	Neutron flux ratio	(A-48)
13	c_i	Precursor concentration	(A-45a)

In order to carry out the transient solution, the variation of each quantity in Table 5-1 with water density and control must be specified. The first nine quantities in Table 5-1 are functions of three variables: axial height, relative water density, $U = \rho_{av}/\rho_{ref}$, and control state, defined in Section 5.3. Specifically, a given parameter (denoted here by Σ) is fit as a quadratic function of U for each control state at each axial height; i.e.,^{Q49}

$$\Sigma^c(z) = \Sigma_0^c(z) \left[1 + a^c(z) (U - U_0) + b^c(z) (U - U_0)^2 \right] \quad (5-35)$$

where \sum_0^c is the value of \sum^c obtained when the relative density U is equal to U_0 , the steady-state density at position (z) . In practice, \sum_0^c is calculated using the base density profile. The density is then perturbed as

$$\rho'(x,y,z) = \rho_0(x,y,z) + \Delta\rho \quad (5-36)$$

where $\Delta\rho$ is constant in position, and Σ is recomputed. This process is repeated for a range of relative densities and the results fit to the form of Equation 5-35. For a given axial height z , this process is repeated for all possible control states. Therefore, for a problem with 10 control states and 24 axial nodal positions, a total of $10 \times 24 = 240$ quadratic fits will be generated for each of the first nine quantities in Table 5-1.

The flux approximation used for each control state and height is in accordance with the procedures outlined in Section 5.3.

The quantities β and λ are weak functions of density and, hence, are not fit as U . A total $\bar{\beta}$ is computed for each axial height and each control state. The individual precursor fractions are given by

$$\bar{\beta}_1 = \bar{\beta} \left(\frac{\beta_1}{\beta} \right) \quad (5-37)$$

where (β_1/β) is constant for the entire core. Also, λ_1 is given as a constant.

Note that the fitting process uses the parameter $U_0(z)$ which is the steady-state density distribution obtained from the 3-D solution. When the fits are applied in the one-dimensional model, this base density is changed to the one obtained with the one-dimensional hydraulics model, as shown in Section 3.2. This procedure ensures that the steady-state one-dimensional solution will be the same as the 3-D average axial solution. Also, reactivity changes will be tied to changes in the "average channel" density, rather than changes in total core density. It is expected that this procedure will work well for situations where the initial power of the core is high and the radial variation in density is not too large. At lower powers the sensitivity of density to quality is large and radial variations in density may be significant and the one-dimensional approach to reactivity feedback will be less accurate. Q2, Q38

6. THERMAL-HYDRAULIC MODEL

The reactor core pressure drop, exit qualities, and water density distribution are calculated by a model designed to predict two-phase flow (steam and water) in transient conditions. The governing five equations in the model consist of a continuity equation of each of the vapor and liquid phases, an energy equation for each phase, and a momentum equation for the mixture. In addition, the location of the "boiling boundary" is tracked using an additional independent equation.

The basic variables consist of volumetric flux, pressure, void fraction, liquid and vapor enthalpies, and the boiling boundary location.

Numerically, an implicit scheme using "field" and "flow" variables is employed, where the flow variables are tabulated at discrete node boundaries and field variables are associated with node interiors. Precautions have been taken to ensure numerical stability.

The implicit equations are solved using a Modified Newton method, which takes advantage of the sparse nature of the non-linear equations.

6.1 TWO-PHASE CONSERVATION EQUATIONS

The one-dimensional two-phase conservation equations of mass, momentum, and energy can be written in many different forms, ranging from the simplest three-equation homogeneous model to a general six-equation two-fluid model. The most general formulation would include two continuity, two momentum, and two energy equations. It also needs empirical correlations for interfacial heat transfer and shear terms. The interfacial shear terms in particular are largely undetermined at present, being complex functions of the local flow regime. In view of this, we have adopted a five-equation model which includes separate continuity and energy equations for each phase, but retains a total (mixture) momentum equation. With this formulation, another equation is needed to specify the problem in the form of a "void fraction correlation."⁷ This correlation has a large data base for steady-state conditions and the uncertainties in using this are considerably less than in specifying interfacial forces.

The five-equation model has as its dependent variables:

$j = j_g + j_l =$ Total volumetric flux

$\alpha =$ vapor volumetric (void) fraction

$P =$ pressure

$h_g =$ vapor enthalpy

$h_l =$ liquid enthalpy

as functions of time and space.

The system of equations meets the following requirements:

1. Separated flow description
2. Capable of handling counter-current flow
3. Capable of handling flow reversals
4. Momentum coupling
5. Thermodynamic non-equilibrium
6. Pressure effects on properties within the core
7. Retain non-linear nature of the equations

The equations can be readily derived using a control volume as shown in Figure 6-1. We use the concept of an infinitesimal interface, where all

phase changes take place. With the notation shown in Figure 6-1, the following equations can be derived:

1. Vapor Continuity

$$\frac{\partial}{\partial t} (\alpha \rho_g) + \frac{1}{A} \frac{\partial}{\partial z} (\rho_g j_g A) = \Gamma_g \quad (6-1)$$

2. Liquid Continuity

$$\frac{\partial}{\partial t} [(1 - \alpha) \rho_l] + \frac{1}{A} \frac{\partial}{\partial z} (\rho_l j_l A) = -\Gamma_g \quad (6-2)$$

3. Vapor Energy

$$\frac{\partial}{\partial t} (\alpha \rho_g h_g^*) - \frac{\alpha}{J} \frac{\partial P}{\partial t} + \frac{1}{A} \frac{\partial}{\partial z} (\rho_g h_g^* j_g A) = \Gamma_g h_{g1}^* + \frac{q''_{wR} P_{Hg}}{A} - \frac{q''_{g1} P_l}{A} \quad (6-3)$$

4. Liquid Energy

$$\begin{aligned} \frac{\partial}{\partial t} [(1 - \alpha) \rho_l h_l^*] - \frac{(1 - \alpha)}{J} \frac{\partial P}{\partial t} + \frac{1}{A} \frac{\partial}{\partial z} (\rho_l j_l h_l^* A) = -\Gamma_g h_{l1}^* \\ + \frac{q''_{wl} P_{Hl}}{A} - \frac{q''_{l1} P_l}{A} + \psi \end{aligned} \quad (6-4)$$

5. Momentum Equation

$$\begin{aligned} \frac{\partial}{\partial t} [j_g \rho_g + j_l \rho_l] + \frac{1}{A} \frac{\partial}{\partial z} \left[\left(\frac{C_R j_g^2 \rho_g}{\alpha} + \frac{C_L j_l^2 \rho_l}{(1 - \alpha)} \right) A \right] \\ = -\frac{\partial P}{\partial z} - \frac{\phi^2 f}{2D_H \rho_l g_c} [\rho_l j_l + \rho_g j_g]^2 - g \cos \theta [\rho_l (1 - \alpha) + \rho_g \alpha] \end{aligned} \quad (6-5)$$

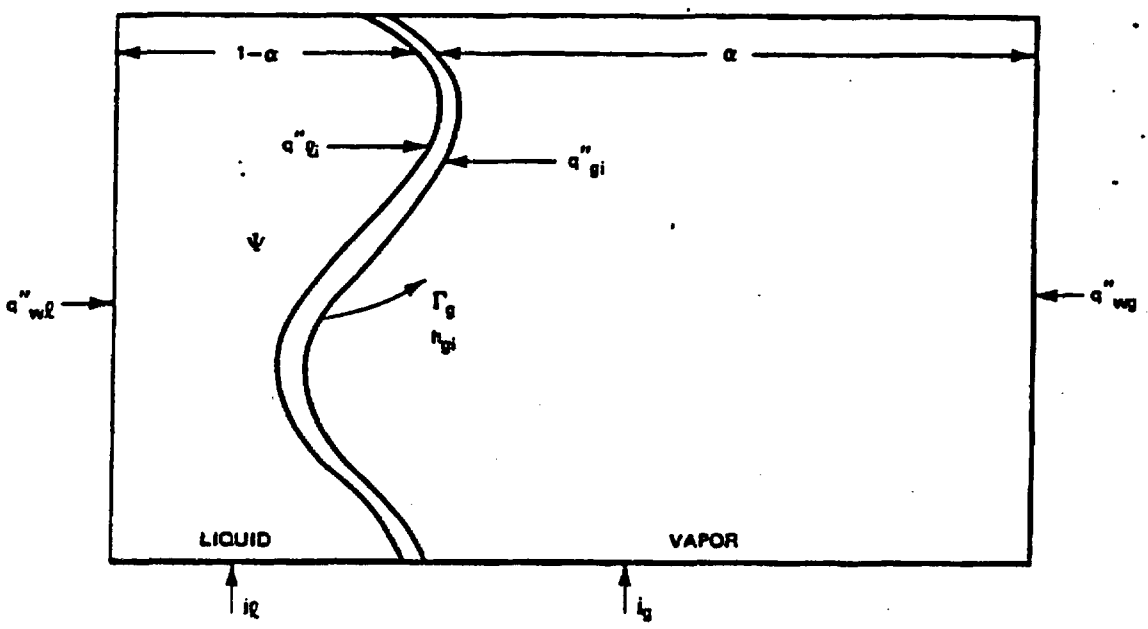


Figure 6-1. Thermal-Hydraulic Control Volume

where

$$C_g = \frac{\langle \alpha v_g^2 \rangle \langle \alpha \rangle}{\langle j_g \rangle^2}, \quad C_l = \frac{\langle (1 - \alpha) v_l^2 \rangle \langle 1 - \alpha \rangle}{\langle j_l \rangle^2} \quad (6-6)$$

In addition, we have the following:

6. Interface Energy Balance

$$(q''_{g1} + q''_{l1}) \frac{P_1}{A} = \Gamma_g (h_{g1}^* - h_{l1}^*) \quad (6-7)$$

7. Drift Flux Relationships

$$j_g = \alpha(C_o j + \bar{v}_{gj}) \quad (6-8)$$

$$j_l = j - j_g = (1 - \alpha C_o)j - \alpha \bar{v}_{gj} \quad (6-9)$$

Equations 6-8 and 6-9 can be used to express j_g and j_l in terms of j and α in the conservation equations.

It is possible to expand the derivative terms in the conservation equations and express them in alternate forms. In particular, the continuity equations can be subtracted from the energy equations to obtain simpler expressions. However, the equations are retained in this form because when differenced, they maintain their "conserving" property.

Note that pressure is assumed to be uniform in both phases. Also, in general $h^* = h + 1/2 v^2 + gz$.

The interface velocity is specified to be $(v_g - v_l)/2$.

8. Boiling Boundary Equation

If $\rho_g, h_g, j_g, \rho_l, h_l, j_l, h_{ld}$ are considered functions of the axial variable z , then the boiling boundary z_{bb} is defined as that value of z for which the mixture enthalpy is equal to h_{ld} , the point at which subcooled boiling begins. In mathematical terms, at $z = z_{bb}$ we must have

$$\frac{\rho_g h_g j_g + \rho_l h_l j_l}{j_g \rho_g + j_l \rho_l} - h_{ld} = 0 \quad (6-10)$$

6.2 THERMAL-HYDRAULIC CORRELATIONS

6.2.1 Interfacial Heat Fluxes

In general, the interfacial heat fluxes are empirically specified in the form,

$$q''_{il(g)} = F_1(T_{l(g)} - T_{sat}) + F_2 q''_{wl(g)} \quad (6-11)$$

where the quantities F_1 and F_2 are functions of pressure and enthalpy. Q16, Q28

6.2.2 Drift Flux Parameters

The parameters C_o and V_{gj} in Equation 6-8 are calculated through correlations based on flow and quality.

6.2.3 Friction Losses

Local irreversible pressure drop losses caused by flow obstructions such as orifices and fuel rod spacers are calculated as

$$\Delta P_{loc} = K_{loc} \frac{G^2}{2g_c \rho_l} \left(1 + \frac{v_{lE}}{v_l} X \right) \quad (6-12)$$

Q16 - Responses to NRC questions on the text are documented in Appendix B. The symbol Q16 denotes that this topic is discussed further in the response to NRC Question 16.

where G is the flow, given by

$$G = \rho_l j_l + \rho_g j_g \quad (6-13)$$

The wall friction losses are given

$$\Delta P_f = f \left(\frac{L}{D_H} \right) \frac{G^2}{2g_c \rho_l} \phi^2 \quad (6-14)$$

where D_H is the hydraulic diameter and f and ϕ^2 are given by correlations involving pressure and flow.

6.2.4 Heat Transfer Coefficients

Regions of applicability for the various correlations for heat transfer coefficients are given in Table 6-1.

Table 6-1
HEAT TRANSFER CORRELATIONS

Criteria			Flow Regime	Heat Transfer Correlation
T_w	T_l	CHF		
$T_w < T_{w_i}$	$< T_{l_i}$	-	Single-Phase Liquid	Dittus-Boelter
$T_{w_i} < T_w < T_{min}$	$> T_{l_i}$ $< (T_{sat} - 1)$	$X < X_c$	Subcooled Boiling	Jens-Lottes
$T_{w_i} < T_w < T_{min}$	T_{sat}	$X < X_c$	Bulk Boiling	Chen
T_{min} = minimum wall temperature for film boiling T_{w_i}, T_{l_i} = conditions at incipience of boiling X_c = transition quality				

6.3 EQUATION SOLUTION

6.3.1 Discretization of Equations

A modified donor cell technique has been employed, similar to that used in the KACHINA code developed at the Los Alamos Laboratory.⁸ The variables are classified into flow variables (j, j_g, j_x) which are tabulated at boundaries between nodes, and field variables (α, P, h_x, h_g) which are defined at the center of the nodes (Figure 6-2). Further, the continuity and energy equations are classified as field equations and integrated from node boundary K to node boundary K+1. The momentum equation (flow equation) is integrated from node center K to node center K+1 (i.e., across node boundary).

We subdivide the channel into nodes by designating the values of z at the nodal interfaces:

$$z_1 = z_2 < z_3 < z_4 < \dots < z_{\text{JOUTLT}} = z_{\text{JOUTLT}+1}$$

The presence of the "zero volume nodes" at either end is to accommodate the boundary conditions. Thus, z_2 corresponds to the inlet and z_{JOUTLT} corresponds to the outlet.

We have associated the index of a field quantity with the index of the nodal boundary immediately below. Thus, z_2 would correspond to an inlet boundary condition for field quantity Q , Q_2 would correspond to that field quantity in the node boundary by z_2 and z_3 , etc.

The convective fluxes $\langle jQ \rangle$ at node boundaries are approximated as follows:

$$\langle jQ \rangle_k = j_k \left[(1/2 + \epsilon_k) Q_{k-1} + (1/2 - \epsilon_k) Q_k \right]$$

$$\epsilon_k = \beta_1 \frac{\Delta t}{\Delta z} |v_k| + \beta_2 \text{sign}(j_k) \quad (6-15)$$

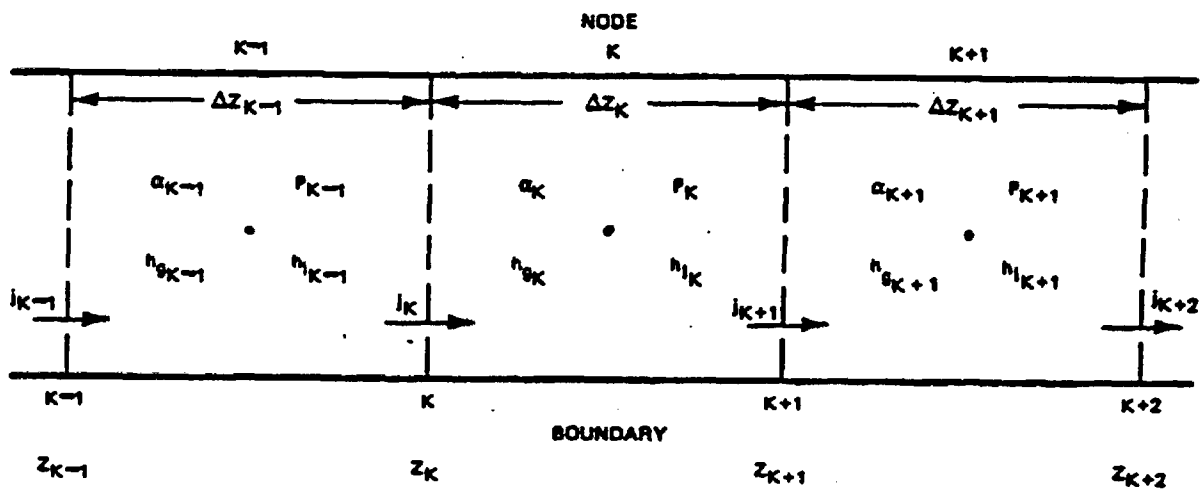


Figure 6-2. Nodalization of Channel

where V_k is the velocity of the particular phase for which the flux is computed, and

$$0 < \beta_1 \leq 0.5$$

$$0 < \beta_2 \leq 0.5$$

so that

$$-\frac{1}{2} \leq \epsilon_k \leq \frac{1}{2}$$

For $\beta_2 = 0.5$ and $\beta_1 = 0$, we have a pure donor cell technique, whereas for $\beta_1 = \beta_2 = 0$ the flux is purely space centered and the method is often unstable. The use of this method assists in reducing truncation error without the necessity of explicit artificial diffusion.^{Q29} The donor cell technique is especially useful for problems involving flow reversals. The time integration scheme is fully implicit.^{Q9} The entire discretization process is described in detail in Reference 9. The discretized equations are:

Momentum

$$\begin{aligned} \rho_i^{k+1} &= \left(\rho_{g,i}^{k+1} j_{g,i}^{k+1} + \rho_{l,i}^{k+1} j_{l,i}^{k+1} \right) - \left(\rho_{g,i}^k j_{g,i}^k + \rho_{l,i}^k j_{l,i}^k \right) \\ &+ \frac{\Delta t}{A_i \Delta x_i} \left\{ \left\langle j_g \left(A_{0g} \frac{C_g j_g}{\alpha} \right) \right\rangle_{i+1/2}^{k+1} - \left\langle j_g \left(A_{0g} \frac{C_g j_g}{\alpha} \right) \right\rangle_{i-1/2}^{k+1} \right\} \\ &+ \frac{\Delta t}{A_i \Delta x_i} \left\{ \left\langle j_l \left(A_{0l} \frac{C_l j_l}{(1-\alpha)} \right) \right\rangle_{i+1/2}^{k+1} - \left\langle j_l \left(A_{0l} \frac{C_l j_l}{1-\alpha} \right) \right\rangle_{i-1/2}^{k+1} \right\} \\ &+ \frac{\Delta t}{\Delta x_i} \left(p_{i+1/2}^{k+1} - p_{i-1/2}^{k+1} \right) + \Delta t \bar{v}_i^{k+1} + \frac{\Delta t \theta^2}{2D_{H_2O} c} \left[\rho_{g,i}^{k+1} j_{g,i}^{k+1} + \rho_{l,i}^{k+1} j_{l,i}^{k+1} \right]^2 \\ &+ \left[\frac{1}{2} \left(\alpha_{i-1/2}^{k+1} \rho_{g,i-1/2}^{k+1} + (1 - \alpha_{i-1/2}^{k+1}) \rho_{l,i-1/2}^{k+1} \right) \right. \\ &\left. + 1/2 \left(\alpha_{i+1/2}^{k+1} \rho_{g,i+1/2}^{k+1} + (1 - \alpha_{i+1/2}^{k+1}) \rho_{l,i+1/2}^{k+1} \right) \right] g \cos \theta \Delta t = 0 \end{aligned}$$

(6-16)

(Here the k index denotes the kth time step.)

Vapor Continuity (Liquid continuity is similar.)

$$\begin{aligned}
 C_{g,i}^{k+1} &\equiv \alpha_{i+1/2}^{k+1} \rho_{g,i+1/2}^{k+1} - \alpha_{i+1/2}^k \rho_{g,i+1/2}^k \\
 &+ \frac{\Delta t}{A_{i+1/2} \Delta z_i} \left[\left\langle j_g^{A_D} \right\rangle_{i+1}^{k+1} - \left\langle j_g^{A_D} \right\rangle_i^{k+1} \right] \\
 - \hat{\Gamma}_g \Delta t &= 0
 \end{aligned} \tag{6-17}$$

where

$$\hat{\Gamma}_g = (\Gamma_g)_{\text{node } i}^{k+1} \tag{6-18}$$

unless node i contains the boiling boundary.

In that case,

$$\hat{\Gamma}_g = (\Gamma_g)_{\text{node } i}^{k+1} \left(\frac{z_{i+1} - z_{bb}}{\Delta z_i} \right) \tag{6-19}$$

with z_{bb} denoting the location of the boiling boundary.

Vapor Energy (Liquid Energy is similar):

$$\begin{aligned}
 E_{g,i}^{k+1} &= \alpha_{i+1/2}^{k+1} \rho_{g,i+1/2}^{k+1} \left[h_{g,i+1/2}^{k+1} + \frac{1}{2} \left(\frac{j_{g,i+1/2}^{k+1}}{\alpha_{i+1/2}^{k+1}} \right)^2 + g \cos \theta z_{i+1/2} \right] \\
 &- \alpha_{i+1/2}^k \rho_{g,i+1/2}^k \left[h_{g,i+1/2}^k + \frac{1}{2} \left(\frac{j_{g,i+1/2}^k}{\alpha_{i+1/2}^k} \right)^2 + g \cos \theta z_{i+1/2} \right] \\
 &- \alpha_{i+1/2}^{k+1} \left(P_{i+1/2}^{k+1} - P_{i+1/2}^k \right)
 \end{aligned} \tag{6-20}$$

$$\begin{aligned}
 &+ \frac{\Delta t}{A_{i+1/2} \Delta z_i} \left[\left\langle j_g A \rho_g \left(h_g + \frac{1}{2} \left(\frac{j_g}{\alpha} \right)^2 + g z \cos \theta \right) \right\rangle_{i+1}^{k+1} \right. \\
 &\left. - \left\langle j_g A \rho_g \left(h_g + \frac{1}{2} \left(\frac{j_g}{\alpha} \right)^2 + g z \cos \theta \right) \right\rangle_i^{k+1} \right] + \frac{\Delta t}{\Delta z_i} A Q_g
 \end{aligned}$$

where

$$\hat{Q}_g = \frac{1}{A_{i+1/2}} (Q_{g1}^{k+1})_{i+1/2} \Delta z_i - \frac{1}{A_{i+1/2}} (q_{wg}^{k+1})_{i+1/2} \Delta z_i - \left(r_g h_{1,g}^* \right)_{i+1/2}^{k+1} \Delta z_i \tag{6-21}$$

with appropriate modifications in the boiling boundary node.

6.3.2 Equation Solution

In both the steady-state and transient conditions, we wish to solve at each value of $t = t_{k+1}$

$$\left. \begin{aligned}
 M_1^{k+1} &= 0 \\
 C_{g,i}^{k+1} &= 0 \\
 C_{l,i}^{k+1} &= 0 \\
 E_{g,i}^{k+1} &= 0 \\
 E_{l,i}^{k+1} &= 0
 \end{aligned} \right\} \quad i = 2, 3, \dots, \text{JOUTLT} - 1 \quad (6-22)$$

$$M_{\text{JOUTLT}}^{k+1} = 0$$

where the terms on the left are defined by Equations 6-16, 6-17, and 6-20.

Define the vector

$$\phi_i = \begin{bmatrix} j_i \\ a_{i+1/2} \\ P_{i+1/2} \\ h_{g,i+1/2} \\ h_{l,i+1/2} \end{bmatrix} \quad (6-23)$$

and the vector

$$F_1^{k+1} = \begin{bmatrix} M_i^{k+1} \\ C_{g,i}^{k+1} \\ C_{l,i}^{k+1} \\ E_{g,i}^{k+1} \\ E_{l,i}^{k+1} \end{bmatrix} \quad (6-24)$$

Then the equations we wish to solve can be written in the form,

$$F(\phi, z_{bb}) = 0 \quad (6-25)$$

$$B(\phi, z_{bb}) = 0$$

where the boundary conditions have been incorporated into ϕ and where $B(\phi, z_{bb})$ denotes the boiling boundary equation (6-10).

We use a modified Newton method to solve (6-25). Let $F'_\phi(\phi, z_{bb})$ denote the Jacobian matrix of partial derivatives of F with respect to the independent variables ϕ . Let $F'_{z_{bb}}(\phi, z_{bb})$ denote the (column) vector of partial derivatives of F with respect to z_{bb} .

Next, let $B'_\phi(\phi, z_{bb})$ denote (row) vector of partial derivatives of B with respect to ϕ and finally $B'_z(\phi, z_{bb})$ the derivative of B with respect to z .

Newton's method for solving Equation 6-25 starting from an initial estimate $\phi^{(0)}, z_{bb}^{(0)}$ can be described as follows:

Solve

$$\begin{bmatrix} F'_\phi(\phi^k, z_{bb}^k) & F'_{z_{bb}}(\phi^k, z_{bb}^k) \\ B'_\phi(\phi^k, z_{bb}^k) & B'_{z_{bb}}(\phi^k, z_{bb}^k) \end{bmatrix} \begin{bmatrix} \Delta\phi \\ \Delta z_{bb} \end{bmatrix} = \begin{bmatrix} F(\phi^k, z_{bb}^k) \\ g(\phi^k, z_{bb}^k) \end{bmatrix} \quad (6-26)$$

If the number of nodes is of moderate size (about 20 to 25), then there is considerable savings in the solution of Equation 6-26 if we take into account the banded structure of F' . Equation 6-26 can be written,

$$\begin{bmatrix} F'_\phi & 0 \\ (B'_\phi)^T & B'_z - (B'_\phi)^T (F'_\phi)^{-1} F'_z \end{bmatrix} \begin{bmatrix} I & (F'_\phi)^{-1} F'_z \\ 0 & I \end{bmatrix} \begin{bmatrix} \Delta\phi \\ \Delta z_{bb} \end{bmatrix} = \begin{bmatrix} F \\ B \end{bmatrix} \quad (6-29)$$

Then $\Delta\phi$ and Δz_{bb} can be computed as,

$$\Delta z_{bb} = \frac{B - (B'_\phi)^T (F'_\phi)^{-1} F}{B'_z - (B'_\phi)^T (F'_\phi)^{-1} F'_z} \quad (6-30)$$

$$\Delta\phi = (F'_\phi)^{-1} F - \Delta z_{bb} (F'_\phi)^{-1} F'_z \quad (6-31)$$

6.4 NOMENCLATURE (All Units are SI Units)

A	Channel cross sectional area, m^2
B	Residual for boiling boundary equation
C_l, C_g	Constants in momentum equation
C_o	Drift flux constant
D_H	Hydraulic diameter, m
F	Residual vector for 5 equation model
G	Total flow, $kg/m^2\text{-sec}$
g	Acceleration of gravity, m/sec^2
$h_l(g)$	Liquid (vapor) enthalpy, joules/kg
h^*	$h + V^2/2 + zg$, total enthalpy, joules/kg

$h_{l(g) \text{ sat}}$	Liquid (vapor) saturation enthalpy, joules/kg
h_{lg}	$h_{gsat} - h_{lsat}$, joules/kg
h_{ld}	Enthalpy at inception of boiling, joules/kg
\bar{h}	Mixture enthalpy, joules/kg
H_g	Interfacial heat transfer coefficient, watt/m ² -°k
J	Mechanical equivalent of heat
j	Volumetric flux, m ³ /sec
$j_{l(g)}$	Volumetric liquid (vapor) flux, m ³ /sec
j_i^k	Volumetric flux at time t_k and mesh interface i, m ³ /sec
K_{loc}	Local loss coefficient
K_f	Friction loss coefficient
P	Pressure, newtons/m ²
ΔP_f	Friction pressure drop, newtons/m ²
ΔP_{loc}	Local pressure drop, newtons/m ²
P_i	Interface perimeter, m
P_H	Heated perimeter, m
$Q_{i+1/2}^k$	Field variable at time t and mesh center node i
"	Wall heat flux to liquid (vapor), watts/m ²
$q_{wl(g)}$	Interfacial heat flux to liquid (vapor), watts/m ²
$q_{l(g)1}$	Interfacial heat flux to liquid (vapor), watts/m ²
$T_{l(g)}$	Liquid (vapor) temperature, °K
T_{sat}	Saturation temperature, °K
$v_{l(g)}$	Liquid (vapor) specific volume, m ³
$v_{l(g) \text{ sat}}$	Liquid (vapor) saturated specific volume, m ³
$v_{l(g)}$	Liquid (vapor) velocity m/sec

NEDO-24154-A

v_{lg}	$v_{lsat} - v_{gsat}$, m^3
v_{gj}	Drift flux constant, m/sec
X	Flow quality
z	Axial position, m
α	Void fraction
Γ_g	Vaporization rate, kg/m^3 -sec
ψ	Volumetric heat generation rate, $watt/m^3$
ϕ^2	Two-phase friction multiplier
$\mu_{l(g)}$	Liquid (vapor) viscosity,
$\rho_{l(g)}$	Liquid (vapor) density, kg/m^3

7. FUEL HEAT TRANSFER MODEL

7.1 MODEL ASSUMPTIONS

The fuel heat transfer model used in the one-dimensional reactor core model provides the time-dependent fuel temperature as input to the Doppler reactivity calculation and provides the cladding wall temperature used in the transient heat flux calculation. A single rod with a radially averaged heat generation rate is used to represent all of the fuel rods in the core. Radial conduction equations are solved for each discretized axial position in the core. Axial conduction is assumed to be negligible. The fuel pellet is divided into seven radial nodes and the cladding into two nodes (see Figure 7-1). The fuel and cladding conductivity and heat capacity are assumed to be temperature dependent. A gap thickness is specified between the fuel and cladding and an input gap conductance is used. Axial and time-dependent gap conductances can be specified. The external heat transfer coefficient and liquid temperature is obtained from the thermal-hydraulic calculation. The heat generation rate in the fuel pellet is obtained from the axial fission distribution determined in the nuclear calculation. The radial heat distribution is assumed to be independent of axial position and independent of time.

7.2 CONDUCTION EQUATIONS

In cylindrical geometry, the partial differential equation governing the temperature can be written

$$\rho C_p \frac{\partial T}{\partial t} = \frac{\partial}{\partial r} \left(k \frac{\partial T}{\partial r} \right) + \frac{k}{r} \frac{\partial T}{\partial r} + Q''' \quad (7-1)$$

where

- ρ = material density
- C_p = heat capacity
- K = conductivity
- T = temperature
- r = radial position
- Q''' = rate of internal heat generation

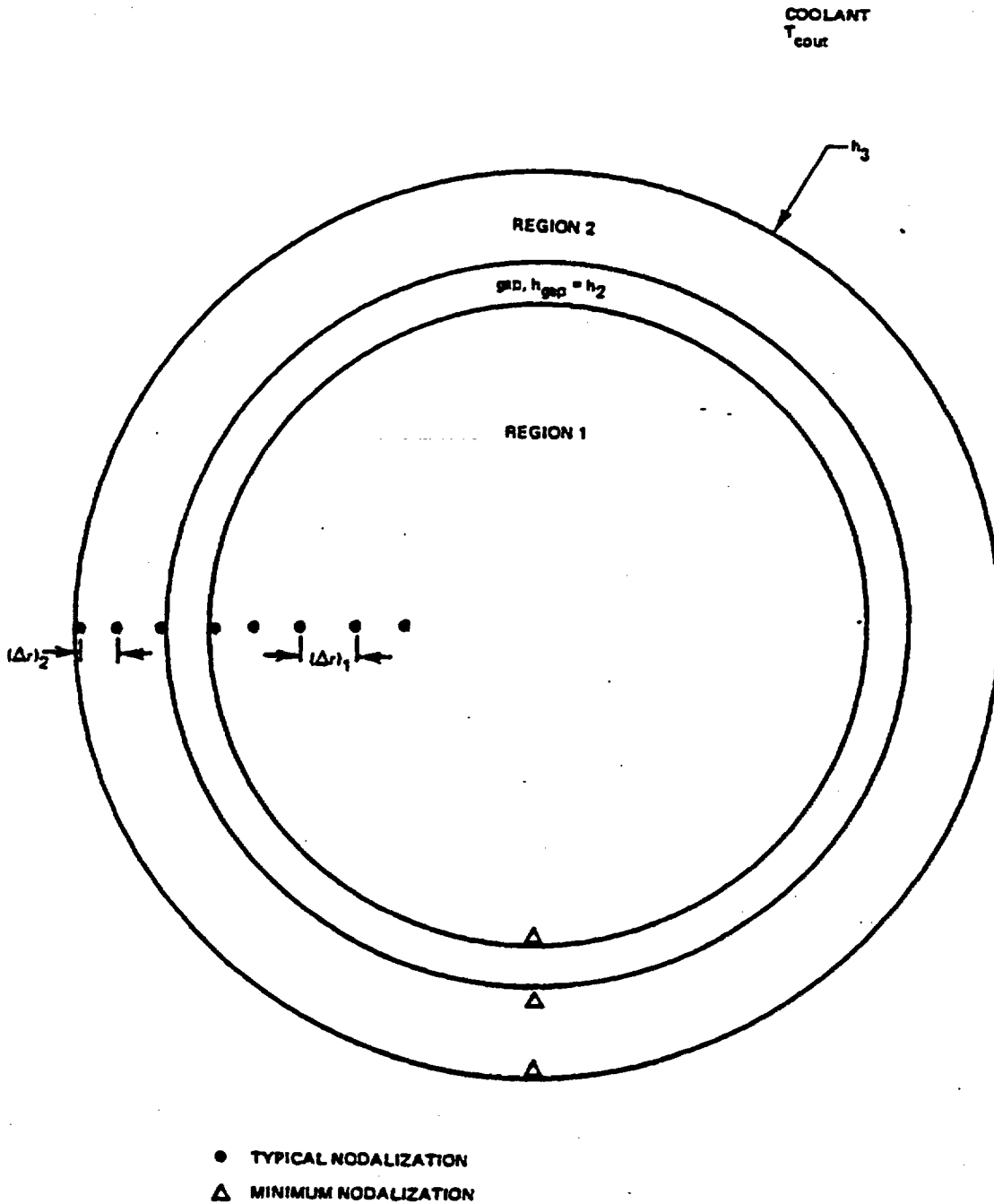


Figure 7.1. Sample Geometry and Nodalization

In carrying out the time integration, the Crank-Nicholson formalism is used. Q40
 This formalism assumes that the temperature varies linearly between time t and $t + \Delta t$.

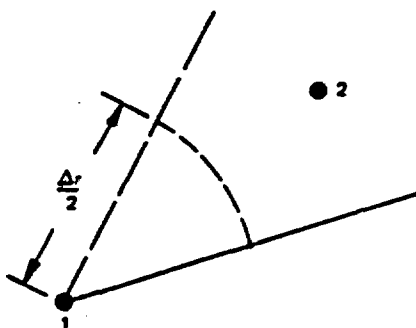
The finite-difference equations can be obtained by considering an energy balance on representative nodes. The conservation of energy equation for this case is

$$\left[\begin{array}{c} \text{rate of} \\ \text{change in} \\ \text{stored energy} \end{array} \right] = \left[\begin{array}{c} \text{rate of} \\ \text{energy} \\ \text{in} \end{array} \right] - \left[\begin{array}{c} \text{rate of} \\ \text{energy} \\ \text{out} \end{array} \right] + \left[\begin{array}{c} \text{rate of} \\ \text{energy} \\ \text{generation} \end{array} \right]$$

In general, three nodes are considered for each finite-difference equation. By definition, consider energy in to be heat transferred from the adjacent node closest to the center of the cylinder to the middle node of the three. Energy out is heat transferred from the middle node to the next node farther from the center. The finite difference equations are of the form,

$$a_i T_{i-1} + b_i T_i + c_i T_{i+1} = d_i \quad (7-2)$$

7.2.1 First Node For Solid Cylinders



Q40 - Responses to NRC questions on the text are documented in Appendix B. The symbol Q40 denotes that this topic is discussed further in the response to NRC Question 40.

$$\begin{aligned} \text{Change in stored energy} &= \rho C_p V \frac{\partial T}{\partial t} \\ &= \frac{(\rho C_p V)}{\Delta t} [T_1(t + \Delta t) - T_1(t)] \end{aligned} \quad (7-3)$$

$$\text{Energy out} = k_s A_m \frac{(\bar{T}_1 - \bar{T}_2)}{\Delta r} \quad (7-4)$$

where k_s is the average of the thermal conductivities at nodes 1 and 2, and

$$\bar{T} = 1/2 [T(t + \Delta t) + T(t)] \quad (7-5)$$

$$V_1 = \frac{\left(\frac{\Delta r}{2}\right)^2}{2\pi} = \frac{\Delta r^2}{8} \quad (7-6)$$

$$A_m = 2\pi \frac{\Delta r}{2} \frac{1}{2\pi} = \frac{\Delta r}{2} \quad (7-7)$$

7.2.2 Interior Nodes

For interior nodes, it is simpler to obtain the finite-difference equations from the partial differential equation than from an energy balance. From Equation 7-1,

The stored energy term is approximated by

$$\frac{(\rho C_p)}{\Delta t} [T(t + \Delta t) - T(t)] \quad (7-8)$$

The first conduction term, containing the thermal conductivity within the derivative, is given by

$$\frac{\partial}{\partial r} \left(k \frac{\partial T}{\partial r} \right) = \frac{1}{(\Delta r)^2} \left[\frac{(k_{i-1} + k_i)}{2} \bar{T}_{i-1} - \frac{(k_{i-1} + 2k_i + k_{i+1})}{2} \bar{T}_i + \frac{(k_i + k_{i+1})}{2} \bar{T}_{i+1} \right] \quad (7-9)$$

where T is a weighted average between the temperatures at the new and old time given by Equation 7-5.

The first derivative term can be approximated by

$$\frac{k}{r} \frac{\partial T}{\partial r} = \frac{1}{2} \frac{1}{r} \left[\frac{(k_i + k_{i+1})}{2} \frac{(\bar{T}_{i+1} - \bar{T}_i)}{\Delta r} + \frac{(k_{i-1} + k_i)}{2} \frac{(\bar{T}_i - \bar{T}_{i-1})}{\Delta r} \right] \quad (7-10)$$

The coefficients, a, b, c, and d are given in Table 7-1.

7.2.3 Last Node of Annular Regions

The coefficients for the last node of an annular region depend upon whether or not the region is adjacent to the coolant. For the last node of any region, the geometry is shown in the following sketch:

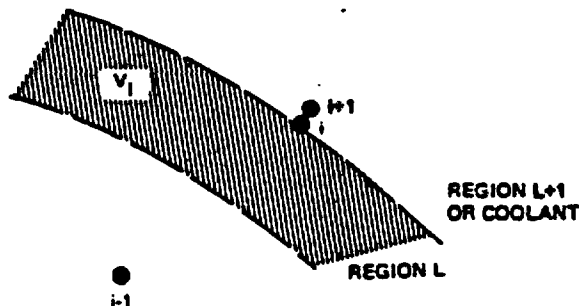


Table 7-1
STEADY - STATE FINITE-DIFFERENCE COEFFICIENTS

Node:	i = 1		2 ≤ i ≤ i _{max} -1	i = i _{max}	
Region:	L = 1		all L	L = LMAX	L = LMAX
Coeff.	Solid Cylinder	L = 1			
a _i	0	$1 + \frac{W_2 h_1}{R(L)}$	$k_a W_2$	$k_a W_2$	$k_a W_2$
b _i	$-\frac{4k_a}{(\Delta r)^2}$	- a _i - c _i	a _i - c _i	- a _i - c _i	$-k_a W_2 - W_2 h_{i+1}$
c _i	$\frac{4k_a}{(\Delta r)^2}$	$k_a W_1$	$k_a W_2$	$W_2 h_{i+1}$	0
d _i	- Q'''	- Q'''	- Q'''	- Q'''	$- Q''' - W_2 h_{i+1} T_{\text{cool}}$

7-6

NEDO-24154-A

If region L is the last region ($L = L + 1$), then \bar{T}_{i+1} is the coolant temperature and if region L is an interior region, \bar{T}_{i+1} is the first node of the next region.

The volume of the last node of any region, per radian, is

$$V_i = \left[\pi r^2 - \pi \left(r_i - \frac{\Delta r}{2} \right)^2 \right] \frac{1}{2\pi} \quad (7-11)$$

$$= \left(r_i - \frac{\Delta r}{4} \right) \frac{\Delta r}{2} \quad (7-12)$$

The mean heat transfer area, per radian, is

$$A_m = \left(r_i - \frac{\Delta r}{2} \right) \quad (7-13)$$

and the surface area of the region, per radian, is

$$A_i = r_i \quad (7-14)$$

The energy into the volume element consists of the energy entering the shaded area by conduction, plus the energy generated. The conduction from $i - 1$ to i is

$$\left(\frac{k_{i-1} + k_i}{2} \right) A_m \frac{(\bar{T}_{i-1} - \bar{T}_i)}{\Delta r} \quad (7-15)$$

If the region is not the last region, the energy out is the energy transferred across the gap:

$$h_{L+1} A_i (\bar{T}_i - \bar{T}_{i+1})$$

If the region is the last region, \bar{T}_{i+1} is replaced by the coolant temperature, which is assumed to be a known quantity.

The stored energy term and the heat generation term are approximated as it was done for the other nodes. The coefficients, a_i , b_i , c_i , and d_i are given in Table 7-2.

When a physical gap exists between two regions, the gap heat transfer is accounted for by using a gap conductance. The heat transfer is based upon the outside surface area of the inner region of the two regions being considered.

Table 7-2
TRANSIENT FINITE-DIFFERENCE COEFFICIENTS

Node:	$i = 1$	$2 \leq i \leq i_{max}-1$	$i = i_{max}$		
Region:	$L = 1$				
Coeff.	Solid Cylinder	$L > 1$	$L < LMAX$	$L = LMAX$	
a_i	0	$\frac{-\sigma W_2 h_2 \Delta t}{\rho C_p \left[1 + \frac{GAP(L-1)}{R(L)} \right]}$	$\frac{-\sigma k_a \Delta t W_2}{\rho C_p}$	$\frac{-\sigma k_a \Delta t W_2}{\rho C_p}$	$\frac{-\sigma k_a \Delta t W_2}{\rho C_p}$
b_i	$1 - c_i$	$1 - a_i - c_i$	$1 - a_i - c_i$	$1 - a_i - c_i$	$1 - a_i - \frac{\sigma \Delta t W_2 h_{2,i+1}}{\rho C_p}$
c_i	$-4\sigma/m_2$	$\frac{-\sigma k_a \Delta t W_2}{\rho C_p}$	$\frac{-\sigma k_a \Delta t W_2}{\rho C_p}$	$\frac{-\sigma \Delta t W_2 h_{2,i+1}}{\rho C_p}$	0
d_i	$(1 - P_{ci}) T_i$ $+ P_{ci} T_{i+1}$ $+ \frac{Q''' \Delta t}{\rho C_p}$	$\frac{(1 - \sigma) \Delta t h_2 W_2 T_{i-1}}{\rho C_p \left[1 + \frac{GAP(L-1)}{R(L)} \right]}$ $+ (1 - P_{ci}) T_i$ $+ \frac{k_a \Delta t W_2 (1 - \sigma) T_{i+1}}{\rho C_p}$ $+ Q''' \Delta t / \rho C_p$	$\frac{(1 - \sigma) k_a \Delta t W_2 T_{i-1}}{\rho C_p}$ $+ (1 - P_{ci}) T_i$ $+ \frac{(1 - \sigma) k_a \Delta t W_2 T_{i+1}}{\rho C_p}$ $+ Q''' \Delta t / \rho C_p$	$\frac{(1 - \sigma) k_a \Delta t W_2 T_{i-1}}{\rho C_p}$ $+ (1 - P_{ci}) T_i$ $+ \frac{(1 - \sigma) W_2 h_{2,i+1} \Delta t T_{i+1}}{\rho C_p}$ $+ Q''' \Delta t / \rho C_p$	$(1 - \sigma) k_a \Delta t W_2 T_{i-1} / \rho C_p$ $+ (1 - P_{ci}) T_i$ $+ W_2 h_{2,i+1} \Delta t T_{i+1} / \rho C_p$ $+ Q''' \Delta t / \rho C_p$
P_{ci}	$\frac{4}{m_2} + C_i$	$(1 - \sigma) \Delta t / \rho C_p$ $\left[W_2 k_a + \frac{W_2 h_2}{1 + \frac{GAP(L-1)}{R(L)}} \right]$	$\frac{(1 - \sigma) \Delta t}{\rho C_p}$ $[k_a W_2 + k_a W_2]$	$\frac{(1 - \sigma) \Delta t}{\rho C_p}$ $[k_a W_2 + W_2 h_{2,i+1}]$	$\frac{(1 - \sigma) \Delta t}{\rho C_p}$ $[k_a W_2 + W_2 h_{2,i+1}]$

7-9

NEDO-24154-A

7.3 NOMENCLATURE.

a_1, b_1, c_1, d_1	Coefficients in finite-difference equations
C	Constant
C_p	Specific heat
(GAP (L - 1))	Radial distance between regions L - 1 and L
h_1	Heat transfer coefficient between a surface and the fluid, or between two regions
k	Thermal conductivity
k_A	$[K(I-1) + K(I)] / 2$
k_B	$[K(I) + K(I+1)] / 2$
m_2	$\rho C_p (\Delta r)^2 / k_B \Delta t$
N	Number of nodes
P_f	Radial peaking factor in a region, a function of r
P_{ci}	Stability (accuracy) parameter defined in Table 2-1
q_1''', Q'''	Heat generation, energy/(time · volume)
R(L)	Outer radius of region L-1
r	Radial coordinate
r_i	Radial location of the i-th node
Δr	Distance between nodes. It can be different for each region.
t	Time
Δt	Time increment
T_1'	Temperature at new time (t+ Δt) at node 1
T_1	Temperature at old time (t) at node 1
\bar{T}	$\sigma T' + (1 - \sigma) T$

NEDO-24154-A

T_{cout}	Fluid temperature outside cylinder
V_i	Volume of ith node
V_0	Constant
$W1_i$	$\left[4 (2r_i + \Delta r) / (4 r_i + \Delta r) \right] / (\Delta r)^2$
$W2_i$	$\left[4 (2 r_i - \Delta r) / (4 r_i - \Delta r) \right] / (\Delta r)^2$
$W3_i$	$\left[8 r_i \Delta r / (4 r_i + \Delta r) \right] / (\Delta r)^2$
$W4_i$	$\left[8 r_i \Delta r / (4 r_i - \Delta r) \right] / (\Delta r)^2$
$W5_i$	$\left[1 + \Delta r / (2 r_i) \right] / (\Delta r)^2$
$W6_i$	$\left[1 - \Delta r / (2 r_i) \right] / (\Delta r)^2$
PL	Density in region L
σ	$\left\{ \begin{array}{l} 0, \quad \text{explicit method} \\ 0.5, \quad \text{Crank-Nicolson method} \\ 1, \quad \text{pure implicit method} \end{array} \right.$

8. REFERENCES

1. R.B. Linford, *Analytical Methods of Plant Transient Evaluations of the General Electric Boiling Water Reactor*, NEDO-10802, February 1973.
2. J.A. Wooley, *Three-Dimensional BWR Core Simulator*, NEDO-20953, May 1976.
3. D.A. Mandell, *CHT - A Program for the One-Dimensional Transient Conduction Heat Transfer in a Cylindrical Geometry*, NEDE-21234.
4. D.E. Patterson and T.H. Bredt, *GEDAC03 - System Overview and Summary*, NEDE-11379, June 1976.
5. C.H. Robbins, *Performance Tests of Axial Flow Primary Steam Separators*, APED-4762, January 1965.
6. H.S. Cheng, *On the Accuracy and Stability of the Variable Implicit Time Integrated Method of the Program TASK*, NEDM-11038-58, July 30, 1971.
7. R.T. Lahey, *Two Phase Flow in Boiling Water Nuclear Reactors*, NEDO-13388, July 1974.
8. F.H. Harlow and A.A. Amsden, *Numerical Calculation of Multiphase Fluid Flow*, J. Computational Physics, B17, 1, January 1975.
9. J.H. Avila, *Solution of Two Phase One-Dimensional Transient Flow Equations*, to be published.

NEDO-24154-A

APPENDIX A

RESPONSE TO NUCLEAR REGULATORY COMMISSION QUESTIONS
ON SECTIONS 1 THROUGH 3 OF VOLUME II

A-1/A-2

QUESTION 1 (Enclosure 2)

In the case of the steamline pressure predictions, "the coarseness of the spatial mesh," which models the steamline, is said to be the cause of "the spreading out of the calculated wave" as compared to measurement. In order to verify this difference, provide a sensitivity study of the effects of spatial mesh sizes. This study should demonstrate the effect of increased noding in the steamline on the steamline pressure predictions. If this sensitivity study does not verify the postulated effect on steamline pressure predictions for the three Peach Bottom-2 turbine trip tests, an alternate explanation and verification should be provided.

RESPONSE

The effect of the mesh size on the steamline pressure prediction can be verified by comparing the results obtained with the three Peach Bottom tests and the KKM steamline results. The Peach Bottom analysis shows a spreading out of the initial pressure pulse relative to the measured data, while the agreement is much better for the KKM steamline pressure. The Peach Bottom steamline is about 400 ft long (100 ft inside the containment and 300 ft outside the containment). Six spatial nodes were chosen to represent this length. The KKM steamline is 327 ft long (93 ft inside and 234 ft outside) and is represented with 7 nodes. The average node length is about 30% smaller in the KKM analysis and the improvement to the steamline pressure prediction is clear by comparing Figures 13-14 and 13-15 with Figures 13-1, 13-5, and 13-9 provided in response to Question 13 of Appendix B, Volume I. Despite this noding effect in Peach Bottom, the dome pressure is simulated quite well by the calculations for all three Peach Bottom Turbine Trips.

NEDO-24154-A

QUESTION 2 (Enclosure 2)

"The fact that heat loss terms are ignored in the transient calculation" was identified as the cause of the discrepancy between the dome pressure predictions and measurements. Provide a calculation to justify the basis for this explanation. Provide all assumptions on surface areas, volumes, specific heat, heat transfer coefficient, reactor coolant temperature, and steam and water flow rates. If this calculation does not fully verify the extent of the discrepancy, additional explanation and verification should be supplied.

RESPONSE

Studies conducted since the time the draft qualification report was issued have shown that a large energy loss rate is required to explain the observed pressure overprediction. (See response to Question 39, Appendix B, Volume I). The exact cause of this peak pressure bias is not known. The audit calculations carried out by BNL indicate a similar bias if a 26% bypass capacity were used, as in the ODYN calculation.

NEDO-24154-A

QUESTION 3 (Enclosure 2)

Provide calculational verification that the core exit pressure oscillations between 0.4 and 0.7 sec are due to "ringing" in the instrument line. This verification should show that the magnitude and frequency of the oscillations correspond to those for the natural frequency of the instrument line. Provide a full explanation and verification of the phenomenon.

RESPONSE

A discussion of sensor line effects on the transient pressure response measurements in the Peach Bottom tests is given in Section B.2.1.1 of the Peach Bottom turbine trip test report (Reference 4).

NEDO-24154-A

QUESTION 4 (Enclosure 2)

For the larger core exit pressure oscillations at times greater than 0.7 sec, the control rod movement has been postulated as the cause. Provide the core exit pressure response to other scram signals which verify this hypothesis. These other scrams should be reactor trips with minimum pressurization transients.

RESPONSE

No other experimental data exist to verify the postulate that the control rod motion was the cause of the sensed core exit pressure oscillations. It is highly unlikely that these oscillations occurred in the reactor exit plenum, because oscillations in the neutron flux would have been observed.

QUESTION 5 (Enclosure 2)

In the evaluation of the neutron flux differences, two major contributors were identified (core pressure and scram motion). The variation due to these contributors should be quantified and the total effect on neutron flux verified.

RESPONSE

The variation in peak neutron flux due to scram initiation time for the Peach Bottom Transient Test conditions is summarized in Table 5-1. The delay time assumed in the model is 0.17 sec for all three tests. A variation of 0.02 sec about the mean was chosen for this analysis. The peak neutron flux is not very sensitive to the scram initiation time in tests numbers 1 and 2, because the rate of void reactivity increase has decreased by the time the scram has started. More sensitivity is observed in the third turbine trip.

Overall sensitivity of flux to pressure variation is difficult to quantify because of the dynamic nature of the problem. A specific assumption about the transient pressure variation has to be made and the transient reevaluated. The qualification report quoted a flux change of 10% due to a 1 psi pressure change. This relationship exists over a very short period of time, while the reactivity is high. No generalizations to other transients can be made about this sensitivity because it was only used to explain differences between the calculated and observed data.

NEDO-24154-A

Table 5-1

PEAK FLUX VALUES AS A FUNCTION OF SCRAM DELAY TIME

Scram Delay Time (sec)	Peak Neutron Flux		
	TT1 (%)	TT2 (%)	TT3 (%)
0.15	330	420	340
0.17	338	438	420
0.19	338	440	560

QUESTION 6 (Enclosure 2)

In order to assure that no unexpected anomalies occur in the usage of ODYN, provide a sensitivity study on the key parameters and explain and verify any observed anomalies. The sensitivity study should be conducted for the Peach Bottom-2 tests, and for turbine trip without bypass and MSIV closure transients for typical BWR licensing conditions. Some of the key parameters which should be varied through the range of potential BWR transient conditions are scram rate, void reactivity coefficient, void distribution, flow rate and distribution, core pressure drop, stopvalve closure time, MSIV closure time (for pressurization transient), core exit pressure, axial power distribution, etc. Refer to the response for other studies requested in these questions as necessary.

RESPONSE

A considerable number of sensitivity studies have been carried out for license basis conditions. Input parameters have been varied in the response to questions in Enclosure 3. The peak neutron flux peak heat fluxes and ACPRs have been tabulated in these responses. Model sensitivities have been carried out in response to the questions in Appendix B, Volume I. Table 6-1 contains a summary of the results of the ODYN model sensitivities.

Table 6-1

SUMMARY OF ONE DIMENSIONAL MODEL SENSITIVITY STUDIES

Model Perturbation	Peak Core Average Heat Flux (% Rated)
(1) Base Case	121.6
(2) Void Response Reduced 15%	117.8
(3) Void Response Reduced 5%	120.6
(4) Void Response Increased 4.8%	122.4
(5) Void Response Increased 14%	123.7
(6) Prompt neutron heating = 0.015%	122.6
(7) Prompt neutron heating = 0.022%	121.4
(8) Bypass flow fraction increased 20%	121.2
(9) Jet pump suction loss coefficient decreased 20%	121.7
(10) Jet pump suction and diffuser losses decreased 20% (increased M ratio 5%)	122.5
(11) Separator L/A decreased 30%	122.0
(12) Separator L/A decreased 90%	120.4
(13) Separator pressure drop decreased by 50%	118.9
(14) Recirculation loop L/A increased by 100%	121.4
(15) Core Pressure drop increased by 0.8% psi (nominal = 24 psi)	121.4
(16) Core pressure drop decreased by 0.7 psi	121.8
(17) Core pressure drop decreased by 2.4 psi	122.3
(18) Carry under fraction = 0.2% (Nominal = 0.1%)	121.4
(19) Carry under fraction = 0.01%	121.7
(20) Steamline pressure drop losses decreased 20%	122.5
(21) Steamline specific heat ratio $\gamma = 1.3$	123.8
(22) Steamline specific heat ratio $\gamma = 1.2$	122.6
(23) Core thermal hydraulic drift flux parameter C_0 increased 10%	121.5
(24) C_0 decreased 10%	121.9
(25) Drift flux parameter V_{gj} increased 20%	121.6
(26) V_{gj} decreased 20%	121.5
(27) Subcooled void model R_1 decreased 20%	121.5
(28) R_1 increased 20%	121.6
(29) Subcooled void parameter R_2^n $n = 0.5$	116.2
(30) R_2^n $n = 1.25$	122.4
(31) R_2^n $n = 1.50$	123.1

QUESTION 7 (Enclosure 2)

In Section 2.1.1 the scram reactivity is compared using one-dimensional and three-dimensional procedures. In the three cases that were presented, the scram reactivity insertion calculated using the one-dimensional model is more conservative than that calculated using three-dimensional model except for the initial stages in the third case. At the initial stages of the scram in the third case, the power predicted by the three-dimensional procedure is higher than that predicted by the one-dimensional procedure. Explain the reason for this nonconservatism, and assess its effect on the neutron flux in the Peach Bottom tests and in Δ CPR prediction. Discuss how the turbine trip without bypass transient would be affected because of these differences in three-dimensional versus one-dimensional procedures.

RESPONSE

The case analyzed in Figure 2-7 of the qualification report is quite similar to the core conditions for Peach Bottom Turbine trip test number one from 50% power. At around 0.1 sec into the scram, the one-dimensional model under calculates the scram reactivity by about 10%. With the large number of control rods in the core, the radial flux distribution is quite complicated, and the approximation scheme chosen to represent the time dependence results in a nonconservative bias. This bias in scram reactivity becomes smaller as the rod insertion fraction increases and is -1% at 0.4 sec. In the analysis of the Peach Bottom test conditions, the one-dimensional scram reactivity model would predict fluxes about 6% lower than the three-dimensional scram curve for that portion of the transient after the start of rod motion. If this particular scram curve were to be used in a turbine trip without bypass transient, there would be no appreciable flux transient at all because the start of rod motion would be triggered by the trip scram mechanism, causing the rods to begin moving about 0.5 sec earlier, so that at 0.4 sec, when the pressure wave hits the reactor core, about \$0.35 negative reactivity has been inserted. At 0.8 sec, about \$3.0 scram reactivity exists, which is much larger than the positive void reactivity contribution.

At end-of-cycle conditions, the scram reactivity increases much more slowly with time, as can be found by comparing Figures 2-2 and 2-4 of the qualification report. In the end-of-cycle case, the most important portion of the scram curve occurs from 0.2 to 1.2 sec after the initiation of rod motion and during the time of the rapid pressure increase. Here the end-of-cycle comparisons show the one-dimensional model to be conservative. Also, biases occurring early in the scram motion, when the total reactivity is small, do not have a significant impact on the transient severity.

QUESTION 8 (Enclosure 2)

In Section 2.1.2, the void coefficient is defined.

- a. Is the void fraction the effective neutron void fraction or is it the void fraction calculated in the thermal-hydraulic analysis?
- b. It is stated that one-dimensional and three-dimensional void coefficients agree to within 5%. Present the details of the wide variety of power levels and control rod configurations to show how this 5% is determined.
- c. How is this uncertainty of 5% introduced in the ODYN model? What is the sensitivity to ΔCPR in the licensing basis transient?

RESPONSE

- a. All void fractions quoted are void fractions calculated by the thermal hydraulic analysis.
- b. Further discussion of the one-dimensional and three-dimensional void response comparisons is presented in the response to Question 2, Appendix B, Volume I.
- c. The difference between one-dimensional and three-dimensional void coefficients is a bias and not an uncertainty. It is shown in the response to Question 2 that this bias is always in the conservative direction for license basis conditions, and, therefore, no model uncertainty is assigned to the one-dimensional collapsing process.

QUESTION 9 (Enclosure 2)

In Section 2.2 thermal and hydraulic models are compared.

- a. Present the details of the standard GE BWR channel hydraulic model referred to in this section.
- b. It is stated that some differences in void fraction exist between the standard GE BWR model and the ODYN code. These are attributed to different numerical treatments and assumption of constant pressure in the standard GE model. No difference is attributed due to the thermal nonequilibrium model and drift flux model in the ODYN code, particularly in the subcooled region. Discuss the sensitivity of the void fractions to these models.
- c. Present all verification details of the standard GE BWR channel hydraulic model with void fraction measurements.
- d. Provide a comparison of the ODYN thermal-hydraulic model with experimental data.

RESPONSE

- a. The details of the standard GE BWR are presented in Chapter 4 of Reference 8.
- b. The model used in the one-dimensional model is a mechanistic subcooled boiling model and is described in more detail in the response to Question 28 in Appendix B, Volume I. This model was used because it is compatible with the separate liquid and vapor continuity and energy equations used in the transient model. The steady-state hydraulics model uses a different model for subcooled boiling in which the subcooled flow quality is determined from the "profile fit", which is a function of the bulk enthalpy and the quantity h_{LD} , the enthalpy at which subcooled boiling begins. The "profile fit" is an analytical expression for the interfacial heat flux up the channel. The sensitivity of the void fractions and transient results to subcooled void models is discussed in the reply to Question 28 of Appendix B, Volume I. The drift flux correlations are identical to those used in the standard GE hydraulic model.
- c. Comparisons with void fraction and pressure drop measurements using the GE correlations are presented in the response to Question 28 of Appendix B, Volume I.

NEDO-24154-A

- d. The ODYN thermal-hydraulic model has been specifically compared to experimental data. It has been compared to the standard GE design models with close agreement. The standard GE design model or equivalent equations have been used to test the appropriate void fractions and pressure drop estimates against experimental data.

QUESTION 10 (Enclosure 2)

In Peach Bottom tests a certain weighted average for 7x7 and 8x8 bundles was used for calculations.

- a. Present the details and basis for the weighting procedure.
- b. Is the same procedure to be used in licensing basis transient analysis?
- c. What is the uncertainty in Δ CPR associated with this procedure in the licensing basis transient?

RESPONSE

- a. In the initial analysis of the Peach Bottom transient, the rod geometry parameters were weighted in proportion to the number of fuel rods of each type in the core. Since that time, a design procedure for transient analysis has been formulated which uses the rod dimensions of the dominant fuel type. That is, the fuel dimensions of the rod type having the largest number in the core is used. The Peach Bottom reactor at end-of-cycle 2 has 576 7x7 bundles and 188 8x8 bundles. Use of the 7x7 parameters rather than the weighted average yielded the same transient results for the Peach Bottom tests.
- b. The dimensions of the dominant rod type will be used in the licence basis analysis.
- c. The 7x7 fuel rods are larger in diameter and therefore have a longer time constant. Therefore, their use will yield a more severe transient than the 8x8 parameters resulting in a conservative Δ CPR estimate. For Peach Bottom-2 this estimate is 0.002 Δ CPR/ICPR greater than the result obtained with average fuel rod parameters. A nonconservative result may be obtained, however, if 8x8 fuel were the dominant type but a significant amount of 7x7 fuel remained in the core. An examination of the current reload configurations shows that when the 8x8 fuel is dominant, there is less than ~25% 7x7 fuel remaining. Based on the sensitivity study quoted above and a 20% loading of 7x7 fuel, the uncertainty connected with this procedure is estimated at ± 0.002 Δ CPR/ICPR.

QUESTION 11 (Enclosure 2)

A value of 1000 Btu/ft²-hr-°F was used for the gap conductance in Peach Bottom tests. It is stated that a 100% change produced only 5% change in peak flux. Describe how the gap conductance was changed. What is the estimated change in ΔCPR?

RESPONSE

Figure 11-1 shows the Peach Bottom Turbine Trip 3 total neutron flux calculated with gap conductances of 1000 Btu/hr-ft² and 500 Btu/hr-ft². Small differences in neutron flux are observed because the entire flux pulse is only about 0.3 sec wide. Therefore, a very fast fuel time constant is needed to produce a moderate density feedback through the rod heat flux. Much larger values of gap conductance will produce changes in the calculated flux response, as evidenced by the response with a gap conductance of 1500 Btu/hr-ft². The estimated difference in ΔCPR/ICPR between these extreme values is 0.005.

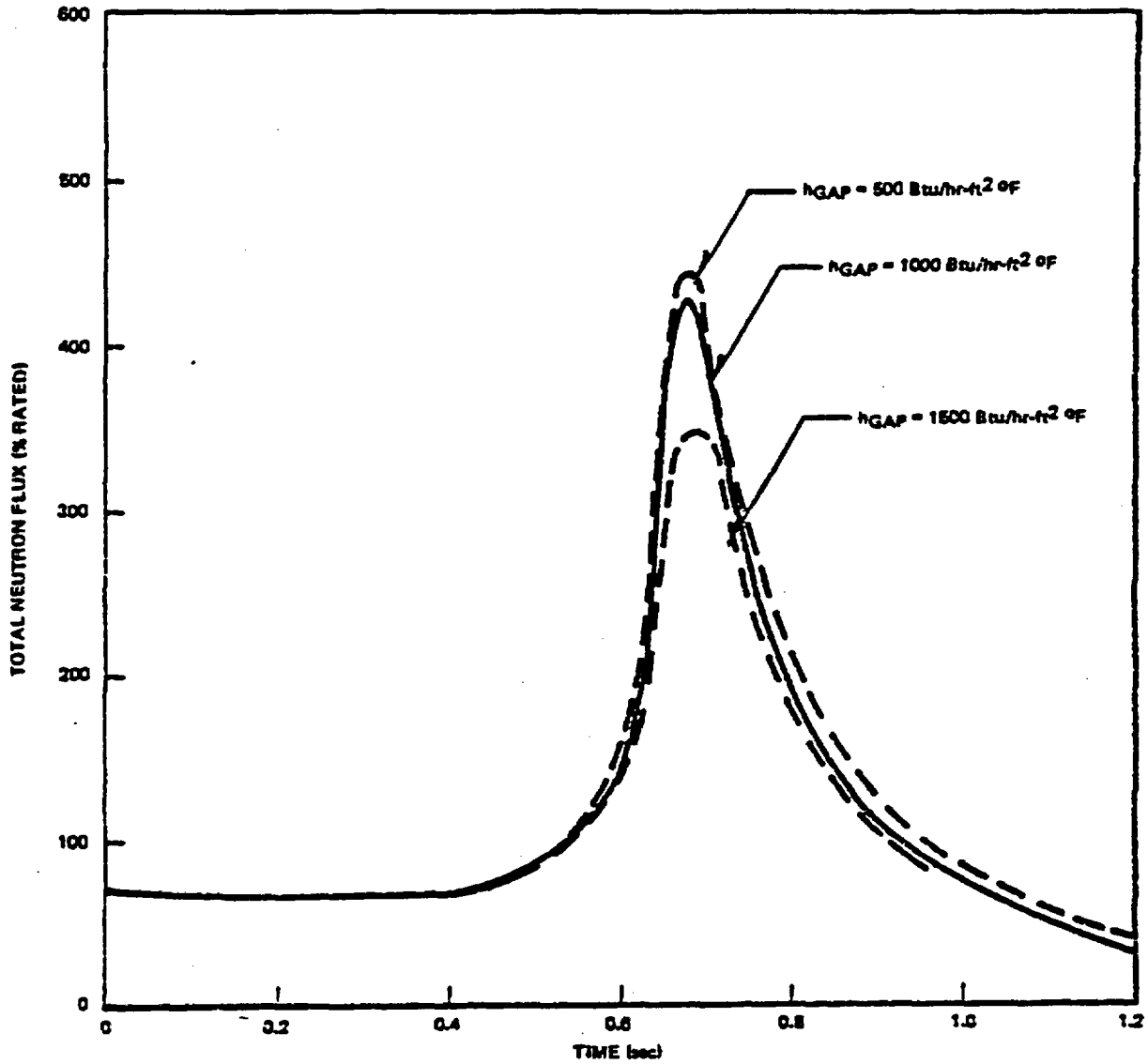


Figure 11-1. Peach Bottom-2 Turbine Trip 3 (69% Power) Neutron Flux

QUESTION 12 (Enclosure 2)

Present the details of instrument line damping and equations for the second-order response, including the characteristics of the transducer. Assess measurement uncertainty for both Peach Bottom and KKM tests.

RESPONSE

A discussion of the instrument line model appears in Section B.2.1.1 of Reference 19. This discussion references three papers which give the details of the equations used. A physical description of the sensor lines is also provided in Appendix B of Reference 4.

NEDO-24154-A

QUESTION 13 (Enclosure 2)

Extend the pressure plots of Figure 3-6 through 3-14 and 3-40 through 3-45 through a period of 3.0 sec to include the peak pressure region both for Peach Bottom and KKM tests.

RESPONSE

Figures 3-6 through 3-14 and 3-40 through 3-45 have been modified to include in excess of 3.0 sec in the qualification documentation.

A13-1/A13-2

NEDO-24154-A

QUESTION 14 (Enclosure 2)

Assess the effect of not considering system heat loss in terms of ΔCPR .

RESPONSE

The current practice of neglecting system heat loss has a negligible effect on ΔCPR . See the response to Question 39 of Appendix B, Volume I.

QUESTION 15 (Enclosure)

It is stated that a 1 psi change in pressure causes a change of 10% in peak neutron flux.

- a. Assess this difference in terms of Δ CPR.
- b. Assess the differences in Δ CPR for the Peach Bottom and KKM tests assuming the calculated conservative neutron flux inputs and the measured pressure inputs.

RESPONSE

- a. It is quite difficult to assess the transient influence of pressure differences on flux calculations without some assumption about how the pressure differences vary in time. The statement about pressure differences in the qualification document was meant to show that small changes in pressure could change the flux near the peak value because the net reactivity was quite high, near β 0.80.
- b. In order to simulate the measured pressure inputs, the Peach Bottom transients have been calculated with a higher bypass capacity (i.e., 35% instead of 26%). (This is not meant to infer that the actual bypass capacity is 35%, but is assumed for pressure simulation purposes only). The core exit pressure traces are shown in Figures 15-1 through 15-3. Critical quality depends directly on pressure and will be influenced mainly by the pressure near the time of peak heat flux, which for the Peach Bottom tests is around 1.1 to 1.2 sec. The 35% bypass calculations show the flux to be virtually identical to the 26% bypass results shown in Question 13. However, after 1.0 sec, the core pressure has been reduced to agree much better with the experimental data. In the case of KKM, the calculated pressure agrees quite well with the experiment out to about 1.8 sec. The Δ CPR/ICPR calculated with these pressure responses are summarized in Table 15-1 along with the data given and previously quoted. Hence, there is negligible difference between Δ CPR's obtained with measured and calculated pressure responses.

NEDO-24154-A

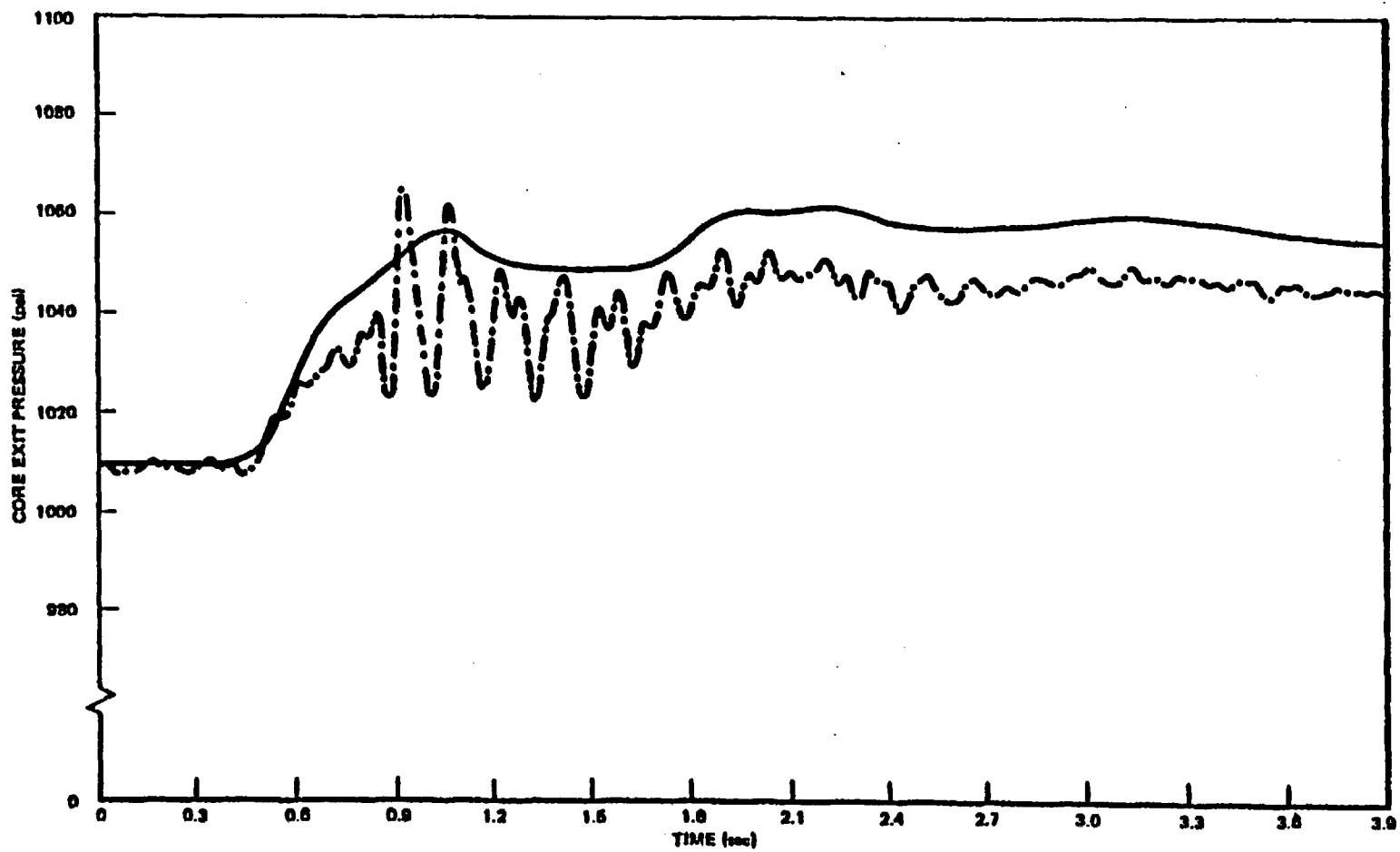
Table 15-1

SUMMARY OF ΔCPR/ICPR RESULTS FOR PEACH BOTTOM TURBINE TRIPS

<u>Test</u>	<u>ΔCPR/ICPR (Data)</u>	<u>ΔCPR/ICPR (26% bp)</u>	<u>ΔCPR/ICPR (35% bp)</u>
PB2TT1	0.170	0.173	0.170
PB2TT2	0.136	0.129	0.135
PB2TT3	0.132	0.141	0.131
KKM	0.077	0.084*	0.084*

*KKM results obtained with 50% bypass.

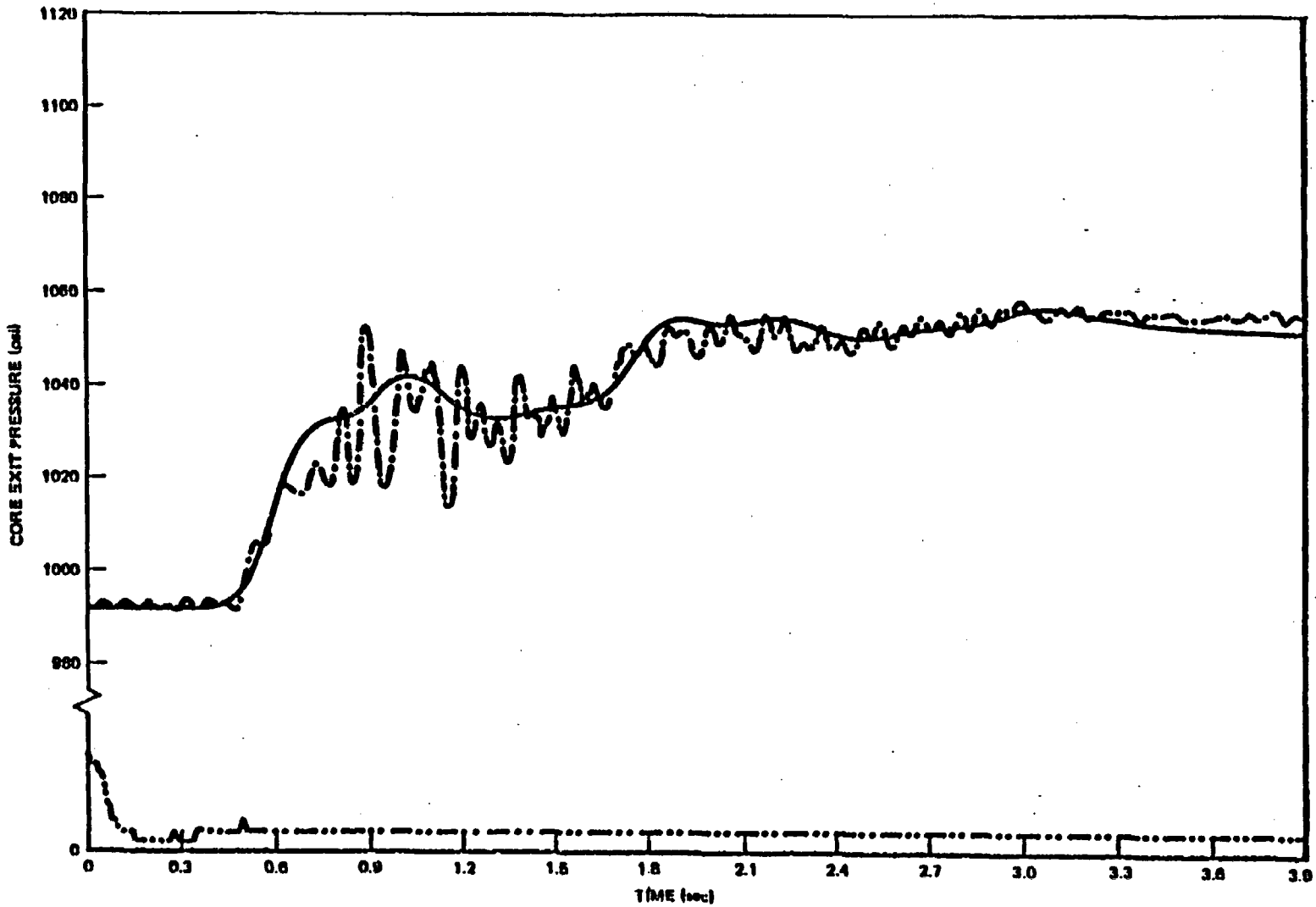
ALS-3



NEBO-24154-A

Figure 15-1. Peach Bottom-2 Turbine Trip 1 Core Exit Pressure (35% Bypass)

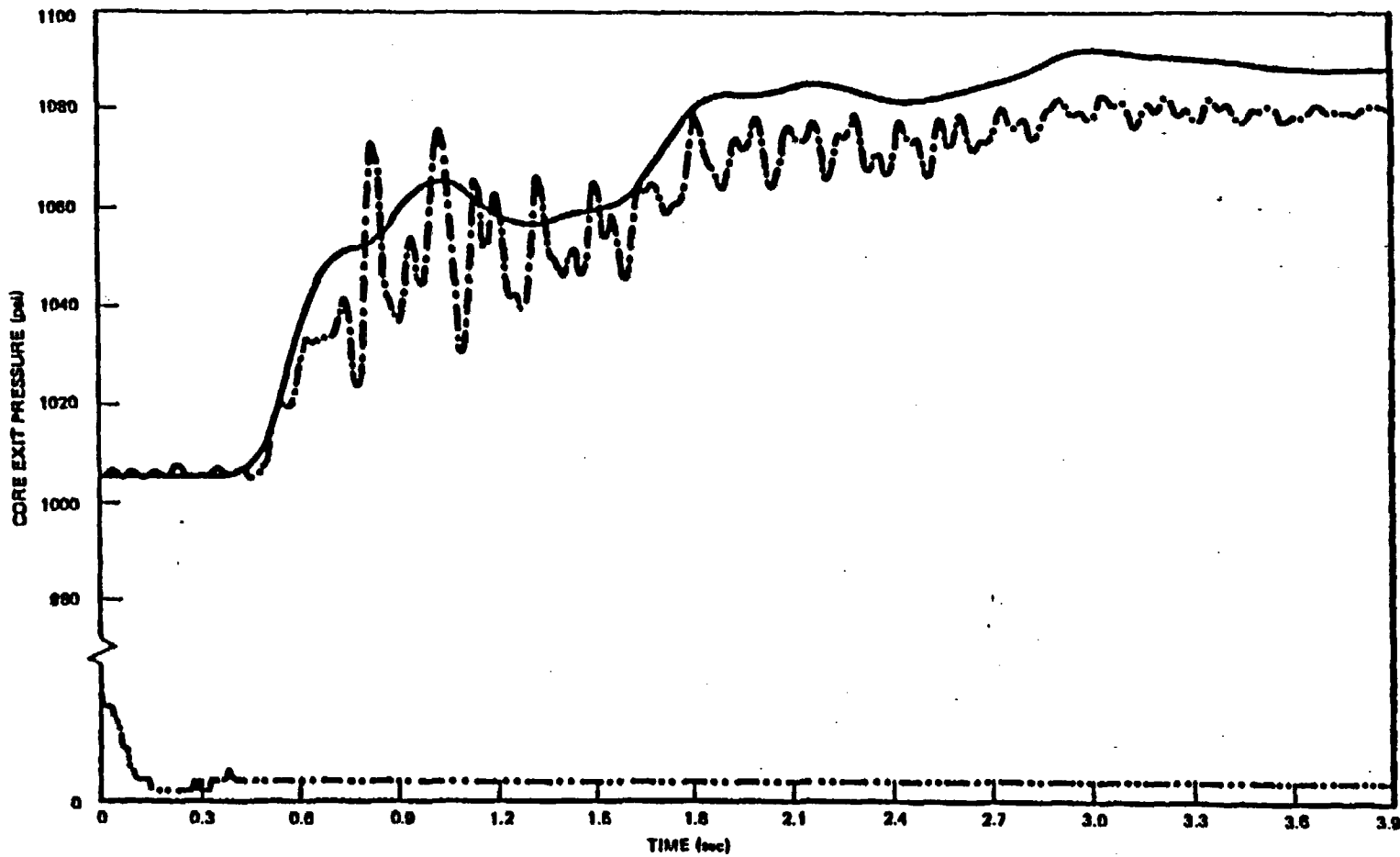
15-4



NEED-24154-A

Figure 15-2. Peach Bottom-2 Turbine Trip 2 Core Exit Pressure (35% Bypass)

ALS-5/ALS-6



NEDO-24154-A

Figure 15-3. Peach Bottom-2 Turbine Trip 3 Core Exit Pressure (35% Bypass)

NEDO-24154-A

QUESTION 16 (Enclosure 2)

Discuss the effect of the uncertainty in the Doppler coefficient on ΔCPR calculations for the turbine trip without bypass transient in a typical BWR/4.

RESPONSE

Uncertainty in the Doppler coefficient and its impact on the transient analysis is discussed in the responses to Questions 12 and 38 of Appendix B, Volume I.

A16-1/A16-2

NEDO-24154-A

QUESTION 17 (Enclosure 2)

It is stated that in the reactor the boiling boundary is different in each channel and the variation in void fraction with axial position is smaller than the one-dimensional estimate. It was also stated that the one-dimensional model represents the average conditions. Present the procedural details for representing the three-dimensional void fraction variation in one-dimensional.

RESPONSE

The procedural details are presented in the One-Dimensional Transient Model report. The effects on the void response and the transient are discussed in the response to Question 2 of Appendix B, Volume I.

A17-1/A17-2

QUESTION 18 (Enclosure 2)

It is stated that measurement uncertainty in pressure is ± 2 psi and in flow it is $\pm 3\%$. This gives an uncertainty of 0.01 in ACPR/ICPR.

- a. Provide ACPR/ICPR versus time curves for all Peach Bottom and KKM tests.
- b. Discuss the effects of instrumentation filters on the uncertainty assessment.
- c. It is noted that the model and data driven ACPR/ICPR values are also within 0.01, although the differences between the experimental and calculated values of pressures may be on the order of 10 psi. Discuss this apparent discrepancy in view of the statement that was made on pressure measurement uncertainty of ± 2 psi and also an earlier statement that 1 psi difference in pressure may make a difference of 10% change in peak neutron flux.

RESPONSE

- a. The General Electric Company does not normally generate plots of critical power ratio (CPR) versus time. Following General Electric Thermal Analysis Basis (GETAB) procedures, the most limiting pressure and power increase transients are evaluated to determine the largest change in the critical power ratio (ACPR). The addition of the ACPR to the safety limit MCPR provides the minimum operating CPR required to avoid violating the safety limit should this limiting transient occur. The operating limit and the safety limit MCPR are independent of the path taken by the transient. Therefore, plots of CPR versus time serve no useful purpose and are not generated.
- b. Instrumentation effects on the experimental uncertainty are discussed in Appendix B of Reference 4.
- c. The draft qualification report unfortunately gives the impression that the ± 0.01 uncertainty was entirely due to the pressure and flow uncertainty. In reality, the change in CPR due to flow and pressure changes are significantly smaller than inferred from the report. In fact, based on ACPR sensitivities in pressurization transients, a 2 psi pressure uncertainty results in a 0.001 uncertainty in ACPR/ICPR, and a 3% flow uncertainty results in a 0.002 ACPR/ICPR uncertainty. The draft report should have stated that the ± 0.01 ACPR/ICPR uncertainty was based purely on a judgment of the uncertainties involved in the entire process of

NEDO-24154-A

evaluating Δ CFR from the experimental data. Based on the pressure sensitivities, the 10 psi pressure difference observed between the calculation and experiment would result in a 0.005 Δ CFR/ICFR. In reality, the dependence on pressure is more complex. A more accurate evaluation of the Δ CFR effects due to pressure is presented in the response to Question 15.

QUESTION 19 (Enclosure 2)

In the meeting on May 3, 1978 to discuss the review of the ODYN computer program, it was stated by General Electric that they would provide a letter discussing the subject of scram reactivity and how it would be included in the ODYN documentation. This documentation of the scram reactivity calculations by General Electric is required to satisfy commitments on, for example, the GESSAR-251 docket. Therefore, General Electric should provide this information describing how they intend to address the topic of scram reactivity.

RESPONSE

The ODYN Engineering Computer Program contains the analytical models for treating the interaction between neutron physics, core thermal hydraulics, and the fuel heat transfer mechanisms. These coupled sets of differential equations are solved so as to include the effects of time dependent variations in the axial direction. The formulation of this model, coupled with the required input from the GE three-dimensional steady-state simulator program, provides a technically sound way of computing scram reactivity.

The required inputs for performing plant transient analyses for reactor scram is reactivity data as a function of control blade insertion. As stated in our previous communication concerning the implementation of the ODYN code, we plan to continue to use the REDY code for analyses of specific transients, even after the NRC has approved the application of ODYN for a prescribed set of transients. In order to use our best technology available, GE plans to use the ODYN code to calculate scram reactivity as an input for those cases where the REDY code will be used to perform the plant transient analysis. This will be implemented by a change to GE's Technical Design Procedures to use the ODYN code to calculate scram reactivity for all cases where it is required as an input for REDY plant transient analysis.

The primary ground rules for this analysis will remain identical to those used in our current Technical Design Procedures. These are:

1. Initial conditions are calculated using the standard steady-state three-dimensional core simulator.

NEDO-24154-A

2. Pressure is maintained at a constant value.
3. Recirculation pump speed is maintained at a constant value.
4. The effects of void collapse in the core due to decreasing fuel surface heat flux are included in the calculation.

Implementation of this improved Technical Design Procedure will assure application of our best technology on a consistent basis.

NEDO-24154-A

QUESTION 20 (Enclosure 2)

Provide References 4, 5 and 6 in MFN 014-78.

RESPONSE

Reference 4 of MFN 014-78 has been published and the Staff has received copies. This report is EPRI-NP-564, dated June 1978.

Reference 5 is attached.

Reference 6 is a standard reference for fluid flow and should be readily available to the Staff.

A20-1/A20-2

Using Equation (A-4), Equation A-83 becomes

$$\pi(\bar{r}, t) = (D_1 B^2 + \Sigma_r) \frac{k_0}{\bar{v}} \phi(\bar{r}, t) \quad (A-84)$$

where

$$\bar{v} = \frac{\sum_g (\nu \Sigma_f \phi)_g}{\sum_g (\Sigma_f \phi)_g}; \quad g = 1, 2, 3 \quad (A-84a)$$

Comparing Equations A-82 and A-84 and noting that $\phi = \phi'$

$$\Sigma_f(\bar{r}, t) = (D_1 B^2 + \Sigma_r) \frac{k_0}{\bar{v}} \quad (A-85)$$

To obtain an expression for $f(z, t)$, substitute Equation A-85 into Equation A-81

$$f(z, t) = \frac{\int_x \int_y (D_1 B^2 + \Sigma_r) \frac{k_0}{\bar{v}} \phi'(\bar{r}, t) \, dx dy}{\int_x \int_y dx dy} \quad (A-86)$$

Following the same procedure used to obtain Equation A-55, Equation A-86 becomes

$$f(z, t) = \left\{ \left(\int_x \int_y \phi' \frac{k_0 \Sigma}{\bar{v}} \, dx dy \right) \left(1 + \overset{\sim}{\text{CDOF}} (\sqrt{T} - \sqrt{T_0}) \right) \right. \\ \left. - k_0 \int_x \int_y \frac{\Sigma}{\bar{v}} \phi' \, dx dy + k_0 \int_x \int_y \phi' \frac{\Sigma_r}{\bar{v}} \, dx dy \right\} / \int_x \int_y dx dy \quad (A-86a)$$

or

$$f(z, t) = k_0 \left[\frac{k_{\Sigma}}{k_0} (1 + \widetilde{\text{CDOP}} (\sqrt{T} - \sqrt{T_0}) - \widetilde{\Sigma} + \widetilde{\Sigma}_r) \right] \quad (\text{A-87})$$

where

$$\widetilde{\Sigma} = \frac{\int_x \int_y \phi' \frac{k_{\Sigma}^*}{V} dx dy}{\int_x \int_y dx dy} \quad (\text{A-88})$$

$$\widetilde{\text{CDOP}} = \frac{\int_x \int_y \phi' \frac{k_{\Sigma}^*}{V} \text{CDOP} \sqrt{T_0} dx dy}{\widetilde{\Sigma} \sqrt{T_0} \int_x \int_y dx dy} \quad (\text{A-89})$$

$$\widetilde{\Sigma} = \frac{\int_x \int_y \frac{\Sigma}{V} \phi' dx dy}{\int_x \int_y dx dy} \quad (\text{A-90})$$

$$\widetilde{\Sigma}_r = \frac{\int_x \int_y \frac{\Sigma_r}{V} \phi' dx dy}{\int_x \int_y dx dy} \quad (\text{A-91})$$

A.6 1-D BOUNDARY CONDITIONS

Let the time-dependent 3-D boundary conditions be expressed as (expanding on the steady-state formulation^{A-1}):

$$-\frac{D(\bar{R}, t) \nabla \phi(\bar{R}, t)}{\phi(\bar{R}, t)} = \Gamma(\bar{R}, t) \quad (\text{A-92})$$

where \bar{R} is the core boundary. To obtain the 1-D boundary condition, rearrange Equation A-92, multiply by the weighting function, ϕ' , and integration over x and y .

$$-(\phi', D\nabla\phi) = (\phi', \phi\Gamma) \quad (\text{A-93})$$

Using Equation A-7, i.e.,

$$\phi = \phi\psi \quad (\text{A-94})$$

in Equation A-93 yields

$$-(\phi', D\nabla(\psi\phi)) = (\phi', \psi\phi\Gamma)$$

Assuming, as was done in Section A-4, that $\psi = \psi'$, and using Equation A-94 yields

$$-(\phi', D\nabla(\phi'\phi')) = (\phi', \phi'\Gamma)\phi' \quad (\text{A-95})$$

where

$$\phi' = \phi/\phi_0$$

Expanding the first term of Equation A-95 yields

$$-\phi'(\phi', D\nabla\phi') - (\phi', \phi'D) \frac{\partial\phi'}{\partial z} = (\phi', \phi'\Gamma)\phi' \quad (\text{A-96})$$

Rearrange Equation A-96

$$-\frac{(\phi'D\phi')}{\phi'} \frac{\partial\phi'}{\partial z} = (\phi', D\nabla\phi') + (\phi', \Gamma\phi') \quad (\text{A-97})$$

Note that

$$D\nabla\phi' = \phi' \frac{D}{D'} \frac{D'\nabla\phi'}{\phi'} = -\phi' \frac{D}{D'} \Gamma' \quad (\text{A-97a})$$

where use has been made of Equation A-92. Inserting this result in Equation A-97 and rearranging yields

$$-\frac{(\phi' D \phi')}{\phi'} \frac{\partial \phi'}{\partial z} = \left(\phi', \phi' \left(\Gamma - \frac{D}{D'}, \Gamma' \right) \right) \quad (\text{A-98})$$

Note that at $t=0$, $\Gamma = \Gamma_0$, $D = D_0$, $\Gamma' = \Gamma'_0$ and $D' = D'_0$; thus

$$-\frac{(\phi'_0, D_0 \phi'_0)}{\phi'_0} \frac{\partial \phi'}{\partial z} = 0 \quad (\text{A-98a})$$

which agrees with the result obtained in Section A.4 that ϕ'_0 is flat. Normally

$$\Gamma = \Gamma_0 = \text{constant}$$

which reduces Equation A-98 to

$$-\frac{(\phi' D \phi')}{\phi'} \frac{\partial \phi'}{\partial z} = \Gamma \left(\phi', \phi' \left(1 - \frac{D}{D'} \right) \right) \quad (\text{A-99})$$

Recall that D' contains no feedback effects.

A.7 DEFINITION OF TRANSIENT REACTIVITY COMPONENTS

In the analysis of reactor transient behavior, it is often convenient to separate the reactivity components due to important changes in reactor parameters such as voids, fuel temperature, and control rod motion. The point neutron kinetics equation is written,

$$\frac{dT}{dt} = \frac{(\beta - \bar{\beta})}{\Lambda} T(t) + \sum_{i=1}^6 \lambda_i C_i(t) \quad (\text{A-100})$$

$$\frac{dC_i}{dt} = -\frac{\beta}{\Lambda} T(t) - \lambda_i C_i(t) \quad (\text{A-101})$$

In terms of the quantities defined above, the amplitude function $T(t)$ is defined to be

$$T(t) = \frac{T}{V} \int_{\omega_0} \bar{\phi}(\bar{r}, t) \phi(\bar{r}, t) d\bar{r}. \quad (A-102)$$

While the remaining quantities are evaluated as

$$C_i(t) = \int W_i(\bar{r}, t) C_i(\bar{r}, t) d\bar{r} \quad (A-103)$$

$$\bar{\beta}(t) = \int \bar{\beta}(z, t) \bar{F} \phi'(z) dz / \int F \phi'(z) dz \quad (A-104)$$

$$\rho_t'(t) = \int M(z, t) \phi'(z, t) dz / \int \bar{F} \phi'(z, t) dz \quad (A-105)$$

$$\Lambda = \frac{T}{V} / \int \bar{F} \phi'(z, t) dz \quad (A-106)$$

Where $M(z, t)$ is defined as

$$M(z, t) = \Gamma_b \left(1 - \frac{D_b(t)}{D_b(t=0)} \right) \delta(z - z_b) + \bar{F} - \bar{\Sigma} - \overline{DBr}^2 \quad (A-107)$$

Throughout the transient, the quantity $M(z, t)$ depends on the void fraction distribution, $\alpha(t)$, control state distribution, $C(t)$, and fuel temperature $T_f(t)$. The various reactivity components can be found by splitting the change in $M(z, t)$ in the following manner:

$$\Delta M_v = M(\alpha(t), C(t), T_f(t)) - M(\alpha(t), C(t), T_f(0)) \quad (A-108)$$

$$\Delta M_c = M(\alpha(0), C(t), T_f(0)) - M(\alpha(0), C(0), T_f(0)) \quad (A-109)$$

$$\Delta M_D = M(\alpha(t), C(t), T_f(t)) - M(\alpha(t), C(t), T_f(0)) \quad (A-110)$$

The reactivity components are then defined as:

Control Reactivity

$$\rho_c(t) = \int dz \Delta M_c(z,t) \phi'(z,t) / \int \bar{F} \phi'(z,t) dz \quad (A-111)$$

Doppler Reactivity

$$\rho_D(t) = \int dz \Delta M_D(z,t) \phi'(z,t) / \int \bar{F} \phi'(z,t) dz \quad (A-112)$$

Void Reactivity

$$\rho_V(t) = \int dz \Delta M_V(z,t) \phi'(z,t) / \int \bar{F} \phi'(z,t) dz \quad (A-113)$$

These definitions ensure that

$$\rho_T(t) = \rho_c(t) + \rho_D(t) + \rho_V(t) \quad (A-114)$$

A.8 NOMENCLATURE FOR APPENDIX A

ϕ_i	3-D neutron flux for i^{th} group; $i = 1,3$
D_i	Fast group diffusion coefficient
ν_i	Neutrons produced per fission for group i ; $i = 1,3$
k_0	Effective multiplication factor for steady state
Σ_{f1}	Macroscopic fission cross section for group i ; $i = 1,3$
Σ_r	Removal cross section for the fast group
B^2	Buckling = $(k_\infty/k_0 - 1)/(M^2 - A_\infty/k_0)$
k_∞	Infinite multiplication factor
M^2	Migration area = $\sum_{i=1}^3 M_i^2$, M_i migration area for group i

$$A_{\infty} = 1/\Sigma_r \left[v_1 \Sigma_i (M_2^2 + M_3^2) + v_2 \Sigma_{f2} M_3^2 \left(\frac{\phi_2}{\phi_1} \right) \right]^{QA8}$$

$$\left(\frac{\phi_2}{\phi_1} \right)^{\infty} \text{ Group 2 to group 1 ratio for an infinite lattice} = \frac{\Sigma_{s1i}}{\Sigma_2}$$

- ψ One-dimensional flux amplitude function
- ψ 3-D flux shape function
- C_i 3-D concentration for ith precursor group
- c_i 1-D concentration for ith precursor group
- K_i 3-D shape function for ith precursor concentration
- w₀ Weighting function for the flux
- w_i Weighting function for the ith precursor
- A (1 - β) (DB² + Σ₁) - Σ₁
- π(\bar{r} , t) 3-D power
- L_f(\bar{r} , t) conversion factor of 3-D flux to power
- f(\bar{r} , t) conversion factor of 1-D flux to power
- ψ(z, t) 1-D power

A.8 REFERENCES

- A-1 J.A. Woolley, *Three-Dimensional EWR Core Simulator*, NEDO-20953, May 1976.
- A-2 A.F. Henry, *Nuclear Reactor Analysis*, MIT Press, Cambridge, Mass., 1975.
- A-3 J.A. Lamarsh, *Introduction to Nuclear Reactor Theory*, Addison-Wesley, Reading, Mass., 1966.
- A-4 A.F. Henry, and N.J. Curlee, *Verification of a Method for Treating Neutron Space-Time Problems*, Nuclear Science and Engineering, B4, M727-744 (1958).

NEDO-24154-A

APPENDIX B

RESPONSES TO NUCLEAR REGULATORY COMMISSION
QUESTIONS ON SECTIONS 1 THROUGH 7 AND
APPENDIX A

NEDO-24154-A

QUESTION 1

Provide References 3, 4, 6, 8 and 9. Provide an appropriate reference for the void fraction correlation used in the model.

RESPONSE

The references requested have been supplied, as available, in Reference 9. The void fraction correlation used in the model is described fully in the response to Question 28 of this question set.

Q1-1/Q1-2

QUESTION 2

The core model including neutronics, thermal-hydraulic and fuel are based on a one-dimensional representation. Describe how radial variations in the core due to a different control state or a stuck rod during the trip would cause deviations from the assumed one-dimensional model. Assess these deviations between the actual three-dimensional representation and the assumed one-dimensional model. Quantify the effect of this uncertainty on ΔCPR.

RESPONSE

As pointed out in the model report, the three main causes of flux level change, as well as flux distribution change, in a BWR core are: (1) void changes; (2) control changes; and (3) fuel temperature changes.

A strict evaluation of the void effects on radial flux distribution during a pressurization transient requires a full three-dimensional evaluation of the turbine trip transients which is currently not available for BWR's. However, much can be learned from the results of the four turbine trip tests outlined in the qualification report.

In the case of the Peach Bottom tests, the entire flux rise is caused by void collapse. Due to the large number of control rods in the core during the steady-state condition, the scram strength was quite large, causing the flux to decrease immediately after the control rods began to move. The experimentally measured flux as recorded by the LPRM signals is plotted for each of the four levels and for each turbine trip in Figures 2-1 through 2-13. Each LPRM response is plotted as a percentage of initial value. All of the curves show all of the flux responses at any one level reaching the same peak value within 5%, indicating that the radial flux distribution remains almost constant during both the void collapse and post-scram parts of the transient. This behavior is noted for all four experiments carried out on the two plants. These experiments present evidence that void collapse effects do not appreciably perturb the radial flux distribution, supporting the use of a one-dimensional neutronics model.

Control rod motion is the most important factor in the reduction of the severity of the transient and can cause significant changes in radial power distribution. When a few rods are inserted into the core at midcycle conditions, for example, the flux in the vicinity of the control rod tips will decrease faster during a scram in those bundles adjacent to control rods. This results in local changes in radial flux shapes as partially inserted control rods move through the core during a scram. The gross radial flux shape also remains constant during the transient as evident in Figures 2-1 through 2-13. The current one-dimensional model contains a procedure which, when used with the three-dimensional collapsing process, accounts for radial flux shape changes by using radial flux shapes adjacent to the control rod tips. (See Chapter 5 of the model report.) Three-dimensional transient scram calculations have been carried out to determine the adequacy of this procedure and the results are described in Reference B-1. The most limiting pressurization transient case occurs at end of cycle, with all of the rods out of the core. In the end-of-cycle case, the radial flux perturbation due to control rod motion is minimal, and the two-dimensional and one-dimensional scram calculations show good agreement, being within 1.0% over the important position the scram curve.

The effect of a stuck rod during a scram is negligible. Scram reactivity calculations carried out with a three-dimensional kinetics code show that a stuck rod has less than a 0.5% effect on scram reactivity. Sensitivity studies determining ΔC_{PR} versus scram speed show that this 0.5% reduction in scram reactivity amounts to less than 0.001 in ΔC_{PR} in a typical load rejection transient. As discussed in the response to Question 1, Enclosure 3, the effect of a stuck rod is conservatively accounted for in the application of the model. Fuel temperature, or Doppler reactivity, is, in general, about 10% of the void reactivity response. Since the void collapse produces small changes in radial flux distributions, Doppler effects do not change the radial flux shape during a pressurization transient.

While the test results and collapsing procedures indicate that a one-dimensional neutronics model is adequate, a one-dimensional thermal-hydraulic model is also used, and the total integrated thermal-hydraulic and neutronic package must be made to respond to changes in core pressure and flow. The core thermal-hydraulic model represents the behavior of a single channel with average power. In a BWR, the density change during a pressurization transient is not entirely uniform. To illustrate this point, refer to Figure 2-14,

which is a schematic of a typical BWR core at full power operation. The overall radial distribution of power consists of a central region of higher power bundles surrounded on the periphery by low power bundles. The low power bundles are orificed to a lower flow rate, but still have a lower power-to-flow ratio than the interior bundles.

For a given pressure increase, the change in void fraction is larger for low quality conditions than high quality conditions. This is illustrated in Figure 2-15, where the change in void fraction for a given pressure change is plotted vs. axial height for a typical low power and high power channel. Above the low power boiling boundary, the change is larger in the low power channel than in the high power channel. Therefore, for pressure increases, the void fraction change will tend to be larger near the outside of the core. The extent of this void change difference is a complicated function of initial quality, perturbation type and axial power distribution. In constructing a one-dimensional collapsed model, a simplified fitting procedure has been adopted which assumes that the change in density is independent of radial position, i.e.,

$$\Delta\rho(x, y, z) = \Delta\rho(z)$$

This procedure has the effect of weighting the reactivity changes in the interior channels more than they would be if the correct radial density change distribution were used. The interior bundles have a larger initial void fraction. Since $\Delta k/\Delta V$ increases with void fraction, the use of a radially constant $\Delta\rho$ tends to overestimate the void reactivity response. This general rule is not strictly true between the high and low power boiling boundaries, but the majority of the reactivity change occurs in the upper half of the core. Some ratios of three-dimensional and one-dimensional reactivity changes due to a 10-psi pressure change are listed in Table 2-1. The first five values in the table have been reproduced from the qualification document. In general, the one-dimensional model overpredicts the reactivity response due to a pressure change. The amount of overprediction is larger for a small reactor core than for a larger reactor such as a generic BWR/6 core design because there are proportionately more peripheral cells in the smaller core. The exception to this general trend is noted in the three Peach Bottom test conditions. In these cases, a considerable number of control rods were inserted, which created additional low power channels in the core interior. It is important to note

that for the full power conditions, the collapsing procedure always tends to overcalculate the void coefficient by margins from as small as 3% to as large as 15%. Therefore, the one-dimensional to three-dimensional collapsing procedure does introduce a bias into the calculations. However, this bias is always in the conservative direction for the license basis initial conditions. Since the collapsing process biases the results in the conservative direction, this procedure does not contribute to an "uncertainty" in ΔCPR .

The quantity $U_0(z)$ will be discussed here rather than Question 6, because it is connected with the one-dimensional core model. The quantity U_0 is the base relative water density used in the density fitting process. When the cross-section fits are generated, a series of collapsed cross sections are calculated at a number of fixed water densities, $\{\rho_1\}$, i.e.,

$$\Sigma_1 = \Sigma(\rho_1) \quad i = 1, 11$$

The quantity U_1 is defined as

$$U_1 = \rho_1 / \rho_B$$

where ρ_B is the saturated liquid density at 1000 psi. The set of cross sections Σ_1 is used to generate a fit of the form

$$\Sigma_1(\rho) = \Sigma_0 (1 + a (U - U_0) + b (U - U_0)^2)$$

where U_0 is the ratio ρ_0 / ρ_B where $\rho_0(z)$ is the average steady-state water density at axial height z . This determines the coefficients Σ_0 , a , and b for each height. Note that, when the fits are generated, U_0 is the three-dimensional relative density. However, when they are used in the one-dimensional model, the one-dimensional estimate of U_0 is used. In the steady-state, this ensures that $\Sigma = \Sigma_0$ and that the one-dimensional axial flux shape is the same as the three-dimensional average axial flux shape. This procedure was also instituted to relate core reactivity changes to density changes occurring in the average channel rather than the full core. In

NEDO-24154-A

general, the one-dimensional estimate for U_0 will be slightly smaller than the three-dimensional estimate, because of the higher density of the peripheral bundles. This also is in a direction to overestimate the void reactivity response and is also partially responsible for the differences given in Table 2-1.

Table 2-1
SUMMARY OF THREE-DIMENSIONAL - ONE-DIMENSIONAL VOID COEFFICIENT COMPARISONS

<u>Plant</u>	<u>BWR Product Line</u>	<u>Number of Fuel Bundles</u>	<u>Power Level (% Rated)</u>	<u>Flow (% Rated)</u>	<u>Exposure Cycle</u>	<u>Ratio $\frac{\Delta k(1D)}{\Delta k(3D)}$ for 10 psi Pressure Change</u>
Plant A	BWR/4	764	48	100	EOC2	0.980
Plant A	BWR/4	764	62	80	EOC2	1.053
Plant A	BWR/4	764	69	100	EOC2	1.075
Plant B	BWR/4	228	77	93	EOC4	1.080
Plant C	BWR/5	560	104	100	EOC1	1.03
Plant D	BWR/4	368	104	100	EOC3	1.103
Plant D	BWR/4	368	104	100	Midcycle 4	1.130
Plant D	BWR/4	368	104	100	EOC4	1.120
Plant E	BWR/4	560	104	100	Midcycle 2	1.145
Plant F	BWR/5	764	104	100	EOC1	1.037
Generic	BWR/6	864	104	100	EOEC	1.058

Q2-6

NEED-24154-A

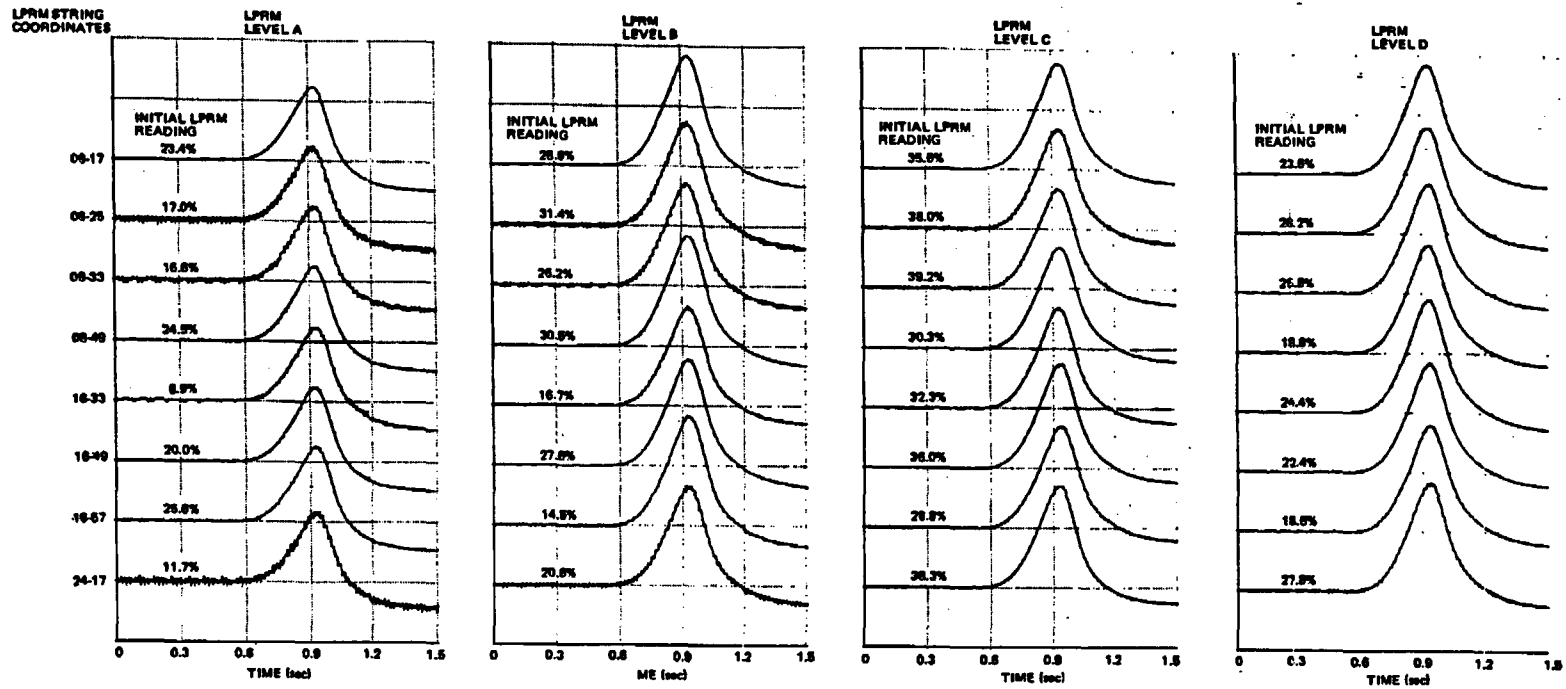


Figure 2-1. Peach Bottom-2 EOC2 Test Turbine Trip Test TTI Core Local Power Monitor Response

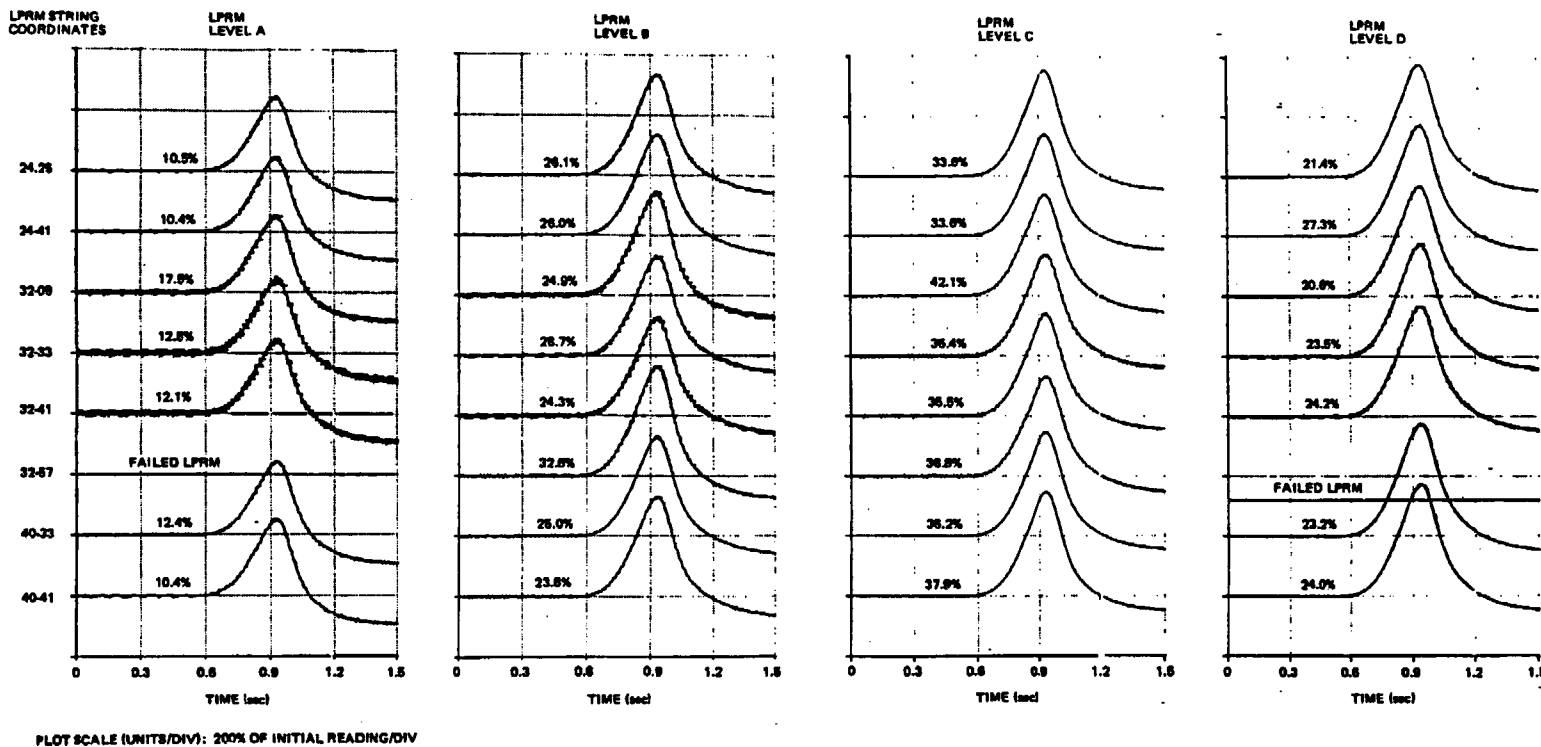
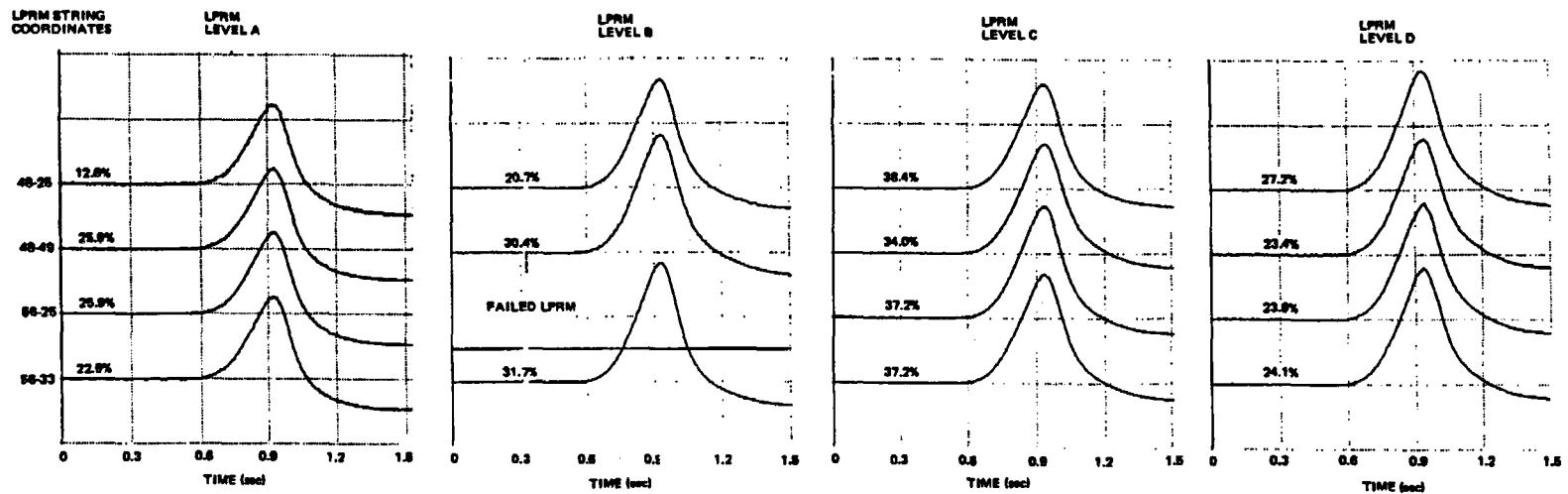


Figure 2-2. Peach Bottom-2 EOC2 Test Turbine Trip Test T11 Core Local Power Monitor Response



PLOT SCALE (UNITS/DIV): 300% OF INITIAL READING/DIV

Figure 2-3. Peach Bottom-2 EOC2 Test Turbine Trip Test T11 Core Local Power Monitor Response

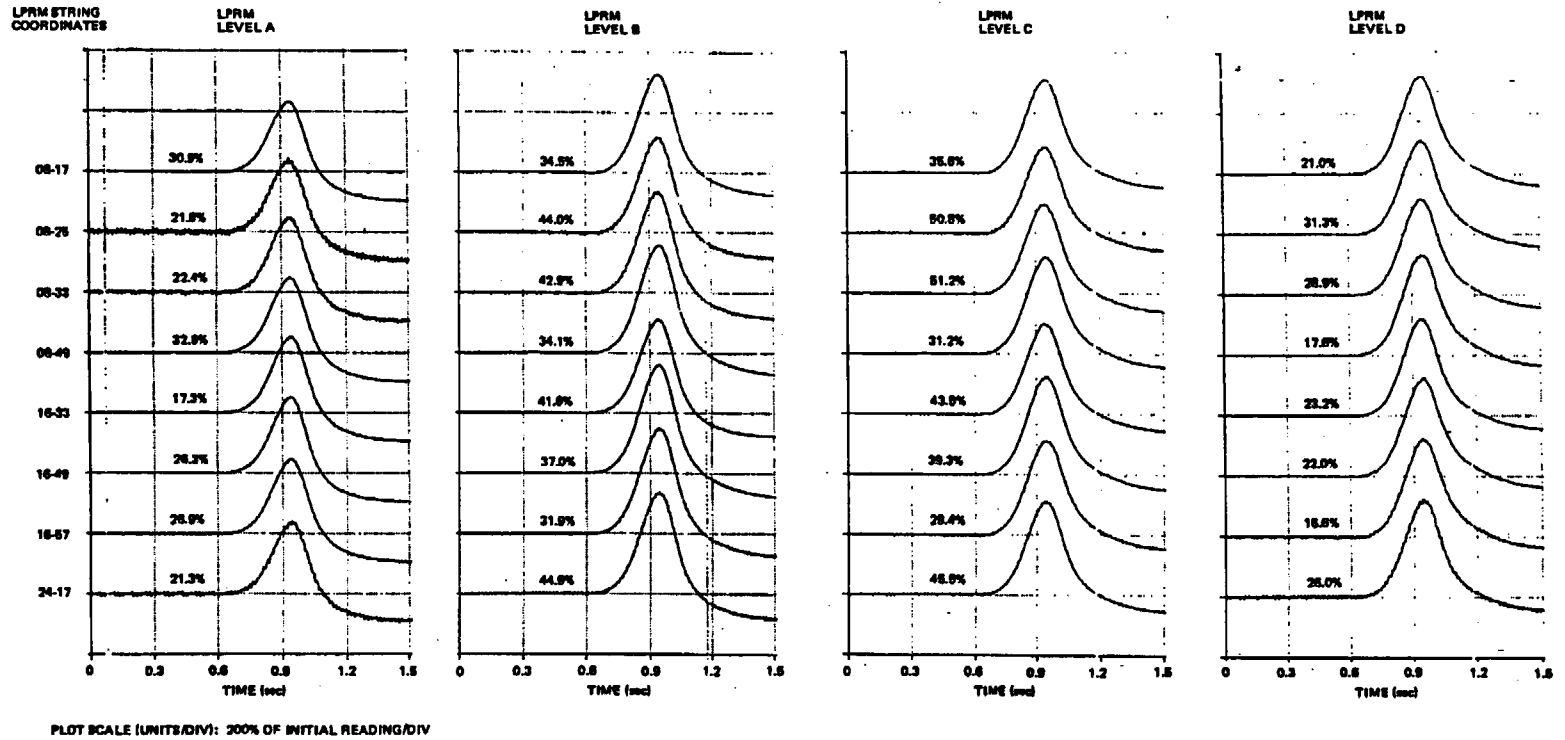
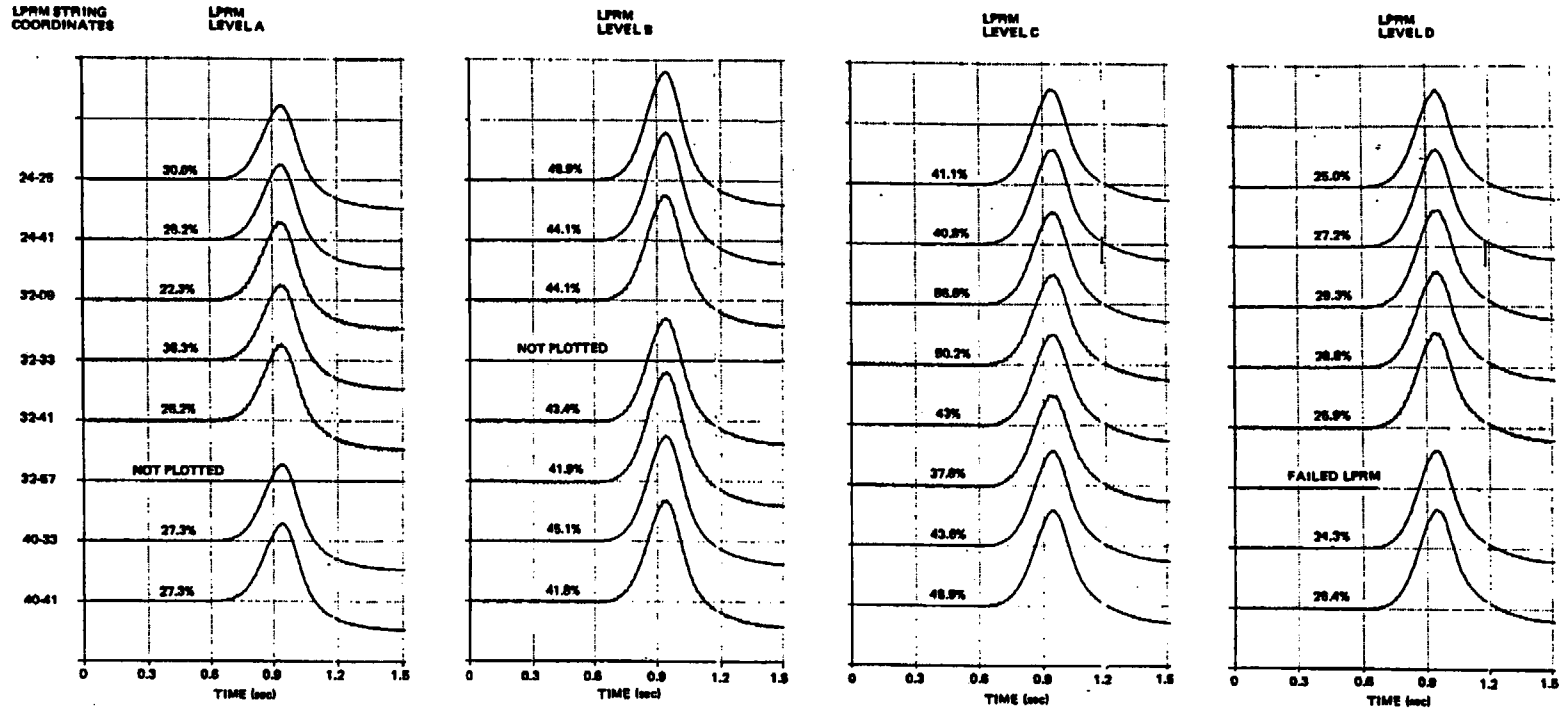
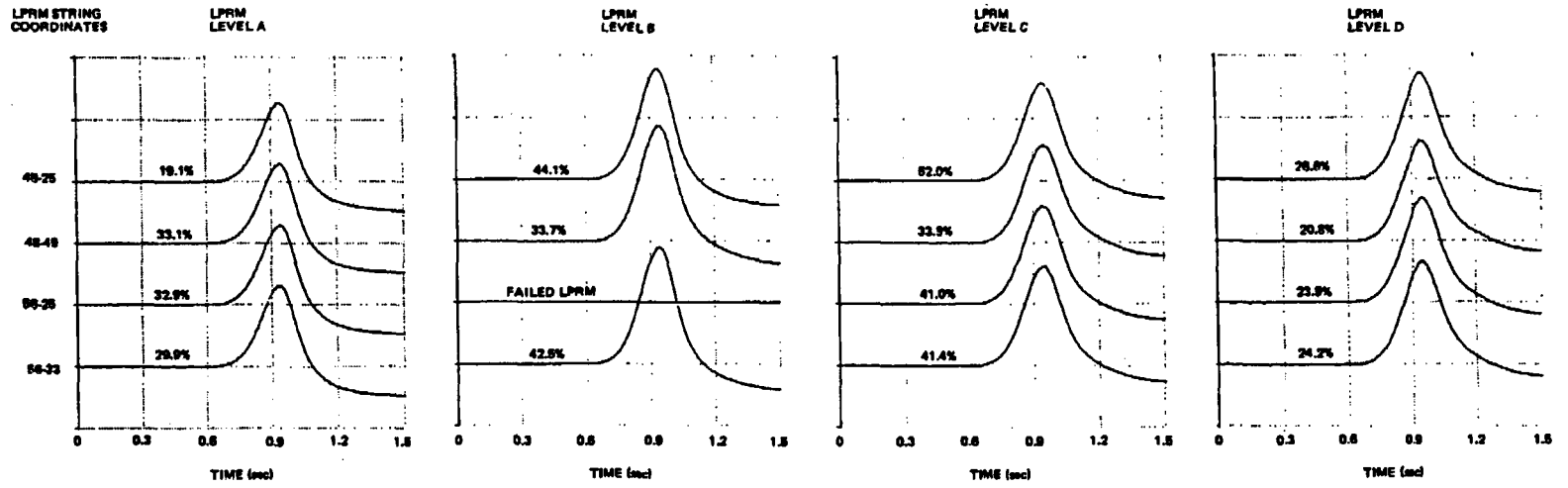


Figure 2-4. Peach Bottom-2 EOC2 Test Turbine Trip Test T12 Core Local Power Monitor Response



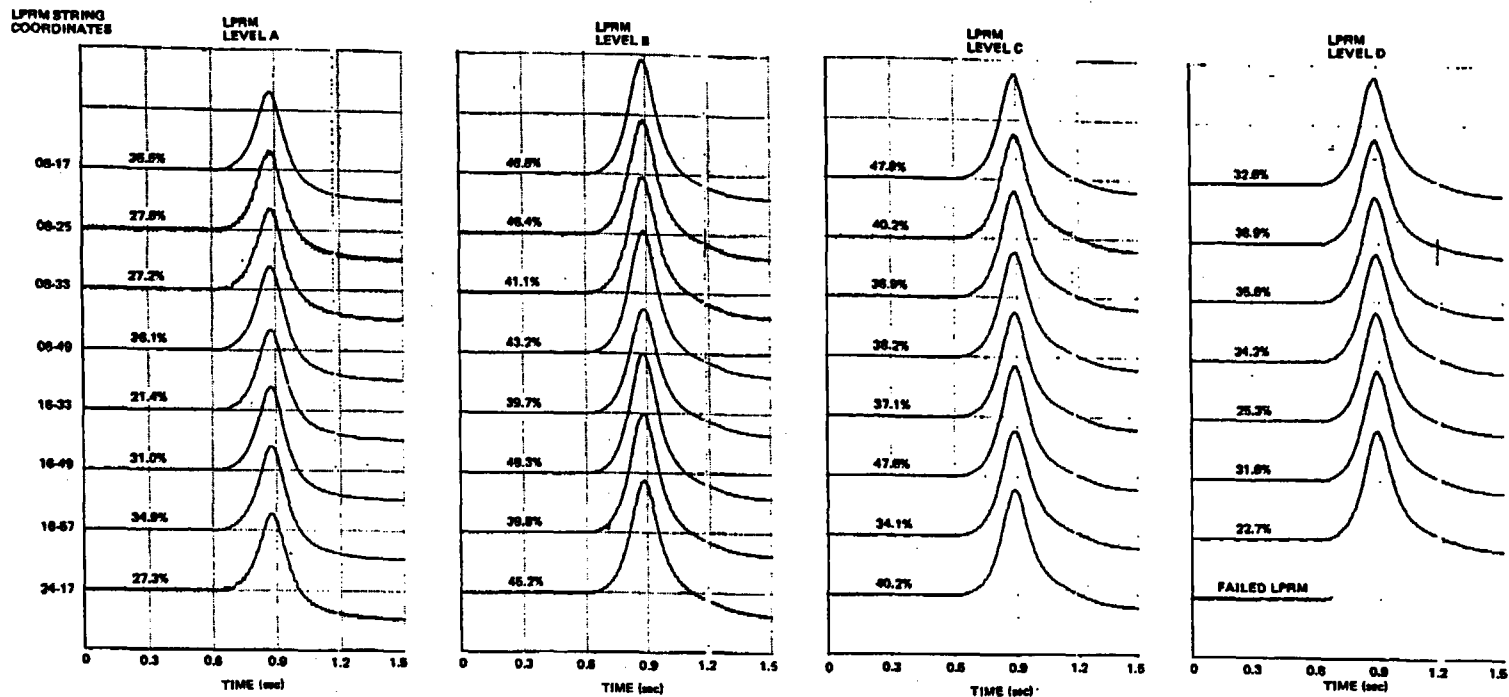
PLOT SCALE (UNITS/DIV): 300% OF INITIAL READING/DIV

Figure 2-5. Peach Bottom-2 EOC2 Test Turbine Trip Test T12 Core Local Power Monitor Response



PLOT SCALE (UNITS/DIV): 200% OF INITIAL READING/DIV

Figure 2-6. Peach Bottom-2 EOC2 Test Turbine Trip Test TT2 Core Local Power Monitor Response



PLOT SCALE (UNITS/DIV): 200% OF INITIAL READING/DIV

Figure 2-7. Peach Bottom-2 EOC2 Test Turbine Trip Test TT3 Core Local Power Monitor Response

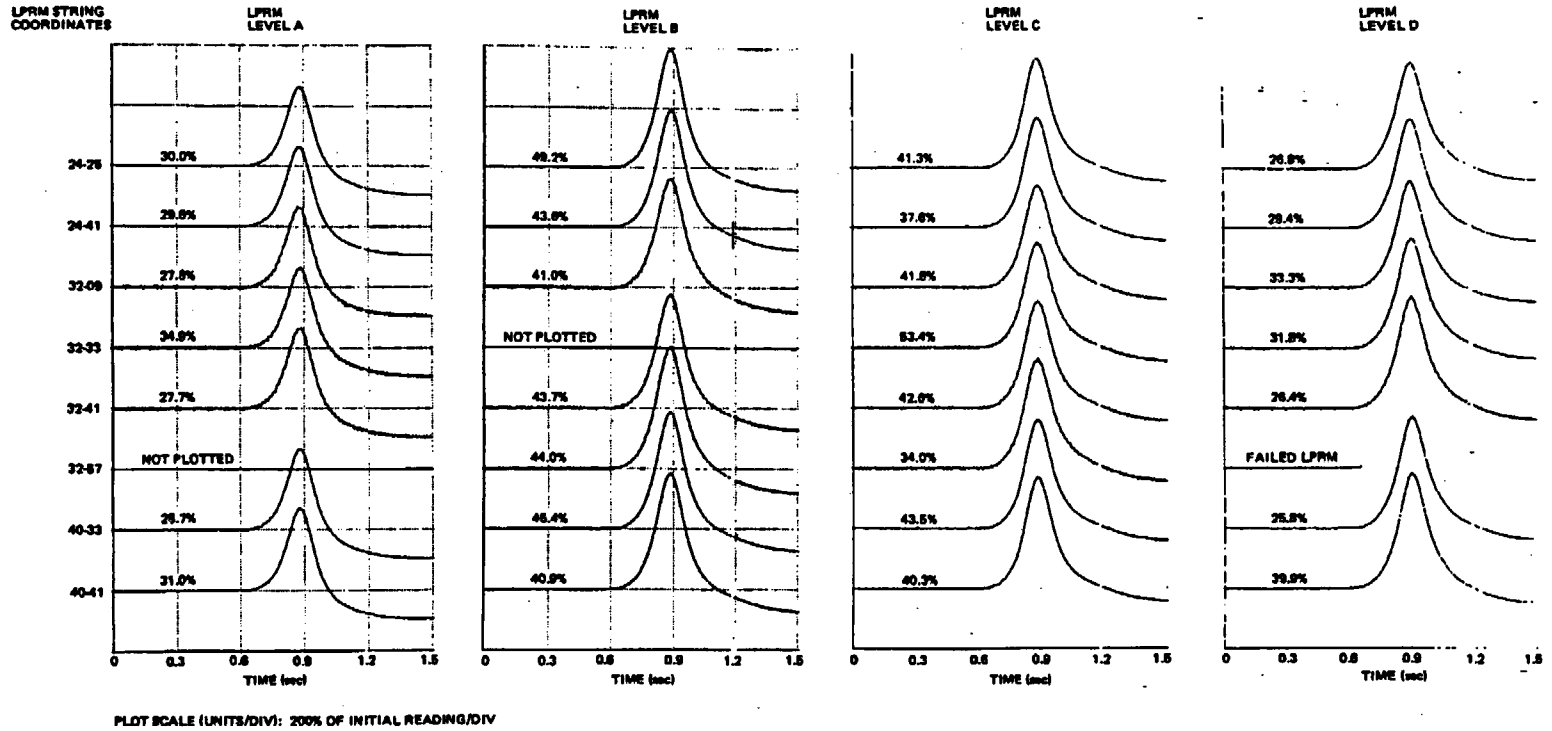


Figure 2-8. Peach Bottom-2 EOC2 Test Turbine Trip Test TT3 Core Local Power Monitor Response

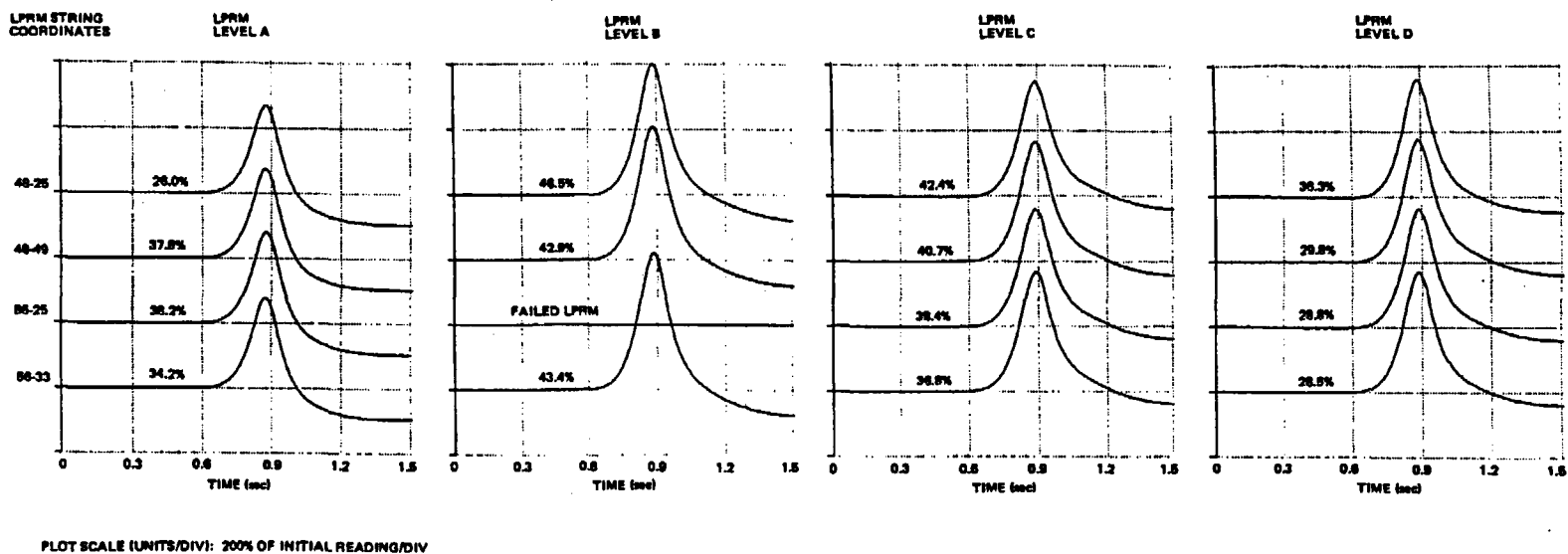


Figure 2-9. Pasach Bottom-2 EOC2 Test Turbine Trip Test TTS Core Local Power Monitor Response

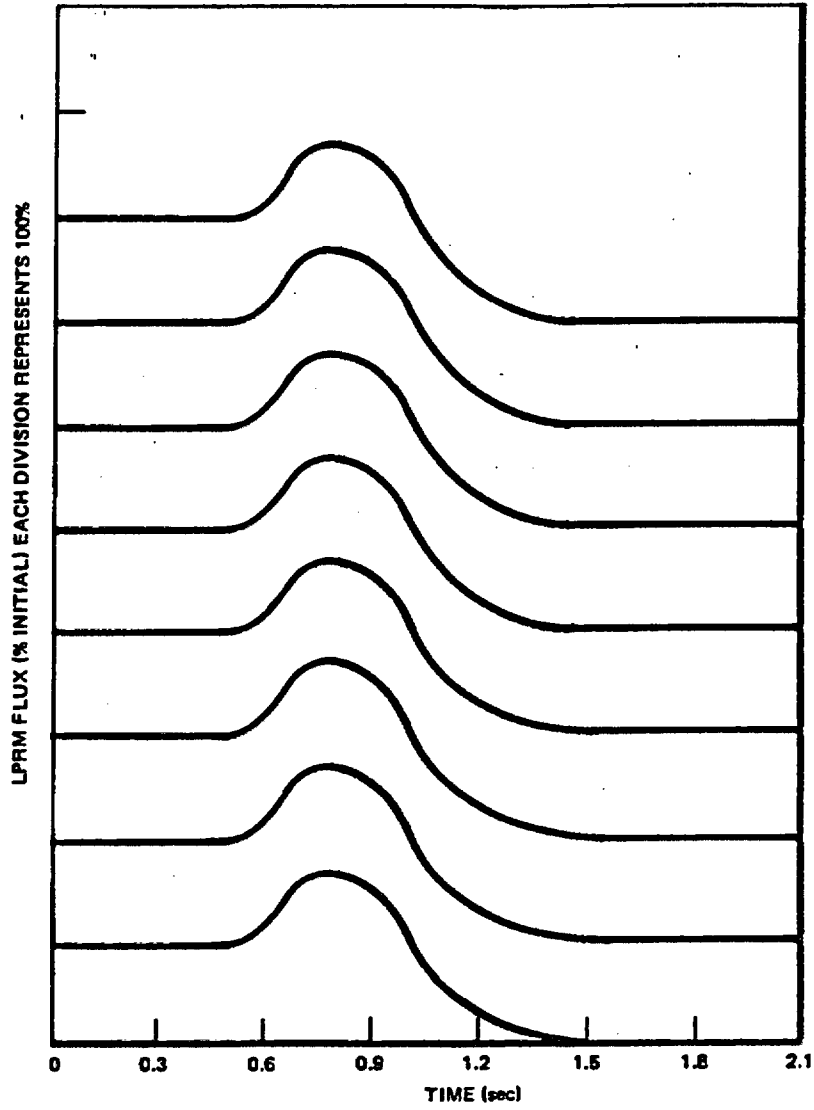


Figure 2-10. A Level LPRM Flux KKM Turbine Trip

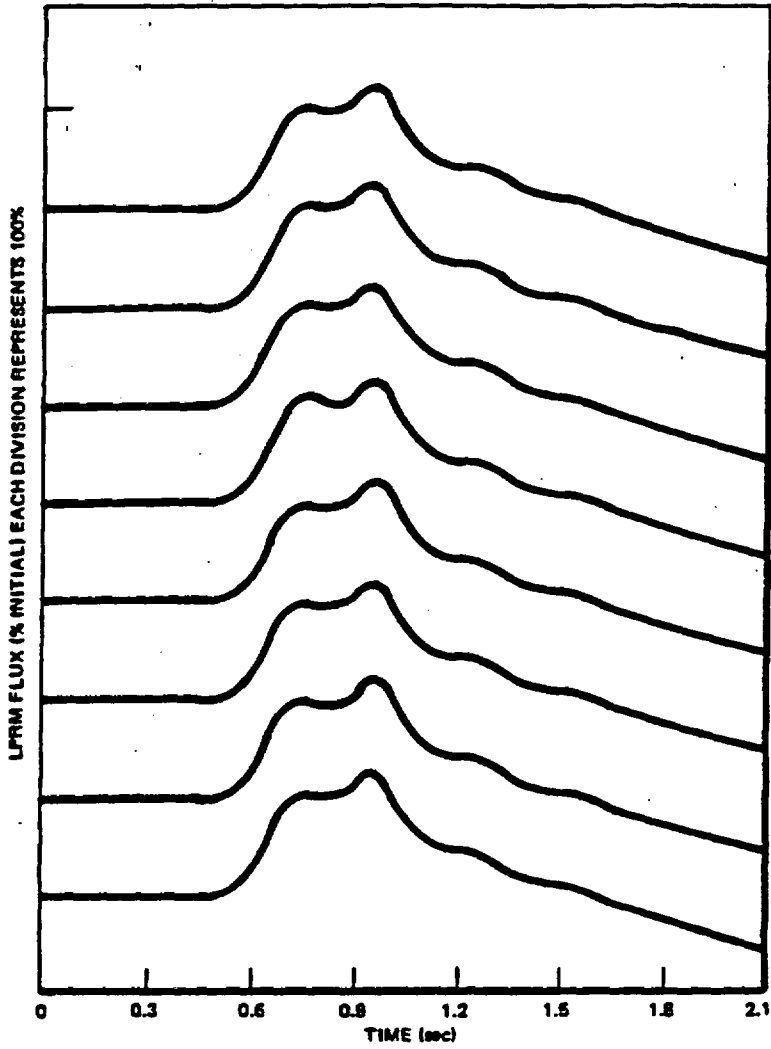


Figure 2-11. B Level LPRM Flux KKM Turbine Trip

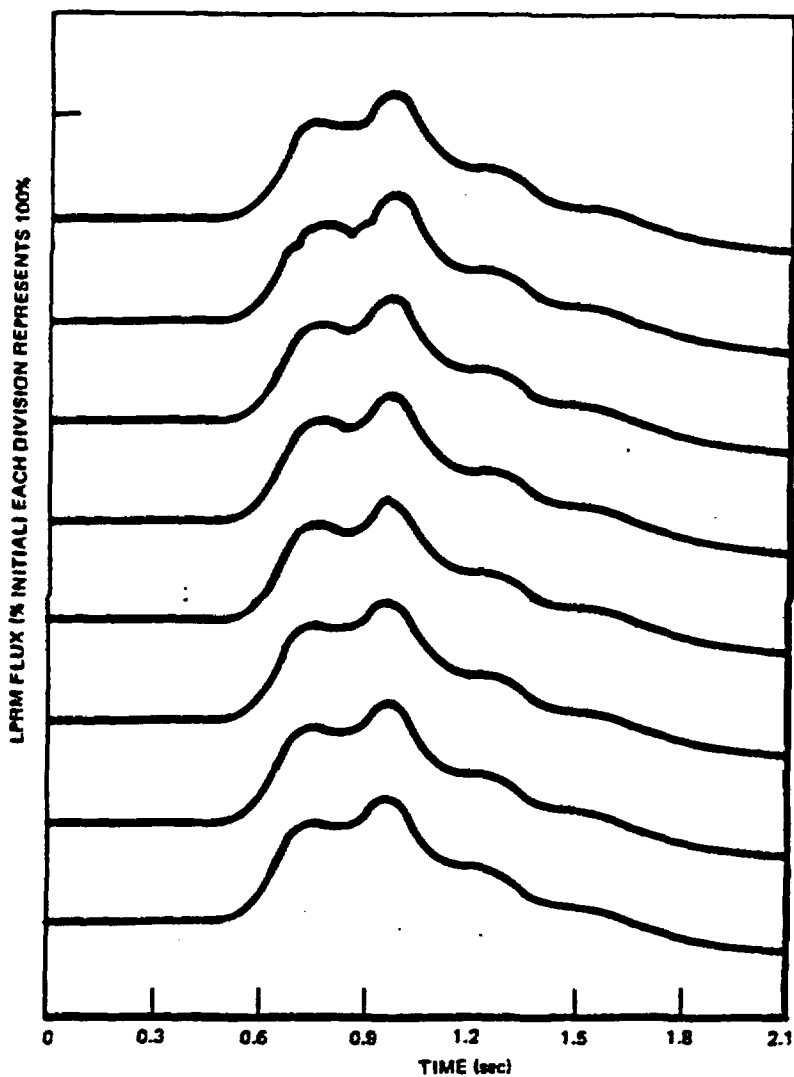


Figure 2-12. C Level LPRM Flux KKM Turbine Trip

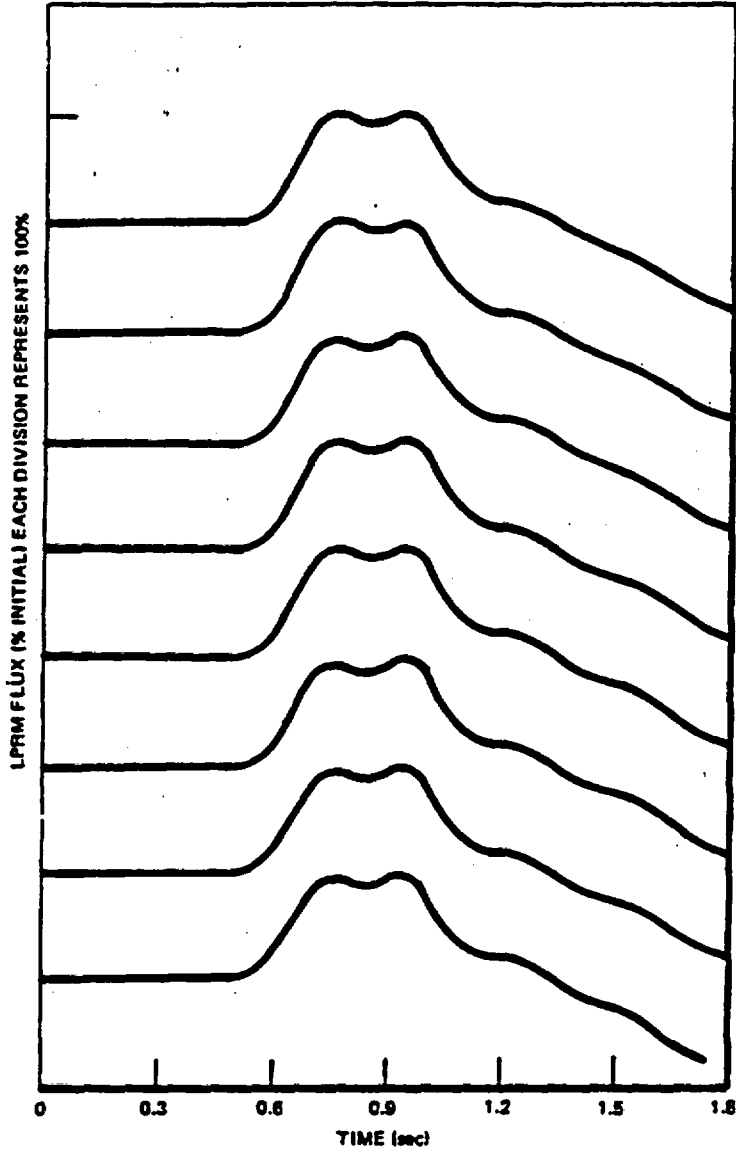


Figure 2-13. D Level LPRM Flux KKM Turbine Trip

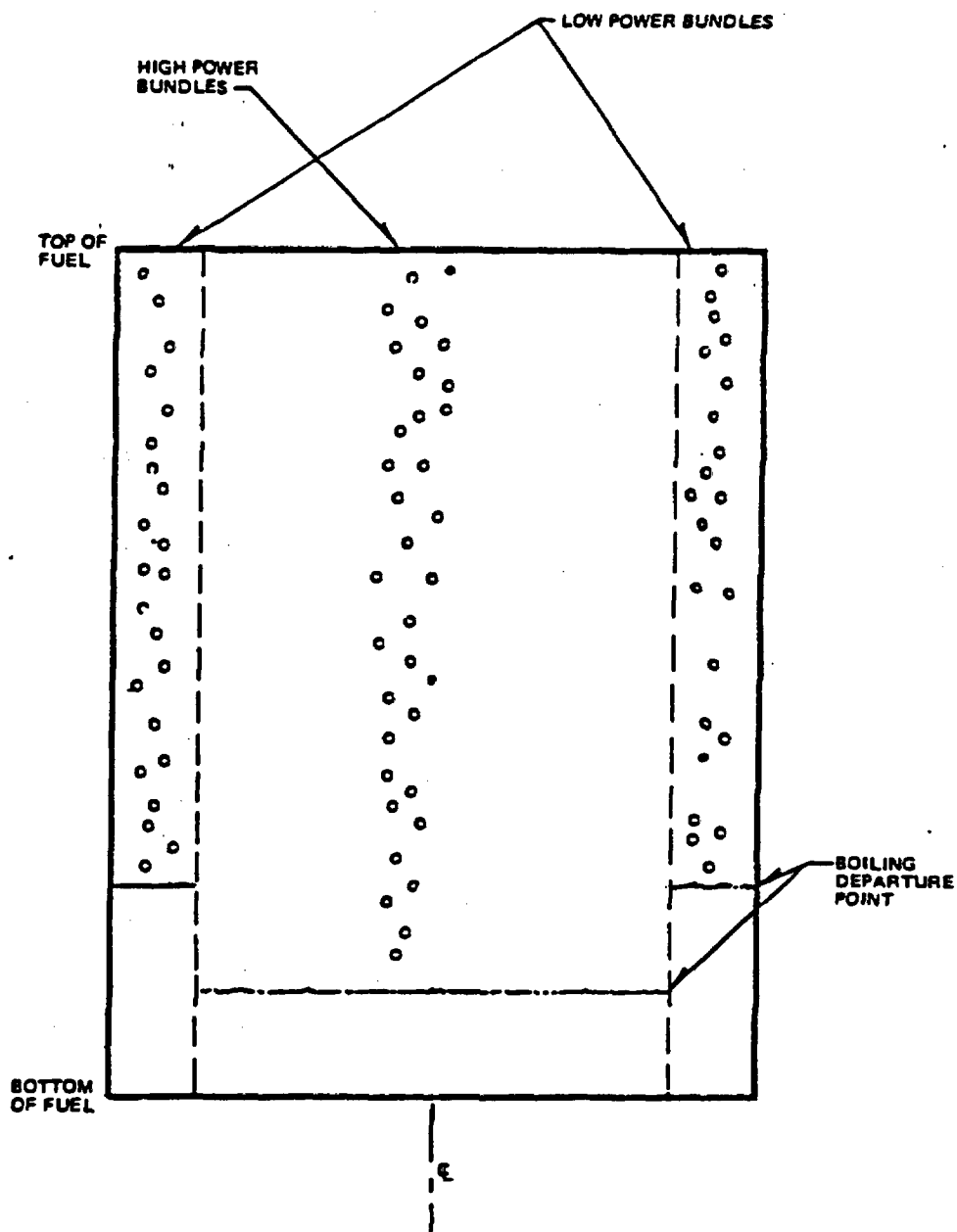


Figure 2-14. BWR Core Schematic

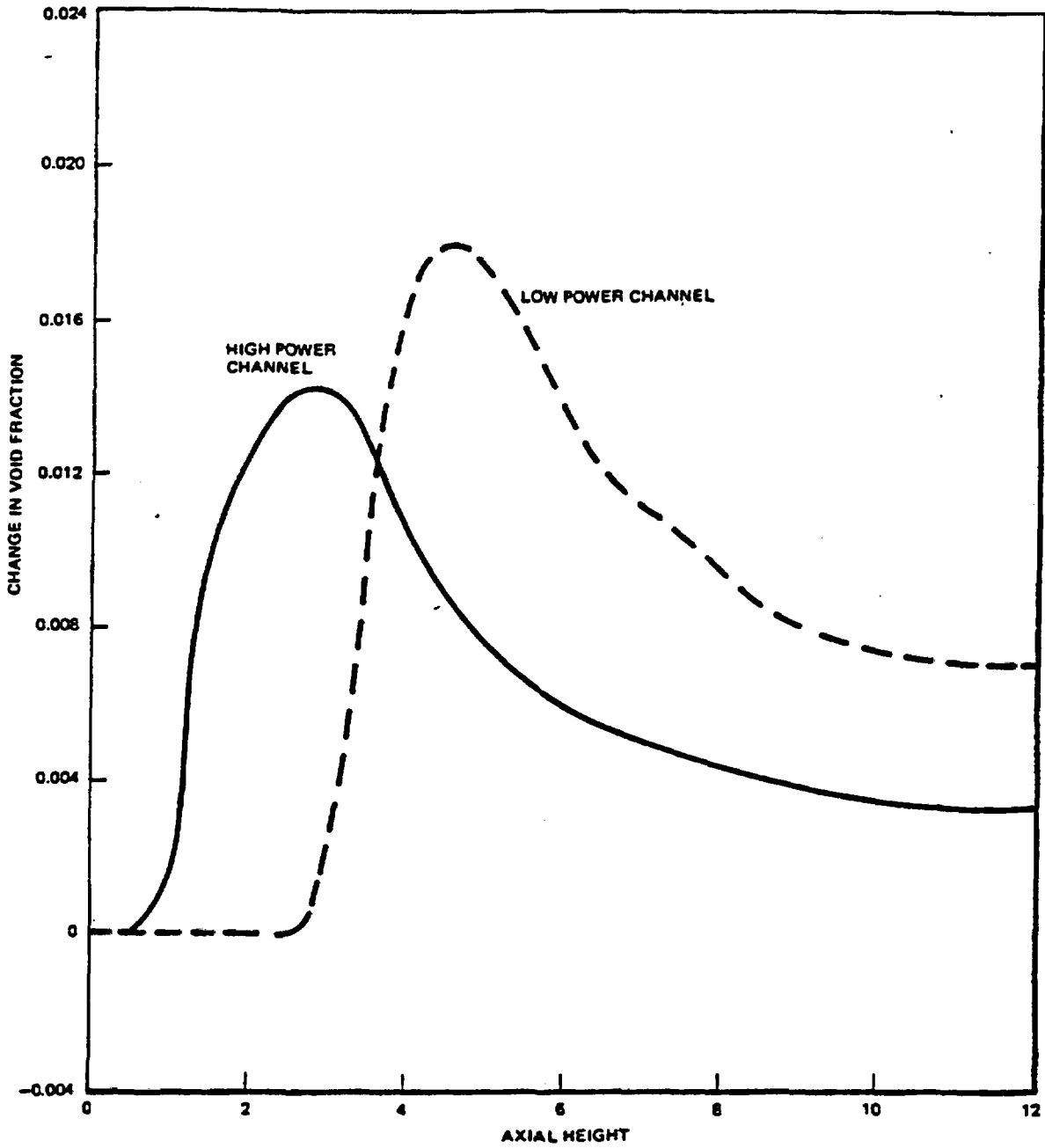


Figure 2-15. Change in Void Fraction for Static Pressure Change

Q2-21/Q2-22

QUESTION 3

Present your methodology for calculation of peaking factors for use in GETAB analysis if the average power level is given by the ODYN code. Discuss the conservatism of your methodology in calculating peaking factors. Provide a sample calculation for peaking factors for a typical BWR/4 such as Peach Bottom.

RESPONSE

There are three peaking factors reported with the GETAB operating limits: (1) a local peaking factor; (2) an axial peaking factor; and (3) a radial peaking factor. The local peaking factor is the design maximum for a particular fuel design, but it is not used directly in the GETAB analysis. Instead, the GETAB analysis uses an R-factor term which considers the distribution of local peaking factors within a fuel assembly. A detailed explanation of R-factor can be found in Appendix III of Reference B-2.

A generic axial power distribution with a peak/average value of 1.4 is used in all GETAB analyses. This axial power distribution is described in Table 5-7 of Reference B-3 and its justification is presented in Appendix V of Reference B-4. The conservatism in this assumed power shape is discussed in the responses to Questions 3, 5 and 6 of Enclosure 3.

The radial peaking factor (or bundle relative power) determined in the process of deriving the GETAB minimum critical power ratio (MCPR) operating limits is determined by an iterative process. To start the iteration, a bundle power is assumed. The GETAB transient is initiated from this bundle power and resulting critical power ratio. The MCPR during this transient is compared with the safety limit MCPR (SLMCPR). The bundle initial power is then adjusted (upward or downward) and the transient is repeated. This adjustment and reanalysis of the transient is performed until the MCPR during the transient is equal to the SLMCPR. The initial bundle power and resulting critical power ratio (MCPR operating limit) are then reported. The bundle radial peaking factor is then derived from:

$$RPF = \frac{BP \times NB}{CTP \times PF}$$

where

- RPF = bundle radial power factor;
- BP = total energy deposited in bundle coolant (MW_c);
- NB = number fuel assemblies in the core;
- CTP = core thermal power (MW_c); and
- PF = fraction of core thermal power deposited in active (in-channel) coolant.

For a typical case (Plant A, EOC 2):

- BP = 6.770 MW_c
- NB = 764
- CTP = 3293 MW_c
- PF = 0.978

and the resulting RPF = 1.606.

QUESTION 4

Provide and discuss the quality of the fit of your decay heat model. Discuss its conservatism, if any.

RESPONSE

The decay heat model implemented in ODYN is identical to the model discussed in Section 2.3 of NEDO-10802, "Analytical Methods of Plant Transient Evaluations for the GE BWR". Generally, the short time response of the decay heat curves is on the order of a 100-sec time constant. This very sluggish behavior is not important in transients where only the short time behavior is significant (less than 5 sec). This can be seen from evaluating $e^{-t/T}$ for $T = 100$ sec and t is chosen on the order of the turbine trip transient maximum heat flux response time, $t = 2.0$ sec, $e^{-1/50} = 0.98$. A change equal to about 2% in the power generation occurs for full power initial power production. Since this variation (i.e., the 2%) in power generation is further restricted by the heat transfer from fuel to moderator, which has a 5-8 sec time constant, the influence on heat flux and moderator density is, for all practical purposes, negligible during pressurization transients.

QUESTION 5

A recent paper, "The Significance of Fast Moderator Feedback Effects in a Boiling Water Reactor During Severe Pressure Transients", by W. Frisch, S. Longenbuck and P. Peternell, published in Nuclear Science and Engineering: 64, 843-848, 1977, indicates that direct heating is a very important parameter in overpressurization transients. Explain how the direct heating effects are considered in the ODYN code. Provide a sensitivity study and discuss the conservatism of the values selected. Quantify the conservatism or the effect of uncertainty on ΔCPR .

RESPONSE

Prompt heating effects are accounted for in the one-dimensional model according to the procedures outlined in Chapter 3 of the model report. The prompt heating fraction is a function of the bundle and channel geometry, as well as the void fraction and control fraction of a particular bundle. Tables 5-1 and 5-2 give a summary of the bundle heating distributions for 7x7 and 8x8 fuel typical of the kind contained in the Peach Bottom-2 reactor. These data were obtained from calculations carried out with the GE lattice physics computer code. The lattice physics heating distributions have been compared to Monte Carlo calculations employing up-to-date nuclear data. These comparisons have been documented in NEDO-23729B-6 (See Tables 4-2 and 4-3. The column labeled "Scatena and Upham" corresponds to the lattice calculations.) The agreement between the lattice calculations and the Monte Carlo results is very good.

The one-dimensional model assumes for lattices of the Peach Bottom type that 2% of the heat is deposited in the channel coolant, 2% in the out-of-channel coolant, and 96% is deposited in the fuel. Tables 5-1 and 5-2 show that, depending on the rod configuration and void fraction, the prompt heat fraction, in the coolant can vary from 0.017 to 0.023 with 0.02 a good average value.

Based on the excellent Monte Carlo agreement, the average in-channel heating fraction is assumed to be larger than 0.016 with 95% certainty. In order to test the sensitivity to these parameters, a series of full power turbine trip calculations have been carried out with varying amounts of prompt heating. The most severe transient was obtained with the 0.016 heating fraction and yielded a $\Delta\text{CPR}/\text{ICPR}$ 0.006 larger than the case with 0.02 prompt heating fraction. The uncertainty in ΔCPR due to prompt heating is $\pm 0.006 \Delta\text{CPR}/\text{ICPR}$.

Table 5-1
SUMMARY OF BUNDLE HEATING DISTRIBUTION FOR A 7x7 D LATTICE

	<u>Uncontrolled</u>			<u>Controlled</u>		
	<u>VF=0</u>	<u>VF=0.4</u>	<u>VF=0.6</u>	<u>VF=0</u>	<u>VF=0.4</u>	<u>VF=0.6</u>
Fuel	0.953	0.953	0.953	0.944	0.943	0.943
Clad	0.009	0.009	0.009	0.009	0.009	0.009
In-Channel Moderator	0.023	0.020	0.018	0.024	0.021	0.019
Leakage Moderator*	0.015	0.018	0.020	0.023	0.027	0.029

*Includes channel wall gamma heating

NEDO-24154-A

Table 5-2

SUMMARY OF BUNDLE HEATING DISTRIBUTION FOR AN 8x8 LATTICE

	<u>Uncontrolled</u>			<u>Controlled</u>		
	<u>VF=0</u>	<u>VF=0.4</u>	<u>VF=0.6</u>	<u>VF=0</u>	<u>VF=0.4</u>	<u>VF=0.6</u>
Fuel	0.951	0.952	0.950	0.943	0.942	0.941
Clad	0.011	0.011	0.011	0.011	0.011	0.011
In-Channel Moderator	0.021	0.019	0.017	0.021	0.020	0.018
Leakage Moderator*	0.017	0.018	0.022	0.025	0.027	0.030

*Includes channel wall gamma heating

QUESTION 6

Provide a good description of the steady-state recirculation system model and initialization process. Justify the selection of plant parameters such as ΔP_{loop} for the analysis. Discuss the conservatism of this value for various transients. Evaluate each component of ΔP_{loop} along the loop and justify with experimental data if possible. Provide sensitivity studies. List in general terms the input parameters and output parameters.

RESPONSE

The steady-state initialization process consists of solving the equations outlined in Chapter 4 with the time derivative terms set equal to zero.

For a particular plant initial condition, the following quantities are input:

- \dot{m}_{RLi} = total flow for loop i
- \dot{m}_{31} = total core flow
- \dot{m}_{1T} = total turbine steam flow
- p = total reactor thermal power
- ΔP_c = steady-state core pressure drop
- P_2 = reactor dome pressure
- L_v = steady-state water level

These input quantities are used in conjunction with other plant inputs to establish the steady-state initial conditions. The remaining quantities (e.g., plant geometry, pressure loss coefficients, separator carryunder fraction, and pump characteristics) are plant-unique but are not changed with operating conditions.

Flow conditions

In the steady state, flow continuity is preserved and can be used to establish the initial conditions (the nomenclature is the same as Chapter 4):

$$m_{13} = m_{1T} \text{ (total vessel steam flow)}$$

$$m_{fw} = m_{1T} \text{ (total feedwater flow)}$$

$$m_{3s} = m_{31} \text{ (total separator flow)}$$

In the bulk water, the carryunder condensation rate is zero and the mass balance at the feedwater sparger yields (Equation 4-27):

$$m_{23} = m_{31} - m_{fw} - m_{cu}$$

This can be combined with Equations 4-22 and 4-23 to yield:

$$m_{cu} = \frac{X_{cu}}{1+X_{cu}} (m_{31} - m_{fw})$$

and

$$m_{23} = m_{22} = \frac{m_{31} - m_{fw}}{1 + X_{cu}}$$

The total steam flow through the separators is obtained from Equation 4-24:

$$m_{12} = m_{13} + X_{cu} m_{22} = m_{13} + X_{cu} (m_{31} - m_{fw}) / (1 + X_{cu}).$$

In the recirc line, the calculation of the drive and suction flows for the jet pump requires a pressure balance, and will be covered below.

Pressures

The plenum exit pressure is obtained from Equation 4-11:

$$P_{1e} = P_2 + \frac{g \rho_1 (\ell_{sep1} + \ell_{SP})}{144 g_c} + \frac{C_{sep} m_{31}^2}{\rho_1 N_{sep}^2}$$

The core pressure is:

$$P_e = P_{1e} - \frac{\ell_1 g \rho_1}{144 g_c}$$

The core inlet pressure is given by:

$$P_I = P_e + \Delta P_c$$

The jet pump throat pressure for loop 1 is obtained from equation (4-80)

$$P_{th1} = P_I - \frac{g}{144 g_c} \Delta Z_{diff} \bar{\rho}_r + \left(K_{dif} \frac{1}{2 g_c \bar{\rho}_r A_{th}^2} \right) \frac{m_{RL1}^2}{144}$$

the downcomer pressure for loop 1 is obtained from Equation 4-79:

$$P_{dwn1} = P_2 + \left[\frac{g}{g_c} \bar{\rho}_b (\Delta Z_b + L_v) - K_b m_{RL1} \right] / 144$$

the jet pump pressure is

$$P_{jet1} = P_{dwn1} - \frac{1}{144} \left(K_{SCT} - \frac{1}{2 g_c \bar{\rho}_b A_{SCT}^2} \right) m_{SCT1}^2$$

Note we have proceeded around two sides of the loop to the jet pump throat pressure on one side and the jet pump suction pressure on the other side. In the steady state, the drive flow is adjusted to obtain a pressure balance around the loop. Specifically, Equations 4-83, 4-91 and 4-85 can be combined to obtain:

$$\left[\frac{(\dot{m}_{RL1} - \dot{m}_{SCT1})^2}{A_{noz}^2} + \frac{\dot{m}_{SCT1}^2}{A_{SCT}^2} - \frac{\dot{m}_{RL1}^2}{A_{th}^2} \right] \frac{1}{\bar{\rho}_r g_c A_{th}}$$

$$= 144 (P_2 - P_e - \Delta P_c) + g_c \left(\bar{\rho}_r \Delta Z_{diff} + \bar{\rho}_r (\Delta Z_b + L_v) \right)$$

$$- \left(K_b + K_{diff} - \frac{1}{2 g_c A_{th}^2 \bar{\rho}_r} \right) \dot{m}_{RL1}^2 - \left(K_{SCT} + \frac{1}{2 g_c A_{SCT} \bar{\rho}_b} \right) \dot{m}_{SCT1}^2$$

All of the quantities in the above equation are known, with the exception of \dot{m}_{SCT1} , which can now be determined. The drive flow is obtained from:

$$\dot{m}_{di} = \dot{m}_{RL1} - \dot{m}_{SCT1}$$

The pressure drop loss terms in the above equation will influence the drive flow obtained for a given core pressure drop. In general, K_b and K_{diff} are considerably smaller than the $1/2g A_{th}^2 \bar{\rho}$ terms and therefore do not contribute very much to the total pressure drop balance. The suction flow loss coefficient is chosen to yield a given jet pump m ratio at rated flow conditions. The jet pump m ratio is defined as:

$$m = \frac{\dot{m}_{SCT}}{\dot{m}_d}$$

and is obtained from test data obtained for a generic jet pump design.

For the drive flow loop, the pump pressure drop is obtained by combining Equations 4-78 and 4-80:

$$\Delta P_{pi} = \left(K_{dwn} + K_d + K_{noz} - \frac{1}{2 \bar{p}_r g_c A_{noz}^2} \right) \frac{\dot{m}_{d1}^2}{144} - \left(K_{SCT} - \frac{1}{2 g_c \bar{p}_b A_{SCT}^2} \right) \frac{\dot{m}_{SCT}^2}{144}$$

For non-jet pump plants the pump pressure drop is computed as

$$\Delta P_{pi} = P_e - P_2 + \Delta P_c - \frac{\bar{p}_b}{144} (L_v + \Delta Z_b) \frac{g}{g_c} - \frac{\bar{p}_r}{144} (\Delta Z_D + \Delta Z_{RL}) + (K_{RL} + K_D + K_{LP}) \frac{\dot{m}_{RL1}^2}{144}$$

and P_{VO1} is given by

$$P_{VO1} = P_2 + \frac{g}{144 g_c} \left(\bar{p}_r \Delta Z_b + \bar{p}_b (L_v + \Delta Z_b) \right) - \frac{K_D}{144} \dot{m}_{RL1}^2$$

Enthalpy

The feedwater enthalpy is adjusted such that the core thermal power yields the appropriate total turbine steam flow. In the steady state, Equations 4-8, 4-13, 4-14 and 4-23 can be combined to obtain:

$$\dot{m}_{1T} = \left[\frac{X_1 h_{fg1} + h_{f1} - h_{f2}}{h_{fg2}} (1 + X_{cu}) - X_{cu} \right] \dot{m}_{31}$$

yielding the required core exit quality:

$$X_1 = \frac{h_{f2} - h_{f1}}{h_{fg1}} + \frac{h_{fg2}}{h_{fg1}} \frac{\frac{m_{1T}}{m_{31}} + X_{cu}}{1 + X_{cu}}$$

The core exit quality can be computed from a heat balance:

$$X_1 = \frac{h_{31} + 948.8 P/m_{31} - h_{f1}}{h_{fg1}}$$

Equating the above two expressions yields the required core inlet enthalpy:

$$h_{31} = h_{f2} - 948.8 P/m_{31} + h_{fg2} \frac{\frac{m_{1T}}{m_{31}} + X_{cu}}{1 + X_{cu}}$$

where P = reactor thermal power (MW).

The feedwater enthalpy can be computed from Equation 4-34, where in the steady state, $h_{33} = h_{31}$:

$$h_{fw} = (h_{31} m_{31} - h_{f2} m_{23} - h_{g2} m_{cu}) / m_{fw}$$

If we substitute derived expressions for m_{fw} , m_{23} , and m_{cu} into the above expressions, the result is:

$$h_{fw} = h_{g2} - \frac{948.8 P}{m_{1T}}$$

which is the gross energy balance for the plant, assuming no external heat losses.

The discussion above shows that the loop pressure drop is required to equal the core pressure drop in the steady-state condition. The core pressure

drop for rated conditions is obtained from the multichannel steady-state hydraulic analysis carried out for each core. The pressure drop correlations used in this case are obtained from experimental data. The multichannel hydraulic analysis technology is described in Reference 8.

At rated conditions, the total loop pressure drop for most plants is about 25 psi. Of this, the majority is comprised of the elevation head in the recirc loop (14 psi).

It is important to point out that in this analysis the total core flow is an input quantity and that the loss parameters are adjusted to yield experimentally determined jet pump m ratios. In this regard, the most important variable is the input core pressure drop, which possibly can influence the dynamic flow behavior.

Sensitivity studies of the recirculation system parameters are included in Question 24. The basis for including these results with Question 24 is that all recirculation system parametrics have been included in one package.

NEDO-24154-A

QUESTION 7

Provide and improve the graphical presentation of the recirculation system model and core model both in steady-state and transient conditions. Show all input and output (data flow) between components of each set of calculations indicating the time sequence and iterative procedures, if any.

RESPONSE

The figures in Revision 1 of the letter report, Reference B-7, describing the one-dimensional transient model have been altered to provide the information requested.

Q7-1/Q7-2

QUESTION 8

Justify the selection of the axial and time variation of the gap conductance as input. Discuss the conservatism of the selected values for different transients. Present the values of the temperature-dependent conduction parameters. Discuss the quality of the fit and conservatism of the selected values. Quantify the conservatism or effect of uncertainty on ΔCPR .

RESPONSE

Core average gap conductance as calculated by the GEGAP Code ("GEGAP-III, A Model for the Prediction of Pellet-cladding Thermal Conductance in BWR Fuel Rods," NEDC-20181, Rev. 1, November 1973), which is approved by NRC, is used in the ODYN licensing calculation for transient safety performance. The calculated core average gap conductance is input for all axial modes and is kept constant during transients.

A sensitivity study performed on a BWR/5 shows that the ΔCPR for the most limiting pressurization event (i.e., load rejection without bypass) decreases by ~12% (~0.02 $\Delta\text{CPR}/\text{ICPR}$) when axial varying gap conductance is used, as calculated by a new model currently under review by the NRC. The normalized axial-dependent gap conductance is shown in Figure 8-1. In Figure 8-1 the initial axial power shape is also shown. It can be seen from Figure 8-1 that most of the high power nodes have higher than core average gap conductance. During the transient, higher gap conductance will lead to faster heat transfer from the fuel to the moderator/coolant, which generates more steam voids. This results in lower stored heat in the higher power nodes. In addition, the faster conversion of fuel energy to steam voids in the core helps to mitigate the transient due to negative void reactivity feedback. Therefore, the transient with axial varying gap conductance is less severe than that with constant gap conductance.

During limiting pressurization transients, it is expected that the fuel gap conductance will be higher than its initial steady-state value due to increase in fuel pellet expansion, fission gas inventory and fuel temperature. As

discussed above, higher gap conductance leads to less severe transient. Therefore, it is concluded that the use of constant (core average) gap conductance in the proposed ODYN licensing calculations is conservative (~0.02 ΔCPR/ICPR).

The thermal parameters are utilized as table values in the ODYN calculation. Linear interpolation is utilized in the table lookup procedure. This is done for calculation efficiency. Values of the thermal parameters are given in the following equations or figures (UO₂ specific heat and thermal conductivity and zircaloy specific heat and thermal conductivity). Figures 8-2 through 8-4 are the UO₂ thermal conductivity and zircaloy parameters. The following equation form is used for specific heat of UO₂:

	<u>Equation Form (Cal/gm-mole - °C)</u>	<u>Range (°K)</u>
1-	$C_p = 19.2 + (1.62 \times 10^{-3}) T - 3.96 \times 10^5 T^{-2}$	298 to 1175
2-	$C_p = 20.58 + (3.132 \times 10^{-4}) T + \frac{(42659)^2}{RT^2} \frac{x}{(1+x)^2}$	1175 to T _{melt}
	$R = 1.987 \text{ (Cal/gm-mole - °K)}$	
	$X = \exp (6.25 - 42659/RT)$	
3-	$C_p = 15.63 + (4.668 \times 10^{-3}) T$	>T _{melt}

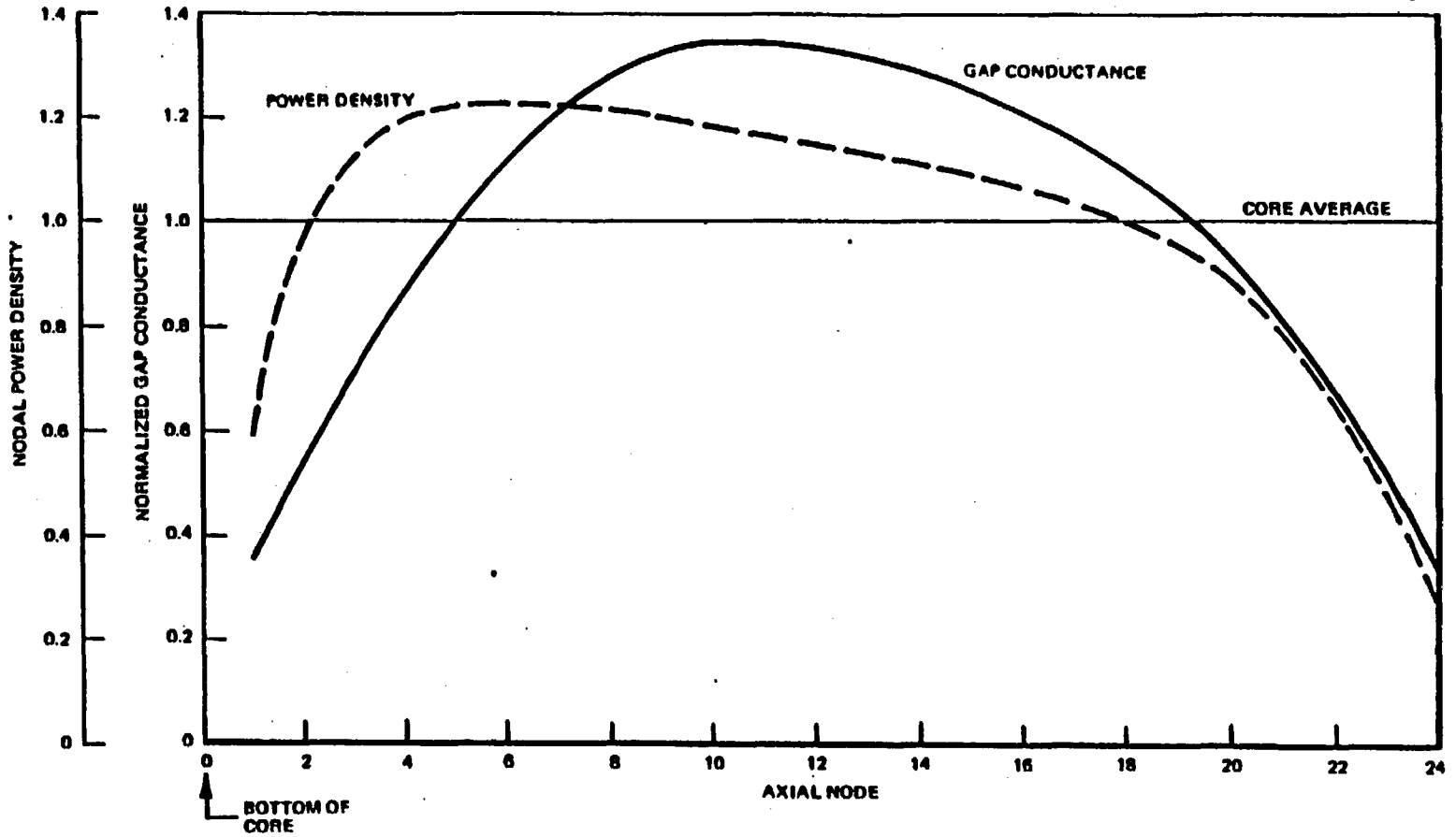
The UO₂ thermal conductivity is based on a value of

$$\int_0^{2805 \text{ °C}} KdT = 93.0 \text{ W/CM}$$

NEDO-24154-A

Uncertainty in these parameters is in the range of $\leq \pm 10\%$. By varying thermal conductivity and specific heat of UO_2 10% in opposing directions, an impact of 20% on the pellet time constant due to thermal variations is obtained. This results in a $\Delta CPR/ICPR$ effect of 0.001. Cladding effects are much smaller in the ODYN impact. Use of the constant gap thermal conductance throughout the transient more than compensates for this effect. The conclusion is that the combination of all thermal parameters in the ODYN program result in a conservative bias in the transient calculations.

08-4



NEEO-24154-A

Figure 8-1. Normalized Axial-Dependent Gap Conductance

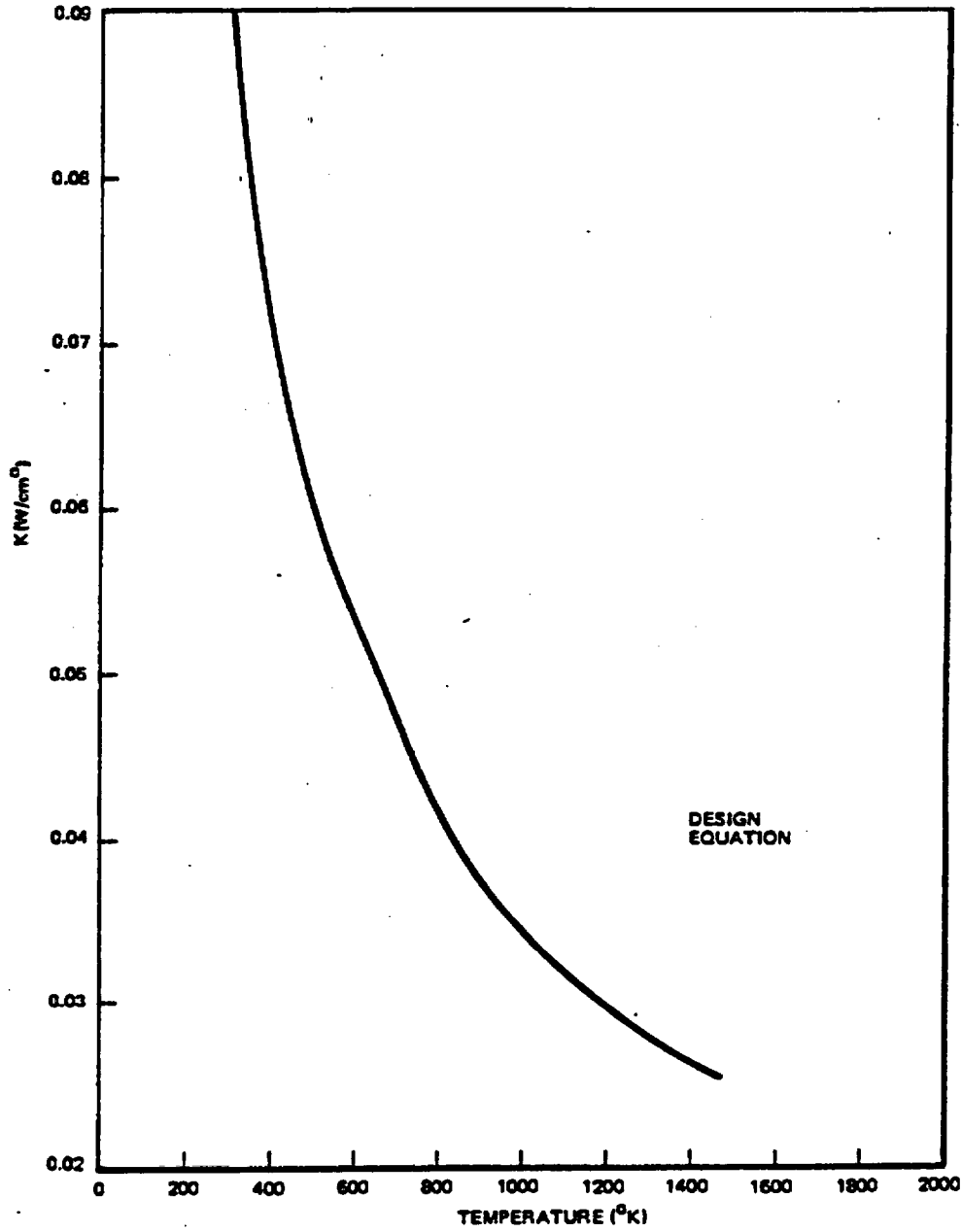


Figure 8-2. UO₂ Thermal Conductivity

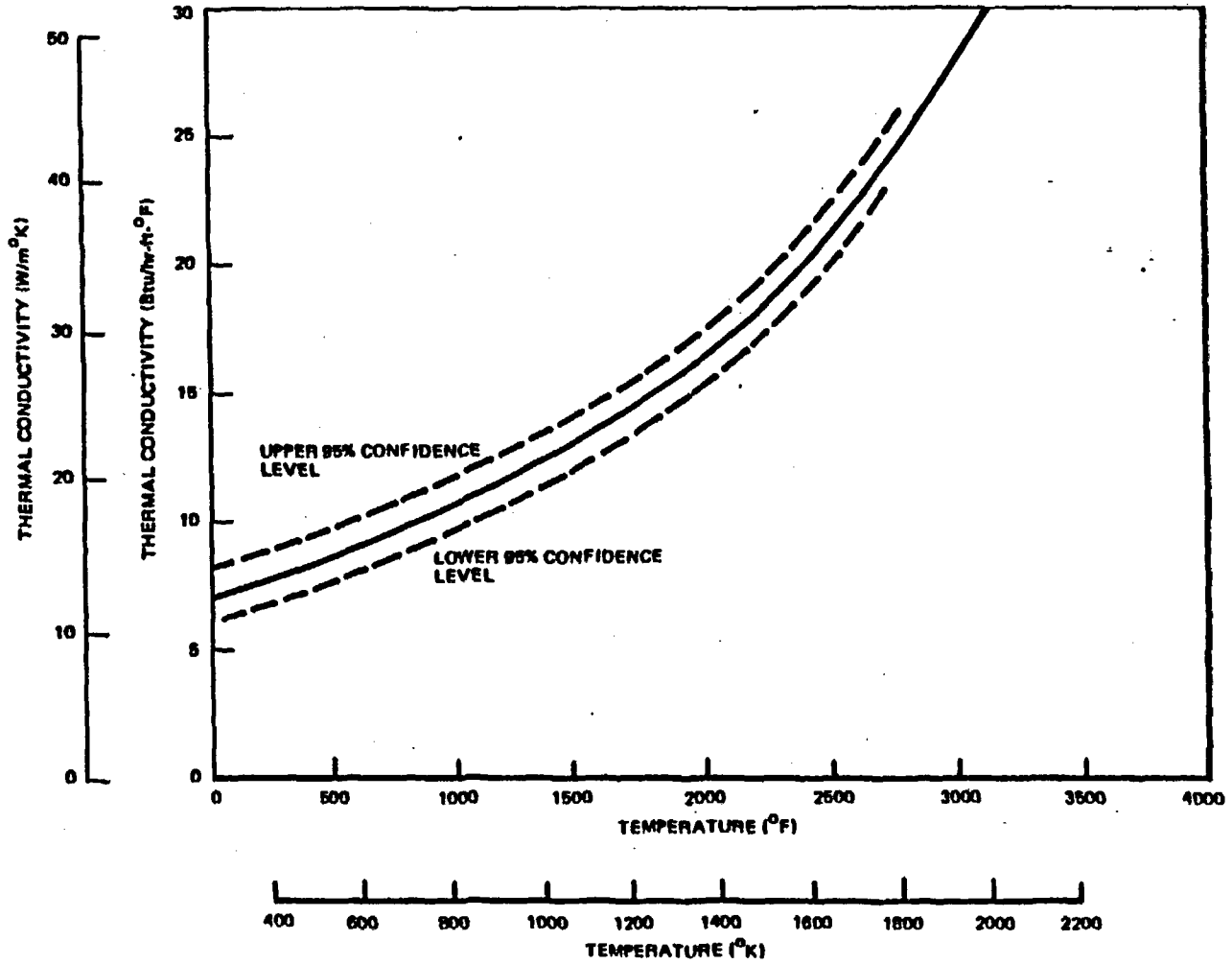
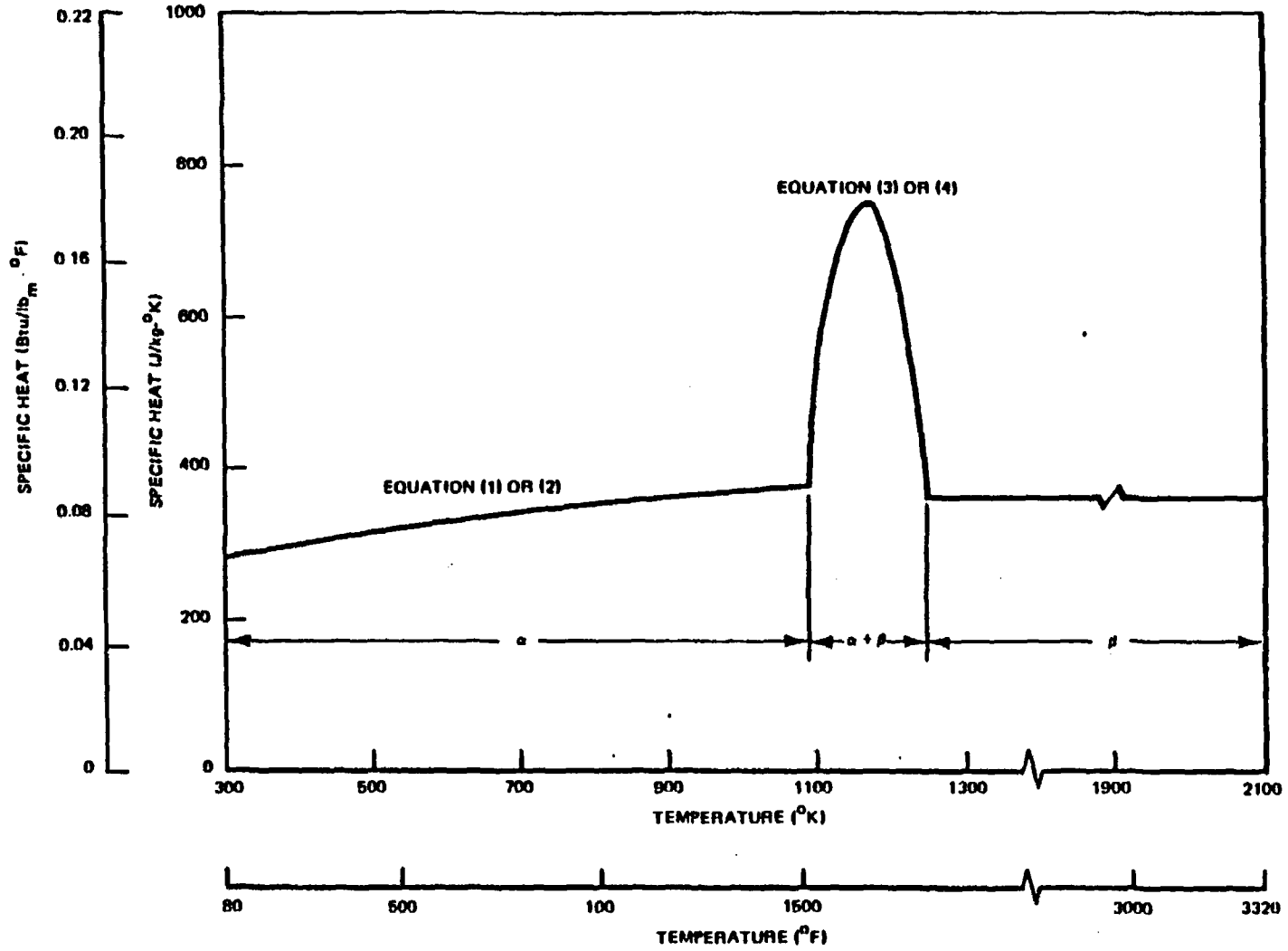


Figure 8-3. Thermal Conductivity of Zircaloy

8-7/08-8



NEDO-24154-A

Figure 8-4. Specific Heat of Zircaloy

QUESTION 9

Discuss the stability of the system and thermal-hydraulics model when the ØDYN code is used with different power distributions and boiling boundary level.

RESPONSE

The one-dimensional transient model has proven to be stable in all of the transients analyzed so far. The vast majority of these transients have been pressurization transients initiated from high power and flow. The initial boiling boundary position ranges from 8 in. to 45 in. above the bottom of the fuel. The model has not been used to analyze low flow/high power conditions, where physical instabilities are more likely to occur.

QUESTION 10

Perform the analysis of the transient presented in NFN 058-78 dated February 7, 1978, with and without control system operation to demonstrate that with the safety system operation alone the results are conservative.

RESPONSE

Abnormal operational transients are defined as events which are results of single equipment failures or single operator errors that can be reasonably expected during any normal or planned mode of plant operations. Control system failures are among the causes. Following the assumed single failure, which is assumed to fail in the worst direction, the resulting transient is simulated in a conservative fashion to show the response of primary system variables and how the various plant systems would interact and function. In the analysis, the plant instrumentation and controls, plant protection and reactor protection systems, except the assumed failure, are assumed to maintain normal operation unless specifically designated to the contrary in order to provide a realistic transient signature. The effects of single failures and operator errors on the transients are also discussed and presented in Chapter 15 of FSAR or PSAR and reload licensing transmittals. In these transients, the consideration of any additional failure (e.g., without control system operation as suggested in the question) is not considered appropriate within the realm of abnormal transient definition.

The probability of the total failure of control systems is considered to be low enough that the event could be classified as an accident should it occur.

Nevertheless, the worst plant control mode is assumed in the transient simulation to provide a conservative safety evaluation to cover all possible plant operation modes. For example, manual flow control mode is assumed in the transient analysis. Furthermore, some control systems are saturated during the transient (e.g., pressure control is saturated during pressurization events) and, consequently, there is no effect on thermal or pressure margin during transients. In addition, most of transients analyzed are mitigated by reactor scram. Thus, the effect of control system operation on the thermal and

NEDO-24154-A

pressure margin is insignificant and minimal. Therefore, it is concluded that although control systems operation is assumed in transient simulations to provide realistic transient signatures, additional failures assumed in these systems would generally not make the transient significantly more severe than the events already presented in the FSAR.

QUESTION 11

In the description of the control system there seems to be a page missing.

RESPONSE

A review of the document indicates all pages and information are in the order planned for publication in the copies within GE. Possibly a printing error has occurred in the copies sent to the staff. The revised document has been reviewed to assure that all information is included and that all normal control functions can be simulated with the information provided when plant data are supplied.

QUESTION 12

Provide a detailed description of the void-quality correlation to obtain $\alpha_{C,B}(z)$ which is used for neutron-effective void correlations. Describe and justify any differences between this correlation and the one used in the thermal-hydraulic calculations. If the correlation contains any empirical factors, discuss their conservatism and experimental data base. Describe how the void fractions in Equation 3-12 are obtained. Justify the form of Equation 3-12. Quantify the conservatism in the empirical factors or effects of uncertainties on ΔCPR .

RESPONSE

The reply to Question 12 contains General Electric Company proprietary information and has been documented separately in Volume III of this report.

QUESTION 13

Derive Equation 3-23. Discuss its basis. Discuss the stability between parallel channels.

RESPONSE

Equation 3-23 is a means of updating the bypass flow fraction during a transient to reflect changes in the pressure drop balance between the active channel and bypass. The bypass flow fraction is defined as:

$$f_{BP} = \frac{m_B}{m_B + m_C} \quad (13-1)$$

where

m_B = total bypass flow, and

m_C = total active channel flow.

We wish to find an f_{BP} at $t + \Delta t$ such that the bypass pressure drop equals the channel pressure drop; i.e.,

$$\Delta P_B (t + \Delta t) = \Delta P_C (t + \Delta t) \quad (13-2)$$

Let us assume that each pressure drop is proportional to the flow squared:

$$\Delta P_B (t + \Delta t) = K_B m_B^2 (t + \Delta t) \quad (13-3)$$

$$\Delta P_C (t + \Delta t) = K_C m_C^2 (t + \Delta t) \quad (13-4)$$

Substituting these expressions into equation (1) yields the requirement that:

$$\frac{m_C}{m_B} = \sqrt{\frac{K_B}{K_C}} \quad (13-5)$$

or

$$f_{BP}(t + \Delta t) = \frac{1}{1 + \sqrt{\frac{K_B}{K_C}}} \quad (13-6)$$

The ratio $\sqrt{\frac{K_B}{K_C}}$ is estimated from the flow and pressure drop at time t ; i.e.,

$$\sqrt{\frac{K_B}{K_C}} = \sqrt{\frac{\Delta P_B(t)}{\Delta P_C(t)}} \frac{m_C(t)}{m_B(t)} \quad (13-7)$$

$$\sqrt{\frac{K_B}{K_C}} = \sqrt{\frac{\Delta P_B(t)}{\Delta P_C(t)}} \left(\frac{1}{f_{BP}(t)} - 1 \right) \quad (13-8)$$

Substitution of Equation 13-8 into 13-6 yields Equation 3-23 in the reference; i.e.,

$$f_{BP}(t + \Delta t) = \frac{f_{BP}(t) \sqrt{\frac{\Delta P_C(t)}{\Delta P_B(t)}}}{1 + f_{BP}(t) \sqrt{\frac{\Delta P_C(t)}{\Delta P_B(t)}} \left(1 - \sqrt{\frac{\Delta P_B(t)}{\Delta P_C(t)}} \right)} \quad (13-9)$$

NEDO-24154-A

Since the time that Equation 13-9 has been derived, studies have shown that it over-corrects the bypass flow fraction, resulting in numerical oscillations in f_{BP} . Therefore, a relaxation parameter u has been added to Equation 13-9, yielding:

$$f_{BP}(t + \Delta t) = \frac{u f_{BP}(t) \sqrt{\frac{\Delta P_C}{\Delta P_B}}}{1 + f_{BP}(t) \sqrt{\frac{\Delta P_C}{\Delta P_B}} \left(1 - \sqrt{\frac{\Delta P_B}{\Delta P_C}}\right)} + (1-u) f_{BP}(t) \quad (13-10)$$

A value of $u = 1/2$ removes the oscillations, still maintaining a bypass-channel pressure drop balance throughout the transient.

QUESTION 14

Discuss the basis for the selection of initial f_{bp} and f_c . Discuss the conservatism of this selection, if any.

RESPONSE

The core bypass flow fraction is an input quantity to the transient model. Its value is obtained from a steady-state analysis of the core hydraulics with a multichannel hydraulics analysis. The basis of this analysis is outlined in Reference B-5. The bypass flow fraction is obtained by requiring a pressure drop balance between the active flow channels and the bypass or leakage flow path. For the vast majority of full power conditions, there is no boiling in the bypass region and a negligible amount of density change occurs there during a pressurization transient. For this reason, the transient response is almost independent of initial bypass flow fraction. The quantity f_c is not defined in the model report.

QUESTION 15

The momentum equation (4-11) does not include forces exerted on the fluid from the walls and assumes one-dimensional flow. In reality, the flow is rotational. Discrepancies from reality are taken care of by using experimental data and a correlation (Equation 4-12) for steady-state. Justify the momentum equation in its present form for its use in transients. Provide the experimental data, if needed more than that in Reference 5, and basis for the correlation and selection of the effective L/A. The correlation (Equation 4-12) should be sensitive to some parameters such as quality, slip and flow rate. Provide information as to sensitivity of this correlation to different parameters. Present experimental techniques, describe experiments and accuracy of measurements. Discuss the variations during the transient and provide sensitivity studies using different C_{sep} and L/A values for a licensing basis transient for a typical BWR/4 such as Peach Bottom.

RESPONSE

The initial application of equations of the form of Equation 4-11 occurred in the earliest history of BWR system simulation. This form was applied in an attempt to find the simplest form applicable to system simulation because of the severely limited computational capabilities of both analog and digital computers available in the early 1960's. At that time, all of the inertial (L/A) and friction loss (K) terms were required to be constant because of computations (either analog or digital) limitations. The question then became one of finding a conservative representation for the transients calculated with reasonable computation cost. Early attempts at simulation fitted the profile of the liquid in the separators based on parabolic axial profiles and estimated the frictional losses in the separators as though they were due to abrupt changes in flow area. These attempts were compared to early data and, by use of constants in the fitting process, were found to yield reasonable although not entirely consistent results. The accumulation of higher quality steam-water data occurred in 1965 and was reported in Reference 5 of the ODYN transmittal letter^{B-8}. These data showed that a good representation of the separator friction pressure drop could be obtained using equations of the form of

Equation 4-12. Reference B-8 indicates that friction head is proportional to volumetric flow rate. Hence, variations of Equation 4-12 are incorporated by transferring to pressure drop. In addition, data from the GE Advanced Technology Laboratories taken during 1965 were reported in References B-9 and B-10. From these data, it was possible to obtain an effective inertial form based on the average flow trajectory of the liquid as it moved along the swirling path prior to discharge from the separators. The flow path and inertial parameter (L/A) was found to be a function of separator inlet quality. The results of such a determination were indicated in Figure 4-3 for an individual separator. Variation of L/A due to the flow rate was found to be negligible (less than 1%) over the range of expected operation and, therefore, was not included in the correlation. The real justification of Equations 4-11 and 4-12 actually exists in the ODYN Qualification Report. A comparison between model and data for the core exit plenum and reactor steam dome shows that good agreement exists in the initial pressure rise. Since only the separator region separates and couples these two regions, this comparison of pressure, particularly for Peach Bottom-2 test data, shows the separator representation is adequate without change for evaluation of large pressurization transients such as turbine trip, load rejection and main steam isolation valve closure.

Sensitivity studies were performed on the inertial terms (L/A). A decrease of 30% in the effective L/A resulted in +0.002 change in $\Delta\text{CPR}/\text{ICPR}$. This is consistent with the uncertainties in the effective L/A and for practical purposes it is negligible. The value of C_{sep} is expected to be conservative as it stands in the model. This is based on the dome to core pressure drop observed at Peach Bottom-2 during the April 1977 testing program. Table 15-1 compares plant data and calculated pressure drops. In all cases, the calculated pressure drop is higher. This is due, principally, to C_{sep} . Sensitivity calculations show that higher values of C_{sep} result in higher $\Delta\text{CPR}/\text{ICPR}$ calculations. Since this is a bias built into the model, uncertainty in this parameter is conservatively accommodated in ODYN.

NEDO-24154-A

Table 15-1
PEACH BOTTOM-2 CORE TO DOME PRESSURE DROP

<u>Case</u>	<u>Calculation (psi)</u>	<u>Plant Data (psi)</u>
TT1	8.3	7.4
TT2	7.3	4.5
TT3	9.7	6.4

Q15-3/Q15-4

QUESTION

Discuss the effects of thermal nonequilibrium vs. equilibrium on the results of a typical licensing basis turbine trip without bypass transient using the ODYN code.

RESPONSE

Thermodynamic nonequilibrium effects are included in the core hydraulic channel model through the use of a subcooled boiling model. Subcooled boiling has a significant effect on the channel void fraction distribution and also on the axial power distribution. The effects of subcooled boiling assumptions on the pressurization transient response is discussed in the reply to Question 28.

NEDO-24154-A

QUESTION 17

Figure 4-1 is insufficient to derive Equations 4-35 through 4-40. Draw the proper figures in detail, indicating the meaning of all symbols on the figures.

RESPONSE

A figure has been added to the revised model report which defines the appropriate quantities in Equations 4-35 through 4-40.

Q17-1/Q17-2

QUESTION

Provide a nodalization diagram for the whole recirculation model showing different pressures in each of the 10 nodes. Justify the selection of only 10 nodes, particularly selections of one node for the vessel, and another node for the downcomer, inlet plenum and the core. Discuss the pressure drops through dryers, downcomer, orifices and the core and justify the selection of one node-single pressure model for these regions. How do these pressure drops change during transients? What type of error is introduced when an iteration is made between the recirculation model and thermal-hydraulic model?

RESPONSE

The attached nodalization diagram (Figure 18-1) indicates the pressure nodes in the ODYN model. Note that the core is nodalized axially as is the steamline.

The justification for this choice of nodes is based on several factors, the most important of which are: (1) the variation of fluid or material properties is negligible over the region; (2) the fluid flowing in the recirculation system is liquid, subcooled and quite incompressible so that acceleration of the flow occurs as a single inertial unit (integral momentum); (3) wave type phenomena demonstrate wave lengths much longer than the nodes; (4) adequate approximation to the phenomena based on the modal representation of a region is made; and (5) the transient pressure drops do not result in significant changes in the approximations (2) through (4) above.

The basis for choosing a single node in the vessel dome is that the pressure drop from the downcomer inlet to the top of the dome is nearly all due to density effects. This amounts to 5 to 6 psi difference from bottom of the dome region to the top. Compared with operating pressures of typically 1000 psia or greater, the difference above results in less than 0.5% change in fluid properties in the dome region. In addition, the dome region is a very large area compared to the height (very little inertial effect). Hence, there is no observable wave response in the dome region. Finally, since the acoustical velocity in steam is ~ 1500 ft/sec, the change of pressure within the dome is effectively instantaneous whenever a flow disturbance is introduced into the reactor vessel.

In the downcomer region during the pressurization transients, the recirculation flow is subcooled by about 20 Btu/lbm. With this degree of subcooling, the change in liquid properties is very small due to pressure. The pressure change from the dome to the bottom of the reactor vessel is about 35 psi, most of which is due to density head and the jet pump diffuser pressure increase. Since the pressure in the downcomer and core inlet is about 1000 psia or greater, the fluid properties vary by less than 0.1%, which is negligible as in the dome region. In addition, sonic speed is in the range of a few thousand feet per second in the downcomer and lower plenum region, which means that similar to the dome region the downcomer and inlet plenum respond to pressure disturbances in the reactor vessel almost instantaneously. This does not mean, however, that flow rate responds instantly to equilibrate pressure disturbance effects, because the recirculation system will require an additional amount of time for fluid acceleration around the loop.

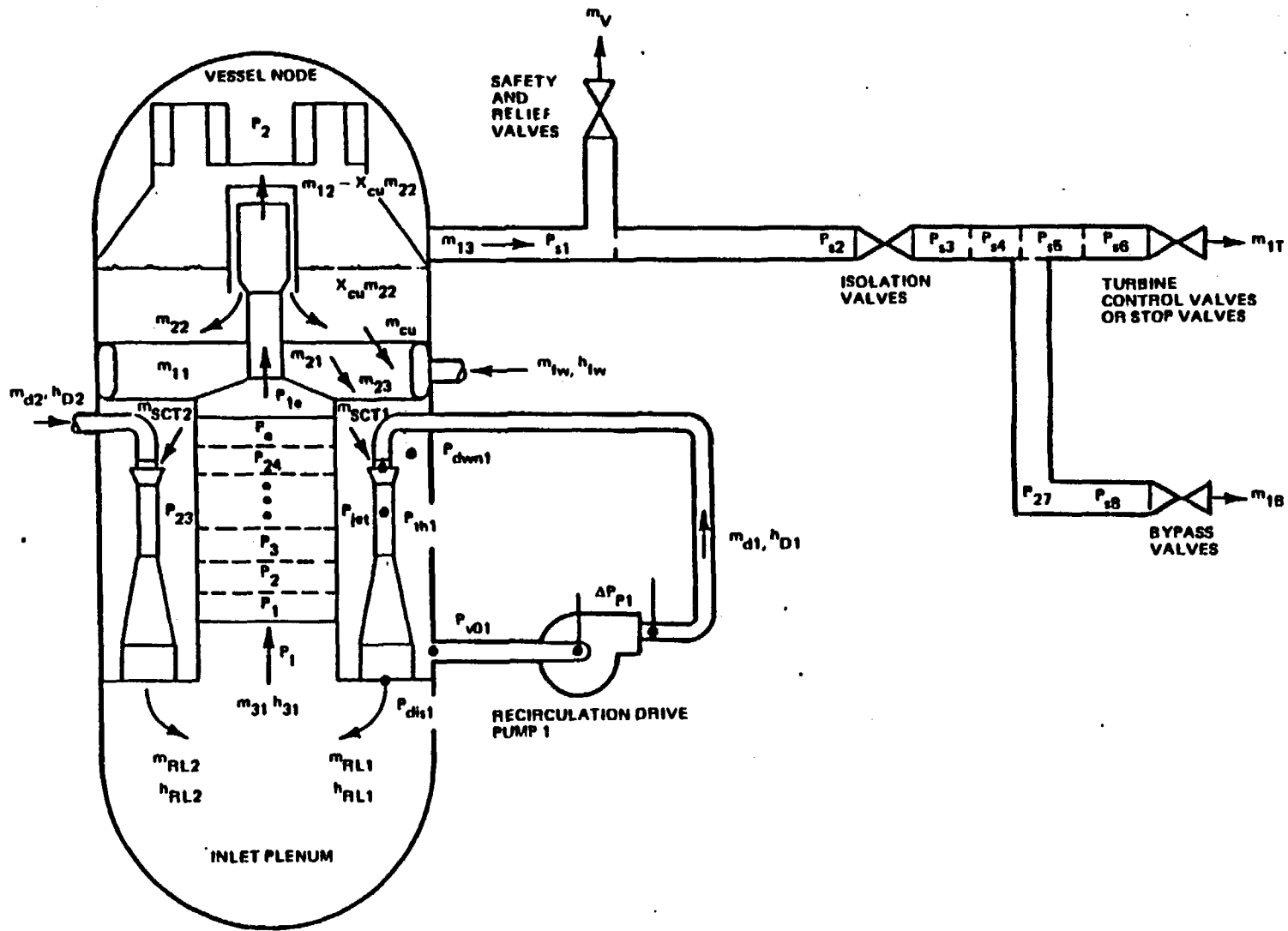
The core is not represented as a single node for pressure calculations in ODYN. The equations in Section 6 require nodal calculation in the core for pressure, density, enthalpy and flowrate. If reference is made to Figure 4-7 (Jet Pump Schematic), please note that the ΔP_{core} is indicated without the nodal structure and P_e , the core exit pressure, is indicated, which may leave the impression that a single pressure is used to represent the core. However, this is not the case as seen by implication from Section 6. The core inlet orifice pressure drop is about 10 psi and is taken into account in the ODYN core. The total core pressure drop is typically 20-25 psi, including the inlet orifice.

The pressure drop through the dryers is >12 inches of liquid water at operating pressure or 0.4 psi.

The pressure drops around the recirculation loop will increase slightly during large pressurization transients. This is due to flow acceleration due to void collapse effects in the core as the vessel is pressurized. These increases in pressure drop are about 15 to 25% or approximately 10 psi from the dome to the core inlet plenum. Such changes do not invalidate any of the arguments above regarding properties in the lumped regions. This is again due to the small pressure drop relative to the absolute vessel pressure at operating conditions of about 1000 psia or higher.

The error introduced in the recirculation-thermal hydraulic model iteration is quantified by two criteria: model stability and accuracy. The iteration procedure is very stable and converges to a relative error criteria on core pressure drop. By choice of the error criteria, this accuracy between models can be as good as desired. Overall accuracy of this method is judged to be excellent for this particular application.

018-4



NEDO-24154-A

Figure 18-1. OLYN Pressure Nodal Diagram

QUESTION 19

Provide a noding sensitivity study for the steamline to show the convergence of the results with 8 nodes for a licensing basis transient for a typical BWR/4. Provide a sensitivity study for different values of γ (the ratio of specific heats for steam) and the values of K (form loss coefficient). Discuss the sensitivity of the results for deviations from the assumption of isentropy and the presence of moisture. Quantify the conservatism in terms of ΔCPR .

RESPONSE

The noding studies performed to date are included in the attached Figures 19-1 and 19-2. These studies show a strong continual improvement out to about 7 nodes where a reasonable approximation is obtained. Further comparison of the 8-node model to the Moody analytical model employing the method of characteristics has also been performed. The comparison of the ODYN steamline model with the method of characteristics model is shown in Figures 19-3 and 19-4. These comparisons were made at various locations along the steamline. The model labeled 8-node model is the ODYN model and the method of characteristics model is identified as the Moody model. The so-called Moody model also includes the convective circulation terms which have been neglected in the ODYN formulation. The comparison case is a turbine stop valve closure simulation along a steamline with constant pressure supply at the inlet to the steamline. Hence, no dome pressure comparisons could be made. Note that the general tendency of the ODYN 8-node model is to overpredict the method of characteristics solution even though all other factors are held constant. The model studies were concluded at this point on the basis that the 8-node model is satisfactory in representation of the steamline response nodes.

Parameter studies of changes in the average specific heat ratio, γ , are shown in Figure 19-5 for changes between 1.10 and 1.30. These values were chosen simply to establish a range of sensitivity. Figure 19-5 shows little sensitivity to specific heat ratio in the dome pressure. The neutron flux peak varies by 10%. The heat flux variation over this arbitrary range is 2.2%.

Uncertainties in specific heat ratio are based on the average specific heat ratio which best matches turbine trip* pressure rate (1.15) compared to the superheated steam maximum from the steam tables (1.25). This uncertainty is $\Delta\text{CPR}/\text{ICPR}$ is ± 0.01 . Actual uncertainties in γ are expected to be significantly less in specific plant analyses. The loss coefficient, K, of the steamline was decreased by 20%. This was based on the upper limit of steamline loss coefficient uncertainty. The results are presented in Figure 19-6. The change in peak neutron flux was -2% and heat flux varied by 1.0%. The $\Delta\text{CPR}/\text{ICPR}$ uncertainty is 0.01 for the steamline loss coefficient. Again, the actual uncertainty is expected to be less in this parameter in specific plant analyses. The presence of moisture in the steamline is extremely low. The amount of liquid entrained in the steam flowing along the steamline is <0.1%. The increase in steamline pressure results in a removal of the mixture from saturated conditions to a mixture consisting of superheated steam and subcooled liquid. By assuming such to be the case, the pressurization is most conservatively represented because of the decreased steam compressibility. The presence of liquid in such small quantities has limited heat absorption capabilities so that little, if any, effect of heat transfer could occur during the pressurization phase. Finally, all of these assumptions are borne out in the comparison of ODYN to the Peach Bottom-2 and KKM data, where a value of specific heat ratio can be adequately determined as 1.15.

The uncertainty in this model for transient initial pressure rate is negligible because it was matched directly to pressure rate data taken at Peach Bottom-2 and other turbine trip tests. Peak dome pressures are conservatively over predicted by the model which are due to nonsteamline effects.

*Peach Bottom-2 data principally.

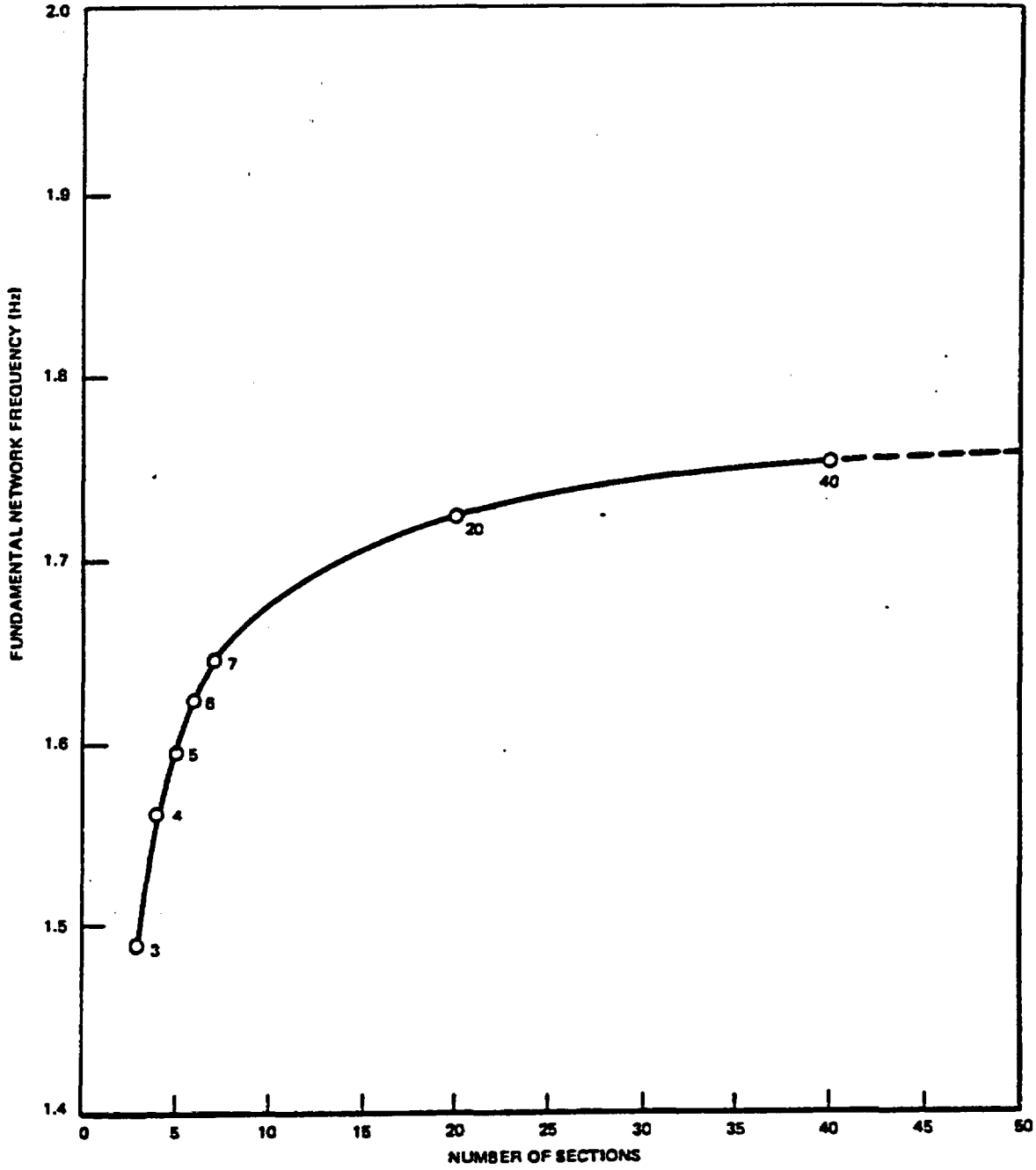


Figure 19-1. Fundamental Frequency

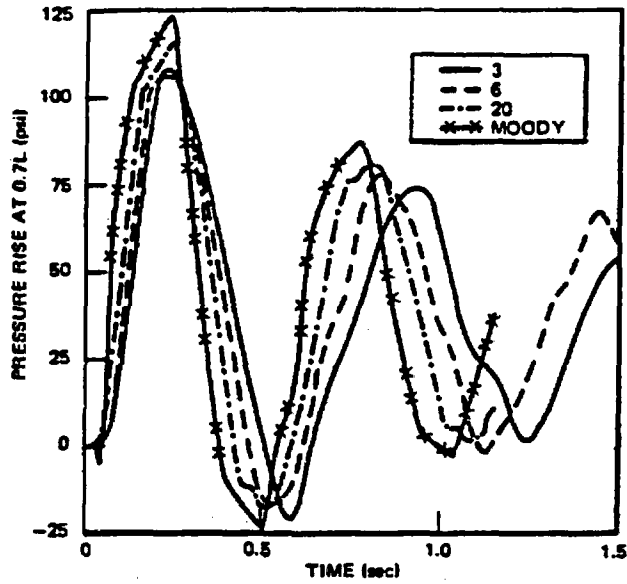


Figure 19-2a. Pressure Rise at 0.7L

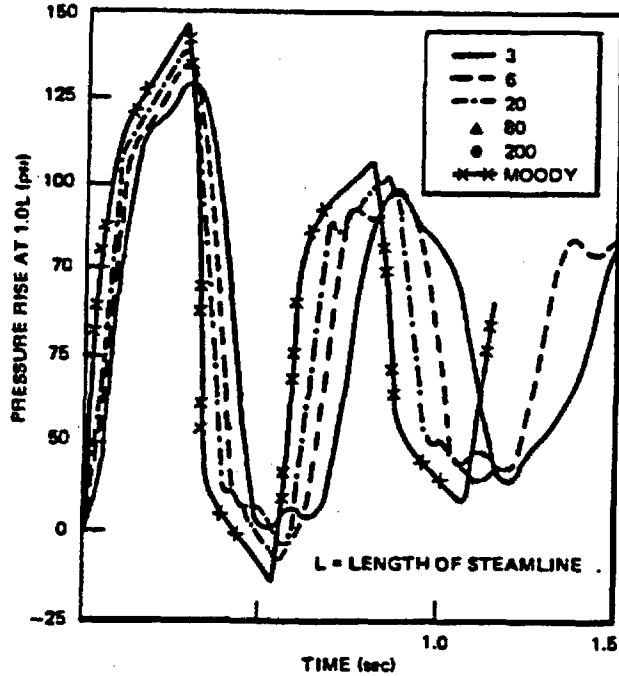


Figure 19-2b. Pressure Rise at 1.0L

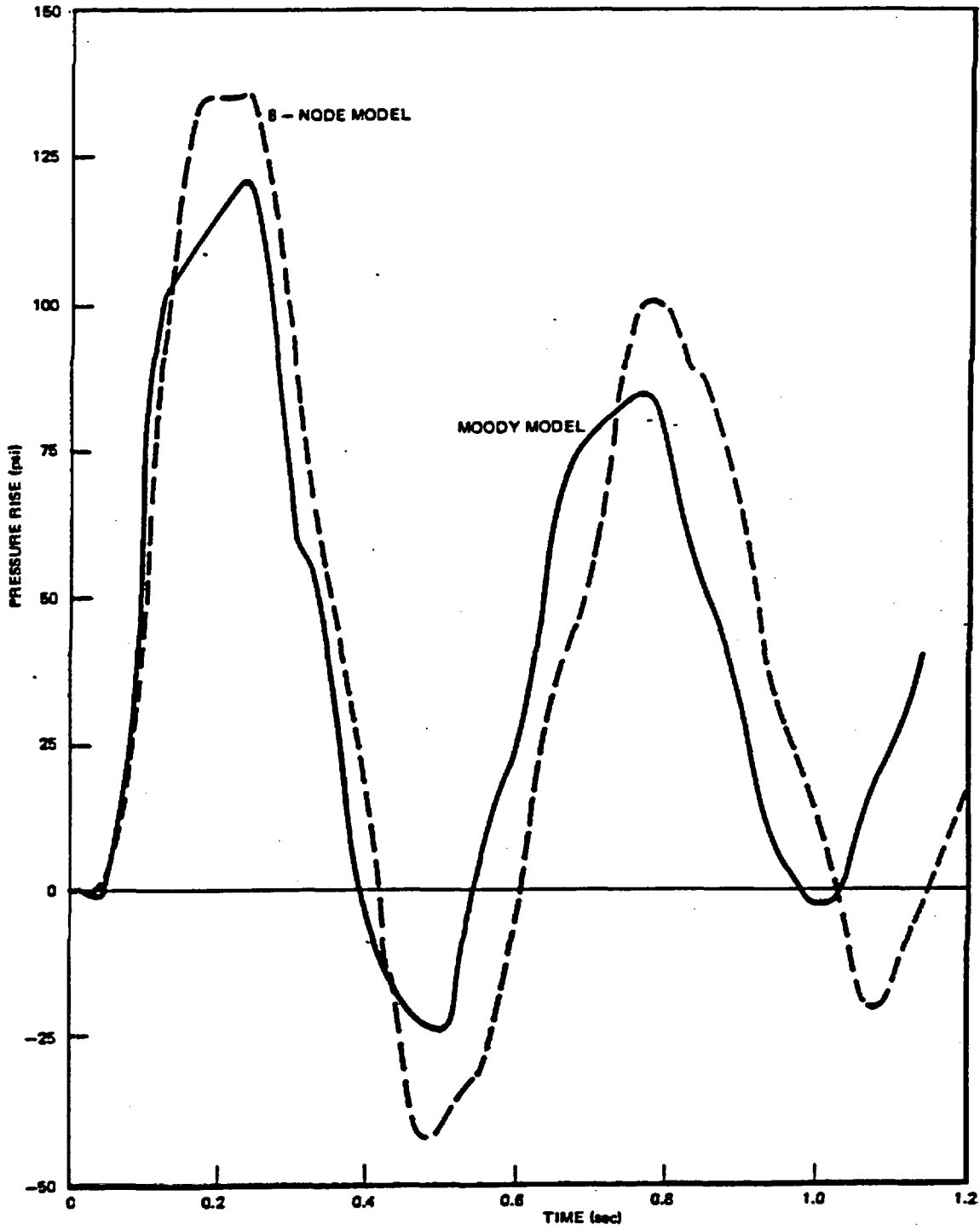


Figure 19-3. Pressure Rise at 2/3 L During Turbine Trip with Constant Dome Pressure

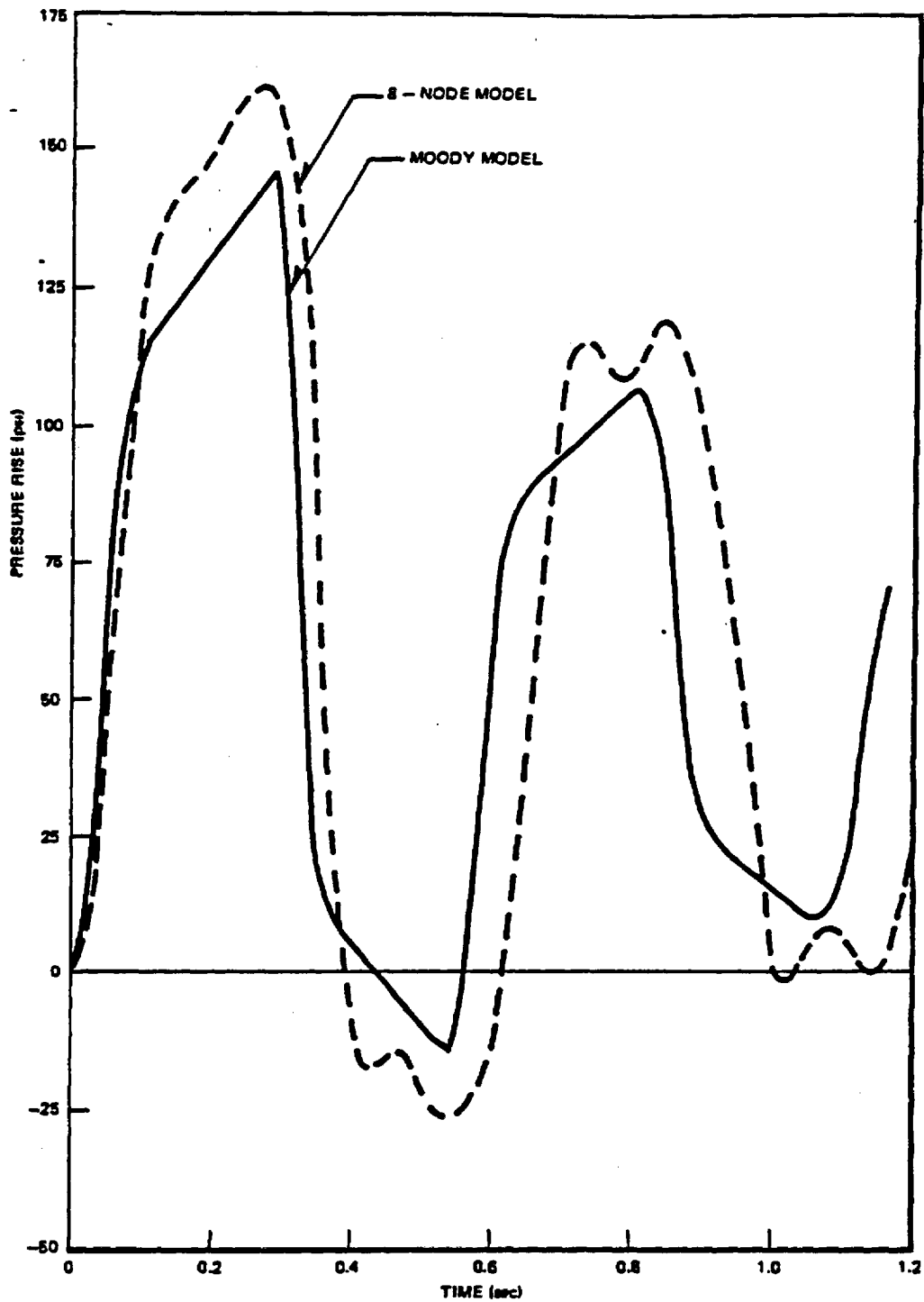


Figure 19-4. Pressure Rise at Turbine During Turbine Trip with Constant Dome Pressure

NEDO-24154-A

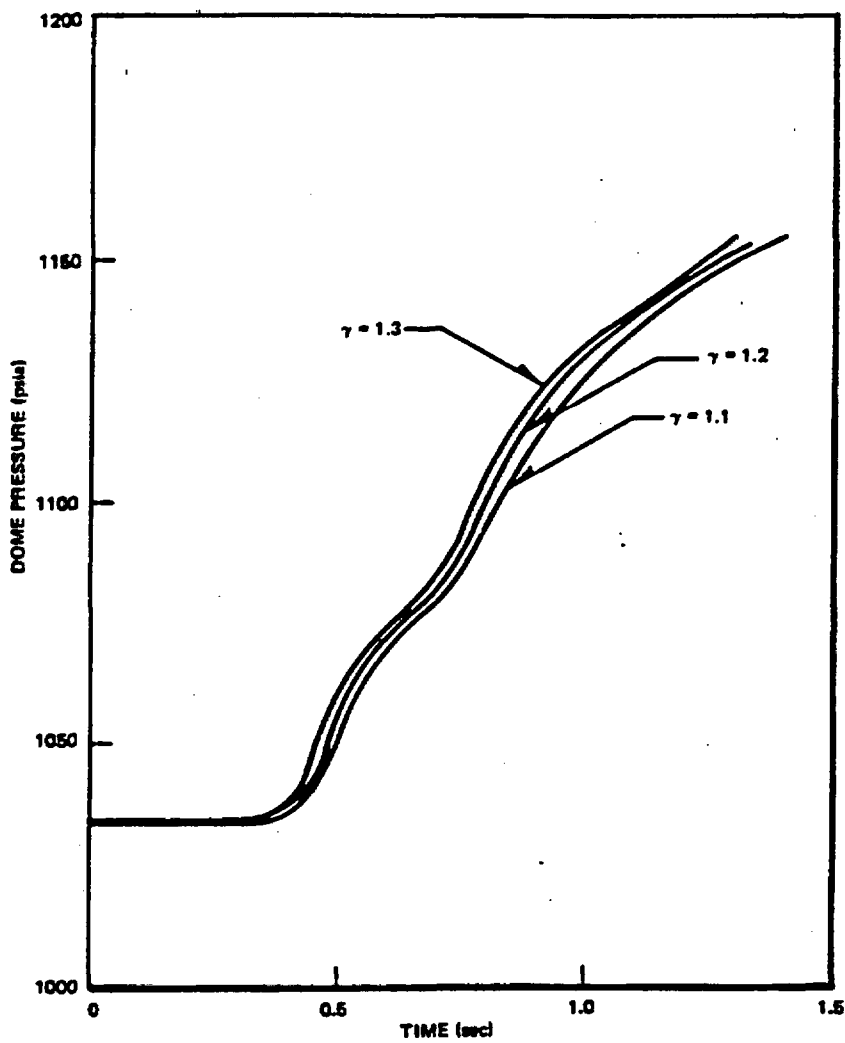


Figure 19-5. Dome Pressure Vs Time - Sensitivity to Specific Heat Ratio, γ

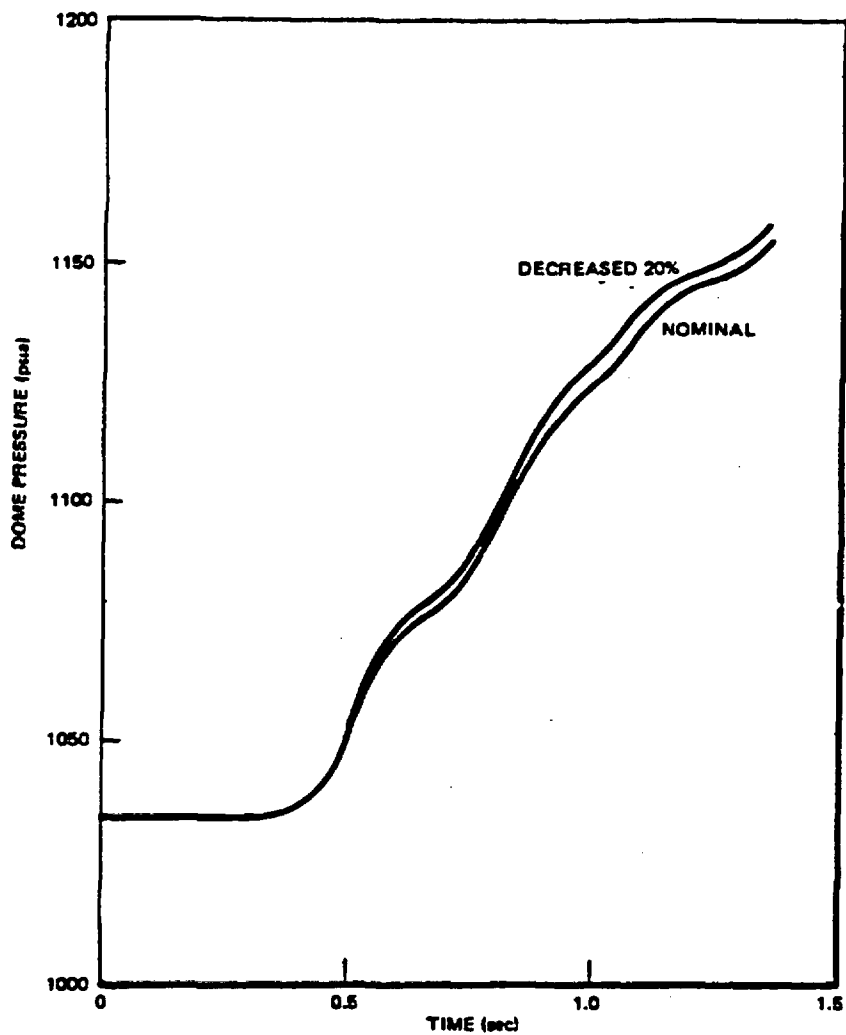


Figure 19-6. Dome Pressure Vs Time-Sensitivity to Steamline Loss Coefficients

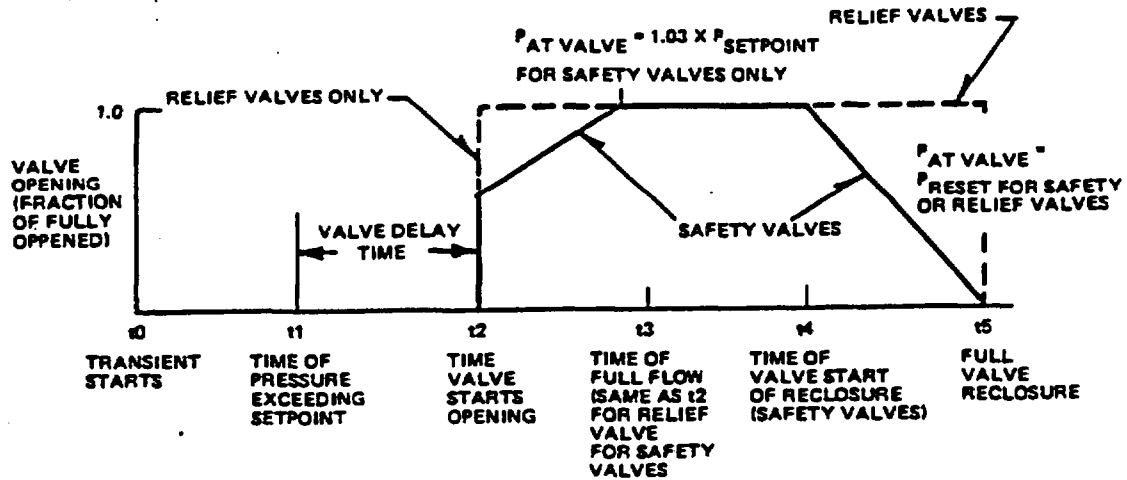
QUESTION 20

Define all notations in the Safety/Relief Valve Model. Describe how the variations of C_{RV} , C_{SV} and f_{SV} are determined and present the nature of the function. Describe how transport delay times are obtained.

RESPONSE

All notation has been defined in Revision 1 of the One-Dimensional Core Transient Model document. The capacity of the relief and safety valves, C_{RV} and C_{SV} respectively, are determined by the nameplate capacities of the safety and relief valves or the minimum specified capacity for plants in the design phases prior to hardware procurement. These valve capacities are, therefore, conservative inputs which are part of the design process. Note that these capacities are both functions of nameplate actuation pressures and not functions of the valve pressure throughout the valve operation. The safety valve characteristic, f_{SV} , is actually applied as indicated in Figure 4-6. This is a linear opening characteristic from 50% of capacity upon initial operation to 100% of capacity when pressure is 103% of the safety valve setpoint. This flow characteristic is an input to the model and, therefore, part of the model application basis. The choice is made such that the input characteristic results in less flow than the actual valve characteristic. The choice will therefore be conservative. Again, the so-called transport delay times are based on equipment design limits or actual valve measurements of the time from start of the valve stroke to full flow through the valves. The choice of transport delay times is also a matter of model input which is a part of the model application basis. One final comment on the modeling of the safety/relief valves is appropriate at this time. In the One-Dimensional Core Transient Model document, there has been no mention of the valve opening delay. In reality, the valves may not open instantaneously when pressure exceeds the setpoint of the valve. Due to the mechanical functions of the valve, there can be a time delay. This delay has been incorporated into the model, although it was not documented. The delay is, in fact, a pure time delay due to mechanical response times which occur prior to valve opening. It is simulated as a time delay effect, not a time constant delay effect. The time line below gives an indication of simulated valve function.

Also note that the safety/relief valve characteristics were indicated on the same figure strictly for convenience. The real safety and relief valves operate with different delay times, flow delay time constants and reseating pressures.



QUESTION 21

Justify the assumption that perfect mixing of suction and drive flows occurs in the jet pump throat.

RESPONSE

The criterion of major concern for designing high efficiency jet pumps is complete mixing of the drive and suction flows. The concern is that a non-uniform velocity profile will flow from the mixer region to the diffuser. If this profile is peaked to the center of the flow channel, the diffuser efficiency can be impaired. In short, the jet pumps are designed to effect complete mixing for effective diffuser utilization.

The measured distribution of flow entering the diffusers of typical jet pumps indicates distributions somewhat like the fully developed turbulent flow for multiple nozzle jet pumps and practically parabolic distributions for single nozzle jet pumps. Such distributions provide good performance of jet pump systems.

The typical BWR/4 jet pump designs yield a nozzle-to-suction velocity ratio of about 3 to 1 at rated conditions. The time to traverse the mixing section of such a pump is about 0.1 sec with velocity of the jet at about 180 ft/sec and velocity of the suction of 60 ft/sec. Mixed velocity is about 80 ft/sec. The inertial frictional time constant of the jet pump system is about 1 sec, which is much longer than the flow transit time. Hence, the mixing effects are practically instantaneous compared to inertial effects on the transient flow. The approximation of instantaneous mixing is well justified in this instance.

QUESTION 22

Present experimental verification for the representation of the jet pump recirculation system and justify the use of the steady-state equations such as Equations 4-67 through 4-69 or Equations 4-84 through 4-91 during transients.

RESPONSE

Experimental verification of the jet pump recirculation system models has been presented in NEDO-10802 in that comparisons to startup pump trip data from Dresden-2 was compared to calculations made by REDY which incorporates the same recirculation system model. These data, presented in Figures 4-10 and 4-11 principally, show that the model predicts somewhat faster coastdown than observed in the plant data. The reasons for this discrepancy is that plant pump inertia was somewhat higher than used in the model and also that plant flow sensors incorporate a filter to smooth the noise in the recirculation flow determination. This filter has a time constant in the range of 0.25 to 0.5 sec.

Additional model verification of the jet pump model is given in NEDO-10802 Amendment 2 where the jet pump model is compared to drive flow oscillations in Figure 1 and a drive flow trip similar to the plant observed pump trips in Figures 2 and 3. These characteristics show the jet pump modeling represents the behavior of the system in both the large transients and the transfer function form.

Equations 4-67 through 4-69 are based on the fact that, during transient and normal operation, the flow in the recirculation system is substantially subcooled. Under normal full power operation, the recirculation system is 10 to 20 Btu/lbm subcooled. An increase in system pressure increases the liquid saturation enthalpy even further. An examination of fluid properties from the 1967 ASME Steam Tables shows that liquids subcooled by this amount are only compressible to 0.3% for a 200 psi pressure change. Such compressibility has been ignored in both the mass and energy balance equations. Further, as the flows mix upon entering the downcomer, the enthalpy change is also due to pressure effects. The change in enthalpy due to 200 psi pressure

change is less than 0.1%. This has also been neglected in the energy balance equations. Note, however, that flow effects for transport along flow channels has been incorporated in Equations 4-56 through 4-64.

The above compressibility arguments also hold in the jet pump mixing region. Since this is the case, the influence on the momentum inertia in the jet pump throat and mixing section due to compressibility is negligible. Further, the recirculation flow is incompressible in the downcomer, drive loop, lower plenum and jet pump diffuser. For this reason, the entire fluid in the recirculation loop must be accelerated enmass due to system transient effects. This paves the way for the integral momentum recirculation system models of ODYN. In this regard, the inertial effects of the jet pump mixing region are taken into account in term identified as \bar{I}_{dif}/A_{dif} . Further accounting for the momentum effects in the jet pump throat would duplicate these inertial terms in the ODYN model and, therefore, be inconsistent with the current formulation. For this reason, the inertial terms (i.e., the transient effects) have been left out of Equations 4-84 through 4-91.

QUESTION 23

Present a figure showing the non-jet pump recirculation system. Present experimental verification for representation of the system.

RESPONSE

The non-jet pump recirculation system description has been expanded and a figure included in Section 4. Experimental verification of the non-jet pump model system is provided in NEDO-10802, Figures 4-13 through 4-15. The data and model comparison is for Oyster Creek Plant startup pump trip transients involving single and multiple pump trips. Generally, very good agreement is demonstrated in the core flow comparisons between data and calculation.

QUESTION 24

The momentum balance equations such as Equation 4-83 describing the recirculation flow model contain terms for mechanical energy on the right side and a term for momentum balance on the left side. In addition, the change of direction of the velocity vector and the forces from the walls are not considered. Justify the use of the equation both in steady-state and transient analyses. Describe how the K values are determined. Provide a sensitivity study using different K values in a turbine trip without bypass transient in a typical BWR/4. Justify the selection of K values and provide a comparison with available experiment data.

RESPONSE

Generally, the geometry of the downcomer region is as shown in Figure 4-7 of the One-Dimensional Core Transient Model. The regions from the bulkwater section into the bulkwater, the jet-pump suction and finally down into the recirculation loop intake can be represented as a series of different flow area channels, where flow is essentially parallel to the axis with local effects due to area changes and pressure forces past internal structural bodies and channel walls within the recirculation flow. Local and wall forces in these types of sections can be represented by viscous loss effects. Because of the turbulent flow in these regions, the viscous loss effects are normally given by flow-squared terms in the equations. This form of the equations for varying area flow channels can be obtained from R. B. Bird, W. E. Stewart and E. N. Lightfoot, "Transport Phenomena," Chapters 6 and 7, John Wiley & Sons, 1960. This form of the momentum equations has been applied consistently throughout the recirculation system. By insuring the system pressure losses and flows are consistent with steady-state calculations, it is possible to determine the loss coefficients consistent with steady-state operation. The K values are determined by the initialization process described in Question 6.

Sensitivities of the recirculation parameters actually extend beyond the loss coefficients. It is possible to recognize these parameters as part of the

recirculation system: inertial parameters (L/A), areas of jet pump components, diffuser loss coefficient, suction loss coefficient, nozzle loss coefficient, m-ratio, core loss coefficient, lower plenum loss coefficient and bulkwater loss coefficient. The impact of varying these parameters is shown in Table 24-1.

There has been no known measurement of operating plant loss coefficients for the downcomer. The jet pump efficiencies have been determined experimentally so that flow and pressure ratios are well-known quantities. Uncertainty in the plant and suction to drive flow ratio is $\leq 5.6\%$. Uncertainties in system loss coefficients, based on engineering evaluation and measurements of jet pumps for flow calibration, are $< 20\%$. The flow areas and jet pump lengths are manufactured to close engineering tolerances so that these parameters vary in a negligibly small manner. The impact of this uncertainty is for all practical purposes zero.

The following have negligible impact on $\Delta\text{CPR}/\text{ICPR}$ for expected order of magnitude variations: (1) drive flow L/A; (2) jet pump areas; (3) nozzle loss coefficients; and (4) lower plenum and bulkwater loss coefficient. Reasonable variations of these parameters did not result in calculated $\Delta\text{CPR}/\text{ICPR}$ impact.

Table 24-1
RECIRCULATION SYSTEM PARAMETER SENSITIVITY

<u>Parameter</u>	<u>Increment</u>	<u>Uncertainty Effect on $\Delta\text{CPR}/\text{ICPR}$</u>
1- Recirculation System L/A	1- Increase by Factor of 2	1- ± 0.002
2- Kdiff	2- Reduced 10%	2- ± 0.001
3- Total jet pump pressure loss	3- Decreased 20%	3- ± 0.01
4- Core Loss Coefficients	4- Increase ΔP 1.5 psi	4- ± 0.0045

NEDO-24154-A

QUESTION 25

Indicate all quantities described in Equations 4-85 through 4-91 in a figure.

RESPONSE

The appropriate quantities have been defined in the revised version of Section 4.

Q25-1/Q25-2

NEDO-24154-A

QUESTION 26

On a non-jet pump recirculation system, provide a figure and define all terms in Equations 4-92 through 4-95 in the figure.

RESPONSE

A non-jet pump recirculation system figure has been provided in the revised version of Section 4.

Q26-1/Q26-2

NEDO-24154-A

QUESTION 27

Correct Figure 6-1.

RESPONSE

This figure has been corrected in the revised version of Section 6.

Q27-1/Q27-2

QUESTION 28

Provide the values of V_{gj} , C_o , F_1 , F_2 , K_{loc} , f , ϕ , T_{wi} , and x_c . Provide the analytical expressions, experimental data and discuss the conservatism of the selected values.

These parameters are important in determining the void fraction and the void collapse during a pressure pulse transient. Provide sensitivity studies for turbine trip without bypass transient for a typical BWR/4 using the values based on either experimental data or analytical considerations. The values chosen should be: (1) nominal; (2) upper bound; and (3) lower bound. The sensitivity studies should include ΔCPR calculations and uncertainties associated with the above parameters should be assessed in terms of ΔCPR .

RESPONSE

The response to Question 28 contains GE Company proprietary information and is documented separately in Volume III of this report.

QUESTION 29

Provide the basis for selection of β_1 and β_2 and discuss the stability and accuracy of the solution.

RESPONSE

The values of β_1 and β_2 currently used in the model are 0.0 and 0.1, respectively. These values were chosen by trial and error. The most accurate result is obtained when both β_1 and β_2 are equal to zero. Hence, the smallest value of β_1 and β_2 needed to achieve numerical stability were selected. The practice of using $\beta_2 = 0.1$ has yielded numerically stable results with a negligible impact on numerical accuracy.

NEDO-24154-A

QUESTION 30

The report contains numerous typographical errors. Some of the symbols are not defined. Correct the errors, define the symbols and present figures showing these symbols where appropriate.

RESPONSE

A review of the model document has been conducted and a revised version has been constructed which will eliminate the majority of the typographical errors.

Q30-1/Q30-2

QUESTION 31

In Equation 5-3, the quantity Γ_b is taken as a constant at the top and bottom of the active core length. The equation accounts for the time variation of the diffusion coefficient. Describe the effect of varying moderator conditions during a transient on the constant Γ_b .

RESPONSE

The boundary condition coefficient Γ will change during a pressurization transient, but this change has a negligible effect on the outcome of the transient. In a full power turbine trip without bypass transient, the average water density at the top of the core changes by about 12% over the first 1.2 sec of the transient. Under conditions where Γ is held constant, the effective value Γ given by:

$$\Gamma = \Gamma_b \left(1 - \frac{D(t)}{D(t=0)} \right)$$

changes from 0 to about 0.1 Γ_b over this 12% range of densities. The parameter Γ_b is generally less than 0.5, so that the total numerical change in Γ is quite small. To verify the magnitude of this effect, a Peach Bottom transient was run where Γ_b was forced to change by a factor of 2 for a 12% density change. This variation is about an order of magnitude more than the variation assumed in the three-dimensional BWR core simulator. The results of this calculation showed a negligibly small effect on the total neutron flux (less than 0.01%). Therefore, the assumption of a constant Γ_0 is adequate for transient applications.

QUESTION 32

Provide the steps leading from Equation 5-6 to Equation 5-9 using the assumption that $C_1(Z,t)$ varies as $\exp(-\lambda_1 t)$.

RESPONSE

Equation 5-9 cannot be derived using the assumption stated in the text. The statement should read: " $C_1(Z,t)e^{-\lambda_1 t}$ varies linearly from t_k to t_{k+1} ". This error has been corrected in the revised text (Reference 2).

QUESTION 33

Provide the steps leading from the left-hand side of Equation 5-14 to the right-hand side of the equation for the assumed behavior of the flux after a cross section change.

RESPONSE

The flux is assumed to behave as $e^{-V\Sigma t}$ after a cross-section change. We also know that $\phi(t) = \phi_k$ at t_k and ϕ_{k+1} at t_{k+1} . Therefore, for $t_k < t < t_{k+1}$

$$\begin{aligned} \phi(t) = & \phi_k \frac{\left(1 - e^{-V\Sigma (t_{k+1} - t)} \right)}{\left(1 - e^{-V\Sigma \Delta t_k} \right)} \\ & + \phi_{k+1} \frac{\left(1 - e^{-V\Sigma (t - t_k)} \right)}{\left(1 - e^{-V\Sigma \Delta t_k} \right)}. \end{aligned} \quad (33-1)$$

The integral

$$\frac{1}{\Delta t_k} \int_{t_k}^{t_{k+1}} \phi(t) dt$$

is evaluated by substituting Equation 33-1 into the integral expression giving:

$$\begin{aligned} \frac{1}{\Delta t_k} \int_{t_k}^{t_{k+1}} \phi(t) dt = & \left(\frac{1}{1 - e^{-V\Sigma \Delta t_k}} - \frac{1}{V\Sigma \Delta t_k} \right) \phi_k \\ & + \left(\frac{1}{V\Sigma \Delta t_k} - \frac{e^{-V\Sigma \Delta t_k}}{1 - e^{-V\Sigma \Delta t_k}} \right) \phi_{k+1} \end{aligned}$$

NEDO-24154-A

QUESTION 34

In deriving the spatial equations (e.g., Equation 5-22), has h been assumed to be a constant in spite of the definition for h given by Equation 5-20?

RESPONSE

The mesh spacing is assumed to be constant in the derivation and the model.

Q34-1/Q34-2

QUESTION 35

The definition for the flux-to-power conversion factor given by Equation 5-32 is not the same as that given by Equation A-87. Explain the difference in the two equations, and state which equation for \bar{F} is actually used for the model.

RESPONSE

Equation 5-32 is used in the model and can be derived from Equation A-87 by making the assumptions expressed in Equations 5-33 and 5-34. These assumptions are made to simplify the numerical calculations and the size of the data file. The approximation was checked against the more exact definition and the resulting power distributions were within 0.5% of each other.

QUESTION 36

Describe and provide results of comparisons, obtained from steady-state calculations, using the one-dimensional core transient model described in the report and the three-dimensional BWR Core Simulator. A wide range of core conditions (flow, pressure, temperature, power level, control rod distributions) and times in cycles including different fuel cycles should be considered.

RESPONSE

The collapsing scheme employed in the generation of nuclear parameters ensures that the steady-state axial power shape and core eigenvalue are identical to the three-dimensional results. The model one-dimensional equation is given by Equation A-2. The steady-state version of this equation is:

$$\frac{\partial}{\partial Z} \bar{D} \frac{\partial \phi_1}{\partial Z} - (\overline{DB}_r^2 - \bar{F} + \bar{E}_r) \phi_1 = 0$$

In the steady state:

$$\bar{F} - \bar{E}_r = \int_x \int_y dx dy \frac{\frac{1}{k_0} \left(k_{\infty}^* \text{GDOP} (\sqrt{T} - \sqrt{T_0}) - 1 \right)}{M^2 - A_{\infty}/k_0} \phi_1^2$$

However, we have defined \overline{DB}_r^2 such that

$$\overline{DB}_r^2 \equiv \int_x \int_y DB^2 \phi_1^2 dx dy = \int_x \int_y \frac{\frac{1}{k_0} \left(k_{\infty}^* \text{GDOP} (\sqrt{T} - \sqrt{T_0}) - 1 \right)}{M^2 - A_{\infty}/k_0}$$

Therefore,

$$\frac{\partial}{\partial Z} \bar{D} \frac{\partial \phi_1}{\partial Z} = 0 \text{ at } t = 0.$$

Also, from Equation A-99, $d\phi_1/dz = 0$ at the problem boundaries at $t = 0$.

Therefore, $\phi = \text{constant}$ in space at $t = 0$.

The flux to power conversion factor, $f(z,t)$ is computed from Equation A-87:

$$f(z,t) = k_0 \frac{\overline{k\bar{\Sigma}}}{k_0} \left[1 + \overline{CDOP} (\sqrt{T} - \sqrt{T_0}) - \overline{\Sigma} + \overline{\Sigma}_r \right]$$

which, when used with the appropriate definitions, reduces to:

$$f(z,t) = \frac{\int_x \int_y \phi \frac{1}{Y} \left\{ \frac{1}{k_0} \left[\overline{k^*} - \overline{CDOP} (\sqrt{T} - \sqrt{T_0}) \right] - \overline{\Sigma} + \overline{\Sigma}_r \right\} dx dy}{\int_x \int_y dx dy}$$

The expression inside the brackets is equal to the fission rate from Equations A-4 and A-5:

$$f(z,t) = \frac{\int_x \int_y \phi \frac{1}{Y} \left(\gamma_1 \overline{\Sigma}_{f1} + \gamma_2 \overline{\Sigma}_{f2} \frac{\phi_2}{\phi_1} + \gamma_3 \overline{\Sigma}_{f3} \frac{\phi_3}{\phi_1} \right) dx dy}{\int_x \int_y dx dy}$$

Table 36-1 contains a list of some of the plants and conditions analyzed with the one-dimensional kinetics model. All of these analyses showed the one-dimensional axial power to be within 0.5% of the three-dimensional average axial power.

NEDO-24154-A

Table 36-1
LIST OF PLANTS AND REACTOR CONDITIONS ANALYZED
WITH 1-D TRANSIENT MODEL

<u>Plant</u>	<u>BWR Product Line</u>	<u>Power Level</u>	<u>Number of Fuel Bundles</u>	<u>Exposure Condition</u>
Plant A	BWR/4	48%	764	EOC2
	BWR/4	62	764	
	BWR/4	69	764	
	BWR/4	104	764	
Plant B	BWR/4	77	228	EOC4
Plant D	BWR/4	104	368	EOC3
	BWR/4	104	368	MidCycle 3
	BWR/4	104		EOC4
Plant E	BWR/4	104	560	EOC2
	BWR/4	104	560	MidCycle 2
Plant F	BWR/5	104	764	EOC1
Plant C	BWR/5	104	560	EOC1
Plant G	BWR/3	104	484	EOC1
	BWR/4	104	560	

Q36-3/Q36-4

QUESTION 37

Discuss and provide results demonstrating the adequacy of a one-group cored model for performing spatial transient calculations.

RESPONSE

The one-group kinetics model employed in the one-dimensional transient model employs collapsed one-dimensional cross sections obtained from three-dimensional flux solutions and infinite medium lattice cross sections. These cross sections will change throughout the transient, depending on the void fraction, fuel temperature, and control at any one time. Use of the one group method implies an instantaneous change in neutron spectrum as the void and control systems change. In order to illustrate the time constants for these spectral changes, we write the three group kinetics equations as:

$$\frac{1}{v_1} \dot{\phi}_1 = \nabla \cdot D_1 \nabla \phi_1 - \Sigma_{R1} \phi_1 + \frac{(1-\beta)}{k} (v_1 \Sigma_{f1} \phi_1 + v_2 \Sigma_{f2} \phi_2 + v_3 \Sigma_{f3} \phi_3) \quad (37-1)$$

$$\frac{1}{v_2} \dot{\phi}_2 = \nabla \cdot D_2 \nabla \phi_2 - \Sigma_{R2} \phi_2 + \Sigma_{S21} \phi_1 \quad (37-2)$$

$$\frac{1}{v_3} \dot{\phi}_3 = \nabla \cdot D_3 \nabla \phi_3 - \Sigma_{R3} \phi_3 + \Sigma_{S22} \phi_2 \quad (37-3)$$

$$C_1 = -\lambda_1 C_1 + \frac{\beta_1}{k} (v_1 \Sigma_{f1} \phi_1 + v_2 \Sigma_{f2} \phi_2 + v_3 \Sigma_{f3} \phi_3) \quad (37-4)$$

where the above equations are a generalization for the time-dependent case of the three-dimensional BWR simulator equations. The notation is the same as used in the BWR simulator report B-11 with C_1 representing the concentration of precursor group 1, β_1 the delayed neutron fraction for precursor group 1, and v_1 the average neutron speed for energy group 1. We express the leakage in groups 2 and 3 in terms of a Buckling expression:

$$-\nabla \cdot D_g \nabla \phi_g = D_g B_g^2 \phi_g \quad (37-5)$$

where

$$g = 2, 3.$$

Also, we define two new variables

$$R_2 \equiv \frac{\phi_2}{\phi_1}, \quad (37-6)$$

$$R_3 \equiv \frac{\phi_3}{\phi_1}. \quad (37-7)$$

The three neutron flux equations can be expressed as equations in ϕ_1 , R_2 and R_3 :

$$\begin{aligned} \frac{1}{v_1} \dot{\phi}_1 &= \nabla \cdot D \nabla \phi_1 - \Sigma_{R1} \phi_1 \\ &+ \frac{(1-\beta)}{k} (v_1 \Sigma_{f1} + v_2 \Sigma_{f2} R_2 + v_3 \Sigma_{f3} R_3) \phi_1 \\ &+ \Sigma_i \lambda_i C_i \end{aligned} \quad (37-8)$$

$$\frac{1}{v_2} \dot{R}_2 + \frac{1}{v_2} \left(\frac{\dot{\phi}_1}{\phi_1} \right) R_2 = -D_2 B_2^2 R_2 - \Sigma_{R2} R_2 + \Sigma_{S1} \quad (37-9)$$

$$\frac{1}{v_3} \dot{R}_3 + \frac{1}{v_3} \left(\frac{\dot{\phi}_1}{\phi_1} \right) R_3 = -D_3 B_3^2 R_3 - \Sigma_{R3} R_3 + \Sigma_{S2} R_2 \quad (37-10)$$

In the steady state, R_2 and R_3 are given by:

$$R_2 = R_2^\infty = \frac{\Gamma_{Sl1}}{\Gamma_{R2} (1 + M_2^2 B_2^2)} \quad (37-11)$$

$$R_3 = R_3^\infty = \frac{\Gamma_{Sl1} \Gamma_{Sl2}}{\Gamma_{R2} \Gamma_{R3} (1 + M_2^2 B_2^2) (1 + M_3^2 B_3^2)} \quad (37-12)$$

Equations 37-9 and 37-10 can be expressed as:

$$R_2 \left(1 + \frac{1}{v_2 \Gamma_{Sl1}} R_2^\infty \frac{\dot{\phi}_1}{\phi_1} \right) = R_2^\infty \left(1 - \frac{\dot{R}_2}{v_2 \Gamma_{Sl1}} \right) \quad (37-13)$$

$$R_3 \left(1 + \frac{R_{23}^\infty}{v_3 \Gamma_{Sl3}} \frac{\dot{\phi}_1}{\phi_1} \right) = R_{23}^\infty \left(R_2 - \frac{\dot{R}_3}{v_3 \Gamma_{Sl2}} \right) \quad (37-14)$$

where

$$R_{23}^\infty = \frac{\Gamma_{Sl2}}{\Gamma_{R3} (1 + M_3^2 B_3^2)} \quad (37-15)$$

Note here that the time constants for changes in R_2 and R_3 are $1/v_2 \Gamma_{Sl2}$ and $1/v_3 \Gamma_{Sl3}$, respectively. Substituting values typical for a BWR:

$$\frac{1}{v_2 \Gamma_{Sl2}} = 8 \times 10^{-6} \text{ sec} \quad (37-16)$$

$$\frac{1}{v_3 \Gamma_{Sl2}} = 8.3 \times 10^{-5} \text{ sec} \quad (37-17)$$

The time constants are several orders of magnitude less than a typical time step of 0.01 sec in the transient solution. Since an implicit flux integration is used,

a "prompt jump" approximation for the flux ratio can be used with good accuracy and the spectral derivative terms can be neglected. Also, examination of a large number of pressurization transient results for typical BWR's shows that a maximum value for $\dot{\phi}_1/\phi_1$ is usually around 10 sec^{-1} and never goes above 20 sec^{-1} . The quantities R_2^∞ and R_{23}^∞ are about 1.0 or 2.0; hence, R_2 and R_3 can be approximated as:

$$R_2 = R_2^\infty \left(1 - \frac{R_2^\infty}{v_2 \Sigma_{sL1}} \frac{\dot{\phi}_1}{\phi_1} \right) \quad (37-18)$$

$$R_3 = R_3^\infty \left(1 - \left(\frac{R_2^\infty}{v_2 \Sigma_{sL1}} + \frac{R_{23}^\infty}{v_3 \Sigma_{sL2}} \right) \frac{\dot{\phi}_1}{\phi_1} \right) \quad (37-19)$$

In the current model, the terms proportional to $\dot{\phi}_1/\phi_1$ are also neglected, giving rise to Equation A-5 in the appendix to the model report. For $\dot{\phi}_1/\phi_1 = 15$, the error in R_3 is still less than 0.3%. Further, it is conservative to neglect these terms. However, the $\dot{\phi}_1/\phi_1$ terms can be retained and substituted into Equation 37-8 to obtain:

$$\begin{aligned} \frac{1}{V} \dot{\phi}_1 = & \nabla \cdot D_1 \nabla \phi_1 - \Sigma_{R1} \phi_1 \\ & + \frac{(1-\beta)}{1} (v_1 \Sigma_{f1} + v_2 \Sigma_{f2} R_2^\infty + v_3 \Sigma_{f3} R_3^\infty) \phi_1 + \Sigma_i \lambda_i C_i \end{aligned} \quad (37-20)$$

resulting in a one-group equation with an effective neutron speed given by:

$$\frac{1}{v} = \frac{1}{v_1} + \frac{1}{v_2} - \frac{(v_2 \Sigma_{f2} R_2^\infty + v_3 \Sigma_{f3} R_3^\infty)}{\Sigma_{R2} (1 + M_2^2 B_2^2)} + \frac{1}{v_3} \frac{v_3 \Sigma_{f3} R_3^\infty}{\Sigma_{R3} (1 + M_3^2 B_3^2)} \quad (37-21)$$

In summary, BWR turbine trip transients can be adequately represented by a one-group, prompt jump approximation and the time constants for spectral change are much smaller than the time scale of pressurization transient calculations.

QUESTION 38

Discuss sensitivities in the cross sections as a function of the reference moderator density fuel temperature and control fraction. How are uncertainties such as these treated in the ODYN code?

RESPONSE

Cross-section uncertainties manifest themselves in transient calculations as biases and uncertainties in void reactivity coefficient, Doppler reactivity coefficient and scram strength. One should evaluate these uncertainties by comparing GE lattice and Monte Carlo calculations. The cross-section data used in the Monte Carlo studies come from the standard ENDFB-4 libraries. The Monte Carlo reactivity calculations have, in turn, been compared to critical experiments representative of BWR configurations.

(1) Moderator Density or Void Reactivity Effects

The uncertainty and bias in moderator density reactivity effects have been estimated by comparing $d k_{\infty}/d\alpha$ values calculated by the GE lattice code with a simulated experimental $d k_{\infty}/d\alpha$. Monte Carlo vs critical experiment comparisons have been used to simulate the experimental values.

The GE Monte Carlo model has been used to simulate a group of five critical experiments. The comparisons are summarized in Table 38-1. These comparisons yield a weighted mean difference between the Monte Carlo criticality and experiment of:

$$\Delta k^{MC \rightarrow Exp} \equiv [k^{Exp} - k^{MC}] = 0.0044 \pm 0.0013 \quad (38-1)$$

This bias and uncertainty is applied to the Monte Carlo estimates at all void fractions and is assumed to be independent.

The derivative of the lattice k_{∞} with respect to void fraction α ($d k_{\infty}/d\alpha$) was evaluated by first calculating the lattice at three void fractions, $\alpha = 0$, $\alpha = 0.4$ and $\alpha = 0.7$. These three values were then used to generate a quadratic fit in void fraction; i.e.,

$$k_{\infty}(\alpha) = k_{\infty}(0) \frac{(\alpha - 0.4)(\alpha - 0.7)}{0.28} - k_{\infty}(0.4) \frac{\alpha(\alpha - 0.7)}{0.12} + k_{\infty}(0.7) \frac{\alpha(\alpha - 0.4)}{0.21} \quad (38-2)$$

This expression can be differentiated to obtain:

$$\frac{d k_{\infty}}{d\alpha} = k_{\infty}(0) \frac{(\alpha - 0.55)}{0.14} - k_{\infty}(0.4) \frac{(\alpha - 0.35)}{0.06} + k_{\infty}(0.7) \frac{(\alpha - 0.2)}{0.105} \quad (38-3)$$

The variance of $d k_{\infty}/d\alpha$ can be evaluated by assuming $k_{\infty}(0)$, $k_{\infty}(0.4)$ and $k_{\infty}(0.7)$ are independent. This yields:

$$\text{Var} \left(\frac{d k_{\infty}}{d\alpha} \right) = \left(\frac{\alpha - 0.55}{0.14} \right)^2 \text{Var} (k_{\infty}(0)) + \left(\frac{\alpha - 0.35}{0.06} \right)^2 \text{Var} (k_{\infty}(0.4)) + \left(\frac{\alpha - 0.2}{0.105} \right)^2 \text{Var} (k_{\infty}(0.7)) \quad (38-4)$$

The variances of the individual k_{∞} values can be determined from the Monte Carlo variances. The $d k_{\infty}/d\alpha$ values are compared for $\alpha = 0.4$ in Table 38-2 for three lattice types typically used in existing BWR's and requisition cores. The weighted mean approach is used to determine the average bias and variance between the Monte Carlo estimates and the lattice code estimates:

$$\text{mean} \left(\frac{d k_{\infty}^{\text{LC}}}{d\alpha} - \frac{d k_{\infty}^{\text{MC}}}{d\alpha} \right) = 0.081 \times 10^{-2}$$

$$\text{Var} \left(\frac{d k_{\infty}^{\text{LC}}}{d\alpha} - \frac{d k_{\infty}^{\text{MC}}}{d\alpha} \right) = 1.18 \times 10^{-5}$$

The final bias and uncertainty in the void reactivity coefficient can be determined by summing the lattice - Monte Carlo bias and the Monte Carlo experiment bias:

$$\frac{d k_{\infty}^{\text{Exp}}}{d\alpha} = \frac{d k_{\infty}^{\text{LC}}}{d\alpha} + \left(\frac{d k_{\infty}^{\text{MC}}}{d\alpha} - \frac{d k_{\infty}^{\text{LC}}}{d\alpha} \right) + \left(\frac{d k_{\infty}^{\text{Exp}}}{d\alpha} - \frac{d k_{\infty}^{\text{MC}}}{d\alpha} \right). \quad (38-5)$$

The second term on the right-hand side involves both a bias and uncertainty and the third term is assumed to have only an uncertainty. The variance in the lattice code to experimental bias is given by:

$$\begin{aligned} \text{Var} \left[\frac{d k_{\infty}^{\text{Exp}}}{d\alpha} - \frac{d k_{\infty}^{\text{LC}}}{d\alpha} \right] &= \text{Var} \left[\frac{d k_{\infty}^{\text{MC}}}{d\alpha} - \frac{d k_{\infty}^{\text{LC}}}{d\alpha} \right] \\ &+ \text{Var} \left[\frac{d k_{\infty}^{\text{Exp}}}{d\alpha} - \frac{d k_{\infty}^{\text{MC}}}{d\alpha} \right]. \end{aligned} \quad (38-6)$$

The variance in the Monte Carlo-experiment bias in $d k_{\infty}/d\alpha$ can be evaluated by substituting the variance obtained from the critical experiments $[\Delta (k^{\text{MC}} - k^{\text{Exp}})]$ into Equation 38-4 for $\alpha = 0.4$. This yields:

$$\text{Var} \left(\frac{d k_{\infty}^{\text{Exp}}}{d\alpha} - \frac{d k_{\infty}^{\text{MC}}}{d\alpha} \right) = 9.68 \times 10^{-6}$$

Therefore:

$$\text{Mean} \left[\frac{d k_{\infty}^{\text{LC}}}{d\alpha} - \frac{d k_{\infty}^{\text{Exp}}}{d\alpha} \right] = +0.081 \times 10^{-2}$$

$$\text{Var} \left[\frac{d k_{\infty}^{\text{LC}}}{d\alpha} - \frac{d k_{\infty}^{\text{Exp}}}{d\alpha} \right] = 2.15 \times 10^{-5}$$

$$\sigma = \sqrt{\text{Var}} = 0.464 \times 10^{-2}$$

From Table 38-2, the values for $d k_{\infty}/d\alpha$ range from 6.6×10^{-2} to 9.2×10^{-2} . Hence, the lattice code bias is about 1% of the average value and the 1 σ uncertainty in this bias about $\pm 6\%$.

The ODYN code uses the infinite lattice data to calculate changes in cross sections with moderator density. As the bias in the infinite lattice data with regard to void coefficient is considered negligible, the ODYN treatment of moderator density effects is considered nominal. There is no treatment of uncertainty in the cross sections due to moderator density in ODYN.

(2) Fuel Temperature

The infinite lattice cross section dependence on fuel temperature is handled by computing a Doppler reactivity decrement, B^{-12} represented by the following expression:

$$\left(\frac{\Delta k}{k} \right)_{\text{Doppler}} = \text{CDOP} (\sqrt{T} - \sqrt{T_0})$$

where

- CDOP = constant of proportionality;
- T = absolute fuel temperature; and
- T₀ = reference fuel temperature.

(3) Control Strength

Calculated results based on the Doppler model have been normalized to Hellstrand's experimental data^{B-14} and this normalized model, when compared to experimental transients performed on the SPERT I^{B-15} and SPERT III^{B-16} reactors, has demonstrated very good agreements. Therefore, the infinite lattice Doppler treatment is nominal. There is insufficient data available to calculate the uncertainty in this treatment of cross-section dependence on fuel temperature; however, based on the two experimental comparisons, a 4% (1 σ) uncertainty is considered a conservative estimate.

The one-dimensional model code employs the nominal CDOP values calculated by the infinite lattice code. Both moderator density and exposure dependence of CDOP are considered. There is no treatment of Doppler reactivity uncertainty in ODYN.

We have again chosen to evaluate possible lattice model uncertainties by comparing lattice control strengths with Monte Carlo results. Here there is a limited amount of data, so a statistical analysis is not possible. Two lattice configurations have been examined at two different void fractions. The results are summarized in Table 38-3. In assigning an uncertainty, we have chosen the largest nonconservative control strength bias, which occurs in lattice A at a 0.40 void fraction. This results in a $\pm 4\%$ uncertainty in control strength.

The ODYN code uses the rod strength predicted by the infinite lattice code. There is no treatment of uncertainty in the cross-dependence on control fraction in the ODYN code.

CDOP is treated as a function of both moderator density and exposure. Design calculations are performed using the standard lattice design code^{B-13} to determine CDOP values at various moderator density and exposure conditions. The functional dependence of CDOP is based on these calculations.

The uncertainty in the infinite lattice cross sections as a function of control fraction is evaluated by considering the control strength Δk_{rod} in terms of the change in k_{∞} ; i.e.,

$$\Delta k_{rod} = k_{\infty}^{uncontrolled} - k_{\infty}^{controlled}$$

Table 38-1

SUMMARY OF MONTE CARLO CALCULATIONS FOR CRITICAL EXPERIMENTS

<u>Critical Experiment*</u>	<u>Monte Carlo Eigenvalue</u>
B&W UO ₂	0.9950 ± 0.0021
BWR Critical (Boron Curtains)	0.9974 ± 0.0024
BWR Critical (Gd rods Core I)	0.9952 ± 0.00096
BWR Critical (Gd rods Core II)	0.9968 ± 0.00106
BWR Critical (Gd rods Core III)	0.9948 ± 0.00099

$$\text{Weighted Mean} = \frac{\sum_i k_i / \sigma_i^2}{\sum_i 1 / \sigma_i^2} = 0.9956 \Delta k^{MC \rightarrow Exp}$$

$$\text{Variance of Weighted Mean} = \frac{1}{\sum_i 1 / \sigma_i^2} = 2.944 \times 10^{-7}$$

$$\text{Sample variance} = \frac{1}{N-1} \sum_i (\Delta k_i - \Delta k)^2 = 1.461 \times 10^{-6}$$

$$\text{Total variance} = (0.2944 + 1.461) \times 10^{-6} = 1.756 \times 10^{-6}$$

$$\sigma = 0.00133$$

$$\Delta k^{MC \rightarrow Exp} = 0.0044 \pm 0.00133$$

*The critical experiment analysis is documented further in "ENDF/B-IV Benchmark Analyses with Full Spectrum Three-Dimensional Monte Carlo Models," C. M. Kang and E. C. Hansen, Trans Am. Nucl. Soc. 27, page 801, November 1977.

Table 38-2
 COMPARISON OF LATTICE PHYSICS CODE AND MONTE CARLO
 VOID COEFFICIENT VALUES

<u>Lattice Type</u>	<u>Lattice Code</u>	<u>Monte Carlo</u>	<u>Var</u>
A	-7.284×10^{-2}	-7.021×10^{-2}	2.034×10^{-5}
B	-9.187×10^{-2}	-9.221×10^{-2}	2.487×10^{-5}
C	-6.631×10^{-2}	-6.865×10^{-2}	0.8051×10^{-5}

$$\text{Weighted Mean} = \frac{\sum_1 \left(\frac{d k_{\infty}^{\text{LC}}}{d\alpha} - \frac{d k_{\infty}^{\text{MC}}}{d\alpha} \right)}{\sum_1 1/\sigma_1^2} = 0.0813 \times 10^{-2} = \frac{\Delta k^{\text{LC+MC}}}{d\alpha}$$

$$\text{Variance of Weighted Mean} = \frac{1}{\sum_1 1/\sigma_1^2} = \pm 4.682 \times 10^{-6}$$

$$\begin{aligned} \text{Sample variance} &= \frac{1}{N-1} \sum_1 \left(\Delta \left(\frac{d k_{\infty}}{d\alpha} \right)_1 - \Delta \left(\frac{dk}{d\alpha} \right) \right)^2 \\ &= 7.182 \times 10^{-6} \end{aligned}$$

$$\text{Total variance} = 1.186 \times 10^{-5} = \text{Var} \left(\frac{\Delta k^{\text{LC+MC}}}{d\alpha} \right)$$

Table 38-3
 COMPARISON OF LATTICE CODE AND MONTE CARLO
 CONTROL STRENGTH CALCULATIONS

		Δk_{rod}^{LC}	Δk_{rod}^{MC}	$(\Delta k_{kd}^{LC} - \Delta k_{kd}^{MC})$
Lattice A	0	0.2621	0.2607 ± 0.0032	+0.0014
Lattice B	0	0.2377	0.2411 ± 0.0038	-0.0033
Lattice A	0.4	0.3148	0.3060 ± 0.0031	+0.0088
Lattice B	0.4	0.2655	0.2763 ± 0.0031	-0.0108

QUESTION 39

Discuss the implications of using a radially averaged heat generation rate rather than a radially dependent heat generation rate. Discuss the conservatism of this assumption in the code. Is it conservative for calculation of the clad temperature? Quantify the effect of this assumption on ΔCPR .

RESPONSE

The radial power distribution within the fuel rod is not uniform (flat) in actual operation. The plutonium buildup and self-shielding of the fuel rods result in a radial power shape peaked quite sharply to the outside of the fuel pellet. Heat transfer from the inside of the pellet to the cladding occurs by diffusion through the fuel material, which is a time-dependent process where the longer the paths of diffusion result in longer traverse times. When power is peaked higher to the outside of the pellet where the average distance from the generation to edge of the pellet is less, the thermal time constant will be lower than in the uniform power production case because a larger portion of the power travels a shorter distance. A reduction in thermal time constant results in faster feedback of heat flux to the moderator-coolant which increases the void fraction, mitigating the pressurization transient to a degree dependent upon the outer radius peaking of the power in the rods. Hence, a uniform (flat) power distribution assumption inside the fuel pellet is conservative for pressurization transients from the power increase conditions. Since this effect is small and the pressurization transients are far from clad temperature limits in the ODYN calculations, the clad temperature impact is not important. Since this effect is conservatively incorporated in ODYN, no evaluation of ΔCPR is warranted.

QUESTION 40

Application of the Crank-Nicholson Method suffers complications when heat generation varies with position and time, when thermal properties vary (as ODYN assumes) and when nonlinear boundary conditions are used. Discuss any restriction on the gap conductances that can be input such that the solutions still remain valid. Radiative heat transfer becomes important in transient gap conductance. This would make h_{gap} highly nonlinear with time. Hence, discuss any restrictions in the calculational method or in input selection.

RESPONSE

The Crank-Nicholson Method suffers complications when time steps are too large relative to thermal time constants and changes of fuel properties occur faster than the time stepping. The BWR thermal time constant is in the range of 5-8 sec compared to 0.01 sec time steps taken in the calculation.* Such extensive time stepping will accommodate all the nonlinearity problems of the fuel behavior. On this basis, there have been no required restrictions on fuel gap conductance during transient calculations. It is also important to note that fuel gap conductance is discussed in Question 8. Since the fuel gap conductance is conservatively held constant in the transient calculations, heat transfer calculations proceed with no difficulties.

Radiation at operating conditions contributes less than 1% to the gap conductance. During power increase transients, the radiant heat transfer component increases because of the fuel temperature increases. This contributes more power to the moderator than assuming the gap conductance remains constant during the transient. Radiation, therefore, results in more moderator voiding, mitigating the pressurization transients somewhat. Since the ODYN heat transfer model ignores the radiant component of heat transfer transient changes, the ODYN calculations will be conservative during the pressurization transients and proceed more smoothly than if the radiant heat transfer effects were included.

* This is the same as the hydraulics time steps. Since the time is synchronized, this eliminates potential gap difficulties.

QUESTION 41

In the description on the control system, it is stated that the systems are simulated through digital logic. Also, the numerical values for response functions, as well as gains and time constants, must be defined for each plant design. Provide a discussion on how response functions, gains and time constants are established and verified for each design.

Furthermore, define what control system failures are evaluated with the code and define those control systems wherein operational credit is taken in the accident analysis. For these defined control systems, provide experimental data that justifies your control system models.

RESPONSE

The response functions, gains and time constants for control systems are determined based on detailed computer simulations of the BWR to achieve stable system control and design objectives. The numerical values are fine-tuned during on-site startup tests.

In the transient safety analysis, the control systems, except the assumed failures, are assumed to maintain normal operation unless specifically designated to the contrary in order to provide a realistic transient signature. Nominal inputs are used in ODYN calculations. The effects of these inputs on thermal and pressure margins, which are insignificant, are discussed in the response to Question 10, Enclosure 1.

Control system failures are evaluated and presented in Chapter 15 of PSAR, or FSAR, or reload licensing submittals. They are:

- (1) feedwater controller failure - maximum demand;
- (2) feedwater controller failure - minimum demand;
- (3) pressure regulator failure - open;
- (4) pressure regulator failure - closed; and
- (5) recirculation flow control failure - increasing flow.

NEDO-24154-A

The effects of single failures and operator errors on the above transients are also discussed and presented in Chapter 15 of PSAR or FSAR or reload licensing submittals. The worst plant control mode is assumed in the above transient simulations.

QUESTION 42

Figure 4-13 provides a block diagram of the valve flow control. Additional description of the control system is required to complete our review of the block diagram. In this regard, provide the following information:

- a. The basis of the gain and lead-lag ratio for the grid compensation function in processing of turbine governor signal.
- b. A description of all function generators used in the control model.
- c. The basis for the selection of the gains and time constants used in the master controller. Also, provide the basis for variations in the gains, if any, in the use of the model. Also provide this information for the flow controller and the flux controller.

RESPONSE

The block entitled, "Grid Compensation Function" in the block diagram (Figure 4-13) is a lead/lag function, the time constants of which are approximately the inverse of the lag/lead function in the pressure regulator. Its purpose is to give the load following loop lead effect to compensate for the lag effect inherent in the pressure regulator. Gain K_G is determined by calculation and verified experimentally both in the field and on the computer.

The control characteristics of valves including flow/position curves as furnished for each plant by the specific equipment reactor are simulated as accurately as reasonably possible. Then, mathematical function generators are devised/adjusted to linearize the steady-state gain curve for each control loop.

The numeric values are adjusted during on-site startup tests to ensure the achievement of stable control and design objectives.

In the transient safety analysis, nominal values are input to ODYN calculations. The effects of these inputs on transient thermal and pressure margins are insignificant and are discussed in the response to Question 10, Enclosure 1.

QUESTION 43

Figure 4-14 provides a block diagram of the motor-generator flow control system. Additional description of the control system is required in order for the staff to complete its review of the block diagram. In this regard, provide the following information:

- a. The basis for the selection of the gains used in the master controller and the speed controller.
- b. A description of the speed demand limits and of the function generator used in the control.

RESPONSE

The speed demand limiter at the output of the Master Control Loop M/A station is set as a function of what speed is necessary to cover the load following range of the automatic load following loop. The function generator in each speed loop is for the purpose of linearizing the steady-state gain characteristic of the fluid coupler.

The selection of the gains used in the master controller and the speed controller is based on detailed computer simulation in order to achieve stable flow control and meet design objectives for load following. The setting is adjusted and fine-tuned during on-site startup test program.

In transient safety analysis, manual flow control is assumed. Therefore, the numerical values of gains have little effect on the transient thermal and pressure margin. A more detailed discussion is presented in the response to Question 10, Enclosure 1.

QUESTION 44

Figure 4-15 provides a block diagram of the feedwater control. Additional description of the control system is required to complete review of the block diagram. In this regard, provide the following information:

- a. Further descriptions of the steam flow gain, the basis of its selection, and its relationship to the steady-state level, power, and steam separator performance.
- b. A description of how the transient response of the steam-driven feedwater pumps is simulated through the rise of the optional compensator.
- c. A basis for the selection of gains and the modeling used to represent the flow controller and the level controller.
- d. A description of the function generators and limits used in modeling the system.

RESPONSE

The gain K_{LS} can be adjusted such that steady-state water level can be automatically changed as a function of steam flow. The theory being that, in order to have a minimum carryunder at low power and minimum carryover at high power, the level should be varied several inches as a function of power level.

The steam-driven feedwater pump and turbine is represented by a third-order differential equation, consisting of a slightly underdamped quadratic represented by the two integrators and the gains K_V , and K_{V2} plus single time constant T_A . The title (optional compensator) for the function determined by K_A and T_A was ill chosen. All three terms of the turbine description generally fall between 0.5 and 1.0 sec and are obtained from the turbine vendor.

The other two "optional compensations" need mention. The K_1, T_1, T_2 function was a lead/lag unit added to inject phase lead to the turbine loops, when the turbine system was first synthesized. It is not used. Function K_2, T_3, T_4 is the lag/lead network which is used in the flow loop when the model represents a single/three-element feedwater control system. When a single/three-element system is used, level controller gains are set to zero and its input feeds directly to the summer showing "optional level setpoint."

When two-loop system is represented, K_2 is turned to zero.

NEDO-24154-A

As with the recirculation system, the attempt is made to represent the flow characteristics of each individual turbine pump or flow control/valve as per vendor specifications. Function generators are used to linearize the steady-state gain curves or at least to make the steady-state gain curves nearly identical for all flow actuators of a given system.

The selection of gains is based on detailed computer simulator in order to achieve stable feedwater control and meet design objectives of the feedwater control system. The gains are adjusted and fine-tuned during onsite startup program.

In transient safety analysis, the nominal specified inputs are used. The effects of these input values on the transient thermal and pressure margin are negligible as discussed in the response to Question 10, Enclosure 1.

QUESTION 45

Figure 4-16 provides a block diagram of the pressure regulator system. Additional description of the control system is required to complete review of the block diagram. In this regard, provide the following:

- a. A description of the modeling of the setpoint adjuster and of the controller that acts upon the pressure error signal. The description is to contain the basis for the gains and time constants used in the model and the selection of numerical values for them.
- b. A description of all nonlinearities presented in the model. The description is to contain the basis and verification of the numerical values selected for the model.

RESPONSE

Figure 4-16 represents a model of a typical BWR pressure regulation system for main steam turbine equipped with Mechanical Hydraulic Control (MHC). Turbine inlet pressure is regulated by a closed-loop feedback control system, through manipulation of the turbine admission valves or steam bypass valves, utilizing the sensed inlet pressure as the feedback signal. For normal operation, the turbine admission valves are designed to regulate steam pressure; however, whenever the steamflow demand exceeds that which can be passed by the turbine admission valves, the pressure control system demands the excess steamflow to be sent to the main condenser through the steam bypass valves. In addition, when the reactor is operating in the automatic load following mode, provisions are made within the pressure control system to allow temporary adjustments to the desired pressure setpoint by means of the setpoint adjuster to permit a faster steam flow response to changes in load demand, thereby utilizing a part of the stored energy capacity in the vessel. The pressure control system is designed to achieve the following design objectives:

1. Steady-State Performance. At steady-state plant operation, the pressure control system maintains primary steam pressure at a nearly constant value, to ensure optimum plant performance. Any limit cycles, or noise, in the system must be of sufficiently small magnitude to avoid premature wear of plant equipment, or compromise of plant operation.

2. Response to Operational Transients. A broad range of routine operational transients must be accommodated without reactor trip, by maintaining pressure within operational bounds or by minimizing pressure induced effects on other reactor systems. The pressure control system must provide responsive, stable performance to minimize vessel water level and neutron flux transients caused by plant normal-operation maneuvers (pressure setpoint changes, level setpoint changes, recirculation flow changes). The pressure control system shall also be designed for operation with other reactor control systems to avoid reactor trip after significant plant disturbances, such as: partial- or full-generator load rejections, loss of one feed-water pump, loss of one recirculation pump, inadvertent opening and closing of relief valves, and steam bypass and main turbine stop-control valve testing.

3. Response to Major Plant-Shutdown Transients. Events which induce reactor trip present significant transients during which the pressure control system must maintain pressure. These transients are characterized by large variations in vessel, steamflow, core thermal-power output, and sometimes recirculation flow, all of which affect vessel water level; hence, the pressure control must respond quickly to stabilize the system pressure and thus aid the feedwater/level control in maintaining water level. The pressure control must also be capable of controlling pressure during normal (main steam isolation valves open) reactor shutdown to control the reactor cooling rate.

4. Plant Startup/Heatup Operation. The pressure control system must provide for automatic control of the reactor system pressure within the bypass steamflow capacity during the plant startup and heatup. This shall permit independent control of reactor pressure and power, during reactor vessel heatup, by varying of steam bypass flow as the main turbine is brought up to speed and synchronized.

NEDO-24154-A

The pressure regulator shown in Figure 4-16 is a proportional plus lag-lead compensation. The proportional gain and lag-lead time constants are determined based upon transient simulations of the BWR to achieve stable pressure control and to achieve the design objectives stated above. The nonlinearities shown on Figure 4-16 are representations of inherent hardware characteristics (such as control value flow vs. value position), electronic functions generators to linearize control value flow to control value demand, hardware limiters and deadband.

The setpoint adjuster consists of a proportional gain plus a lag filter. It is switched into service only during automatic load-following operation. The proportional gain and the time constant are chosen for stable pressure operation such that a certain power change rate is achieved by manipulation of the reactor recirculation flow. On-site startup test participation by control system design engineers ensures that the gains and time constants are optimally tuned to achieve the stated design objectives.

The numerical values for the gain and time constants used in transient safety analysis are nominal specified values. The effect of these numeric values on thermal and pressure margins is insignificant as discussed in the response to Question 10, Enclosure 1.

QUESTION 46

In a discussion of the reactor safety system, the operation of a flux filter is presented. It is stated that the flux filter may be switched in or out of the high flux scram circuit. Provide the basis for the use of the flux filter in the system. Also, quantitatively, describe the time impact upon the trip of the safety system in the use of the filter in the most limiting flux event, and for the bypass of the filter. The flux filter is presented as a double lead-lag filter with the lead lag ratio less than one. Provide the basis for the selection of the lead-lag ratios.

RESPONSE

The use of a double lead/lag filter in the model is for flexibility of simulation. In the actual simulation of the high flux scram circuit only the natural system response delay is considered. That is, in the licensing application of the model for transient analysis, the flux filter simulation:

$$N_s = \frac{K_s (1 + T_2s) (1 + T_3s) N}{(1 + T_1s) (1 + T_4s)} \quad (1)$$

is converted to

$$N_s = \frac{N}{1 + T_4s} \quad (2)$$

by inputting the following:

$$K_s = 1.0$$

$$T_1 = T_2$$

$$T_3 = 0.0$$

NEDO-24154-A

and the input value for T_4 is the equipment specified maximum allowable APRM flux sensor time constant. This is to simulate the sensed neutron flux by relating the actual neutron flux through a sensor time constant. The use of this sensor time constant delays the scram initiation time by about a time interval equal to one time constant. This makes the simulation more realistic, and at the same time, more conservative.

QUESTION 47

Discuss the uncertainties in gains and time constants in control and protection systems.

RESPONSE

The uncertainties in the reactor protection system parameters are accounted for by using conservative maximum specification inputs to the ODYN licensing basis calculations. Specifically, the "safety limits" of the reactor protection system instrument setpoints and instrument characteristics are used. If there are no safety limits specified, the maximum allowable uncertainties specified for instrument setpoints or instrument characteristics are added to the nominal values specified. The uncertainties are added in such a way that it makes the simulated transients more severe from peak power and pressure consideration.

Uncertainties in control system have little effects on the transient thermal and pressure margins as discussed in the response to Question 10, Enclosure 1.

QUESTION 48

Discuss the uncertainties in the overall calculations due to heat loss.

RESPONSE 48

Heat losses during a transient are assumed to be negligibly small in the one-dimensional model. This assumption is conservative for peak pressure and flux calculations.

In order to estimate the magnitude of possible heat loss, a simple heat loss model was added to the BWR plant model. In this model, the vessel dome and intervals are assumed to be equal to the steam temperature in the steady state. During the pressurization transient, the saturation temperature of the steam will increase. The heat loss is assumed to be:

$$Q_{\text{loss}} = A_{\text{VI}} h (T_{\text{SAT}} - T_{\text{VI}})$$

where

A_{VI} = area of vessel and intervals exposed to steam;

T_{SAT} = saturation temperature of steam;

T_{VI} = temperature of vessel and intervals; and

h = heat transfer coefficient

This model was tested for the Peach Bottom turbine trip number 1 test conditions. The value of the heat transfer coefficient was varied to determine the effect on peak dome pressure. It was found that, for the Peach Bottom -1 turbine trip, a peak energy loss of 77 MW, or 5% of the initial thermal power, was required to reduce the peak pressure by 8 psi. Based on this large energy loss rate needed to sustain a small pressure loss, it has been concluded that heat loss effects have a negligibly small effect on peak pressure estimates.

QUESTION 49

The manner in which General Electric treats Doppler and void reactivity effects in preparing ODYN input is discussed in the report. However, the manner in which moderator temperature effects in the nonboiling portions of the moderator are included in the cross sections is not discussed. Results obtained by our consultants indicate that the moderator temperature effect is important and should be included in the calculations. State whether or not the moderator temperature effect is included in the ODYN calculations. Discuss the effect and provide quantitative results for the Peach Bottom Unit 2 turbine trip tests.

RESPONSE

In the one-dimensional model, cross sections are assumed to be only functions of the fuel temperature and moderator density. Moderator temperature effects on the neutron scattering law and thermal neutron spectrum are neglected. The reactivity effects of moderator temperature changes are illustrated in Table 49-1 where lattice calculations of reactivity changes due to changes in moderator temperature are tabulated for 0% void fraction and 40% void fraction.

During a typical pressurization transient, the change in moderator temperature is small. At the peak of the flux transient, the temperature change is less than 1°C in the subcooled region and less than 4°C in the saturated region. This amounts to a reactivity change of $2.2 \times 10^{-4} \Delta k$, a small percentage (2.7%) of the total void reactivity change. Since it is a negative reactivity component, it is conservative to neglect it. Further, its effect on the flux transient and ΔCPR is negligible.

Table 49-1
 REACTIVITY EFFECTS OF MODERATOR TEMPERATURE CHANGE
 (BOL LATTICE CONDITIONS)

<u>Void Fraction</u>	<u>Temperature Change</u>	<u>Reactivity Change</u>	<u>$\Delta k / \Delta T, (^{\circ}C)^{-1}$</u>
0%	+66°C	-0.0033	-0.5007×10^{-4}
40%	+14°C	-0.0007	-0.5000×10^{-4}

REPLIES TO NRC QUESTIONS
ON APPENDIX A

QUESTION 1

On page A-3 of the report, it is stated that Henry suggests that $\phi(z,t)$ be normalized according to Equation A-11. However, a perusal of Henry's book indicates that he normalized the quantity $\phi(z,t)/V$ - a number density. Therefore, discuss the consequences of the two different normalization procedures with respect to the derivations presented in Appendix A of the report.

RESPONSE

There are no consequences resulting from defining the one-dimensional neutron flux as done in Equation A-11. Henry notes (p. 300) that he uses the number density rather than the flux to conform to convention. And it is the convention to write point kinetics equations in terms of the neutron density. However, in Appendix A of Reference 1 a one-dimensional kinetics equation is being derived rather than point kinetics, and normally space-dependent kinetics equations are in terms of flux rather than number densities.

Since V is constant and only one energy group is being considered, Equation 7.3.1 of Henry's book can be cast in the same form as Equation A-11 of Appendix A.

Considering the above statement and collapsing only in the x and y direction, Equation 7.3.1 becomes:

$$T(z,t) = \int_x \int_y \omega(\bar{r}) \frac{1}{V} \phi(\bar{r},t) dx dy.$$

Since V is assumed constant, it can be pulled out of the integral.

Thus:

$$T(z,t) = \frac{1}{V} \int_x \int_y \omega(\bar{r}) \phi(\bar{r},t) dx dy.$$

Multiplying by v :

$$v T(z,t) = \phi(z,t) = \int_x \int_y \omega(\vec{r}) \phi(\vec{r},t) dx dy.$$

Note that the above equation is very similar to Equation A-11. The only difference is that in Appendix A the weighting function is assumed to be a function of space and time.

QUESTION 2

In Equation A-15 the first term is assumed to be negligible since $1/V$ is very small and ψ varies slowly with time. However, as control rods move during a scram, the shape function ψ surely must change. Therefore, discuss the effect of scram on this term with respect to its being negligible as compared to other terms in the equation.

RESPONSE

Appendix A has been amended so that the above assumption is not made. Instead, it is shown that for $1/v$ constant, and $\omega_0 = \phi$, the left-hand side of Equation A-15 becomes:

$$\left(\phi, \frac{1}{v} \frac{\partial \psi}{\partial t} \right) \phi = \left(\phi, \frac{1}{v} \psi \right) \frac{\partial \phi}{\partial t} = \frac{1}{v} (\psi, \phi) \frac{\partial \phi}{\partial t}$$

This means that Equation A-64 should be:

$$\frac{T}{v} = \iint \phi^{-2} \frac{1}{2v} dx dy.$$

This change has been incorporated into the revised version of Appendix A. Transient studies have been run which incorporate the revised definition of $1/V$. These studies show that the $1/V$ term contributes a negligible amount to the calculated neutron flux in a typical turbine trip transient.

Question 3

In Equation A-25, the precursor decay constant is assumed to vary both with time and with space. Since six precursor groups are being used with experimentally determined β 's and λ 's, explain the assumed variation of λ with space and time. In Equation A-26, for example, it is not varied as per Equation A-25.

RESPONSE

The text of Appendix A has been changed (Reference 2) so that the λ_1 's are constants. (Equation A-25 has been eliminated.)

NEDO-24154-A

QUESTION 4

In Equation A-1, the leakage term is represented as $D_1 \nabla^2 \phi_1$. However, since a perturbation theory analysis is used to derive effective cross sections, explain why the leakage term is not represented as $\nabla \cdot D \nabla \phi$ in the analysis.

RESPONSE

The spatial gradient of the fast diffusion is neglected because the fast diffusion coefficient, D_1 , is fairly constant for BWR's. This is consistent with the assumption made in the three-dimensional BWR Core Simulator Topical Report (Reference 3).

NEDO-24154-A

QUESTION 5

The shape function for the delayed neutron precursors K_1 should be related to K_1 and δK_1 by an equation similar to the one for ψ' , ψ'' and $\delta\psi'$ given by Equation A-21. Please provide this equation in the text with appropriate definitions.

RESPONSE

The requested information has been added to the text of the revised ODYN technical document.

A5-1/A5-2

QUESTION 6

Equation A-54 was the defining equation for $\bar{\beta}$ and was used in defining F in Equation A-57. In Equation A-67 another defining equation is used for β . Although the two equations for β have similar forms, justify the use of Equation A-67 rather than A-54 for $\bar{\beta}$.

RESPONSE

Equation A-54 can be written as:

$$(1) \quad \bar{\beta} = \frac{(\phi', \beta F \phi')}{(\phi', F \phi')}$$

where:

$$(2) \quad F = \frac{1}{k_o} \frac{k_m^* D_1}{M^2 - A_m/k_o} (1 + \overline{CDOP} (\sqrt{T} - \sqrt{T_o})) - \frac{D_2}{M^2 - A/k_o} + \sum_{r1}$$

Rearranging

$$(3) \quad F = \frac{1}{k_o} \frac{D_1}{M^2 - A_m/k_o} \left[k_m^* + k_m^* \overline{CDOP} (\sqrt{T} - \sqrt{T_o}) - 1 + \frac{(M^2 - A_m/k_o)}{D_1} \sum_{r1} \right]$$

Recall that:

$$(4) \quad \sum_{r1} = \frac{D_1}{M_1^2}$$

Substituting (4) into (3) yields:

$$(5) \quad F = \frac{1}{k_o} \frac{D_1}{M^2 - A_m/k_o} \left[k_m^* + k_m^* \overline{CDOP} (\sqrt{T} - \sqrt{T_o}) - 1 - \frac{M^2 - A_m/k_o}{M_1^2} \right]$$

Carrying out an order of magnitude analysis one finds that:

$$(k_{\infty}^* + k_{\infty}^* \overline{\text{CDOP}} (\sqrt{T} - \sqrt{T_0})) \approx 1.$$

The magnitude of the remaining term within the brackets,

$$\left(1 - \frac{M^2 - A_{\infty}/k_0}{M_1^2}\right),$$

is not as readily evident. The term can be rearranged as follows:

$$(6) \quad \left(1 - \frac{M^2 - A_{\infty}/k_0}{M_1^2}\right) = \frac{M_1^2 - M_2^2 + A_{\infty}/k_0}{M_1^2}.$$

However:

$$(7) \quad M^2 = M_1^2 + M_2^2 + M_3^2.$$

Thus, substituting (7) into (6) yields:

$$(8) \quad \left(1 - \frac{M^2 - A_{\infty}/k_0}{M_1^2}\right) = \frac{M_2^2 - M_3^2 + A_{\infty}/k_0}{M_1^2}.$$

The fast group migration area, M_1^2 , is approximately an order of magnitude greater than the numerator and thus (8) can be neglected with respect to K_{∞}^* . Thus, (5) can be written as

$$(9) \quad F = \frac{1}{k_0} \frac{D_1}{M^2 - A_{\infty}/k_0} k_{\infty}^* \left(1 + \overline{\text{CDOP}} (\sqrt{T} - \sqrt{T_0})\right)$$

Substituting (9) into (1) yields:

$$\frac{\left(\phi', \frac{\beta D_1 k_{\infty}^*}{M^2 - A_{\infty} / k_0}, \phi' \right)}{\left(\phi', \frac{D_1 k_{\infty}^*}{M^2 - A / k_0}, \phi' \right)}$$

This is equivalent to Equation A-67. The revised text of Appendix A includes the above approximation.

QUESTION 7

Equation A-57 was the defining equation for \bar{F} . In the equation after Equation A-67 another definition is presented for \bar{F} . Although the two equations are somewhat similar, justify the use of the second equation rather than Equation A-57 for \bar{F} .

RESPONSE

The equation after A-67 has been corrected so that it is the same as A-57.

QUESTION 8

The equation for A_{∞} given on page A-24 differs from that given in the report on the three-dimensional BWR Core Simulator by a leakage factor which comes from the flux ratio $(\phi_2/\phi_1)^{\infty}$, and Equations 3-4b and 3-11 from the report on the three-dimensional BWR Core Simulator. Please explain the difference in the definitions of A_{∞} used in the two reports.

RESPONSE

The two equations are the same if the definition of $(\phi_2/\phi_1)^{\infty}$ is used in the equation for A_{∞} on page A-24; i.e.

$$(1) \left(\frac{\phi_2}{\phi_1} \right)^{\infty} = \frac{\Sigma_{S1} l_1}{\Sigma_2}$$

The above relationship comes from Equation 3-1b of the report on the three-dimensional BWR Core Simulator for the zero leakage case.

Substituting (1) into the equation for A_{∞} from page 24 yields:

$$A_{\infty} = \frac{\gamma_1 \Sigma_{f1}}{\Sigma_{R1}} (M_2^2 + M_3^2) + \frac{\Sigma_{S1} l_1}{\Sigma_{R1}} \frac{\gamma_2 \Sigma_{f2}}{\Sigma_{R2}} M_3^2$$

(Note typo in equation for A_{∞} in p. 24. The Σ_1 inside brackets should be Σ_{f1} .)

This equation is the same as that in the report on the three-dimensional BWR Core Simulator, B-11 Equation 3-11.

Equation 3-11 of the Simulator report also contains a typographical error. The coefficients of Σ_{f1} and Σ_{f2} should be ν_1 and ν_2 , respectively.)

NEDO-24154-A

Appendix B

REFERENCES

- B-1. Letter, MFN 014-78, E.D. Fuller to D.F. Ross, "Transmittal of Draft of ODYN Qualification Report," dated January 13, 1978.
- B-2. NEDE-10358-PA, "General Electrical Thermal Analysis Basis Data, Correlation and Design Application," January 1977.
- B-3. NEDE-24011-P-3, "Generic Reload Fuel Application," May 1977.
- B-4. NEDO-10958-A, "General Electric Thermal Analysis Basis Data, Correlation and Design Application," January 1977.
- B-5. NEDE-24811-P, "Generic Reload Fuel Application," Chapter 4, Hydraulic Model Description, May 1977.
- B-6. C. L. Martin, "Nuclear Basis for ECCS (Appendix K) Calculations," NEDO-23729, November 1977.
- B-7. Letter, MFN 462-78, E. D. Fuller to D. F. Ross, "Transmittal of ODYN Computer Code Model Description," dated December 2, 1977.
- B-8. C. H. Robbins, "Performance Tests of Axial Flow Primary Steam Separators," APED-4762, January 1965 (1978 Summary).
- B-9. I. H. Edelfelt, "APED Axial Steam Separator Computer Program," 65GL10, January 1965.
- B-10. E. L. Lusterader, "Axial-Flow Steam Separator and Dryer Development," 65GL11, January 1965.
- B-11. J. A. Wooley, "Three-Dimensional BWR Core Simulator, NEDO-20953, May 1976.
- B-12. R. C. Stirn et. al. Generation of Void and Doppler Reactivity Feedback for Application to BWR Design, December 1975 (NEDO-20964)
- B-13. C. L. Martin, Lattice Methods Physics Verification, July 1976 (NEDO-20939).
- B-14. E. Hellstrand, et. al., "The Temperature Coefficient of the Resonance Integral for Uranium Metal and Oxide" Nuclear Science and Engineering, 8, 497-506 (1960).
- B-15. R. C. Stirn et al. Rod Drop Accident Analysis for Large Boiling Water Reactors, March 1972 (NEDO-10527).
- B-16. C. F. Stuart, SPERT Reactivity Tests, February 1974 (NEDO-20315).